2026

An Investigation into Methods to Advance Microplastic Retrieval, Detection and Characterisation Using Forensic Science and Machine Learning Approaches

A PhD Submitted to the University of Staffordshire

OSBORNE AMY O

MSci, PgCHPE

SUPERVISORS: PROFESSOR CLAIRE GWINNETT, PROFESSOR MOHAMED SEDKY

A THESIS SUBMITTED IN PARTIAL FULFILMENT OF THE REQUIREMENT OF THE UNIVERSITY OF STAFFORDSHIRE FOR THE DEGREE OF DOCTOR OF PHILOSOPHY

Acknowledgements

I want to express the most enormous thank you to my supervisor, Professor Claire Gwinnett, who has provided me invaluable support throughout my whole academic journey by providing emotional support, advice, and some incredible opportunities to get involved in research and projects. I would also like to thank my second supervisor Professor Mohamed Sedky for his support with everything machine learning, without your help I probably still wouldn't know where to start.

I would also like to sincerely thank Professor Andrew Jackson for his support throughout my PhD. You may not have been an official supervisor, but your support was just as valuable and helpful. I truly would have been lost without your support with statistics. In addition, I would like to thank Will Bailey for his insight and help in presenting the machine learning data.

I would also like to thank all the other academic and technical staff who helped me throughout my academic journey, in particular Sarah Appelbee for her support with the Raman analysis and Dr Alision Davidson for her support and encouragement.

The biggest thank you also goes to my fellow PhD students in S419: Dr Mia Abbott, Dr Ross Kwok, Dr Megan Needham, Dr Keith Silika, Dr Angela Bonner, Robin Parsons, Dr Laura Wilkinson, Elli Toulson and Dr Thomas Bird. Without you guys, I would have probably dropped out.

Thank you, also to my work family in the tech team; Robin Parsons (So good you get two mentions), Suzy Walley, Jade Wilson, Leah Taylor, Vicky McQuillan, Saxon Costello, Saima Hanif, Dr Tom Bird, Aimee Simmill and Liz Deakin. Thank you for keeping me going in the last few months.

Last but certainly not least, I would like to thank my family for their unwavering support. In particular, I would like to thank my Mum, who has listened to me rant and cry even when she has no idea what I'm talking about.

Abstract

The analysis of microplastics is a quickly growing area of interest as more is learnt about sources and their potential effect on the environment are discovered. As the field of microplastic research is very interdisciplinary, there are various diverse approaches to microplastic research, with different methods being deployed and different priorities being investigated depending on what is being studied. As a result of this, there is a lack of standardisation in the techniques used and even what is considered a microplastic can differ between different studies. This makes it difficult to fully compare different studies and get a clear interpretation of the presence and effects of microplastics. Machine learning has the potential to help streamline and speed up microplastic research by automating the detection of microplastics, allowing more research to be conducted in a shorter period of time.

The aims of this thesis were to investigate currently used methods of extraction and analysis and propose a new standardised approach to the retrieval and characterisation of microplastics. These methods were tested in a laboratory simulation experiment, the results of which will inform a field study conducted on samples taken from the Hudson River. In addition, the use of machine learning to automate the detection of microplastics was investigated.

These aims were met by a variety of methods. Firstly, the currently used methods of extraction and analysis were investigated by completing a comprehensive literature review to identify gaps in knowledge and areas that could be standardised and improved to help streamline microplastic research. The use of Easylift® was investigated as a method of retrieval for microplastics on filter papers to aid in the maximisation of microplastics collected and facilitate subsequent analysis. The tape was tested with two different filter papers (glass and cellulose filter papers) and two different filtration methods (Buchner filter and glass frit) to determine if one method resulted in a greater percentage of microplastics retrieved. The funnel and filter combination found to have the highest retrieval rate with Easylift® was cellulose filter paper with the glass frit, as it had a mean recovery rate of

99.16% with a standard deviation of 0.96% points. The glass filter paper with the Buchner filter combination resulted in the lowest retrieval rate (91.21% with a standard deviation of 2.03%).

From the literature review conducted, it was found that the samples are often searched for using a stereomicroscope. Then, the polymer type is confirmed by either Fourier transform infrared spectroscopy (FTIR) or Raman spectroscopy. The inclusion of Polarised light microscopy (PLM) as a method of searching and further characterisation was employed to determine if potential microplastics were missed by stereomicroscopy, and if the advantages of PLM were beneficial to the characterisation and interpretation process and if certain features meant that microplastics were more likely to be missed. A study was conducted where the sample slide was searched first by stereomicroscopy and then with PLM. The inclusion of PLM found an additional 549 particulates over the 244 sample slides subsection used in this study. The PLM found a significant number of colourless particulates that were missed by the stereomicroscope search, finding 371 (67% of those found by PLM) more colourless particulates compared to the 285 (21% of those found by stereomicroscopy) colourless particulates found with the stereomicroscope. The use of PLM also allowed for the samples to be characterised further than it was possible with the stereomicroscope, including birefringence, sign of elongation, cross-sectional shape and presence of delusterant. These features allowed for contamination to be identified with a greater level of discrimination. Finally, the use of machine learning was investigated as a method of automating the detection process, using 3102 images taken from the ‘Hudson River samples’, which were comprised of water and air samples. The images were split into training, validation, and test set with a 70% (2171), 20% (621), and 10% (310) split. The training was undertaken with YOLOv5, YOLOv7 and YOLOv8 three times for each algorithm, once with 25 epochs, once with 100 epochs and once with the augmented training set with 100 epochs. It was found that YOLOv5 performed the worst out of all algorithms investigated with an F1 score of 0.278; YOLOv5 also had the lowest mAP50 with a mean of 0.191, meaning that it had inaccurate bounding boxes. YOLOv7, with 100 epochs,

had the best all-round performance, with the correct identifications for most classes, including microfibres and fragments.

This research has contributed to the knowledge of microplastic analysis by applying a forensic science approach to the methods used in the collection and characterisation of microplastics. A new novel method of collecting microplastics from the surface of filter papers was proposed, and the inclusion of PLM was recommended to provide greater characterisation of microplastics. Certain features were recommended to be recorded, including colour, presence of delusterant and birefringence. These features allowed for potential sources of contamination to be identified and removed and potential sources of microplastics to be investigated. Furthermore, the implementation of machine learning to automate the detection of microplastics would allow the research process to be greatly sped up, allowing more research to be conducted in a shorter period of time, helping to increase knowledge of the problem and potential solutions to be identified.

Contents

Table of Tables

Table of Figures

Chapter 1 Literature Review

1.1 What are Microplastics and what are the Sources?

Microplastics as a source of pollution in the the environment was first discussed in 2004 in a study researching pollution levels in marine sediments, which reported finding an abundance of microfibres in the samples (Thompson., *et al.*, 2004). Prior to this, it was generally assumed that plastic disappeared as it degraded (Cassidy & Aminabhavi, 1981). There are several different types of microplastics, including fragments, which are small pieces of plastic that have uneven, jagged edges as they are produced through the breakdown of larger plastic items. Films are thin pieces of plastic such as from a plastic bag. Pellets, such as microbeads, are designed for cosmetic use. Microfibres are produced from shedding clothes; microfibres are defined as having a longer length than cross-sectional shape (Miller *et al.*, 2017). Microplastics are most commonly described as being smaller than 5 mm (<5mm) (Fendall & Sewell., 2009), and nanoplastics are smaller than 1 µm (Xu *et al.*, 2023a). Although some studies use slightly different size definitions, for instance, Costa *et al.* (2010) classifies microplastics as being less than 1 mm. There are also further issues with the definition of microplastics as under some definitions of polymers and plastics, rubber would be excluded, due to the presence of the elastomers that are not present in plastic and the fact that rubber can be natural (ISO 472, 2013), however, rubber from tyres has been reported as a microplastic in numerous studies (Free *et al.*, 2014 & Kole *et al.*, 2017). Due to this discrepancy, it can make comparing literature difficult, as some studies will use different definitions of microplastics, which may result in plastics that would have been included under one definition being excluded in another, meaning depending on the definition used, there would be an under or overcount of microplastics (Hartmann *et al.*, 2019). It is also important to consider items of anthropogenic origin that would not be classed as microplastic but may be harmful to the environment. For instance cotton and wool would be considered a natural material, but the process of manufacturing garments often involves adding potentially harmful chemicals such as dyes and

cleaning chemicals (Stone *et al.*, 2020). These natural materials are often not reported or investigated in microplastic literature but may be more prevalent in the environment than microplastics (Stanton *et al.*, 2019).

In this thesis, microplastics will refer to synthetic materials under 5 mm. Anthrogopenic particulates refer to both microplastics and natural materials that have been processed by humans, such as cotton. Microfibres will refer to both natural and synthetic fibres that are anthropogenic in origin unless otherwise stated.

1.1.1 Wastewater Treatment Plants

One source of microplastic pollution into the environment is wastewater treatment plants (WWTPs) (Dris *et al.*, 2015b). This is because microfibres produced by washing clothes, microbeads and glitter from personal care products are likely to end up in a WWTP (Ziajahromi *et al.*, 2017). Napper and Thompson (2016) conducted a study investigating the number of fibres discharged from a washing machine; they found that a 6 kg load of acrylic cloths could release approximately 728,789 fibres per wash, meaning a large number of microfibres end up in a WWTP every time the washing machine was used. Carr, Liu & Tesoro (2024) found a large quantity of blue polyethylene particulates in WWTP effluents that were identified as potentially originating from toothpaste. Studies of WWTPs have shown that they can remove around 99% of microplastics from the wastewater (Magnusson & Norén, 2014). Wastewater treatment plants tend to share a similar design, however, the processes that they use to filter the effluent can differ. The main treatments that can be found are aeration, flocculation, and sedimentation (Habib, Thiemann & Al Kendi, 2020). Aeration involves using air blowers, pumps and diffusers to oxygenate the aeration tanks. They often work in conjunction with the microorganisms present in activated sludge to remove organic compounds (Asadi *et al.*, 2017). Flocculation uses a chemical coagulant to bond together particulates to form larger particulates that are more easily removed as they will settle. The most common coagulants used are inorganic metal salts, including aluminium sulphate and ferric chloride; in recent years, more efficient polymeric flocculants

(coagulant aids) have been used to advance the flocculation process (Lee, Robinson & Chong, 2014). Sedimentation is used to remove solid materials in the wastewater treatment plant as the heavy materials will settle on the bottom after flocculation allowing the material to be separated with specialised tanks (Prata, 2018). Primary treatment at a wastewater treatment plant can remove around 65% of plastic contamination, and secondary and tertiary filtration techniques can remove approximately 95% of plastic contamination, preventing it from entering the water environment (Burns & Boxall, 2018). In a study investigating the effectiveness of secondary wastewater treatment processes removing 1-6.3μm polystyrene spheres, 94.9% of the 1μm spheres were removed, and 76% of the 6.3μm spheres were removed. They found that common WWTP treatment chemicals ferric chloride, polyaluminum chloride and cationic polyamine enhanced the removal of microplastics with ferric chloride and polyaluminum chloride being a more effective method than the use of polyamine. Their findings suggest that chemical coagulation is an important process in the removal of microplastics and that refinement of the dose can lead to a more effective method of removal, with a smaller dosage of coagulant being needed for the larger microplastics than the smaller size fraction (Rajala *et al.*, 2020). As this study used seeded samples with only one polymer type and microplastic type, the results may differ if, for instance, microfibres were present in the samples or plastics that were used were not 'clean' as the samples used in this study were. This is further supported by Shahi *et al.* (2020), who found that the physical shape, size and surface morphology produced noticeable differences in the flocculation and coagulation process of microplastics with a small, smooth and spherical shape having the lowest retrieval rate with both alum coagulant and alum coagulant combined with polyamine-coated sand.

Even though WWTP's are able to remove a high volume of microplastics that pass through them, they have been found to still release a large number of microplastics into the freshwater environment. Talvitie *et al.* (2017) found that WWTPs release between $1.7x10^6$ and $1.4x10^8$ microplastics per day after treatment and filtering. While Murphy *et al.* (2016) found that approximately $6.5x10^7$ microplastics were discharged per day. These two studies

demonstrate that WWTPs are a major contributor to microplastic pollution in freshwater environments, despite how effective the filtration techniques implemented are.

1.1.2 Atmospheric Pollution

Other potential sources of microplastic pollution include atmospheric deposition, with ambient outside air containing between <1 to >1000 microplastics per metre^3 (O'Brien *et al.*, 2023). The most commonly encountered microplastic type in atmospheric samples is microfibres (Ahmad *et al.*, 2023). The sources of these microfibres are likely to be from clothing as they will shed fibres through abrasion, movement and when washed (Jahandari, 2023., & Stanton *et al.,* 2023). Other sources of atmospheric microplastic pollution include nail salons from acrylic nails and tyre wear (O'Brien *et al.*, 2023).

Atmospheric transport of microplastics can impact remote locations that otherwise would have been pristine (Bank & Hansson, 2019). Terrestrial microplastics have been demonstrated to be transported to the ocean via atmospheric transport; for instance, microbeads and other suspended atmospheric microplastics have been found in sea air (Liu *et al.*, 2019). With one study indicating that the source of the microplastics found may have been 95km away (Allen *et al.*, 2019). Bergmann *et al.* (2019) found microplastics in snow samples in both the Alps and the Arctic with a mean concentration of $9.8 \times 10^3 \pm 6.9 \times 10^3$ particulates per litre with the Alps having a higher concentration of microplastics than the Arctic. This would suggest that weather conditions provide a method of transport for microplastics. However, this number is comprised of both natural and synthetic fibres, so the concentration of microplastics is likely to be lower. This study was also conducted using citizen scientists, and although they were instructed in contamination prevention methods, contamination is still likely to have occurred.

It is estimated that the annual exposure of atmospheric microplastics in cities for adults is 7.37×10^4, and for children is 1.06×10^5, which is comparable to the amount estimated to be consumed from food and water (Xu *et al.*, 2024).

It has been projected that wind transportation is responsible for 7% of primary microplastic pollution in the ocean (Boucher & Friot., 2017). Dris *et al.* (2016) found an atmospheric fallout of 2-355 microplastic particles per m^2 per day in Paris, which is similar to the results found in another study by Cai *et al*. (2017), where atmospheric fallout of 175 to 313 particles per m^2 per day in Dongguan, China was found. A study into atmospheric microplastic pollution in London found a fallout of 771 ± 167 particles per m^2 per day, with fibres accounting for 510 to 925 microplastic particles per m^2 per day; they were also able to estimate that the particulates could have travelled between 12 and 60 km with assuming a 5 m s^{-1} wind speed (Wright *et al.*, 2020). However, they also found that precipitation did not affect microplastic deposition, suggesting that the source of the microplastics originated from the city itself. Klein and Fischer (2019) have found a link between the number of atmospheric microplastics detected, storm events and wind speeds, but no links to precipitation were observed. Ward *et al.* (2024) found that fibres tended to travel further than spheres, with the fibres being deposited over a 32% bigger area. However, there is no statistical difference in distance travelled when they are smaller than 6µm. This study demonstrates that both size and shape have an impact on how far the microplastics can travel, so both should be considered when considering atmospheric microplastic pollution.

1.1.3 Abrasion of Tyres

The abrasion of tyres has also been found to generate microplastics (Kole *et al., 2017)* and is estimated to be responsible for one-third to half of all microplastics unintentionally released into the environment (Giechaskiel *et al.*, 2024). Leads & Weinstein (2019) investigated microplastic concentrations in water and sediment in the Charleston Harbour estuary; of the microplastics identified, 17.1% (n=639) were classified as tyre wear particles. Of these, only a small subset of the suspected tyre wear particles was confirmed with FTIR, meaning that the percentage of tyre wear particles could be lower than reported. Tyre wear particles have also been found to be ingested by fish in urban estuaries, as Parker *et al*. (2020) found tyre wear

particles in 14% of fish sampled. This demonstrates that not only are tyre wear particles contributing to microplastic pollution, but they also pose a risk to wildlife. It has been estimated that globally, 2907 kilotonnes of tyre wear particles are generated every year (Evangeliou *et al.*, 2020), illustrating that microplastic pollution originating from tyre wear is a major contributor.

1.2 What are the Issues Caused by Microplastics?

Microplastics are small enough to be consumed by several organisms, but the long-term effects of both microplastics in the environment and microplastic consumption are still relatively unknown (Farrell & Nelson, 2013. & Wright, Thompson & Galloway., 2013). Several factors could influence why microplastics are ingested, including the colour, size, shape, density, age and polymer type (Chouchene *et al*., 2023). The colour of the microplastic could affect its bioavailability by appearing visually similar to the organism's target food (Botterell *et al.*, 2019). In a study investigating the colour of microplastic fragments consumed by *Psalidodon eigenmanniorum* when they are exposed to red, green, yellow, white, black and blue microplastic fragments, it was found that yellow and blue fragments were more frequently consumed by the fish, and white fragments were consumed the least (Ríos, Tesitore & Teixeira de Mello., 2022). In another study, the most common colours found in the gastrointestinal tract of commercial fish were black (46.9%), followed by blue (29.4%) (Koraltan, Mavruk & Güven., 2022). These studies demonstrate that organisms demonstrate a selective feeding behaviour, meaning they are more likely to ingest microplastics of a certain colour compared to others, although it could be due to the fact that some colours have a higher abundance in the environment than other causing them to be consumed more frequently. The shape of the microplastics may also impact the likelihood of ingestion, for instance, Steer *et al.* (2017) found that microfibres were the most dominant shape of microplastic found to be ingested by fish larvae in the English Channel. In addition to being consumed, there is evidence that microplastics also interact with organisms by bioadhesion, meaning that they adhere to the surface of the organism, this is an underinvestigated pathway for microplastics, and the effects are

unknown, but some studies show that for certain species the level of bioadhesion is greater than ingestion (Kalčíková, 2023).

Plastic can act as a vector that transfers chemicals to marine organisms; approximately 84% of plastic treated in the North Pacific Accumulation zone had at least one chemical on the surface of the plastic at higher concentrations than those found in the sediment (Chen *et al.*, 2018). Microplastics can also act as a vectors, spreading harmful bacteria and organisms to new environments, including pathogens that are harmful to humans, such as *Vibrio spp*. (Zettler, Mincer & Amaral-Zetter, 2013). Walkinshaw *et al.* (2020) conducted a literature review of studies looking into microplastic contamination of different species, and they concluded that, while all species investigated showed signs of microplastic contamination, organisms at lower trophic levels have a higher risk of microplastic contamination than those at higher trophic levels. In addition to spreading harmful bacteria, they can also impact internal bacteria populations; for example, when mussels were exposed to microplastics over a seven day period followed by a seven day with no microplastic exposure there was a substantial effect noted on the levels of Spirochaetes and *Proteobacteria* when compared to mussels that had not been exposed to microplastics, this change facillitatated intestinal inflammation and enabled the proliferation of pathogenic species within the mussels (Li *et al*., 2024a).

Cole *et al.* (2015) found that prolonged exposure of copepods to microplastics greatly reduced reproductive output and led to decreased feeding behaviours. This demonstrates that microplastic ingestion is having an impact on the organisms that consume them. Farrell and Nelson (2013) found the trophic transfer of microplastics between mussels and crabs, and Nelms *et al.* (2018) found trophic transfer between wild mackerel and captive grey seals; this indicates that microplastics can move up the food chain, causing bioaccumulation and biomagnification (Galloway, Cole & Lewis, 2017). This trophic transfer has the potential to reach humans and adversely affect human health (Wang *et al.*, 2018). It has been projected that regular consumers of European shellfish may consume 11,000 microplastics every year (Karami *et al*., 2017). A study by Horton *et al.* (2018) found that when

Daphnia Magna consumed polystyrene microplastics over 72 hours no adverse effects were observed concerning their survival and mobility. Although this study did not investigate the effects of prolonged exposure, it is possible that microplastic consumption could have adverse consequences after this time. They also used clean polystyrene beads in their study, and it is unclear whether the results are due to the fact that the plastic was clean, that polystyrene beads were used, the exposure time or a combination of some or all of these factors. Although other studies, for instance, Lei *et al.* (2018) found that when zebrafish ingested plastics it caused cracking of villi and enterocytes. They also found that exposure to plastics reduced reproduction rates and increased mortality, with effects increasing as the microplastic size decreased. This would indicate that as the plastic degrades into smaller and smaller pieces, it may produce more negative effects on biota. There is a potential for plastics to cause more harm as they reach nanoplastic size (<1 μm) as they can cross the cell membrane and affect the cells' ability to function (Liu *et al,* 2021c). Besseling *et al*. (2014) has found a 67.7% rate of malformed offspring when Daphnia were exposed to 32 mg/l of aged nanoplastics, however when pristine nanoplastics were used, the rate of malformed offspring dropped to 0.3% at 32 mg/l and 12.1% at 155 mg/l. This study would indicate that it is potentially the leaching of chemicals from the plastic as it degrades which may have a bigger impact on the organism than the presence of plastic alone. They also found that the effects were not observed until 30 mg/l which is a much higher concentration of plastics than has currently been reported. When Rainbow trout were co-exposed to nylon microfibres and a virus (*Salmonid Novi rhabdovirus*), the mortality rate increased dramatically from 20% when exposed to only the virus to 80% when co-exposed to both; this indicated that microplastics could decrease an organism's ability to fight off a viral infection and allow easier access to the organism by irritating the fish's gills and digestive tract (Seeley *et al.*, 2023). This study further demonstrates that the presence of microplastics may have multiple harmful effects that go further than the physical effects of the presence of microplastics. When mice were exposed to polystyrene microplastics through intratracheal instillation, it was found that inhalation of microplastics results in autophagic cell death in the bronchial epithelial cells,

which resulted in an inflammatory response from the lungs (Jeon *et al.*, 2023). This study demonstrates that ingestion is not the only pathway for microplastics into biota and that it will have potentially harmful effects when inhaled. Another study investigating the effects of microplastics and nanoplastics on male reproductive toxicity in mice found that after a 12-week exposure period, there were several effects found, including an increase in spermatogenesis disorders and physiological abnormalities in the sperm (Gao *et al.*, 2023). The biodegradable polymer Polylactic acid (PLA) was given to mice in a repeated oral gavage study over 28 days; they found that the plastics incompletely degraded in the gastrointestinal tract, transforming into oligomer nanoplastics, increasing their toxicological effects as they are now more bioavailable and increasing toxicity. The study also found the presence of PLA in the mice's blood, brain, liver, spleen, lungs, kidneys, and epididymis, but was absent from their heart and testis (Liang *et al.*, 2024).

1.2.1 Human Health and Plastic, what is Currently Known?

Human health effects of microplastics are a cause for concern, as the effects have not been fully investigated and observed, and as they are ubiquitous in the environment, it has been observed that humans are ingesting (Alberghini *et al.*, 2023) and inhaling microplastics (Chen, Li & Wang, 2023). In addition to this, while the skin membrane will not allow most microplastics to pass through, nanoparticles may be able to pass through open wounds, sweat glands and hair follicles (Schneider *et al.*, 2009). 'Ultra fine particles or nanoparticulates' smaller than 0.1 μm are able to translocate transcellularly through the alveolar epithelium, these small particles also generate more pulmonary inflammation, leading to coughs and worsening of asthma symptoms (Schraufnagel, 2020). Microplastics have been found in human heart tissue and blood samples (Yang *et al.,* 2023b), arteries (Liu *et al.*, 2024), gallstones (Zhang *et al.*, 2024), hip and knee joints (Li *et al.*, 2024b), placenta (Zhu *et al.*, 2023) and in the testis and semen (Zhao *et al.*, 2023).

A study investigating the effects of the exposure of polyethylene on the human gut microbiota and intestinal barrier, using an adult vitro gut model, found an increase in the potentially harmful pathobionts, *Desulfovibrionacae*

and *Enterobacteriaceae*, while simultaneously finding a decrease in beneficial bacteria such as *Christensenellaceae* (Fournier *et al.*, 2023). These studies demonstrate that the presence of microplastics is likely to have an impact on human health, but more research is required to fully understand the possible short- and long-term health complications that could arise as a result of exposure to microplastics.

Another area to consider is the presence of pathogens on the surface of the microplastic, as a variety of infectious disease agents, including viruses, bacteria, fungi, and parasites, can be transported on the surface of microplastics (Beans, 2023). Plastic is a suitable vector for these communities because it is more resistant to degradation than other natural floating debris, and it has a hydrophobic surface that promotes colonisation from bacterial communities and biofilm production (Zettler, Mincer & Amaral-Zetter, 2013). Research has also shown that the microbial communities on microplastics are vectors for increased antibiotic resistance as the accumulation of pollutants and bacterial communities on the surface of the microplastics generate conditions that encourage a high transfer rate and evolution of antibiotic resistance genes (Liu *et al.*, 2021b). A study found the presence of antibiotic-resistant bacteria being between 100-5000 times higher on the surface of microplastics than the surrounding water (Zhang *et al.,* 2020); this could potentially be of great concern to human health through the production of ‘superbugs’ that are antibiotic resistant.

1.3 Macroplastics to Microplastics

Plastics that enter the environment will degrade, producing microplastics through several different mechanisms such as photodegradation, thermal degradation, hydrolysis, and biodegradation (Singh & Sharma. 2008; Andrady., 2011; & Cassidy & Aminabhavi., 1981). There tends to be some visual indications that the plastic is undergoing degradation, including, crazing, cracking, erosion, discolouration, phase separation (Singh & Sharma., 2008), changes in surface texture, and the production of biofilms (Shah *et al.*, 2008). As a biofilm is produced the plastic will become negatively buoyant and sink beneath the water (Cole *et al.*, 2011) changing the environmental conditions the plastic is exposed to.

Photodegradation degrades plastic by the impurities and extraneous groups absorbing energy from sunlight; the energy absorbed promotes it to an excited singlet state. This singlet state produced is then converted to a triplet state capable of breaking bonds, cleaving the polymer chain and generating radical pairs which form peroxy radicals with oxygen attracting hydrogen forming hydroperoxide groups; these groups also absorb energy, breaking weak O-O bonds and forming alkoxy and hydroxyl radicals, leading to hydrogen abstraction, chain scission, and rearrangement (Singh & Sharma., 2008). The changes will cause the plastic to become brittle and fragment into smaller pieces, and mechanical properties such as tensile strength also deteriorate (Cassidy & Aminabhavi., 1981). Each polymer type will have a different optimum wavelength of UV light that causes the most photodegradation; for example, it is 300 nm for polyethylene and 370 nm for polypropylene (Singh & Sharma., 2008). The deeper the plastic is in the water column, the wavelengths of light that reaches the plastic will change, wavelengths <320 are attenuated in the first six inches of the water column, (De Haan., 1993). Photodegradation is the most common form of degradation for plastics that are left at ambient conditions; when submerged, the effects of photodegradation are decreased (O'Brine & Thompson, 2010).

Biodegradation is caused by microorganisms such as bacteria and fungi that form a biofilm on the surface of the plastic that is capable of breaking down materials into CO_2, H_2O, methane and inorganic compounds or biomass

(Singh & Sharma., 2008). A biofilm is defined as a population of microbial cells that attach to the surface of an object (Stepanović *et al.*, 2004). These microorganisms that form a biofilm on the surface of plastic are known as Plastisphere organisms (Keswani *et al.*, 2016). The presence of a biofilm on the surface of the plastic changes its buoyancy, causing it to sink under the surface of the water (Zettler, Mincer & Amaral-Zettler, 2013). There are four stages in the production of biofilms: the first being adsorption of dissolved organic molecules, followed by the attachment of bacterial cells, then attachment of unicellular eukaryotes and finally the attachment of larvae and spores. After the biofilm has been produced, other organisms, such as algae, will also then attach to the surface, increasing the level of biofouling (Lobelle & Cunliffe., 2011). There are numerous factors that will influence biofilm production: the surface chemistry and structure for example the polymer type which has the largest effect on biofilm production, and size or age. Environmental conditions the plastic is exposed to includes temperature, light, nutrients, oxygen, salinity, pressure, and movements between different environments (Harrison et al., 2018). Tender *et al*. (2017) conducted a study into microbial growth on two polymer types, they found that the levels microbial cell density was five times higher on a biodegradable plastic bag than on the polyethylene bags. Lobelle and Cunliffe (2011) conducted a study investigating biofilm produced on polyethylene bags immersed in seawater. A biofilm was observable after one week of submersion; they found that plastic was neutrally buoyant by the third week of submersion and sunk below the surface. They identified *Pseudomonas* and *Arthrobacter* present in the biofilm, both of which are able to biodegrade polyethylene. When the biofilm was removed, the plastic regained its positive buoyancy. Freshwater and marine environments share some similar features, however, there is less research into biofilms produced in freshwater environments than those produced in marine environments (Harrison *et al.*, 2018) therefore the biofilms formed in freshwater environments could differ from those produced in marine environments. In freshwater environments, the location of the plastic is the greatest influencing factor on biofilm production, followed by the polymer type (Tender *et al.*, 2017). Chen *et al.* (2019) found that when plastic was placed in a freshwater lake, biofilm production differed depending on the

season, with it taking three days in spring and summer and nine days in winter; in addition to this, the biofilm produced in summer was much denser than the one produced in winter. They also found that the proportion of different species present in the biofilm was different for each season.

The type of degradation that the plastic has undergone will change the features that can be observed. For instance, photodegradation will cause yellowing of plastic (Singh & Sharma., 2008). The location of the plastic will also influence the degradation rates of the plastic Arias-Villamizar & Vázquez-Morillas (2018) found that plastic degraded faster in a marine environment than in a freshwater environment, as there were higher levels of microbial activity and salinity. The polymer type has been shown to influence how fast a plastic will degrade O'Brine and Thompson (2010) conducted a study looking into how polyethylene degraded compared to a biodegradable corn-starch alternative. After 40 weeks submerged in seawater, 100% of the surface area for a biodegradable plastic carrier bag had disappeared, while the polyethylene bag had only decreased by 2%. This indicated that biodegradable plastics degrade faster than conventional plastics. Although this study only investigated the surface area and tensile strength of the plastics, meaning it does not provide any information on how the plastic has degraded and at what point in time the signs of degradation will occur. They also only looked at degradation in salt water, so the results are likely to differ in different conditions. For instance, the tensile strength of plastics has been shown to decrease faster when left exposed to the air than when submerged in water, as it was exposed to more UV light and so was able to photodegrade to a greater extent than the submerged plastic (Andrady, 2011). This demonstrates that there are different factors which will influence the speed of degradation depending on where in the environment the plastic is left to degrade. Ikada (1999) conducted an experiment to observe the features of plastic as it degrades using SEM; when the plastic was left in activated sludge, semi-spherical holes formed on the surface that would grow gradually larger in size whilst still maintaining their shape. Whereas when the plastic was left to degrade in soil, random shaped holes were observed, and the plastic began to crack after ten weeks. Although there

were no results on how the plastic may degrade when they are in either fresh or saltwater.

1.4 Microplastics in Freshwater Environments

Freshwater systems could be a major contributor to marine microplastics, and more research is needed to determine the levels of plastic pollution in freshwater environments (Dris *et al.*, 2015b). A study into the microplastic pollution in the Nida River, Poland, found 245 ± 21 microplastics per litre (Bhat & Janaszek., 2024). Research into the Danube River has reported a higher mass of plastic compared to that of larval fish, with plastic being found to weigh 4.8 ±24.2 g per 1000 m^{-3}, and fish larvae 3.2 ±8.6 g per 1000 m^{-3} (Lechner *et al.*, 2014), however, this study used visual sorting with the naked eye, so many microplastics were likely to have been missed. The study was also conducted from April to June when there are likely to be more fish larvae present in the water, and they do not provide any data to compare the levels of pollution with the rest of the year. Miller *et al*. (2017) assessed the levels of microplastic pollution in the Hudson River finding a concentration of 0.98 microplastics/l^{-1} and 233 microfibres over 142 samples. Although, in subsequent analysis half of these were identified as natural fibres. They estimated between 200 and 800 million microfibres were discharged from the Hudson per day, with an average of 300 million per day. This study was only investigating microfibre pollution meaning that the data may not be representative of the total microplastic pollution which is likely to be much higher. In another study, the surface waters of the East River and Long Island Sound USA were sampled for microplastics and anthropogenic pollution using the grab sample method (see section 1.5, for more information on Grab samples). 97% of the samples taken contained anthropogenic particulates with the two hotspots found correlating with either high population density or areas of high shipping traffic (Miller *et al.*, 2024). Faure *et al*. (2015) conducted a study into Swedish lakes; over all of the sediment samples, there was an overall population of 1300±2000 microplastics/m2 in the water samples, an average of 43,000 particles/km^2 over three lakes. Although, in this study, a neuston net with a mesh size of

333µm was used; meaning any microplastics that are smaller than the mesh will not be retained, indicating that the population of microplastics in the water column was higher. For instance, one study into microplastic pollution in the Seine used two different mesh sizes to sample the water column; when the 80 µm mesh was used, a microplastic concentration between 0.003 to 0.106 particles/L^{-1} was found. Whereas when a mesh of 330 µm was used, a concentration of between 0.00028 and 0.00045 particles/L^{-1} was recorded (Dris *et al.*, 2015a). This study demonstrates that microplastic pollution does exist in the Seine, albeit in low concentrations, but the use of two different mesh sizes demonstrates how many microplastics can be lost even when using small mesh sizes, due to this it is likely that even the 80µm mesh would have lost some microplastics that were too small to be retained by the net. Small rivers that run through moderately populated catchment areas also have a high level of microplastic contamination in some cases higher than those found in larger rivers,

The concentration of microplastics in freshwater environments is likely to change as it travels through different environments and sources of pollution, Peters and Bratton (2016) found that the concentration of microplastics found in the stomachs of sunfish in the Brazos River Basin was the highest in urban areas followed by downstream locations and the lowest concentration of microplastics were found in upstream locations. Microplastic concentrations have also been found to increase in areas near and downstream of wastewater treatment plants (Mintenig *et al.*, 2017). A small river in Oker Northern Germany was found to have an overall microplastic pollution level of 63 microplastics per m^{-3}, they also found higher concentration of microplastics in the urban areas (71/m^{-3}) than the rural areas (51/m^{-3}) (Büngener *et al.*, 2024). There is also the potential for temporal differences in microplastic concentrations, for instance, Nel, Dalu and Wasserman (2018) found greater microplastic concentrations in river sediment in winter due to increased sediment deposition caused by reduced river flow. Although the overall microplastic concentration does not increase the further downstream the samples are taken, Miller *et al*. (2017) found similar microplastic concentrations at the start of the Hudson River to those

found at the end of the river, although there were hotspots in certain areas such as near large cities. The cause for these findings was not investigated during this study; however, one possible explanation is that they were only sampling the surface of the water, and large quantities of plastics may be present further down the water column as the plastic settles while they degrade and are retained in the river sediment (Nizzetto *et al.*, 2016).

1.5 Collection and Analysis

One of the main challenges to microplastic research is that there is no standardised approach to collecting or analysing microplastics, which makes the comparison of different studies more challenging as they would have used different methods (Barrows *et al*, 2017). In addition, the definition of what size parameters constitute a microplastic varies from study to study, the most widely used size range is less than 5 mm in size (Thompson *et al.*, 2009), but other size parameters, such as being less than 1 mm in size are also commonly seen in literature (Van Cauwenberghe *et al.*, 2013. & Browne *et al.*, 2011). There are three main approaches used as sampling methods: bulk sampling, volume-reduced, and selective sampling (Hidalgo-Ruz *et al.*, 2012). Table 1.1 shows what methods of collection and analysis various papers have employed. Selective sampling is not used frequently in microplastic research as it would be difficult to visually detect the smaller size fractions and so would only be an appropriate method when interested in the larger size fractions of plastic. Each approach uses different methods of collecting microplastics, meaning they are likely to collect microplastics in different quantities and sizes. For example, selective sampling uses visual inspection to manually remove microplastics, suggesting those that are very small or have no features that stand out such as being a bright colour are unlikely to be collected. In contrast, bulk sampling removes an entire volume of the matrix being investigated (e.g. sediment or water), meaning that it will gather all microplastics present within the area samples Barrows *et al*. (2017) produced the ‘grab method’ a form of bulk sampling for retrieving microplastics in water to collect a representative sample. This method involved collecting a one-litre water sample. The study found that the ‘grab

method' recovered three orders of magnitude more microplastics than the more commonly used neuston net. This method was further adapted by Miller *et al*. (2017) to collect water from the top 8-18 cm by using a metal bucket that has been triple rinsed. The collected water is then decanted into a clean 1-litre glass jar with a metal lid.

The location that samples are taken from also varies from study to study; for instance, sediment samples have been taken 1 cm from the surface (Browne *et al.*, 2011) from a 5 cm depth (McDermid & McMullen., 2004., & Song *et al.*, 2015), 10 cm depth (Horton *et al.*, 2017), 15 cm depth (Dris *et al*, 2015b) and 28 cm depth (Claessens *et al.*, 2011). As the samples have been collected from different depths, the results found are not easily comparable, as there is likely to be a change in the concentration of microplastics as the depth of the sediment sample increases.

There are several techniques implemented to separate microplastics from the sediment, the most commonly used is density separation which involves using a NaCl solution to separate plastics based on their density as the plastics have a lower density than the sediment and so will be suspended in the liquid whilst the sediment sinks to the bottom allowing separation (Hidalgo-Ruz *et al.*, 2012). However, there are different techniques to collect the microplastics, Crawford and Quin (2017) used a method of density separation where the sediment was agitated for two minutes before being allowed to settle for ten minutes, after which time the supernatant was extracted using a three-necked flask and a vacuum for filtering; this process was repeated three times to ensure optimum extraction of microplastics. Other methods have involved using an air pump to agitate the sediment whilst more NaCl was being pumped in, causing the excess NaCl to overflow, bringing the separated microplastics with it, which is then caught by a glass vessel (Nuelle *et al.*, 2014). There are also different concentrations of NaCl used, for instance, the most commonly found one is 1.2kg/l (Browne *et* al., 2011), but filtered seawater has also been used (Turra *et al.*, 2014), ZnCl is another method employed as it has a higher density and so will retrieve plastics with a higher density that NaCl may not retrieve (Lahens *et al.*, 2018). As different studies are using different techniques to extract

microplastics it is possible that the results produced would be different if another technique had been implemented, for instance, it is very unlikely that all the microplastics were removed during filtration with the seawater, meaning that some could remain to contaminate the sample, while NaCl may not recover as many microplastics as ZnCl as it has a lower density and any plastics with a high density such as PVC would not be extracted. Density separation has been found to be an ineffective method of extraction in instances where there is a high proportion of organic matter, for example, wastewater treatment samples, this is because these organic substances exhibit densities similar to the plastic being extracted from the sample (Tagg *et al.*, 2015).

Table 1.1 A table to show how different studies collect and analyse microplastic samples.

Study	Sample type	Collection method	Sequential analysis methods	Characteristics reported
Yin *et al.* (2022)	Sediment	- Grab	- Stereomicroscopy 20-100x - FTIR	- Microplastic type - Polymer type - Size - Colour
Stanton *et al.* (2019)	Water	- Volume reduced	- Stereomicroscopy 16-160x - Optical microscope 100x - FTIR	- Microplastic type - Polymer type - Colour
	Air	- Bulk		
Kapp & Yeatman (2019)	Water	- Grab - Volume reduced	- Stereomicroscopy 15-120x - Hot needle test - Raman spectroscopy	- Microplastic type - Polymer type - Size
Miller *et al.* (2017)	Water	- Grab	- Stereomicroscopy 45x - FTIR	- Microplastic type - Polymer type - Size - Colour
Faure *et al.* (2015)	Water	- Volume reduced	- Stereomicroscopy - FTIR	- Microplastic type - Polymer type - Size
	Sand	- Bulk		

Van Cauwenburg *et al.* (2013)	Sediment	- Bulk	- Microscope - Raman spectroscopy	- Polymer type
Dris *et al.* (2016)	Air	- Bulk	- Stereomicroscope - FTIR	- Microplastic type - Polymer type - Size
Horton *et al.* (2017)	Sediment	- Bulk	- Light microscope 6x - Raman spectroscopy	- Microplastic type - Polymer type - Size -Colour
Lechner *et al.* (2014)	Water	- Volume reduced	- Visual inspection	- Microplastic type
Wang *et al.* (2017)	Water	- Volume reduced	- Stereomicroscopy 160x - Scanning electron microscopy - FTIR	- Microplastic type - Polymer type - Size - Colour
Laju *et al.* (2022)	Water	- Volume reduced	- Stereomicroscopy 40x - FTIR - Scanning electron microscopy	- Microplastic type - Polymer type - Size - Colour -Surface characteristics - Inorganic elemental composition
	Sediment	- Bulk		
Banik *et al.* (2024)	Water	- Volume reduced	- Stereomicroscopy - FTIR	- Microplastic type - Polymer type - Size - Colour
	Sediment	- Bulk		
Rosso *et al.* (2024)	Snow	- Bulk	- Microscope - FTIR	- Polymer type - Size
Dowarah *et al.* (2020)	Bivalves		- Nile red & fluorescent microscope 40-100x - Raman	- Polymer type - Size
Parker *et al.* (2020)	Fish		- Stereomicroscopy 10-110x -Hot needle test - FTIR	- Microplastic type - Polymer type - Size - Colour

Eriksen *et al.* (2013)	Water	- Volume reduced	- Scanning electron microscopy	- Microplastic type - Presence of Biofilms - Surface morphology -Elemental composition - Size - Colour
Sierra *et al.* (2020)	Water	- Volume reduced	- Polarised light microscopy x4-x100 - Confocal Raman - Near infrared spectroscopy - Scanning electron microscopy	- Microplastic type - Optical activity - Polymer type - Elemental composition - Size
Büngener *et al.* (2024)	Water	- Volume Reduced	- Stereomicroscopy 40-50x - Macroscope 80x - FTIR	- Microplastic type - Polymer type - Size - Colour

Table 1.1 shows that the majority of microplastic studies use a stereomicroscope to visually search for potential microplastics, which is then confirmed with either Fourier transform infrared spectroscopy (FTIR) or Raman spectroscopy to produce a polymer identification. Some papers have used a method called the hot needle test, which uses a hot needle to confirm if the object is a polymer and determine its melting point; this method is a cheap and quick method of identifying if an item is synthetic; it does not give an accurate indication of the polymer type (Lusher *et al.*, 2017). This method would cause damage to the polymer, altering its optical properties, meaning that it would then be difficult to do some subsequent analysis, such as polarised light microscopy, which is commonly used to analyse fibres within forensic science. The majority of studies use FTIR to determine polymer type, and the remainder use Raman spectroscopy. FTIR works by exposing the sample to infra-red radiation, which affects the molecule's atomic vibrations, producing a specific absorption or transmission of energy that can

be used to identify the bonds present in the molecule (Nandiyanto, Oktiani & Ragadhita, 2019). Meanwhile, Raman uses a two-photon inelastic light scattering event to produce ‘Raman scattering’ and provide information on the molecule's structure through molecular vibrations (Araujo *et al.*, 2018). Both techniques have advantages and disadvantages; for instance, they are both non-destructive, but Raman spectroscopy can struggle with fluorescent samples (Xu *et al.*, 2019). It is, though, able to analyse microplastics down to 1μm, meaning that it can characterise microplastics that would be too small for FTIR analysis (Fu *et al*., 2020). FTIR may not be suitable for samples smaller than 5μm as they are unlikely to produce enough absorbance for an interpretable spectrum to be produced, FTIR will also have issues with complex environmental matrices, which can make the identification of smaller samples difficult (Xu *et al*., 2019). A further limitation of FTIR is that black particles absorb strongly in the infrared range and can lead to total absorption, resulting in difficulties in the interpretation of results and can lead to an underestimation of microplastic populations (Stock *et al.*, 2022).

Another method being used in Table 1.1 is Scanning electron microscopy (SEM); in this method, the sample is scanned with a highly excited electron beam (Yadav *et al.*, 2023). SEM coupled with an energy dispersive X-ray (EDS1) is able to differentiate carbon-based materials such as plastics from non-polymers, as the plastics will show carbon-specific signals that differ from those found in non-plastic materials (Blair *et al.*, 2017). The technique is, though, unable to identify the specific polymer present or its quantity (Yadav *et al.*, 2023). SEM can also be used to determine the presence of a biofilm and observe the plastic surface morphology to look for signs of degradation (Eriksen *et al*., 2013).

The fluorescent dye Nile Red has also been applied to microplastic research to help detect microplastics. The dye absorbs onto the surface of the microplastics using van der Waals interactions and dipole interactions in polar polymer types, allowing them to become visible when exposed to blue light (450-510 nm) (Maes *et al*., 2017). The technique is fast and easy to use as it requires minimal training to use effectively (Sturm *et al.*, 2023). This method does, however, have some drawbacks, such as the dye can make

the determination of the original colour of the microplastics difficult; in addition to this there are instances where Nile Red is unable to stain some coloured microplastics due to the presence of the dye used in their production meaning that the method will not stain all microplastics that may be present in a sample (Shruti *et al.*, 2022). Both synthetic fibres and natural fibres will also fluoresce with this method, meaning that other methods are still needed to differentiate and identify the synthetic microplastics from other materials within the sample (Galvão *et al.*, 2023).

1.6 Forensic Fibre Analysis

Microfibres are one of the most common shapes of microplastics found in literature (Woodall *et al.*, 2015). In study investigating marine sediments in Belgium, 59% of the microplastics found were microfibres, 25% were granules, 12% were microbeads, and 4% were plastic films (Claessens *et al.*, 2011). Due to microfibre prevalence, researchers must be able to characterise fibres, which is traditionally a forensic application, meaning that the techniques used in forensic science can be transferred to microplastic research.

Microplastic research could benefit from applying forensic techniques to analyse and quantify microplastics to get the most information out of the plastics found. Currently, many papers do not quantify microplastics beyond type, colour and polymer type (see Table 1.1) (Bagaev *et al.*, 2017., Free *et al.*, 2014. & Kang *et al.*, 2015). Some studies also only use a stereomicroscope with a maximum magnification of x40 to find and characterise microplastics (Dris *et al.*, 2015a., Bagaev *et al.*, 2017. & Miller *et al.*, 2017), meaning that the microplastics cannot be quantified to the same extent as forensic fibre analysis as the microscope cannot observe the plastics at a high enough magnification to observe any inclusions on the surface or the cross-sectional shape of the fibre that using polarised light microscopy (PLM) can observe as it can achieve greater magnification than the stereomicroscope (Kasetty, Rammanohar & Ragavendra, 2010). This allows the fibre to be characterised to a greater extent with the PLM; for

instance, a common forensic approach is to identify the cross-sectional shape of the fibres (Grieve, Biermann & Schaub, 2005); this has relevance to microplastic analysis as different cross-sectional shapes will have different surface areas and as such will have different toxicological effects as some will be able to accumulate more persistent organic pollutants (POPs) as they have a greater surface area. Other characteristics used to identify synthetic fibres include identifying the presence of delusterant, colour, birefringence and fluorescence (Buzzini & Massonnet, 2015). All these attributes allow the fibre to be characterised further than polymer type, potentially allowing for trends and potential sources to be identified; for instance, in a forensic case, the 'Atlanta child murders' a green trilobal fibre could be linked back to a particular carpet manufacturer, these fibres were then linked to a carpet in the suspect's parents' house (Palenik, 1999). This case demonstrates how valuable the information that can be gained from fibre evidence is. Applying the same techniques to microplastic research will allow for greater characterisation of the samples, meaning more trends and possible sources of the plastics can be identified. Forensic fibre work also provides methods of retrieving fibres from surfaces, mainly through tape lifting (Robertson & Roux, 2018). A method of recovery implemented in this research study is the use of Easylift®; Easylift® was developed at the University of Staffordshire as a new method of retrieving fibre evidence from crime scenes and allowing the fibre's optical properties to be recorded without the need to dissect the tape as it is non-birefringent and so does not interfere with analysis using a polarised light microscope (Gwinnett & Jackson, 2013). 'Easylift®' has been used by Staffordshire police to retrieve fibres from places such as seat belts and windows (Jackson & Gwinnett, 2013). In this instance, it will be used to extract microplastics from filter papers once the samples have been filtered see Chapter 2 for more information.

Forensic fibre analysis often has large quantities of samples that need processing, which costs a lot in terms of both time and money (Robertson & Roux, 2018). Large-scale data needs to be collected to fully understand the effects of microplastics on the environment and their prevalence. This also has large implications regarding time and cost, as collecting, processing, and

analysing samples is very time-consuming. To overcome this, an automated system of detecting and characterising microplastics and forensic fibres is needed, as it will allow the time taken to analyse samples to be greatly reduced, thus decreasing the cost and time required to fully process samples, allowing more research to be done in a shorter period of time.

Another potential issue with microfibres is contamination prevention, as fibres are commonly found in laboratory conditions and in clothes (Woodall *et al.*, 2015). Due to this, it is beneficial to apply forensic approaches to fibre analysis and contamination prevention to microplastic research to ensure accurate quantification of microplastics in the environment. A process that automatically detects and categorises fibres would be very beneficial to forensic fibre analysts as it would reduce the time required to fully process the fibre, increase consistency, and remove any potential human errors that may arise (Langdon *et al.*, 2003).

1.7 Machine Learning

Machine learning has many applications, especially when used in conjunction with image processing. Artificial intelligence allows computers to understand observations, as computer vision works from a mathematical and logistical standpoint, and image processing is seen as mapping. This means that if the algorithm knows the domain in which the observed data is constrained, the analysis can become automated (Sonka, Hlavac & Boyle, 2014). Machine learning and image processing have been used to detect oil spills from satellite radar images by training it to recognise oil spills and disregard natural occurrences such as rain and algae, which can appear similar on the satellite image (Kubat, Holte & Matwin, 1998). This approach could be applied to microplastic analysis, allowing the automatic detection and characterisation of microplastics, speeding up the analysis time.

Machine learning systems can come in various categories that are based on whether they are using supervised, unsupervised, semi-supervised or reinforcement learning; this can be further categorised into whether they are using an online or batch learning process and whether they have an instance-based or model-based approach (Géron, 2019). In unsupervised

learning, the machine is given the input but not the output, so it has to find hidden trends from the data provided (Zanero & Savaresi, 2004); some common unsupervised algorithms include K-means, Hierarchical cluster analysis, Isolation Forest, anomaly and novelty detection and Principal component analysis (Géron, 2019). Whereas in supervised learning, the machine is given both the input and the output, allowing it to learn from the training sets provided; it will then be able to identify objects included in the training without them being labelled (Lloyd, Mohseni & Rebentrost, 2013) some common supervised learning algorithms include: K-Nearest Neighbour, Decision Trees and Random Forest, neural networks and linear regression (Géron., 2019). Supervised learning has been implemented in the determination of sex from skeletal remains, which had an overall accuracy of 95% (Bewes *et al.*, 2019), demonstrating the wide applications of supervised learning to classify objects. Both approaches have benefits and limitations, for instance, unsupervised learning can produce some unpredictable outputs (Woźniak, Wyrzykowski & Belokurov, 2012); this would mean that the classifications would need to be checked by a human operative to verify the classifications, whereas supervised learning is only able to identify objects that it has been taught in its training sets if something new appears it will not know how to classify it (Dakka, Ipeirotis & Sacco, 2009). Although, this can be overcome with a comprehensive training set. Semi-supervised algorithms use partially labelled data, and an example of this is photo-hosting systems where the user will upload their photo, and the system will cluster the photos it believes are of the same person; this part is unsupervised. The user can then provide a label for one image, which will be applied throughout the dataset; these processes tend to use both supervised and unsupervised algorithms (Géron, 2019). In reinforcement learning, the system observes the environment and makes decisions as to what actions to perform; if it performs well, it gets a reward, and if it does not, it receives a negative reward; from this, it is able to identify the best strategy to solve the problem. Reinforcement algorithms include Proximal policy optimisation, Trust region policy optimisation and Deep deterministic policy gradients (Henderson *et al.*, 2017).

Random Forest is a commonly used algorithm for image classification that produces multiple decision trees where the different classifiers are produced using a random vector sampled independently from the object being identified. Every decision tree's outcome will then 'cast a vote' to identify the input vector with the identification with the most votes being used to identify the object (Pal, 2005). Decision Trees classify objects from a starting root node down to a leaf node which provides the identification of the object. Each decision tree generated contains one or more leaf nodes and internal nodes; the internal nodes will have at least one child node that corresponds to one of the possible values for each classification; these nodes lead to a leaf node that provides the classification for the decision tree (Raileanu & Stoffel, 2004). The Random Forest classifiers measure the impurity of an identification using the Gini index; this allows the chance of a misclassification to be determined (Davidson, 2009). The more trees there are in a random forest, the more robust the classification systems are. This will, however, result in a reduction in speed, which will slow down any real-time prediction and classifications, meaning it would be unsuitable for applications such as traffic predictions (Ahmad *et al.*, 2018).

K-Nearest Neighbour is another algorithm used for classification and regression, it is based upon a distance function to determine the difference or similarity between two inputs, with an unknown input being classified using the classification of its nearest neighbour if there are several neighbours close to the input then it will classify the input with the most 'votes' (Rajagopalan & Lall, 1999). K-Nearest Neighbour has the advantage of being simple to implement, and the training is fast; it is also a robust technique to use when there is noisy training data or a large training set; however, it can become biased by the value of K, it has computation complexity, memory limitation issues and can be led astray by irrelevant attributes leading to an inaccurate classification (Bhatia & Vandana, 2010).

You Only Look Once (YOLO) is a single-stage object detection framework that is faster compared to two-stage approaches (Koirala *et al.*, 2022). The algorithm is able to detect and classify objects in real-time by using a convolutional neural network (CNN) (Naseri & Ali, 2022). The algorithm has

been frequently used due to its ability to have a high accuracy whilst having a small model size and being able to be trained on a single Graphic processing unit (GPU) (Solawetz. & Francesco, 2024). The algorithm works by splitting the image into a grid; the grid cell that the centre of an object being detected falls into is responsible for detecting that object, each grid square will calculate a confidence score for each bounding box that indicates how confident the model is that a correct prediction has been made (Redmon *et al.,* 2016).

Support Vector Machine is also used for classification and regression; it separates clusters and classifies unknown objects by separating the hyperplane; the unknown object is then classified depending on which side of the hyperplane it falls. Several potential hyperplanes will be tested to find the maximum margin separating the hyperplane, by selecting this hyperplane it will maximise the classifiers' ability to predict the classification of unseen examples. The Support Vector Machine can still deal with outliers and anomalies through the use of a soft margin, that allows some data points to be classified despite being on the other side of the hyperplane (Noble, 2006). Support vector machines are good with unstructured and semi-structured data such as images and text, it is also possible to add additional dimensions to the data through the use of the kernel function allowing the generation of two-dimensional classifications from one-dimensional data (Noi & Kappas, 2017).

Background subtraction (BGS) models are used to detect moving objects by labelling pixels that are significantly different from the background (Benezeth *et al.*, 2010). For BGS algorithms to be successful, they need to be able to cope with variations in illumination conditions, be able to disregard the movement of small elements in the background and be capable of adding additional elements to the background model (Parks & Fels, 2008). Parks & Fels (2008) compared seven different background subtraction algorithms including both recursive methods; Running Gaussian Average (RGA), Gaussian mixture model (GMM), GMM with an adaptive number of Gaussians (AGMM), approximated median filtering (AMF); and non-recursive

methods; Median filtering, Mediod filtering and EigenBackgrounds (EigBG), using seven outdoor and six indoor video sequences. They found that all the algorithms tested had a performance difference of less than 10%. The Mediod filtering algorithm outperformed the others investigated when the recall was >0.85, but when the recall was <0.85 GMM and AGMM algorithms performed the most successfully. None of the algorithms were able to consistently create a high-quality foreground mask. The authors recommend the AMF if computational efficiency or memory requirements are a priority, but if a more theoretically sound BGS is required, then Mediod filtering or AGMM would be the more appropriate algorithm to implement.

Lorenzo-Navarro *et al*. (2018) tested several algorithms (K-Nearest Neighbour (K-NN), C4.5, Random Forest (RF), Support Vector Machine (SVM), and adaptive boosting (AdaBoost)) ability to detect microplastic particulates, They found that RF with ReliefF used prior to training to maximise the separation of the classes had the best overall, accuracy (96.6%), precision (96.6%) and recall (96.6), however, when comparing the ability of the algorithms used on their own, RF still outperforms the other algorithms investigated with accuracy (96.4%), precision (96.5%) and recall (96.4%). However, this study was only interested in producing a microplastic count and classifying it into broad categories: fragment, line, pellet, and tar. The study did not attempt to classify the microplastic further than this; they also predominantly used microplastics in the larger size fraction, meaning that it may not be as accurate with smaller microplastics. In another study comparing the RF, KNN and SVM algorithms for land coverage classification, they found that overall classification results ranged from 90-95% successful identification with the support vector machine classifier generating the most accurate results with the least sensitivity to training sample size. RF was the second most accurate followed by KNN. The difference between the accuracy of classification results of KNN compared to RF increased as the training sample size increased (Noi & Kappas, 2017). Khan & Ahmed (2019) also compared the use of these three algorithms to detect snow conditions; they found that SVM produced the most accurate results (95.9%), followed by RF (94%) and then KNN (93.1%). KNN also performed the worst on all

the image classification weather conditions and had the most false negatives.

1.8 Automated Detection

The field of forensic science has been trying to develop a system of automating fibre detection for several years, for instance, the Foster and Freeman Fx5 fibre finder system and the Cox analytical Maxcan fibre finder (Langdon *et al.*, 2003). Paulsson & Stocklassa (1999) produced a system to identify fibres based on their colour using image processing. However, this system struggled with debris contamination, pale fibre colours and fibre aggregation. More recently, Wetzer and Lohninger (2018) have attempted to develop an automated method of identifying forensic fibres using image processing and were able to produce a system that is able to optically match fibres and cope with contamination by dirt, air bubbles and changes in focus, although some fibres were not fully detected as it only detected some of the fibre and not its full length leading to an overcount. Sermier *et al*. (2006) conducted a study to compare the Maxcan fibre finder system to manual analysis, they found that the automatic system tended to be more efficient than the analyst, although when an experienced examiner was used and allowed sufficient time they were just as efficient as the Maxcan system. However, the system itself had several issues; for instance, the system struggled to detect pale and very dark fibres as it struggled to differentiate strong colours and pale colours from Newton's rings. One of the benefits of this system is that it is not influenced by the diameter of the fibre which the analysist was influenced by, in particular by the presence of microfibres. This provides support for the production of an automated system for microplastics as it is not affected by the presence of microfibres, which are one of the most abundant microplastics. The SHUTTLE project has developed a SMMART microscope capable of hyperspectral, fluorescence and polarimetry (Balas *et al.*, 2023) to automatically locate and identify trace evidence from crime scenes using a range of microscope techniques including, polarised light, transmitted light, fluorescence and absorption microscopy (Bijker, 2023). A study into the use of the SMMART microscope found that it was able to speed up trace evidence analysis on tape lifts containing hairs, textile fibres,

sand, pollen, glass, skin and blood up by a factor of 178.6 (Balas *et al.*, 2023). The microscope uses images of the tape lift, and the trace evidence undergoes colour and spectroscopic analysis. The images produced are processed by artificial intelligence. This data is then compared to the internal databases to search for the identification of the different types of evidence present in the sample. (SHUTTLE, 2022).

Microplastic research is going through the process of becoming automated. Primpke et al. (2017) used focal plane array (FPA) FTIR microscopy and image analysis to create an automated method of polymer detection for microplastics. The system developed was able to identify size, count and polymer type with a good level of reliability and accuracy, however, the time taken to complete the analysis was still high compared to manual methods meaning that it is not saving time for analysts. Although it was able to detect and identify more of the smaller particles than the manual methods, demonstrating that it is still a useful tool for identification of analysis. Jia *et al.* (2022) used a laser direct infrared (LDIR) imaging system (8700 LDIR) and FTIR to automate the identification of microplastics in soil samples after extraction and acid digestion of the soils. The software scans the selected area and identifies non-particle areas as background; it would then perform a morphological identification and collect an infrared spectrum to identify the particulate. Giardino *et al.* (2023) used Nile red staining, and a Python script called ‘MicroplasticsLab’ that segments the image to quantify and measure microplastics on the filter membrane. The method implemented had an average image processing time of 10 seconds and was able to identify microplastics with a deviation of 8% compared to the manual count. This approach was able to solve the ‘halo’ effect that can be observed with fluorescent samples, leading to fewer errors and misattribution of microplastic shapes. Tang *et al.* (2024) used a digital slide scanner VS120 and the image processing software ‘MPs-Counter’ to semi-automate the quantification of spherical microplastics. It was able to detect microplastics down to 1µm with an error rate below 0.6%. The samples used in this study were clean fluorescent polystyrene microbeads stored in ultra-pure water, meaning it is not a representation of environmental samples and so the

performance is likely to vary when it is exposed to a sample with background debris and various shapes and sizes of microplastics.

Lorenzo-Navarro *et al.* (2018) have attempted to produce a system to count and classify microplastics 1-5mm using machine learning and computer vision. They used a variety of different classifiers (KNN, C4.5, RF, and SVM) to determine which was the most accurate. They found that the RF classifier was the most accurate, with an overall accuracy of 96.6%. In the more recent study, they used the previously tested algorithms and a three-level cascade classifier, SVM, to classify lines, then RF to classify pellets, followed by Principal component analysis with RF to classify organic, tar and fragments. They found that all the algorithms tested had comparable performance, but SVM had the highest accuracy at 88.3%, and the cascade classifier had an accuracy of 91.1% (Loranzo-Navaro *et al.*, 2020). While it is able to identify microplastics with high accuracy, it does not fully classify the microplastics beyond type and colour, leaving a potential for natural microfibres to be identified as synthetic. This demonstrates that there is still room for improvement in automated methods of characterising microplastics and fibres. Wang *et al*. (2024) used flow cytometry and machine learning to differentiate microplastics from natural particulates in aqueous suspensions. They tested both supervised (Random Forest) and unsupervised approaches (viSNE maps) (see Section 1.7). They found that they were able to accurately measure microplastics in the suspension with both machine learning methods, with accuracies of over 93% achieved. They were, however, unable to differentiate between different size fractions and polymer types. viSNE was able to identify microplastics when the microplastic content was less than 20%; when samples contained a microplastic content higher than 20%, there was a slight over-estimation, which could then be further exacerbated by the presence of diatoms and suspended biofilms. Random Forest also struggled with samples with a suspended biofilm but performed well when microplastic content was less than 40% (1.6% absolute deviation compared to theoretical content). If microplastic content was above 40% Random Forest performance decreased. While this method provides no characterisation of the microplastics detected it can be used as a rapid

screening method to give indications of the level of microplastic contamination within a sample in a time-effective method.

1.9. Knowledge gaps

The field of microplastics research has evolved considerably in the last few years, with more sample types being analysed and new techniques applied to detect and characterise the samples. As of yet there is not a method that facilitates extraction from filter paper in the field, allowing the samples to be stored without risk of loss or contamination. This also means that the bulk samples either have to be taken back to the laboratory for filtration (Haque, Holsen & Baki, 2024 & Yang *et al.*, 2023c), or the filter papers are stored in a container until analysis (Cunningham *et al.*, 2022 & Soininen *et al.*, 2024). This potentially limits the quantity of samples being taken or reducing the amount of data obtained from the samples due to time constraints and allowing the potential for loss and contamination of samples. In addition, at the time of writing there has been no published research into the potential for stored samples to become contaminated or for sample loss to occur. A method of extraction from filter papers that allows the samples to be stored long term without risk of loss or contamination would be beneficial to the field of microplastic research. It could also then facilitate inter-laboratory studies, by allowing the samples to be easily sent to different facilities allowing results to be validated by other researchers, creating more reliable data and allowing for samples to be re-analysed as new techniques emerge.

There is also no research into the potential rates of loss of microplastics during filtration, by knowing what is likely to be lost during filtration it allows for the final count to be adjusted if necessary. It also means that the most appropriate filter and funnel combinations can be chosen depending on what equipment is available to maximise the microplastics' recovery, resulting in more accurate reporting of pollution levels.

The most common method of searching for microplastics after filtration is stereomicroscopy (Ding *et al*. 2025., Mutlu *et al*, 2025., Vithatabandhu, *et al*, 2025. & Zhang *et al*, 2025), see table 1.1 for more examples of studies and

the methods that they use. Stereomicroscopes typically have a magnification in the range of 40-160x (Laji *et al*, 2022. & Wang *et al*, 2017). This level of magnification may not be high enough to be able to reliably detect all microplastics present in the samples. In addition, it is not a high enough magnification to be able to fully observe the detected microplastics to characterise features such as cross-sectional shape, presence of inclusions and internal and surface features that aid in the identification of synthetic and anthropogenic materials. Being able to identify these features and rule out natural material at the microscopy stage will also save time during confirmatory testing e.g. FTIR or Raman as less time will be spend on obtaining spectra from non-anthropogenic materials that look similar to some microplastics, for example some species of diatoms look visually similar to microbeads and at lower magnifications if can be hard to conclusively identify them as natural.

Polarised light microscopy (PLM) has been used in a few studies as the primary method of detection; Zhang *et al.* (2024) used PLM to detect microplastics in nasal lavage fluid using a treated filter membrane to allow the samples to be viewed under crossed polars: Dam *et al*. (2024) used compared the used of Nile red and fluorescence microscopy with PLM in the identification of microplastics in black soldier fly larvae. They found that PLM was a simple high throughput method of analysis PET and LDPE microplastics. They also note that plastic, plant material and cuticle all had strongly distinguishing features under crossed polars, which allowed for their quick identification. Due to these advantages PLM was found to be the preferred method of analysis in this study. Sierra *et al.* (2019) used PLM as the primary method of detection of isolated particulates in a glass petri dish to examine them under crossed polars. Any optically active particles were manually removed with tweezers and mounted on a slide for confocal Raman analysis. All of these studies use PLM as a method of detection instead of stereomicroscopy, demonstrating that PLM is a useful method of detection due to its ability to observe the sample under crossed polars, which increases the contrast between the particulates and the background, this is a particularly useful approach for synthetic materials as their interference

colours under crossed polars allows them to be easily detected. There is currently no research comparing the use of stereomicroscopy to the use of PLM as a method of detection, to determine if PLM results in more microplastics being detected due to the increased magnification, control over illumination and use of crossed polars. All of these studies also do not implement an additional technique possible with the use of PLM, which is calculating the birefringence of the microfibres present in the samples. By calculating the birefringence, more information is gained about the fibre including an indicative polymer identification.

Most studies report what quality control and contamination preventions steps they have taken, but do not state if/how contamination is identified and removed from the final count (Mia *et al*, 2024., Muhtadi *et al*, 2025. & Wu *et al*, 2024). Another approach taken is to blank correct by removing any microplastics that have the same size, colour and type category as found in the blanks taken (Alava *et al.*, 2021. & Miller *et al*, 2017). In addition, most research reports colour, polymer type, size and microplastic types (See table 1.1.) being able to characterise the microplastics beyond these features such as cross-sectional shape and presence of delusterant allows greater discrimination between legitimate microplastics and contamination, as more features are being observed to inform this identification. The greater level of characterisation of samples will allow for the possibility of potential sources to be identified, e.g. trilobal fibres are used very often for carpets, if there is a large quantity of trilobal fibres in a sample, looking in the vicinity for carpet manufacturers may allow the source to be identified.

In order for microplastics research to advance, the speed of research needs to increase, one possible way of achieving this is the use of machine learning to automate the detection of microplastics. As of yet there is no fully robust automated method of achieving this trained on large quantity of real sample images. Being able to quickly detect the microplastics allows real time indication of plastic pollution providing faster insights into levels of contamination. It will also save the researchers 1000’s of man hours that can now be spent characterising the microplastics and developing strategies to

help eliminate microplastic pollution, and a greater understanding of the impact of its presence in the environment and on human health.

1.10 Thesis Rationale

Microplastic pollution is becoming a growing area of concern as the long-term effects of plastic pollution on the environment and human health is still relatively unknown. In order to fully understand its potential effects, research on microplastic pollution needs to be accelerated and standardised.

One potential way to speed up research is to automate the detection and analysis of microplastics, as this would mean that a large number of samples could be analysed in a shorter time frame than it would take a human analyst. An automated method of analysis would also potentially reduce the number of microplastics that were missed or misidentified due to human error.

In order for an automated system to work the microplastic samples have to be presented in a consistent and standardised way, such as mounted on a glass microscope slide. The use of Easylift®, a forensic tape developed at Staffordshire University, is a potential method of presenting microplastic samples to an automated system as it is non-birefringent and allows the samples to be seen against a clear background.

In microplastic research, there is also an issue with inconsistent methods being used for analysis and different features being observed; this thesis proposes to use a forensic fibres analysis approach, such as identifying its cross-sectional shape to categorising microplastics that would allow more information to be observed and potential sources and contamination to be determined. Through the use of a standardised method of processing samples it would allow an easier comparison of results from different studies allowing a greater understanding of microplastic pollution.

1.11 Thesis Aims

The aims of this thesis are as follows:

1. To investigate the application of Easylift® as a new method of extracting microplastics from filter papers and what explore techniques its use is compatible with.
2. To generate an extensive and representative training data set to automatically detect microplastics and investigate its efficacy.
3. To investigate the use of Polarised light microscopy as a method of microplastic screening and analysis.
4. To test the use of the machine learning algorithm YOLO as an automated method of detecting microplastics.

1.12 Thesis Structure

Chapter 2 will examine the use of Easylift® as a method of retrieving microplastics from filter papers and what the percentage recovery of microplastic is when it is used. This chapter will also examine potential methods of analysis that are used in microplastic research and if they are compatible with the use of Easylift®.

Chapter 3 will focus on the findings of the Rozalia project 2019 Hudson River expedition. This study was used as a field trial of Easylift® its use as a method in the field will also be evaluated in this chapter. The samples taken during this expedition were used to generate the images for the training data set. It will also investigate the use of polarised light microscopy as a method of searching for and analysing microplastics. This chapter will investigate if PLM and stereomicroscopy are comparable methods or if one is potentially able to find or locate more microplastics. It will also investigate the characteristics of the microplastics found by each method to determine if certain characteristics are more easily identified with one method over the other.

Chapter 4 will examine the generation of an extensive training dataset and the efficacy of the YOLOv5, YOLOv7, and YOLOv8 algorithms as a method of automating microplastic analysis using the training data.

Chapter 5 will summarise the overall conclusions reached throughout this thesis and discuss what further work could be completed to further advance the research competed in this thesis.

Chapter 2 Improved Method for the Retrieval of Microplastics from Water Samples Using a Forensic Fibre Recovery Approach

The findings of this chapter have been published in Environmental Advances. (Gwinnett, Osborne & Jackson., 2021).

2.1. Introduction

2.1.1 Microplastics and Extraction of Water Samples

Microplastics have been found in several different environments and ecosystems (Blettler *et al.*, 2018); the effects of the presence of microplastics in the environment are still relatively unknown (Carbery, O'Connor & Thavamani, 2018). See Section 1.2 for more information on what is known about the effects of microplastics. To better understand how prevalent microplastics are in the environment, accurate and reliable data is required. There is potential for microplastics to be lost at every stage of collection and analysis. However, there is very little research into how much of the sample is potentially being lost at each stage, so understanding where and how these losses occur is important to maximise the recovery of microplastics. During the collection of the sample stage, several methods have been used previously, including the neuston net, which involves dragging a net behind a boat to collect samples from either the surface water or the water column (Hidalgo-Ruz *et al.*, 2012) see Section 1.5 for more information on methods of collection. The use of mesh does mean that it is likely that microplastics that are smaller than the diameter of the mesh will not be retained and, as such, lead to a misrepresentation of the microplastic population (Barrows *et al.*, 2017).

Table 2.1 A table to show the proportion of different neuston net mesh sizes used in 33 microplastic studies taken from Hidalgo-Ruz *et al.* (2012).

mesh size (μm)	sea surface	water column
50–290	2	2
300–390	13	2
400–505	5	1
600–1000	6	-
1500–3000	3	-
not specified	6	2

[a]N = 33 studies; note that the sum of cases exceeds the total number of studies, because several studies took both water column and sea surface samples.

The larger the mesh size used, the more microplastics are likely to be lost. Dris *et al.* (2015) used two different mesh sizes when they were investigating the microplastic concentration in the Seine River: 80µm and 330µm. When the 330µm net was used, a concentration of between 0.00028 to 0.00045 particles/l^{-1} was recorded, whereas when the 80µm was used, a concentration of between 0.003 to 0.106 particles/l^{-1} was found. This demonstrates that there is a difference in the quantity of microplastic being retained by each net, with the smaller mesh showing a higher microplastic concentration than the larger mesh. Table 2.1 demonstrates the range of different mesh sizes used in 33 different microplastic studies taken from Hidalgo-Ruz *et al.* (2012). It shows that there is a large array of mesh sizes used ranging from 50-3000µm this potentially can lead to a large disparity between results, making comparisons between studies difficult. From Table 2.1, it is evident that most studies use neuston nets with relatively large mesh sizes, with 15 out of 33 studies using a mesh over 600µm, meaning that it is likely that most studies that used a neuston net are reporting inaccurate microplastic concentrations. Barrows *et al.* (2017) compared the concentrations found when using a neuston net with a mesh size of 335 µm, to taking 1-litre grab samples. They found that the grab samples recovered three orders of magnitude more microplastics than the neuston net, finding 5.9 ±4.4 microplastics per litre, whereas the neuston net found 0.005 ± 0.004 per litre. This demonstrates how large the potential for microplastic loss is when using the neuston net to collect samples. In a study by Kapp and Yeatman (2018), grab and neuston net samples (100µm mesh size) were

compared they found that a larger proportion of the samples taken with the neuston net contained microplastics (92%) compared to the grab sample (75%). This is likely due to the neuston net sampling a larger volume of water than the grab sample. They also found a higher concentration of fibres in the grab samples (58%) than those recovered by the neuston net (48%). In addition to this, the grab samples contained a higher proportion of microplastics between 100-333µm (76%) than the neuston net (51.3%); these findings highlight the potential disadvantages of using either method. As the grab sample collects a smaller sample, there is a higher potential for variability between repeat samples. Although it allows greater uniformity in the amount of samples taken and can help to reduce contamination of samples (Miller *et al.*, 2017).

While there is some research into the effectiveness of some methods of extracting microplastics during sampling, there is no research into the potential loss rate during the filtering process, and in some cases, papers do not state what method of filtration is used.

Table 2.2 A table to show what equipment is used in different microplastic studies to filter water samples.

Reference	Method of filtration	Filter paper
Stanton *et al.* (2019)	Filtered under vacuum	Mixed cellulose membrane filter
Leslie *et al.* (2017)	Filtered under vacuum	Glass filter paper
Miller *et al.* (2017)	Filtered under vacuum	Mixed cellulose membrane filter
Dyachenko, Mitchell & Arsem (2017)	Buchner filtration	Membrane
Barrows *et al.* (2017)	Glass frit	Mixed cellulose membrane filter
Lahens *et al.* (2018)	Glass frit	Glass filter paper
Lusher *et al.* (2015)	Bucher filter	Glass filter paper
Wang *et al.* (2017)	Filtered under vacuum	Glass filter paper
Lusher *et al.* (2014)	Buchner funnel	Glass filter paper

Cordova, Hadi & Prayudhu (2018)	Filtered under vacuum	Cellulose filter paper
Ebere *et al.* (2019)	Not filtered under vacuum	Cellulose filter paper
Woodall *et al.* (2014)	Filtered	Glass filter paper
Kanhai *et al.* (2018)	Buchner filtration	Glass filter paper
Dris *et al.* (2016)	Filtered	Quartz-fibre GF/A

Table 2.2 Shows what different methods for extracting microplastics from water samples have been used in different studies several of the studies did not specify what kind of filtration mechanism they used, only stating that the sample was filtered under vacuum. This is of significance as if there is a difference in the ability of different methods to successfully retrieve microplastics, then it would be difficult to compare studies where it is not stated what method was used. Most studies used a glass filter paper to filter the water. Other filter papers used are cellulose filter papers and mixed cellulose membrane filters; it is also unknown if the filter type will affect the recovery rate of microplastics.

2.1.2 The Use of Tape Lifting in Forensic Science Fibre Recovery and its Links to Microplastic Work

There is an overlap between the fields of microplastic research and forensic science in terms of forensic fibre analysis, as fibres can be of evidential value (Grieve *et al.*, 2018). Due to the varying nature of the surface's fibre evidence needs to be retrieved from, there are several approaches to collecting fibre evidence including, tweezers, vacuuming, taping, combing and sweeping (Robertson & Roux, 2018). One of the most common techniques applied to retrieve fibres in forensic science is a tape lift (De Wael, Gason & Baes, 2008), which involves adhering a colourless transparent plastic film with an adhesive on one side to a surface and removing it to collect any fibres on the surface, this tape would then be secured to a suitable backing such as an acetate sheet (Robertson and Roux, 2018). Tape lifting is often the preferred method because it fixes the fibres in place, preventing loss and any potential further contamination of the

sample, allows the sample to be stored for a long period of time, is easy to apply and has a high recovery rate (De Wael, Gason & Baes, 2008). These benefits could be transferred to microplastic research.

Once collected, the tapes are searched using a low-power stereomicroscope to find any fibres of interest and compare them to control fibres taken, for instance, from a suspect's clothing (Sermier *et al.*, 2006). After identification of a target fibre, it would be retrieved from the tape lift via a tape dissection and remounted on a glass microscope slide so that optical properties can be observed (Jones & Coyle, 2011). See Figure 2.5 for more information on tape dissection. Once removed from the tape lift the fibre will be examined with polarised light microscopy (PLM) as it allows the determination of the optical properties of the fibre (Buzzini & Massonnet, 2015). A forensic fibres expert will typically categorise the fibres according to colour, cross-sectional shape, dimensions, presence of delusterant and birefringence (Wiggins., 2018). The most significant of these is the birefringence, as it allows the polymer type of the fibre to be indicatively determined (Grieve, 1983). Birefringence is the difference between the perpendicular and parallel refractive index of the fibre; the birefringence value provides insight into the polymer type of the fibre being investigated (Nayak, Padhye & Fergusson, 2012). For more information on birefringence, see Section 2.2.1.1. One issue with tape lifting is the need for dissection; this is because the acetate and the tape are birefringent and so would interfere with polarised light microscopy, leading to an inaccurate birefringence value being calculated (Robertson & Roux, 2016).

Typically, in microplastic research, researchers will leave the microplastics in situ on the filter paper (Barrows *et al.*, 2017. & Miller *et al.*, 2017) or manually retrieve the fibre with tweezers (Talvitie *et al.*, 2017). In doing this, there is the potential for fibres to be lost, move and become contaminated. Therefore, the application of tape lifting to microplastic research should be investigated as it could help to prevent the loss of microplastics and prevent contamination.

2.1.3 Aims and Objectives of the Study

The aim of the study is to investigate the retrieval rate of different filter and filter paper combinations and how effective Easylift® is as a method of recovery.

The objectives of this study are as follows:

1) To investigate and evaluate the different properties of Easylift® to facilitate the analysis of microplastics.
2) Determine if microfibres are being lost during the filtration of water samples.
3) If so, determine if the filter paper type or funnel used impacts the amount of microfibres lost through filtration.
4) Determine the efficacy of Easylift® as a method for retrieving microfibres from the surface of two different filter papers (Cellulose and glass fibre) after two different filtration techniques (Buchner and glass frit).

2.2 Easylift®

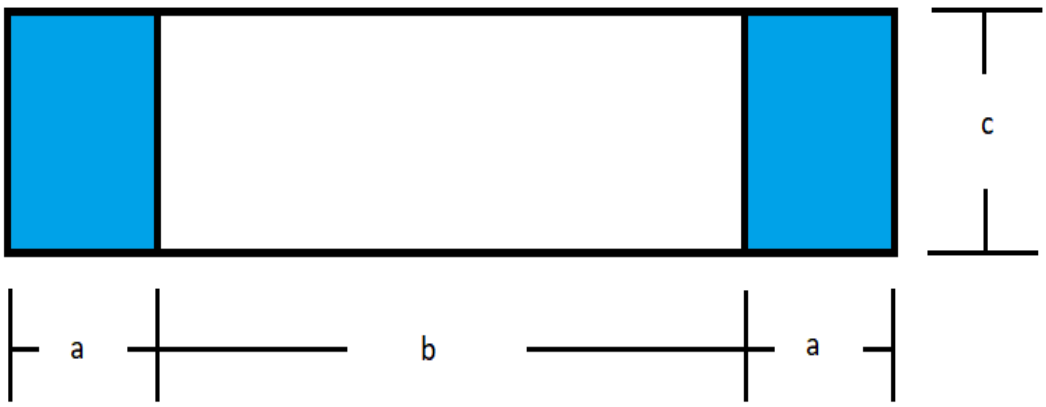

Figure 2.1 A diagram demonstrating a piece of Easylift® tape: a is 25 mm, b is 75 mm and c is 25mm.

Figure 2.1 demonstrates a diagram of a piece of Easylift® tape. Each tape has blue tabs (a) for easy use and sample collection and a transparent adhesive tape that is 75 mm by 25 mm (b) for adhering to a microscope slide.

Easylift® is a tape lift developed for retrieval of fibres from crime scenes; what sets Easylift® apart from other commonly used tapes such as J-Lar is that it is essentially non-birefringent, allowing for the microplastics to be characterised by polarised light microscopy in situ. The ability to analyse microplastics in a sealed environment offers many benefits including the ability to store samples for long periods of time, prevent loss of samples and prevent further contamination of the samples from the point of tape lifting. This will prevent the potential loss of evidence and save time and expense (Jackson & Gwinnett, 2006). The ability to store samples also allows for the sample to be analysed by multiple examiners, meaning results could be verified. As stated in Section 1.9 the ability to affix samples to a secure slide in the field means that more time can be spend in the field gathering samples rather than having to analyse in the field or bring all samples back to the laboratory this also means that findings can be ratified and validated. Other methods of tape lifting could be implemented that provide the storage benefit including, J-lar, gelatine lifters etc these methods do not however allow the characterisation of the samples in situ as easily as Easylift® does, as it would require the samples to be dissected from the tape to undergo further analysis reintroducing the potential for contamination and loss. These methods may be beneficial if the researcher is only interested in being able to visually observe the samples, but as this thesis aims to investigate the use of PLM alongside Easylift®, it was the only method tested.

Figure 2.2 shows A decision tree showing the how the use of Easylift® as a method of recovery was decided upon

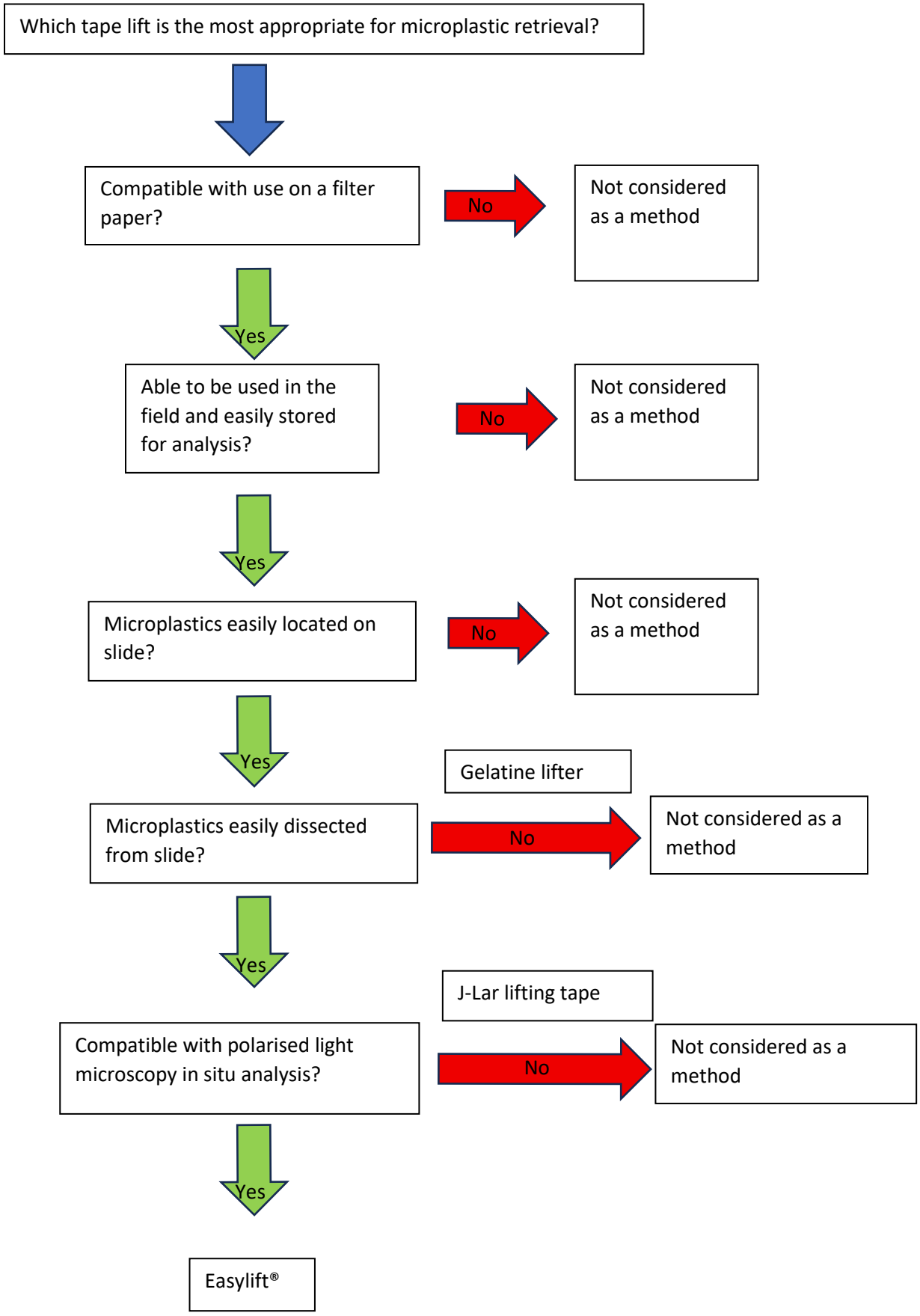

Figure 2.2 A decision tree showing the how the use of Easylift® as a method of recovery was decided upon.

2.2.1 The Properties of Easylift®

This investigation aims to establish the compatibility of Easylift® with *in situ* microplastic analysis using a variety of analytical techniques.

2.2.1.1 Easylift® and Polarised Light Microscopy

Polarised light microscopy (PLM) is a method of analysis commonly used in forensic fibre analysis that allows observations to be made with the human eye to allow the birefringence and sign of elongation of the fibre to be established, which can be highly discriminating when used in conjunction as it allows the fibres polymer type to be determined (Brinsko, Sparenga & King, 2016). The majority of microplastics will exhibit birefringence, meaning PLM can be used as a method to characterise microplastics.

As discussed in Section 2.1.2. the tapes and backing material used to retrieve fibres are birefringent, meaning that it will interfere with the examiners' ability to characterise any fibres contained within the tape lift using PLM. The solution to counteract this in forensic science is to dissect and remove the fibre from the tape lift and then remount on a glass slide (Robertson & Roux, 2018), as the glass from the slide is essentially non-birefringent; however, this process is time-consuming and there is the potential for sample loss to occur (Paulsson & Stocklassa, 1999). Whereas Easylift® is by design essentially non-birefringent, as a result, any particulates held within the Easylift® tape lift, and a glass microscope slide can be analysed using PLM without the need to dissect the tape and remove the particulate of interest.

As synthetic fibres vary in chemical composition and optical properties, their refractive indices vary. Synthetic fibres split light into two beams. These two light beams have different refractive indices, one being n-perpendicular and the other n-parallel. The difference between these two refractive indices is the fibres' birefringence value, which indicates the fibres' polymer type. A list of birefringence values can be seen in Table 2.3.

When the n-parallel is greater than n-perpendicular, they are said to have a positive sign of elongation, and if the opposite were true, it would have a negative sign of elongation (Gorski & McCrone, 1998). The birefringence of the fibre can be calculated when the fibre is in the diagonal North-West South-East position with the fibre between two pieces of crossed polaroid this causes the fibres' interference colours to become visible (Reffner, Kammrath & Kaplan., 2020). Figure 2.3 shows a trilobal nylon fibre in-plane light and under crossed polars demonstrating the fibres interference colours.

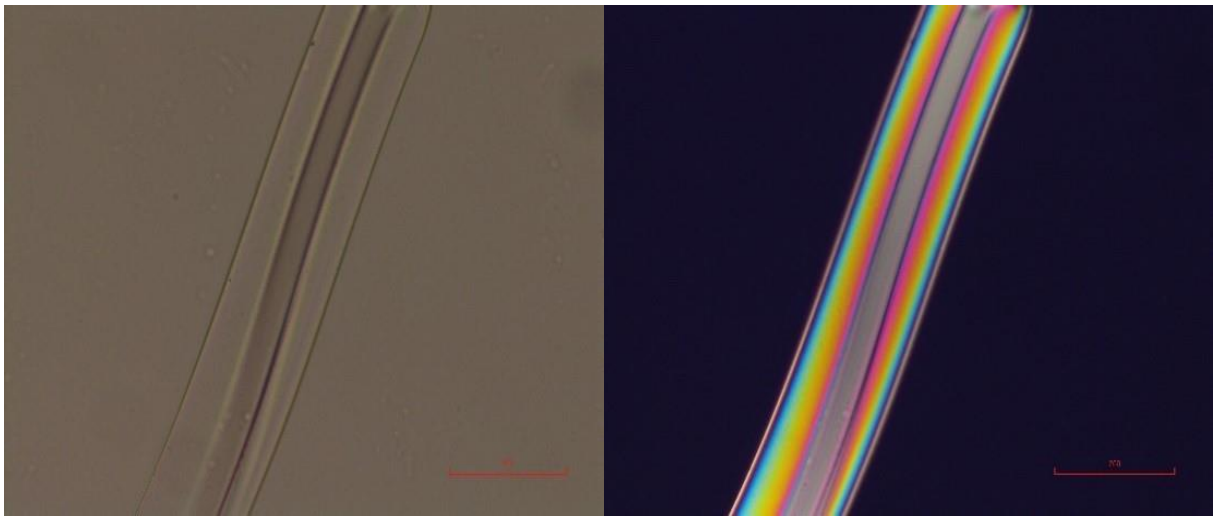

Figure 2.3 A colourless trilobal Nylon fibre under plane light (left) and under crossed polars (right) taken x200 magnification on a Nikon eclipse E400 polarised light microscope.

It is possible to determine the optical path difference of the fibre with a quartz wedge with a varying optical path difference that is pushed through the accessory slot of the PLM; as the wedge is moved through the accessory slot the interference colours will change at the point where the quartz wedge and the fibre have the same optical path difference the fibre will become black, this is known as 'compensation black' the optical path difference can then be determined using the Michel-levy chart (Gorski & McCrone, 1998). This value, in conjunction with the thickness of the fibre, can be used to calculate the birefringence of the fibre in the calculation:

$$birefringence = \frac{Optical\ path\ difference}{(thickness\ of\ fibre\ (\mu m) x 1000)}$$

Table 2.3 Typical sign of elongation and birefringence ranges for different fibres derived from Heuse and Adolf's Standort diagram (Palenik, 1992).

Fibre type	Birefringence range	Sign of elongation
Acetate: Diactetate	0.002-0.005	Positive
Actetate:Triacetate	0.000-0.001	Positive/Negative
Acrylic	0.001-0.005	Negative
Modacrylic: Verel®	0.000-0.001	Negative
Modacrylic: Dynel®	0.002-0.005	Positive
Aramid: Kevlar®	0.200-0.710	Positive
Aramid: Nomex®	0.120-0.230	Positive
Rayon (Viscose)	0.020-0.028	Positive
HT Viscose	0.035-0.039	Positive
Cupro	0.021-0.037	Positive
Lyocell	0.044	Positive
Flurocarbon	0.039	Positive
Nylon: Nylon 6	0.049-0.061	Positive
Nylon: Nylon 6,6	0.056-0.063	Positive
Polyolefin: Polyethylene	0.050-0.052	Positive
Polyolefin: Polypropylene	0.028-0.034	Positive
Polyester: PET	0.147-0.175	Positive
Polyester: PBT	0.148-0.150	Positive
Polyester: PCDT	0.098-0.102	Positive
Polyester: PEN	0.273	Positive
Saran	0.008	Negative
Spandex	0.010	Positive

Sulfar	0.111	Positive
Vinal	0.025-0.030	Positive
Vinyon (Cholorfibre)	0.002-0.005	Positive

Without Easylift®	With Easylift®
(a) 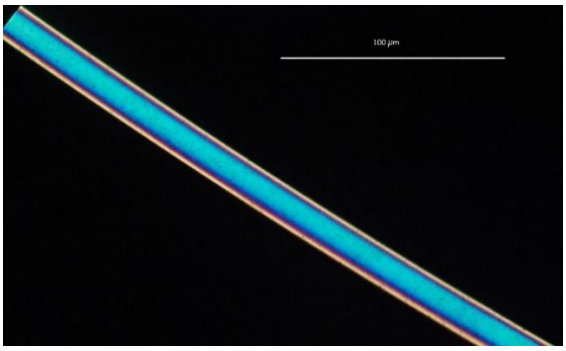	(b) 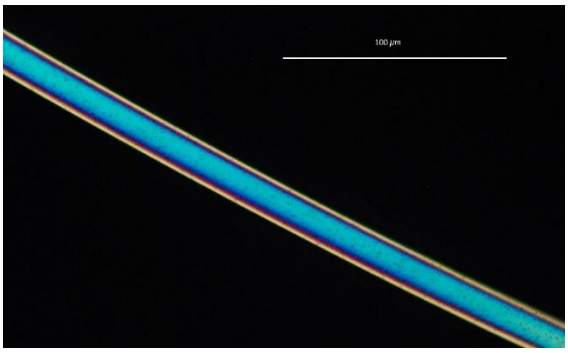

Figure 2.4 Interference colours seen in a colourless (i.e. white) nylon fibre when viewed between crossed polars. The scale bar is 100µm long in each image.

The fibre used in Figure 2.4 was examined and imaged under crossed polars using a Microtec polarised light microscope, and the camera used was a Nikon D80 DSLR with a Nikkor 35mm 1:1 lens (settings were F stop of 1.8, a shutter speed of 1/20s, ISO of 1600, auto white balance with no zoom applied). The fibre was orientated with its long axis positioned in the Northwest to Southeast position so that its interference colours are visible. In image (a) of Figure 2.4, there was no Easylift® in the light path, and the fibre was mounted in DPX on a glass microscope slide. To produce image (b) of Figure 2.4, Easylift® was adhered to the underside of the microscope slide, after which the fibre was re-examined and imaged in the same manner described above. This was undertaken to allow the same fibre to be viewed with and without Easylift® without the need to extract the fibre from the DPX mountant, which can result in loss or damage to the sample.

Figure 2.4 shows a colourless cylindrical nylon fibre between crossed polars with and without the presence of Easylift®. The fibre's maximum optical path difference will vary at any given thickness along its length. Its maximum thickness and cross-sectional shape contribute to its interference colours,

which are visible when the fibre is placed under crossed polars in Northwest to Southeast diagonal position. As the fibre in Figure 2.3 exhibits clear bands of colour, it is a good example to demonstrate that the addition of Easylift® into the light path did not impact upon the interference colours exhibited. In addition, the background colour in image b remained uniformly black as far as the human eye can detect when Easylift® was placed into the light path. This, in addition to the lack of a change in interference colour between the two images, demonstrates that Easylift® is essentially non-birefringent and provides support that the birefringence and sign of elongation of the MP particles can be determined by PLM using a first-order red tint plate and/or quartz wedge as it is unaffected by the presence of Easylift® in the light path.

Some fibres exhibit pleochroism under plane polarised light, where the fibre will exhibit different colourations when observed in different orientations due to the preferential transmission and absorbance of different wavelengths of light along the different vibration directions within the fibre (Brinsko, Sparenga & King, 2016). Figure 2.5 demonstrates a fibre that exhibits dichroism (a form of pleochroism) in-plane polarise light; the colour change that results from the rotation of the fibre can be seen unaltered in the presence of Easylift®. From the images in Figure 2.5, it can be seen that the presence of Easylift® in the light path has no impact on the ability to observe the fibres dichroism, further displaying Easylift®'s compatibility with characterising particulates with PLM. It is recommended in forensic casework to check fibres for dichroism as a further characteristic to compare fibres to control fibres (De Wael., 2021)

Without Easylift®	With Easylift®
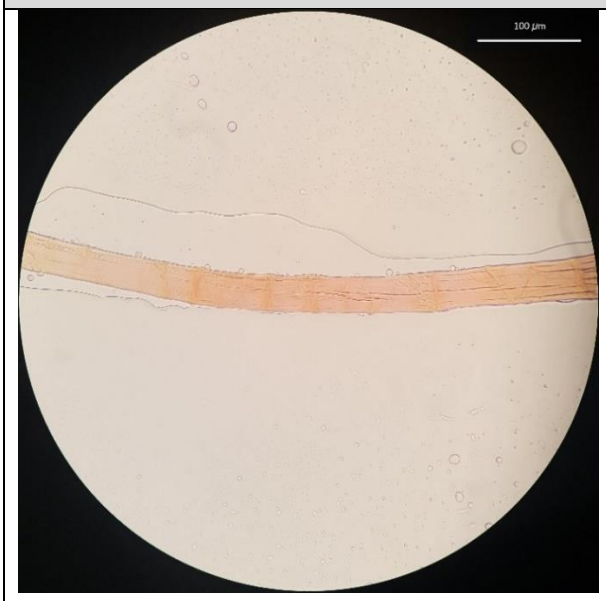	
	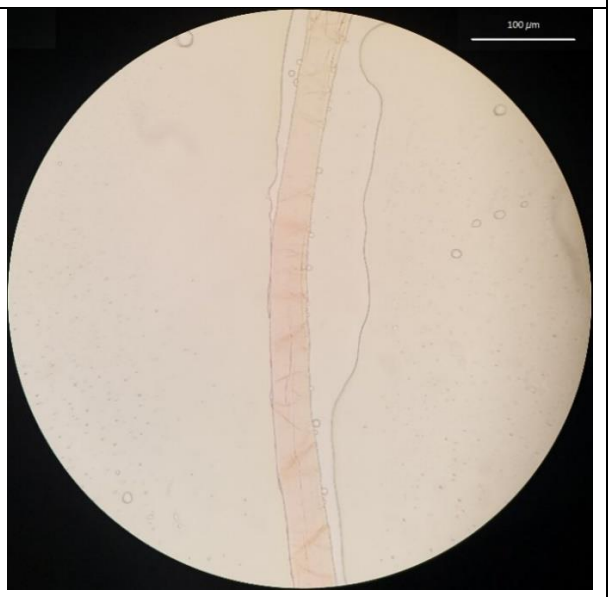

Figure 2.5 A red fibre in transmitted plane-polarized light demonstrating a colour change due to the fibre's dichroism, the fibre can be seen unaltered and with the addition of Easylift®.

The images shown in Figure 2.5 were taken in plane-polarised light, not under crossed polars. The fibre was first positioned on its long axis in the East-West position without the addition of Easylift® being placed on the light path. A Glass coverslip with Easylift® adhered to it was carefully placed on top of the slide coverslip so that the fibre could be imaged with the addition of Easylift® in the same place. The fibre was then rotated to the North-South position, and the process was repeated first without the presence of Easylift®

and then with the addition of Easylift® in the light path. All four images were taken using a Samsung SM-G973F (Samsung Galaxy S10) camera that was held approximately 1 cm away from the eyepiece. The Camera settings were: F2.4, 1/90s. 4.32 mm, ISO 125, auto white balance, and no flash.

2.2.1.2. Easylift® and FTIR

Fourier Transform Infrared (FTIR) spectroscopy is commonly utilised in microplastic research as a method for polymer type identification (Bayo, Olmos & López-Castellanos, 2020., Miller *et al.* 2017. & Nelms *et al.* 2018) See Table 1.1 for more information on the methods frequently used in microplastic research. FTIR uses infrared radiation to promote the vibrational energy levels of the molecule to an excited state. The absorption of infrared radiation occurs when a photon transfers to a molecule, promoting it to a higher energy state, resulting in the vibrations of the molecular bonds within the molecule caused by bending, wagging, deformation and stretching of the bonds at different wavenumbers in the infrared region of a light spectrum. The wavenumber that each absorbance peak is a result of different properties within the molecule, meaning that it creates an identifying 'fingerprint' allowing the molecule to be identified (Chen *et al.*, 2015). Plastic polymers have very individualising infrared spectra with distinct band patterns, meaning it is an effective method of identification of microplastics (Hidalgo-Ruz *et al.*, 2012). FTIR can identify microplastics down to around 10-20 µm in size in its smallest dimension (Araujo *et al.*, 2018).

The purpose of the experimental work described in this section is to explore:

- The ease with which a microplastic particle can be extracted from an Easylift® tape lift by dissection.
- Whether once removed from the tape lift the microplastic particle can be successfully characterised by Fourier Transform Infrared (FTIR) spectroscopy.

In order to meet these aims, a control FTIR spectrum of a 2x2 mm piece of blue polypropylene film that would serve as the microplastic of interest was created. After the spectrum was obtained, the film was mounted on a glass microscope slide using Easylift®. It was then dissected and removed from the

tape lift; the process for this can be seen in Figure 2.6. Once extracted from the tape another FTIR spectrum of the film was obtained, along with a spectrum of the adhesive and non-adhesive side of Easylift®, so that the effect of being in a tape lift could be established.

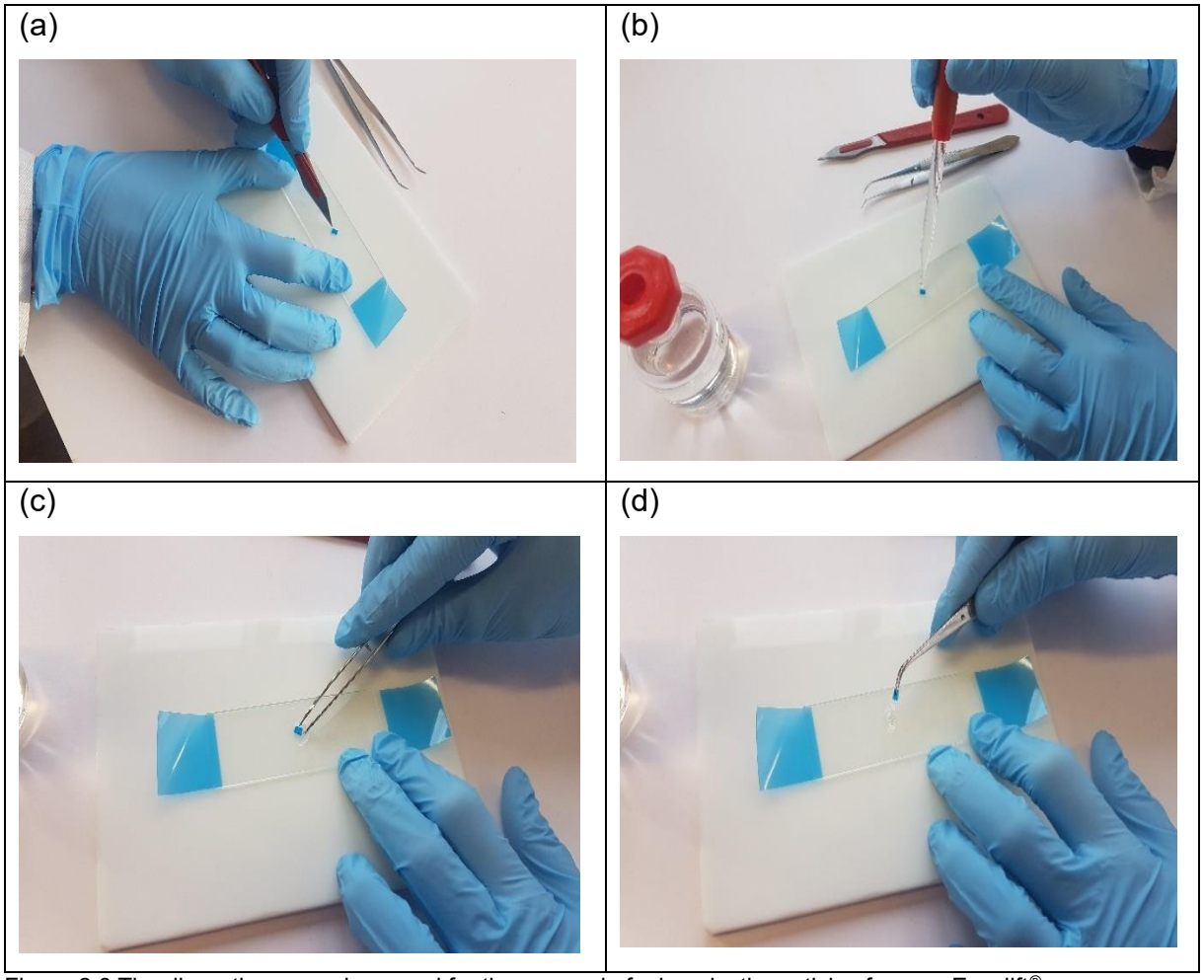

Figure 2.6 The dissection procedure used for the removal of microplastic particles from an Easylift® tape lift. (a) Using a scalpel, the tape is cut through to the microscope slide, creating a 'V'-shaped flap over the particulate of interest. (b) a drop of TissueClear® solvent is placed over the incision and left for 3-5 seconds. (c) using metal jeweller's tweezers, the V-shaped flap is lifted. (d) the particle of interest is removed from underneath the tape.

All FTIR spectra were obtained using the same instrumental settings in Figure 2.7. They were all obtained using Attenuated Total Reflectance (ATR) FTIR spectroscopy, using a Thermo Nicolet, Avatar 370 spectrometer which uses OMNIC software. The FTIR was set up to average over 32 scans with a resolution of 4 cm^{-1}. The FTIR was equipped with a Specac Golden gate single reflection diamond ATR accessory with a ZnSe focusing element.

All self-adhesive tapes, Easylift® included, have several strong absorption bands in the infrared region, meaning that *in situ* analysis is unlikely to

produce productive results. However, it is possible to extract the microplastics from the tape lift. This process is shown in Figure 2.5; once extracted from the tape lift, it is then possible to characterise the microplastic with FTIR. Figure 2.7 demonstrates the FTIR spectra for the microplastic of interest before and after being encased in Easylift®, the spectra remain virtually unchanged after being mounted in Easylift® demonstrating the compatibility of Easylift® and FTIR, once any particulates of interest have been extracted.

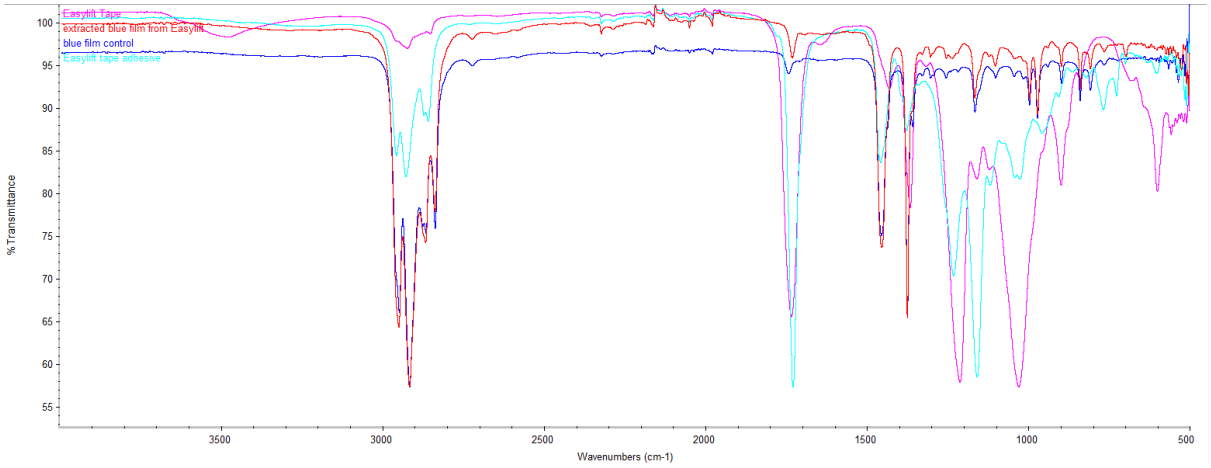

Figure 2.7 FTIR spectra of the Easylift® tape (pink) and its adhesive (pale blue), plus those of a fragment of blue-coloured plastic film taken before it was tape lifted with Easylift® (dark blue) and after dissection from the lift so created (red). Produced by Professor Claire Gwinnett.

2.2.1.3 Easylift® and Confocal Raman

Raman spectroscopy has also been used in microplastic research to classify the polymer types of the suspected microplastics (Lenz *et al.* 2015., Saeed *et al*. 2020. & Wolff *et al*. 2019). As with FTIR, Raman is a form of vibrational spectroscopy. The frequency shifts that occur when the light is scattered by the molecules can either be positive or negative; the magnitude of the scattering is known as the Raman frequency. The resulting Raman frequencies for the molecule make up the Raman spectrum (Woodward, 1967). Raman uses the inelastic scattering of light, also called 'Raman scattering', to provide information on the molecule's structure through molecular vibrations (Araujo *et al*., 2018). If the photon produced by the inelastic light scattering has a lower frequency than the original photon, it produces Stokes Raman scattering, and if the photon has a higher frequency

than the original, it produces anti-Stokes Raman scattering. The technique measures the shift produced to generate the spectrum. The resulting shift in wavelength will depend on the chemical composition of the molecule being analysed (Rostron, Gaber & Gaber, 2016). Raman spectroscopy is also able to analyse microplastics down to 1 µm, meaning that it is able to characterise microplastics that would be too small for FTIR analysis (Fu *et al.*, 2020). Figure 2.8 shows the spectra obtained from a plastic fibre contained within an Easylift® tape lift using confocal Raman microspectroscopy.

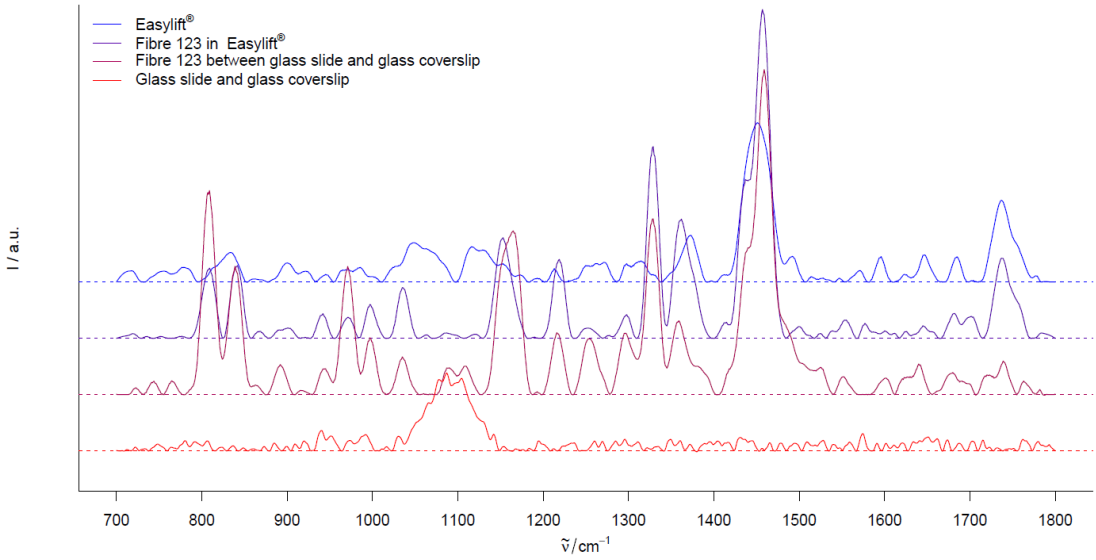

Figure 2.8 Raman spectra demonstrating the profile produced by a synthetic fibre contained in an Easylift® tape lift created using confocal Raman microspectroscopy. Produced by Professor Claire Gwinnett

Table 2.4 Salient peaks of the Raman spectra shown in Figure 2.7

Peak position /cm^{-1} [(s) = sharp (b) =broad]	Easylift®	Fibre 123 in Easylift®	Fibre 123 between glass slide and coverslip	Glass slide and coverslip
808(s)	No	Yes	Yes	No
840(s)	No	Yes	Yes	No
971(s)	No	?	Yes	No
997(s)	No	Yes	Yes	No
1035(s)	No	Yes	Yes	No

~ 1095(b)	No	No	Yes	Yes
~ 1155(b)	No	Yes	Yes	No
1218(s)	No	Yes	Yes	No
1255(s)	?	?	Yes	No
1296(s)	?	?	Yes	No
1328(s)	No	Yes	Yes	No
1360(s)	No	Yes	Yes	No
~1455(b)	Yes	Yes	Yes	No
1738(b)	Yes	Yes	Yes	No

Figure 2.8 shows four spectra obtained by confocal Raman spectroscopy, two of these spectra are from a colourless polyolefin fibre (taken from sample number 123 of the Microtrace Forensic Fibre Reference Collection) held between Easylift® and a glass microscope slide or a glass coverslip and microscope slide. Two blank spectra were also obtained, which are visible in Figure 2.8. One blank was taken off the Easylift® tape, and the second blank was taken off the glass coverslip on a microscope slide. The salient peaks of all four spectra are summarised in Table 2.4. Of the 14 peaks listed, two peaks (1455 and 1738 cm^{-1}) are present in the spectra for Easylift®, and one peak (1095 cm^{-1}) is present in the spectra of the glass coverslip. The remaining 11 peaks can be unambiguously assigned to have originated from the fibre used, with seven peaks appearing in both spectra for the fibre, demonstrating the compatibility of Easylift® and Confocal Raman spectroscopy.

The spectra exhibited in Figure 2.8 were obtained using a method adapted from Lepot *et al*. (2008). The results were obtained using a Renishaw inViva Raman Microscope with a Leica microscope, using a ×20 objective lens for simultaneous illumination and data collection. An excitation wavelength of 514nm was used, laser intensity was 50 mW, and the integration time used was 4 seconds. Once the spectra were obtained, the results were imported into R version 3.6.3 (R Core Team, 2020) as x, y coordinate data using RSTUDIO Desktop Open-source Edition version 1.2.5033 (RStudio, n.d.). The spectra were then processed using the hyperSpec package version

0.99-20200213 (Beleites & Sergo, 2020) to correct baseline drift and enhance the signal-to-noise ratio using LOESS smoothing.

The two central spectra in Figure 2.8 were created by analysing a colourless cylindrical polyolefin fibre (number 123 of the Microtrace Forensic Fibre Reference collection) by the method described above. A spectrum was first obtained from the fibre mounted in between a coverslip and a glass microscope slide; a spectrum was also taken of the coverslip and the microscope slide without the fibre being present. The same fibre was then mounted onto a glass microscope slide using Easylift®, and a spectrum was recorded of the fibre within the tape lift; a spectrum was also recorded for the Easylift® tape for comparison purposes.

The instrumental setup used in this investigation was based on the results of the initial optimisation trials, wherein the laser intensity and integration times were varied. A noteworthy result of this investigation found that when the laser intensity was set to 100mW and integration time was set to 1 second the fibre used was visibly damaged whilst no deformation or melting of the Easylift® was observed.

A Study by Poli, Littli & Lavagnolo (2024) used Easylift® to a method of extraction as described in Section 2.3 of this thesis, as part of the study they conducted a validation study to assess Easylift®'s compatibility with Raman. They mapped the surface of the microscope slide with an inViva Renishaw micro-Raman. They were able to conclude that the background signals displayed a Pearson's correlation below their chosen threshold, indicating that the glass slide and Easylift® tape could not be mistaken for microplastics. While the Pearson's correlation for microplastics within the sample were significantly higher than the threshold value often over 0.75, demonstrating Easylift®'s compatibility with Raman analysis.

2.2.1.4 Easylift®'s Interaction with Unpolarised Ultraviolet and Visible Light

As demonstrated in Figure 2.9, Easylift® is essentially transparent to visible light (Wavelengths of light 400 to 700 nm), and it shows a transmission rate of >80% to ultraviolet light that is within the wavelength range of 300-400 nm. Figure 2.10 also demonstrates Easylift®'s compatibility with microspectrophotometry. Due to Easylift®'s transparency within the ultraviolet range, there is a potential that Easylift® may be compatible with dyes commonly used in microplastic research including, Nile red, fluorescein isophosphate and Safranine T (Lv *et al.*, 2019b. & Shahi *et al.*, 2020).

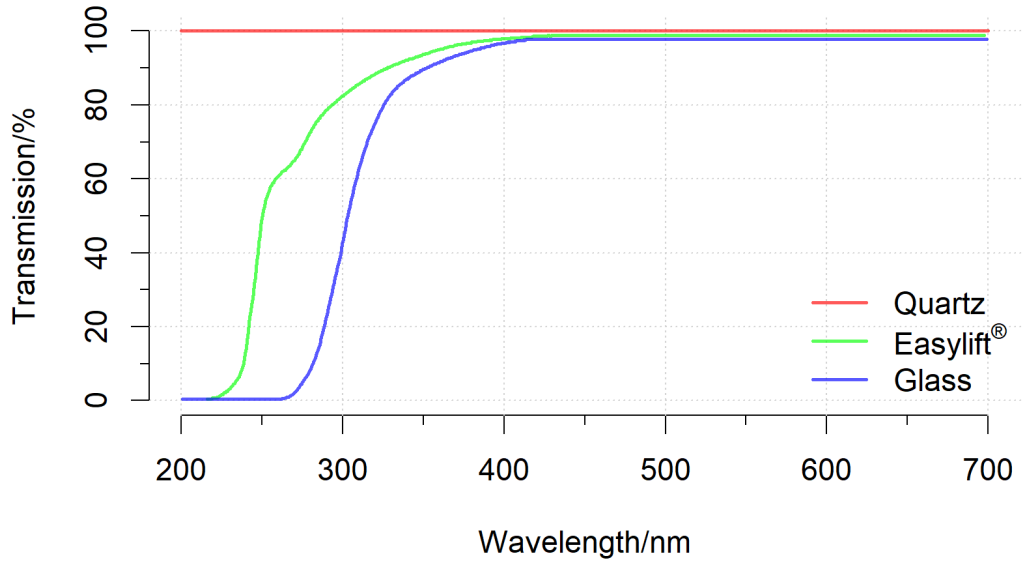

Figure 2.9 Ultraviolet-visible transmission spectra (redrawn from spectra provided by Jaap van der Weerd and Linda Alewijnse of the Netherlands Forensic Institute). Produced by Professor Andrew Jackson.

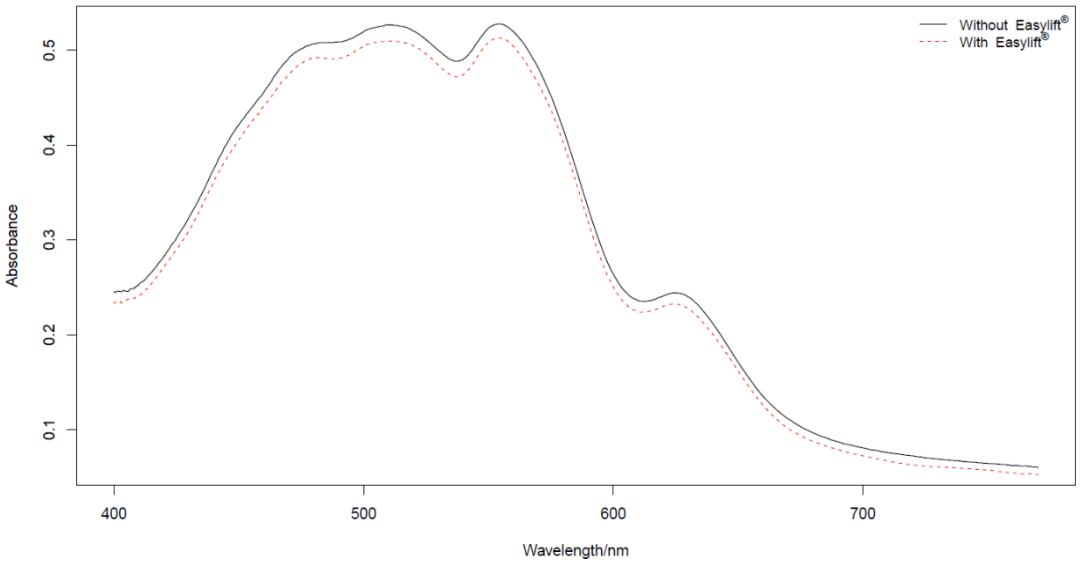

Figure 2.10 Visible spectra obtained by Microspectralphotometry from a red nylon fibre. The spectral data were recorded by Chris Hunter of SMCS Ltd.

As demonstrated by Figure 2.11 the transparency of Easylift® discussed above means that Easylift® is compatible with fluorescence microscopy. The images shown in Figure 2.11 were captured using a LUMNIA-FLHS modular microscope with a hyperspectral camera, thus also illustrating the potential for microplastics held under Easylift® to be characterised using hyperspectral microscopy.

Illuminated with white light from below	Fluorescence consequent on oblique laser excitation from above
(a) 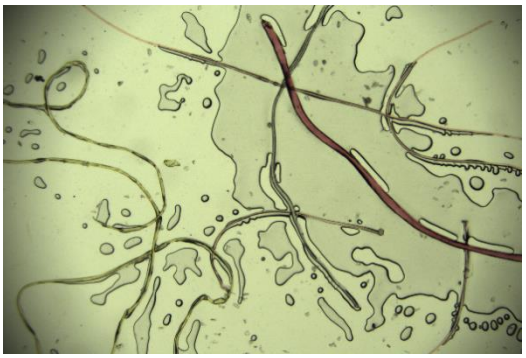	(b) 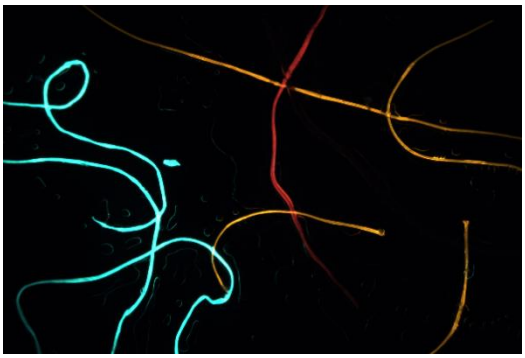

Figure 2.11 Images of fibres held in Easylift® demonstrating Easylift®'s compatibility with fluorescence microscopy and hyperspectral imaging. Images taken by Nathanail Kortsalioudakis, courtesy of Costas Ballas and Nathanail Kortsalioudakis of SPECTRICON.

The original transmission spectra used to create Figure 2.9 were recorded at the Netherlands Forensic Institute by Linda Alewijnse during a research project led by Jaap van der Weerd. The spectra were recorded in the 200-700 nm wavelength, and a spectrum of Easylift®, a glass slide and a quartz slide were recorded. These spectra have been recreated in Figure 2.8. The spectra were recorded using a Perkin Elmer Lambda 35 spectrometer; for the glass and quartz slide, the sample was placed over the instrument measuring beam. To record the spectra for Easylift®, the tape was held by its adhesive tape in a cardboard frame. This frame was then placed in the instrument to allow the spectra for Easylift® to be recorded. The research mentioned above only required a subset of the spectra that were recorded, so the spectra that were of interest were replotted using R version 3.6.3 (R Core Team, 2020) through RStudio Desktop Open Source Edition version 1.1.447 (RStudio, n.d.), using functions from the packages; jpeg version 0.1-8.1 (Urbanek, 2019), countcolors version 0.9.1 (Weller, 2019a), colordistance version 1.1.0 (Weller., 2019b) and imager version 0.42.1 (Barthelme., 2020).

The spectra shown in Figure 2.10 were recorded by Chris Hunter of SMCS Ltd (http://www.smcs.co.uk/) using an SMCS mspt MicroSpec with 0.8 nm wavelength accuracy taken across the visible spectrum. Both spectra displayed were taken using a red nylon trilobal fibre (number 87 in the Microtrace Forensic Fiber Reference Collection manufactured by BASF USA) that has been mounted in DPX on a glass microscope slide with a glass coverslip. An Easylift® tape was placed on top of the slide before the spectra titled 'With Easylift®' were recorded.

The images shown in Figure 2.11 were taken using a LUMNIA-PLHS modular scientific microscope developed and distributed by SPECTRICON http://www.spectricon.com/spectral-imaging-products/lumnia-flhs/. Both images were taken by Nathanail Kortsalioudakis using the microscope's MuSES-HS hyperspectral camera using both of its sensors. Image (a) shows the specimen was illuminated with white LED (wavelength 400-720 nm), and image (b) the specimen was illuminated with fluorescent light with the wavelengths 445, 500 and 600 nm (Full width and half maximum (FWHM) ± 40nm) excited by light wavelengths of 405, 473 and 532 nm. The excitation

radiation was provided from above using the microscope's ring-shaped Polyline diode laser array that surrounds its objective lens. The instrument's notched filtering system, located in the light path between the sample and the camera, was used to effectively eliminate a wavelength band 4 nm wide that includes the wavelength of the laser light. This filtering system, coupled with the oblique illumination geometry, allows this microscope to achieve a high signal-to-noise ratio in fluorescence imaging. The fibres shown in Figure 2.11 are fibres from a red wool jumper, yellow polyester from a high visibility vest and peach-pink and white acrylic from a jumper. These were held on a glass microscope slide by a piece of Easylift®.

2.2.1.5 Easylift® and Mounting Mediums

Easylift® removes the need to dissect the tape lift before Polarised light microscopy (See section 2.2.1.1), saving the examiner time and preventing loss or contamination of the sample. When making traditional microscope slides, a mounting medium that at least initially is a liquid is placed between the microscope slide and coverslip; the mounting medium serves a number of purposes.

1. It adheres the coverslip to the slide, trapping the specimen between them.
2. If the specimen is thin enough, it restricts it to lie in what is essentially a single plane.
3. It controls the refractive index (RI) of the specimen's environment.

Easylift®'s adhesive performs the first two of these functions and so can be used successfully without the requirement for a mounting medium; it is, however, compatible with both aqueous and non-aqueous mounting mediums including, DPX, Entellan®, Fluromount™ and CC/Mount™. This means that a mounting medium can be used when control over the refractive index of the sample's environment is required, see appendix A.2 for more information.

2.3 Investigation into the recovery rates of microfibres from water using different filtering systems and Easylift® tape

2.3.1 Pilot Study

2.3.1.1 Method

The pilot study was conducted to investigate whether Easylift® was an appropriate method to retrieve microplastics from filter paper and if microplastics are lost during filtration and retrieval. During the study, 25 fluorescent polyester fibres taken from a high visibility jacket were manually retrieved using jewellers' tweezers and seeded into one litre of tap water.

This sample was then filtered under vacuum using a ceramic Buchner funnel and a Whatman® 70 mm cellulose filter paper catalogue number 1003 070.

Once filtration of the sample was finished, the glass bottle used to contain the sample was rinsed with 10ml of water and filtered to retrieve any microplastics that may have become adhered to the side of the glass bottle, the Buchner funnel was also rinsed.

The filter paper was then removed with the jewellers' tweezers and, placed in a glass petri dish and covered with an acetate sheet with a grid drawn on so that the fibres retrieved by the filtration process could be counted with a UV torch that emitted a light of 395 nm, to determine how many were retrieved or lost. Once determined, the microfibres were retrieved with Easylift® whilst the filter paper was still damp, ensuring the whole surface of the filter paper was tape lifted; the full Easylift® procedure can be found in Appendix A.2. The tape was then adhered to a glass microscope slide and the UV torch was used to count the number of microfibres retrieved by Easylift® from the filter paper. This procedure was repeated 15 times.

2.3.1.2 Results and Discussion

Table 2.5 The results of the pilot study seeding 1 litre of water with 25 fluorescent fibres to test the efficacy of Easylift®.

Sample	Percentage of fibres recovered by the filter paper	Percentage of fibres recovered from the filter paper with Easylift®	Overall percentage recovered
1		93	/
2	96	96	96
3	54	93	50
4	100	100	100
5	84	100	84
6	68	100	68
7	100	96	96
8	88	100	88
9	80	100	80
10	84	100	84
11	68	100	68
12	68	100	68
13	100	100	100
14	76	100	76
15	100	100	100
Mean	78	99	76
Range	46	7	50
Standard deviation	14.5	2.6	14.8

Table 2.5 shows the results of the pilot study; the percentage recovered by the filter paper for sample one is missing due to an error in the number of fibres added to the sample; full results can be found in Appendix A.3 Table A.1. From the results, it is apparent that microfibres are being lost during filtration with between 54-100% of microfibres being retrieved. There are a few potential areas for this loss, one being that the fibres remained in the glass bottle, became stuck in the small gap between the Buchner funnel

walls and the filter paper or on the funnel walls or the fibre was not retained by the filter paper and so passed through the filtration system without being retained.

The results also show that Easylift® was successful in collecting microfibres from the filter paper with between 93-100% with an overall 99% success rate of microfibres being collected via tape lifting.

During this experiment, only one filter paper type and funnel type were investigated. As other methods are used in microplastic analysis, more methods need to be investigated to determine if one method is able to retain more microplastics than others.

One issue that needs to be considered with this data is the small sample size could produce inaccurate data as one fibre would be the equivalent of 4% of the sample, meaning the loss of one fibre could skew the results and produce inaccurate results, for instance, if two fibres are not retained by the filter paper that translates to an 8% loss. To combat this, the sample size will be increased to help prevent data skews.

2.3.2 Main Study

2.3.2.1 Experimental Design and Materials

During the simulation experiment, target microfibres were suspended in tap water, and the seeded water was filtered under vacuum using a Vacuubrand® PC 3012 VARIO by Buchner filtration, and then the microfibres were recovered from the filter paper via tape lifting (see Section 2.1.2). The target microfibres that were used were fluorescent polyester fibres from a high visibility jacket; these microfibres were chosen due to the fluorescent properties of the fibres that allowed them to visibly fluoresce when exposed to a UV torch that emits light at 395 nm. Illumination of the fibres by a UV torch was conducted in a darkened room whenever a count of target microfibres was undertaken. The tape used in this experiment was Easylift® (see Section 2.2); Easylift® is manufactured by Tecman Ltd.

The experiment has a balanced 2 x 2 factorial design, in which the dependent variables are the recovery rate of target microfibres retrieved from the filter paper by Easylift® and the recovery rate of the filtration apparatus used to filter the microfibres from water. The independent variables were the filter type and Buchner funnel used, with each independent variable having two levels. The two levels for the filter type used are cellulose filter paper (Whatman catalogue number 1003 070 pore size 6 µm) or glass microfibre filter papers (Whatman catalogue number 1820 070 pore size 0.7 µm), both of which are 70mm in diameter. The two levels for the funnel type are a ceramic Buchner filter (available from Fisher Scientific catalogue number 10771752), or a glass frit (available from RESTEK catalogue number KT953825-0000). These methods were chosen as they are methods of filtration often used in microplastic research (see Table 2.2).

An A&D Company Ltd HR-250A analytical balance was used to weigh all samples to determine the mass of water present in each filter at the point that tape lifting occurred. This was conducted in duplicate so that the mass could be included as a covariate during hypothesis testing; the results are available in Appendix A.3 Table A.2

2.3.2.2 Experimental Procedure

During experimentation, there were three repeats undertaken for each of the four unique combinations of the independent variables. For each procedure investigated, the following method was followed:

Between 121 and 394 (inclusive) target microfibres were removed from a high visibility jacket using sandpaper and collected into a pre-weighted, clean, dry ceramic evaporating basin, and the exact number of microfibres was determined (c_1). The basin was reweighed to determine the mass of the fibres used (f) (Average weight 0.0028 g). the fibres were then transferred by washing into 10 L of tap water that was distributed into ten clean 1 L glass bottles so that the microplastic sample was not as concentrated and to make it more realistic to water samples taken of environmental samples.

An unused air-dry filter of one of the two types being investigated (see Section 2.3.2.1) was placed in a clean petri dish, and the mass of this combination was determined (p_1) by weighing on an analytical balance. The filter was then placed into one of the two funnel types being investigated; the funnel and filter paper were then observed using a UV torch to ensure that the set-up was free from any contamination from fluorescent fibres. The water in each bottle was then vacuum filtered through the assembled filter set-up, and the inside of each bottle was rinsed with 100 ml of tap water; this water was then also filtered through the same filter. After all the water from the bottles and rinse water had been filtered, the inner sides of the filter used were rinsed with 50 ml of water. 3-7 seconds after the last of the water had passed through the filter, the vacuum was broken.

The filter was then immediately removed from the funnel and placed back into the petri dish, which was then re-weighed, allowing the combined mass of the dish, the damp filter, and the target microfibres to be determined (p_2). The number of target microfibres on the filter paper was then counted (c_2).

For each filter, an unused piece of Easylift® was removed from its backing, and its adhesive-coated side was then applied and removed from the surface of the filter, the same piece of Easylift® was then reapplied until the whole surface of the filter paper had been in contact with the tape, this process is visualised in Figure 2.12. The number of target microfibres present on the tape was then counted (c_3) with the aid of the 395 nm UV torch.

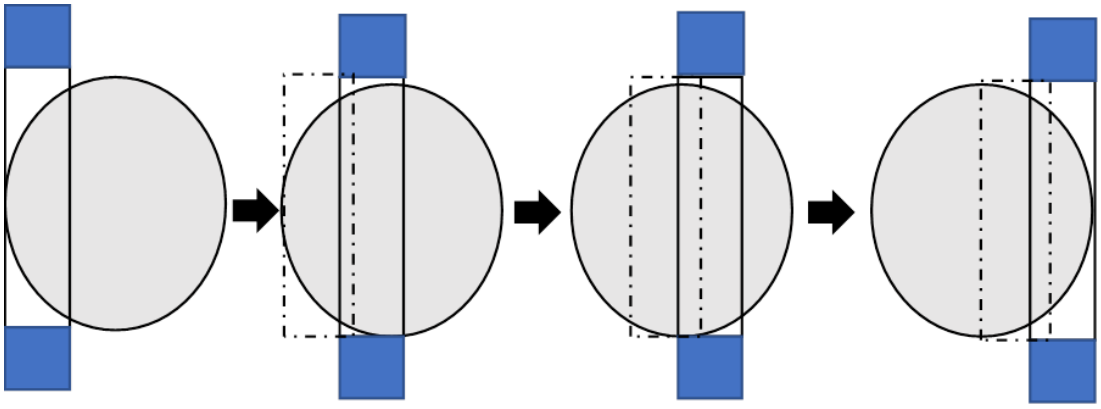

Figure 2.12 A diagram to demonstrate how Easylift® is used to retrieve microplastics from a filter paper.

When tape lifting, it is best that the filter paper is slightly damp. This is because when the filter is dry, the tape will collect more fibres from the filter, which may overload the sample and make identification of microplastics difficult to find and identify. If the filter is too wet, the tape may lose some of its tackiness, preventing it from collecting potential microplastics and may mean that the tape loses some of its ability to protect the sample from contamination, Figure 2.13 demonstrates six images demonstrating an Easylift® tape lift after it had been used in either a dry, damp or wet cellulose or glass filter paper. For each image, the adhesive side of the Easylift® tape was brought into repeated contact with the filter paper in the manner shown in Figure 2.12. In each case, the tape was then adhered to an unused glass microscope slide. For each of the two images labelled ‘air-dry filter’ there was no pre-treatment of the filter paper before it was tape lifted. The images labelled ‘damp filter’ each of the filters was separately pre-treated by placing it within a ceramic Buchner filter and filtering 1 litre of tap water through the system under vacuum. The Vacuum was broken approximately 5 seconds after the last traces of water had passed through the filter. For the images labelled ‘wet filter’, each filter was separately pre-treated by saturating it with distilled water over the whole surface of the filter paper. All images were taken with a Nikon AF-S Nikkor 10-70 mm camera under identical illumination conditions using the ambient light present within the room, with each glass slide placed on a dark card with the Easylift® tape facing the camera.

Filter type	Air-dry filter	Damp filter	Wet filter
Cellulose	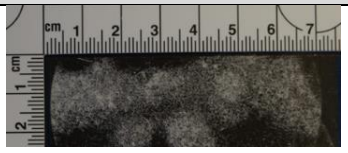		
Glass fibre	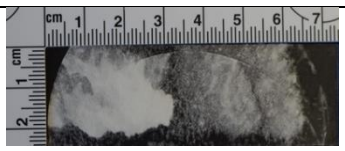	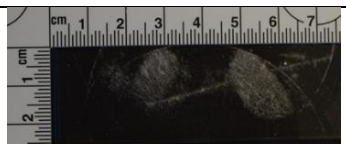	

Figure 2.13 Images of Easylift® tapes that had been used to tape lift clean filters of varying water content.

The mass of water present in the filter at tape lifting (w) could not be determined by oven drying the filter to a constant mass, as when tape lifting the filter, the tape will also collect fibres that originate from the filter paper. To estimate the total mass of water in each filter at the point of tape lifting, 20 of each of the cellulose and glass filter paper were weighed whilst air dry, these filters were then placed in an oven at 105 ºC for 16 hours and then re-weighed (Results are in appendix A.3 Table A.2). The mean mass difference for each filter (d) was then used in the calculation of w:

$$w = (p_2 - p_1 - f) + d$$

The target microfibre count allowed the percentage of fibres present on the filter that was recovered on the tape ((c_3/c_2) x 100%) to be determined for each repeat. The percentage of fibres present in the water that was extracted by filtration before tape lifting was also calculated (c_2/c_1) x 100%).

A blank sample of 10 L of tap water was also filtered using the same method as described above, using a cellulose filter paper and the ceramic funnel. This blank was found to contain one fibre that was indistinguishable from the target microfibres. This was considered to be within the likely margin of error in the count data, and so the data was not adjusted to account for contamination.

2.3.2.3. Statistical Analysis

The analysis of the data from the seeded experiment described above was conducted by four linear models:

- Model 1: A balanced 2x2 factorial ANOVA The dependent variable was the percentage of target microfibre particles present on the filter paper that was recovered by the tape, and the independent variable was the filter paper and funnel type used.
- Model 2: An ANCOVA The dependent variable was the percentage of target microfibre particles present on the filter that was recovered by the tape, and the independent variable was the filter paper and funnel

type. With the mass of the total water content on the filter paper at the point of tape lifting is included as a covariate.

- Model 3: an ANOVA conducted to find whether models 1 and 2 have a statistically significant difference.
- Model 4: A balanced 2x2 factorial ANOVA with interaction conducted to test the effect of filter type and funnel type on the percentage of target microfibres present in the water that were extracted onto the filter before tape lifting.

For all tests conducted, the significance threshold used was 0.05 (95% confidence). In Models 1, 2 and 4, a Shapiro Wilk test and a Levene's test were conducted to test the data for deviation from the assumptions that underpin the accuracy of the models concerned and no deviation was found (Jackson, Osborne & Gwinnett, 2020). The results of these tests can be found in Appendix A.3 Figures A.6 and A.7.

Two sets of simple effects tests were carried out after Model 1 was undertaken. One tested the effect of funnel type with fixed levels of filter type, and the other tested the effect of filter type at fixed levels of funnel type. Within these two sets, a Bonferroni adjustment was made to the p values to control the familywise error rate. It was also recognised that the two sets of simple effects could constitute a family. To allow for this, two values of alpha were used one without the Bonferroni correction (0.05) and one with the Bonferroni correction (0.025). The following significance categories were created: if the adjusted p-value is > 0.05, then it is not significant. If it is less than or equal to 0.05 adjusted p-value but >0.025, then the significance is discussable. If the adjusted p-value $\leq$0.025 then the result is significant. Any discussable p values would be those that have demonstrated significance and had only one set of simple effects tests undertaken.

The effect size measures implemented for models 1, 2 and 4 were eta squared and omega squared, and Pearson r was used for the tests of the simple effects. The threshold values used as cut points to categorise effect sizes are:

- For partial eta squared, small = 0.0099, medium = 0.0588 and large = 0.1379 (Richardson, 2011, citing Cohen, 1969 pp. 278-280).
- For omega squared, small = 0.01, medium = 0.06, and large = 0.14 (Field, Miles & Field, 2012 p 455).
- For Pearson r, small = 0.10, medium = 0.30 and large = 0.50 (Cohen, 1988 pp. 79-81).

The analysis was performed using RStudio Desktop Open-Source Edition version 1.2.5033 (RStudio, n.d.), running R version 3.5.1 (R Core Team, 2018), with the following packages loaded for use in statistical testing: gvlma version 1.0.0.3 (Pena and Slate, 2019), effects version 4.1-1 (Fox & Weisberg, 2019), car version 2.1-5 (Fox & Weisberg, 2011) and phia version 0.2-1 (De Rosario-Martinez, 2015).

All of the raw data, the code that was used to analyse it and the output from that code have been published as a data set (Jackson, Osborne & Gwinnett., 2020).

2.3.2.4 Results and Discussion

2.3.2.4.1 The Recovery of Microfibres in the Seeded Study

The seeded study described in Section 2.3.3.1 aimed to investigate the effect of filter type and funnel type on the rate of recovery for target microfibres from the filter papers using Easylift® as a method of recovery. The percentage recovery rate at each instance can be seen in Table 2.6. Figure 2.14 shows the rate of recovery of target microfibres grouped by funnel and filter type. Part (a) of Figure 2.15 shows the mean values for the rate of recovery with 95% confidence intervals grouped by filter and funnel type, while part (b) shows the rate of recovery with 95% confidence intervals grouped by filter and funnel type adjusted to control for the effect of the total mass of water on the filter paper at the point of tape lifting. Full results are available in Appendix A.3 Table A.3.

Table 2.6 A table to show the results of the seeded study when microfibres were seeded into 10 litres of water with both a glass frit or ceramic Buchner funnel or a cellulose filter paper or a glass microfibre filter paper.

Sample	% Recovered on the filter	% Recovered by Easylift®	% Recovered overall
Condition Cellulose filter paper and Buchner filtration			
1	91.14	97.14	88.54
2	92.47	99.55	92.05
3	94.95	98.94	93.94
Mean	92.85	98.54	91.51
Range	3.81	2.41	5.4
Standard deviation	1.93	1.25	2.74
Condition Glass filter paper with Buchner filtration			
1	91.87	88.95	81.73
2	80.99	91.84	74.38
3	89.21	92.86	82.84
Mean	87.36	91.21	79.65
Range	10.88	3.91	8.46
Standard deviation	5.67	2.03	4.60
Condition Cellulose filter paper with Glass frit			
1	92.98	98.11	91.22
2	95.73	99.36	95.12
3	93.37	100	93.37
Mean	94.03	99.16	93.24
Range	2.75	1.89	3.90
Standard deviation	1.49	0.96	1.95
Condition Glass filter paper with Glass frit			
1	90.11	95.12	85.71
2	95.54	98.45	94.06
3	96.23	96.08	92.45

Mean	93.9	96.55	90.74
Range	6.12	3.33	8.35
Standard deviation	3.35	1.71	4.43

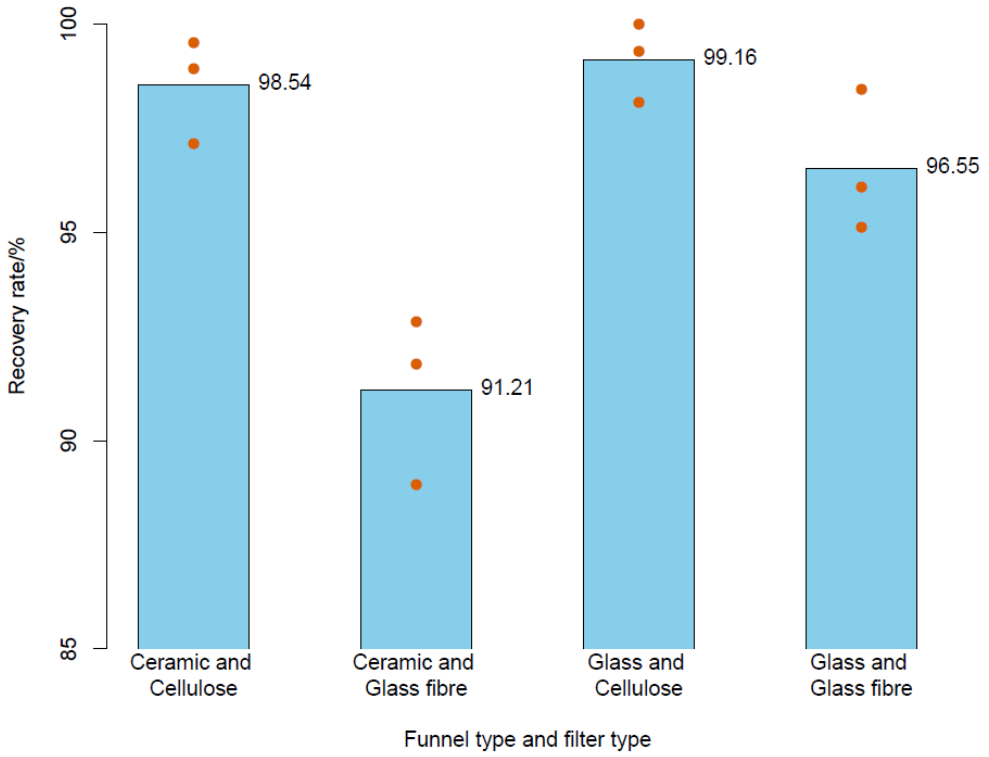

Figure 2.14 Mean target MP fibre recovery rates from filters by tape lifting with Easylift®, grouped by funnel type and filter type, with mean values and raw data points shown. Produced by Professor Andrew Jackson.

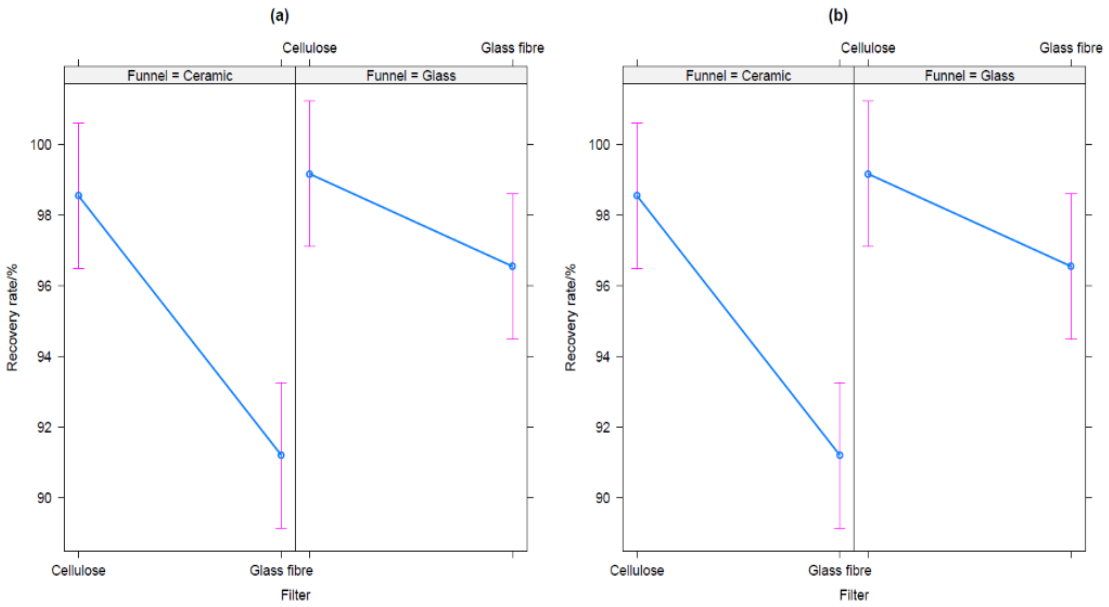

Figure 2.15 Interaction plots showing means and 95% confidence intervals for the target MP fibre recovery rate from filters by tape lifting with Easylift®, grouped by funnel type and filter type. Part (a) shows the means and 95% confidence intervals as revealed by ANOVA. Part (b) shows the same as (a) except in this case the statistics shown have been adjusted by ANCOVA to control for the effect of the total mass of water in the filter at the point of tape lifting. Produced by Professor Andrew Jackson.

As outlined in Section 2.3.3.3 both an ANOVA (model 1) and an ANCOVA (model 2) were used to test the effect of filter type and funnel type on the rate of target microfibres recovery from filters using Easylift®. Table 2.7 Shows the summary of the ANOVA (a) and the ANCOVA (b) which reveal the main effect of the independent variables (filter type and funnel type) is significant, as is the effect of the interaction between them. Partial eta squared: $\left(\frac{degrees\ of\ freedom\ x\ F\ model}{degrees\ of\ freedom\ x\ F\ model + degrees\ of\ freedom\ error}\right)$ Measures the proportion of variation explained by an independent variable after removing variance from other predictor variables, allowing the determination of how large an effect the independent variables have on the dependent variables (Richardson, 2011). Partial eta squared can provide a positive bias in the calculation of the effect size as it explains sample variance and not population variance (Mordkoff, 2019). In this case, all the combinations have a large effect size in Table 2.7 a, and in Table 2.7 b, all but the covariate have a large effect size, with the covariate having a medium to large effect size indicating that the independent variables (the funnel type in Table 2.7a or the filter type in Table 2.7 b) had a large effect on the dependant variable (percentage of target microfibre particles present on the filter that was recovered by the tape).

Omega squared:

$$\frac{Sum\ of\ squares\ between\ groups - (degrees\ of\ freedom\ between\ groups) x\ mean\ square\ within\ groups}{Sum\ of\ squares\ total + mean\ squares\ within\ groups}$$

Is an effect size used to measure the analysis of variance in ANOVAs to show how much of the variance in the dependent variable can be explained by the independent variable (Kroes & Finley, 2023). It is recommended as it is a less biased alternative to partial eta squared (Mordkoff, 2019). All but the funnel category in Table 2.7 b have a small effect size with omega squared; this indicates that a small amount of the variance of the dependent variables can be explained by the independent variables.

Table 2.7 ANOVA summary for Model 1 (a) and ANCOVA summary for Model 2 (b). The cut points (i.e. benchmark or threshold values) of partial eta squared and omega squared used to categorise the effect size magnitude are given in Section 2.3.3.3. The covariate in (b) is the absolute water content (in grams) of the filter at the point of tape lifting. Produced by Professor Andrew Jackson.

(a)

Term	Degrees of freedom	F	p	Significant at > 95% confidence	Partial eta squared	Omega squared
Filter	1	31.130	0.001	Yes	0.796 (>large)	0.001 (<small)
Funnel	1	11.162	0.010	Yes	0.583 (>large)	0.000 (<small)
Filter:Funnel	1	7.015	0.029	Yes	0.467 (>large)	0.000 (<small)
Residuals	8	NA	NA	NA	NA (NA)	NA (NA)

(b)

Term	Degrees of freedom	F	p	Significant at > 95% confidence	Partial eta squared	Omega squared
Covariate	1	0.691	0.433	No	0.090 (medium-large)	0.000 (<small)
Filter	1	17.127	0.004	Yes	0.710 (>large)	0.021 (small-medium)
Funnel	1	6.591	0.037	Yes	0.485 (>large)	0.007 (<small)
Filter:Funnel	1	7.417	0.030	Yes	0.514 (>large)	0.008 (<small)
Residuals	7	NA	NA	NA	NA (NA)	NA (NA)

This interaction effect, shown by these tests in Figure 2.13 and Figure 2.14, shows that for each funnel type, changing the filter type from cellulose to glass fibre was typically accompanied by a reduction in the number of microfibres recovered, and this effect was more visible when the ceramic filter was used. In addition, when cellulose filters were used, the rate appears largely unaffected by funnel type, this was not the case for the glass filters as the rate of retrieval decreased when switching from the glass frit to the ceramic funnel. To test the significance of these interactions, simple effects analysis was carried out based on model 1, the results of which are displayed in Table 2.8.

Table 2.8 The results of simple effects analysis of each of the effect of funnel type at fixed levels of filter type (a) and the effect of filter type at fixed levels of funnel type (b). Produced by Professor Andrew Jackson.

(a)

Funnel type 1	Funnel type 2	Filter type	Difference of means between funnel types	Better funnel type	Degrees of freedom	F	Adjusted p	r	Significant at > 95% confidence	Effect size magnitude
Ceramic	Glass	Cellulose	-0.617	Glass	1	0.240	1.000	0.171	No	small-medium
Ceramic	Glass	Glass fibre	-5.334	Glass	1	17.937	0.006	0.832	Yes	> large
Residuals	NA	NA	NA	NA	8	NA	NA	NA	NA	NA

(b)

Filter type 1	Filter type 2	Funnel type	Difference of means between filter types	Better filter type	Degrees of freedom	F	Adjusted p	r	Significant at > 95% confidence	Effect size magnitude
Cellulose	Glass fibre	Ceramic	7.327	Cellulose	1	33.850	0.001	0.899	Yes	> large
Cellulose	Glass fibre	Glass	2.610	Cellulose	1	4.295	0.144	0.591	No	> large
Residuals	NA	NA	NA	NA	8	NA	NA	NA	NA	NA

These tests revealed that tape lifting resulted in a higher mean target microfibre recovery rate from the filters when used with the:

1) Cellulose filter paper and glass frit funnel combination (m = 99.16%, s_{n-1} = 0.96 % points) to when the cellulose filter paper was used with the ceramic funnel (m = 98.54%, s_{n-1} = 1.25% points), however, this difference is not statistically significant.
2) Glass filter paper and glass frit funnel combination (m = 96.55%, s_{n-1} = 1.71 % points) to when the glass filter paper was used with the ceramic funnel (m = 91.21%, s_{n-1} = 2.03 % points) and this is a statistically significant difference.
3) Ceramic funnel and cellulose filter combination (m = 98.54%, s_{n-1} = 1.25% points) to when the ceramic funnel was used with glass filter paper (m = 91.21%, s_{n-1} = 2.03 % points), and this was a statistically significant difference.
4) Glass frit funnel and cellulose filter combination (m = 99.16%, %, s_{n-1} = 0.96% points) to when the glass frit funnel was used with the glass filter paper (m = 96.55%, s_{n-1} = 1.71 % points), but this is not a statistically significant difference.
5) The Pearson r effect sizes for Table 2.8 a, show a small-medium effect size for the funnel types when a cellulose filter paper was used and a large effect size for the type of funnel used when the glass filter paper was used.
6) The Pearson r effect size for Table 2.8 b shows a large effect size for both filter combinations when used with either a ceramic filter or the glass frit.

The interaction effect displayed in Figure 2.15 and Table 2.8 could be explained by an observation made during the experimentation. This is because when the glass filter paper was used in combination with the ceramic funnel, the glass filter was pliable, and so when under vacuum, would form visible dimples where the holes of the ceramic funnel were located, which did not occur when the cellulose filter was used with the ceramic funnel. Microfibres that settled into those dimples were less likely to be retrieved by the Easylift® tape. This dimpling of the glass filter paper did

not occur when the glass filter paper was used in conjunction with the glass frit, as it provides even support across the surface of the filter paper. It was also noted that when the ceramic funnel was used, after filtration, a few target microfibres were found outside the filter's edge at the base of the ceramic funnel. These microfibres were, therefore, not recovered by the filter paper. Furthermore, as shown in Figure 2.13, the tape lift will remove fibres that originate from the filter paper, but the degree to which this happens can be decreased by increasing the filter's water content. Whilst these fibres are distinguishable from any microplastics, their presence can increase sample processing time by masking and hiding potential microplastics. Also, if using the cellulose filters, then there is a possibility that the examiner will be unable to differentiate between cellulose fibres and white cotton fibres, which is detrimental to studies such as Stanton *et al.* (2019) as they were looking for anthropogenic materials, including cotton. As previously discussed, increasing the water content of the filter decreases the amount of filter paper fibres lifted during tape lifting. In the experiment, the vacuum was stopped between 3-7 seconds after the last visible traces of water had passed through the filter paper. Meaning the filter was damp at the point of tape lifting. However, some issues may arise if the water content of the filter is too high, as it impairs the tapes' ability to recover microplastics. This provides *prima facie* reason to hypothesise that the water content of the filter at the point of tape lifting will have an impact upon the recovery rate of microplastics.

This hypothesis was tested by adding the total mass of water in the filter at the point of tape lifting as a covariate to model 1 to produce the ANCOVA in model 2. The outcome of the F tests performed using model 2 is shown in part (b) of Table 2.7. As discussed above, like model 1 this shows both of the main effects and the effect of the interaction between them to be significant.

However, from part (b) of Table 2.7, the effect of the covariate was not found to be significant. Table 2.9 shows that the qualitative examination of the proportion of the dependent variables' variance explained by models 1 and 2 shows the inclusion of the covariate to create model 2 provides very little improvement compared to model 1. Furthermore, the ANOVA in model 3

was used to compare these nested models quantitatively, and this did not demonstrate any statistically significant differences between them [F = 0.6907, p = 0.4334].

Table 2.9 Model 3 (a) Measures of variance explained by each of Model 1 (ANOVA) and Model 2 (ANCOVA) when they are treated as multiple linear regressions. Each of these models was built with the percentage target MP particle recovery rate from the filter with the tape as the dependent variable (DV) (see Table 2.7 for the independent variables and the covariate). Multiple R2 measures the proportion of the DV's variance that the model explains. Shrinkage provides an estimate of how that proportion would diminish if the model were applied to the population and adjusted R2 is multiple R2 – shrinkage. (b) shows the results of an ANOVA to test for variance between the two models. Produced by Professor Andrew Jackson.

(a)

	Multiple R^2	Adjusted R^2	Shrinkage
Model 1	0.860	0.808	0.052
Model 2	0.873	0.800	0.073
Difference	-0.013	0.008	

(b)

```
Model 1: recovered_on_tape ~ Filter * Funnel
Model 2: recovered_on_tape ~ abs_water + Filter * Funnel
  Res.Df    RSS Df Sum of Sq      F Pr(>F)
1      8 19.034
2      7 17.324  1    1.7094 0.6907 0.4334
```

In this experiment, the absolute water content of the filter papers at the point of tape lifting ranged from 0.432 g to 0.790 g (m = 0.622 g and s_{n-1} = 0.117 g). Based on the observations discussed above, it can be concluded that within the range displayed and with the experimental set-up used, the data does not support the hypothesis that change in the water content affects the rate at which tape lifting can recover microfibres from the filter used. There is also no observable evidence that variation in the time at which the vacuum is disconnected from the Buckner flask has a visible impact on the recovery rate of tape lifting.

However, it cannot be completely ruled out that the water content of the filters that were tape lifted may have suppressed the microfibre recovery rate

compared to that that would have been obtained on dry filter papers. This was, however, not viewed to be an issue in this study as:

1) There were combinations of filter and funnel type used in the study in which the recovery rate was observed to have been reliably high.
2) Tweezers can be used to manually retrieve any unrecovered microfibres from the surface of the filter paper.

The data also allowed the calculation of the percentage of target microfibres recovered on the filter paper prior to tape lifting. The effect of each filter type and funnel type on microfibres recovered by the filter was tested by ANOVA model 4, the results of which are shown in Table 2.10, this revealed no significant effects of filter and funnel type on the recovery of microfibres by the filter paper. This is not unsurprising as:

- The target microfibres used were much larger than the pores in both filter types.
- There was nothing about the design of either funnel that would suggest that one would extract microfibres at a better rate than the other.

Table 2.10 ANOVA summary for Model 4 was built to test the effect of filter type and funnel type on the percentage recovery of the target MP particles from the water by filtration. Produced by Professor Andrew Jackson.

Term	Degrees of freedom	F	p	Significant at > 95% confidence	Partial eta squared	Omega squared
Filter	1	1.878	0.208	No	0.190 (>large)	0.000 (<small)
Funnel	1	3.669	0.092	No	0.314 (>large)	0.000 (<small)
Filter:Funnel	1	1.788	0.218	No	0.183 (>large)	0.000 (<small)
Residuals	8	NA	NA	NA	NA (NA)	NA (NA)

Table 2.10 shows a large effect size for all categories with partial eta squared and a small effect size when omega squared is used. Partial eta squared contains a positive bias when compared to omega squared (Mordkoff, 2019). The effect of the effect size for the effect of filter type and funnel type on the percentage recovery of the target MP particles from the water by filtration is likely to be small.

2.3.2.4.2 The Optical Properties of Filter Paper Fibres

As previously discussed, the use of Easylift® to recover microplastic pollutants from filter papers offers several potential benefits, including the compatibility with highly discriminating optical techniques, allowing characterisation *in situ* on the tape lift. However, as noted in Section 2.3.3.4.1, the process of tape lifting the filter's surface also recovers fibres that originate from the filter paper itself. This means fibres from the filter will be present during any *in situ* characterisation of microplastics found on the tape. For this characterisation to be successful, it has to be possible to discriminate between the microplastics and any fibres that originate from the filter paper. As microplastics come in many colours, shapes and sizes it would be unlikely for a microplastic to be sufficiently similar to the filter fibres to cause confusion between the two. To further differentiate between filter fibres and microplastics their optical properties can be examined. Figure 2.16 shows a colourless nylon fibre surrounded by fibres from either the glass filter paper or the cellulose filter paper the fibres are mounted on a glass microscope slide with Easylift®. Images (a) and (c) are images taken using plane-polarised light, allowing the optical properties of the fibres to be observed, the optical properties will differ based on the polymer type and thickness of the fibre. These images show that there is a degree of similarity between the nylon fibre and the fibres that originate from the filter papers, this is particularly evident in image (a). Although there are some similarities the fibres originating from the filter are easily discernible from the nylon fibre. Images (b) and (d) show the same field of view as images (a) and (c), but the images are taken whilst the specimens were between crossed polars, allowing for there to be more of a contrast between the filter fibres and the nylon fibre, this is especially noticeable in image (b) as unlike the cellulose filter fibres glass is essentially non-birefringent meaning that it is virtually invisible when under crossed polars (Yang *et al.*, 2012) while as cellulose is birefringent (Uetant, Koga & Nogi, 2019) it does not have this benefit.

	In plane-polarised light	Between crossed polars
A colourless nylon fibre with glass filter paper fibres.	(a) 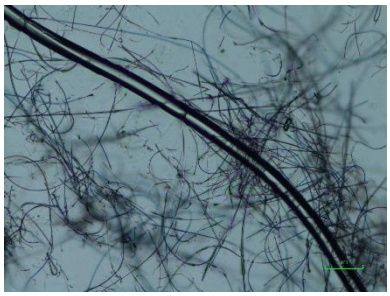	(b) 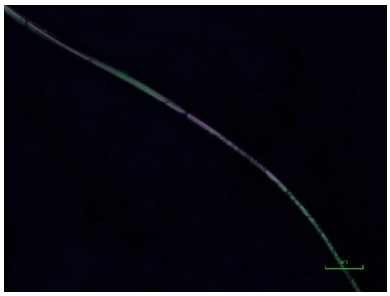
A colourless nylon fibre with cellulose filter paper fibres.	(c) 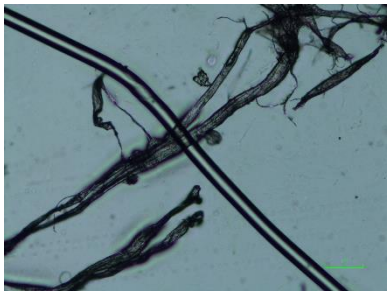	(d) 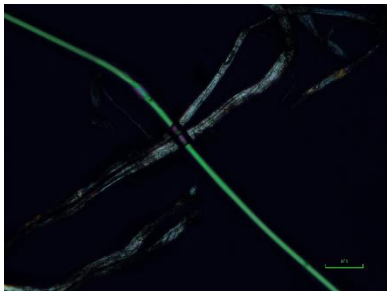

Figure 2.16 Images of two nylon fibres from the same source. One of these is with glass filter paper fibres, the other with cellulose filter paper fibres and are both shown as observed in each of transmitted plane-polarised light and between crossed polars. For each image of this figure, the specimen is held between Easylift® and a glass microscope slide. Scale bar is 50 µm.

As the vast majority of plastic fibres are birefringent (Palenik, 2018) and so combined with the invisibility of the glass filter fibres between crossed polars can be used to provide a high degree of visibility for a large number of microplastic particulates, that may happen to be morphologically similar.

As demonstrated in Figure 2.17, which demonstrates cotton fibres with either glass or cellulose filter paper fibres. It is easy to discern the difference between glass filter fibres and the colourless cotton used. However, cotton is cellulosic (De Wael & Lepot, 2012), meaning that it can be difficult to distinguish between the cotton fibres and the cellulose fibres from the filter paper (see parts (c) and (e) of Figure 2.17). This is important for studies on microplastic pollution, which is also interested in the prevalence of anthropogenic cotton fibres in the natural environment.

	Without silicone oil	With silicone oil
A white cotton fibre with glass filter paper fibres	(a) 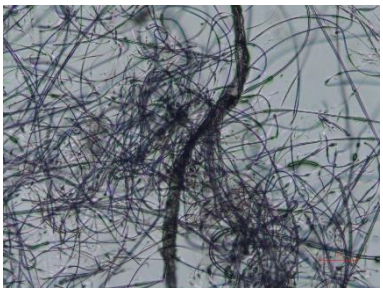	(b) 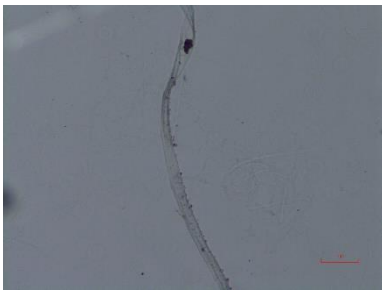
A white cotton fibre with cellulose filter paper fibres	(c) 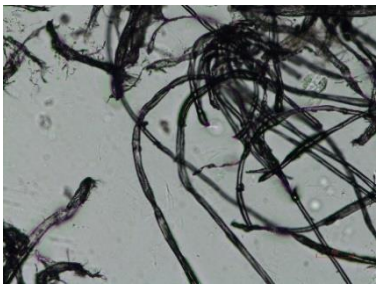	(d) 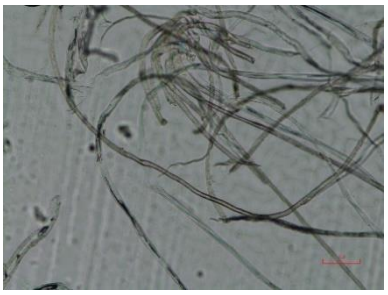
A blue cotton fibre with cellulose filter paper	(e) 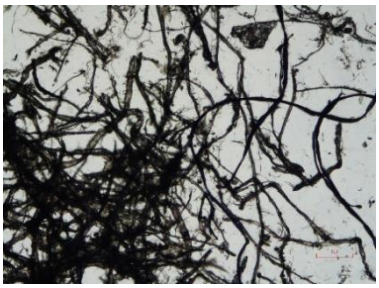	(f) 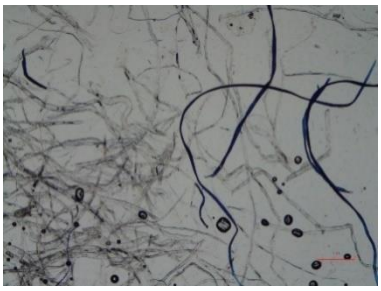

Figure 2.17 Images of cotton fibres with either glass or cellulose filter paper fibres, each taken with and without a mountant. In these images, the mountant is a silicone oil with a refractive index of 1.5280 and the light used to illuminate the specimens is not polarised. For each image of this figure, the specimen is held between Easylift® and a glass microscope slide.

For studies interested in the presence of materials like cotton, the glass filter fibres have a secondary property that can be utilised to help further differentiate between fibres of interest and glass filter fibres. This is because glass has one refractive index; the fibres are also colourless and have a low opacity. This means that in the presence of a mountant with a suitable refractive index, the glass fibres can be made to effectively disappear from view whilst the cotton fibres are still visible. This is illustrated in Figure 2.17 images (a) and (b), with image (a) being of a colourless cotton fibre surrounded by glass filter paper fibres encased in Easylift®, whereas image (b) shows the same location but a small v was cut in the Easylift® tape around the cotton fibre and silicone oil with a refractive index of 1.5280 was

placed over the cut and allowed to seep under the tape immersing the fibres, and rendering the glass fibres virtually invisible. This also means that any microplastic particles present on the slide that are either coloured or possess a noticeably different refractive index to that of the mountant will also be visible. As the glass fibres are essentially non-birefringent, the invisibility of those fibres will be maintained when viewed under crossed polars, allowing birefringent microplastics to be even more clearly visible when viewed under such illumination conditions.

Images (d) and (f) of Figure 2.17 were produced in the same manner as image (b), using cellulose filter paper fibres rather than glass fibres; as can be seen in these images, the cellulose fibres remain visible when a mounting agent is used. This is because cellulose fibres have internal structures which cause a difference in the fibre's refractive index, meaning that the boundaries between these structures show relief, making them visible, and so the fibres will not disappear as the glass fibres will do when a suitable mounting agent is used. This means that the difficulty in differentiating the cellulose fibres from the cotton fibres remains difficult, as shown in images (c) and (d), where the cotton fibre cannot be easily distinguished from the surrounding cellulose fibres. Images (e) and (f) show the same principle displayed in images (c) and (d), but a blue cotton fibre was used instead of a colourless cotton fibre to make the contrast between the cellulose fibres and the cotton fibres more apparent.

Easylift® is compatible with a range of mounting materials including both temporary and permanent mounts (Stuer, 2016), as displayed in Figure 2.16 and Appendix A.2. However, the use of an additional mountant can also have negative effects; for instance, there is a potential that it would render any colourless, transparent, non-birefringent microplastic, that happens to have a sufficiently similar refractive index invisible. However, this would be incredibly unlikely given the wide range of such properties in microplastic particulates. Another disadvantage is that the mountant may leave a residue on the microplastic that is dissected from the tape lift for further analysis. Although, any such residues can be removed by washing with a suitable solvent (Kirkbride and Tungol, 1999).

2.3.2.5 Limitations

1) As discussed in section 2.3.3.4.1, it was not found that tape lifting removed all microfibre particulates present on the filter papers. As a whole, it was found that tape lifting recovery rates ranged from 89-100% across all combinations investigated, with a mean and standard deviation of 96.4% and 3.5% respectively. For model 1, the adjusted R^2 value is 0.808 (see Table 2.10); this suggests that within the experimental set-up used, approximately 81% of the variance seen in the recovery rates is controlled by the choice of filter and funnel type. From this and the data presented in Figure 2.14 and Figure 2.15, it can be determined that optimisation of the filter and funnel type can be expected to produce a recovery rate greater than 96.4% with a standard deviation of less than 3.5% points. It is, however, unlikely that any optimisation would lead to a 100% recovery rate with a standard deviation of 0% points. As discussed in 2.3.3.4.1, some of the losses of target microfibres were observed to be caused by the fibres settling on the inner surface of the funnel but not the filter paper, these were therefore not extracted as only the surface of the filter was tape lifted, it is, however, possible to also tape lift the inside of the funnel to collect any such microfibres. When tape lifting the surface of the funnel care must be taken not to tear the tape when removing it from the surface of the funnel as Easylift® can be prone to tearing or sticking to itself when used on smooth curved surfaces.
2) The simulation experiment had three repeats for each of the four unique combinations of its factor level. This sample was sufficient to detect any significant interactions in models 1 and 2. Therefore, this experiment is fit for purpose despite the small sample size. However, the results of this study are contingent upon the specific experimental set-up used in this study. With this knowledge and the findings of the seeded study, it can be concluded that pretesting prior to the adaption of tape lifting into any microplastic sampling protocol is highly advisable.
3) The seeded experiment did not detect an effect of the absolute water content on the filter paper at the point of tape lifting on the recovery rate

of microfibres. This does not, however, mean that no such effects occurred, for example, it is possible that no effects were detected as the range of water contents used in this experiment was too small to be significant. This holds out the possibility, as noted in section 2.3.3.4.1, that the presence of water on the filter paper at the point of tape lifting suppressed the rate of microfibre recovered using Easylift®. Although, it is noteworthy that the best combination of filter and funnel type (cellulose filter and glass frit) produced a recovery rate of 99.16% with a standard deviation of 0.96% points. This suggests that if the effect was present, the effect of the suppression was very small in this experiment set up.

4) It is evident from the seeded study that tape lifting of the damp filter papers not only recovered the target microfibres present but also collected fibres that originate from the filter paper used. While this effect is not desirable, it is ultimately not an issue as polarised light microscopy can be used to easily distinguish between sample microplastics and filter fibres. Also, as outlined in section 2.3.3.4.2, the use of a mountant with a refractive index suitable similar to that of the glass fibres can be used to make those fibres effectively disappear.
5) As part of contamination control measures, it has been recommended that studies investigating microplastic pollution use triple-distilled water (Stanton *et al.*, 2019) or Millipore water (Nelms *et al.*, 2018. & Woodall *et al.*, 2015) to rinse equipment before it is used. Tap water was used in this study as the amount of water required in this study excluded the use of triple-distilled or Millipore water for reasons of practicality. The use of tap water may have introduced contaminant fibres into the study. However, the blank procedure performed indicates that this is unlikely to be an issue.
6) The effects of biofilms on the microplastics have not been investigated in this study. In addition, in the seeded study, only the target fibres were suspended in the water, which may limit the generalisability of the results to real-world samples. The presence of a biofilm and or suspended materials might have an impact on the tape-lifting process. It is also possible that the presence of any biofilms of suspended material may interfere with any subsequent *in situ* analysis whilst on the tape lift.

7) As outlined in section 2.2.1.1, polarised light microscopy is an effective means of characterising anthropogenic textile fibres whilst they are held *in situ* in an Easylift® tape lift. To a large degree, this is because:
    1) The range of birefringence values of these fibres and their range of thicknesses are such that the measurable optical path difference is frequently seen.
    2) Birefringence values can be an effective means of distinguishing between anthropogenic synthetic fibres of different polymer types. For instance, Palenik, (2018) states that polypropylene tends to exhibit birefringence in the range of 0.028-0.034 whilst polyethylene is in the range of 0.050-0.052. Unfortunately, such a clear distinction between polymer types is not always possible, for instance, nylon 6 has a range of 0.049-0.061, which encompasses the birefringence range for polyethylene (see Table 2.3 for a full list of birefringence ranges). It should be noted, however, that when the birefringence does not provide sufficient discriminating power for microplastic characterisation, there are other characteristics that could be examined to do so, such as cross-sectional shape, fluorescence, colour, presence of inclusions such as delusterant, all of which can be readily determined *in situ* on Easylift® tapes.
8) As outlined in sections 2.2 and 2.3.3.4.1 Easylift® is designed to enable the characterisation of microscopic particulates using a range of optical techniques without the need to dissect from the tape lift. There are, however, several techniques that cannot be undertaken *in situ*, for instance, the analysis of colour and colourants. In the forensic science context, colour is determined using microspectrophotometry (MSP) as it can be used to discriminate between fibres from different sources (Biermann & Wiggins, 2018. & Palenik, Beckert & Palenik, 2016). As shown in section 2.2 Easylift® is compatible with microspectrophotometry. However, if the aim is the identification of colourants present rather than colour then microspectrophotometry is not sufficient and further testing is needed, for instance, thin-layer chromatography (Biermann & Wiggins, 2018). Thin-layer chromatography cannot be used *in situ* on the Easylift® tape, however, thin layer chromatography and other techniques such as

infrared spectroscopy can be conducted once the particulate has been dissected from the tape lift.

2.3.2.6 Conclusions

The seeded study described in this chapter provides evidence of the potential of tape lifting as a method of post-filtration microplastic recovery during the analysis of water samples. As it allows for the rapid preparation of samples for subsequent examination with a wide range of optical techniques including polarised light microscopy. Easylift® also offers a secure storage environment for microplastics preventing contamination and loss of the samples which as discussed in Section 1.9 would greatly benefit the field of microplastic research by facilitating inter laboratory research and validation of findings by independent researchers.

In the seeded experiment, filter type and funnel type were found to produce a significant interaction effect on the rate of microfibre recovery post-filtration. Under the conditions outlined in section 2.3.3.1 and with the optimal choice of filter and funnel type, tape lifting can be used to reliably collect all but a small percentage of microfibres. The best funnel and filter combination was found to be cellulose filter paper with the glass frit as it had a mean recovery rate of 99.16% with a standard deviation of 0.96% points. The water content of the filter paper was also not found to affect the rate at which tape lifting can recover microfibres from the filters used when looking at the range of water contents observed in this study before tape lifting.

A statistically significant difference was only found when comparing the glass filter paper and glass frit funnel combination (m = 96.55%, s_{n-1} = 1.71) with the glass filter paper with the ceramic funnel (m = 91.21%, s_{n-1} = 2.03) P value = 0.006. A statistically significant difference was also found when comparing the ceramic funnel and cellulose filter combination was used (m = 98.54%, s_{n-1} = 1.25) with the ceramic funnel with the glass filter paper (m = 91.21%, s_{n-1} = 2.03) P = 0.001.

The glass filter paper with the Buchner filter combination resulted in the lowest retrieval rate (91.21% with a standard deviation of 2.03%), This could

be explained through an observation made during the experiment. As the glass filter paper is very pliable when under vacuum, the filter will form dimples on the surface where the holes on the Buchner funnel are. These holes tended to trap smaller microfibres, making them less likely to be retrieved by the Easylift® tape lift, as mentioned in Section 1.9 knowing the potential loss rates of each filter funnel combination allows the most appropriate method to be implemented to maximise the microplastics' recovery, resulting in more accurate reporting of pollution levels. In addition, by knowing what is likely to be lost during filtration it allows for the final count to be adjusted if necessary.

It was found that the tape lifting of the damp filter papers not only recovered the target microfibres present but also collected fibres that originate from the filter paper used. While this effect is not desirable, it is ultimately not an issue as polarised light microscopy can be used to easily distinguish between sample microplastics and filter fibres. In addition, if the filter was slightly damp, fewer fibres would be retrieved than if the filter was dry. Meaning that it is best to extract the microfibres from the filter paper soon after filtration rather than allowing the filter paper to dry before tape lifting.

Easylift® was also demonstrated to be compatible with a number of techniques that can be used *in situ* such as polarised light microscopy which allows the polymer type of the microplastic to be determined via calculation of its birefringence. Easylift® is also compatible with confocal Raman spectroscopy allowing for a confirmatory technique to be used without the need to dissect the microplastic in question from the tape lift. If, however, the microplastic needs to be removed for the tape lift so that it can undergo further analysis such as FTIR, as the microplastic is readily dissected from the tape lift.

Chapter 3 Development of an improved method of processing microplastic samples – Easylift® field trial and the addition of polarised light microscopy for the detection of microplastics

3.1 Introduction

3.1.1 Microplastic Detection

The identification of microplastics can be challenging due to a number of features, including size, shape, colour, and the presence of background and natural materials obscuring the sample. Due to these factors, it can make their accurate detection challenging so a variety of techniques are often implemented (Shim, Hong & Eo Eo, 2017). The most commonly used first step is to use stereomicroscopy to locate and identify potential microplastics see Table 1.1(Dris *et al.*, 2016., Norén, 2007. & Prata *et al.*, 2020a). Even an experienced microplastic researcher can make errors in the identification of microplastics in the presence of natural materials such as diatoms and chitin (Viršek *et al.*, 2016). Dyachenko, Mitchell & Arsem, (2017) tested the use of stereomicroscopy as a screening method with a spiked sample containing a known number of 200 µm polystyrene beads, and they found that 87% of the microbeads were confirmed microscopically. However, as they only investigated one size of 'clean' microbeads, this may not be comparable to environmental samples. For instance, another study using environmental samples from the sea surface and beach sand found that using stereomicroscopy to screen microplastics led to a significant underestimation of fragmented microplastics and microfibres were significantly overestimated in both sample types (Song *et al.*, 2015). Viršek *et al*, (2016) found an error rate of misidentification ranging from 20-70%, with the error rate increasing as the size of microplastics decreases. In such instances where the use of stereomicroscopy alone is not enough to identify microplastics, there are some techniques used to aid the differentiation of natural and synthetic particles, such as using Nile red to stain microplastics, causing them to fluoresce under certain wavelengths of light (Prata *et al.*, 2020b). Some

stereomicroscopes will also have a fluorescent attachment, meaning that they can be used in conjunction with Nile red (Wang *et al.*, 2019).

The dye in Nile red absorbs onto the surface of the microplastics using van der Waals interactions and dipole interactions in polar polymer types, allowing them to become visible when exposed to blue light (450-510 nm) (Maes *et al.*, 2017). The affinity of the dye and the microplastics can be increased with heat during the dyeing phase as this loosens the polymer chain; when the sample is then allowed to cool to room temperature, the dye becomes encapsulated in the polymer matrix. This means that there is improved stability and extending the lifetime of the effects of the Nile Red dye (Shruti *et al.*, 2022). The technique is fast and easy to use as it requires minimal training to be implemented effectively. It is also time-saving in studies with a large number of samples that require quantification (Sturm *et al.*, 2023). A study that tested the recovery rate of Nile Red with a sand sample spiked with Polyethylene, found a recovery rate of 98 ± 3% (Shim *et al.*, 2016). Its use has also resulted in an increase in the detection of microplastics from smaller size fractions <1mm (Erni-Cassola *et al.*, 2017). This method does, however, have some drawbacks, such as the presence of the Nile Red dye can make the determination of the original colour of the microplastics challenging; in addition to this there are instances where Nile Red is unable to stain some coloured microplastics due to the presence of the dye used in their production meaning that the method will not stain all microplastics that may be present in a sample (Shruti *et al.*, 2022). Both synthetic fibres and natural fibres will also fluoresce with this method, meaning that other methods are still needed to differentiate and identify the synthetic microplastics from other materials within the sample (Galvão *et al.*, 2023). Research has also been done to try to automate the detection of microplastics to eliminate human error in their detection and speed up analysis (Primpke *et al.*, 2020). PerkinElmer has developed the Spotlight 400, an FTIR microscope to rapidly image and analyse large sample areas (PerkinElmer, 2023); this technique has been applied to microplastic samples and has been found to be able to identify microplastics down to 6.25 µm in three minutes per sample (Liu *et al.*, 2021a). When the spotlight was

combined with Nile Red, it was able to identify 78% of the luminescent particles assumed to be microplastics, later confirmed with FTIR, while the remaining 22% were either organic in nature or solidified oil components (Kang *et al.*, 2020). Principal component analysis has been used with Raman spectrometry image mapping, where the sample was scanned with the x20 or x100 objective. The synthetic material was able to be separated from the organic material through the use of the generated Raman spectra (Luo *et al.*, 2022).

Polarised light microscopy (PLM) is a widely used technique in Forensic science as a method of fibre examination, as it is able to provide information about the polymer type through the determination of its birefringence value. In addition to this PLM can provide other characterising information such as surface characteristics such as the fibre's diameter, cross-sectional shape, and presence of delusterant (Farah *et al.*, 2015). PLM is also used to detect microplastics, although less commonly used, Sierra *et al.,* (2019) used PLM to identify optically active particulates in their sample as an initial identification approach, although they did not use PLM to determine the fibre's birefringence and provide an initial polymer identification nor did they investigate any other features present such as the cross-sectional shape to help further identify synthetic materials before any further techniques are implemented. PLM has recently been used to classify microplastics from Antarctic samples (Cunningham *et al.*, 2022) and the Long Island Sound, USA (Miller *et al.*, 2024). In these studies, PLM was used to provide polymer type and allow a greater level of classification such as cross-sectional shape to group microplastics into those that may be from a similar source this also helped to identify and remove contamination from the final microplastic count. The analysis used in these studies was informed by the findings of this thesis.

Examiners tend to use strict criteria to identify and classify microplastic particles, Norén, (2007) outlined some stipulations the particulates have to follow to be considered a microplastic, such as having no cellular or organic structures visible within the particulate, fibres need to be equally thick along their entire length, the microplastic needs to exhibit a homogenous colour

throughout, and if particulates are colourless, they are examined under high magnification and with a fluorescence microscope to determine if it may have an organic origin. However, these criteria may eliminate potential microplastics as it has not taken into account that not all synthetic fibres will be equally thick along its entire length due to factors such as its cross-sectional shape and damage caused during or after manufacture. The colour is also not always homogenous throughout the fibre; examples of these exceptions can be seen in Figure 3.1. In addition, this enumeration alone is not enough to fully comprehend the extent of microplastic pollution (Rivers, Gwinnett & Woodall, 2019), as there needs to be a holistic approach taken to understand microplastic pollution, including investigating potential sources of the pollution and the processes involved in their journey into the environment.

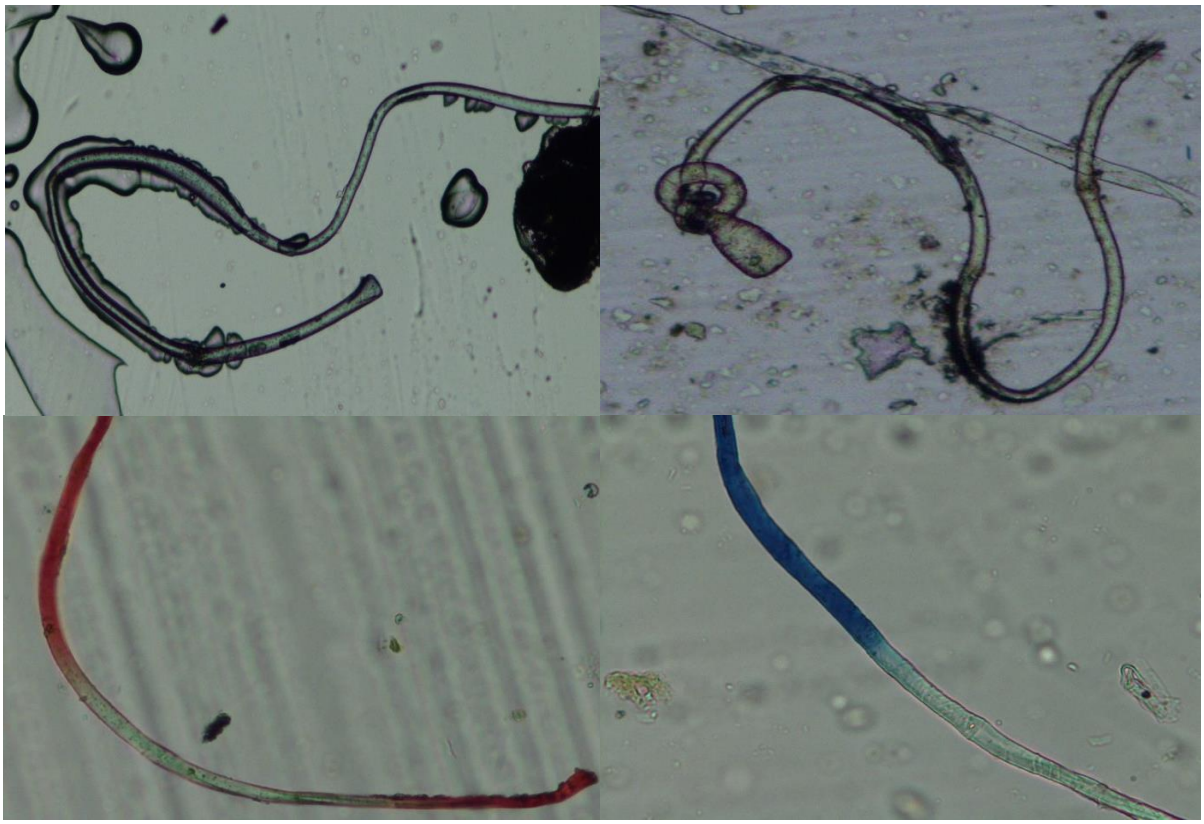

Figure 3.1 A series of synthetic fibres found in environmental samples taken from the Hudson River (top left and right) demonstrating an uneven thickness along the fibres length and, images demonstrating a fibre without homogenous colouration (bottom left and right).

3.1.2 Properties of Synthetic and Textile Fibres

There are several different methods of producing synthetic fibres depending on the polymer being used. Melt spun fibres are commonly made of nylon, polyesters and polyolefins (Ziabicki, 1976); this is because for melt spinning to be successful, the polymer needs to become fusible below the degradation temperature, have a high enough molecular weight to prevent filament breakdown when under strain but low enough to not have too high a viscosity that hinders the ability to process the polymer, and have small polydispersity to allow the melt flow to be constant (Misra *et al.*, 1995). The molecular chains need to have enough mobility that they are able to orient in the direction of the fibre when put under strain and have a high purity and uniformity (Hufenus *et al.*, 2020 & Qin *et al.*, 2018). When melt spinning polymers the polymer pellets run through a screw extruder to melt and pressurise the polymer, a melt pump is used to ensure that there is a constant throughput rate. The liquid polymer is extruded through spinneret holes that form the cross-sectional shape of the resulting fibre; after leaving the spinneret, the fibres are spun into the quenching chamber or a water bath to cool and solidify the fibre (Hufenus *et al.*, 2020). If a polymer does not meet the criteria for melt spinning such as acrylics, there are alternative production processes that can be used. Two further techniques are wet and dry spinning in these techniques, the polymer is dissolved in a solvent and extruded through a spinneret hole, in wet spinning the fibre then goes into a coagulant bath that removes the solvent from the fibre and in dry spinning the solvent is left to evaporate leaving the fibre behind (Craig, Knudsen & Holland, 1962). Depending on which method is used, the cross-sectional shape of the fibre will be altered; variations in the solvent and temperature used will also impact the shape, with lower temperatures producing less cylindrical cross sections (Bell & Dumbleton, 1971).

The cross-section of synthetic fibres is chosen depending upon their intended purpose, for example trilobal fibres are often used for carpet fibres as they have an increased durability (Chadhuri, 2018), or some fibres are made hollow to increase the insulation properties of the fibre (Grieve,

Biermann & Schaub, 2005). Table 3.1 shows a selection of commonly encountered cross-sectional shapes used for synthetic fibres. Cylindrical fibres are a very commonly used cross-sectional shape for garments (Jones & Coyle, 2011). Under the microscope, they look like a tube that will have a relatively consistent width along its length. Bilobal fibres are produced using two spinneret holes that creates a fibre with the appearance of two cylindrical fibres 'stuck together', when being observed with a microscope the central cleft should be observable twisting along the length of the fibre at some points only one lobe may be observable. A trilobal fibre is composed of three lobes in a pyramid formation. When observed with a microscope, it will look like a larger lobe with a smaller lobe meandering from side to side along the length of the fibre; it may also twist so the lobe that runs along the top will change. The ratio of the three lobes can vary, with some lobes being longer and more apparent than others. Delta fibres are extruded through a triangular spinneret hole rather than a circular one, giving it a triangular cross-sectional shape. Some delta fibres are more exaggerated and may appear similar to a trilobal fibre, and some are more rounded, and the shape may be more difficult to observe as it appears similar to a cylindrical fibre. In both instances, employing microsectioning on the microscope to observe the whole fibre will aid in the identification of the cross-sectional shape. Square fibres are extruded through a square-shaped spinneret hole; they can appear similar to delta fibres, but as the fibre twists, the square cross-sectional shape should be identifiable by the number of corners that run along the fibre. Flat fibres look like a squashed cylindrical fibre, they can be identified by how the fibre twists when the whole length is observed as the thinner side of the fibre will become visible.

Table 3.1 Commonly found synthetic cross-sectional shape.

Cross-sectional shape	Transverse view	Longitudinal view	Example image
Cylindrical	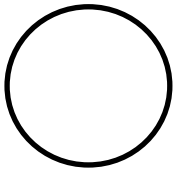		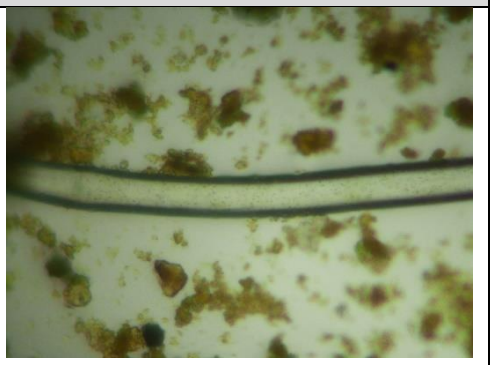
Bilobal	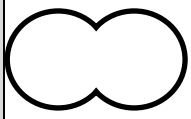	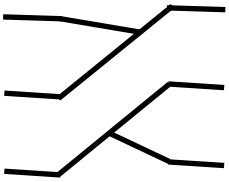	
Trilobal	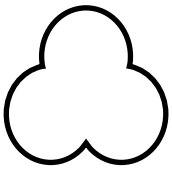	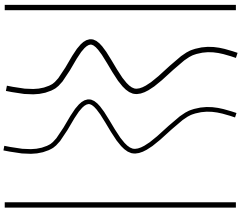	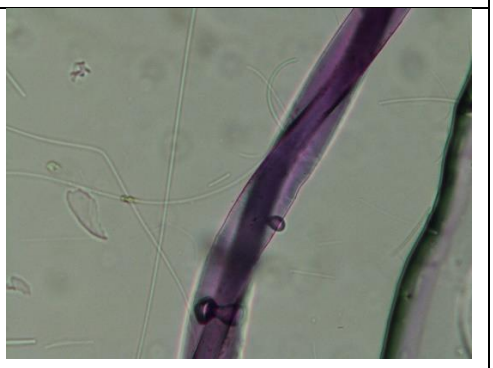
Delta	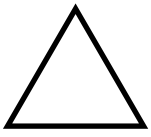	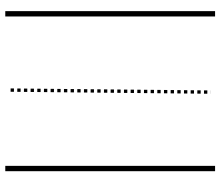	

Square	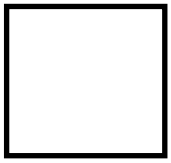	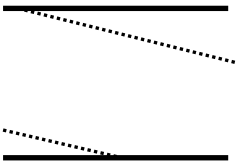	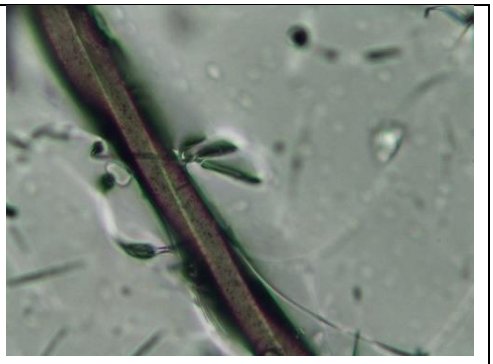
Flat		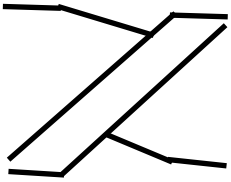	

Many textile fibres are comprised of naturally occurring materials such as cotton, viscose, and wool (Muthu *et al.*, 2012). Natural fibres can be split into three broad categories depending on their origin: vegetable, animal, and mineral (Chandramohan & Marimuthu, 2011). Vegetable fibres, also known as cellulosic fibres, are fibres that are comprised of cellulose; they are mainly sourced from seeds (cotton), bast (flax & hemp), and leaf (abaca) (Carr *et al.*, 2008). Animal fibres are mainly comprised of proteins, they are sourced from animal hair (wool, cashmere, and mohair), silk fibres from the dried saliva of bugs and insects when they are creating cocoons (silk) and avian fibres taken from birds (feathers) (Chandramohan & Marimuthu, 2011). Mineral fibres are fibres that have been sourced from minerals and altered to fulfil a purpose. They are asbestos, the only naturally occurring mineral fibre, ceramic fibres (glass fibres) and metal fibres (aluminium fibres) (Chandramohan & Marimuthu, 2011). Cotton is the most commonly used seed fibre as it is responsible for roughly half of all textile fibres produced annually (Nayak *et al.*, 2020). Cotton fibres can be readily identified with a microscope by its ‘kidney shaped’ cross sectional shape, the presence of a lumen and convulsions along the length of the fibres, PLM is also able to observe changes in the transmitted interference colours due to the reversals

in the direction of the spirals (fibril) when a first order red tint plate is used (Gordon, 2009). Flax fibres also have characteristic features that aid in their identification, it has a polygonal cross-section with clockwise twists, thick cell walls with a small lumina. There are some features that are common in all bast fibres for instance dark dislocations in the formation of an 'X' that run perpendicular along the length of the fibres (Nayak *et al.*, 2020). Hemp and jute also both have a polygonal cross-sectional shape but they both have counterclockwise twists, and hemp has closely packed transverse striations and the fibre ends rounded, blunt or forked tips while jute has a lumen of irregular width and the fibre ends in pointed tips (Carr *et al.*, 2008). Textile silk fibres are comprised of filaments that are joined together in pairs covered in sericin, silk fibres have a smooth, uniform surface and a delta cross-sectional shape, while natural silk has a ribbon cross-sectional shape and fine longitudinal lines (Nayak *et al.*, 2020).

3.1.4 Identifying Anthropogenic Materials - Recommended Features to Observe

This study has a strong reliance on the ability to correctly identify and tell the difference between natural and anthropogenic particulates, this section will give a brief guide on the factors that indicate an anthropogenic particulate and features that indicate natural material. A number of features will be discussed below; none should be used in isolation but rather a combination of the following features can help to identify if a particulate is natural or anthropogenic.

3.1.4.1 Colour

The colour of the particulate is a good indicator as to whether it is anthropogenic or not, particularly when it is exhibiting vibrant colours that are unlikely to occur naturally, for instance, blue, purple and red. These colours are a result of pigments and dyes. As stated above, the presence of colour alone should not be used to determine the classification as there will be exemptions such as brightly coloured natural materials like coral particulates, feathers and some flower materials, e.g., brightly coloured petals. In addition

to this not all textile fibres are dyed and coloured so other features need to be considered (Grieve, 1983).

3.1.4.2 Internal Features

Another feature that is important to observe and consider is the presence of any internal features as it can provide information on the structure of the particulate and indicate if there are any additives. Plant-based particulates will exhibit features such as the presence of a lumen (Berghjord & Holst, 2010) and specialised cells like chloroplasts (Cox *et al.*, 1987). Different natural fibres may exhibit different internal structures and features which allows an identification to be made and a determination of whether the particulate is anthropogenic in nature, see resources such as Summerscales & Gwinnett (2017) for information on what features to look for when identifying anthropogenic textile fibres.

Synthetic fibres can also have internal features known as additives or inclusions that are added into the polymer mix during production, the presence of these features is a good indicator that the particulate is synthetic (Palenik, 2018). These inclusions can be produced accidentally during production such as air bubbles and stress marks produced during the extrusion process of a polymer fibre (Robertson and Grieve, 1999). Or deliberately added during manufacture to serve a purpose. For instance, delusterant (titanium dioxide) is added to synthetic fibres to remove some of the lustre of the fibre, making it less bright (Brinsko, Sparenga & King, 2016). The presence and absence of delusterant is an important feature to observe in synthetic fibres (De Wael, 2021).

3.1.4.3 External Surface Features

The outer surface of the particulates will also have features that can indicate whether the particulate is anthropogenic in origin or natural. Natural fauna such as diatoms (microscopic algae with a silica shell) are commonly found in water samples and some can be confused with microbeads when there is not adequate magnification to observe them due to their uniform circular appearance (Brownlee et al., 2022, & Carson *et al.*, 2013). But when viewed

under a high enough magnification, the external features are observable, including pitting and regular mosaic patterns (See figure 3.2, two diatoms at x400 magnification where the surface features are observable).

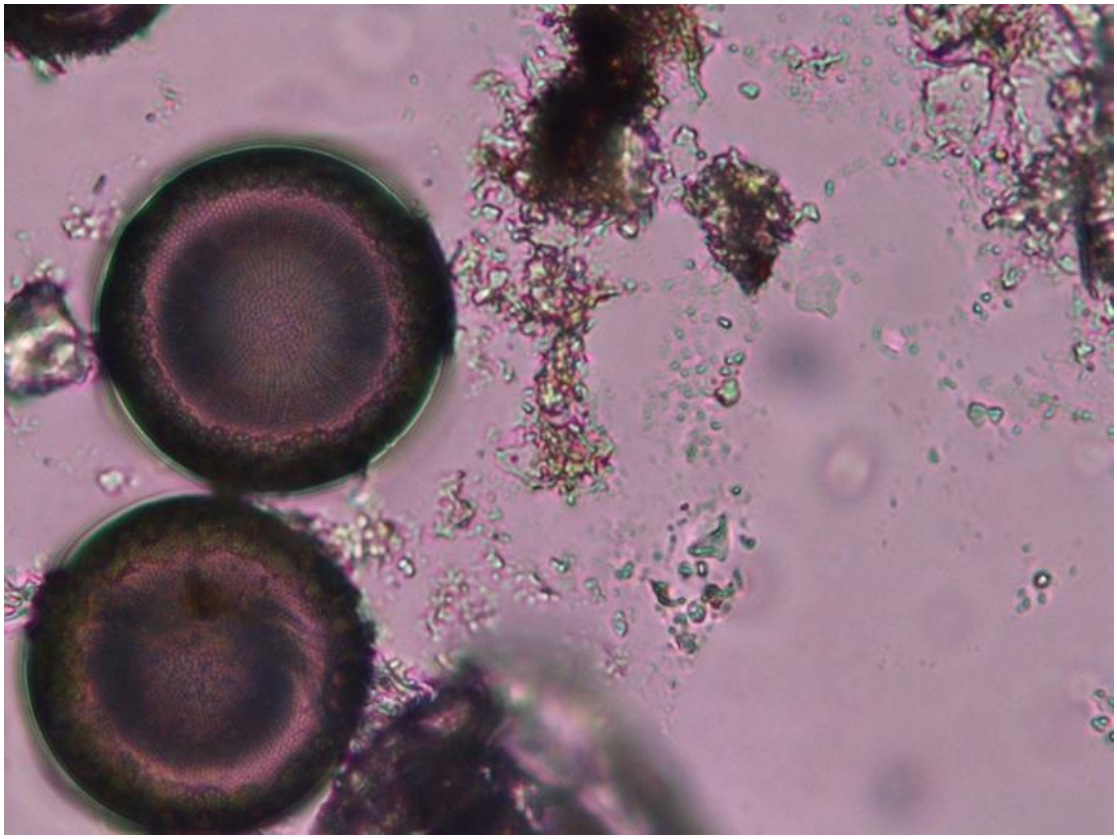

Figure 3.2 an image of diatoms (In the Stephanodiscus genus) at x400 magnification.

Pollen grains can also be readily mistaken due to their round shape, but surface features, including dimpling, spikes and cleavages, are observable and allow for its identification (Radja *et al.*, 2019). When examining fibres, the surface may appear to be covered in scales of varying shapes and sizes, these scales indicate the presence of hair. Hair could be either natural or anthropogenic, the former from animals in the environment and the latter from textile materials. Sheep, rabbit, alpaca and other animals' hair are regularly used in textiles (Kerkhoff *et al.*, 2009), but a large majority are dyed to colour the material. This dye is a useful indicator that it is a textile fibre rather than a naturally occurring hair fibre.

3.1.4.4 Cross-Sectional Shape

Synthetic fibres can be produced with different cross-sectional shapes (the shape when the fibre is observed in the transverse position); this feature is a useful indicator that the fibre is anthropogenic and also synthetic (Xu, Pourdeyhimi & Sobus, 1993), meaning it is a useful feature to look for when only looking for synthetic materials. Originally, synthetic fibres were produced by extruding a liquid polymer through a spinneret hole. This would create a fibre with a cylindrical cross-sectional shape (Taylor, 1990). However, non-cylindrical cross-sectional shapes are being produced more commonly through changes in the spinneret conditions and altering the shape of the spinneret holes (Holme, 1999). For instance, acrylic fibres can be either wet spun or dry spun but depending on the method used the cross-sectional shape will be different (Craig, Knudsen & Holland, 1962 & Holme, 1999). In the manufacture of melt-spun fibres such as nylon, polyester, and polypropylene the cross-sectional shape is changed by altering the shape of the spinneret holes to create shapes including bilobal, trilobal and delta (Hufenus *et al.*, 2020), fibres with these cross-sectional shapes are easily differentiated from natural fibres as they do not occur naturally, see table 3.1 for examples of cross-sectional shapes.

Natural anthropogenic fibres can also have distinctive cross-sectional shapes that can aid in identification. For example, cotton fibres have longitudinal twists giving it a ribbon shape, while ribbon shape synthetic fibres do exist, other features including a non-uniform thickness along the length and a collapsed lumen identify the fibre as being cotton (Tedesco & Browne, 2021).

3.1.4.5 Optical Properties

All synthetic fibres, with the exception of glass fibres and Vinyon HH (Johri, 1979), are anisotropic, meaning that they possess two refractive indices. The two refractive indices are at 90° to each other; the difference between these two indices is the fibres birefringence value, which gives an indicative identification of the polymer type. The calculation of the birefringence (see Section 2.2.1.1) is helpful in the identification of anthropogenic natural fibres and synthetic fibres. Some natural materials, such as quartz, also have a birefringence value and exhibit interference colours, so this feature should be

used in combination with the previously discussed features to make an identification.

3.1.5 Aims and Objectives of the Study

The aim of the study is to investigate whether the addition of PLM to the search process is beneficial for the detection of anthropogenic materials in addition to stereomicroscopy.

The objectives of this study are as follows:

1) To build on the evaluation of the use of Easylift® from Chapter 2 during a field trial
2) To determine if there is a benefit to adding PLM to the process of searching for microplastics with stereomicroscopy, or as a standalone technique.
3) To investigate whether certain characteristics, e.g. colour, microplastic type or size, influence whether they are found with stereomicroscopy or PLM.

3.2 Method

3.2.1 Sample Collection

Between 25/06/2019 and 12/07/19, the Rozalia project ran an expedition to investigate microplastic pollution in the Hudson River Entitled “The Hudson River Mountains to the Sea, Seafloor to the Sky Microplastic Sampling and Technology Expedition”. This expedition was funded by the National Geographic Society, Kilroy Realty Corporation and Schmidt Marine Technology Partners. The expedition conducted a range of different studies and collected a total of 447 samples: 227 water, 163 air and 57 soil samples. Samples were taken from the headwaters of the Hudson River, Lake Tear of the Clouds (44.17°N, −73.96°W) to Ambrose Light (40.74°N, −73.96°W), where the Hudson River meets the Atlantic Ocean. In the main Hudson River study, the whole of the river (315 miles) was sampled every three miles; samples were taken aboard the American Promise, white water rafting, by dingy and taken from the shore see Figure 3.3 to see the location of each sample site. The Hudson River was investigated in this study as it was building on research by the Rozalia project 3 years prior (Miller *et al.*, 2017),

where the same sample sites were used, but only surface water samples were taken allowing for some temporal comparisons to be made. The project aimed at creating a 4D heatmap of the Hudson River by sampling the full water and air column. The river also encompasses a variety of different environments and population types producing more representative samples that can be used to train an automated method of detecting microplastics, see Chapter 4 for more information.

Figure 3.3 A map to show sample locations along the Hudson River colour-coded by collection platform: American Promise (red), dinghy (black), shoreline (blue), and white-water raft (purple), produced by Brooke Winslow.

During the expedition, a separate study into the microplastic pollution surrounding wastewater treatment plants (WWTP) was completed, in this study, three WWTP's were investigated: Hudson River WWTP, Yonkers WWTP and East River WWTP; the location of each can be seen in Figure

3.4. Each WWTP was sampled in 27 locations: every half mile from 2 miles north to 2 miles south.

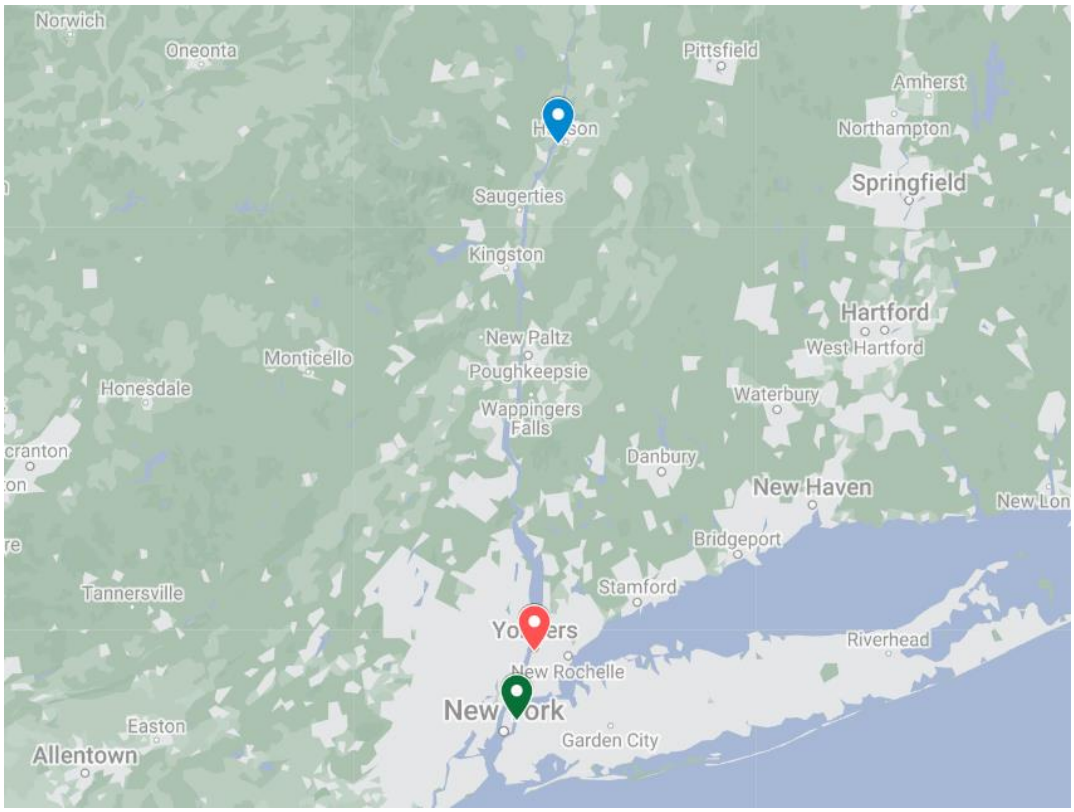

Figure 3.4 A Map to show the locations of the three wastewater treatment plants investigated: Hudson (blue), Yonkers (Red) and East River (Green).

3.2.1.1 Water Samples

In the Hudson study 227, 1 litre water samples were taken: 107 surface water samples, 58 samples from the middle of the water column and 62 samples from 1 meter off the riverbed.

In the WWTP study 27, 1 litre water samples were taken during this study at three wastewater treatment plants: Hudson River WWTP, East River WWTP and Yonkers WWTP, with 81 samples total. For each WWTP Surface, middle and bottom water samples were taken every half mile from 2 miles north of the WWTP to 2 miles South of the WWTP.

The surface samples were obtained using a galvanized steel bucket (size = 4.73 L) attached to a polypropylene rope that was thrown off the side of the boat to collect a sample of the surface water. This water was then used to triple rinse a clean 1 litre glass jar to avoid potential contamination. The jar was then filled, and the lid secured, until the sample was filtered.

Samples taken from the middle and bottom of the water column were collected using a 5 L General Oceanics Niskin bottle with a 4.39 mm aperture opening. A 4.54 kg weight was attached to the bottom of the Niskin bottle to ensure that the Niskin bottle remained vertical. The Niskin bottle was supported by a polypropylene safety line and lowered into the water by the side of the boat. Once the correct depth had been reached, either the mid-point in the water column or 1 meter from the bottom, the messenger was released to trigger the closure of the Niskin bottle. The Niskin bottle was then raised back onto the boat ensuring that it remained upright. Once aboard a 1 litre glass jar was triple rinsed with the water collected by the Niskin bottle and then filled to the top and sealed until filtration.

Filtration of the samples was undertaken in the galley on the boat. During filtration, contamination was prevented using the protocols outlined in Miller & Gwinnett (2021) including turning off all fans and reducing the number of crew allowed in the sample processing area. The water samples were filtered under vacuum using a portable vacuum pump, with a ceramic Buchner filter and Whatman number 3 cellulose filter paper (Whatman catalogue number 1003 070, pore size of 6 µm). Once all the samples had gone through filtration the glass jar was rinsed with triple distilled water which was also filtered. Once filtration was complete, the filter, whilst still damp, was tape lifted with an Easylift® tape. See section 2.2 for more information on Easylift® and Figure 2.11 for a diagram of how the Easylift® was used to retrieve microplastics from the surface of the filter paper. One piece of Easylift® was used per filter paper. The Buchner funnel was also tape lifted near the seams, where microplastics could have been trapped and not collected by the filter paper. Once tape lifted the Easylift® tape was adhered to a glass microscope slide and labelled with an indelible pen on one of Easylift® tapes' two blue tabs. The filter paper would then be observed at x30 on a stereomicroscope to see if any potential microplastics had not been retrieved, if a potential microplastic was located it was retrieved with jewellers' tweezers and a small corner of the Easylift® tape would be pulled up so that it could be sealed within the tape lift.

3.2.1.2 Air Samples

During the expedition 163 air samples;108 low and 54 high air samples were taken during this study. The air samples were taken using a Leland legacy air filter pump set at 8 litres/hour left for thirty minutes to filter the particulates onto a 70 mm 0.7 µm pore size Whatman glass filter GF/A (Catalogue number 1820 070). The low water samples were taken from 15 m above the water's surface, and the high air samples were taken from 9 m above the water's surface. Once sampling was complete the filter was placed in a metal container to transport it to the sample processing area. The filter was extracted from the metal container with metal jewellers' tweezers and placed on a ceramic plate with a drop of triple distilled water on it to moisten the filter paper whilst ensuring any potential contamination from the water would not be present on the surface of the filter paper. Whilst the filter was still damp, it was tape lifted with an Easylift® tape. See Figure 2.11 for a diagram of how the Easylift® was used to retrieve microplastics from the surface of the filter paper. One piece of Easylift® was used per filter paper. Once tape lifted Easylift® was adhered to a glass microscope slide and labelled with an indelible pen on one of Easylift® tapes' two blue tabs. The filter paper would then be observed at x30 on a stereomicroscope to see if any potential microplastics had not been retrieved, if a potential microplastic was located it was retrieved with jewellers' tweezers and a small corner of the Easylift® tape would be pulled up so that it could be sealed within the tape lift.

3.2.2 Analysis

For all samples taken from the Hudson River in conjunction with the Rozalia project 2019 expedition, a two-stage examination procedure was implemented. The first stage of examination involved observing each sample mounted with Easylift® on a glass microscope slide with a Nikon Stereomicroscope at x30 magnification; the entire surface of the slide is searched systematically 1 cm x1 cm square at a time. Any materials of anthropogenic origin, including textile fibres, fragments and microbeads, were marked with an indelible pen on the surface of the Easylift® tape so that it could be relocated and further analysed. The stereomicroscope was also chosen for the first stage of analysis as it is often used in microplastic

research to find and classify microplastics (Barrows et al., 2017., Dris et al., 2016. & Prata et al., 2020a).

After stereomicroscopy, the samples underwent another level of searching using a Microtec Polarised light microscope (PLM) firstly the locations marked during stereomicroscopy were observed to determine if they were potentially of anthropogenic origin (see section 3.1.4. for information on how the particulates were identified). If the particulate was determined to be anthropogenic then its features would be characterised and recorded in a spreadsheet, the particulate would then be circled and numbered on the slide. If it was determined to not be anthropogenic then no further analysis took place. The entire slide was then searched at x40 under crossed polars; this allows any interference colours to be observed, making plastic materials more visible; see Section 2.2.1.1 and Section 3.1.4.4 for more information about polarised light microscopy. The slide was then searched again under plane polarised light at x100 to search for smaller microplastics that may be missed. Any materials of interest found during these stages would undergo characterisation with the PLM, including noting its; colour, type (e.g., fibre or fragment), cross-sectional shape, presence of inclusions such as delusterant, width, length where applicable, sign of elongation and birefringence to give an indication of polymer type. Each item of interest had been observed it was then imaged with the Nikon DS-L3 camera attachment, to create a training data set to produce an automated method of detecting microplastics (See Section 1.7, 4.1.6 and 4.1.7 for more information). Each item of interest was imaged at x40, x100, x200 and x400 under plane polarised light multiple images of each item were taken at different orientations and if the item displayed birefringence it was imaged under crossed polars at x400 magnification. Images of the background of the slide were also taken at varying magnifications, and images of items such as diatoms and natural materials were taken to ensure that there was a wide variety of materials represented in the training data used in Chapter 4.

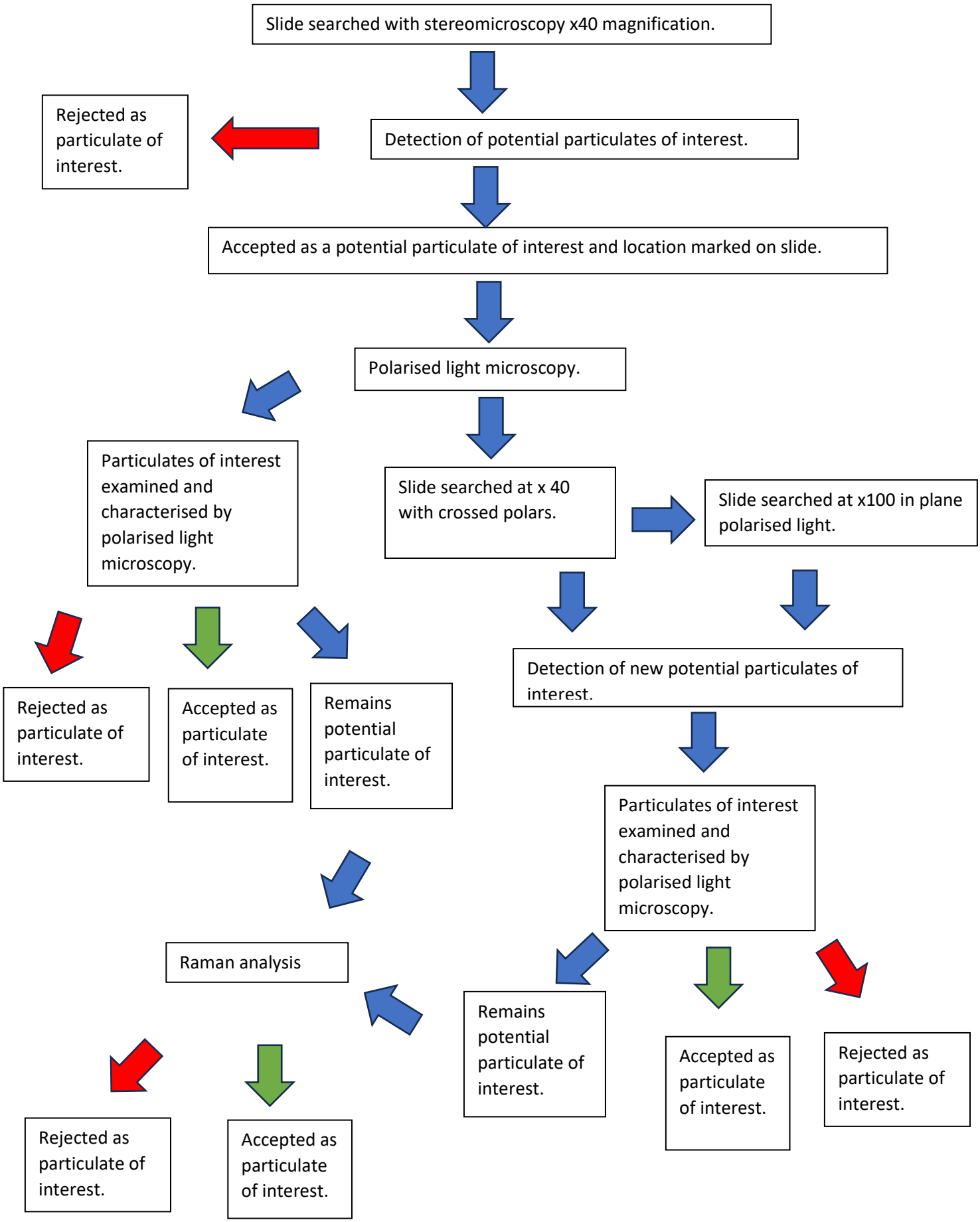

Figure 3.5 A flow diagram to demonstrate how the slides were searched after extraction with Easylift®.

For those samples where it was not possible to obtain a polymer identification using the PLM, and for a sub-selection of samples (54 sample slides), all items identified as being synthetic underwent Raman analysis using a Renishaw inViva Raman Microscope with a Leica microscope to confirm polymer type. Using a ×20 objective lens for simultaneous illumination and data collection. An excitation wavelength of 514 nm was used, laser intensity ranged from 1-50 mW, and the integration time used ranged from 5-10 seconds. The resulting spectra were then compared to a collection of known Polymer spectra generated using the Microtrace Forensic Fibre Reference collection to identify the polymer type. See Figure 3.5 for a flow diagram to demonstrate the search process used in this study.

Once all analysis was complete, each microplastic was compared to the controls taken. Easylift® was used to create ambient controls to assess potential contamination to the samples by affixing them sticky side up to surfaces in the laboratory station. Reference control samples were taken during the expedition, including the crew's clothing and any ropes present on the boat, to identify and eliminate potential contamination. These samples were taken by either collecting a sample of fibres from the garments and cutting a piece of the rope off and packaging them into a paper wrap to be mounted in DEPEX after the expedition has finished. Another approach used was that the garment was tape lifted with Easylift® and adhered to a glass microscope slide for analysis. These samples included the ‘white main lines’ of the boat, ‘blue rope’ from the air sampler, ‘yellow and black safety line’ for the Niskin bottle and air support’, the ‘Niskin puller line’, ‘gally line controls’, ‘orange and silver bucket line’, ‘Bounty paper towel’, ‘yellow cotton t-shirt’, ‘denim 71% cotton 29% polyester shorts’, ‘nylon bird print shorts’, ‘blue and black ‘Everlast’ shoes’, ‘grey and khaki pants 91% nylon 3% elastin’, ‘blue face buff polyester’, ‘black sandals’, ‘grey and black gloves polyester’, ‘blue cotton expedition t-shirt’, ‘pink shoes’, ‘black shoes’, ‘yellow bandana cotton’, ‘red and blue bandana’, ‘grey shorts’, ‘blue polyester 1’, ‘blue polyester 2’, ‘grey shorts polyester and spandex’, ‘denim shorts’, ‘green silk shorts’, ‘ Patagonia trousers polyester’, ‘blue sun shirt’, ‘beige shorts’, ‘blue shorts polyester cotton and elastane’, ‘grey shorts polyester’, ‘87% polyester top’,

‘black fleece’, ‘blue Patagonia fleece’, ‘blue skort’, ‘pink skort’, ‘blue polyester shorts’, ‘billabong inner fabric’, ‘billabong seam and fabric’, ‘dark blue expedition t-shirt polycotton blend’, ‘white American magic shirt’, ‘red jacket 100% Nylon’, ‘ black Patagonia buff vest 100% polyester’, ‘pink leggings 90% nylon 10% spandex’, ‘navy jacket polyester’, ‘blue leggings 82% polyamide 18% elastin’, ‘bright blue Rozalia shirt polycotton blend’, ‘navy blue Rozalia fleece 100% polyester’, ‘grey shorts pink trim 100% polyester’, ‘grey Rozalia shirt polycotton blend’, ‘floral shorts cotton’, ‘blue & green trek pants 63% polyamide 26% polyester 11% elastin’ and ‘red shorts 100% cotton’.

The research design was completed by Rachael Miller at the Rozalia project with method development fed in from Claire Gwinnett at the University of Staffordshire informed from the findings of Chapter 2. During sampling, all crew were responsible for aiding the collection of samples from the river. The 3 members of the crew from the University of Staffordshire also filtered the water samples and tape lifted both water and air samples in the galley of the boat and searched the slides using stereomicroscopy. Analysis of all sample slides by polarised light microscopy and Raman spectroscopy was completed at the University of Staffordshire by Amy Osborne.

3.3 Results and Discussion

3.3.1 Field Trial of Easylift®

This was the first time Easylift® had been used in the field as a method of retrieving and storing microplastic samples from the filter papers, and so is a valuable indicator as to how successful its use would be in large scale microplastic field studies. In this study the water samples were filtered in the boats’ galley and then immediately tape lifted with Easylift® to retrieve and preserve the sample.

This section will discuss and evaluate the performance of Easylift® during the 2019 Rozalia project field trial.

3.3.1.1 Retrieval

From the findings of Gwinnett, Osborne & Jackson (2021) (See Chapter 2) Easylift® was found to have a retrieval rate of 98.54% when retrieving microfibres from a cellulose filter paper when a Buchner funnel was used, so it could be expected that the recovery rate should be at a similar level in the field trial. Once a filter paper had been tape lifted with Easylift®, the filter paper would then be searched at x30 magnification with the stereomicroscope to look for any potential anthropogenic materials that may not have been collected by the tape lift. If any such material was found remaining on the filter paper, they were collected with jeweller tweezers and the corner of the Easylift® tape was lifted, and the material was deposited underneath it, and the tape lift was stuck back down onto the microscope slide. Over all the samples taken on the course of the expedition, there were only a handful of occasions (an estimate of under 20 occasions) where something was found left on the filter paper. However, a precise number of instances is not able to be provided as it was not recorded at the time of the expedition. This would suggest that Easylift® was successful in its role of retrieving the majority of potential anthropogenic materials. It is possible that there were anthropogenic materials left on the filter paper that were not found during the search with the stereomicroscope. This is due to several factors as the filter only had a quick search with the stereomicroscope at a x30 magnification smaller particulates are less likely to be observed especially as the filter paper does not provide the best background for successfully observing potential microplastics as it is not transparent (Sun *et al.*, 2019). The presence of debris on the filter paper is also likely to be a factor in whether any remaining particulates are observed, as it can mask and obscure them from sight. The filter paper was also not exhaustively searched due to time constraints while aboard the research vessel. Easylift® was successful in retrieving the particulates from the filter papers, but the level of particulates that may have remained on the filter paper is likely to be underestimated. While the laboratory study results in Chapter 2 demonstrate that Easylift® can achieve a retrieval rate of 98.54%, this study was done using clean water samples, meaning that there would be no debris on the

filter paper that could prevent any microplastics being collected, it would also mean that all the microplastics on the slide could be viewed unobscured allowing them to be quantified more easily. The laboratory study also used only fluorescent yellow fibres that were easily visible both under UV light and reflected light from the stereomicroscope, whereas the environmental samples contained various colours, sizes and shapes of microplastics, some of which may not be as visible and easy to identify as yellow fibres. Due to these factors the retrieval rate could be lower than the 98.54% reported in the laboratory trial. In the dataset, there was an underrepresentation of some microplastic types, namely microbeads and films; this could be because they were not present in the sample to be retrieved by Easylift®. It cannot be ruled out, however, that Easylift® may not have been successful in their retrieval, as microbeads and films have not been investigated in a laboratory trial in the same way that microfibres have been and their morphology and potential difference in size may impact their retrieval rate. After the filtering was complete, the filter funnel would also be tape lifted to collect any microplastics that may have become trapped between the filter paper and the funnel. When filtering the non-porous surface of the funnel, Easylift® would occasionally tear. The tape was still useable, but care would need to be taken when adhering the two halves onto the microscope slide. In order to prevent tearing this tape lifting should be done with care should be taken when using the tape lift on the hard curved surface of a filter funnel.

3.3.1.2 Debris

In Gwinnett, Osborne & Jackson (2021) clean water was used, meaning that this is the first time the effect of debris and biological materials found in natural aquatic environments on Easylift®'s ability to collect microplastics. In particularly debris-heavy samples, such as those taken from the bottom of the water column, the tape lift could become saturated with the debris; if too much was adhered to the tape lift, it can lose its tacticity, impairing Easylift®'s ability to seal onto the slide. If this happened it could cause the tape to peel of the microscope slide this leaves room for contamination of the sample to occur or loss of microplastics from the tape lift. To combat this effect, if there

was an excess of debris on the filter paper, then multiple strips of Easylift® were used to prevent this loss of tacticity.

3.3.1.3 Moisture

While discussed in Section 2.3.2.4.1, the effect of water content was not found to have a significant impact on the retrieval of microfibres, the moisture level of the filter paper was observed to affect the retrieval rate of background fibres with Easylift® in Gwinnett, Osborne & Jackson (2021) as seen in Figure 2.12. This effect was continued to be observed during the field trial. If the filter paper was not left under vacuum for an extra few seconds after the last traces of visible water passes through it would be too damp when tape lifting and potentially leave behind more microplastics. If the filter is too damp, the tape will also lose its tacticity, impairing Easylift®'s ability to seal onto the slide. As the air samples did not involve water, they were dry when it came to tape lift them. But as it was found that dry filter papers release more filter fibres than slightly damp ones. During the field trial, the filter paper would be slightly moistened by pipetting 1 ml of triple distilled water underneath the filter paper. By adding the water under the filter paper rather than on top, it prevented any potential contamination that may have been present in the triple distilled water.

3.3.1.4 Controls

During the field trial Easylift® was used to create ambient controls to assess potential contamination to the samples by affixing them sticky side up to surfaces in the laboratory station. Using Easylift® rather than a damp filter allowed for the presence of airborne cotton to be observed, which may have been obscured by a cellulose filter paper. Using Easylift® also meant that all contamination that adheres to the tape is permanently trapped on its surface. In contrast, the damp filter papers may not retain all contamination that lands on them, and all contamination may not be successfully retrieved from the surface of the filter.

3.3.1.5 Integrity and Storage

An advantage of using Easylift® in the field is that it allows for easy storage and preservation of samples. As the filters are tape lifted immediately after filtration, the potential for loss of microplastics and contamination of airborne microplastics is reduced. The microscope slides can then be securely stored in microscope slide boxes indefinitely, awaiting analysis, allowing for greater sample generation as time does not need to be spent on the analysis of samples during the field experiment. The samples taken in 2019 are still intact and maintain their integrity six years after their extraction. It is expected that they will retain their integrity for many years if stored in a microscope slide box out of direct sunlight. This could also allow for confirmation of results produced, as the samples can easily be sent to other laboratories for ratification of results or further analysis with further techniques that may not be available to the original laboratory. This could facilitate a laboratory network to enable microplastic studies to be conducted regardless of the infrastructure and equipment available at the sampling location. As infrastructure is often a limiting factor to microplastic research, the ability to collaborate between different laboratories is very important (Bakir *et al.*, 2024).

3.3.1.6 Analysis

The samples were analysed whilst still mounted to the slide with Easylift®. A first search was done with a stereomicroscope, followed by a second search using a Polarised light microscope. As Easylift® is effectively non-birefringent, it allows for the analysis of the samples under crossed polars within the same focal plane without the need to remove the sample from the tape lift. This allowed for the successful identification of birefringence for the majority of microfibres; the birefringence value was used to identify the polymer type. Introducing PLM into the searching and analysis process, allows for a quick and cost-effective polymer identification of fibres. This technique is not, however, useful for the polymer identification of fragments and films as the thickness is not possible to measure in the same way it can

be measured with fibres. Fragments, films and fibres that were unable to be identified with the PLM underwent further analysis with a confocal Raman microscope. The confocal Raman microscope is able to provide a polymer type in situ without the need to dissect the material out of the tape lift. The use of PLM allows for rich information about the microplastics to be observed, including colour, cross-sectional shape, delusterant and inclusions, sign of elongation and polymer type. All these features allow for more accurate elimination of crew clothing contamination rather than excluding all blue polyester, it can be narrowed down further to a blue polyester with delusterant and a similar width, meaning that there will be a more accurate estimation of the level of microplastic pollution, and information about potential sources of microplastic contamination can be achieved.

3.3.1.7 Recommendations

Easylift® was successfully used as a method of retrieving anthropogenic particulates from filter papers during this field trial. The samples were then successfully stored without degradation to the samples so they could be analysed after the field element of the expedition was finished. The ability to store the samples long-term also allows for the facilitation of multiple laboratories to analyse the samples and validate findings, which is not currently undertaken due to the risk of loss and contamination. There were, however, some challenges in its use for instance if the filter paper was tape lifted whilst it was still damp the tape may struggle to lift all the particulates from the surface of the filter paper. As such, there are some recommendations for the optimisation of the use of Easylift® in the field;

1. It is recommended that the sample is filtered under vacuum to remove excess water from the surface of the filter paper, whilst still leaving the filter sufficiently damp that it does not extract too many filter paper fibres. In instances where it is not possible to use vacuum filtration the filter paper should be left for a longer period of time to try and mitigate the effect of excess water on Easylift®'s tacticity.

2. For optimum extraction, the filter paper should be tape lifted while still slightly damp, 3-5 seconds after the last traces of water have passed through the filter paper when using a vacuum filter.
3. If an air sample is being collected dampen the filter paper with 1 ml of triple distilled water from behind.
4. Carefully tape lift the inside of the Buchner filter to collect any particulates that were trapped between the filter and the funnel.
5. If the filter paper contains a lot of background debris, then multiple tape lifts should be used.
6. When filtering, a cover should be placed over the Buchner funnel to prevent atmospheric contamination.
7. After tape lifting check the filter paper with a stereomicroscope to look for any particulates of interest that may not have been retrieved.
8. Store the tape lifts in a microscope slide box out of direct sunlight and high temperatures.
9. An upturned Easylift can be affixed to a surface to collect atmospheric controls during filtration.

3.3.2 The use of PLM as a Method of Detection

Table 3.2 A table to show the comparisons between stereomicroscopy and polarised light microscopy.

	Stereomicroscopy	Polarised light microscopy
Maximum magnification	x160	x1000
Average magnification	x20-100	x400
Light setting options	-Reflected light -Transmitted light -Bulb brightness	-Transmitted light -Plane polarised light -Polarised light -Condenser settings -Bulb brightness -Iris settings -Köhler illumination
Approximate cost of equipment (£)	500-2500	1000-8000
Required accessories		- Quartz wedge - 530nm first order red tint plate - Stage micrometre - Eye piece scale

Optional accessories	-Camera - Software to measure items	-Rotating stage -XY stage -Tilting compensator -Camera
Average time per slide (experienced examiner)	10 minutes	30-60 minutes
Observable features	-Colour -Microplastic type -Approximate width and length	-Colour -Microplastic type -Width and length -Cross-sectional shape -Presence of delusterant and other inclusions -Sign of elongation -Birefringence -Polymer type -Indication if it is natural or synthetic.

The use of PLM has several benefits over using standard stereomicroscopy, firstly, as shown in Table 3.2, being that the PLM offers a greater level of magnification and control over the lighting conditions that are illuminating the sample (McCrone, 1994) for instance, the PLM allows the sample to be observed under Köhler illumination and has a greater level of control over the amount of light the sample is being exposed to. These features allow the enhanced ability to observe the anthropogenic particulates by increasing or decreasing the contrast, these features also allow for greater detail about the particulate of interest to be observed, such as cross-sectional shape, presence of delusterant or the presence of surface scales which all help to gain an accurate identification of the particulate of interest and whether it is from an anthropogenic source or not. Another benefit of the PLM is the ability to observe the particulates in both plane polarised light and under crossed polars. The ability to observe the particulates under crossed polars allows the interference colours of any birefringent particulates to become visible (Stoeffler, 1996). An example of a fibre under plane polarised light and under crossed polars can be seen in Figure 3.6. The ability to see the fibres against a black background with the interference colours visible allows for increased contrast, which helps to detect anthropogenic materials that exhibit birefringence, especially colourless particulates that may be easily missed

without appropriate contrast being provided. As nearly all particles will exhibit birefringence the use of PLM is a valuable addition as a technique to detect anthropogenic particulates.

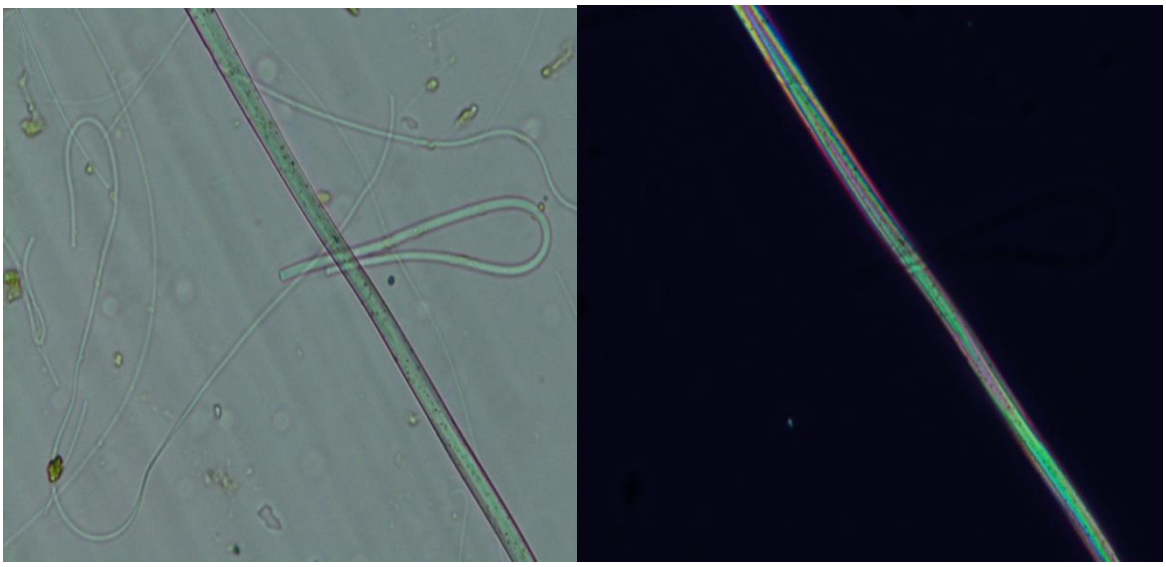

Figure 3.6 a colourless microfibre mounted with Easylift® under plane polarised light (left) and the same fibre under crossed polars x400.

In addition to being able to observe the optical properties of a particulate, it is possible to calculate its birefringence value, which can be used to provide a preliminary polymer identification (Reffner, Kammrath & Kaplan., 2020). Based upon these advantages, it can be expected that the use of stereomicroscopy followed by the use of PLM is likely to result in the detection of further anthropogenic particulates that were not detected by the initial search with the stereomicroscope. Further to this, the expectation is that there will be a difference in the ability to detect colourless particulates between the two methods. In this study over the 244 sample slides analysed, stereomicroscopy identified 1331 particulates in the first stage search, and PLM found an additional 549 in the second stage search. Of the subsection of samples where all suspected synthetic materials underwent analysis with Raman microscopy, only one particulate was found to have an incorrect polymer identification as PLM identified it as polyester and Raman indicated it was Nylon. This is likely as the microfibre was dark blue and thin, making determining its optical path difference more complicated, making it likely that it was an order out. No particulates identified as synthetic by PLM were found to not be synthetic after Raman analysis was conducted. A large

number of particulates, however, were not able to gain an identification by Raman analysis, either due to their colour or the presence of a biofilm, meaning the rate of misidentification by PLM could be higher.

Figure 3.7 shows the amount of each colour detected using the stereomicroscope and the polarised light microscope, respectively, and Figure 3.8 shows the percentage proportion of each colour detected using the stereomicroscope and the polarised light microscope, respectively. Colourless microplastics make up a significant portion of those detected using PLM (67%) compared to stereomicroscopy (21%). The number of colourless microplastics found with the stereomicroscope found in this study is consistent with those found in literature; Wang *et al*. (2017) found a concentration of 24.7% of colourless microplastics found in the Hanjiang River and Yangtze River. This is likely because brighter colours are more easily detected compared to colourless particulates (Hartman *et al.*, 2019). These results would indicate that a large proportion of colourless microplastics are not being detected when stereomicroscopy is being used as the primary method of detection; this is particularly apparent in Figure 3.6 where the number of colourless particulates found with the PLM is higher than those found with the stereomicroscope.

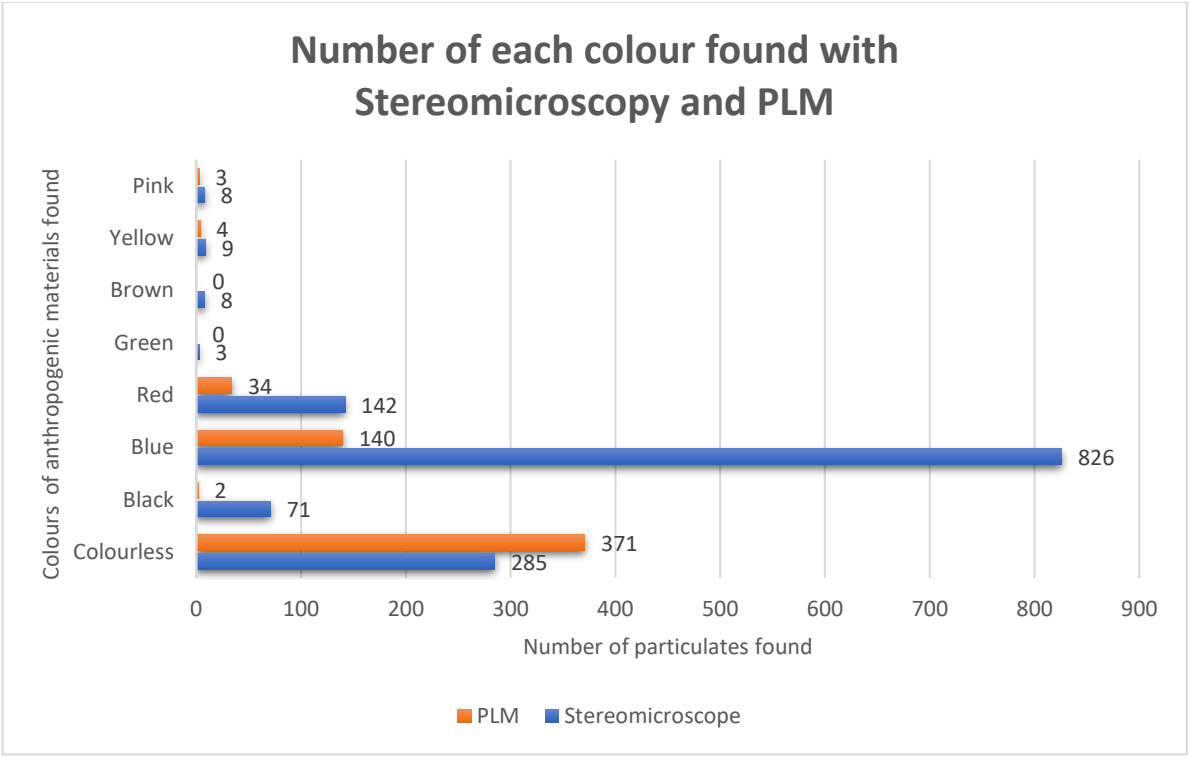

Figure 3.7 A Bar chart to show the number of each colour found with stereomicroscopy and PLM.

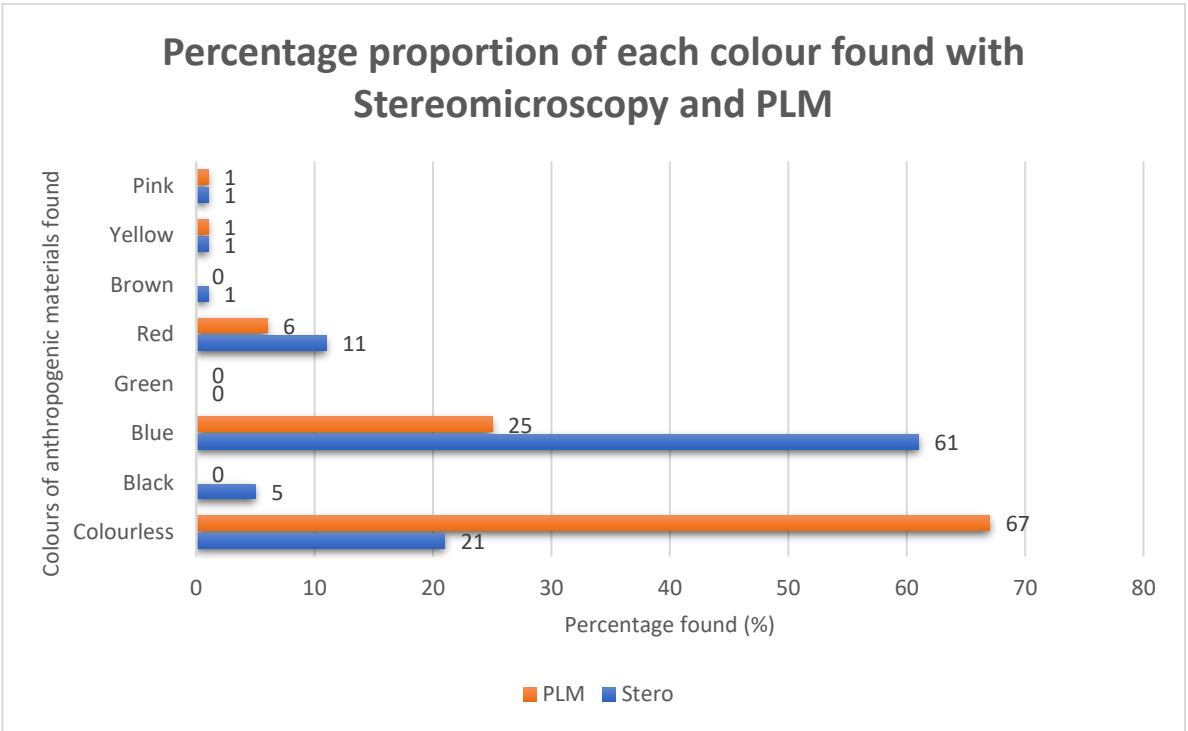

Figure 3.8 A bar chart to show the percentage proportion of colours found with the stereomicroscope and PLM.

This could be due to several factors, including lighting, magnification, the inability to observe interference colours on the stereomicroscope, and the

contrast to the background. As the stereomicroscope only has limited lighting settings, as seen in Table 3.2, it may not be possible to adjust the settings so that appropriate contrast is produced to adequately detect colourless microplastics from the colourless background. This is one aspect that the use of a PLM is beneficial as it is possible to adjust the amount of light illuminating the sample to a greater degree than the stereomicroscope. In addition to this, the PLM's ability to observe the sample under crossed polars making the interference colours of any microplastics present observable (McCrone, 1994) would further allow for the detection of microplastics that may not be easily observed with the stereomicroscope, see Figure 2.2 to see an example of a colourless fibre under plane polarised light and under crossed polars. These results do not account for the size or the type of microplastic being observed so it is possible that there are more confounding factors as to why some microplastics were not detected using the stereomicroscope. It is also possible that it was not the use of the PLM that was solely responsible for the detection of these missed microplastics but rather the action of a second search that located these microplastics and that many of them may have been detected in a secondary search of the slide with the stereomicroscope. However, it is likely that the colour of the microplastic is indeed playing a role in whether it was detected with the stereomicroscope and that the use of PLM may be an appropriate method to locate microplastics due to its increased ability to observe colourless microplastics. These samples also encompass both water and air samples so there could be a difference in the colours detected in the water samples opposed to the air samples due to a difference in background materials between these two sample types.

Figure 3.9 shows two pie charts that display the number of each microplastic type found with either stereomicroscopy. From these graphs, it is apparent that the distribution between the two categories appears very even, with fibres accounting for 86% and 90% and fragments accounting for 14% and 10% in the stereomicroscope and PLM categories, respectively. This indicates that the microplastic shape has no effect on the likelihood of it being found with either the stereomicroscope or the PLM, but rather it is the

combination of other feature such as colour or size that may determine how likely it is to be detected. However, there is an overrepresentation of microfibres and fragments in the data, with only one microbead and film found in each category, so it is possible that there could be an observable difference in the types of microplastics being detected in one method over the other if they were more represented in the data set.

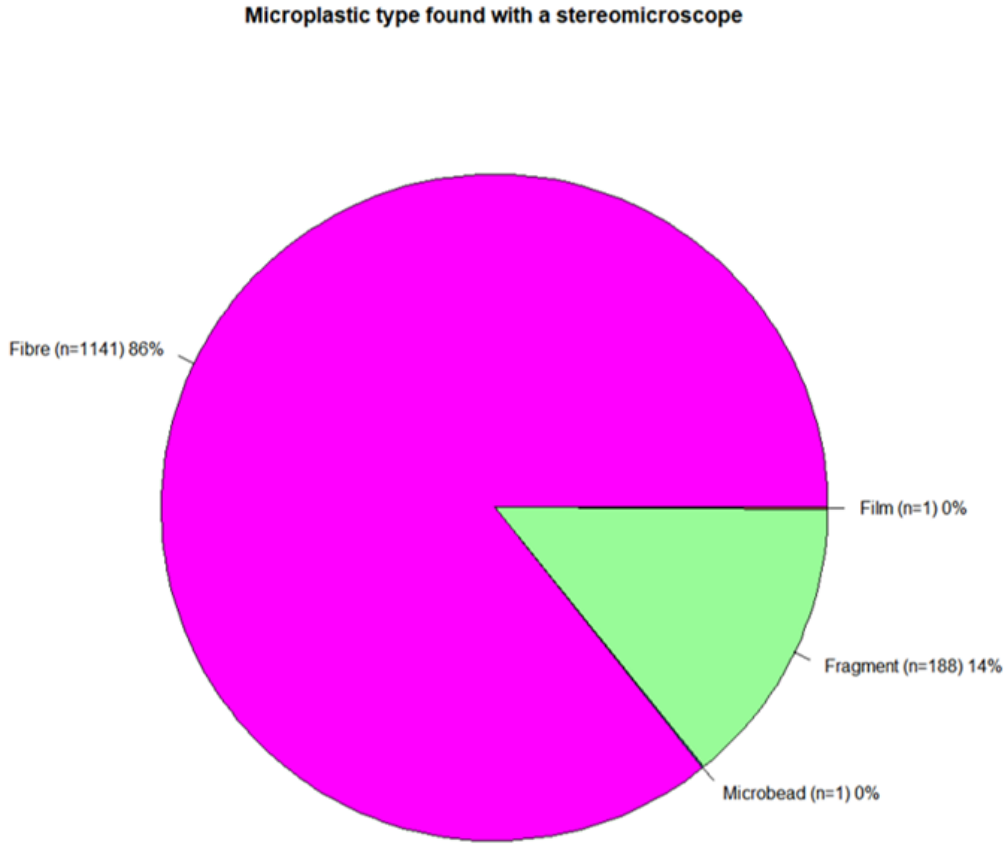

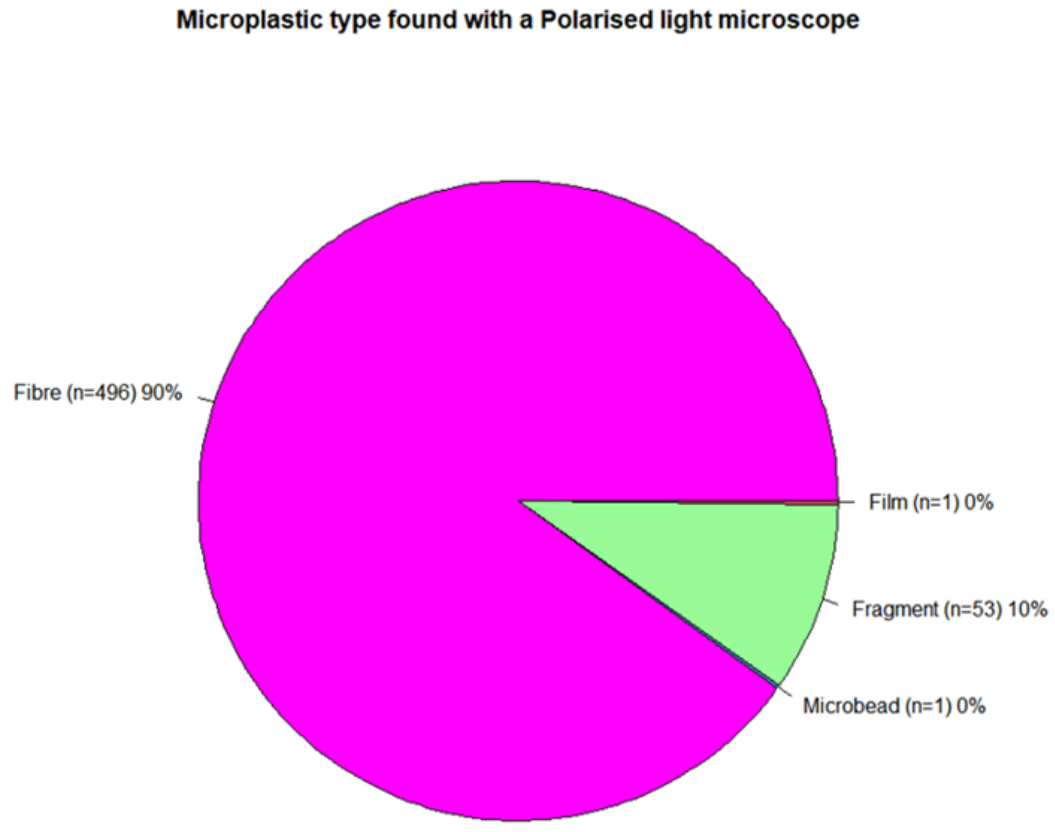

Figure 3.9 Pie charts to show the number of each microplastic type found with either the Stereomicroscope or the PLM.

Figure 3.10 demonstrates a boxplot displaying the ranges of widths µm found with either the stereomicroscope or the PLM. From this graph, it is evident that there is no substantial difference between the two categories; there are, however, more large outliers in the stereomicroscope category. Width is also not the longest measurement for the microplastics and so not the best indicator of whether the size of the microplastic is a factor in whether it is located with the stereomicroscope in the first search or PLM in the second. The length of the microplastic would be the best measurement to take to investigate this; however, in this study, it was not possible to take a length measurement for each microplastic in the same way that the width was taken. This is because when measuring the fibres, they could turn back on themselves and knot, making it impossible to gain an accurate measurement. This means that the length measurements recorded in this study would have a skew towards the smaller length microplastics, and so would not provide an accurate insight into the role length has on the ability to detect a microplastic. However, it is to be expected that smaller microplastics are going to be more easily located when a higher magnification is used.

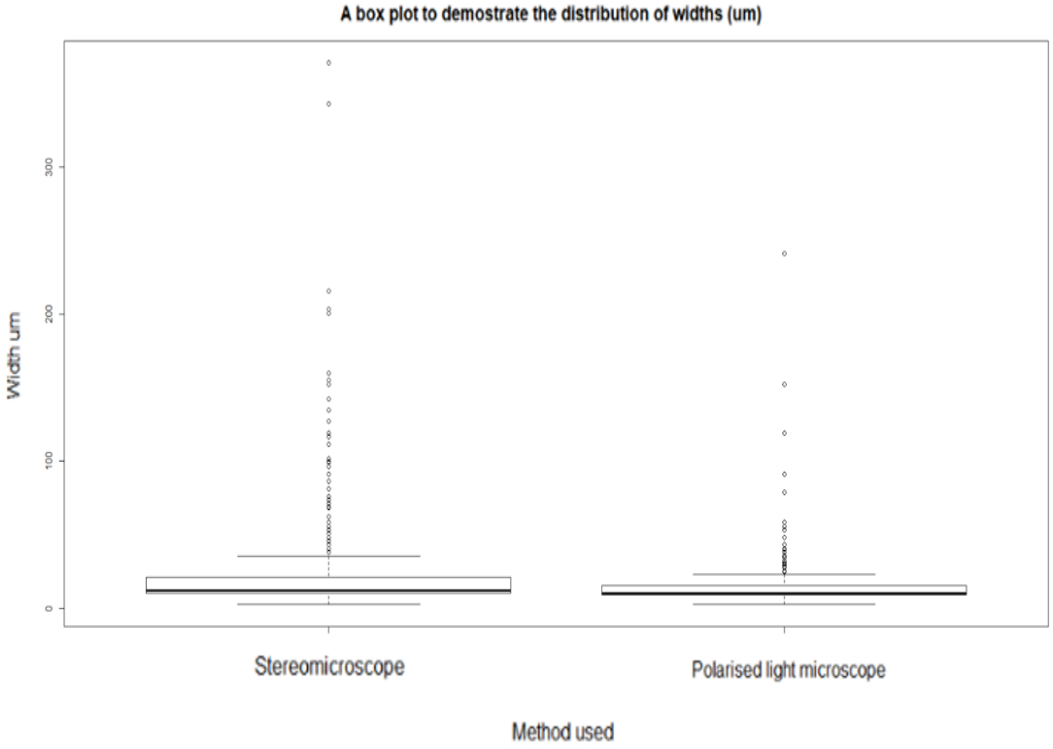

Figure 3.10 A boxplot to show the distribution of widths µm found with either the Stereomicroscope or the PLM

A logistic regression was undertaken to determine if characteristics of the anthropogenic materials can be used to determine the likelihood of being located with a stereomicroscope, the results can be seen in Table 3.3. From the results, colour seems to be the biggest predictor of whether or not it would be detected by stereomicroscopy. With colourless being the biggest predictor as it has a value of β estimate of -4.03724, meaning the stereomicroscope is less likely to detect it, it also has a p-value (8.88×10^{-8}) under 0.05 meaning that these results are significant and being colourless is a good predictor of whether stereomicroscopy will locate the particulate. Some of the other colours looked at includes purple, green and grey. The p-values for each of these categories are all >0.05 meaning that there is not a significant relationship between these colours and their use as predictors as to if they will be detected by stereomicroscopy or not, although this could be because they have a relatively small sample population which could explain the non-significant results. Blue, orange, pink and red have a p-value <0.05 meaning they are significant predictors of whether they will be detected by stereomicroscopy. Microplastic type is not a good predictor of whether it will

be detected by stereomicroscopy as all p-values are >0.05, meaning that there is not a significant relationship between microplastic type and which method detects them, which is backed up by the findings in Table 3.3. The cross-sectional shape does not appear to be a good predictor of stereomicroscopes ability to detect a particulate as all the β estimates are small, and the p-values do not indicate a significant relationship between cross-sectional shape and whether it was detected using stereomicroscopy or PLM. The presence of delusterant is also not a useful predictor, although there is a small difference between low to no delusterant and a medium level of delusterant that indicates the more delusterant present, the more likely it is to be found with the stereomicroscope, which would be expected as delusterant would make a microfibre more visible, however, this is not a statistically significant predictor of whether the level of delusterant will affect whether it is found with stereomicroscopy or not. The identification of the particulate also does not seem to be a useful predictor, polyvinyl chloride has a β estimate of -16.95 which means that stereomicroscopy would be unlikely to locate it, however, there is only one PVC particulate in this dataset and so this is not a reliable indicator. Hair is the only identification with a p-value <0.05 indicating a significant relationship it also has a positive β estimate, meaning that the identification being hair is a significant indicator that it is likely to be detected with stereomicroscopy, this could be because hairs on average have a large width and features like a medulla that make them easier to detect (Deedrick & Koch, 2004). The logistic regression carried out has a calculated McFadden's pseudo R^2 value of 0.1950978. A McFadden pseudo R2 value between 0.2-0.4 represents an excellent fit for the produced model (Zhou, Kuttal & Ahmed, 2018); as the calculated pseudo R2 value is close to 0.2, it can be interpreted as a good fitting model. A p-value for the R^2 of 0 was also calculated, which indicates that the calculated R^2 value is not due to chance. Figure 3.11 shows the results of a logistic regression to calculate the predicted probability of each particulate being detected with stereomicroscopy based on their characteristics including what sample type it was, sample location, microplastic shape, colour, cross-sectional shape, presence of delusterant and identification, plotted on a scatter plot. Most of the blue marks denoting stereomicroscopy are clustered

around 1, this indicates that the model has correctly predicted the probability of being detected with stereomicroscopy as high. In addition, most of the red marks denoting PLM are nearer to 0, indicating that the model correctly predicted that there was a low probability of being detected by stereomicroscopy and a higher chance of being detected by PLM. There are some points of uncertainty around 0.5, this means that the model was less confident at predicting the probability of these particulates being detected with stereomicroscopy, this could however, be because there may be particulates with overlapping characteristics and features. This graph shows that a large quantity of particulates that were given a low predicted probability of being detected were located using the PLM. This demonstrates that the stereomicroscope is consistently missing anthropogenic materials with certain characteristics mainly those that are colourless. But it is sufficient for locating a large majority of anthropogenic particles; 70.7% of the particulates in this study, this does, however, constitute 29.3% being missed if the stereomicroscope was used as the only method of searching. It also has not been investigated whether the PLM would be able to find all of the anthropogenic materials identified by the stereomicroscope if it had been used as the primary method of detection, this would be beneficial to investigate as it is possible that there are some characteristics that the PLM may have struggled to find if they had not already been identified by the stereomicroscope. It does, however, suggest that the particulates found with PLM were not found only due to a second search being undertaken but that PLM provides benefits that allow the detection of particulates that are easily missed by stereomicroscopy.

Table 3.3 A logistic regression was performed to investigate what factors affect which method the particulate was found with. Intercept = Found with Stereomicroscopy

```
Call:
glm(formula = Method ~ ., family = "binomial", data = data)

Deviance Residuals:
    Min       1Q   Median       3Q      Max
-2.7057  -1.0118   0.5443   0.6316   1.7293

Coefficients:
                                  Estimate Std. Error z value Pr(>|z|)
(Intercept)                        4.77139    1.28023   3.727 0.000194 ***
`MP type`Film                    -15.79318 1455.39833  -0.011 0.991342
`MP type`Fragment                 -0.95361    1.52054  -0.627 0.530562
`MP type`Microbead                -2.63011    2.01433  -1.306 0.191655
ColourBlue                        -1.79993    0.75728  -2.377 0.017461 *
ColourBrown                       11.02849  499.93049   0.022 0.982400
ColourColourless                  -4.03724    0.75488  -5.348 8.88e-08 ***
ColourGreen                       11.57467  807.01212   0.014 0.988557
ColourGrey                        11.78556  698.64304   0.017 0.986541
ColourMultiple                    12.25532  840.27452   0.015 0.988363
ColourOrange                      -3.39141    1.26258  -2.686 0.007229 **
ColourPink                        -3.34416    1.14047  -2.932 0.003365 **
ColourPurple                      11.66544 1019.28007   0.011 0.990869
ColourRed                         -2.13587    0.77791  -2.746 0.006039 **
ColourYellow                      -1.65311    1.32829  -1.245 0.213301
`cross sectional shape`Cylindrical -0.48864    0.58547  -0.835 0.403940
`cross sectional shape`Delta      -0.56067    0.67340  -0.833 0.405072
`cross sectional shape`Fragment    0.05429    1.61490   0.034 0.973183
`cross sectional shape`Irregular  -0.56765    0.65972  -0.860 0.389542
`cross sectional shape`Multilobal -0.37739    0.92518  -0.408 0.683342
`cross sectional shape`Ribbon     -0.34671    0.83538  -0.415 0.678122
`cross sectional shape`Square     -0.33051    1.43010  -0.231 0.817230
`cross sectional shape`Tape       -0.78078    1.10157  -0.709 0.478455
`cross sectional shape`Trilobal   -0.05296    1.46015  -0.036 0.971067
DelusterantLow                    -0.85769    0.75518  -1.136 0.256064
DelusterantMedium                  0.07768    0.82421   0.094 0.924915
DelusterantN/A                    -0.68424    0.74649  -0.917 0.359350
IdentificationAnthropogenic        1.68795    1.26459   1.335 0.181949
IdentificationCotton              -0.10598    0.84991  -0.125 0.900767
IdentificationHair                 1.32298    0.66889   1.978 0.047942 *
IdentificationNylon               -0.62918    0.64483  -0.976 0.329191
IdentificationPolyester            0.12174    0.59167   0.206 0.836984
IdentificationPolyethylene        -2.60599    1.69883  -1.534 0.125032
IdentificationPolyethylene/Nylon  -0.34786    1.07321  -0.324 0.745842
IdentificationPolypropylene        0.69350    0.70118   0.989 0.322645
IdentificationPolyvinyl Chloride -16.95397 1455.39767  -0.012 0.990706
IdentificationSynthetic            0.12291    0.63050   0.195 0.845437
IdentificationUNKN                -0.04566    0.87981  -0.052 0.958614
---
Signif. codes:  0 ‘***’ 0.001 ‘**’ 0.01 ‘*’ 0.05 ‘.’ 0.1 ‘ ’ 1

(Dispersion parameter for binomial family taken to be 1)

    Null deviance: 2275.1  on 1880  degrees of freedom
Residual deviance: 1831.2  on 1843  degrees of freedom
AIC: 1907.2

Number of Fisher Scoring iterations: 14
```

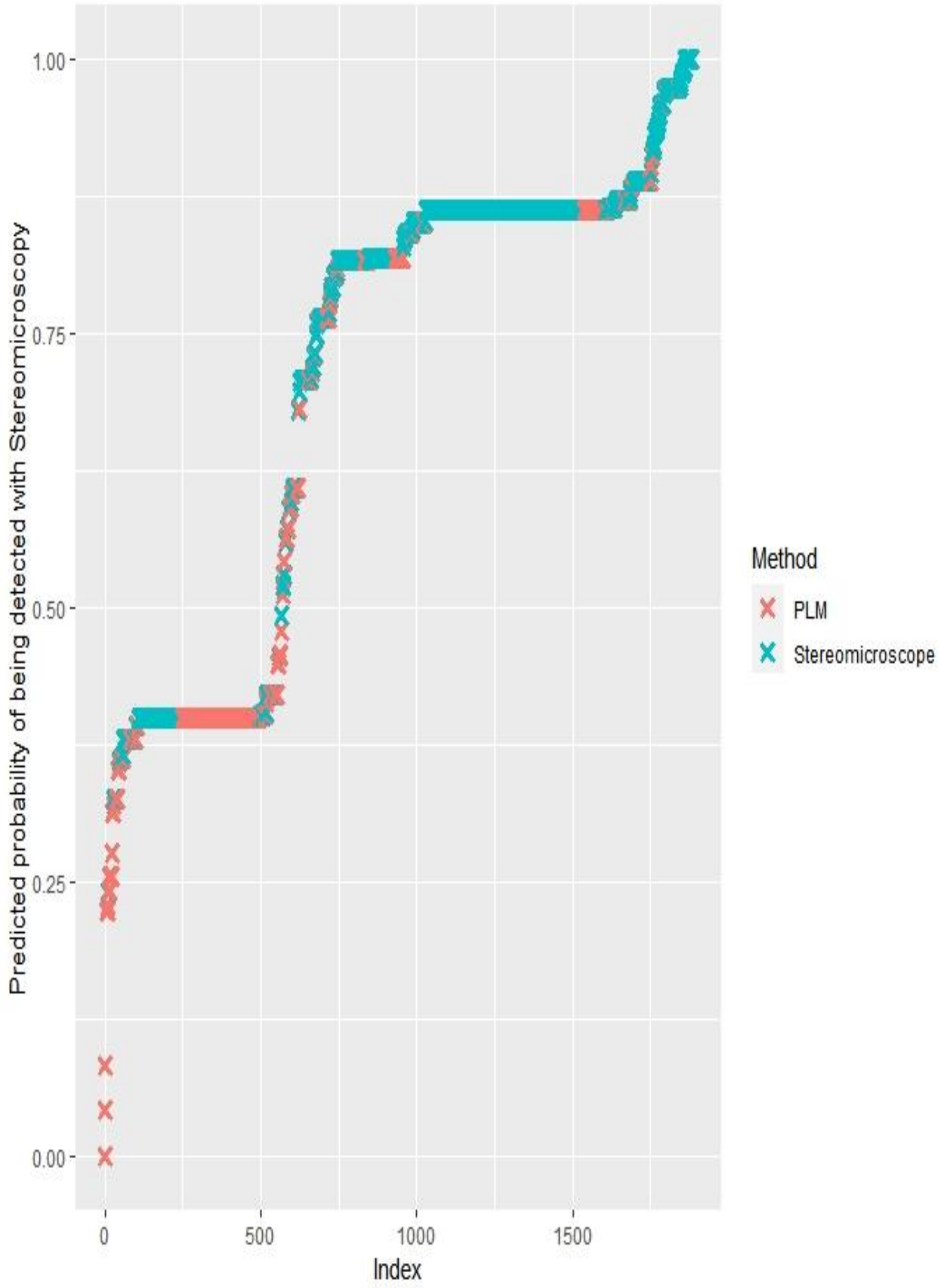

Figure 3.11 A logistic regression scatter plot to show the predicted probability of being detected with stereomicroscopy and which method was responsible for detecting it.

Another element that is important to examine when comparing the two methods is how many additional particulates were found in each sample slide. Figure 3.12 shows a scatter plot with the number of particulates found by stereomicroscopy plotted against the number of additional particulates found with PLM, and Figure 3.13 shows a Bland-Altman plot of the mean number of particulates found plotted against the difference between the two methods (the number of additional particulates found by PLM) for each sample slide. In figure 3.13 the positive mean difference (bias) line is above 0 this indicates that PLM consistently found more particulates than stereomicroscopy.

The darker the plot point, the more values fall at that data point. In most instances PLM found at least one additional particulate with the average being an additional 2.3 more particulates being found with the PLM after a search with stereomicroscopy. The most extreme difference observed is one particulate being found with stereomicroscopy and an additional 12 found with PLM, the majority of these additional particulates being colourless, which may indicate why certain samples will have a higher proportion of particulates found by PLM. The more particulates found by stereomicroscopy the less particulates are found with PLM, this could be due to the random distribution of particulates, or the ones found in these samples happen to have characteristics that are more easily discernible with the stereomicroscope. One possible explanation is the presence of contamination; if a sample slide had a high concentration of contamination from the blue cotton t-shirts worn during the expedition, then a higher proportion of the particulates are likely to be found with the stereomicroscope as the blue fibres are easy to locate with the stereomicroscope. The effect of which is explored in Figure 3.14 and Figure 3.15, which shows the percentage of contamination and blue particulates, respectively, against the total number of particulates found per slide. They both seem to demonstrate the same pattern: as the number of particulates increases, so does the level of contamination and particulates that were identified as being blue, as they both have a very similar mean of around 50% of particulates. Both graphs show a positive trend line although the presence of contamination has a stronger trend line ($R^2 = 0.5314$) than presence of blue ($R^2 = 0.3238$). This is

likely due to the inclusion of the air samples where fewer blue particulates were identified, and a large proportion was identified as contamination due to the ability to identify white cotton. However, the high number of contamination/ blue particulates per slide would indicate why the number of particulates found by PLM does not increase with the number of particulates on the slide, as the contamination tends to have characteristics that make it easy to find particulates with the stereomicroscope such as bright colours.

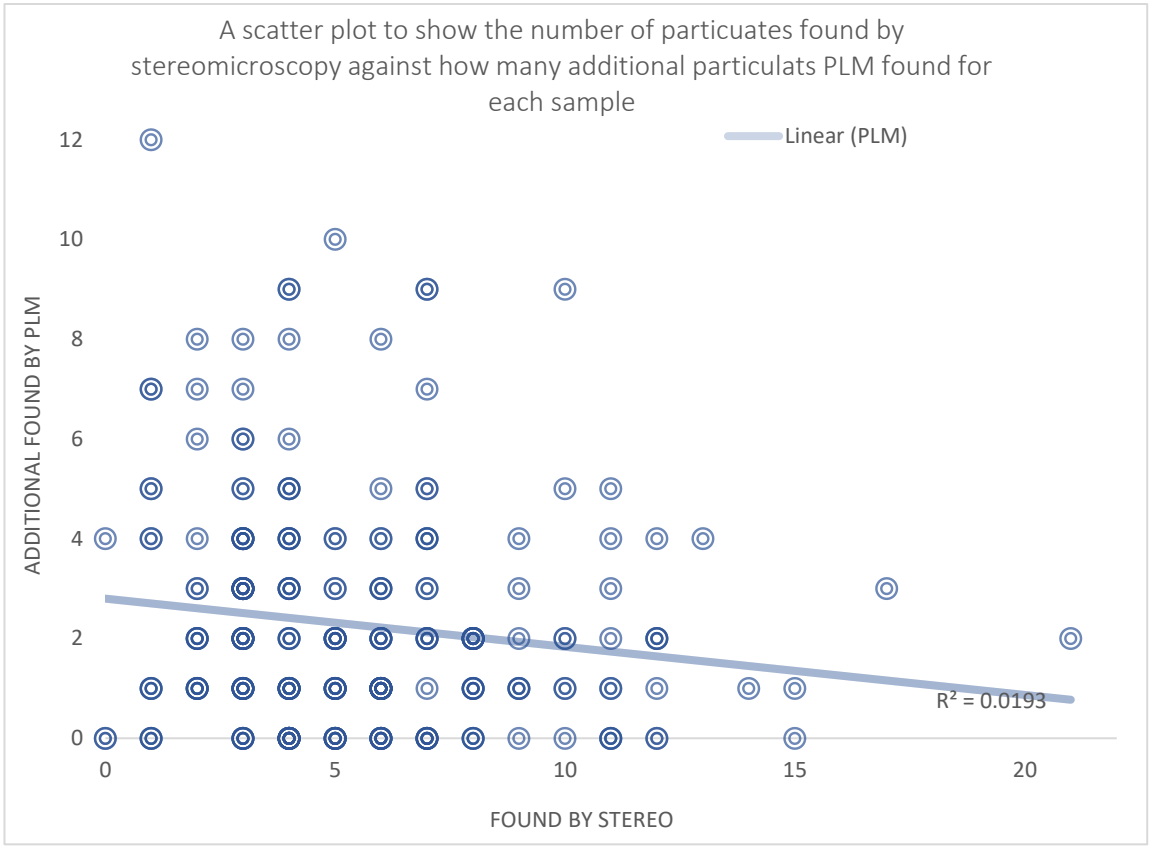

Figure 3.12 A scatter plot showing the number of particulates located using stereomicroscopy against the addition number found by PLM for each sample.

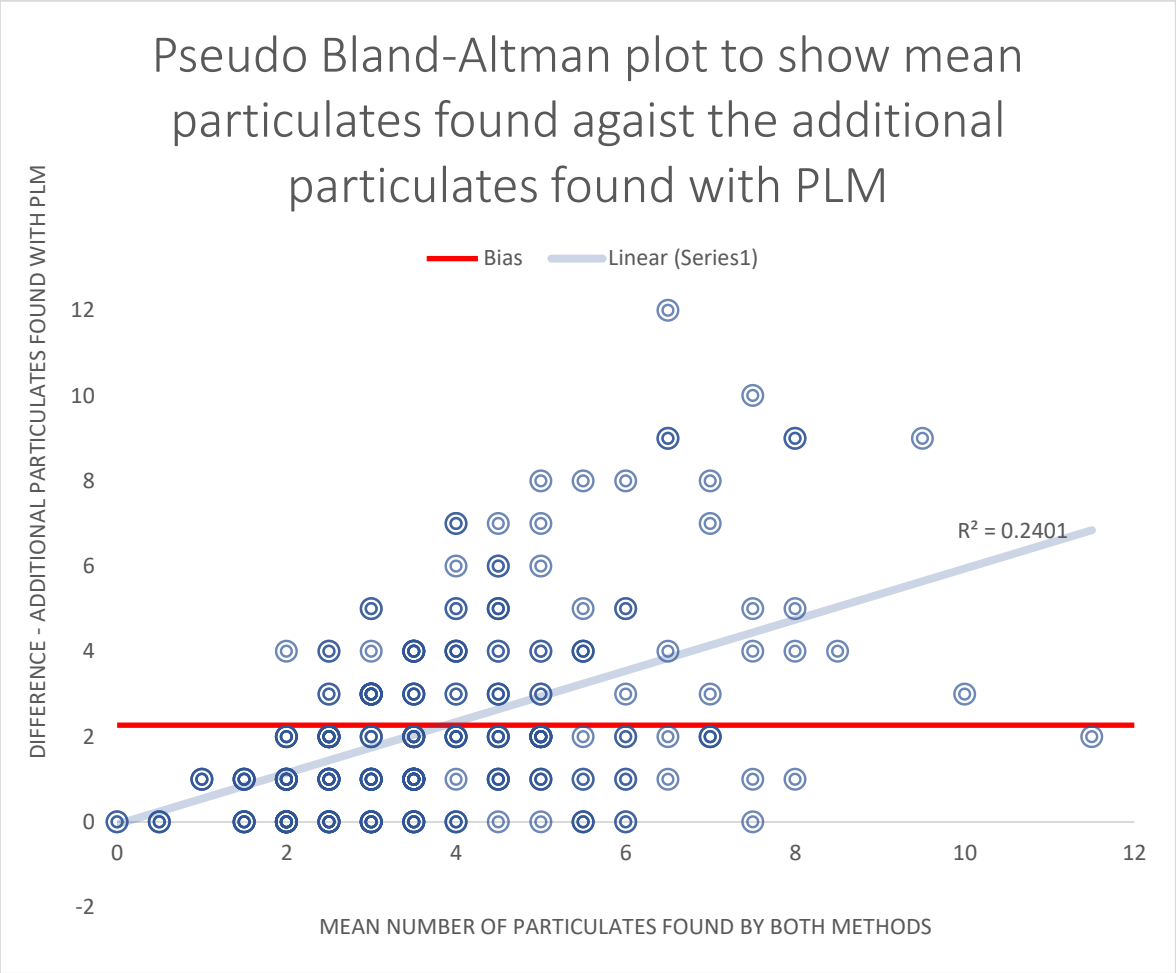

Figure 3.13 A Pseudo Bland-Altman plot to show the mean number of particulates found by both methods against the difference between the two methods.

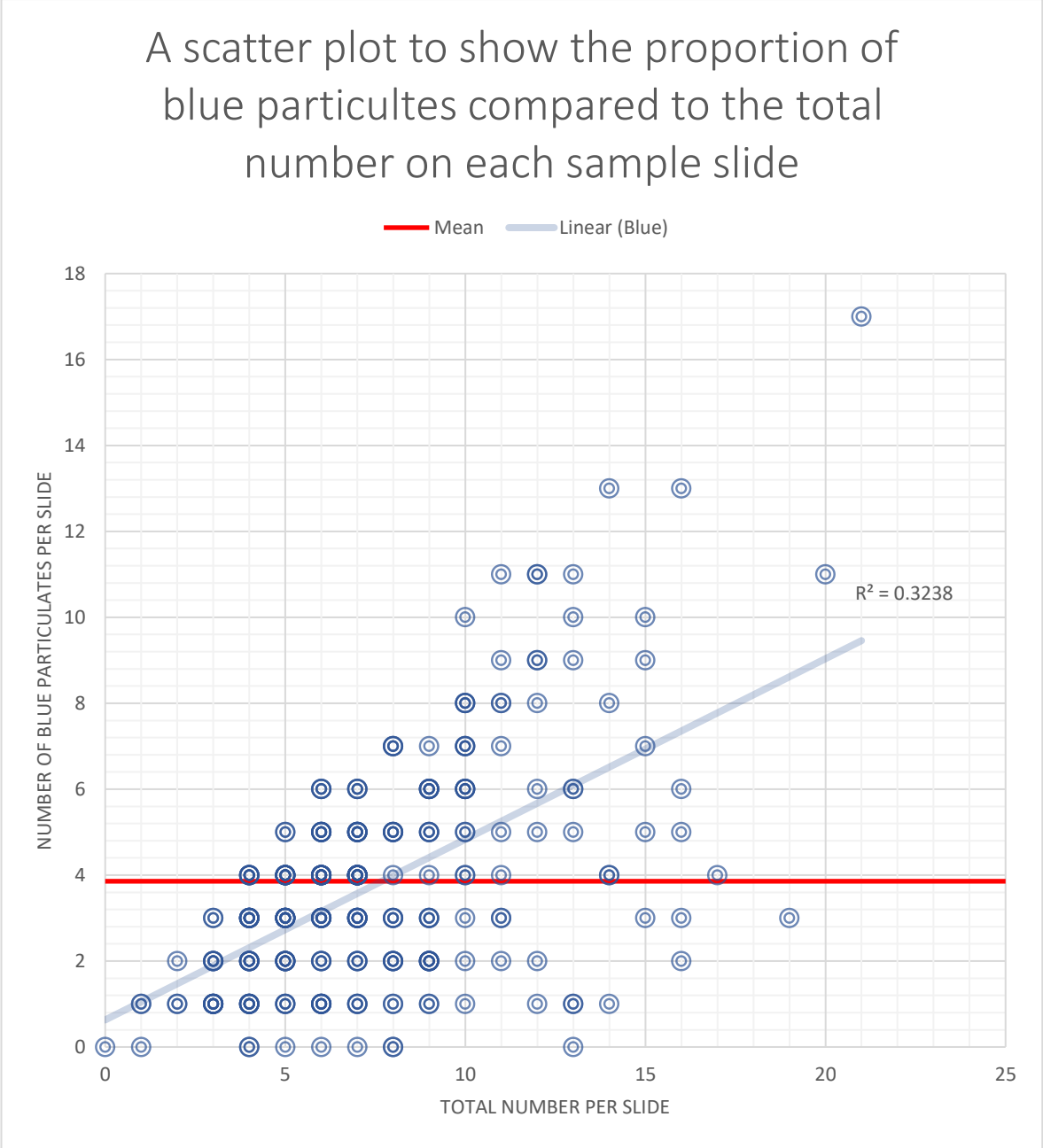

Figure 3.14 A scatter plot to show the total number of blue particulates compared to the total number on each sample slide.

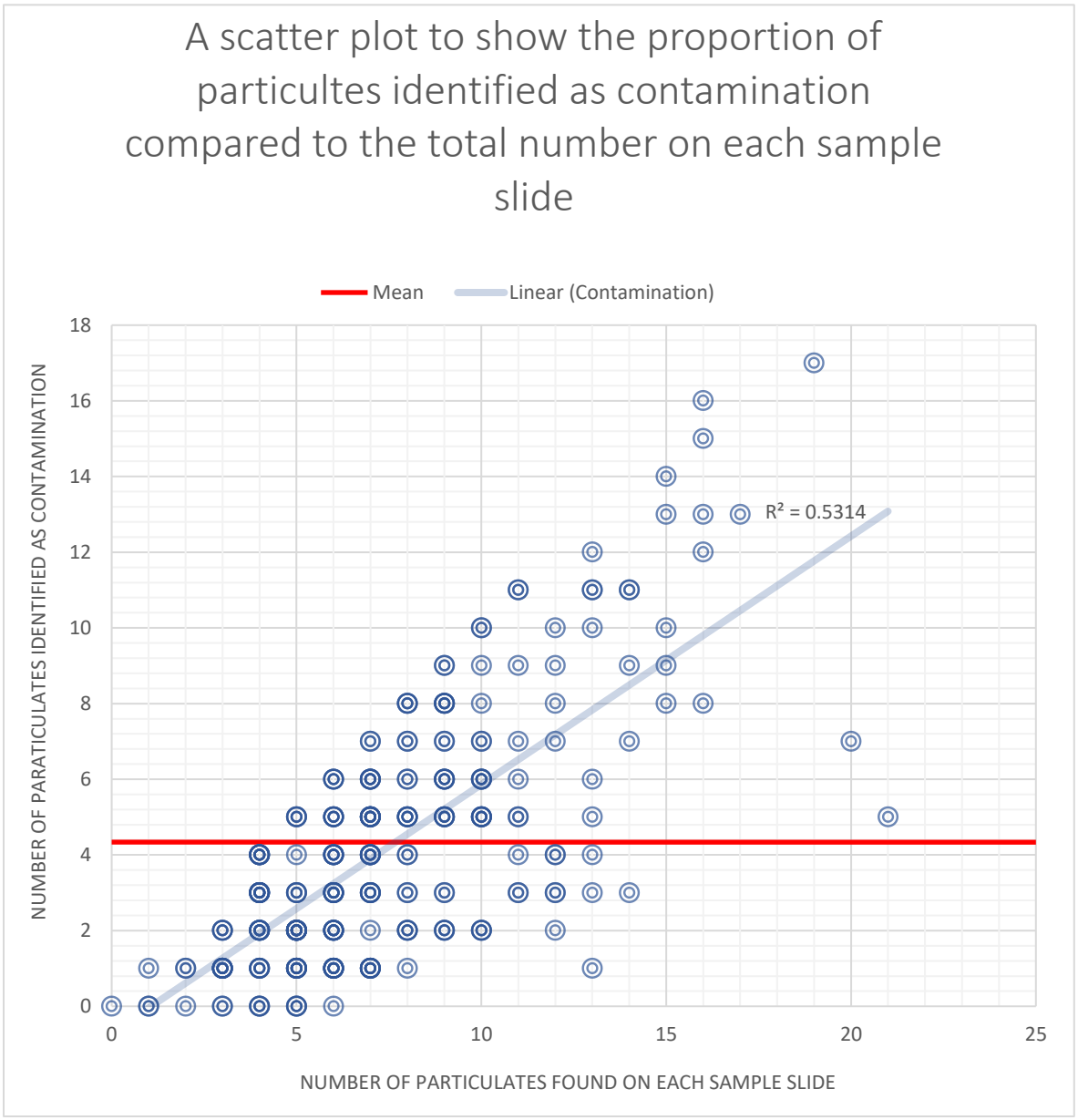

Figure 3.15 A scatter plot to show the percentage of particulates identified as contamination compared to the total number on each sample slide.

3.3.2.1 Application of data from the Hudson River.

The increased characterisation of the microplastics found in the samples has the potential to identify a potential source and as discussed in Section 1.9 being able to characterise the microplastics beyond these features such as cross-sectional shape and presence of delusterant allows greater discrimination between legitimate microplastics and contamination, as more features are being observed to inform this identification. Figure 3.16 shows a map of the Hudson River with the magnitude of microplastic pollution found in orange. Potential sources of industrial microplastic pollution including ferry ports and wastewater treatment plants have been marked on the map with black circles. If samples could be obtained from these, and any other potential source identified, comparisons could be made to determine if the microplastics may have originated from these areas. In addition, the increased level of detail recorded allows for greater discrimination when identifying any potential contamination from crew clothing in the samples. Figure 3.17 shows a map of the Hudson River showing a subsection of the microplastic pollution (blue) and particulates that were identified as contamination (green). From the data displayed in figure 3.17, contamination was successfully identified in every sample, in some samples the total identified as contamination was far higher than those identified as microplastic pollution. Had it not been possible to characterise the microfibres to the extent that they were characterised in this study it would have been more difficult to identify contamination from actual microplastic pollution, leading either to the levels of microplastic pollution being overestimated or more microplastics being excluded as contamination than needs to be resulting in an underestimation. Both outcomes would provide an inaccurate indication of the levels of microplastic pollution in the river.

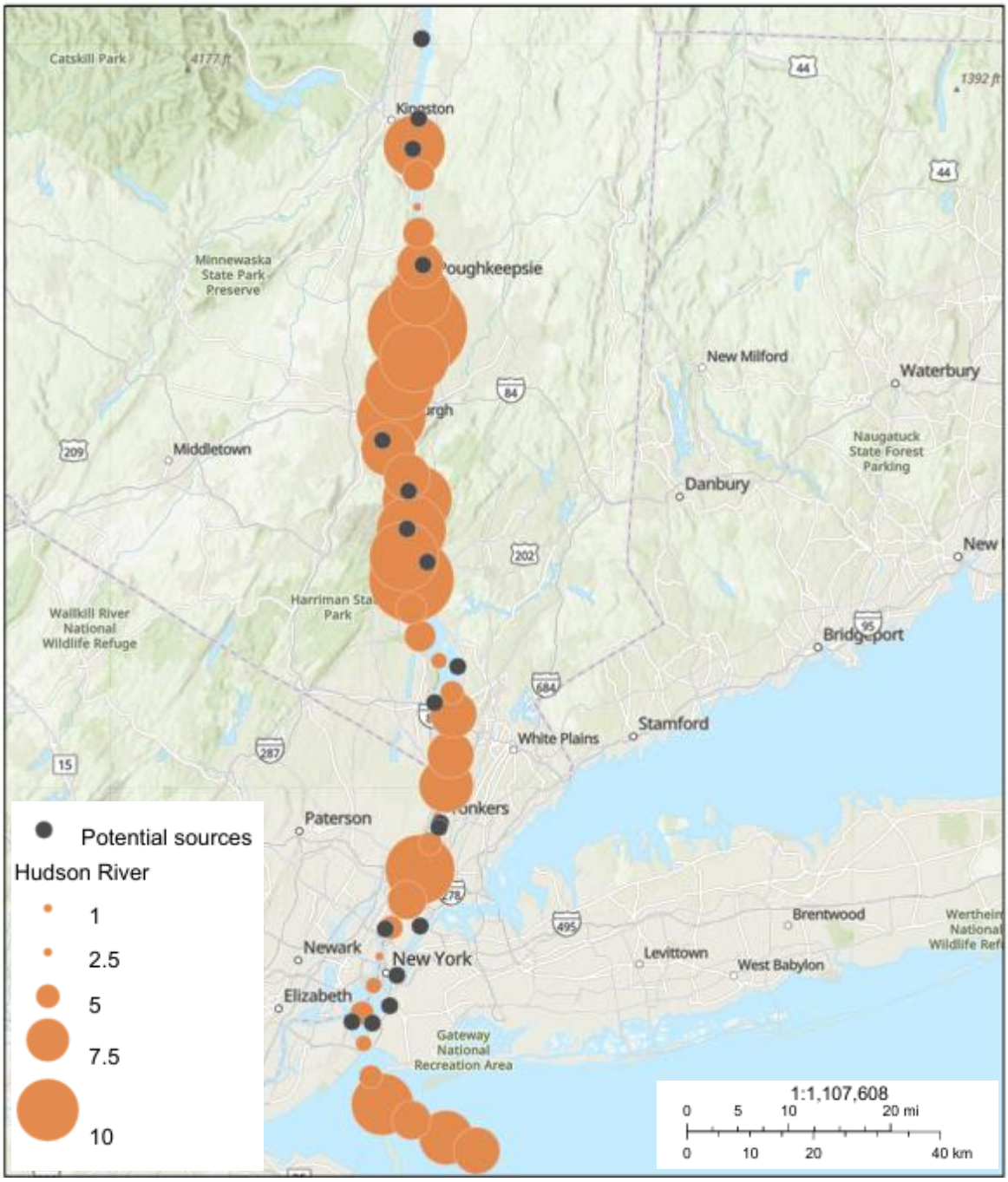

Figure 3.16 A Map of the Hudson River showing a subsection of the magnitude of microplastic pollution (Orange) found during the Rozalia project Hudson River expedition. Potential sources of pollution have been marked with Black circles.

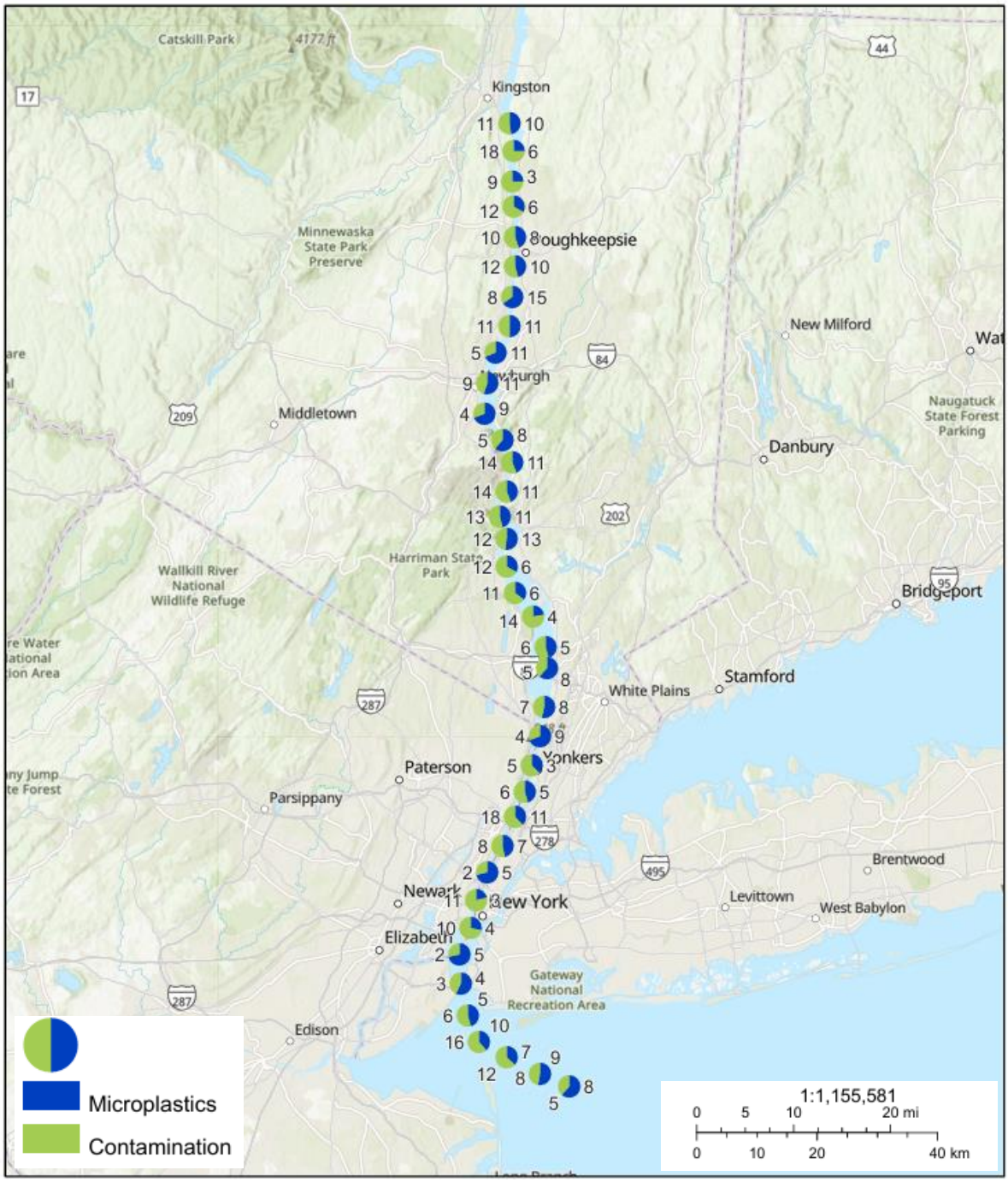

Figure 3.17 A Map of the Hudson River showing a subsection of the microplastic pollution (Blue) and particulates that were identified as contamination (Green) found during the Rozalia project Hudson River expedition

3.3.2.2 Evaluations and Limitations.

In this investigation of the sample slides, the primary focus was not the investigation of the use of PLM in the search process but rather the microplastic pollution along the entire Hudson River. Due to this, the method was focused on characterising the large volume of sample slides whilst trying not to slow down analysis times. Size dimensions were not taken for all identified particulates particularly fibres, due to difficulty accurately being able to measure the length of long and twisting fibres, in some cases the particulate may also have been partially obscured by background debris and so gaining an accurate measurement of dimension is not possible. Furthermore, no measurements were taken for items such as cotton to save time during the analysis process. This means that the effect of size on the ability of the two different techniques to locate them cannot be conclusively determined. This would be valuable to investigate in future studies to determine how size may play a role in the ease of detection between the two investigated methods.

During the analysis of the sample slide when there was a misidentification found by stereomicroscopy but deemed by PLM to not be anthropogenic in origin, these particulates were not characterised. It may be beneficial to know the characteristics of the items that were misidentified by stereomicroscopy to determine if there are any trends that may indicate what is potentially causing false positives when the stereomicroscope is used.

This study was not designed to investigate whether searching the slide with PLM followed by stereomicroscopy yields similar results. This would be valuable to investigate as it would conclusively demonstrate that either the act of second searching the slide is the main cause for finding more anthropogenic particulates or the use of PLM facilitates the detection of anthropogenic particulates that are potentially easily missed by stereomicroscopy.

All the sample slides used in this study were analysed by the same researcher, meaning there should be no differences between what is

identified as an anthropogenic particulate and what is excluded, ensuring consistency in the results. This, however, is not guaranteed as it is possible that, over time, the decision-making process is altered and evolves as more samples are observed. In addition, as only one analyst was examined it is possible that another analyst would have found different particulates with the stereomicroscope, so it would be beneficial to repeat this experiment with different analysts to determine if the same results are obtained.

A further benefit of using PLM is that it enhances the ability to identify contamination with a greater level of confidence and exclusion criteria. By fully characterising a sample of fibres from each crew member's clothing, any corresponding fibres found with the same characteristics (colour, width, presence of delusterant, cross-sectional shape and birefringence id) would be removed from the final count of anthropogenic materials. Using this many characteristics in the exclusion criteria ensures that fibres that are similar but do not share all the required characteristics are not incorrectly removed; for instance, a colourless cylindrical nylon fibre is unlikely to have originated from the same source as a cylindrical colourless nylon fibre with delusterant present, and such eliminating it as contamination would not be accurate.

3.4 Conclusion

The aim of this chapter is to assess an improved method of processing microplastic samples by assessing the use of Easylift® in a field study and investigating whether including Polarised light microscopy is a beneficial addition to the analysis workflow. This was completed by evaluating Easylift®'s performance in the 2019 Rozalia project Hudson River field trial to determine if it is logistically appropriate to employ in the field and to see how it handles. The use of PLM was also employed on these samples after a search with stereomicroscopy to see if PLM is able to find any trends in what microplastics are potentially often missed when only searching with a stereomicroscope.

Easylift® was found to be an effective method to retrieve microplastics from filter papers in a field study, as it was successfully used on over 500 samples that encompass air, water, and soil samples. During the searches of the filter

paper post tape lift there was only a small number of particulates that were not retrieved across all samples. The sample slides were able to be stored after extraction and there were no visible signs of degradation five years after extraction, meaning that they can be left to be analysed after the field trial is over. The level of moisture on the filter paper affects the tacticity of Easylift®'s adhesive which can affect the recovery of any particulates on the filter paper and cause the tape to not securely adhere to the microscope slide meaning that the sample is open to loss and contamination, due to this it is best to filter the sample under vacuum so that the excess water will be removed from the surface of the filter paper.

The use of PLM as an additional method of analysis was investigated by searching each slide with a stereomicroscope followed by the PLM. The addition of PLM found a further 549 particulates over the 244 sample slides subsection used in this study. The PLM found a significant number of colourless particulates that were missed by the stereomicroscope search finding 371 (67% of those found by PLM) more colourless particulates compared to the 285 (21% of those found by stereomicroscopy) of colourless particulates found with the stereomicroscope. This demonstrates that the PLM is able to identify a large number of colourless particulates of interest that would have been missed, had only the stereomicroscope been used to locate potential anthropogenic particulates. In addition, a logistic regression found a statistically significant relationship between the effect of the method used and the particulate being colourless (P-value = 8.88×10^{-8}).

The width does not seem to have an effect on which method the particulates are found with. This could be because it is the other features, such as the colour, that are more of an indicator of how easy it may be to locate. It could also be that neither method was better at finding smaller methods or neither method found them at all, meaning that the effect of size is present, but the methods used were not appropriate for their detection. The smaller size fractions could also simply not be present in the sample either due to their absence in the environment, or because they are not retained by the filter paper or not successfully lifted by Easylift®. In addition, the size data produced in this study is skewed as the length was only taken for a handful

of samples and width was not taken for certain materials, for instance, cotton, to save time as the results in this study were not optimised for this purpose but rather to generate the data for the Hudson River expedition. Due to this, it is not possible to conclusively determine how much of a role size has an impact on its detection with either stereomicroscopy or PLM.

As the number of particulates on the slide increases the number detected by PLM does not increase as would be expected. This could be because the contamination was not removed from the data analysis as this study was investigating to see if there was a difference in the particulates found with stereomicroscopy and PLM. The crew wore blue cotton t-shirts while sampling, these fibres tended to be easily found with the stereomicroscope, so if samples had high levels of contamination, it is likely that most of it would have been found with the stereomicroscope, which could explain why as particulates on the slide increases the proportion found with the PLM does not also increase. The addition of PLM also allowed a greater level of characterisation of the microplastics found by allowing the determination of birefringence, sign of elongation, presence of delusterant and cross-sectional shape of fibres. By collecting this information, a more accurate assessment of sources of contamination can be made, and information on potential sources to be investigated. As discussed in Section 1.9 knowing if a particular type of microplastic is likely to be missed, alternative approaches such as the inclusion of PLM can be adopted to maximise detection and gain the most accurate population of microplastic levels in the environment.

3.5 Further Work

Due to the findings of this study, several areas have been identified that need further investigation and improvement to understand the data within this study further. Firstly, the study should be repeated using PLM as the first method of searching. This would conclusively determine whether the use of PLM was beneficial or whether the action of a second search is what is responsible for finding further particulates. A double-blind study could also be conducted so that it is known exactly what is on each slide, and a separate examiner searches and records microplastics on the slide. This would allow

the determination of how accurate the two methods are and if there is a common particulate type that is missed by both methods.

Further investigations also need to be made into the effect of size on detection as it was not possible to accurately ascertain from the data used in this study. The length and width data could also be taken for more particulates in the data used in this study to improve the dataset used. An investigation also needs to be carried out to determine if Easylift® has a limit of extraction by testing it with a smaller size fraction; this would allow the determination of whether Easylift® is able to extract small particulates, which would explain their absence in the sample slide if this was found to be the case.

Chapter 4 Investigating the use of YOLO software to create an automated method of detection of microplastics and anthropogenic materials.

4.1 Introduction

4.1.1 Machine Learning and its Uses

Machine learning is the application of programming computers so that they learn from supplied data (Géron, 2019). Broadly speaking, it is a classification of algorithms that is capable of automatically producing predictive models by detecting patterns in data (Christin, Hervet & Lecomte, 2019). The use of machine learning has progressed rapidly in the last few decades due to the development of new algorithms, availability of online data and low-cost computation (Jordan & Mitchell, 2015). Machine learning has been used for a number of different applications, including for the interpretation of genomic data sets (Libbrecht & Noble, 2015), comparison of handwriting evidence (Neupane *et al.,* 2024), in cancer prognosis and prediction (Kourou *et al.*, 2015), finding child sexual abuse texts on the dark web forums (Ngo, Mckeever & Thorpe, 2023) and predicting weather forecast uncertainty (Scher & Messori, 2018). A large number of algorithms have been used and developed in machine learning to encompass a wide variety of different types of data and problems that may be encountered (Jordan & Mitchell, 2015). A branch of machine learning is deep learning, which is capable of learning without supervision from unlabelled data by finding patterns; it is commonly used as an exploratory tool to group similar data together. Deep learning is also capable of learning from supervised data, where in traditional machine learning the algorithm additionally needs information on what to search for in the form of colour, size etc, to be stated in terms of patterns in pixels through the use of bounding boxes, deep learning is capable of detecting and obtaining features from the data just by being told that an item is present in the image and it will figure out what it looks like itself (Christin, Hervet & Lecomte, 2019).

Supervised learning is one of the most common forms of machine learning that involves giving the algorithm labels to train it how to classify data (Géron, 2019). In machine learning, the algorithm learns how to classify objects by repeatedly testing the different search parameters against the training data set (LeCun, Bengio & Hinton, 2015).

Unsupervised learning is an alternative technique where the data is supplied to the algorithm unlabelled, and the algorithm will learn from the data without being taught what anything is. It will then attempt to group and cluster the data based on hidden structures in the data (Géron, 2019). This approach is useful in anomaly detection to find outliers in a set of data, for example, fraudulent transactions on credit cards (Zanero & Savaresi, 2004). One of the common types of unsupervised learning is hierarchical cluster analysis in which the algorithm will cluster similar data points in the context of the of the issue being investigated (Dell'Anna *et al.*, 2009).

4.1.2 Image Classification Techniques

Image classification is a technique in computer vision that classifies images using segmentation, key feature extraction and matching identification (Bharadiya, 2023). Object detection in image classification is one of the most difficult problems in machine learning, as it aims to localise and detect different objects within an image or video and assign a label to the bounding box (Shaifee *et al.*, 2017). Datasets provides the framework for training and evaluating supervised learning machine learning models for object detection (Long *et al*., 2021. & Paullada *et al.*, 2021). In order to create an accurate method of automated detection a large and representative dataset is required (Xu & Goodacre, 2018). All datasets are prone to limitations and biases such as the use of an analyst with subjective judgements and biases during the dataset production that can impact the algorithms accuracy, although a rigorous error analysis can be employed to assess how useful the dataset is in practice (Paullada, *et al.*, 2021). The most difficult part of creating a dataset is not generating the images but annotating the data, this is due to the fact that the labels have to be generated by a human annotator. This is an extremely time-consuming effort (Gauen *et al.*, 2017). The

annotation can also lead to issues where subjective values, judgments and biases of the annotator may generate a data set bias, as annotating the dataset is a form of ‘interpretive work’ and can result in the amalgamation of target labels (Paullada *et al.*, 2021).

Image segmentation is the process in which the image is split into significant non-overlapping areas (Egmont-Peterson, Ridder & Handels, 2002). Classic segmentation was presented for use in greyscale images, where the division of the images is based on grey-level similarities and the edge is detected with grey-level discontinuity as the areas where there is a large change in the level of grey is likely to be the boundary of a different region or object (Yu *et al.*, 2023). This technique is also capable of colour image segmentation by clustering pixels by their colour and using the mean colour of a cluster to reduce the number of different colours in the image to make it simpler to detect the contour of each object present in the image (Géron, 2019). Another technique is collaborative or co-segmentation, which extracts common regions from multiple images rather than one image as with classical segmentation. This method does require prior training with classic segmentation so that this knowledge can be used to segment similar objects (Yu *et al.*, 2023).

Machine learning has developed to include biologically inspired computational models called artificial neural networks (ANN), the most common ANN is a convolutional neural network (CNN) these CNNs are often used to resolve image-driven and pattern recognition tasks (Géron, 2019). CNNs are ‘translation invariant’ which means that they are able to locate and recognise patterns regardless of where in the image it is located, this is due to the number of convolutional layers (Bharadiya, 2023). These neural networks have a large number of connected computational nodes (neurons) that work together to learn from the provided input, these models also use multiple hidden layers (deep learning) that make decisions based upon the previous layer to improve the final output (O’Shea & Nash, 2022). CNNs are also capable of hierarchical feature extraction, which is made up of several layers of convolutional and pooling layers that will progressively extract features from the image at differing levels of abstraction. This technique

allows the CNN to identify complex patterns and structures in the data, producing more accurate identifications (Bharadiya, 2023). A CNN has been used to screen for microplastic contamination in soil samples; the CNN used seven layers (four convolutional and three fully connected). There were 32 filters used in the first convolutional layer, which was increased by a factor of two for each convolutional layer, this system generated an accuracy of 78.5%. This model was able to differentiate between low and high levels of contamination in the samples, it did, however, suffer from overfitting where the model memorised irrelevant background information resulting in a lower accuracy, this could be counteracted by supplying the model with more training samples (Ng, Minasny & Mcbratney, 2020). Other studies have found that using a one-dimensional CNN significantly outperforms other more traditional machine learning algorithms (Huang *et al*, 2022).

4.1.3. Uses of the Software 'You Only Look Once' (YOLO) in Automated Detection

You only look once (YOLO) is a real time single stage object detection framework that is faster compared to two stage approaches (Koirala *et al.*, 2022). The algorithm is able to detect and classify objects in real-time by using a convolutional neural network (CNN) (Naseri & Ali, 2022). The models have been frequently used due to its ability to have a high accuracy whilst having a small model size and being able to be trained on a single Graphic processing unit (GPU) (Solawetz. & Francesco, 2024). The algorithms work by splitting the image into a grid, the grid cell that the centre of an object being detected falls into is responsible for detecting that object, each grid square will calculate a confidence score for each bounding box that indicates how confident the model is that a correct prediction has been made (Redmon *et al.,* 2016).

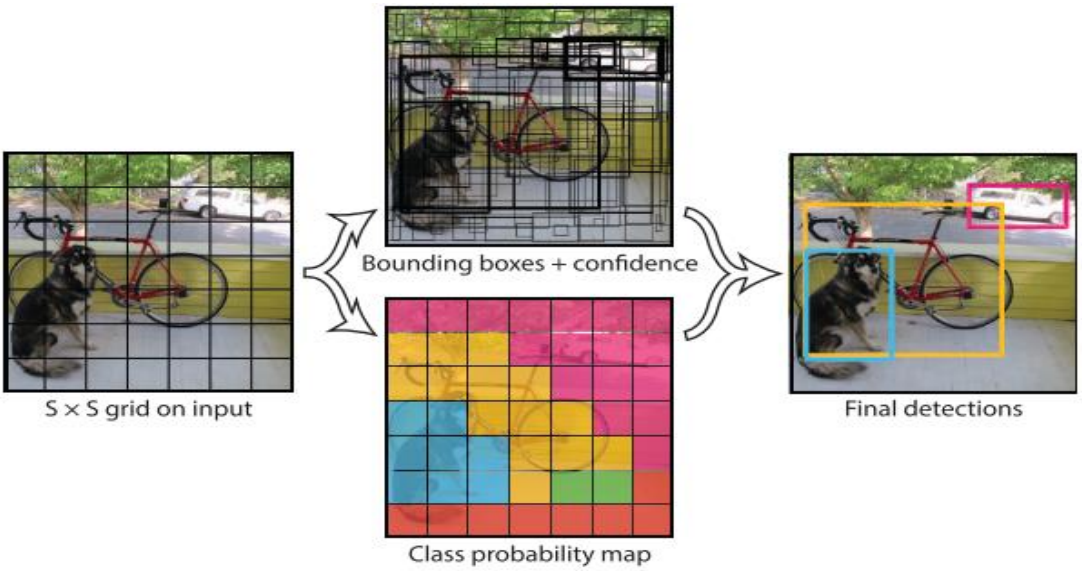

Figure 4.1 An image to demonstrate how YOLO's model works to produce predictions taken from Redmon *et al* (2016).

YOLO has several advantages over other traditional algorithms; including that it is very fast as it runs at 45 frames per second (with a Nvidia Titan-X GPU) (Shafiee *et al.*, 2017), YOLO also produced an average level of precision more than twice the size of other comparable image detection algorithms (Redmon *et al*, 2016). As YOLO reasons each image globally to create its predictions, meaning it will see the image in its entirety during the training and test phases, it makes half the amount of background errors as the comparable algorithm Fast R-CNN. The algorithm does, however, struggle to localise some objects precisely, particularly those that are very small (Redmon *et al.*, 2016).

YOLO has been used in a number of different applications, it has been used in conjunction with the algorithms CAD3 and CNN to detect and classify leukocytes in leukaemia with 3060 microscope images (80-20% test train split), they were able to achieve an accuracy of 94.3% (Abas, Abdulazeez & Zeebaree, 2022). YOLO v4 has also been used to detect drones, by training with images of drones at different distances and with different environmental conditions, they also trained the model to detect birds and planes as these may be confused with drones, the model was able to identify drones with 98.3% accuracy, with the main issue with the detection model being the ability to detect similar small objects at varying distances (Naseri & Ali, 2022). There has been various versions of YOLO released over time; YOLO,

YOLO2, YOLOv3, YOLOv4, YOLOv5, YOLOv6, YOLOv7, YOLOv8, YOLOv8, YOLO-NAS, YOLO-World and YOLOv9 (Nelson., 2021). This study is investigating the use of YOLOv5, YOLOv7 and YOLOv8 for microplastic detection.

4.1.3.1 YOLOv5

YOLOv5 is a fairly recent version of YOLO that uses a lightweight network architecture, that has had a state-of-the-art performance on several object detection benchmarks (Talaat & ZainEldin, 2023). It was the first of the YOLO models to connect predicting bounding boxes with the class labels for an end-to-end differentiable network (Solawetz, 2020). YOLOv5's structure consists of a 'backbone', that isolates important features from the image (Fang *et al.*, 2021). The 'neck' which produces feature pyramids that help with generalising object scaling allowing the algorithm to cope with the same object with different sizes and scales. The 'neck' uses a Path Aggregation Network (PANet) to facilitate the flow of information. The PANet pools to connect feature grids to all feature layers allowing any useful information obtained from each layer to be communicated directly to the subnetwork (Cheng & Zhang, 2020). The final stage is the 'head', which produces anchor bounding boxes and generates the final output vectors and class probabilities and bounding boxes for the detected objects (Fang *et al.*, 2021). YOLOv5 trains very quickly meaning that it cuts down on training time and costs (Nelson, 2021).

4.1.3.2 YOLOv7

YOLOv7 has a higher accuracy and detection speed when compared with other algorithms, allowing for real time detection (Sun *et al.*, 2023). YOLOv7 uses group convolution (using multiple kernels per layer leading to multiple channel outputs for each layer) to expand the channel used and the number of elements of the computational blocks. The same group convolution and channel multiplier is applied to all computational blocks in the computational

layer. This then produces the feature map, which is calculated by shuffling the computational blocks into groups according to a chosen group parameter; all groups are then concatenated together. After this, the groups are added to the feature maps to perform a merge cardinality (Wang, Bochkovski & Liao, 2022).

4.1.3.3 YOLOv8

YOLOv8 is a ‘single pass’ object detection model, meaning it is capable of identifying objects in a single pass, as a result it is very quick and efficient (Abdulla., 2023). It has a measured high level of accuracy (Solawetz. & Francesco, 2024). YOLOv8 has a similar structure to YOLOv5 with a backbone to extract characteristics from the images, a neck that merges the features created by the backbone to create feature pyramids that combine lower-level features into high level representations. And the head that predicts the target category (Yang *et al.,* 2023a). But has had several architectural changes in comparison to YOLOv5 (Solawetz. & Francesco, 2024). YOLOv8 does not use any anchors, meaning that it implies rather than predicting distance from a known anchor box, and it estimates the centre of the object (Nelson, 2021). Employing anchor-free predictions will lower the number of box predictions, making post-processing less challenging as it expedites the non-maximum suppression (NMS), which sorts through potential detections following interference (Talaat & ZainEldin, 2023).

4.1.4 Creating a Training Dataset

To produce an accurate method for detecting anthropogenic particulates and microplastics it needs to be trained to detect the wide range of different characteristics such as colour, shape and internal features that can be present. These features can also be affected by the presence of background materials, various lighting conditions and orientations of the microplastics on the slide. The larger the dataset the more accurate and transferable to different microplastic samples the model will be (Cubaynes & Fretwell, 2022).

Creating a comprehensive training dataset is an important step in producing a model that is able to accurately identify microplastics. It is important that there is a balanced dataset with good representations of all classifications used, as it will create a bias towards the more represented classes, and the training for the smaller classes will not be sufficient (Susan & Kumar, 2021). When there is an imbalance, using accuracy as a metric to evaluate the model is unreliable as it will provide an over-optimistic estimation of the model's ability to classify minority classes (Chicco & Jurman, 2020). One method of increasing the data set and its robustness is to augment the images being used, which involves altering the image (Yang *et al*, 2023a). Some types of augmentation include rotation, blurring, mirroring, cropping, scale, greyscale, colour saturation and altering the brightness and exposure (Xu *et al.,* 2023). Including augmented images in the dataset can improve the model's performance, although it is unable to overcome all biases that may be present in the dataset (Shorten & Khoshgoftaar, 2019).

4.1.5 Uses of Machine Learning with Microscope Images

Machine learning has been used to identify other particulates. For instance, Gonçalves *et al*. (2016) used image processing to classify and identify 23 different types of pollen with four different algorithms: K-nearest neighbour (KNN), J48, C-support vector classification (C-SVC) and Sequential minimal optimisation (SMO). They found no statistically significant difference between the human (67% accurate) and computer classification (66% accurate), but the computer tended to produce more consistent classifications. Machine learning has also been used in conjunction with FTIR to identify different pollens, this combination of FTIR and KNN produced an accuracy of 84% (Dell'Anna *et al.,* 2009). Different types of microscopy images have been used to train datasets, for instance, Anderson, Vega & Kovscek (2020) used images of shale taken with Transmission X-ray Microscopy and Focused ion beam-scanning electron microscopy to characterise the shale and enhance the image quality using machine learning techniques. Das *et al.* (2013) used light microscope images to detect the presence of the malaria parasite by combining a statistical learning technique, Bayesian statistics, with the

Support vector machine (SVM) for a high classification accuracy, they found that when 19 discriminating features were used the Bayesian approach had a higher accuracy of 81%, while if only nine discriminating features were used SVM had the highest accuracy of 83.5%. Other projects have tried to automate the assessment of damage to hairs using images from a Scanning electron microscope, using K-nearest neighbour, achieving an 87% accuracy in its classifications (Chu *et al.*, 2020).

4.1.6 Machine Learning for Fibre and Microplastic Identification.

Machine learning has been used to automate the detection of fibre analysis, Wetzer & Lohninger (2018) used the algorithm Otsu's method that automatically finds the optimal threshold based on pixel distribution to detect fibres on a tape lift. In a test with 77 images of tape lifts on a light microscope, the system was able to identify all the fibres that manual searching was able to locate, although some fibres were not fully detected along its whole length due to background debris and fibres twisting. Machine learning was used to detect asbestos on SEM images by training on 100 images using U-Net Semantic Segmentation model, they were able to achieve a 95% success rate (Biswas & Biswas, 2021). Lorenzo-Navarro *et al*. (2021) looked into using deep learning to automate the classification and detection of microplastics between 1-5mm. They used U-net for particle segmentation and VGG16 for classification; an average accuracy of 98.11% was found. In another study by Lorenzo-Navaro *et al*. (2020), they tested a three-level cascade classifier using SVM, RF and Principal component analysis with RF to identify fragments lines, pellets, organic and tar in images of microplastics ranging from 1-5 mm. The resulting model produced an accuracy of 91.1%, a precision of 91.35, and a recall of 91.1%; the metric produced from this model shows that it is performing well in the identification of microplastics. This model does, however, concentrate on the larger size fraction of microplastics that are visible to the naked eye and so would not be appropriate for microscopic samples. The microplastics were also presented to the model cleaned and laid out with no overlapping, meaning that sample

pretreatment is required before it can be used to quantify the microplastics. Other attempts have combined hyperspectral imaging with a one-dimensional convolutional neural network to detect and classify forensic fibres in comparison to four traditional machine learning models, K-NN, SMV, RF and partial least squares-discriminant analysis (PLS-DA); they found that the one-dimensional convolutional neural network consistently outperformed the four traditional methods with RF having the highest accuracy of the four methods at 91.4%, whilst the one-dimensional convolutional neural network generated an accuracy of 98.6% (Huang *et al.*, 2022). Machine learning methods have been used on environmental samples collected with a neuston net from a freshwater environment; these samples were then visually sorted with a x40 microscope and distributed over separate filters based on their colour. A 12-mega pixel smartphone camera was then used to acquire images of the filters. The samples were classified using K-Nearest Neighbour (supervised) and K-Means Clustering (unsupervised) to classify them as either pellets, lines, fragments, or fibres. K-nearest neighbour was able to classify the microplastics with an accuracy over 0.9, and K-Means Clustering indicated that there was a probable undercount of some microplastic shapes due to the methodology used as the neuston net was unlikely to sample microfibres adequately (Massarelli, Campanale & Uricchio, 2021). While these samples were obtained from environmental samples, the microplastics being laid out on filter papers so that there is no overlap adds a time-consuming step into the process meaning that the models produced may not be able to identify microplastics that have not been separated from each other. YOLOv8 has been used to identify four types of microplastics on aluminium oxide filters and glass slides, with 755 images using an 80-20 split. The model produced had a high mAP of 94.6%. This model only had the classification ‘particle’; this means that the model generated is unable to distinguish between different microplastic shapes as it was only focused on detection for further analysis with FTIR (Xie, Gowen & Xu, 2024). YOLOv5 was used to differentiate plastics and microorganisms from the marine environment on filter papers, 300 images of plastics and microorganisms on a filter paper were used to produce this model in a 50-25-25 split, and the classifications plastic and worm were used. They found that at 30 epochs, all

plastics and microorganisms were correctly identified, but there were also a high number of false positives and duplicate identifications (Shishkin & Grekov., 2023).

As discussed in Section 1.9, as of yet there is no robust, infallible method of automated detection for microplastics using machine learning that has been effectively applied to and trained on a large number of different environmental samples. As the background material in different environments varies greatly depending on where the sample is taken. For instance, the diatom's shape and size can be vastly different if samples at the source of the river compared to those found in saltwater environments (Pellondo'u, Toya & Novelyn, 2023). there is a need for a system that is able to successfully identify and classify microplastics to speed up research, in both fibres and microplastic research, the current automated numeration methods for fibres seems to be an issue as they are long, thin and tend to overlap themselves meaning that often the fibre will be counted as multiple microfibres (Paulsson & Stocklassa, 1999. & Wetzer & Lohninger, 2018).

4.1.7 Other Forms of Automated Detection for Fibres and Microplastics

There have been other approaches to automating the analysis of microplastics and forensic fibres that are using different methods of automating microplastic analysis. For example, the Foster and Freeman Fx5 fibre finder was developed to automatically search forensic tape lifts for coloured fibres using a high-resolution colour scanner with ten narrow band filters ranging from 390-750 nm (Wiggins, Turner & Miles, 1999). This system could differentiate between similar fibres in most instances when the control sample was adequately represented. This system was not tested on samples with high levels of background noise and was unable to detect fibres that were completely perpendicular to the tape in the same orientation as the scanning beam (Sermier *et al.*, 2006). The 'Maxcan fibre finder' was another attempt to automate the analysis of forensic tape lifts; this system used the hue, saturation, and luminance model to determine the colour of the fibres (Langdon *et al.*, 2003). This system performed at least as well as manual

searches, where the Maxcan had a detection rate between 98-100% and the manual search had a detection rate of between 61-100%. The system would however, struggle to identify pale pink fibres where the detection would fall to 67%, this was considered to be due to the systems inability to differentiate the fibres from newton rings present in the tape lifts. The system was not affected by the fibres' diameter, whereas the manual searching was affected by the fibres' diameter (Sermier *et al.*, 2006).

There has also been movement towards automation within microplastic analysis. A semi-automated approach has been trialled using a LabRAM HR800 Raman micro-spectrometer with a Horiba Scientific Particle Finder module for LabSpec6 attachment to locate and characterise microplastics. This system had an identification rate of 75%, but the success of particulate identification would decrease with particle size (Frère *et al.*, 2016). Primpke *et al*. (2017) has used FTIR microscopy and image analysis using Python ad Simple ITK image processing modules to automate the detection of microplastics. They were able to map the presence of synthetic and natural material on a membrane filter paper and determine the polymer type by comparing it to reference samples. They also found that the automated method was able to detect microplastics smaller than 30 μm that manual searching was not able to detect. The automated approach also found seven times as many polymer particulates as the manual method, demonstrating how beneficial applying an automated approach may be for microplastic detection.

The SHUTTLE project has developed a SMMART microscope capable of hyperspectral, fluorescence and polarimetry (Balas *et al.*, 2023) to automatically locate and identify trace evidence from crime scenes using a range of microscope techniques including, polarised light, transmitted light, fluorescence and absorption microscopy (Bijker, 2023). The microscope uses samples mounted on a tape lift, which are then imaged, and the trace evidence undergoes colour and spectroscopic analysis. The images produced in the previous step are processed by artificial intelligence. This data is then compared to the internal databases to search for the identification of the different types of evidence present in the sample. The

smart microscope has been successfully used to quantify textile fibre shed and identify blood and skin cells (SHUTTLE., 2022). A recent study found that the SMMART microscope was able to speed up trace evidence analysis containing hairs, textile fibres, sand, pollen, glass, skin and blood by a factor of 178.6 (Balas *et al.*, 2023).

4.1.8 Evaluating Machine Learning Prediction Models

There are several different performance metrics that can be used to evaluate the performance of a prediction model, including accuracy, F-Score, Area under the ROC curve, average precision and squared error (Caruana & Niculescu-Mizil, 2006). See Table 4.1 for examples of how different performance metrics are calculated.

Table 4.1 Equations commonly used as performance metrics.

True predictive rate/Precision = $\frac{True\ positives}{True\ positives + False\ positives}$
Accuracy = $\frac{True\ positives + True\ negatives}{True\ positives + False\ positives + True\ negatice + False\ negatives}$
True positive rate/Recall/sensitivity = $\frac{True\ positives}{True\ positives + False\ negatives}$
F-score = $2\ x\ \frac{Precision\ X\ Recall}{Precision + Recall}$
True negative rate/Specificity = $\frac{True\ negatives}{False\ positives + True\ negatives}$

The F1 score is the measure of the model's accuracy; it is the harmonic mean of precision and recall (Padmanaban & Parthiban, 2016). The closer the F-score is to 1, the better the model is at classifying objects (Tomar & Agarwal, 2014). An area under the curve-Receiver Operating Characteristic curve (AUC-ROC curve) is a performance metric used to evaluate classification models; the ROC is a probability curve, whilst the AUC is the measure of separability that demonstrates how competent the model is at distinguishing between different classes. The higher the AUC value is, the better the model is at predicting classifications (Narakhede, 2018). To create a ROC (Receiver Operating Characteristic) curve performance metric the number of successful identifications and unsuccessful identifications

produced by the classification scheme is displayed in a confusion matrix (Bradley, 1997) an example of a confusion matrix can be seen in Table 4.2. A ROC graph is made by plotting the true positive rate on the y-axis and false positive rate on the x-axis an example of a ROC curve can be seen in Figure 4.2. On a ROC curve graph, the closer the curve is to 100% on the y-axis, the better the model is at accurately classifying the objects with a curve at 100%, meaning that the model produced a perfect classification system (Fawcett, 2006).

Table 4.2 An example of a confusion matrix.

		Predicted	
		Positive	Negative
Actual	Positive	True Positive (TP)	False negative (FN) type II error
	Negative	False positive (FP) Type I error	True Negative (TN)

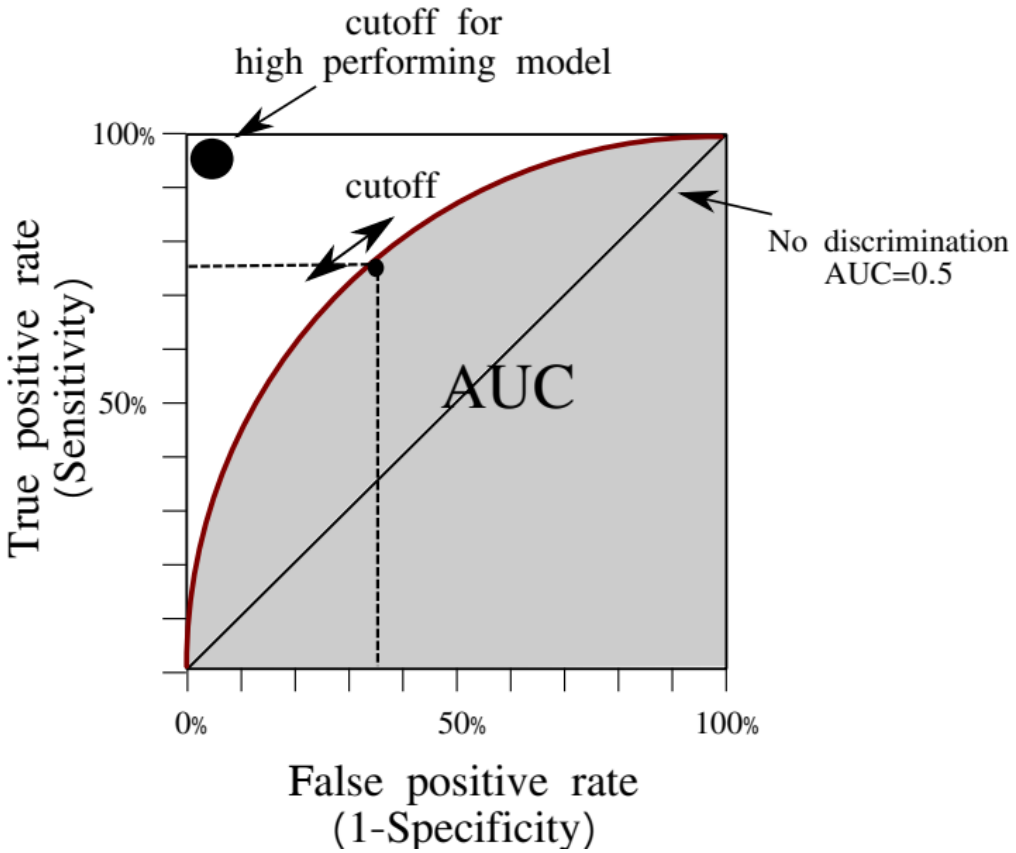

Figure 4.2 An example an ROC curve with the area under the ROC curve shown taken from Rodríguez-Hernández, Pruneda & Rodríguez-Díaz (2021).

4.1.9 Aims

1) To generate a comprehensive dataset of images using samples taken from the Hudson River.

2) To create an annotation system to classify objects in the dataset.

3) To train and test the dataset with the algorithms YOLOv5, YOLOv7 and YOLOv8 to determine the most appropriate algorithm for detecting microplastics by comparing the identification rates and metrics.

4.2 Method

4.2.1 Creation of the Dataset

The dataset was created using samples from the 2019 Hudson River expedition. See Section 3.2 for details on how the samples were collected. The samples were mounted on an Easylift® tape lift placed on a glass microscope slide. The images were taken on a Nikon Eclipse E400 POL polarised light microscope with a DS-L3 Nikon camera attachment. Each particulate of interest was photographed at each magnification (x40, x100, x200 and x400) under plane polarised light, and known synthetic microfibres were photographed twice at each magnification and under crossed polars at x400 magnification to observe their interference colours. A total of 13,992 images were taken these comprised of 8927 images from water samples from a saltwater environment to the freshwater source of the Hudson River. 3989 images taken from air samples; 330 images taken from soil samples. A further 746 images were taken of known textile fibres mounted with Easylift® a selection of these samples also used DEPEX as a mounting agent.

4.2.2 Annotation of the Dataset

Of the 13992 images taken 3102 images were annotated using the Computer Vision Annotation Tool (CVAT) (Sekachev *et al.*, 2020). There are many different objects that need to be accurately annotated to produce a comprehensive training data set. In this study, the objects were split into 21 classes.

4.2.2.1 Microfibre

Microfibres are microplastics that have longer length than width (Miller *et al.*, 2017) they are often shed from clothing. Microfibres tend to make up a large majority of the microplastics found within research (Kapp & Yeatman, 2018, Napper. *et al*, 2021 & Zaki *et al.*, 2021). They need a large representation in the data set due to this and the fact that there is a large variation in possbile fibre characteristics that need to be accounted for such as cross sectional shape and the presence of delusterant. See Figure 4.3 for examples of images of microfibres

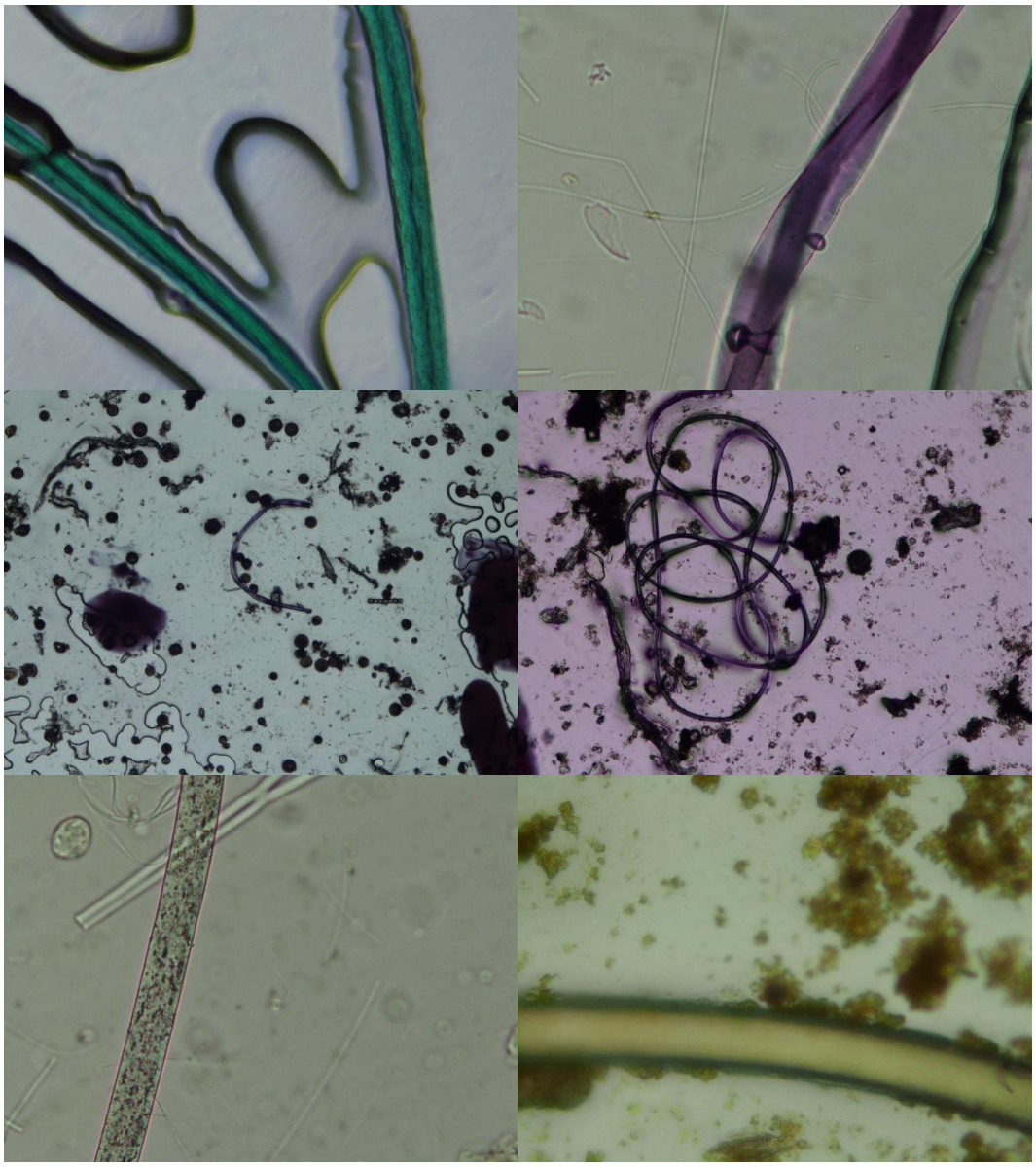

Figure 4.3 A selection of fibres, top left green Bilobal fibre x400, top right purple trilobal fibre x400, middle left blue square fibre x40, middle right long blue cylindrical fibre x100, bottom left colourless cylindrical fibre with delusterant x400, bottom right colourless cylindrical fibre x400.

4.2.2.2 Fragment

Fragments are produced through the degradation of larger items of plastic and often have an irregular shape and jagged edges (Hidalgo-Ruz *et al.*, 2012). They are often found in microplastic studies and are the second most abundant type of microplastic behind fibres (Leads & Weinstein, 2019 & Zaki *et al.*, 2021). A large number of blue fragments were found during this study, so there may be an overrepresentation of blue fragments within the data set. See Figure 4.4 for examples of images of fragments.

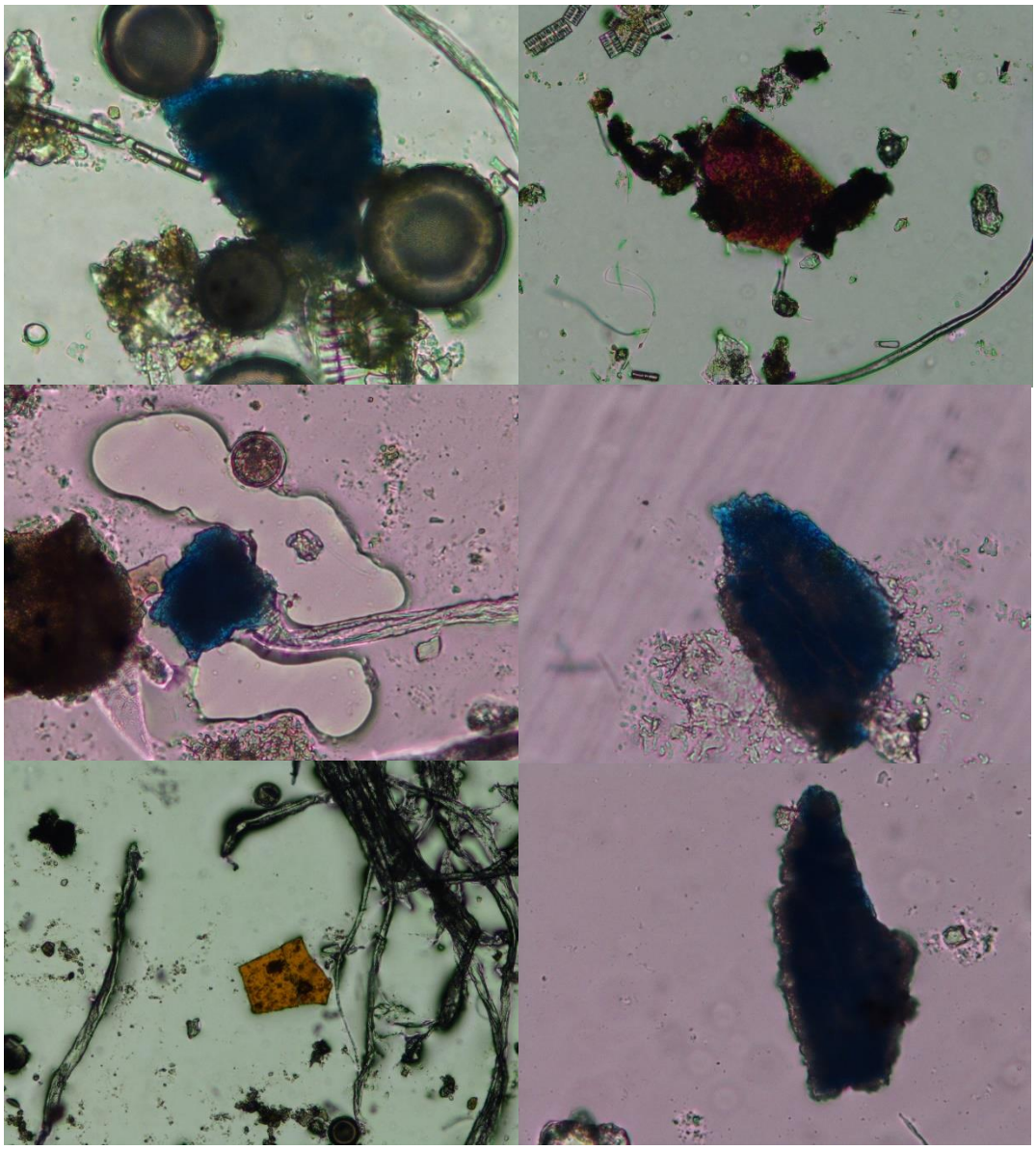

Figure 4.4 A selection of fragments, top left blue fragment x400, top right red fragment x200, middle left blue fragment x400, middle right blue fragment x400, bottom left orange fragment x200 bottom right blue fragment x400.

4.2.2.3 Microbead

Microbeads are small spherical microplastics that are manufactured for facial scrubs (Ziajahromi *et al.*, 2017); their concentrations are relatively low compared to the other microplastic types at 5% (Liu *et al.*, 2019) or not at all (Free *et al.*, 2014 & Lv *et al.*, 2019a). Very few microbeads were found in this study, meaning that there will be an underrepresentation of microbeads in the training data set. See Figure 4.5 for examples of images of microbeads.

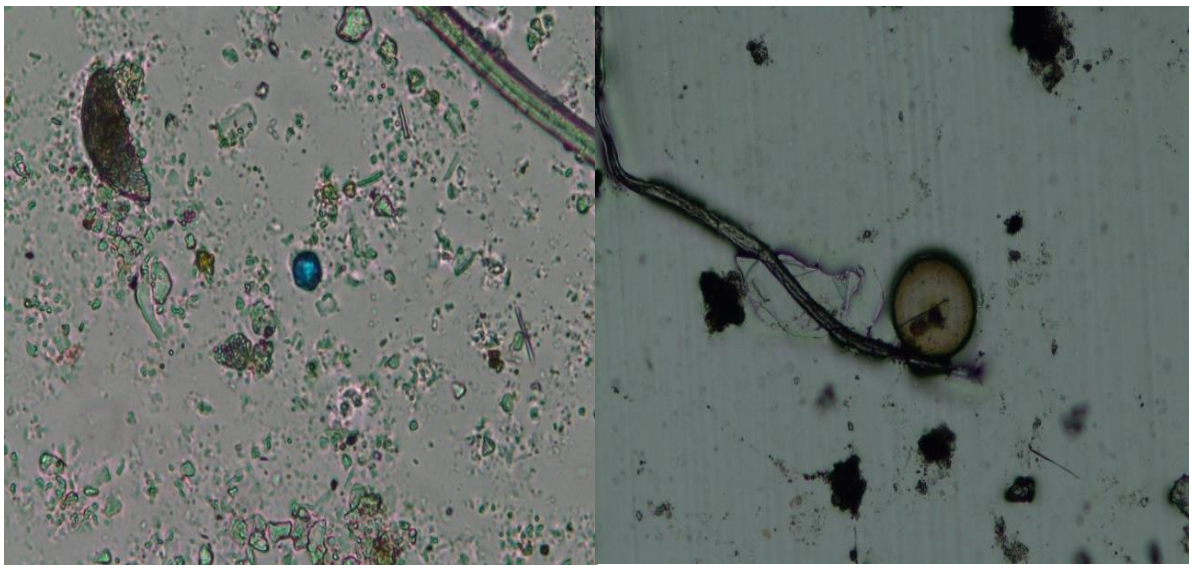

Figure 4.5 Left a blue microbead x400, right a colourless microbead x100.

4.2.2.4 Film

Films are thin pieces of plastic created from the breakdown of larger items of plastic, such as plastic bags (Free *et al.*, 2014). Their concentrations can vary depending on the medium being investigated, with 12-18% having been found in WWTPs (Blair, Waldron & Gauchotte-Lindsay, 2019 & Lv *et al.*, 2019a) to very low levels in river sediment (Horton *et al.*, 2017). Very few films were found in this study, meaning that there will be an underrepresentation of films in the training data set. See Figure 4.6 for an example of a film.

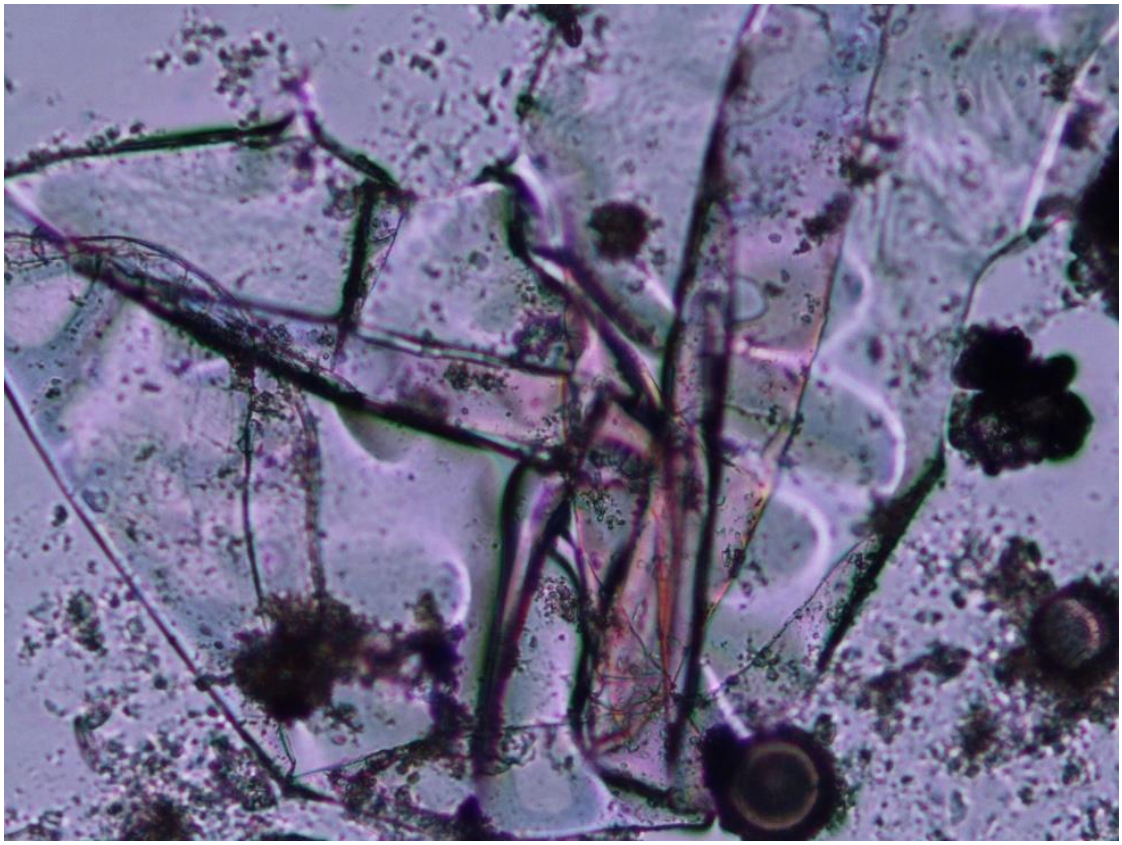

Figure 4.6 A colourless film x400.

4.2.2.5 Background Material

Background material encompasses all the sediment, silt and debris that will be present in any natural sample that is taken. The levels and types of background material vary depending on the sample type, with air samples containing less background material and soil samples the most. The levels also vary depending on where the sample was taken, with samples taken at the bottom of the water column tending to contain more debris than those at the surface. Figure 4.7 shows examples of images of background material. However, there can still be a large number of background material tags in images that are not overwhelmed with background material. This is demonstrated in Figure 4.8, which shows the number of background material tags that are still needed in images where there appears to be very little background material and debris.

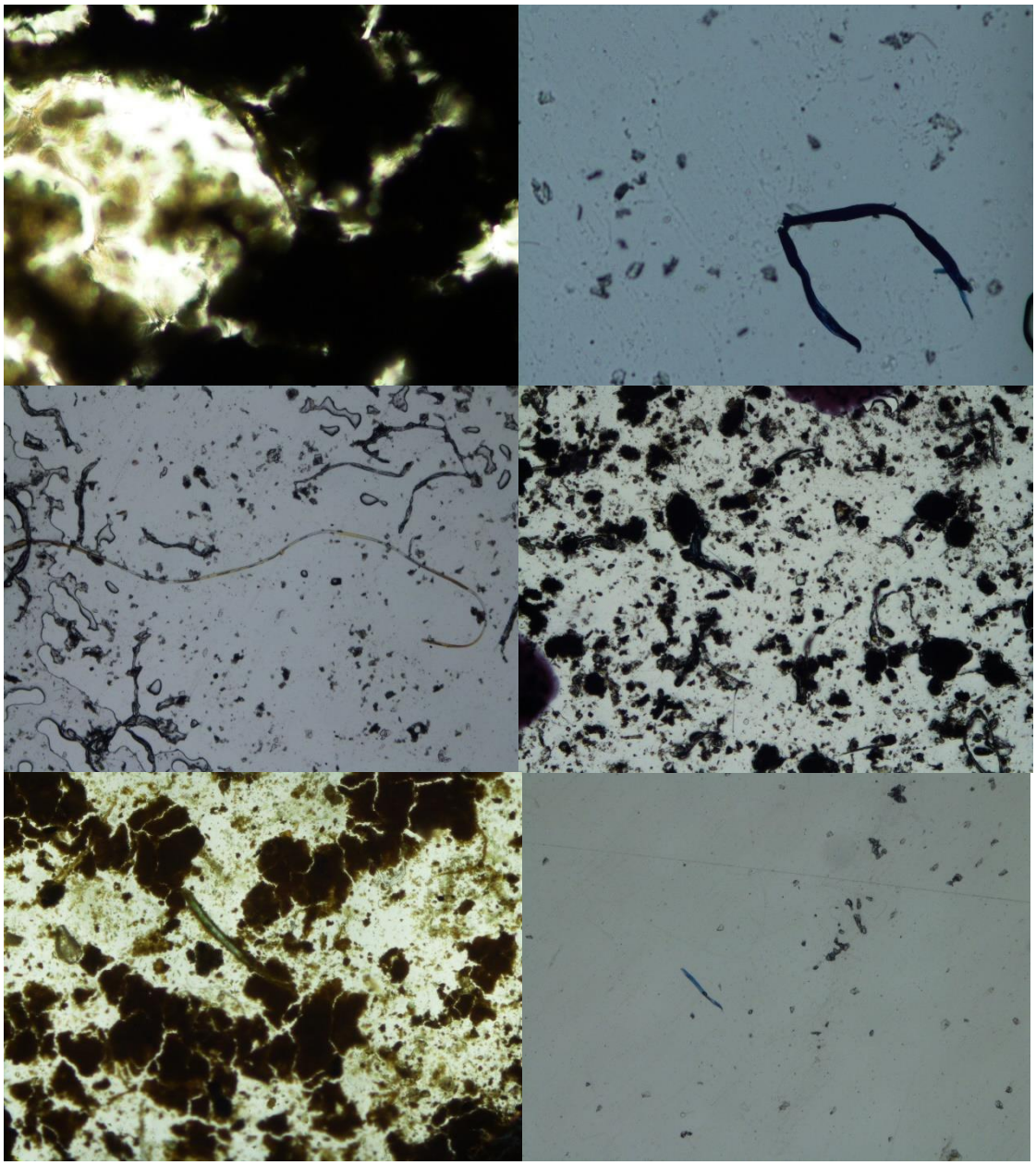

Figure 4.7 a selection of images to show the different levels of background materials that could be present in the images. Top left an image of a soil sample showing a microfibre being masked by background material x100, top right an air sample showing a piece of cotton with minimal background material x100, middle left a water sample from the middle of the water column x40, middle right a water sample from the bottom of the water column x40, bottom left a soil sample x40, bottom right an air sample x40.

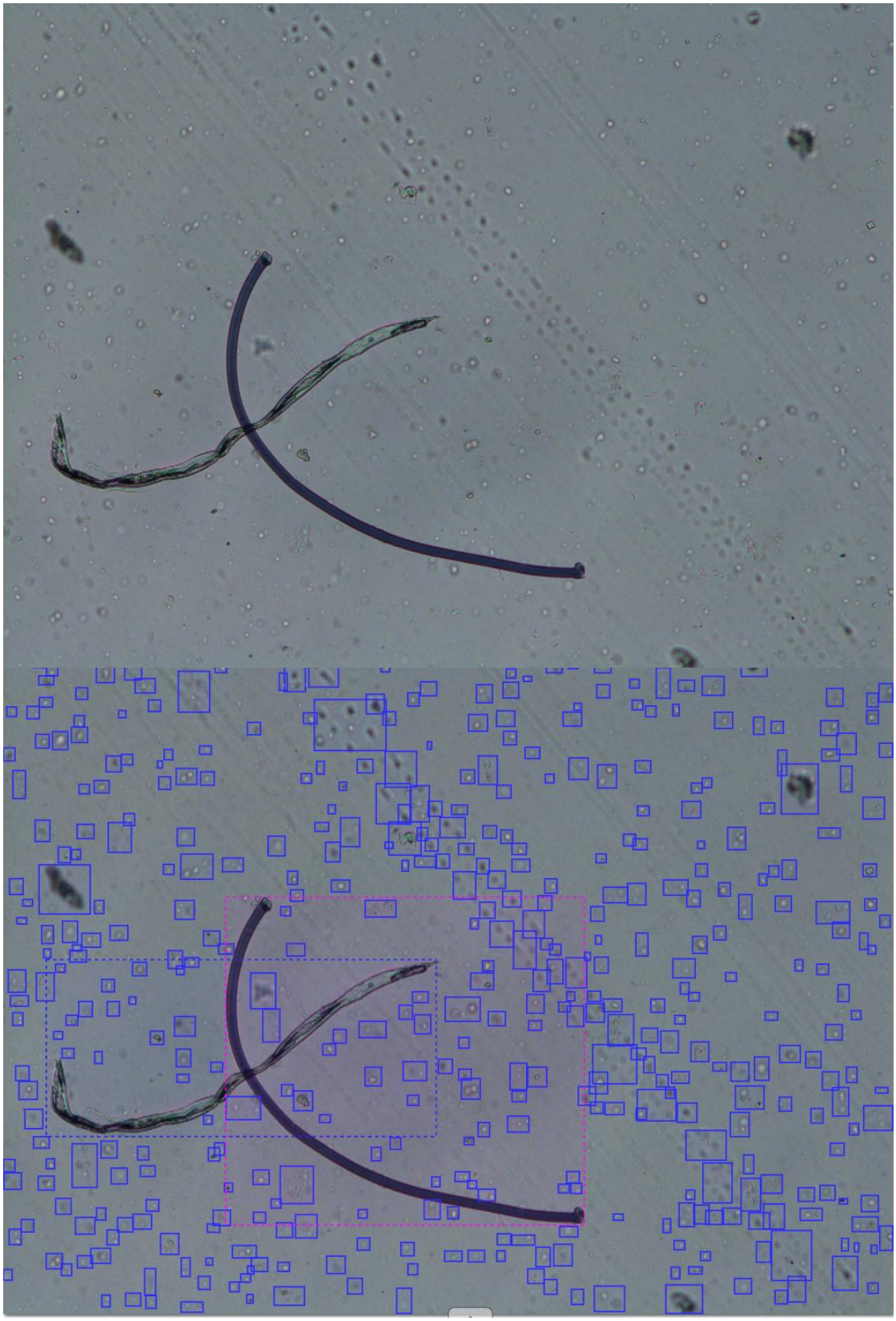

Figure 4.8 An image of a blue microfibre from an air sample without tags (top) and with tags (bottom) images to demonstrate the number of background material tags needed in an image that appears relatively clean.

4.2.2.6 Cellulose Filter Fibre

Cellulose filter fibres were used for the water samples and are frequently collected by the Easylift® tape. As the filter paper is cellulosic, it is difficult to differentiate colourless cotton fibres from cellulose filter fibres (Gwinnett, Osborne & Jackson, 2021). Examples of cellulose filter fibres can be seen in Figure 4.9, with some examples annotated in red boxes.

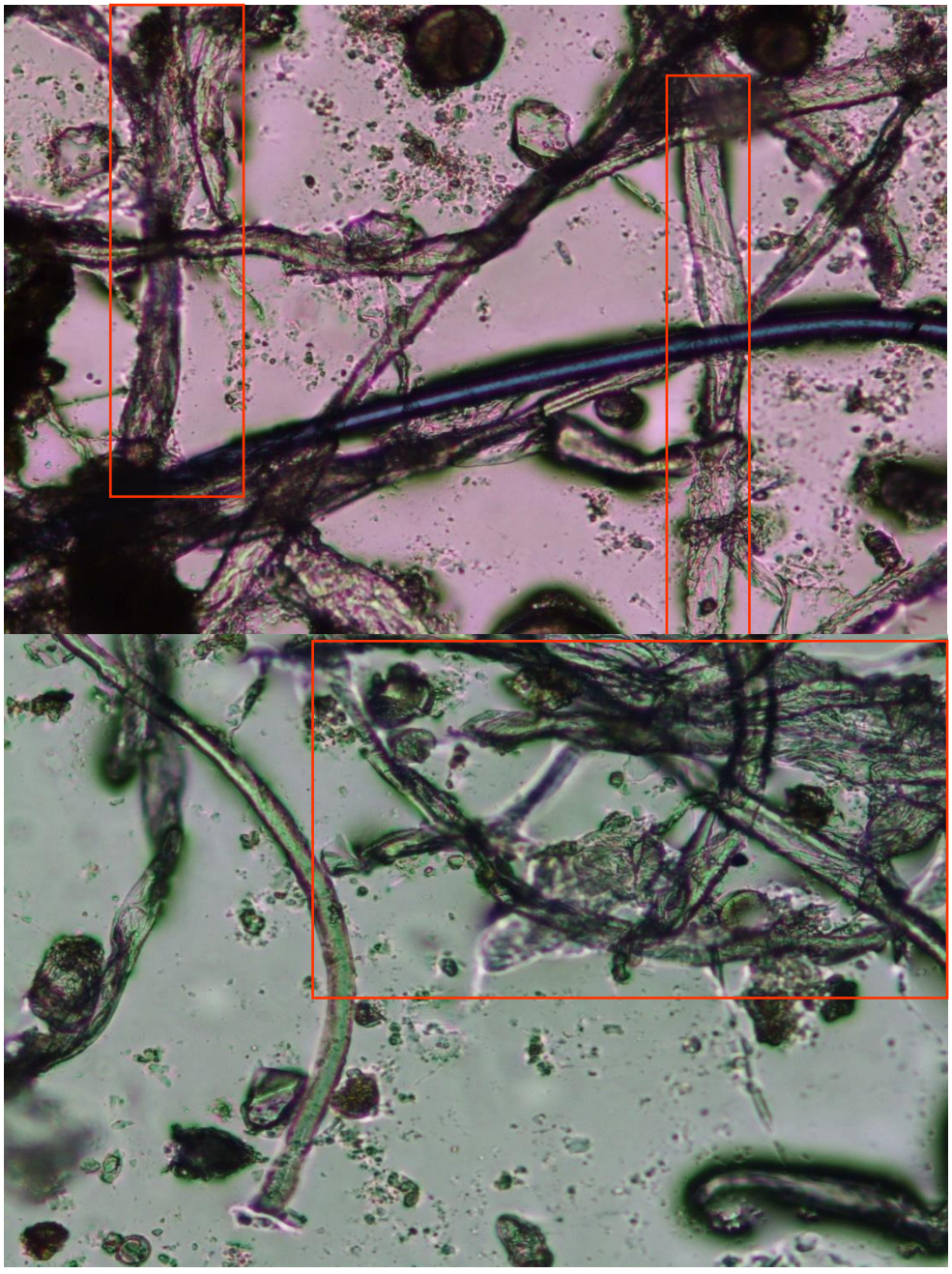

Figure 4.9 Two images showing examples of images with cellulose filter fibre present x200.

4.2.2.7 Glass Filter Fibre

Glass filter fibre paper was used for the air samples during this study. These thin cylindrical fibres do not exhibit any birefringence. They sometimes fold over and resemble the eye of a needle. Figure 4.10 shows some examples of images with glass filter fibres; some examples have been highlighted with red boxes.

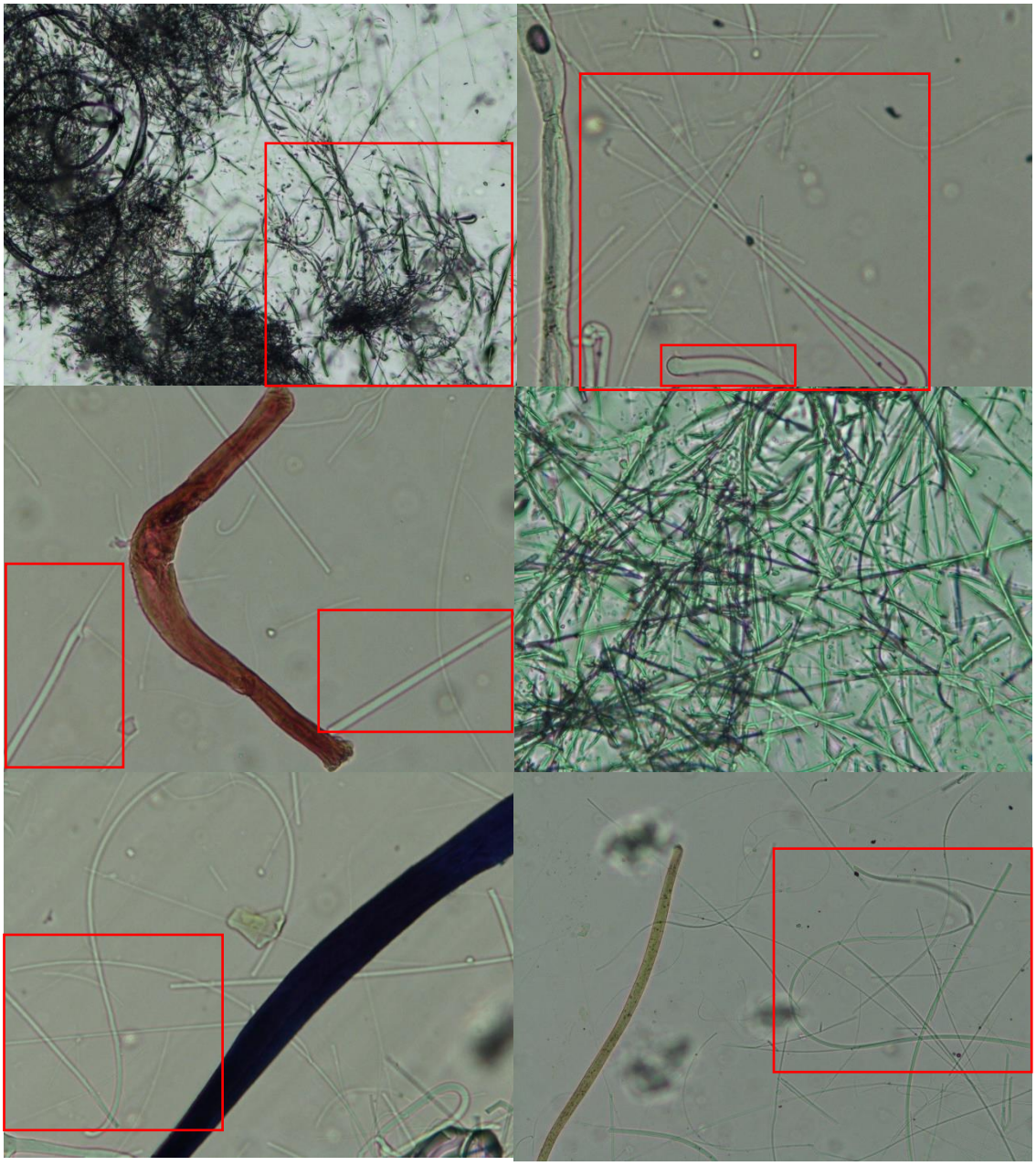

Figure 4.10 A selection of images displaying glass filter fibres. Top left a high-density collection of glass filter fibres x100, top right a colourless cotton fibre surrounded by glass filter paper x400, middle left red microfibre surrounded by glass filter fibres x400, middle right a collection of glass filter fibres x400, bottom left blue cotton fibre surrounded by glass filter fibre x400, bottom right yellow microfibre surrounded by glass filter fibres x200.

4.2.2.8 Diatom

Diatoms are eukaryotic phytoplankton that occur in all the world's oceans rivers and lakes. Their appearance depends on the aquatic environment in which they are located (Zhou *et al*., 2020). Some diatoms can appear similar to microplastics, for instance, microbeads. Examples of the different diatoms found can be seen in Figure 4.11.

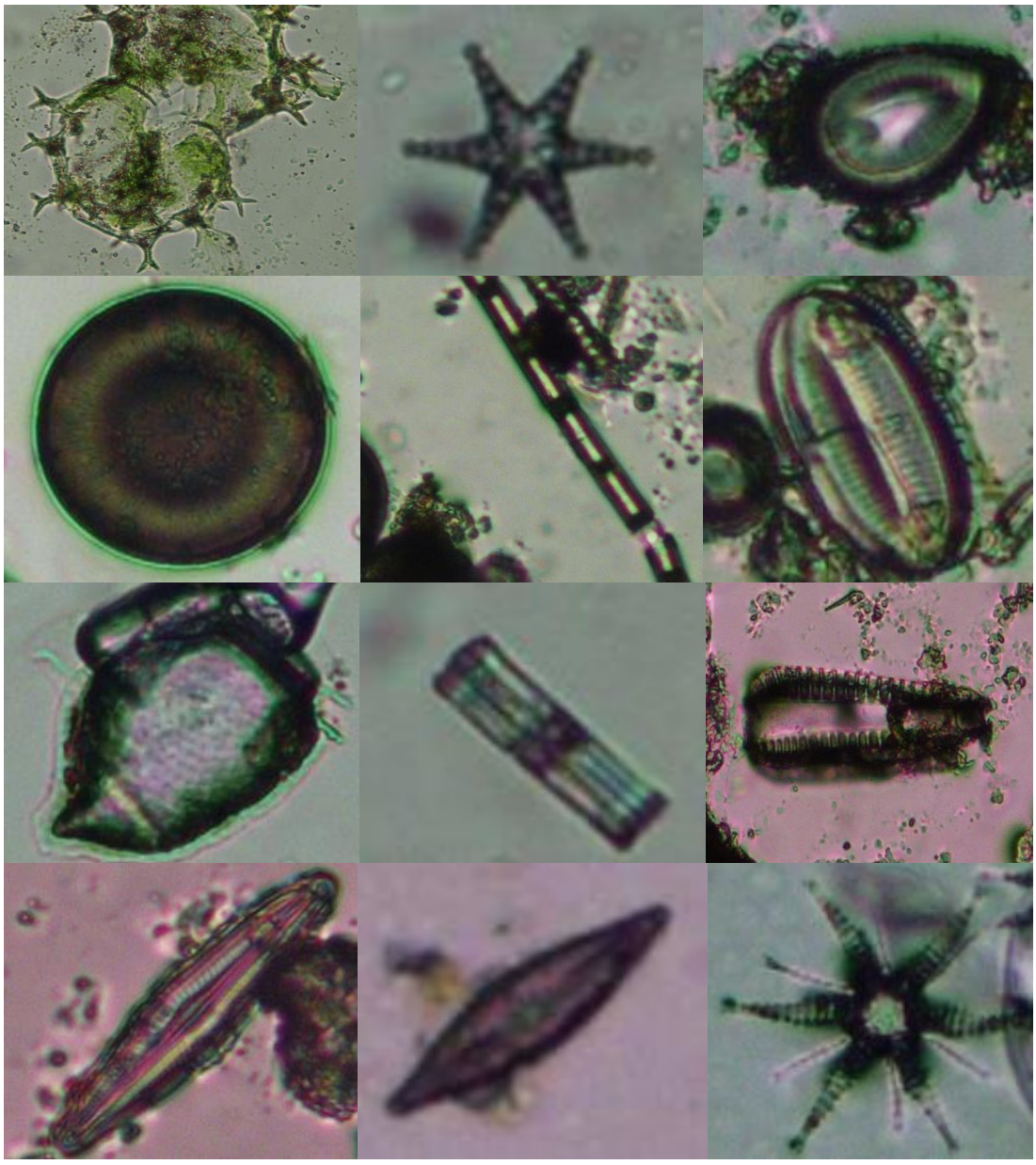

Figure 4.11 A selection of some of the different types of diatoms encountered along the Hudson River.

4.2.2.9 Cotton

Cotton fibres were often encountered in the samples taken as the crew wore blue cotton t-shirts. Being able to identify cotton fibres is of interests as while they are not synthetic, they are anthropogenic in nature and have often been dyed which may also be harmful to the environment. Examples of cotton fibres can be seen in Figure 4.12.

Figure 4.12 Top left a colourless cotton fibre x100, top right red cotton fibre x200, bottom left blue cotton fibre x400, bottom right blue cotton fibre x400.

4.2.2.10 Hair

This tag includes all hair that cannot be attributed to textile use this includes human hair and some animal hair that has made its way into the sample. Hair can appear very similar to microfibres. Examples of hairs can be seen in Figure 4.13.

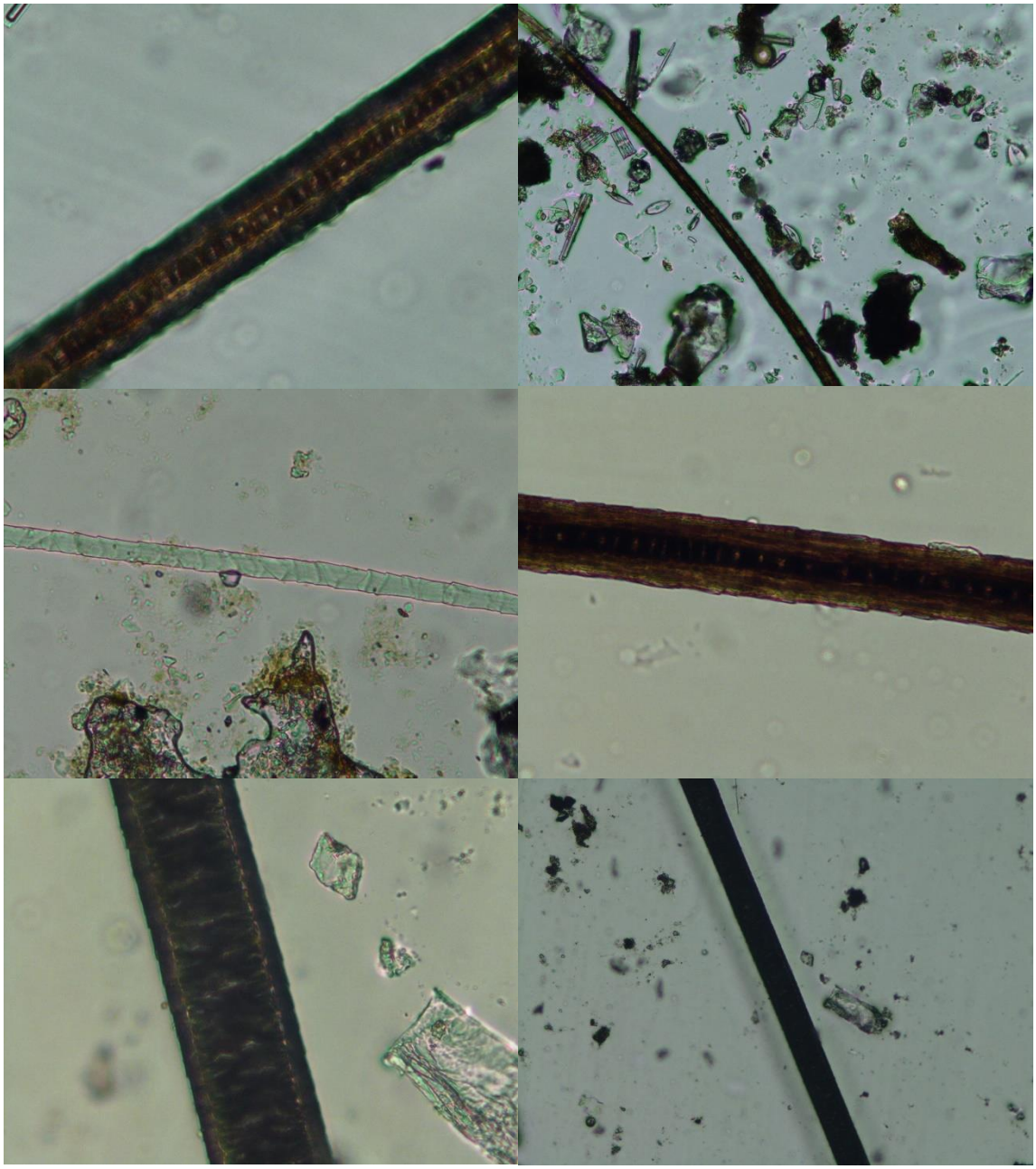

Figure 4.13 A selection of different hairs, top left brown hair x400, top right brown hair x200, middle left colourless hair x400, middle right x400, bottom the same brown hair x 400 (left) x 100 (right).

4.2.2.11 Hair Textile

Textile hairs include items such as wool and hairs that are processed or dyed, making them anthropogenic in origin. The most common feature of these fibres is the presence of dye. Examples of textile hairs can be seen in Figure 4.14.

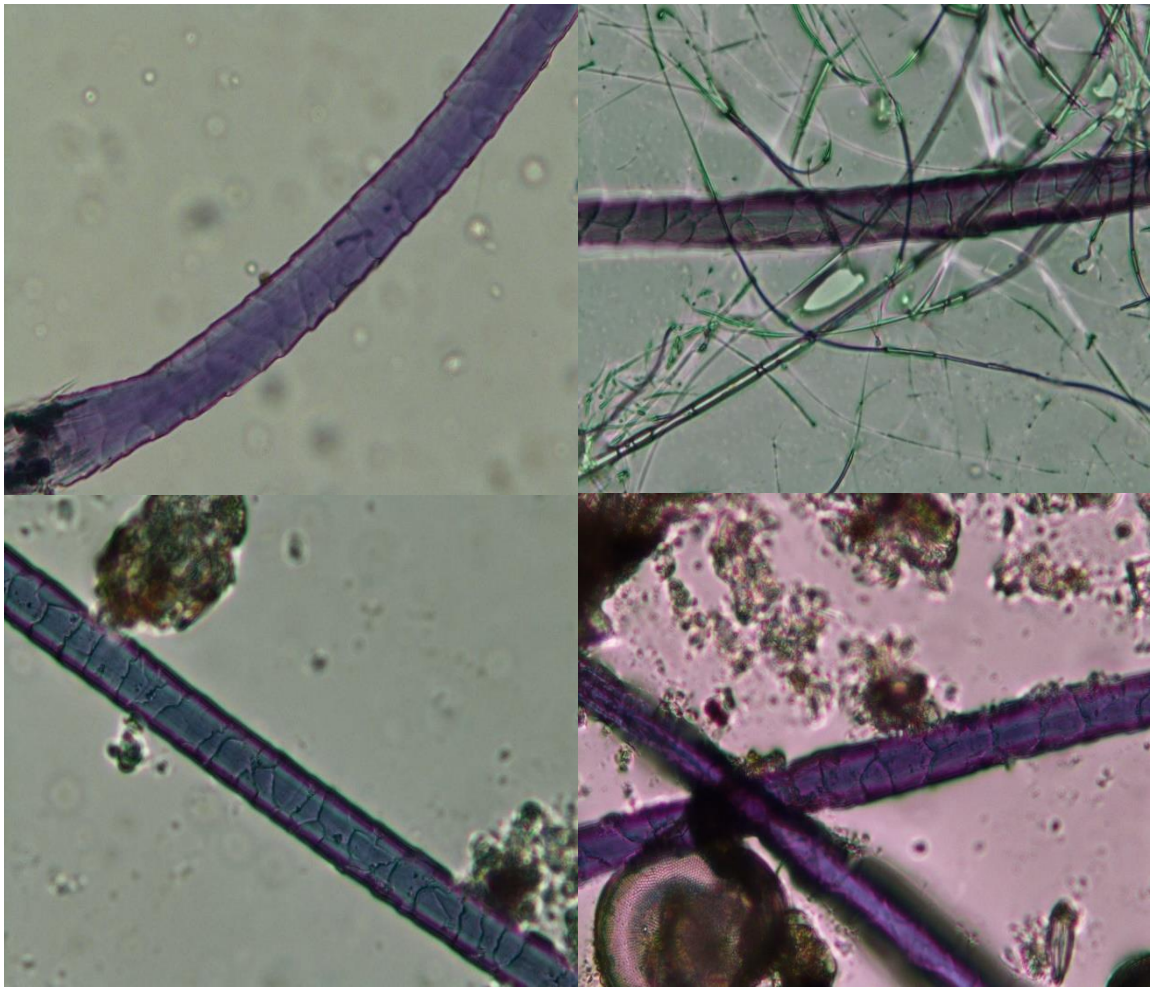

Figure 4.14 A selection of blue textile hairs x400.

4.2.2.12 Air Bubble

Air bubbles can form on the tape lift as the excess water evaporates of the slide, some of the air bubbles can appear visually similar to dark fibres. Examples of images containing air bubbles can be seen in Figure 4.15.

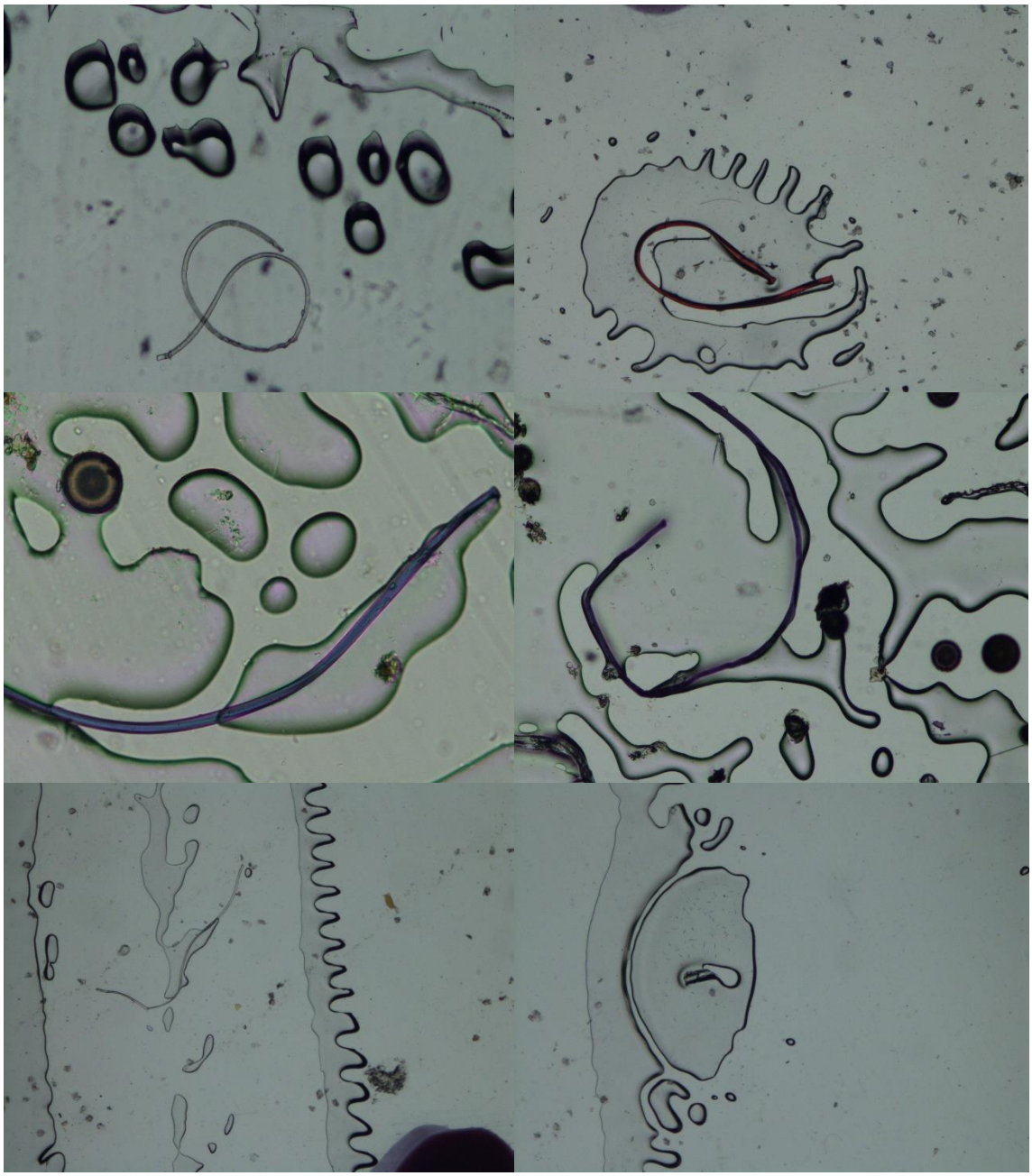

Figure 4.15 A selection of images of air bubbles, top left a colourless microfibre surrounded by air bubbles x100, top right a red microfibre within an air bubble x40, middle left blue microfibre surrounded by air bubble x200, middle right blue microfibre surrounded by air bubbles x100, bottom left colourless microfibre surrounded by air bubbles x40, bottom right small colourless microfibre within an air bubble x40.

4.2.2.13 Pen

Pen was used to mark the slide during the searching stage to indicate where a potential anthropogenic particulate was on the slide; as such, it appears in several photos. Examples of images containing pen can be seen in Figure 4.16.

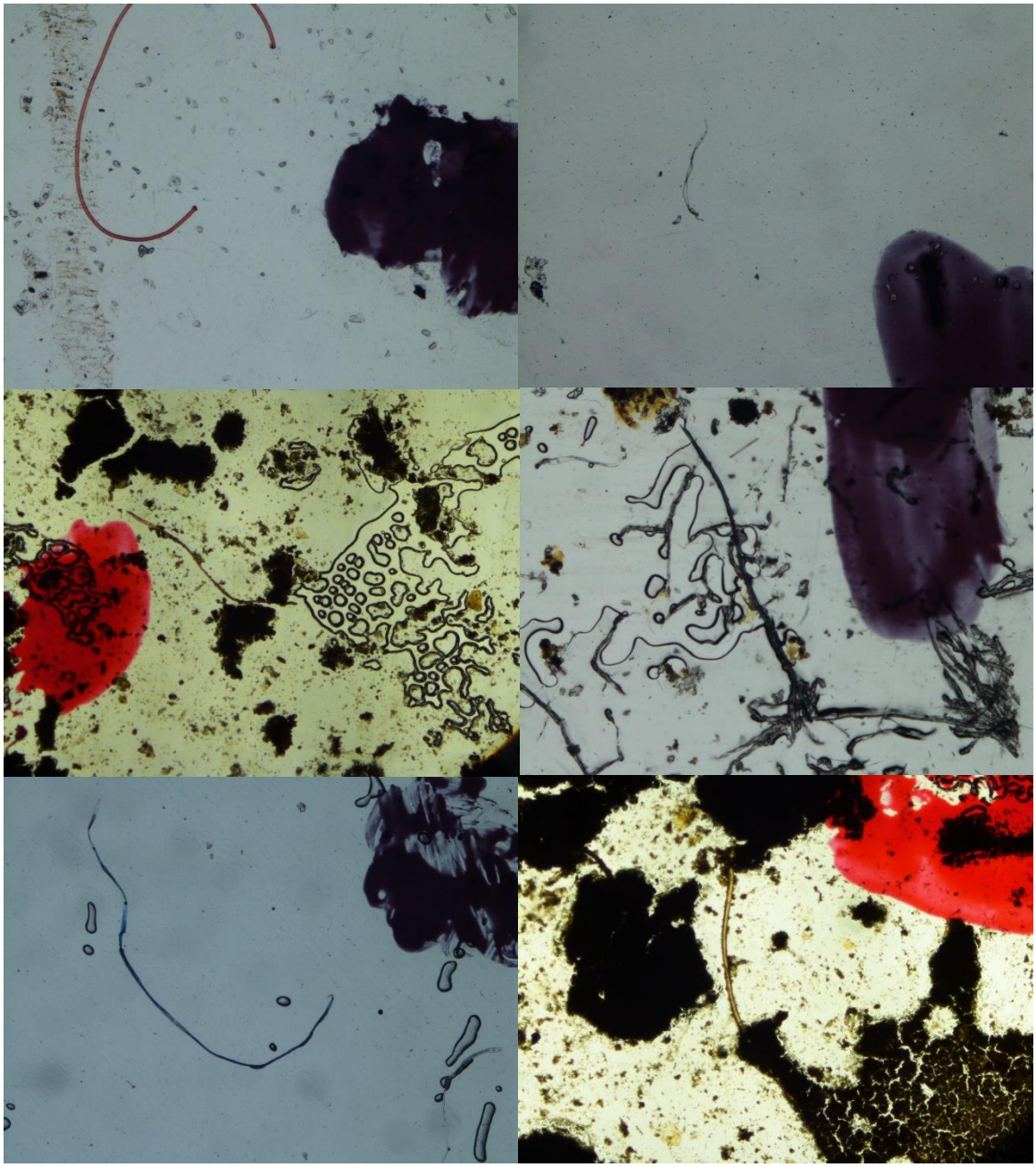

Figure 4.16 A selection of images demonstrating the use of pen to mark areas of interest in the slide x40.

4.2.2.14 Natural Material

This tag encompasses any natural material that may be present on the slide this includes plant matter, minerals and natural fibres that are not of anthropogenic origin. Examples of natural materials present in the samples can be seen in Figure 4.17.

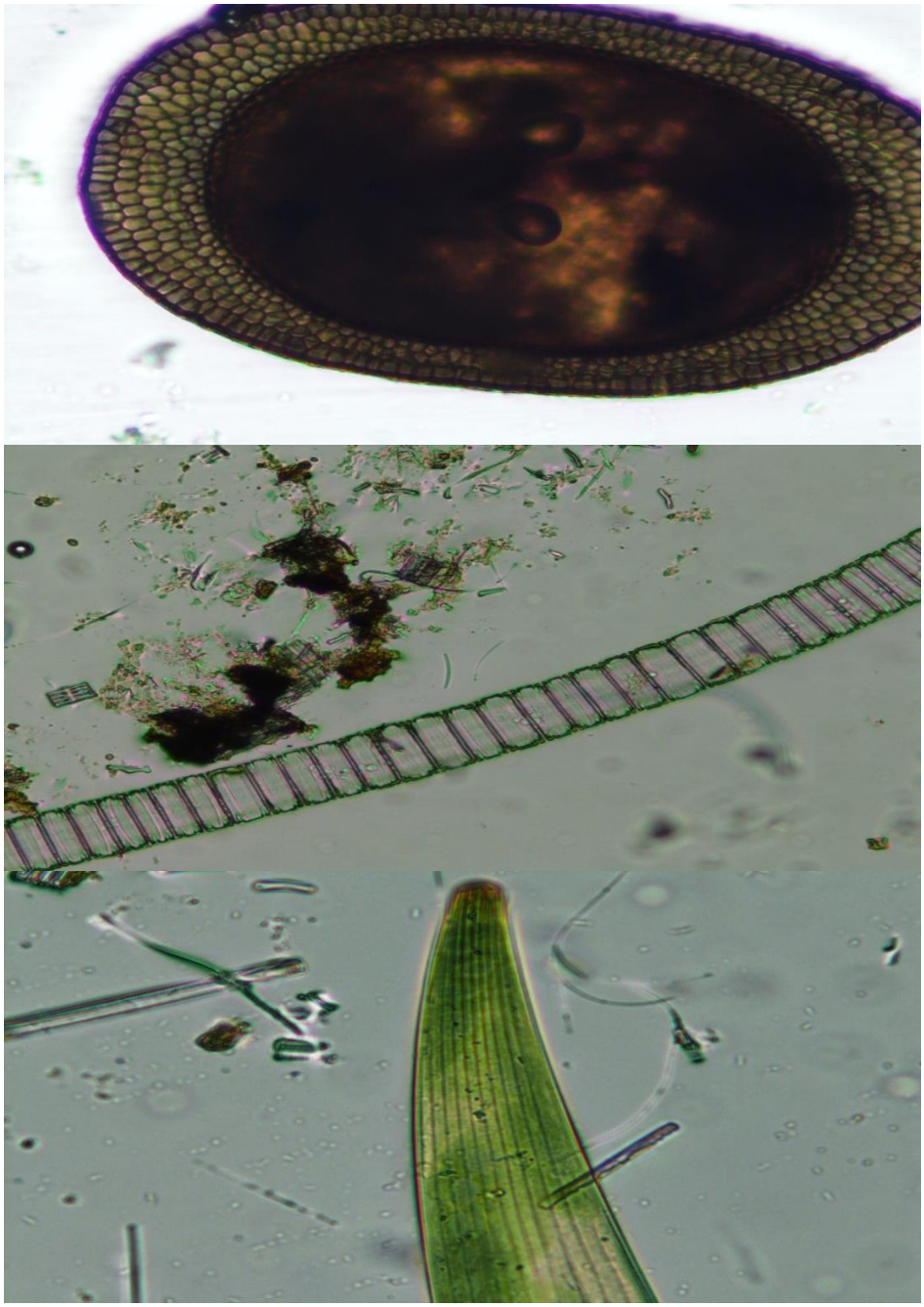

Figure 4.17 Three images demonstrating natural material.

4.2.2.15 Insect Matter

As the samples are from a natural environment, there will be a level of insect matter found in the sample. This includes aquatic insects and terrestrial insects that have made their way into the water samples. Some examples of the insect matter found in the samples can be seen in Figure 4.18.

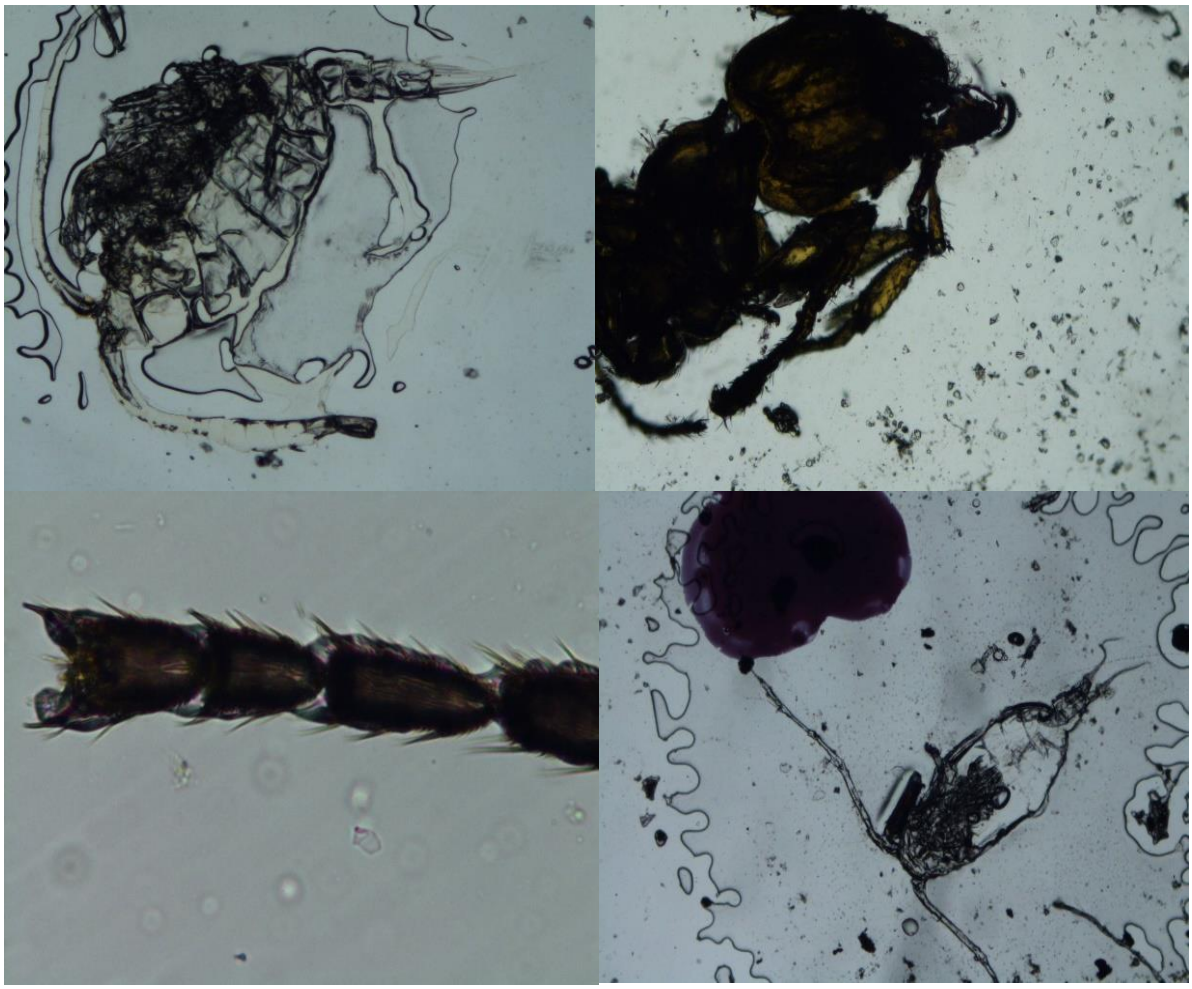

Figure 4.18 Top left an aquatic insect x40, top right an ant x 400, bottom left a spider leg x400, bottom right an aquatic insect x40.

4.2.2.16 Salt

Salt naturally occurs in aquatic systems in different concentrations; as the water evaporates, it will leave behind salt crystals that may crystalise onto an anthropogenic particulate. Examples of salt crystals can be seen in Figure 4.19.

Figure 4.19 Examples of salt crystals.

4.2.2.17 Edge of Slide

Some of the anthropogenic particulates are located near the edge of the microscope slide meaning that it will appear in some of the images and so needs to be included in the annotations. Examples of images showing the edge of the slide can be seen in Figure 4.20.

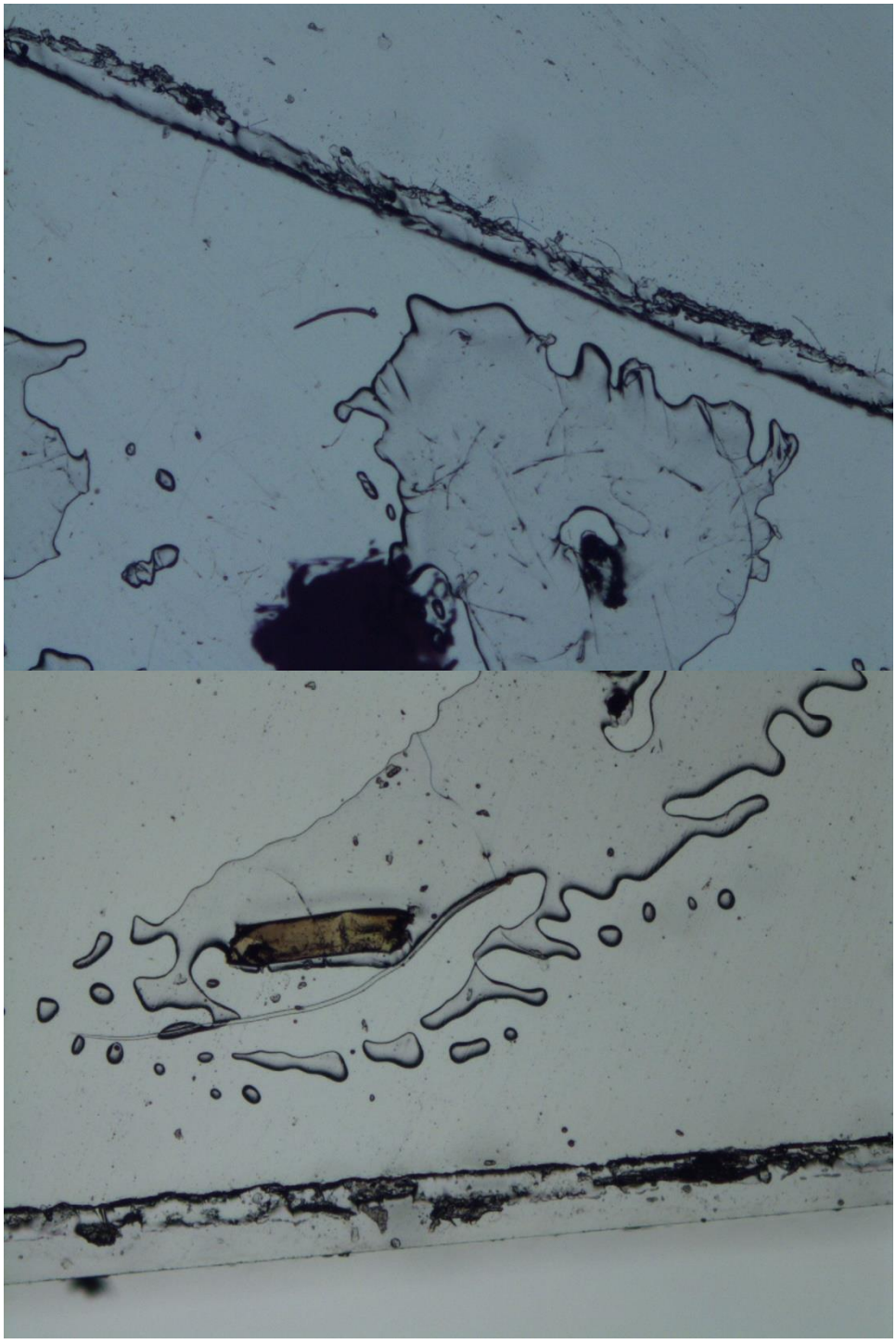

Figure 4.20 Two images showing the edge of the microscope slide x40.

4.2.2.18 Easylift® Tab

In the same way that the edge of the slide can be in some of the images the blue tab of the Easylift® tape also appears in some of the images when items of interest are positioned near to it. Examples of images showing the Easylift® tab can be seen in Figure 4.21.

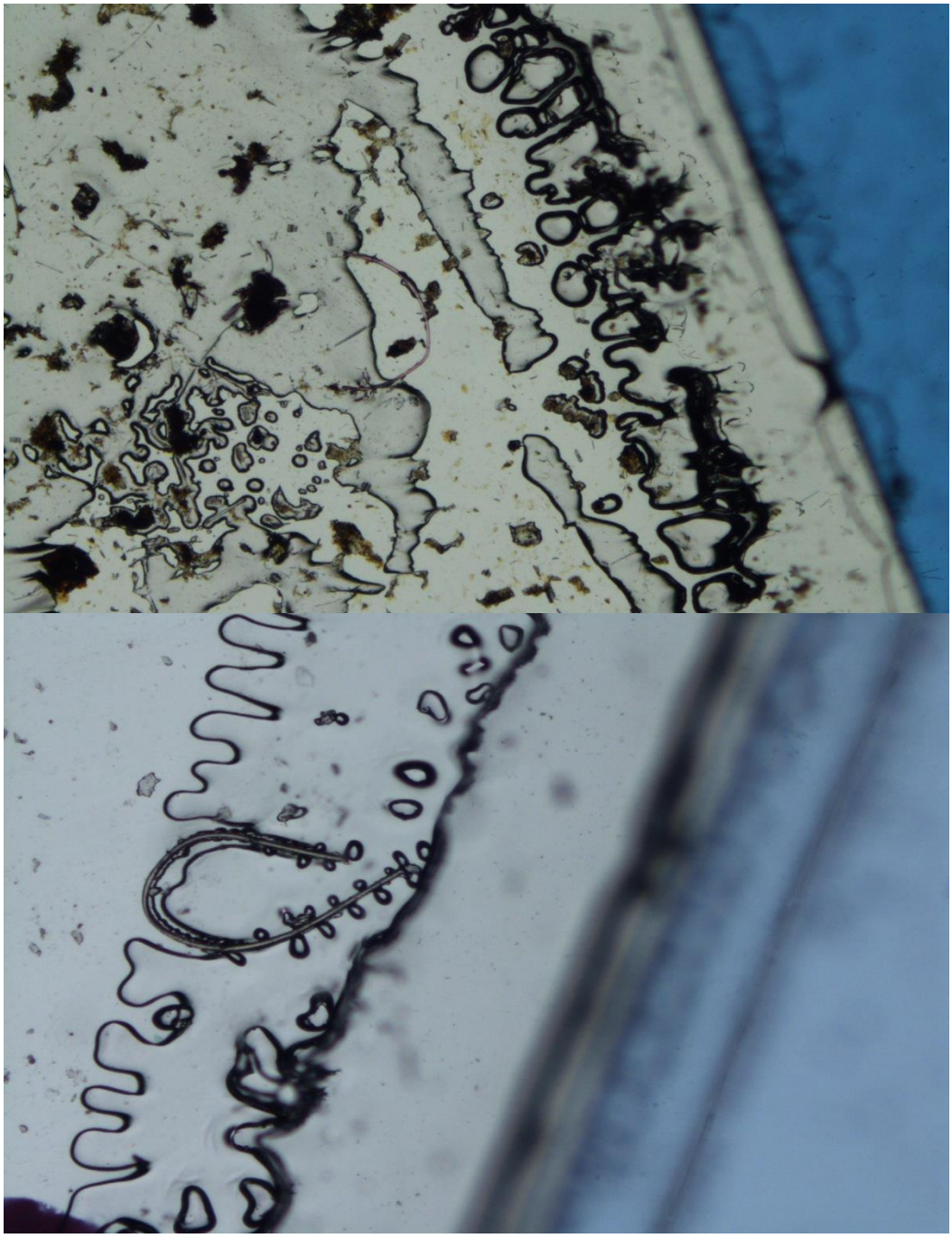

Figure 4.21 Two images that shows Easylift®'s blue tab in the image x40.

4.2.2.19 Sand

Sand was present in the soil samples, and some of the bottom of the water column samples were particularly murky. An example of an image with sand can be seen in Figure 4.22.

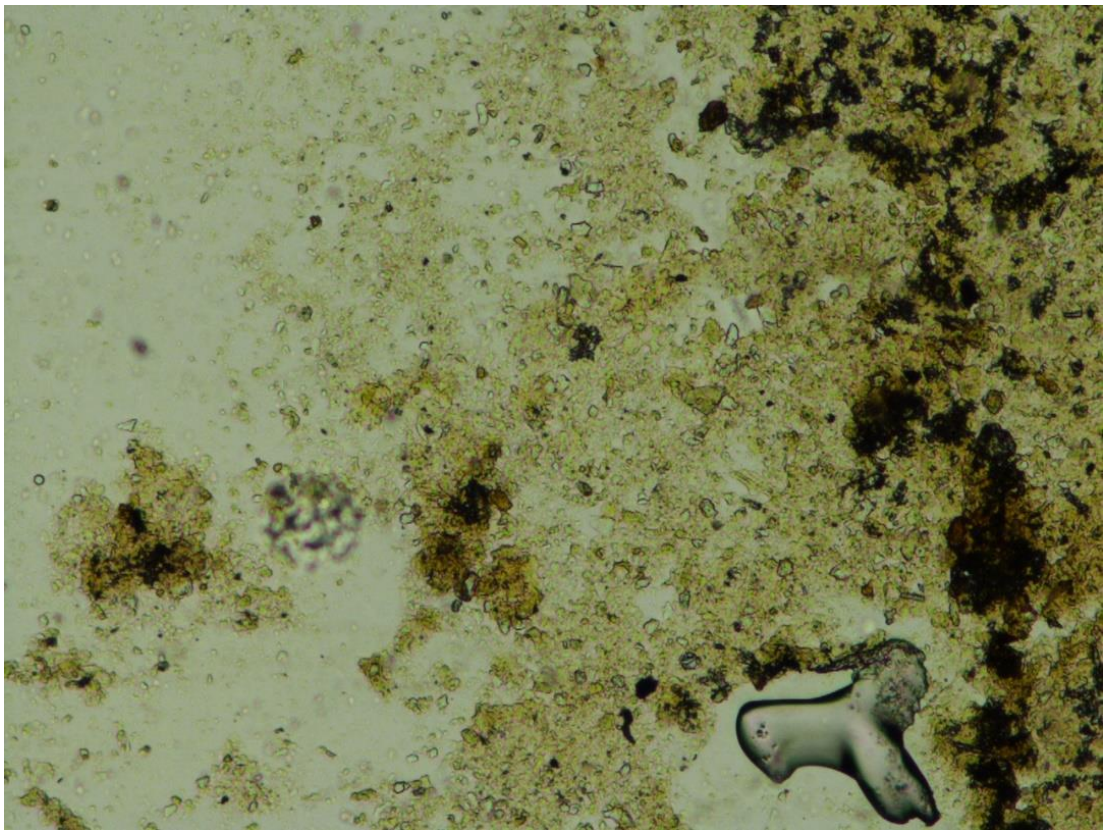

Figure 4.22 An image of a sample slide that contains sand x100.

4.2.2.20 Anthropogenic

Some items cannot be conclusively identified but are known to be of anthropogenic origin either through the presence of dye or internal characteristics for example cotton fibres can identified by its kidney shaped cross sectional shape, the presence of a lumen and convulsions along the length of the fibres (Gordon, 2009). Type of anthropogenic fibres include materials such as cupro, viscose, and other cellulosic fibres. Some examples of anthropogenic fibres can be seen in Figure 4.23.

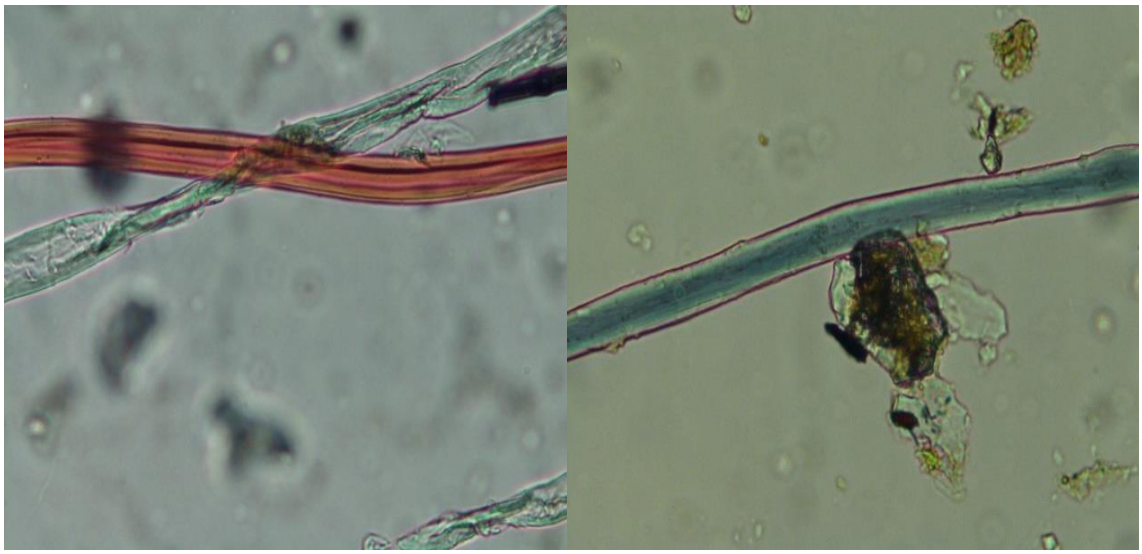

Figure 4.23 Two examples of fibres that were identified as anthropogenic x400.

4.2.2.21 Unknown

Some material found during analysis could not be definitively identified and so were given the identification of unknown. An example of something with an unknown classification can be seen in Figure 4.24.

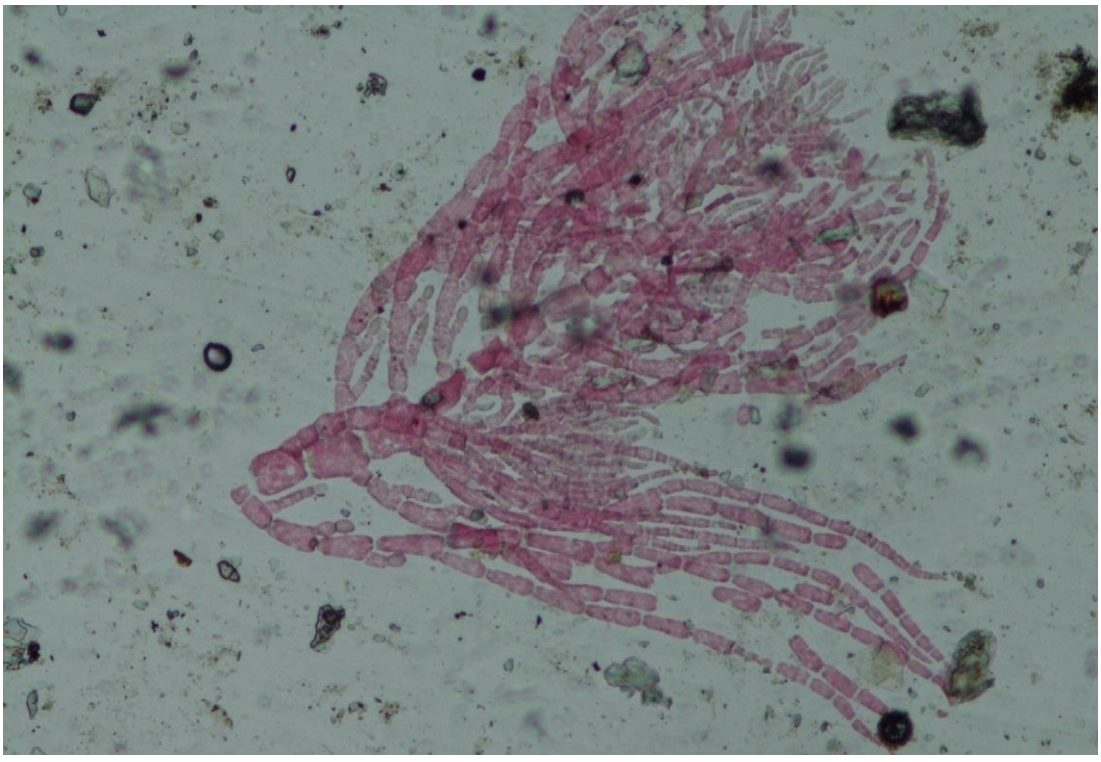

Figure 4.24 An Image of something that was given the unknown classification x200.

4.2.3. Training the Dataset

The 3102 images and annotations were uploaded to Roboflow (Dwyer & Nelson, 2022) and split into training, validation, and test set with a 70% (2171), 20% (621), 10% (310) split as this split has previously been used in literature (Xi *et al.*, 2020, Revi *et al.*, 2021, Effendi, Ramadhan & Hidayat, 2023. & Himami, Bustamam & Anki, 2021). Table 4.3 shows the breakdown of the populations of the different classifications used.

A second dataset was created by randomly augmenting the training images using Roboflow. The augmentations used were flipped horizontally and vertically, rotated 90 ° clockwise, counterclockwise, and upside down, and a 4% blur was applied. This increased the number of training images to 6504.

Table 4.3 A table to show the number of each class represented in the 3102 images in the dataset.

Class	Total	Train	Validation	Test
All	260818	180012	55121	25685
Air bubble	14323	10101	2796	1426
Anthropogenic	39	30	6	3
Background material	224347	155060	47202	22085
Sand	0	0	0	0
Cellulose filter paper	4023	2719	917	387
Cotton	1081	709	248	124
Diatom	10144	6695	2434	1015
Easylift® tab	11	7	4	0
Film	0	0	0	0
Edge of slide	55	37	13	5
Fragment	281	257	89	35
Glass filter fibre	3384	2267	823	294
Hair textile	74	56	11	7
Hair	75	58	11	6
Insect matter	11	8	3	0
Microbead	4	3	1	0
Microfibre	2075	1480	387	208
Natural material	182	121	38	23
Pen	524	347	116	61
Salt	72	48	18	6
Unknown	13	9	4	0

Training was undertaken with YOLOv5 (Jocher *et al.*, 2022), YOLOv7 (Wang, Bochkovski & Liao, 2022) and YOLOv8 (Jocher, Chaurasia & Qiu, 2023) three times each to test if different settings would help improve the models performance. They were trained once with 25 epochs (the number of times the whole dataset is passed through the algorithm) (Li *et al.*, 2021, & Ghosal & Sarkar, 2020), once with 100 epochs (Li *et al.*, 2021., Chen, Yoo & Fang, 2022. & Ieamsaard, Charoensook & Yammen, 2021), and once with the augmented training set with 100 epochs. The training was conducted using public Google Collaborate notebooks using the V100 GPU by following the open-source code provided in each notebook.

4.3 Results and Discussion

The images taken on the Hudson River were used in this study as they encompass a wide range of environmental conditions, from freshwater to salt water. Meaning that they would generate a comprehensive data set that would contain a wide range of different materials as the environment changed, e.g. the levels of salt or the population of diatoms changes along the course of the river. The images were also from environmental samples meaning that they would be representative of the type of samples being taken in microplastic research and so the resulting models should be able to cope with any environmental microplastic sample. Controlled laboratory images were also included in the dataset to increase the representation of microfibres in the dataset and to include some fibre types that were not well represented in the dataset such as bilobal fibres and green fibres.

The Classes laid out in Section 4.2.2 were chosen to account for anything that was likely to appear in the sample images was able to be placed into one of the classifications. A large number of classes were chosen as opposed to ‘microplastic’ or ‘not microplastic’ so that information could be gleaned about what classifications are being confused for others, meaning that the dataset can be better evaluated. It also meant that the classification of anthropogenic materials that would have fallen into ‘not microplastic’, such

as cotton, could also be identified by the resulting model, allowing for greater detail to be gained from the samples being investigated.

A 70:20:10 split was used as it is a commonly used breakdown of data in machine learning (Xi *et al.*, 2020. Revi *et* al., 2021. Effendi, Ramadhan & Hidayat, 2023. & Himami, Bustamam & Anki, 2021). Himami, Bustamam & Anki (2021) trialled a 70:20:10 split and a 60:20:20 split to detect pathologic myopia; they found that the 70:20:10 split overall performed the best in the majority of models produced.

YOLO was selected as the algorithm being investigated as it is one of the faster single-stage detectors available, being able to identify and classify objects in a single pass-through of the network (Nelson, 2021). It is also frequently used in research (Yang *et al.*, 2023a, Talaat & ZainEldin, 2023, Jung & Choi, 2022. & Naseri & Ali, 2022). As it has the advantage of speed it lends itself to detecting and classifying the microplastics in real time (Naseri & Ali., 2022). The ability to detect in real time would be invaluable to microplastic research and greatly speed up the analysis process allowing research to be completed in shorter periods of time. In addition YOLO has several other advantages over other traditional algorithms such as Random Forest or R-CNN including that it uses a global context awareness when analysing the images, meaning that the algorithm looks at the entire image and uses context from that background to help inform identifications reducing the number of false positives when there are complex backgrounds (Redmon *et al.*, 2016). YOLO is also able to maintain a high accuracy when dealing with images that contain overlapping objects and multiple object classification by applying techniques such as non-maximum suppression (Buhl, 2024) both of which are features very commonly seen in images of microplastic samples.YOLOv5 was selected as one of the versions of YOLO to test as it was the first of the YOLO models to connect predicting bounding boxes with the class labels for an end-to-end differentiable network and performed better and was faster than the previous iterations of YOLO (Solawetz., 2020). It also has the benefit of a small memory requirement and the ability to be used in real-time with a better background area distinction in comparison to other models (Shishkin & Grekov, 2023). In addition YOLOv5

can very easily be scaled and applied on mobile devices allowing in field analysis to be undertaken (Solawetz, 2020).YOLOv7 was also chosen as it had a different structure to YOLOv5 through the addition of the extended efficient layer aggregation and adding model scaling techniques and has been shown to have a faster and more accurate performance (Solawetz, 2024). YOLOv8 was selected as, at the time of training it was the latest version of YOLO available. In addition, it has a measured high level of accuracy (Solawetz. & Francesco, 2024). YOLOv8 also has have several architectural changes in comparison to YOLOv5 (Solawetz. & Francesco, 2024). YOLOv8 does not use any anchors, meaning that it implies rather than predicting distance from a known anchor box, and it estimates the centre of the object (Nelson, 2021).

4.3.1 YOLOv5

4.3.1.1 YOLOv5 Training with 25 Epochs

Table 4.4 shows the metrics produced for each classification when trained with YOLOv5 for 25 epochs. The precision (Also known as positive predictive value) was fairly high at 0.68 compared to some of the single classes in this model, the precision measures the proportion of positive identification that were correct, meaning in this instance 68% of positive identifications were true positives. Whereas the recall (also known as the true positive rate) measures the proportion of actual positives that were identified correctly for this model. The recall was low at 0.108, this means that the model correctly identified 10.8% of objects, a successful algorithm will have a high precision that remains high as the recall increases (Padilla, Netto & da Silva, 2020) indicating that it is consistently correctly identifying the classification of the objects. There are various metrics to help evaluate precision and recall together including the F1 score, which is the harmonic mean of precision and recall with a score of 1 meaning the model has perfect precision and recall and 0 meaning either the precision and or recall are 0. The F1 score for this model was 0.186, which is very low and indicates that the model is not performing well in correct identifications. The overall results for mAP50 and mAP50-95 were also low; these metrics show how much overlap there is

between the ground truth data and predicted data, which helps to demonstrate both an identification was successful and if the predicted bounding box was placed in the correct location. Meaning for mAP50 if the predicted bounding box has an overlap of 50% or more with the ground truth bounding box, the identification is considered successful, and in mAP50-95, which looks at the range of overlap between 50-95% between the predicted bounding box and the ground truth bounding box in 0.5 increments and averages them for the overall mAP50-95 value (Géron, 2019). As the results for both of these metrics were low, this means that the algorithm was not accurately placing the predicted bounding box. There are several classifications that have a precision of 1 but a recall, mAP50 and mAP50-95 of 0, this means that for this classification there were not successful identifications. Overall, this model was most successful at identifying air bubbles and background material.

Table 4.4 A table to show the overall precision, recall, F1 score, mAP50 (a metric to evaluate how successful an identification is when the Intersection Over Union (IOU) or the overlap between the predicted and actual bounding box is 50%) and mAP50-95 a metric to evaluate how successful an identification is when the IOU is 50-95%) when the images are trained with YOLOv5 and 25 epochs.

Class	Precision	Recall	F1 score	mAP50	mAP50-95
All	0.68	0.108	0.186	0.0895	0.0414
Air bubble	0.31	0.405	0.351	0.312	0.158
Anthropogenic	1	0	0	0	0
Background material	0.263	0.436	0.328	0.351	0.134
Cellulose filter fibre	0.196	0.0414	0.068	0.0461	0.0174
Cotton	0.351	0.19	0.247	0.151	0.0591
Diatom	0.281	0.121	0.169	0.129	0.0748
Easylift tab	1	0	0	0	0
Edge of slide	1	0	0	0	0
Fragment	0.441	0.221	0.294	0.145	0.0647
Glass filter fibre	0.271	0.00365	0.007	0.0293	0.0101
Hair textile	1	0	0	0	0
Hair	1	0	0	0.0912	0.0476

Insect matter	1	0	0	0	0
Microbead	1	0	0	0	0
Microfibre	0.24	0.336	0.28	0.161	0.053
Natural material	1	0	0	0	0
Pen	0.563	0.293	0.385	0.284	0.168
Salt	1	0	0	0	0
Unknown	1	0	0	0	0

The dataset trained with YOLOv5 with 25 epochs did not yield satisfactory results. Figure 4.25 shows the confusion matrix for plotting the actual identification provided to the algorithm against the predicted identification, with the true positives being those in which the actual identification and predicted identification are the same. The confusion matrix shows that the algorithm could not correctly identify the different classes with a good level of accuracy. Air bubbles were correctly identified in 25% of cases (699 identifications, the misidentifications for air bubbles were, background material 16% (447 identifications) and diatoms 5% (140 identifications). Anthropogenic material had no correct identifications, there were however, 17% (1 identification) identified as cotton. Background material had a true positive identification rate 41% (19353 identifications). Cellulose filter fibres were correctly identified 1% of the time (9 identifications). The misidentifications for cellulose filter fibres were air bubble 5% (46 identifications) and background material 9% (83 identifications). Cotton was correctly identified in 1% of cases (3 identifications). The misidentifications for cotton were background material 1% (3 identifications) and microfibres 12% (30 identifications). Diatoms were correctly identified correctly 4% of the time (97 identifications). The incorrect identifications for diatoms were air bubbles 7% (170 identifications) and background material 19% (463 identifications). Easylift® tab had no correct identifications, but there were misidentifications, background material and microfibre were both 8% (2 identifications). The edge of the slide also had no correct identification, with a misidentification for background material of 12% (1 identification). Both the Easylift® tab and the edge of the slide are underrepresented in the dataset,

so to improve the identification of these classes, their representation should be increased. Fragments were correctly identified 8% of the time (7 identifications). The misidentifications for fragments were air bubbles 1% (1 identification), background material 31% (28 identifications), microfibre 3% (3 identifications) and pen 4% (4 identifications). Glass filter fibres had no correct identifications. The misidentifications for glass filter fibres were air bubbles 2% (16 identifications) and background materials 12% (99 identifications). Hair textile and hair both had no correct identifications, and the only misidentification for both classes was microfibre. This misidentification is easily explainable as hairs and microfibres can have a similar appearance to each other. To resolve this problem and improve the overall performance of the algorithm, there are a number of steps that can be taken, including changing the number of epochs used when training the model, as the more times the training data is passed through the algorithm, the prediction errors will decrease (Géron, 2019). However, there will be a point where the errors will start to increase again, which indicates that the model is overfitting the training data set; this means there is an optimum number of epochs before the accuracy of the model starts to decrease (Lee & Lee, 2018). Another way to solve the problem would be to increase the representation of each class in the training data set either by adding more images or by adding an augmentation to the existing images because, naturally the representation of each class increases with the number of images used to train the more data the algorithm has to learn the better its performance metrics will be (Shahinfar, Meek & Falzon, 2020). Insect matter and microbeads both had no correct identifications or misidentifications, this is likely because they are underrepresented in the dataset. The model was able to correctly identify a microfibre in 16% of instances (61 correct identifications); the misidentifications were air bubbles and background materials 1% (3 identifications). Natural material had no correct identifications; the misidentifications for this class were background material 16% (6 identifications), cellulose filter fibres and cotton 3% (1 identification). Pen was correctly identified 17% of the time (20 identifications), the misidentifications were air bubble 3% (3 identifications), background material 25% (29 identifications) and fragments 7% (8 identifications). Salt was not

correctly identified by this model but there were misidentifications for air bubble 6% (1 identification) and background material 50% (9 identifications).

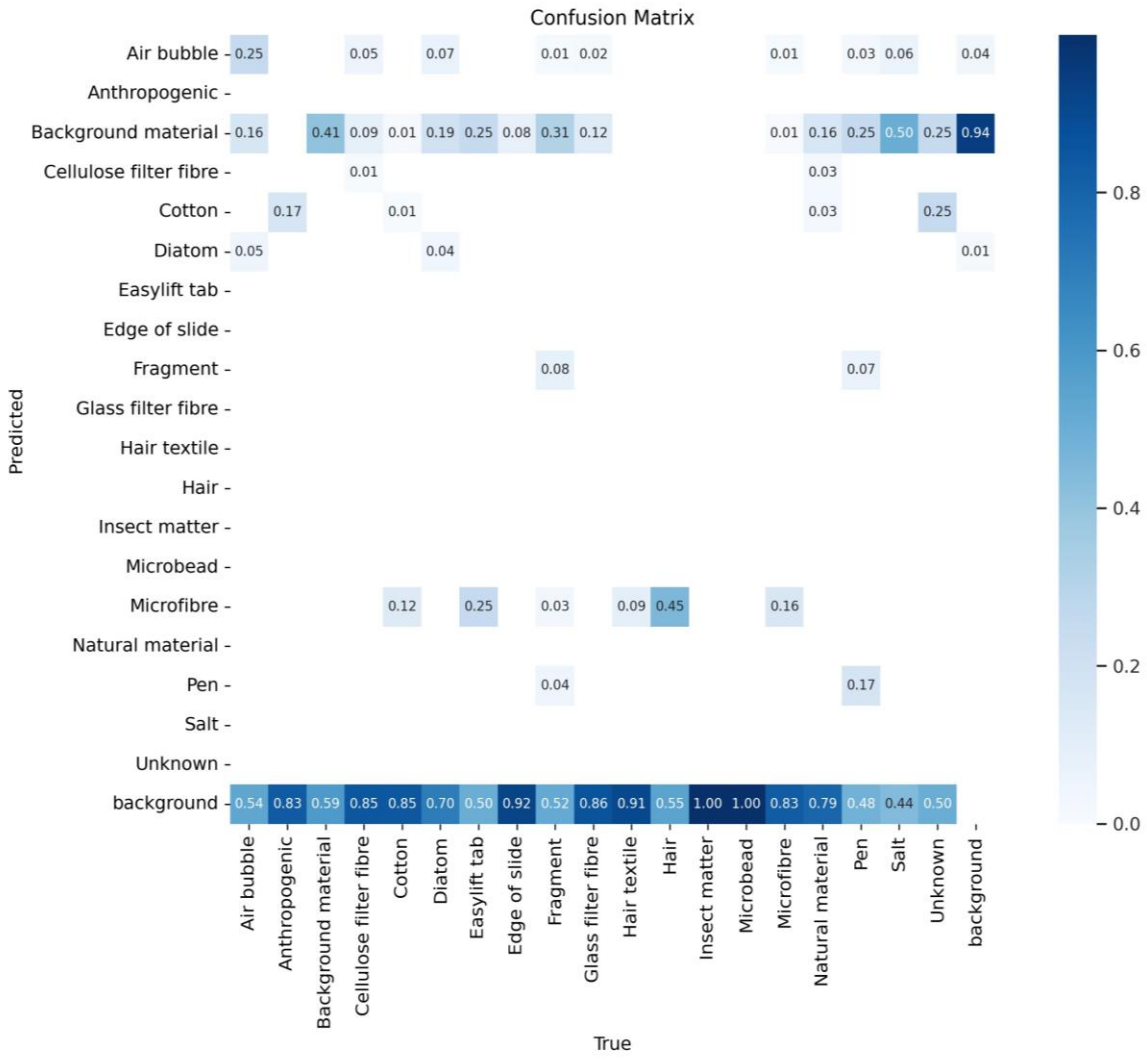

Figure 4.25 A confusion matrix to show how successful the algorithm was at correctly predicting each class when trained with YOLOv5 for 25 epochs.

Figures 4.26 and 4.27 show a precision-confidence and a recall-confidence curve respectively for the model produced by training the dataset with YOLOv5 with 25 epochs. From these graphs, it is apparent that the model does not have a good recall as all classes are 0.15 at a 0.0 confidence threshold, meaning that the model produces the best recall when there is a low confidence threshold used, which leaves the model open to false positives (Nurmaini *et al.*, 2023). Conversely the precision of the model is shown to be high with all classes were 1.0 at a 0.902 confidence threshold.

However, in order to fully evaluate the model's ability to classify objects, precision and recall need to be considered together.

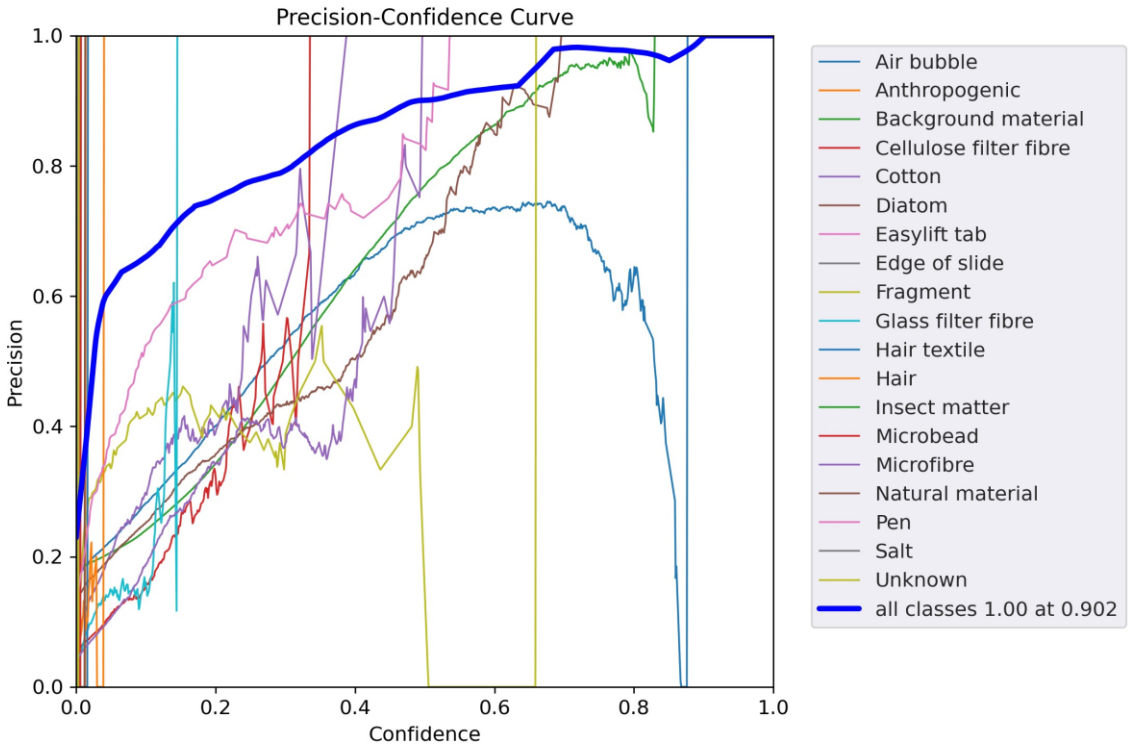

Figure 4.26 A precision-confidence curve to evaluate the model YOLOv5 when trained for 25 epochs.

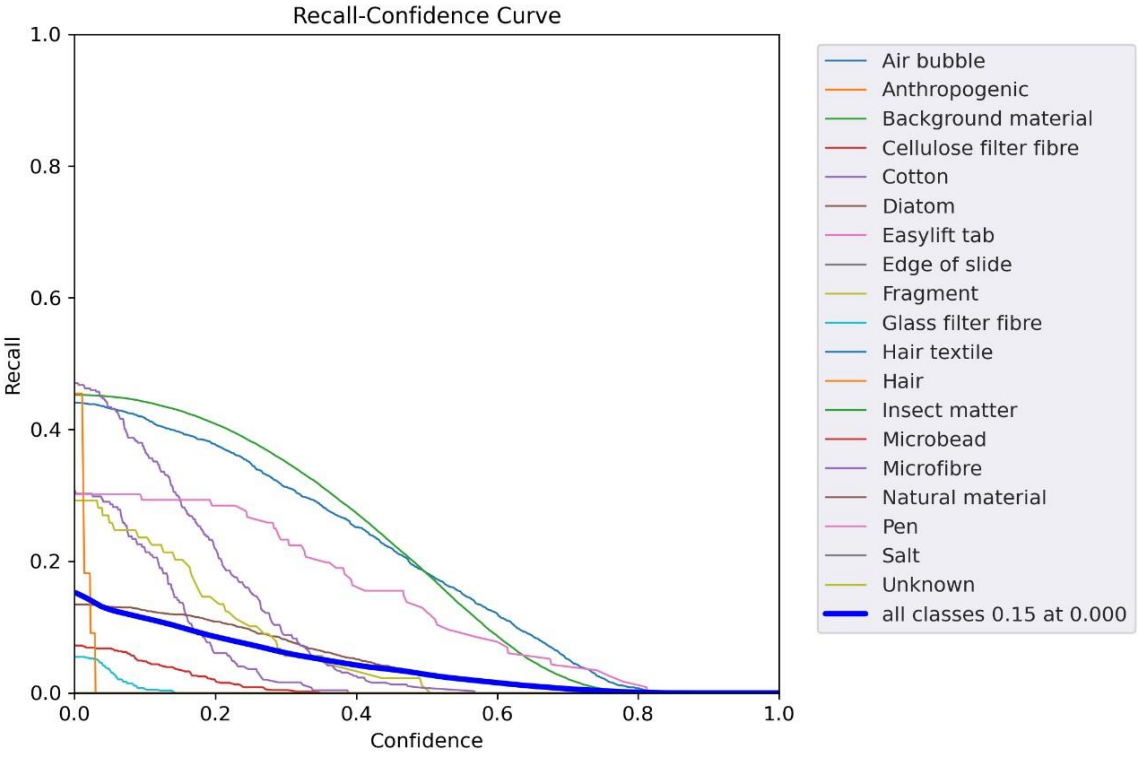

Figure 4.27 A recall-confidence curve to evaluate the model YOLOv5 when trained for 25 epochs.

Figure 4.28 shows the F1-confidence curve produced when that dataset was trained with YOLOv5 for 25 epochs. This figure helps to visualise the balance between the algorithm's precision and recall, against various confidence thresholds to allow the selection of a confidence threshold that balances precision and recall or prioritises on over the over depending on what is required of the algorithm (if the score is under the minimum threshold the algorithm will ignore the prediction) if the confidence threshold is too low there will be more false positives and it if is too high there will be more false negatives (Nurmaini *et al.*, 2023). As the confidence threshold decreases the F1 score has decreased, all classes had an F1 score of 0.11 at a confidence threshold of 0.130 which is very low and indicates a poorly performing model.

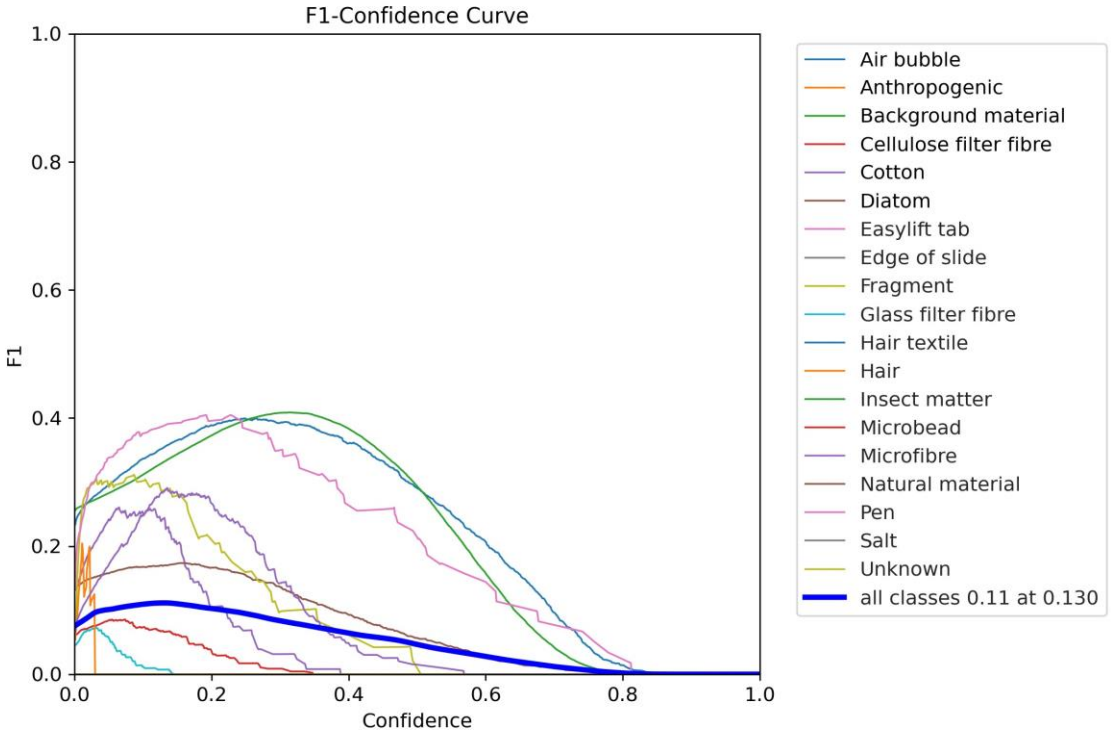

Figure 4.28 An F1-confidence curve to evaluate the model produced using YOLOv5 when trained for 25 epochs.

Figure 4.29 shows the precision-recall curve produced when training the dataset with YOLOv5 for 25 epochs. A high area under the curve means that there is a high recall and precision (Géron, 2019). From the graph we can

see that the model is most successful at identifying air bubbles, background material and pen, while all classes have an area under the curve of 0.089, this is a very low metric that indicates that the model is not performing well and would not be a good model to implement in its current form for the identification of microplastics.

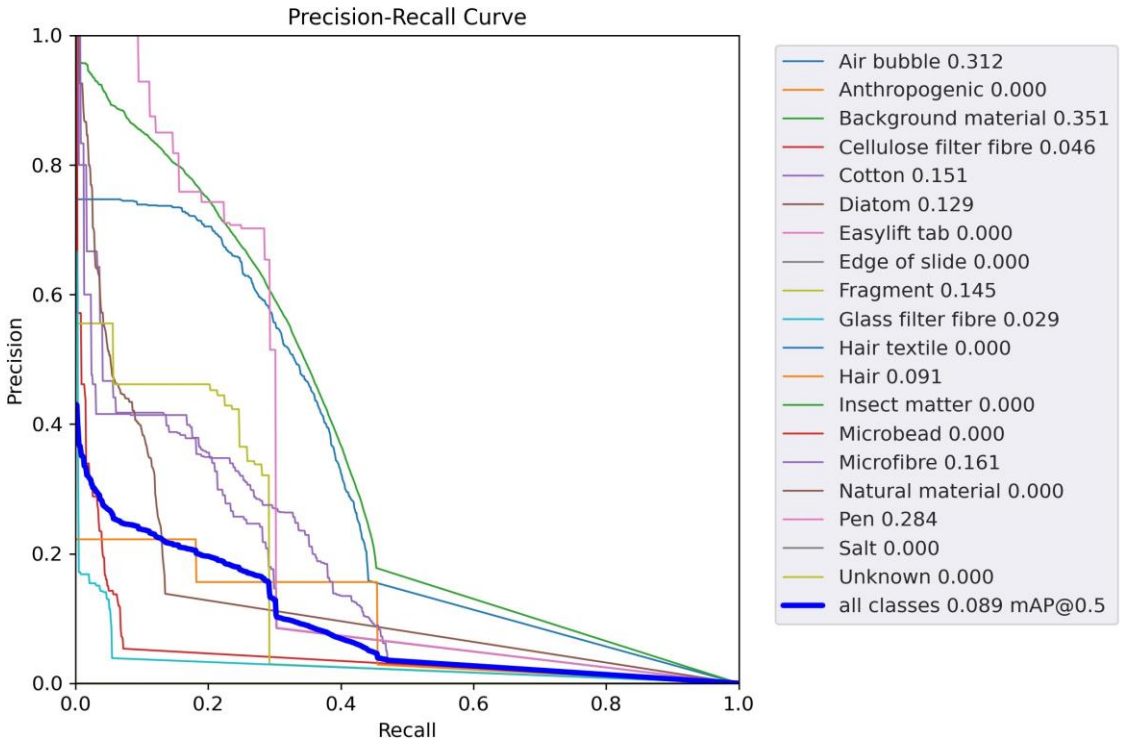

Figure 4.29 A Precision-Recall curve to evaluate the model YOLOv5 when trained for 25 epochs.

4.3.1.2 YOLOv5 Training with 100 Epochs

Table 4.5 shows the metrics produced for each classification when trained with YOLOv5 for 100 epochs. The precision for all classes is 0.787, meaning that 78.7% of positive identifications were true positives. The recall is 0.196, meaning 19.6% of objects were correctly detected. The overall F1 score is 0.314, which is still low and indicates a poorly performing model. These metrics are an improvement from YOLOv5 being run with 25 epochs, but as the recall is still fairly low the model will potentially have more false positives. The mAP50 and mAP50-95 also increased, showing that the model is better

at placing bounding boxes after 100 epochs than 25. The algorithm is most successful at identifying air bubbles, background material, fragments, microfibres and pen. There are still some classes that are not successfully being identified, namely anthropogenic, Easylift® tab, edge of slide, hair textile, hair, insect matter, microbead, natural material and salt, but this could be due to an underrepresentation of those classifications in the dataset.

Table 4.5 A table to show the overall precision, recall, F1 Score, mAP50 (a metric to evaluate how successful an identification is when the Intersection Over Union (IOU) or the overlap between the predicted and actual bounding box is over 50% the identification is successful) and mAP50-95 a metric to evaluate how successful an identification is when the IOU is 50%-95%) when the images are trained with YOLOv5 and 100 epochs.

Class	Precision	Recall	F1 Score	mAP50	mAP50-95
All	0.787	0.196	0.314	0.213	0.122
Air bubble	0.547	0.588	0.567	0.586	0.333
Anthropogenic	1	0	0	0	0
Background material	0.441	0.489	0.464	0.451	0.188
Cellulose filter fibre	0.473	0.292	0.361	0.269	0.134
Cotton	0.571	0.371	0.450	0.381	0.217
Diatom	0.631	0.362	0.460	0.442	0.258
Easylift tab	1	0	0	0	0
Edge of slide	1	0	0	0	0
Fragment	0.701	0.337	0.455	0.423	0.284
Glass filter fibre	0.336	0.239	0.279	0.2	0.0769
Hair textile	1	0	0	0.0266	0.0213
Hair	1	0	0	0.183	0.119
Insect matter	1	0	0	0	0
Microbead	1	0	0	0	0
Microfibre	0.574	0.471	0.517	0.467	0.26
Natural material	1	0	0	0.0329	0.0178
Pen	0.683	0.576	0.625	0.593	0.415
Salt	1	0	0	0	0
Unknown	1	0	0	0	0

Figure 4.30 shows the confusion matrix produced when the dataset was trained with YOLOv5 for 100 epochs. Air bubbles were successfully identified in 54% of instances (1510 identifications), and the model confused air bubbles for background material in 9% of cases (252 identifications) with cellulose filter paper in 1% of cases (28 identifications). The remaining identifications were predicted as being ‘background’ (1006 identifications) and so were not detected by the model. No objects that were supplied to the model as anthropogenic were correctly identified, but 17% (1 identification) were identified as cotton and microfibres, respectively, as these are both forms of anthropogenic fibres (Gordon., 2009) these identifications are not necessarily incorrect. A conclusive identification beyond that they were anthropogenic in origin was not able to be obtained manually. 49% (23129 identifications) of background material was identified correctly with the remainder of those that were not correctly identified being predicted as background (false negative). Cellulose filter fibres were correctly identified in 24% of instances (220 identifications); the model did have some false negatives, including 5% (46 identifications) identified as air bubbles, 10% (92 identifications) identified as background material and 60 % (550 identifications) categorised as ‘background’. The predictions of air bubbles could be due to the fact that the filter fibres are colourless and so an edge of a cellulose filter fibre may appear similar to the edge of an air bubble; there is also likely to be instances where air bubbles and cellulose filter fibres are in close proximity and may be present within each other’s bounding boxes, which could lead to the errors in predictions. Object overcrowding is a common issue with microscope images used in machine learning as the images often contain a large number of items of interest overlapping each other. This is very true with microplastic samples, particularly microfibres. This overcrowding can cause a barrier to automatic detection and segmentation of individual objects (Zinchuk, Grossenbacher-Zinchuk, 2020). This issue would also be difficult to overcome as the model would need to be trained with realistic examples of images that it might encounter, and if it was trained with images made to have no overlap, it might then struggle to identify objects from environmental samples which is the goal of the model being tested in this project. Cotton was successfully identified in 29% (72

identifications) of predictions, misidentifications were 1% (3 identifications) identified as air bubbles, 1% (3 identifications) identified as background material, 6% (15 identifications) identified as cellulose filter paper, 10% (25 identifications) identified as a microfibre and 52% (550 identifications) were identified as 'background'. The misidentification of cellulose filter paper can be attributed to the fact that cotton and the filter paper fibres are visually similar to each other, as both are cellulosic in nature (Sczostak, 2009). Diatoms were successfully identified in 30% (730 predictions) of predictions, misidentifications were 2% (49 identifications) air bubbles, 15% (365 predictions) background material, and 53% (1290 predictions) were identified as background as so were not located by the model. As diatoms are small and come in a variety of different shapes (Carson, 2013), the model may struggle with their identification, especially as some of them are perfectly spherical and can look similar to a microbead. No diatoms were misidentified as microbeads in this model. However, there is a lack of representation of microbeads in the dataset, so both diatoms and microbeads would need to be better represented in the dataset to counteract potential misidentifications on unknown environmental samples. The Easylift® tab was not successfully identified in this model, misidentifications were 25% (1 identification) and background material 25% (1 identification), although this class was only represented in the validation set 4 times, meaning that the representation of this class in the dataset needs to be increased. The edge of slide also did not have any correct identifications, 15% (2 identifications) were incorrectly identified as cotton, and 8% (1 identification) were identified as cellulose filter paper, this could be because all of the cellulose filter fibres and a large number of cotton fibres were colourless, and so may have appeared similar to the edge of the microscope slide, to counter act this the representation of the edge of slide class could be increased. Fragments were correctly identified 24 % of the time (21 identifications); as this is a microplastic, the level of identification is not satisfactory to be used as a method of identification. Misidentifications were background material 30% (27 identifications), diatoms 2% (2 identifications) and pen 4% (4 identifications). Glass filter paper was correctly identified in 20% (165) of identifications, with misidentifications including background material for 8% (66 identifications)

and air bubbles for 3% (25 identifications). It is possible that the glass filter paper was mistaken for air bubbles as the edge of an air bubble would appear very similar in appearance to a glass filter fibre. The background material misidentification could be explained as there was a lot of glass filter fibres it was impossible to separate the background material and the glass filter fibres in the bounding boxes. Both textile hair fibres and hair were not correctly identified; textile hair was misidentified as fragments in 9% of identifications (1 identification). This could be due to the hair being dyed a synthetic colour such as blue, which was a common colour for fragments to be. The textile hair was also mistaken for cotton in 18% of identifications (2 identifications). Hair was misidentified as a microfibre in 82% of identifications (9 identifications). This is likely as hair can appear visually similar to a cylindrical synthetic fibre, especially when there are no observable features such as the medulla or the scale pattern visible in the image. Hair was also misidentified as cotton in 9% of identifications (1 identification). Both hair and textile hair only have 11 images each in the validation set so there may not be enough representation in the data set to accurately identify these two classes. Insect matter appeared one time in the validation set and was misidentified as ‘background’ this would be because it is severely underrepresented in the and because the class would cover a wide variety of materials that may appear for example, across the whole dataset a spider’s leg, an ant and several aquatic organisms were classified as insect material. Microbeads were also only represented once in the validation set, it was incorrectly identified as background material, this class needs to be better represented in the data set in order to produce a robust method of microplastic identification. Microfibres were correctly identified in 44% of identifications (170 identifications), this is an improvement from 16% when run for 25 epochs, but as the rate of identification is less than 50% it is not a reliable method for correctly identifying the presence of microfibres. Misidentifications include 5% cotton (19 identifications), 1% cellulose filter fibre (4 misidentifications), and 2% air bubbles (8 identifications). Natural material was not correctly identified in this model, misidentifications of natural material were 18 % background material (7 identifications), 3% cellulose filter fibre (1 misidentification) and 5% cotton (2 identifications). Pen was correctly

identified in 49% (57 identifications), the most common misidentification was background material 14% (17 identifications). Other misidentifications were air bubble and cellulose filter fibre (3%) (3 identifications) and fragments and microfibre 1% (1identification). Salt was not correctly identified by this model; this is likely because that images used to train and test the model were from the upper Hudson River where salt levels were low compared to saltwater samples. The most common misidentification was background material at 72% of identifications (13 identifications), salt was misidentified as an air bubble in 6% of identifications (1 identification).

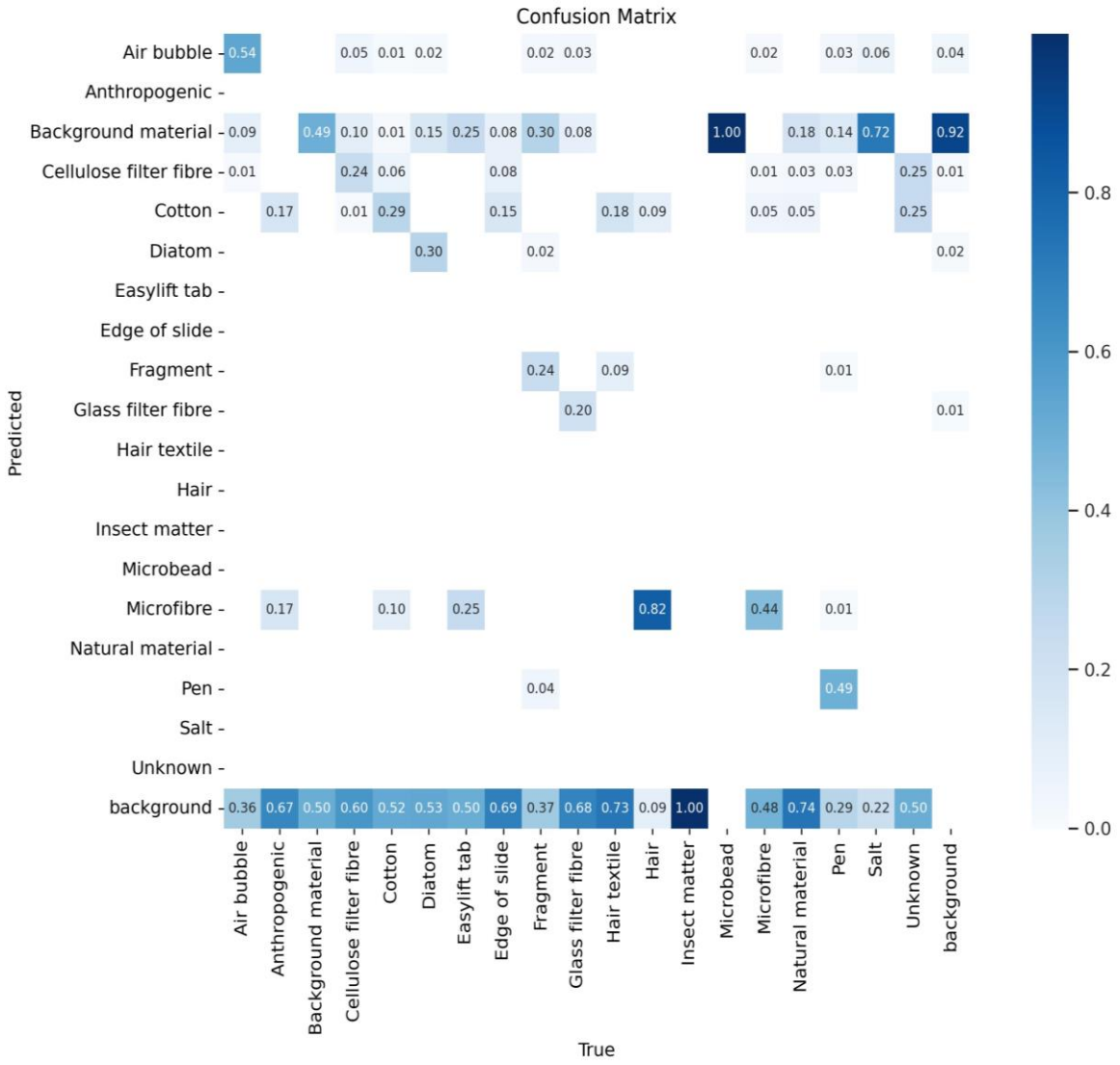

Figure 4.30 A confusion matrix to show how successful the algorithm was at correctly predicting each class when trained with YOLOv5 for 100 epochs.

Figure 4.31 shows a precision-confidence curve, and Figure 4.32 shows a recall-confidence curve when the dataset was trained with YOLOv5 for 100 epochs. From these two graphs, the model's precision is high, with all classes having a precision of 1.00 at a confidence level of 0.902, whereas the recall is very low for this model, with all classes having a recall of 0.29 at a confidence of 0.0. These two metrics together show how well the model performs at correctly identifying the different classes; a good model will have a high precision and recall.

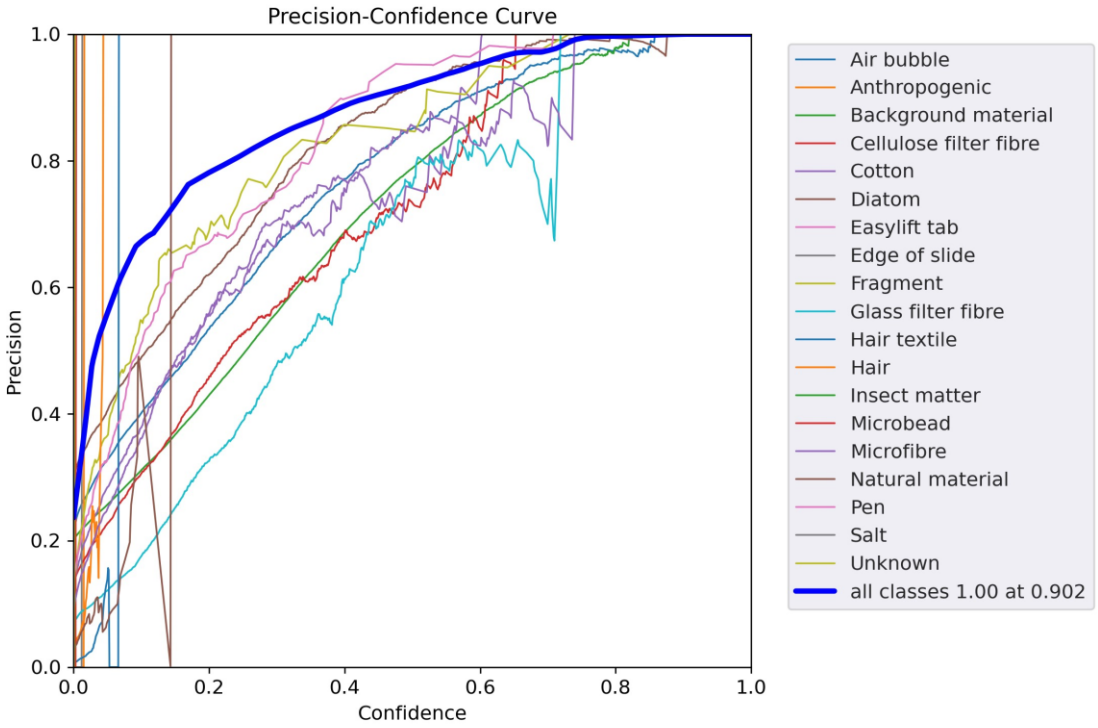

Figure 4.31 A precision-confidence curve to evaluate the model YOLOv5 when trained for 100 epochs.

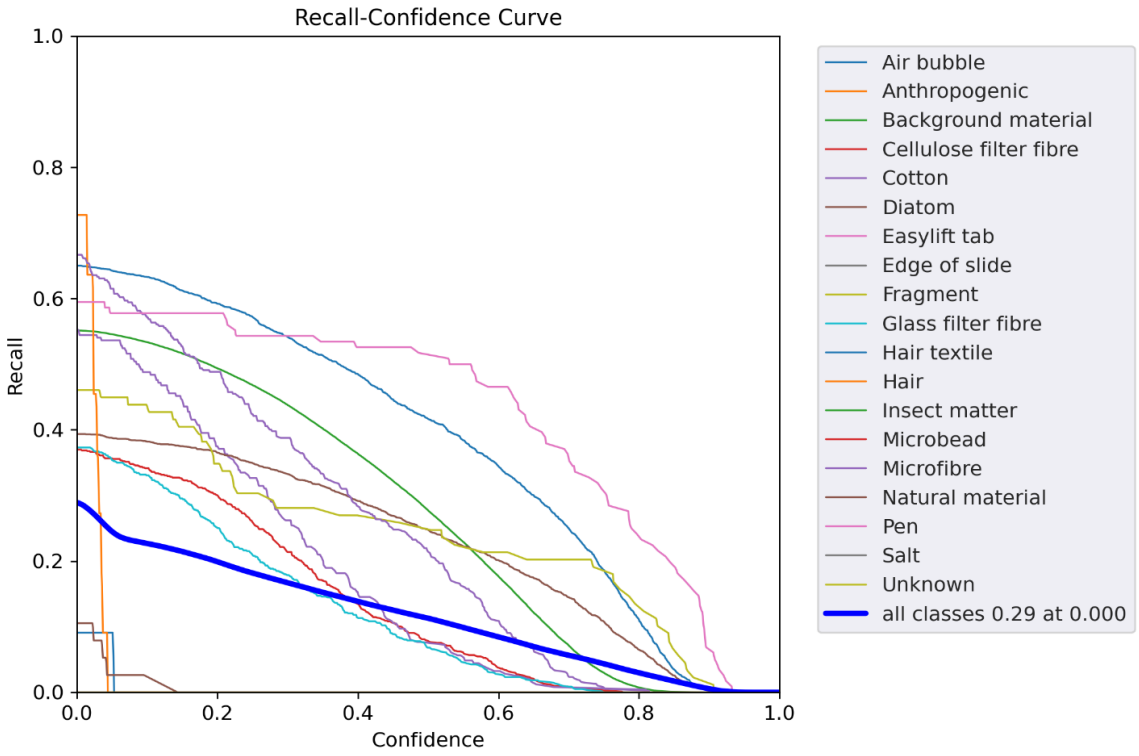

Figure 4.32 A recall-confidence curve to evaluate the model YOLOv5 when trained for 100 epochs.

Figure 4.33 shows an F1-confidence curve to evaluate the model by taking both precision and recall into consideration. All classes are at 0.22 at a confidence of 0.197, after this point the F1 score begins to decrease. The model overall performs best in the identification of pen, followed by air bubble and background material.

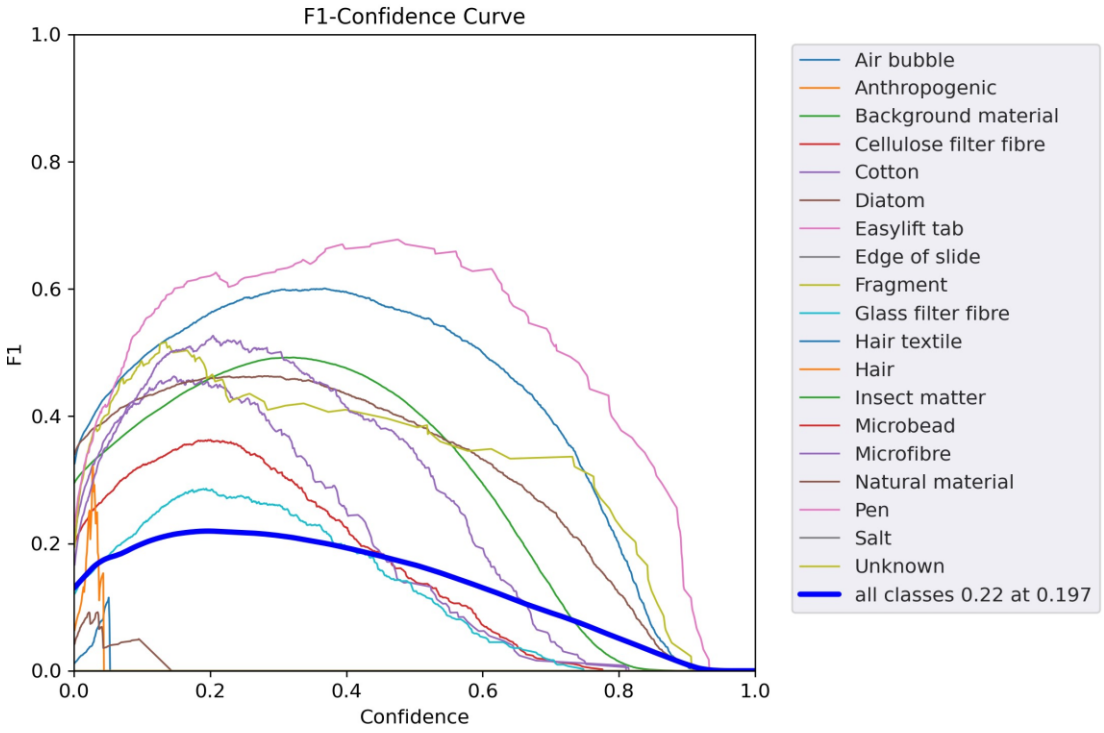

Figure 4.33 An F1-confidence curve to evaluate the model produced using YOLOv5 when trained for 100 epochs.

Figure 4.34 shows a precision-recall curve for the model produced by training with YOLOv5 for 100 epochs, the higher the area under the curve and the closer to the top right-hand corner, the better the model was at correctly identifying that class. The model was most successful at identifying pen with and area under the curve of 0.586, followed by microfibres with an area under the curve of 0.467. The model was least successful at identifying salt, unknown, microbeads, edge of slide and Easylift® tab with an area under the curve of 0.0 meaning no correct identifications were made for these classes. Overall, the model had an area under the curve of 0.213, indicating that the model has not performed well in the identification of microplastics.

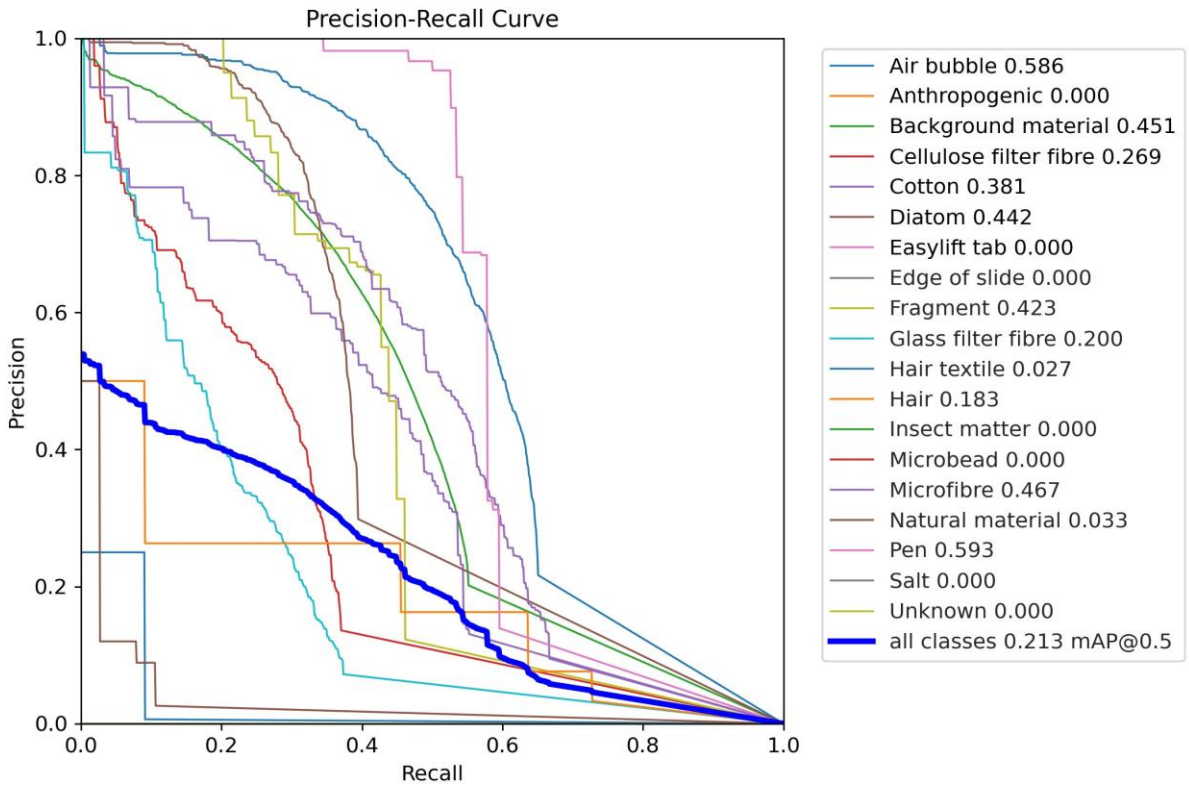

Figure 4.34 A Precision-Recall curve to evaluate the model YOLOv5 when trained for 100 epochs.

4.3.1.3 YOLOv5 Training with Augmented Data and 100 Epochs

Table 4.6 shows the metrics produced for each classification when trained with YOLOv5 for 100 epochs with augmented images used in the training data see Section 2.2.3 for more information on the augmented images. The precision for all classes is 0.728, meaning that 72.8% of positive identifications were true positives. The recall is 0.217, meaning 21.7% of objects were correctly detected. The recall metric is still low compared to the precision, meaning there is a higher chance of false positives. The Overall F1 score was 0.334, which is low and means that the model is not performing well overall. From the metric shown in Table 4.6 the model is most successful at identifying air bubbles, pen and microfibres. The most accurate bounding boxes were made for air bubbles, pen, microfibres and fragments.

Table 4.6 A table to show the overall precision, recall, F1 Score, mAP50 (a metric to evaluate how successful an identification is when the Intersection Over Union (IOU) or the overlap between the predicted and actual bounding box is over 50% identification is successful) and mAP50-95 a metric to evaluate how successful an identification is when the IOU is 50-95%) when the augmented images are trained with YOLOv5 and 100 epochs.

Class	Precision	Recall	F1 Score	mAP50	mAP50-95
All	0.728	0.217	0.334	0.269	0.162
Air bubble	0.708	0.626	0.665	0.673	0.399
Anthropogenic	1	0	0	0.0099	0.00396
Background material	0.564	0.466	0.510	0.475	0.203
Cellulose filter fibre	0.606	0.335	0.431	0.375	0.208
Cotton	0.566	0.3	0.392	0.395	0.222
Diatom	0.706	0.431	0.574	0.496	0.285
Easylift tab	0	0	0	0	0
Edge of slide	1	0	0	0.127	0.0927
Fragment	0.742	0.483	0.585	0.542	0.375
Glass filter fibre	0.49	0.318	0.386	0.315	0.138
Hair textile	1	0	0	0.076	0.046
Hair	1	0	0	0.263	0.197
Insect matter	1	0	0	0	0
Microbead	0	0	0	0	0
Microfibre	0.678	0.509	0.581	0.6	0.345
Natural material	1	0	0	0.0715	0.0312
Pen	0.781	0.664	0.718	0.689	0.536
Salt	1	0	0	0	0
Unknown	1	0	0	0	0

Figure 4.35 shows the confusion matrix produced when the dataset was trained with YOLOv5 for 100 epochs with an augmented training dataset. Air bubbles were correctly identified in 62% of cases (1734 identifications), this is an improved identification compared to the model produced without augmented images, with 224 more correct identifications. However, there are still 29% (811) of air bubbles not being detected by this model. This may be

due to the location of these air bubbles within the image if they are near other materials the model may not be able to distinguish between the two objects. Air bubbles were misidentified as background material 7% of the time (196 identifications) and as cellulose filter paper 1% of the time (28 identifications). There were no correct identifications for anthropogenic materials, however 33% (2 identifications) were identified as microfibres which they would appear visually similar to, as anthropogenic materials is a class for items with no confirmed identifications such as cotton etc, there will be a large variety of features present in this class, and these features are likely to overlap with other classes that could be classed as anthropogenic but have known identifications. As such this will be a challenging class to correctly predict, and it may be that while the analysist was not able to correctly assign an identification further than anthropogenic it does not mean that the algorithm was necessarily wrong if it classifies an item as a microfibre or cotton. In addition to this there is an under representation of this class as it only occurs if a conclusive identification further than anthropogenic in origin cannot be reached. The background material classification was correctly identified in 51% of predictions (24073 identifications), the remaining background material classifications were not detected by the algorithm. Cellulose filter fibres were correctly predicted 33% of the time (303 identifications). Only 1% (9 identifications) were misidentified as cotton which is surprising as they are visually very similar when the cotton is colourless, and colourless cotton is represented in the data set. Other misidentifications for cellulose filter fibres were air bubbles 3% (27 identifications) and background material 13% (119 identifications). Cotton was correctly predicted in 33% of identifications (82 identifications). Like with cellulose filter fibre cotton was only misidentified as cellulose filter paper in 6% of identifications (15 identifications), this implies that the model may be able to accurately distinguish between the two classes. Other misidentifications for cotton are air bubbles 1% (3 identifications), background material 1% (3 identifications) and microfibres 11% (27 identifications). Diatoms were correctly predicted in 40% of identifications (974 identifications), misidentifications for the diatom class were background material 13 % (316 identifications) this is likely as diatoms were very small and would be very

close to background material and debris and so would not be easily excluded from each other's respective bounding box; and air bubble 1% (27 identifications). Easylift® tab was not correctly identified in this model, misidentifications for Easylift® tab were, background material 25% (1 identification) and microfibres 50% (2 identifications). As this is an underrepresented class it is not a surprise that it has not been accurately predicted by the model, the presence of the classification within the data set should be increased in order to improve the correct classification rate. The edge of the slide was also not correctly predicted in this model, the misidentifications produced were, background material 8% (1 identification), cellulose filter fibre 8% (1 identification), cotton 8% (1 identification) and pen 15% (2 identifications). Fragments were correctly predicted by this model 38% of identifications (34 identifications). The misidentifications for fragments were, air bubble 2% (2 identifications), background material 29% (26 identifications) and pen 2% (2 identifications). A large number of fragments (28% or 25 fragments) were not detected by the algorithms this is a high number of microplastics be to be missed by the model and this would need to be improved before it could be used to classify samples. The glass filter fibre classification was correctly identified in 34% of identifications (280 identifications). The misidentification for this class were air bubble 1% (8 identifications) and background material 7% (58 identifications). Textile hair fibres were not detected by this model, but a misidentification of microfibre was predicted in 36% (4 identifications) of identifications, this is a reasonable misidentification as they will both look very similar to each other especially if the textile fibre presents no features such as the medulla or a cuticle pattern in the images. Hair textile also had a 27% (3 identifications) misidentification rate for cotton. Hair also was not successfully identified by the model and had an 82% (9 identifications) microfibre misidentification rate, and 9% (1 identification) for cotton. Insect matter was not detected by the model and there were no misidentifications for this classification. Microbeads were also not detected by the model, and the one instance of microbeads was misidentified as background material. Microfibres were correctly identified in 52% of classifications (201 identifications) this is a higher level of accuracy than some other classes but as the primary purpose of this algorithm is to

identify microplastics the error rate is still too high to be used reliably. Misidentifications for microfibres were air bubble 2% (8 identifications), cellulose filter fibre 2% (8 identifications) and cotton 7% (27 identifications). Natural material was not correctly identified by this model, the misidentifications were, air bubble 3% (1 identification), background material 24% (9 identifications), cellulose filter fibres 3% (1 identification), cotton 5% (2 identifications), glass filter fibres 3% (1 identification) and microfibre 8% (3 identifications). There is a large variation in the misidentifications for this classification, this is likely due to the large variation of visual appearance in this class and overcrowding in the images. Pen was correctly identified in 62% of identifications (72 identifications), the misidentifications for this class were air bubble 3% (3 identifications), background material 11% (9 identifications), cellulose filter fibre 1% (1 identification) and fragment 1% (1 identification). Salt was not correctly identified by the algorithm, and 78% of the salt objects were misidentified as background material. Overall, this model is most successful at identifying pen, microfibres, background material and air bubbles. The most common misidentifications were air bubble, background material, cellulose filter fibres, glass filter fibres and microfibres.

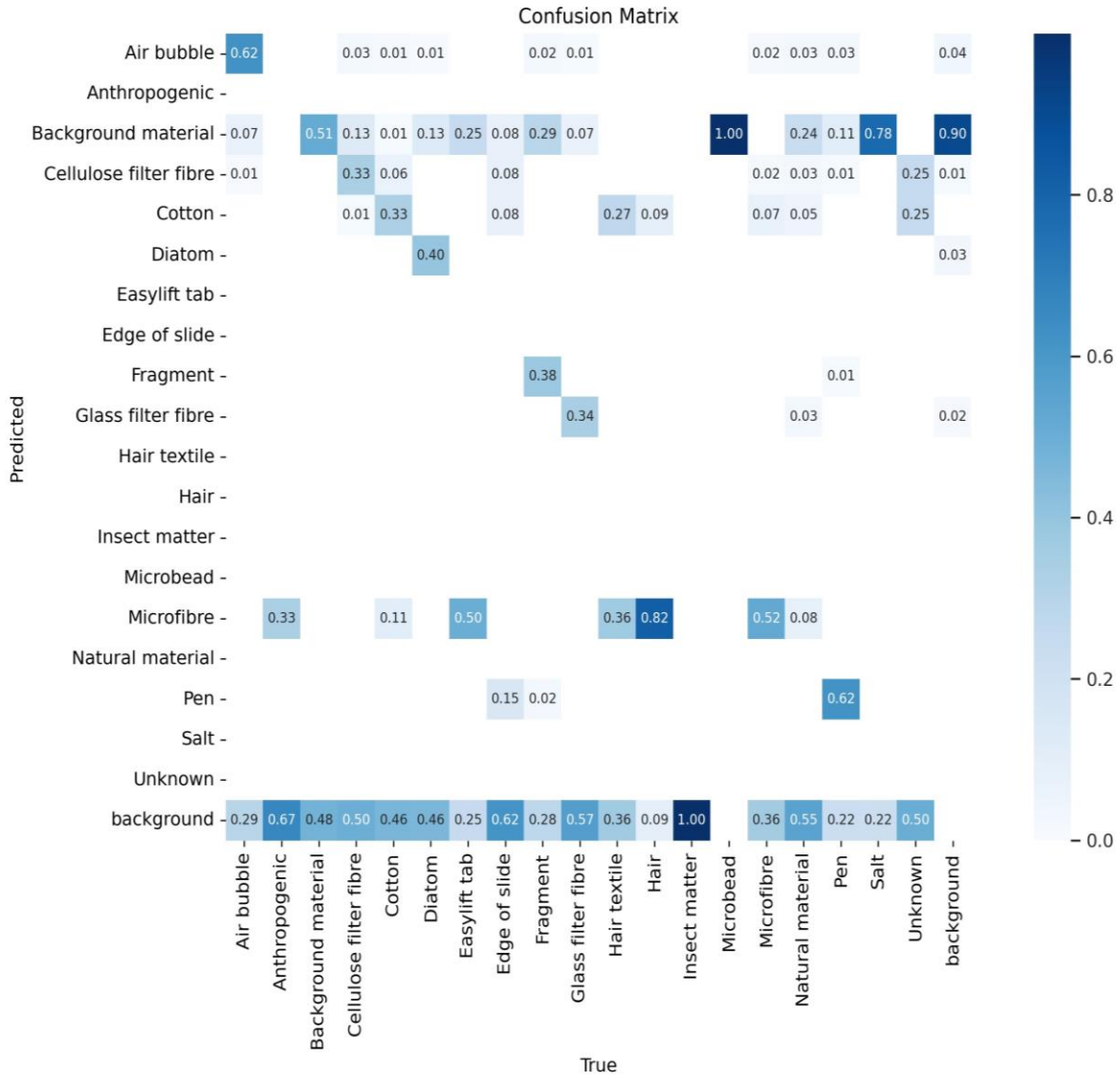

Figure 4.35 A confusion matrix to show how successful the algorithm was at correctly predicting each class when trained with augmented images using YOLOv5 for 100 epochs.

Figure 4.36 shows a precision-confidence curve, and Figure 4.37 shows a recall-confidence curve when the dataset was trained with YOLOv5 for 100 epochs and augmented images were used in the training dataset. From these two graphs, it can be seen that the model's precision is high, with all classes having a precision of 0.89 at a confidence level of 0.916, whereas the recall is very low for this model, with all classes having a recall of 0.38 at a confidence of 0.0. Pen, air bubbles and fragments had the best recall in this model.

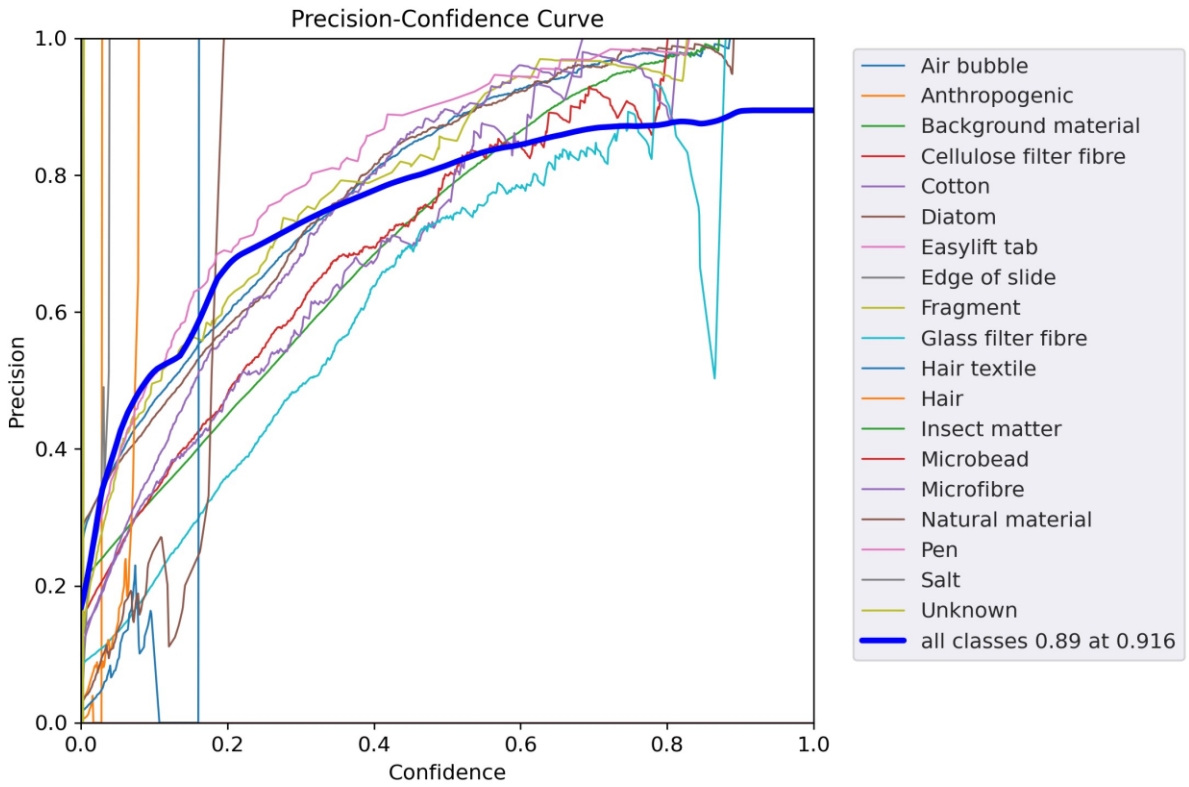

Figure 4.36 A precision-confidence curve to evaluate the model when trained with augmented images using YOLOv5 for 100 epochs.

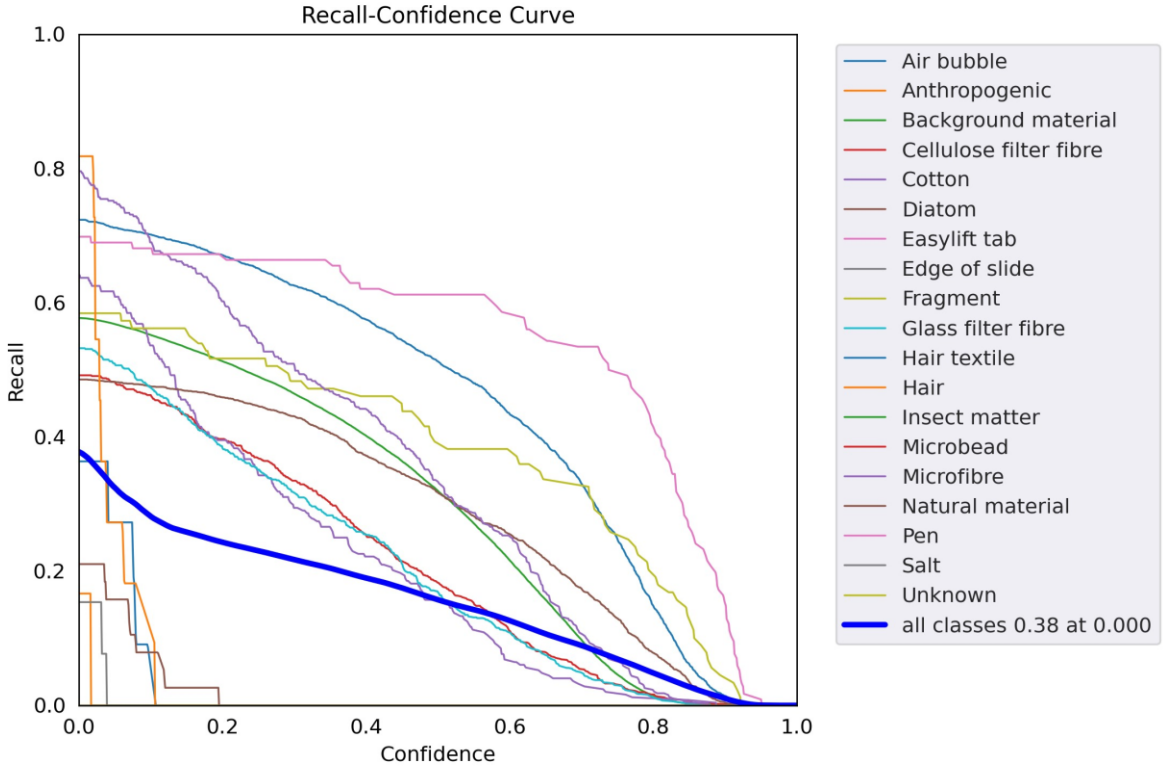

Figure 4.37 A recall-confidence curve to evaluate the model when trained with augmented images using YOLOv5 for 100 epochs.

Figure 4.38 show a F1-confidence curve when the dataset was trained with YOLOv5 for 100 epochs and augmented images used in the training dataset. All classes are at 0.25 at a confidence of 0.292, after this point the F1 score begins to decrease. The model overall performs best in the identification of pen, followed by air bubble, fragments and microfibres.

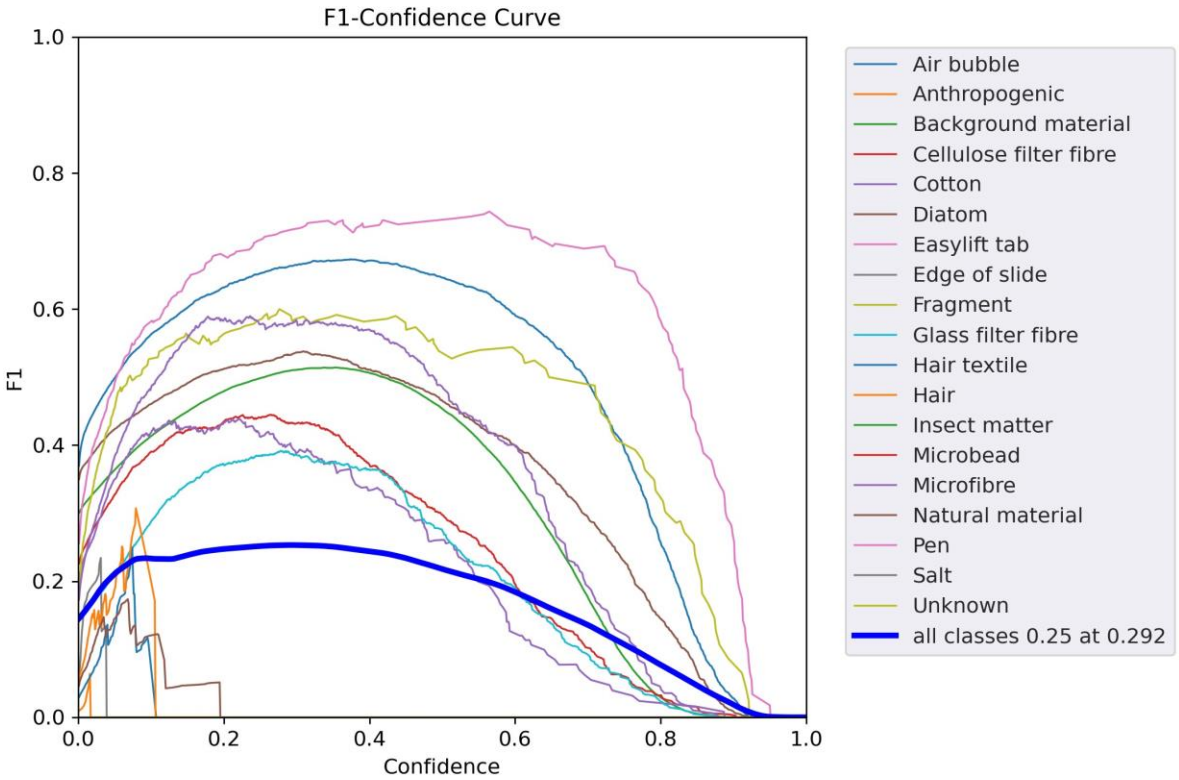

Figure 4.38 An F1-confidence curve to evaluate the model produced when trained with augmented images using YOLOv5 for 100 epochs.

Figure 4.39 shows a precision-recall curve for the model produced by training with YOLOv5 for 100 epochs and augmented images used in the training dataset. The model was most successful at identifying pen with and area under the curve of 0.689, followed by air bubble with an area under the curve of 0.673 and microfibres with an area under the curve of 0.600. The model was least successful at identifying salt, unknown, microbeads, edge of slide and Easylift® tab with an area under the curve of 0.0 meaning no correct identifications were made for these classes. Overall, the model had an area under the curve of 0.269, indicating that the model has not

performed well in the overall classification of objects commonly found in microplastic samples.

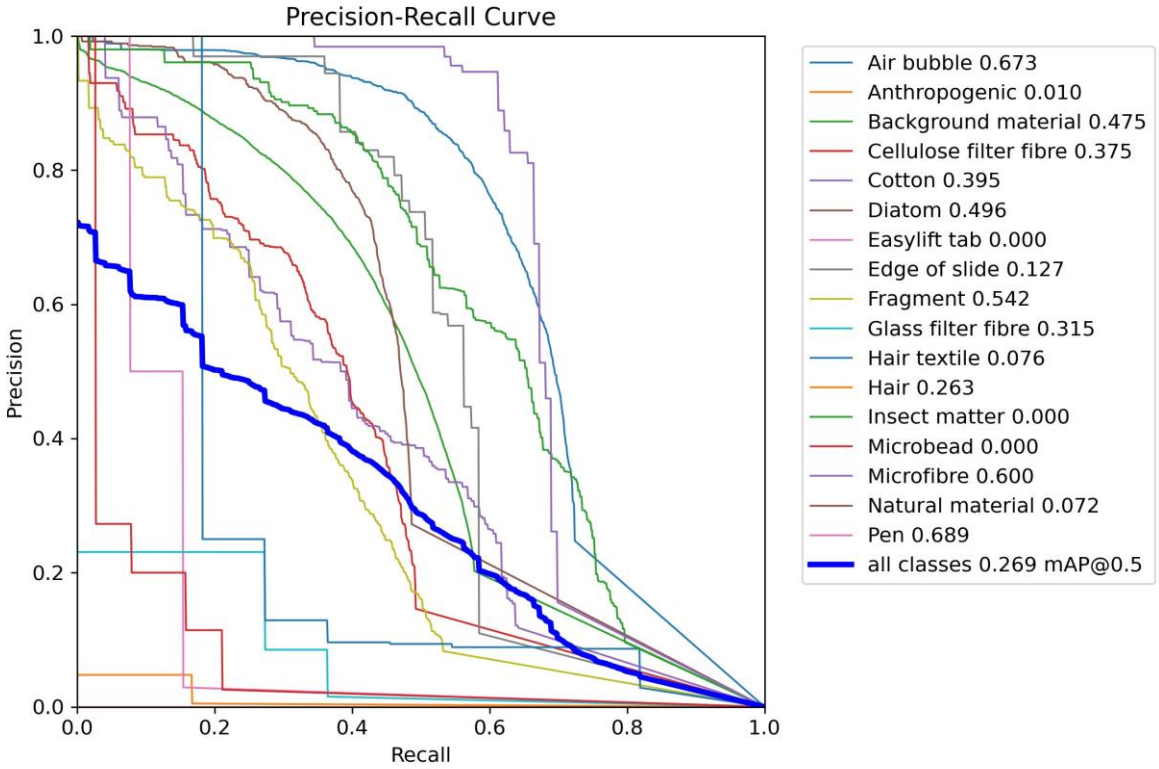

Figure 4.39 A Precision-Recall curve to evaluate the model when trained with augmented images using YOLOv5 for 100 epochs.

4.3.2 YOLOv7

4.3.2.1 YOLOv7 Training with 25 Epochs

Table 4.7 shows the metrics produced for each classification when trained with YOLOv7 for 25 epochs. The precision for all classes is 0.843, meaning that 84.3% of positive identifications were true positives. The recall is 0.332, meaning 33.2% of objects were correctly detected. The recall metric is still low in comparison to the precision meaning that there is a higher chance of false positives. The Overall F1 score was 0.476, which is low and means that the model is not performing well overall in the identification of all classifications. From the metric shown in Table 4.7 the model is most successful at identifying air bubbles, pen, fragments, and microfibres. The most accurate bounding boxes were made for air bubbles, pen, microfibres, air bubble and fragments.

Table 4.7 A table to show the overall precision, recall, F1 Score, mAP50 (a metric to evaluate how successful an identification is when the Intersection Over Union (IOU) or the overlap between the predicted and actual bounding box is over 50% identification is successful) and mAP50-95 a metric to evaluate how successful an identification is when the IOU is 50-95%) when the images are trained with YOLOv7 and 25 epochs.

Class	Precision	Recall	F1 Score	mAP50	mAP50-95
All	0.843	0.332	0.476	0.354	0.244
Air bubble	0.795	0.809	0.802	0.834	0.543
Anthropogenic	1	0	0	0.0231	0.0195
Background material	0.663	0.529	0.588	0.556	0.241
Cellulose filter fibre	0.596	0.7	0.644	0.647	0.403
Cotton	0.71	0.552	0.621	0.63	0.451
Diatom	0.775	0.665	0.716	0.688	0.423
Easylift tab	1	0	0	0	0
Edge of slide	1	0	0	0	0
Fragment	0.898	0.685	0.777	0.719	0.558
Glass filter fibre	0.593	0.601	0.597	0.602	0.344
Hair textile	0.999	0.0909	0.166	0.194	0.188
Hair	1	0	0	0.065	0.0623
Insect matter	1	0	0	0	0
Microbead	1	0	0	0	0
Microfibre	0.756	0.705	0.730	0.781	0.586
Natural material	0.313	0.105	0.157	0.101	0.0824
Pen	0.919	0.871	0.894	0.878	0.727
Salt	1	0	0	0.000688	0.00055
Unknown	1	0	0	0	0

Figure 4.40 shows a confusion matrix produced when the dataset was trained with YOLOv7 for 25 epochs. Air bubbles were correctly identified in 82% of cases (2293 identifications), this is a good level of positive identification, air bubbles were misidentified as background material in 3% of identifications (84 identifications). There is still a false negative rate of 14% (391 air bubbles) for the air bubble classification. Anthropogenic and salt were not detected and had no misidentifications, this may be due to low representation in the dataset and overcrowding in the images that the class is present in this may improve if the model is run for more epochs. Background material was correctly identified 56% of the time (26433 identifications), there were no misidentifications for background material, but a large false negative rate of 43%. Cellulose filter fibre had a correct prediction rate of 63% (578 identifications). The misidentifications for cellulose filter fibres were, air bubble 1% (9 identifications), background material 11% (101 identifications), cotton 2% (18 identifications), diatoms 1% (9 identifications) and microfibre 1% (9 identifications). Cotton had a correct prediction rate of 57% (141 identifications). The misidentifications for cotton were background material (2 identifications), cellulose filter fibres 2% (5 identifications), diatom 1% (2 identifications), microfibres 9% (22 identifications) and natural material 1% (2 identifications). Both cotton and cellulose filter fibres have a very low rate of misidentifications for each other, which is a good outcome for this model as both cotton and cellulose filter paper are cellulosic and so will look very visually similar to each other. Diatom has a correct prediction rate of 70%, the only misidentification was 4% (97 identifications) as background material. This misidentification is not unexpected as the diatoms were ubiquitous over the sample slides and there are occasions where a diatom could not be excluded from a background material bounding box. Easylift® tab, edge of slide, hair, insect material and salt were not detected by the model, all occurrences of these classes were not classified by the model and so were false negatives. Fragments had a positive identification rate of 81% (72 identifications), the only misidentification was for microfibre 1% (1 identification). The remaining fragments were classified as false negatives. The correct identification rate for fragments is good for this model but could still be improved as the more

accurate the positive identification rates the better the model will be at detecting the microplastics. Glass filter fibres have a correct prediction rate of 61% (502 predictions). The misidentification for glass filter fibres were background material 5% (41 identifications) and air bubble 1% (8 identifications). Hair textile only had a correct prediction rate of 17% (2 identifications) and no misidentifications all remaining hair textile objects were false negatives. Microfibres had a correct prediction rate of 68% (263 identifications) but a wide variety of misidentifications; air bubble 1% (4 identifications), anthropogenic 1% (4 identifications), cotton 6% (23 identifications), hair textile 1% (4 identifications), hair 2% (8 identifications) and natural material 1% (4 identifications). While microfibres had a bigger variety of misidentifications the actual level of misidentification was fairly low for each of the classifications misidentified. Natural material had a correct prediction rate of 19% (7 identifications). The incorrect identifications for natural material were cotton 5% (2 identifications), microfibre 5% (2 identifications) and unknown 10% (4 identifications). It is interesting that 10% were classified as unknown when the model made no identification for unknown, this could be because there is likely to be some visual similarities between those classified as unknown and natural materials as both do not have a conclusive identification and so there will be lots of characteristics shared between both classes. Pen had a correct prediction rate of 90% (104 identifications) this is a very high correct prediction rate for this model. Pen had a misidentification rate of 1% (1 identification) for air bubble, background material, diatom, Easylift® tab, edge of slide and fragment. Overall, this model is most successful at identifying pen, microfibres, fragments, diatoms, background material and air bubbles. The most common misidentifications were air bubble, background material and microfibres.

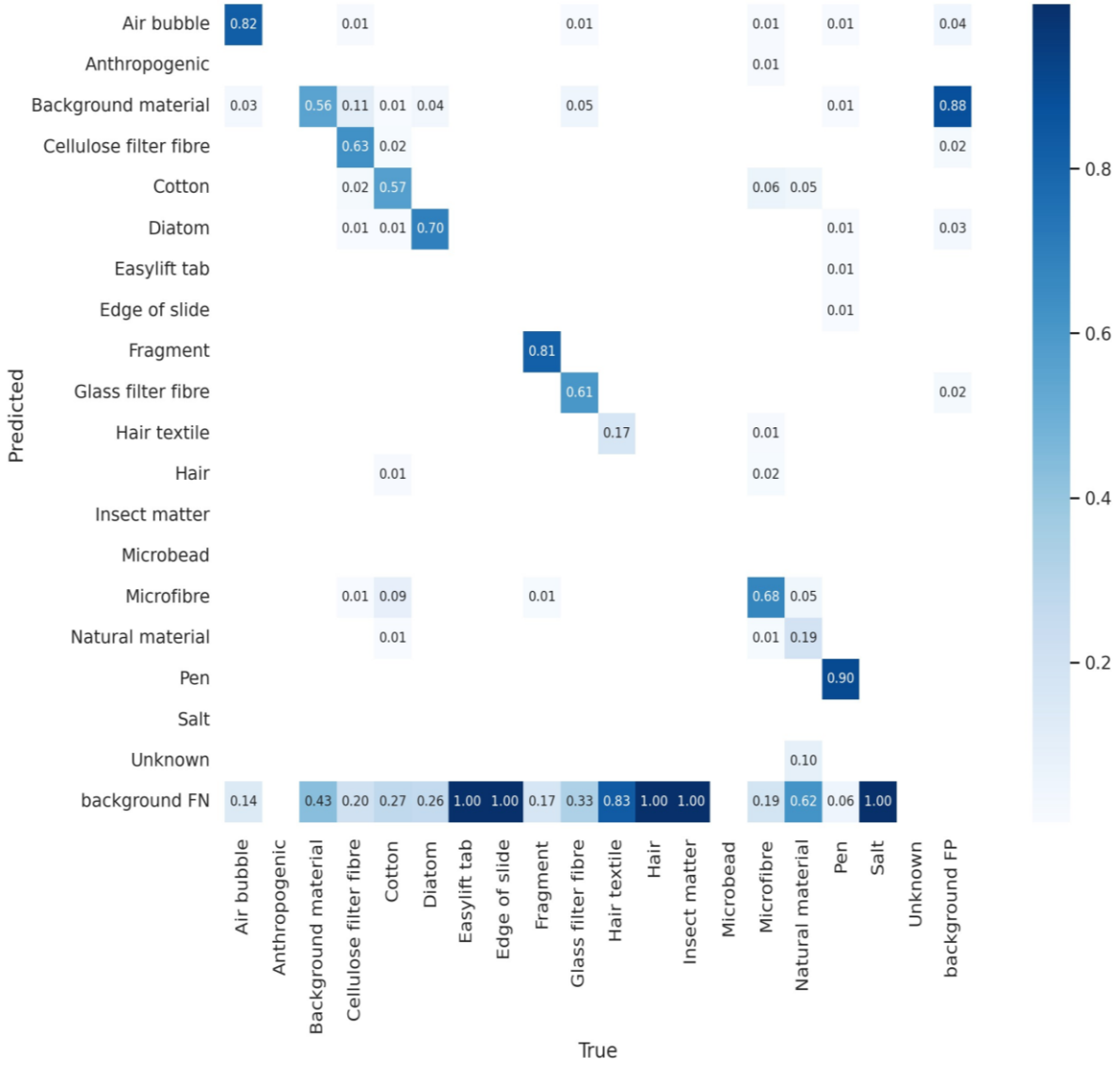

Figure 4.40 A confusion matrix to show how successful the algorithm was at correctly predicting each class when trained using YOLOv7 for 25 epochs.

Figure 4.41 shows a precision-confidence curve and figure 4.42 shows a recall-confidence curve when the dataset was trained with YOLOv7 for 25 epochs. From these two graphs it can be seen that the model's overall precision is high with all classes being having a precision of 1 at a confidence level of 0.941, whereas the overall recall is relatively low for this model with all classes having a recall of 0.53 at a confidence of 0.0. However, some of the classes are performing far better than others which is bringing the average down. For instance, pen, air bubble and fragments have a good recall level for this model.

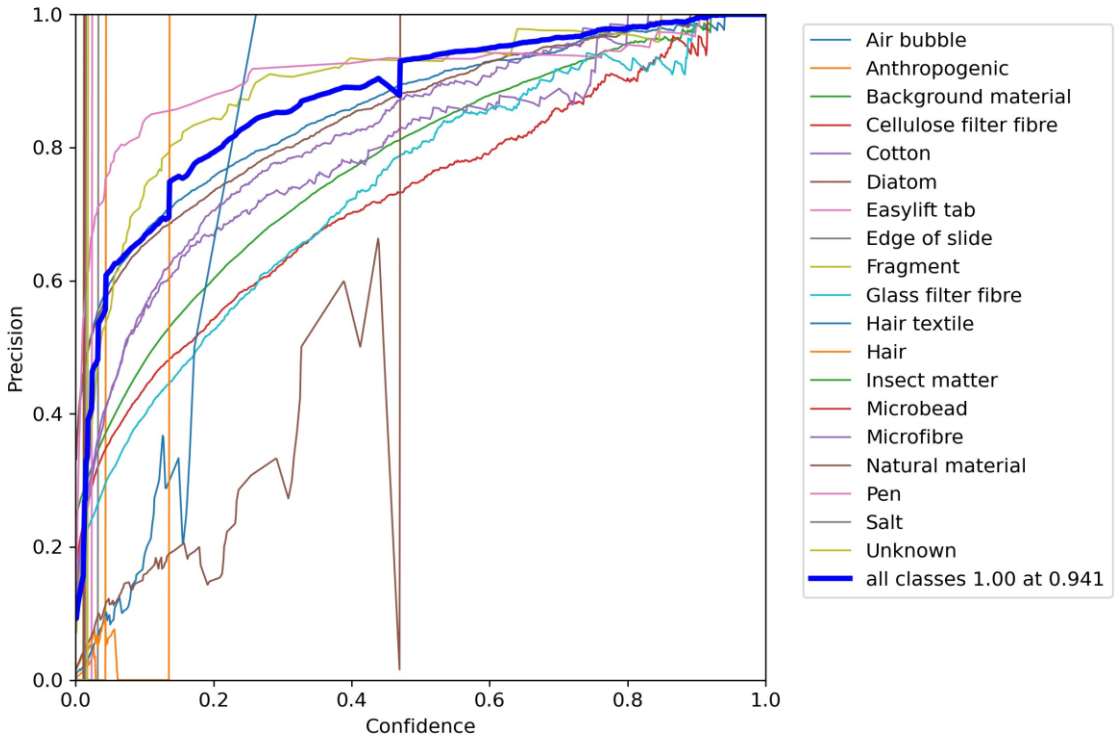

Figure 4.41 A precision-confidence curve to evaluate the model when trained using YOLOv7 for 25 epochs.

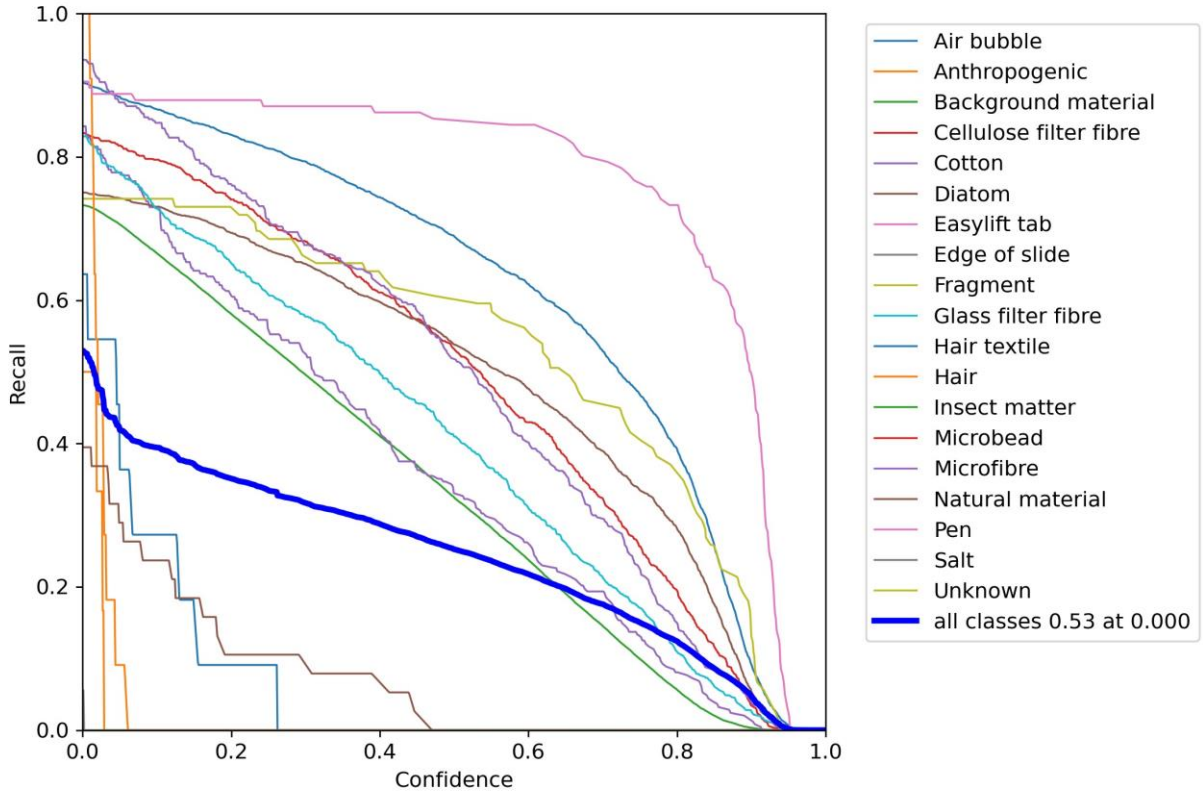

Figure 4.42 A recall-confidence curve to evaluate the model when trained using YOLOv7 for 25 epochs.

Figure 4.43 shows an F1-confidence curve when the dataset was trained with YOLOv7 for 25 epochs. All classes are at 0.35 at a confidence of 0.261, after this point the F1 score begins to decrease. This average is being lowered by the underperforming classes namely, natural material, hair, anthropogenic and hair textile. All the other classes are performing well above the average for all classes. The model overall performs best in the identification of pen, followed by air bubble, fragments, diatoms and microfibres.

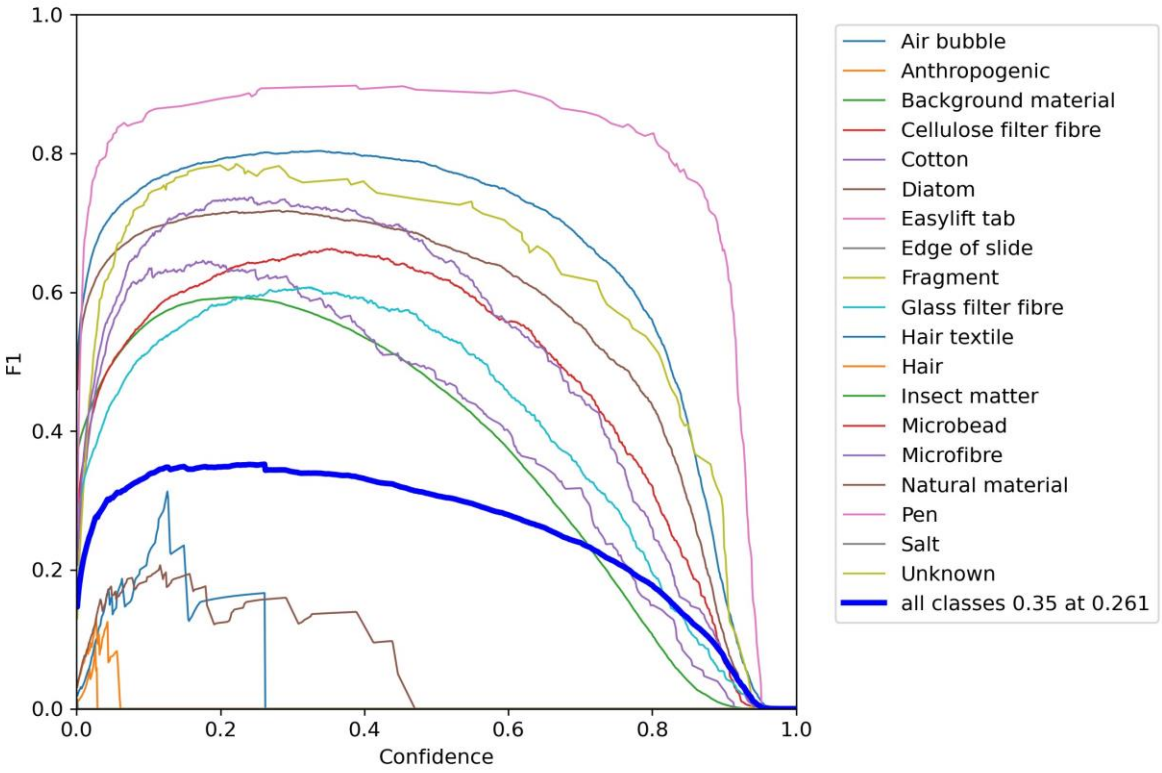

Figure 4.43 An F1-confidence curve to evaluate the model produced when trained using YOLOv7 for 25 epochs.

Figure 4.44 shows a precision-recall curve for the model produced by training with YOLOv7 for 25 epochs. The model was most successful at identifying pen with and area under the curve of 0.878, followed by air bubble with an area under the curve of 0.834, microfibres with an area under the curve of 0.781 and fragments with an area under the curve of 0.719. The

model was least successful at identifying unknown, microbeads, edge of slide and Easylift® tab with an area under the curve of 0.0 meaning no correct identifications were made for these classes. Overall, the model had an area under the curve of 0.354 indicating that the model has not performed well in the overall classification of objects commonly found in microplastic samples, but it has performed well in the detection of microplastic microfibres and fragments which is the main goal of this model.

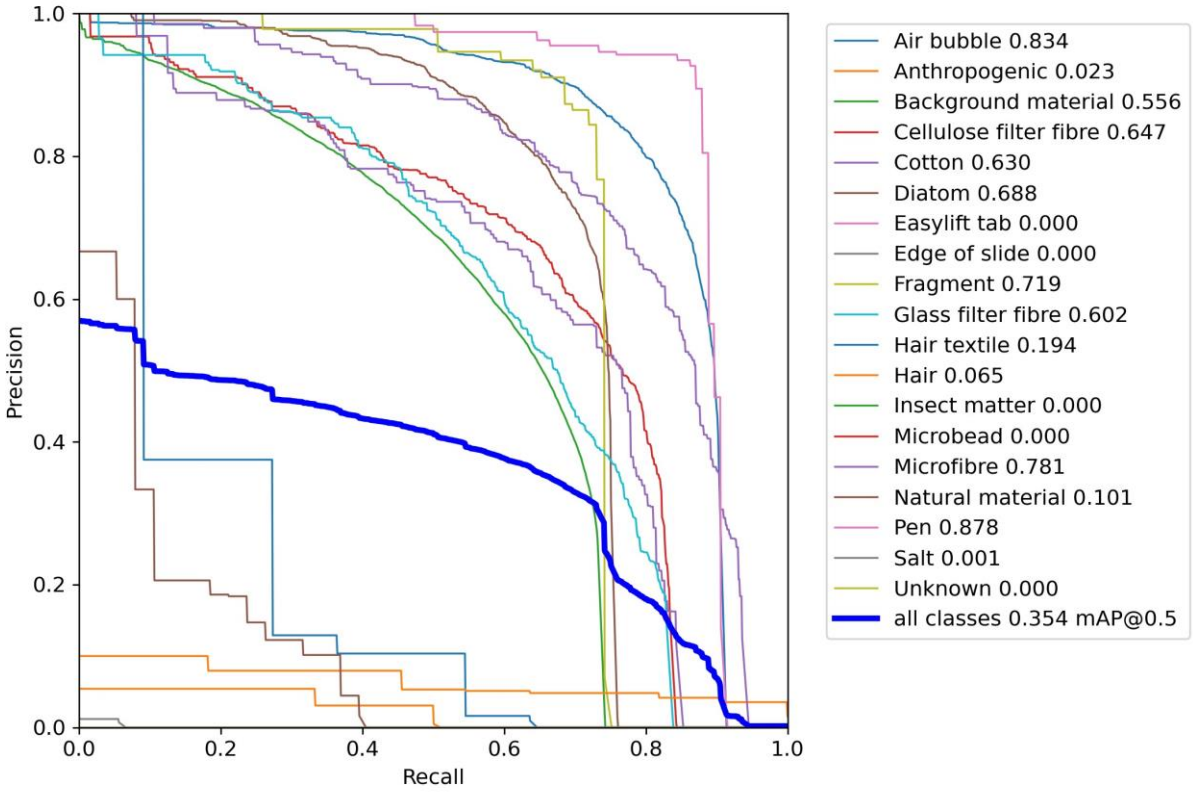

Figure 4.44 A Precision-Recall curve to evaluate the model when trained using YOLOv7 for 25 epochs.

4.3.2.2 YOLOv7 training with 100 epochs

Table 4.8 shows the metrics produced for each classification when trained with YOLOv7 for 100 epochs. The precision for all classes is 0.715 meaning that 71.5% of positive identifications were true positives. The recall is 0.463, meaning 46.3% of objects were correctly detected. The recall metric is still low in comparison to the precision meaning that there is a higher chance of false positives. The Overall F1 score was 0.562, which is still fairly low but an improvement from previous models discussed. From the metric shown in

Table 4.8 the model is most successful at identifying air bubbles (F1 score 0.796), pen (F1 score 0.901), fragments (F1 score 0.742), and microfibres (F1 score 0.755). The most accurate bounding boxes were made for air bubbles, pen, microfibres, air bubble and fragments. The precision for this model is lower than the model produced for 25 epochs, this could be because the model has begun to reach the point of over fitting where the model is no longer improving with each epoch (Géron, 2019). However, the recall, F1 score, and mAP metrics are higher than the 25-epoch algorithm, meaning this is unlikely to be the case. Another possible explanation for this decrease, is that the classes, edge of slide, hair and anthropogenic are now being detected which has brought their precision down from 1 reducing the models overall precision but actually means that the model is performing better as can be seen in the increased recall value.

Table 4.8 A table to show the overall precision, recall, F1 score, mAP50 (a metric to evaluate how successful an identification is when the Intersection Over Union (IOU) or the overlap between the predicted and actual bounding box is over 50% identification is successful) and mAP50-95 a metric to evaluate how successful an identification is when the IOU is 50-95%) when the images are trained with YOLOv7 and 100 epochs.

Class	Precision	Recall	F1 score	mAP50	mAP50-95
All	0.715	0.463	0.562	0.455	0.319
Air bubble	0.765	0.83	0.796	0.819	0.538
Anthropogenic	0.495	0.167	0.250	0.207	0.177
Background material	0.616	0.586	0.601	0.55	0.238
Cellulose filter fibre	0.596	0.712	0.649	0.683	0.397
Cotton	0.731	0.645	0.685	0.683	0.467
Diatom	0.755	0.716	0.735	0.708	0.446
Easylift tab	1	0	0	0	0
Edge of slide	0.538	0.538	0.538	0.538	0.357
Fragment	0.702	0.787	0.742	0.802	0.609
Glass filter fibre	0.54	0.647	0.589	0.593	0.334
Hair textile	0.512	0.545	0.528	0.485	0.446
Hair	0.369	0.586	0.453	0.369	0.326
Insect matter	1	0	0	0	0

Microbead	1	0	0	0	0
Microfibre	0.689	0.834	0.755	0.814	0.592
Natural material	0.365	0.316	0.339	0.305	0.223
Pen	0.906	0.897	0.901	0.9	0.722
Salt	1	0	0	0.115	0.0746
Unknown	1	0	0	0.123	0.11

Figure 4.45 shows a confusion matrix produced when the dataset was trained with YOLOv7 for 100 epochs. Air bubbles had a true positive identification rate of 82% (2293 identifications), 4% (112 identifications) were misidentified as background materials. The model has a low rate of misidentification for the air bubble class. Anthropogenic material had a true positive identification rate of 50% (3 identifications), the remaining 50% were false negatives and not detected by the model. Background material had a true positive rate of 62% (29265 identifications), there were no misidentifications for background material and the remaining objects were not detected by the algorithm; the false negative rate for background material is likely to always be a bit higher than the other classifications as it was so ubiquitous within each image, and it was a subjective opinion as to what was within each bounding box. Some bounding boxes contained many small bits of background material that the algorithm could identify individually. Conversely, the algorithm could be grouping background materials that had their own individual bounding box. Cellulose filter fibres had a true positive identification rate of 67% (614 identifications). Misidentifications for cellulose filter fibre were air bubble 1% (9 identifications), background material 10% (92 identifications) and cotton 2% (18 identifications). Cotton had a true positive rate of 73% (181 identifications), misidentifications for cotton were, background material 2% (5 identifications), cellulose filter fibre 3% (7 identifications), diatoms 1% (2 identifications), microfibre 3% (7 identifications) and natural material 2% (5 identifications). Diatoms had a true positive identification rate of 73% (1777 identifications), with the only misidentification being background material 4% (97 identifications), this is a good rate of detection for the diatom classification, as with other

classifications they suffer from image overcrowding and could be easily missed or misclassified, particularly on images with a lower magnification. Easylift® tab, insect matter, salt and unknown all had no positive identifications and were not detected by the model. The edge of the slide had a true positive identification rate of 64% (8 identification); the only misidentification was for the Easylift® tab at 9% (1 identification); this is likely because the Easylift® tab is on the edge of a slide is often going to be present in the same image. Fragments have a true positive identification rate of 80% (71 identifications), misidentifications for fragments were, background material 9% (8 identifications), and microbead and microfibre were both 1% (1 identification). This is a good identification rate for fragments in addition only 10 fragments were wrongly classified and a further 8 missed meaning that this model is able to identify the majority of fragments. Glass filter fibre had a true positive identification rate of 64% (527 identifications), the misidentifications for glass filter fibres were, background material 6% (49 identifications) and cellulose filter fibres 1% (8 identifications). Hair textile had a true positive identification rate of 67% (8 identifications) the only misidentification was for microfibres at 22% (2 identifications). Hair had a true positive identification rate of 50% (5 identifications), with the remaining 50% (5 identifications) being identified as microfibres. It is unsurprising that both hair and hair textile have misidentifications for microfibres as they will both be visually similar to microfibres as they fit the definition for a fibre. Microbeads were not detected and had no misidentifications; this may be due to low representation in the dataset and overcrowding in the images that the class is present in this may improve if the model is run for more epochs. Microfibres had a true positive detection rate of 74% (286 identifications), the misidentifications for microfibre were, anthropogenic 1% (4 identifications), background material 2% (8 identifications), cellulose filter fibre 1% (4 identifications), cotton 8% (31 identifications), and natural material 1% (4 identifications). This model has a good correct prediction rate for microfibres, but there are still some misidentifications being made and microfibres being missed by the model. Natural material had a true positive prediction rate of 43% (16 identifications). The misidentifications for natural material were, background material 4% (2 identifications), cellulose filter paper 11% (4

identifications), cotton 18% (6 identifications), diatoms 4% (2 identifications) and glass filter fibres 4% (2 identifications). Pen had a true positive detection rate of 94% (109 identifications), the misidentifications for pen were, background material 2% (2 identifications) and diatoms 1% (1 identification). On the whole, this model has performed well the majority of classes have a positive identification rate over 60%, there is still room for improvement, however, as there are still regular misidentifications.

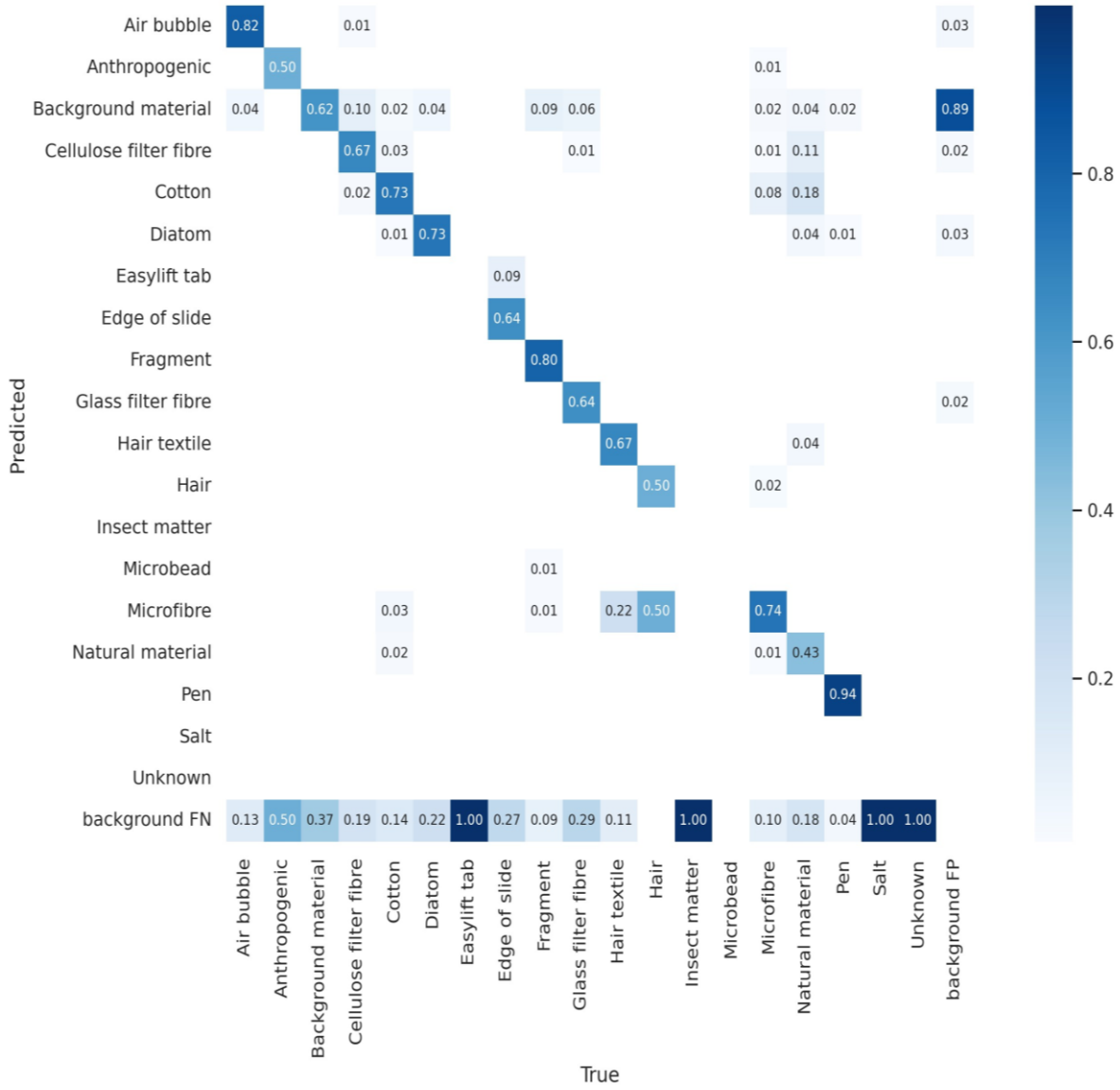

Figure 4.45 A confusion matrix to show how successful the algorithm was at correctly predicting each class when trained using YOLOv7 for 100 epochs.

Figure 4.46 shows a precision-confidence curve and Figure 4.47 shows a recall-confidence curve when the dataset was trained with YOLOv7 for 100 epochs. From these two graphs the model's precision is high with all classes being having a precision of 1.0 at a confidence level of 0.961. The recall is lower than precision with all classes having a recall of 0.61 at a confidence of 0.0. This on the surface does not seem like the model has performed well for recall, but this is because the average is being brought down by a few underperforming classes, like unknown and salt that had no correct identifications. Other classifications are performing very well for recall with pen, air bubble, microfibre and fragments having the best recall in this model.

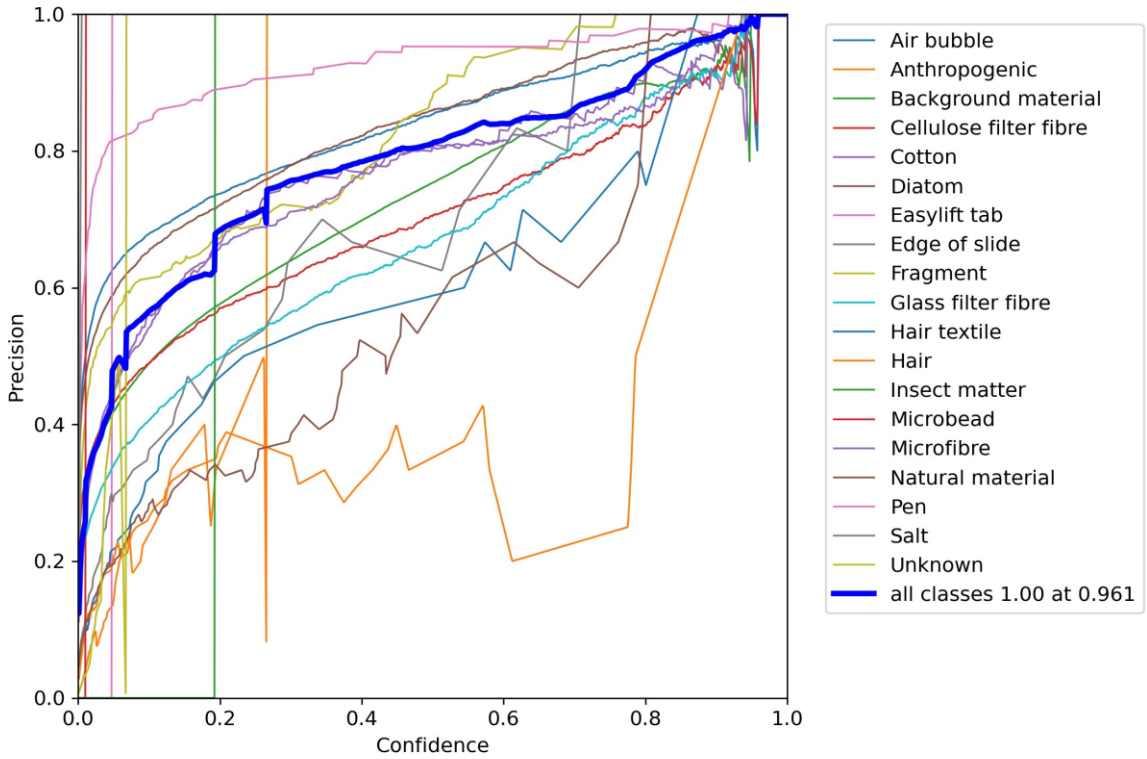

Figure 4.46 A precision-confidence curve to evaluate the model when trained using YOLOv7 for 100 epochs.

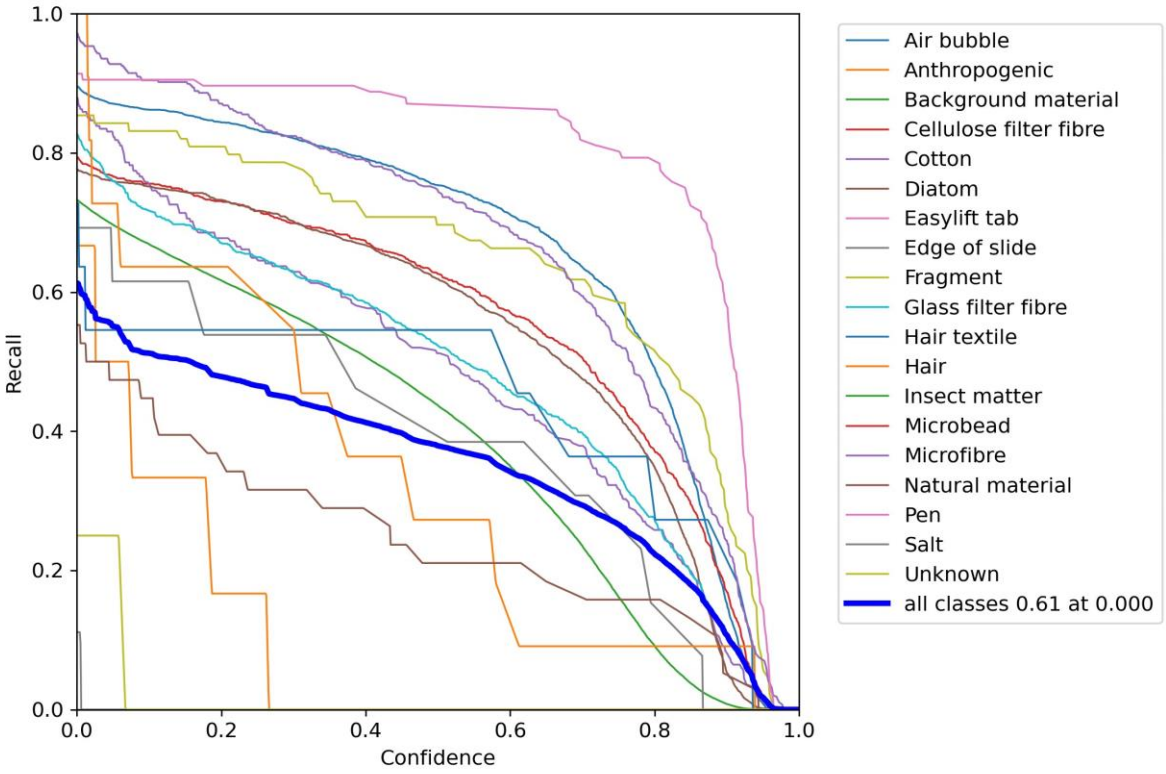

Figure 4.47 A recall-confidence curve to evaluate the model when trained using YOLOv7 for 100 epochs.

Figure 4.48 shows a F1-confidence curve when the dataset was trained with YOLOv7 for 100 epochs. All classes are at 0.45 at a confidence of 0.260, after this point the F1 score begins to decrease. This average is, however, being brough down a few underperforming classes including, natural material, hair, anthropogenic, salt, unknown and hair textile. All the other classes are performing well above the average for all classes. The model overall performs best in the identification of pen, followed by air bubble, fragments, microfibres and diatoms.

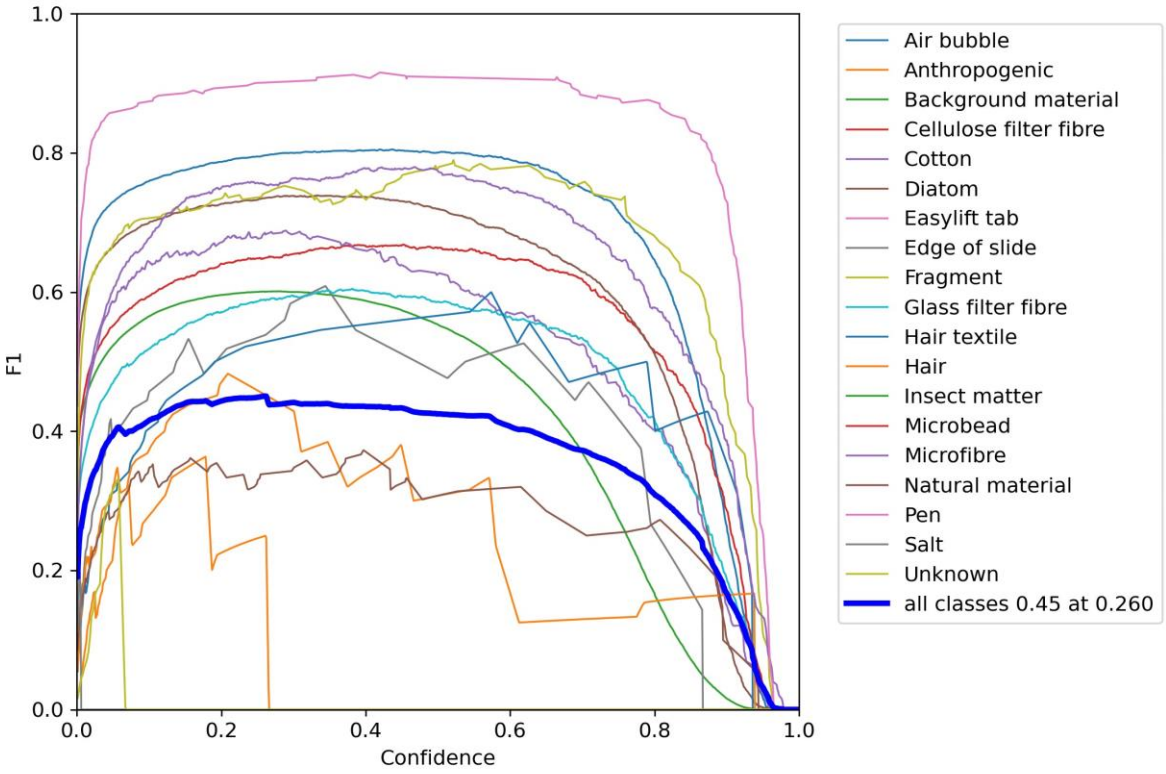

Figure 4.48 An F1-confidence curve to evaluate the model produced when trained using YOLOv7 for 100 epochs.

Figure 4.49 shows a precision-recall curve for the model produced by training with YOLOv7 for 100 epochs. The model was most successful at identifying pen with an area under the curve of 0.900, followed by air bubble with an area under the curve of 0.819, microfibres with an area under the curve of 0.814 and fragments with an area under the curve of 0.802. The model was least successful at identifying microbeads, insect matter and Easylift® tab with an area under the curve of 0.0 meaning no correct identifications were made for these classes. Overall, the model had an area under the curve of 0.455, indicating that the model has not performed well in the overall classification of objects commonly found in microplastic samples.

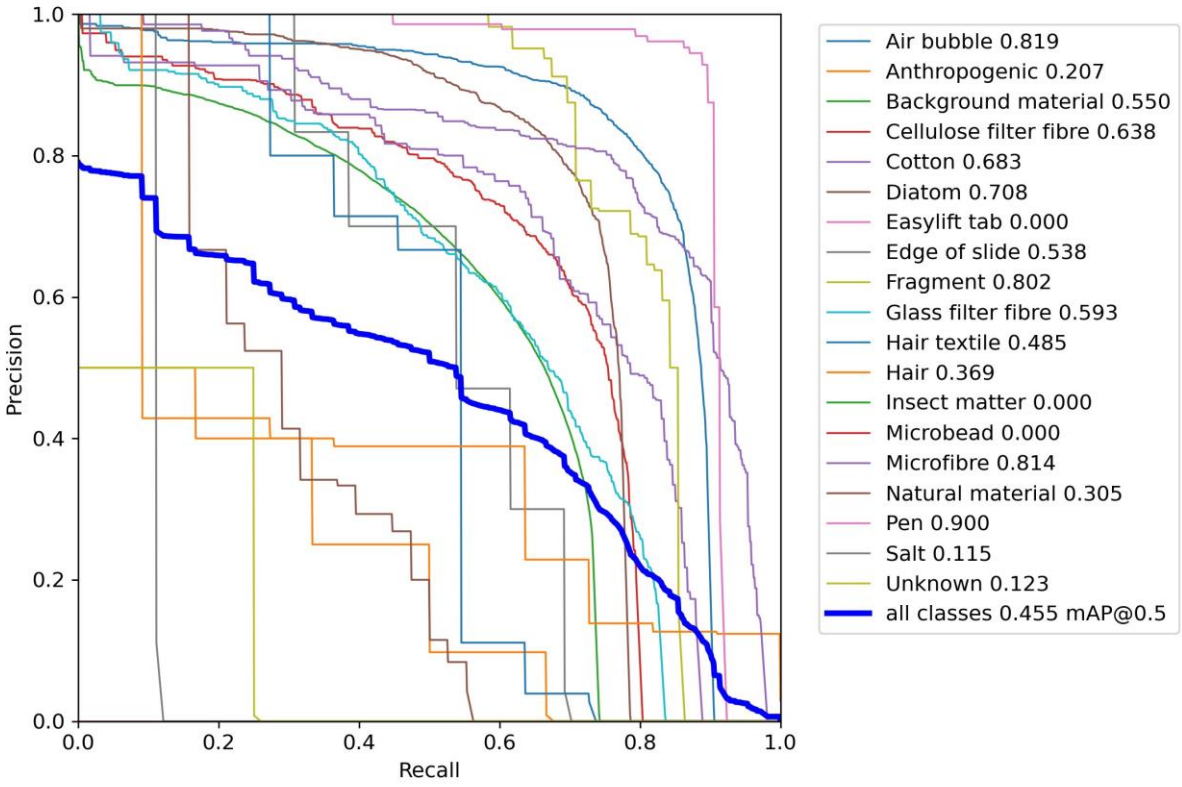

Figure 4.49 A Precision-Recall curve to evaluate the model when trained using YOLOv7 for 100 epochs.

4.3.2.3 YOLOv7 Training with Augmented Data and 100 Epochs

Table 4.9 shows the metrics produced for each classification when trained with YOLOv7 for 100 epochs with augmented images used in the training data. The precision for all classes is 0.611, meaning that 61.1% of positive identifications were true positives. The recall is 0.56, meaning 56% of objects were correctly detected. For this model the precision and recall are closer to each other. The F1 score for all classes is 0.584, which is still a low F1 score. Some classifications performed very well in this model with pen performing the best with a F1 score of 0.878, which is a very good result. Microfibres and fragments also performed well in this model with both having an F1 score over 0.750 which would be considered successful, meaning that this model is able to correctly identify microplastics with a good level of success and reliability. According to Table 4.9 the model also had some success with microbeads as it had a precision of 0.997 and a recall of 1, meaning that it had a 100% success rate for identifying microbeads, but as this is a very underrepresented class in the data set (only one instance) this

does not fully demonstrate how well the model may or may not be able to identify microbeads. The dataset would need to be expanded to include more microbeads to be able to say with confidence how successful it was at identifying microbeads.

Table 4.9 A table to show the overall precision, recall, F1 Score, mAP50 (a metric to evaluate how successful an identification is when the Intersection Over Union (IOU) or the overlap between the predicted and actual bounding box is over 50% identification is successful) and mAP50-95 a metric to evaluate how successful an identification is when the IOU is 50-95%) when the augmented images are trained with YOLOv7 and 100 epochs.

Class	Precision	Recall	F1 Score	mAP50	mAP50-95
All	0.611	0.56	0.584	0.542	0.394
Air bubble	0.754	0.832	0.791	0.815	0.532
Anthropogenic	0.407	0.5	0.449	0.495	0.424
Background material	0.58	0.584	0.582	0.522	0.223
Cellulose filter fibre	0.544	0.71	0.622	0.611	0.387
Cotton	0.657	0.748	0.700	0.712	0.491
Diatom	0.721	0.68	0.700	0.658	0.404
Easylift tab	1	0	0	0.249	0.174
Edge of slide	0.486	0.692	0.571	0.541	0.412
Fragment	0.812	0.779	0.795	0.791	0.609
Glass filter fibre	0.505	0.525	0.515	0.462	0.262
Hair textile	0.492	0.636	0.555	0.553	0.459
Hair	0.323	0.608	0.422	0.39	0.348
Insect matter	0	0	0	0	0
Microbead	0.997	1	0.998	0.995	0.796
Microfibre	0.706	0.832	0.764	0.83	0.634
Natural material	0.462	0.368	0.410	0.314	0.226
Pen	0.868	0.888	0.878	0.889	0.738
Salt	1	0	0	0.0908	0.0574
Unknown	0.296	0.25	0.271	0.383	0.311

Figure 4.50 shows a confusion matrix produced when the dataset was trained with YOLOv7 for 100 epochs and augmented images were used in the training dataset. Air bubble had a true positive detection rate of 81% (2265 identifications), the only misidentification was background material 4% (112 identifications). Anthropogenic material had a true positive identification rate of 40% (4 identifications), the misidentifications for anthropogenic material were, background material 20% (2 identifications) and microfibres 20% (2 identifications). The misidentifications for anthropogenic are understandable as it is a small, underrepresented class, that is a result of being unable to provide a conclusive identification further than it being anthropogenic in origin, and so the features of this class are going to be very varied. Background material had a true positive identification rate of 57% (26905 identifications), there were no misidentifications for this classification only false negatives. Cellulose filter fibres had a true positive identification rate of 66% (605 identifications). There were some misidentifications for cellulose filter fibres, they were, air bubble 1% (9 identifications), background material 9% (84 identifications), cotton 2% (18 identifications), diatoms 1% (9 identifications) and microfibre 1% (9 identifications). Cotton has a true positive identification rate of 70% (174 identifications), the misidentifications for cotton were, background material 3% (7 identifications), cellulose filter fibres 3% (7 identifications), diatoms 1% (2 identifications), glass filter fibre 1% (2 identifications), microfibres 5% (12 identifications) and natural material 2% (5 identifications). Both cotton and cellulose filter fibres have several different classification misidentifications, but the level of misidentification for each other is low. This is good as cotton would be counted in studies that are looking at all anthropogenic pollution such as Stanton *et al.* (2019) whereas cellulose filter fibres would not as they have originated from the filter paper used. Diatoms had a true positive detection rate of 67% (1631 identifications), the only misidentification was for background material 4% (97 identifications). Easylift® tab, insect matter, microbead and salt all had no correct positive identifications, and so were not detected by this model, this is likely due to the underrepresentation of these classes in the dataset. The

edge of the slide had a true positive identification rate of 64% (8 identifications), the misidentifications for this classification were, air bubble 7% (1 identification) and Easylift® tab 14% (2 identifications), as the number of instances for this classification are low the representation of the class needs to be increased to have a more accurate indication of the level of success of identification. Fragments had a true positive identification rate of 81% (72 identifications) this is a good identification rate for fragments. The misidentifications were background material 4% (3 identifications), cotton 1% (1 identification), microbead 1% (1 identification) and microfibre 1% (1 identification). It is interesting that there was a misidentification for microbeads as they had such a low representation within the dataset, but they can appear very similar to fragments in an image where microsectioning to see the 3D shape is not possible. Glass filter fibre had a true positive identification rate of 50% (412 identifications) the only misidentifications was background material 5% (41 identifications), this is likely due to the overcrowding of the microscope images and the fact that the glass filter fibres are long and thin meaning they are likely to be close to other objects and appear within their bounding box. Hair textile had a true positive identification rate of 50% (6 identifications), the misidentification for textile hair was microfibres 40% (4 identifications), this is likely due to the fact that they both fit the definition of fibres and the natural features of hair are not visible in every image. Hair had a true positive identification rate of 42% (5 Identifications) and the misidentifications were for microfibres 58% (6 identifications), as with hair textile the classification hair will appear very visually similar to microfibres and as microfibres make up a larger proportion of the data set it is not unsurprising that the misidentifications for both hair and hair textile were microfibres. Microfibres had a true positive identification rate of 79% (306 identifications). The misidentifications for microfibres were cotton 5% (19 identifications) and, air bubble, anthropogenic, background material, cellulose filter fibre, fragment, hair and natural material 1% (3 identifications respectively). The level of correct identification for microfibres is good with the majority being correctly detected. Natural material had a true positive identification rate of 46% (17 identifications). The misidentifications were background material, cotton and unknown 4% (1 identification

respectively) and fragments and microfibres 8% (3 identifications). Pen had a true positive identification rate of 94% (109 identifications), the misidentifications were, background material and diatoms 1% (1 identification respectively). This is a very good performance for the identification of this classification, with the vast majority being correctly identified. Overall, the model has performed very well in the detection of microplastics, and most classes having a correct detection rate of over 50%.

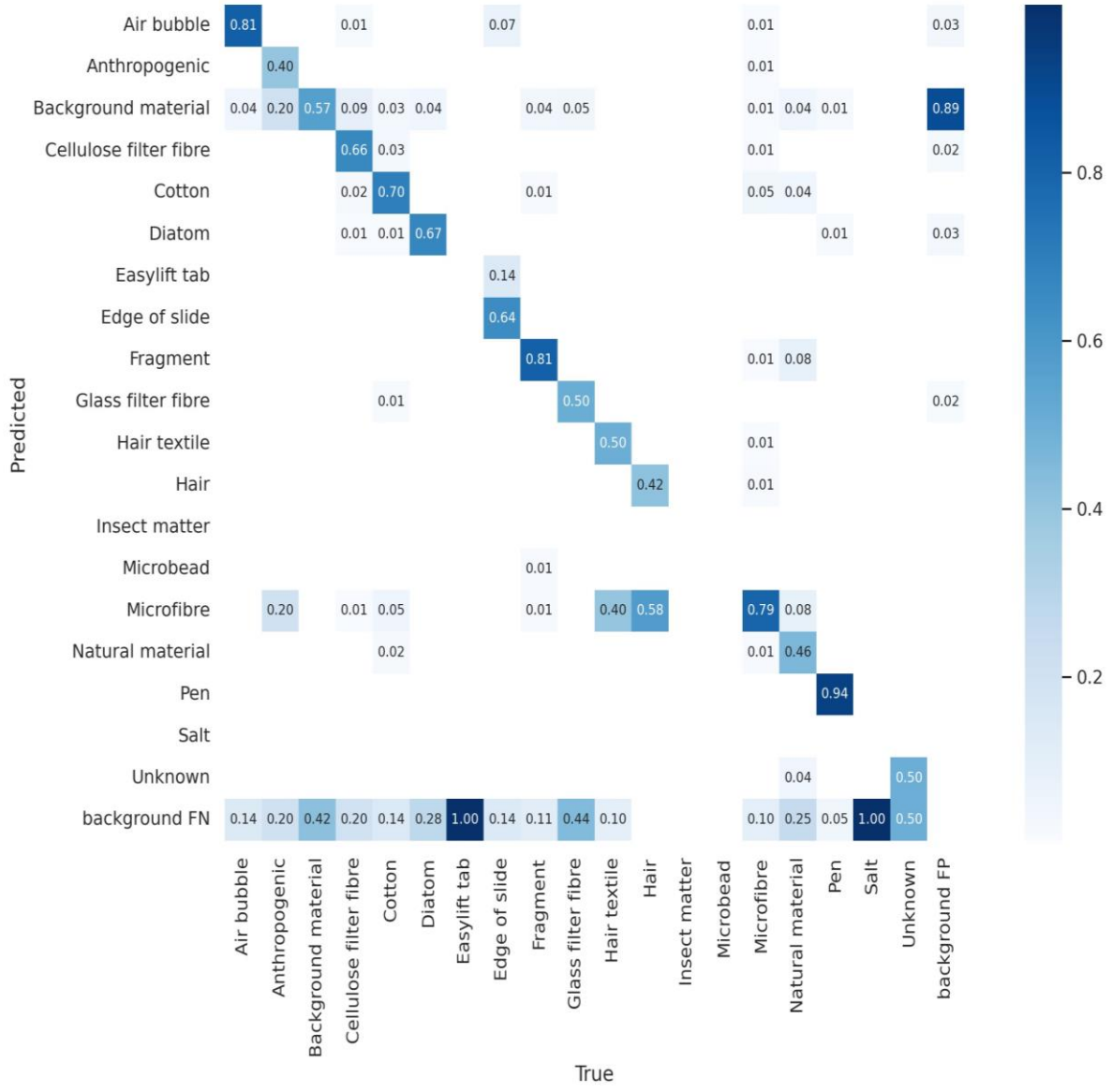

Figure 4.50 A confusion matrix to show how successful the algorithm was at correctly predicting each class when trained with augmented images using YOLOv7 for 100 epochs.

Figure 4.51 shows a precision-confidence curve and Figure 4.52 shows a recall-confidence curve when the dataset was trained with YOLOv7 for 100 epochs with augmented images used in the training dataset. From these two graphs the model's precision is high with all classes being having a precision of 1.0 at a confidence level of 0.961. The recall is lower than precision with all classes having a recall of 0.70 at a confidence of 0.0. This on the surface does not seem like the model has performed well for recall, but this is because the average is being brought down by a few underperforming classes, like unknown and salt that had no correct identifications. Other classifications are performing very well for recall with pen, air bubble, microfibre and fragments having the best recall in this model.

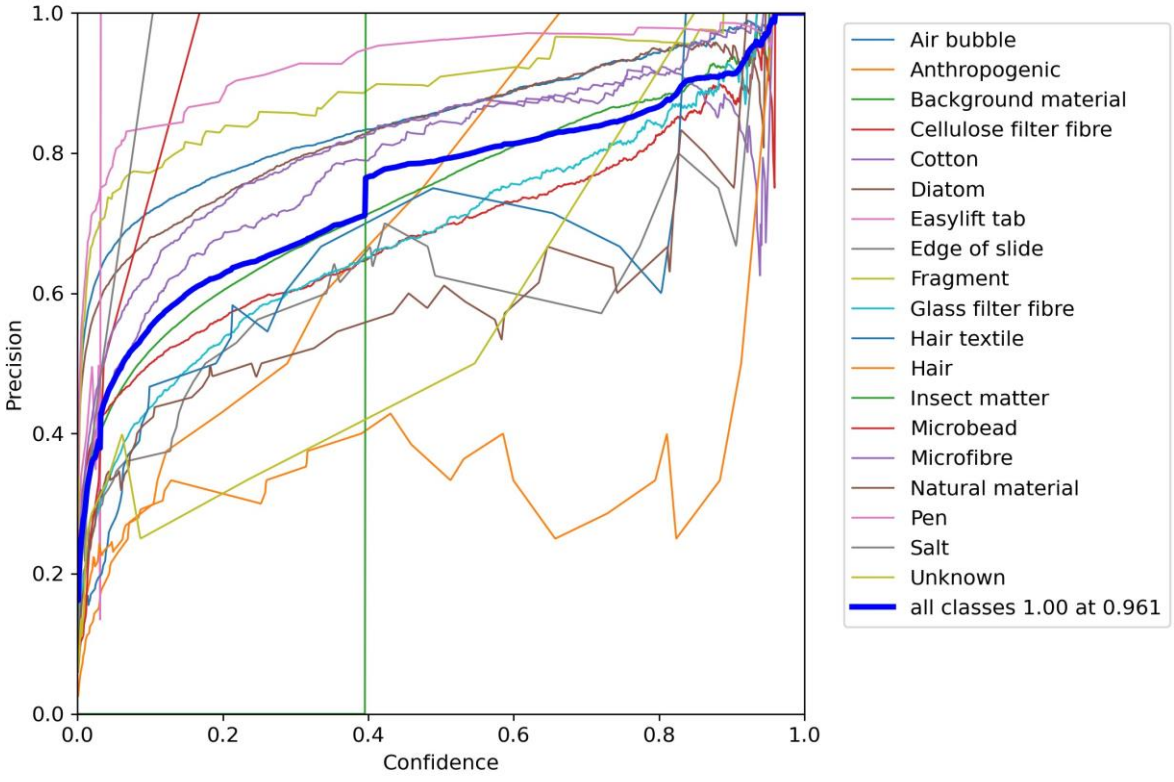

Figure 4.51 A precision-confidence curve to evaluate the model when trained with augmented images using YOLOv7 for 100 epochs.

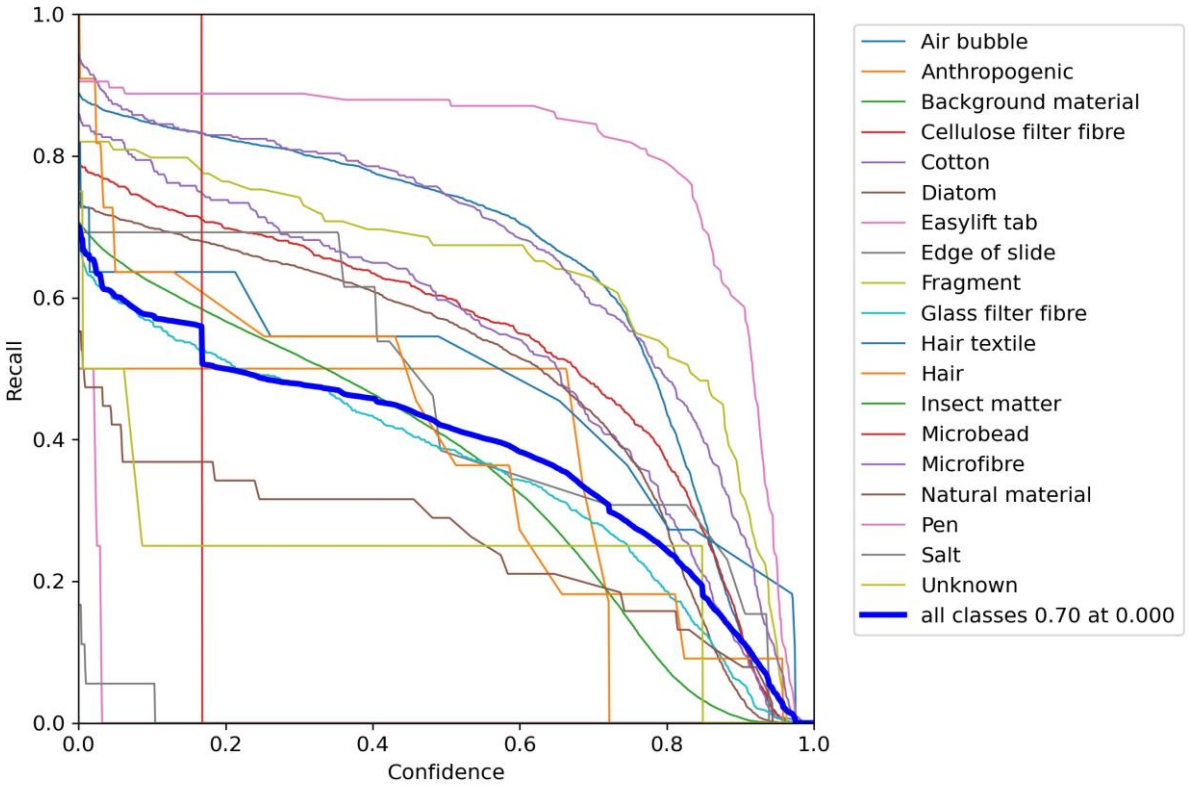

Figure 4.52 A recall-confidence curve to evaluate the model when trained with augmented images using YOLOv7 for 100 epochs.

Figure 4.53 shows a F1-confidence curve when the dataset was trained with YOLOv7 for 100 epochs and augmented images used in the training dataset. All classes are at 0.53 at a confidence of 0.167, after this point the F1 score begins to decrease. The model overall performs best in the identification of pen, followed by air bubble, fragments and microfibres.

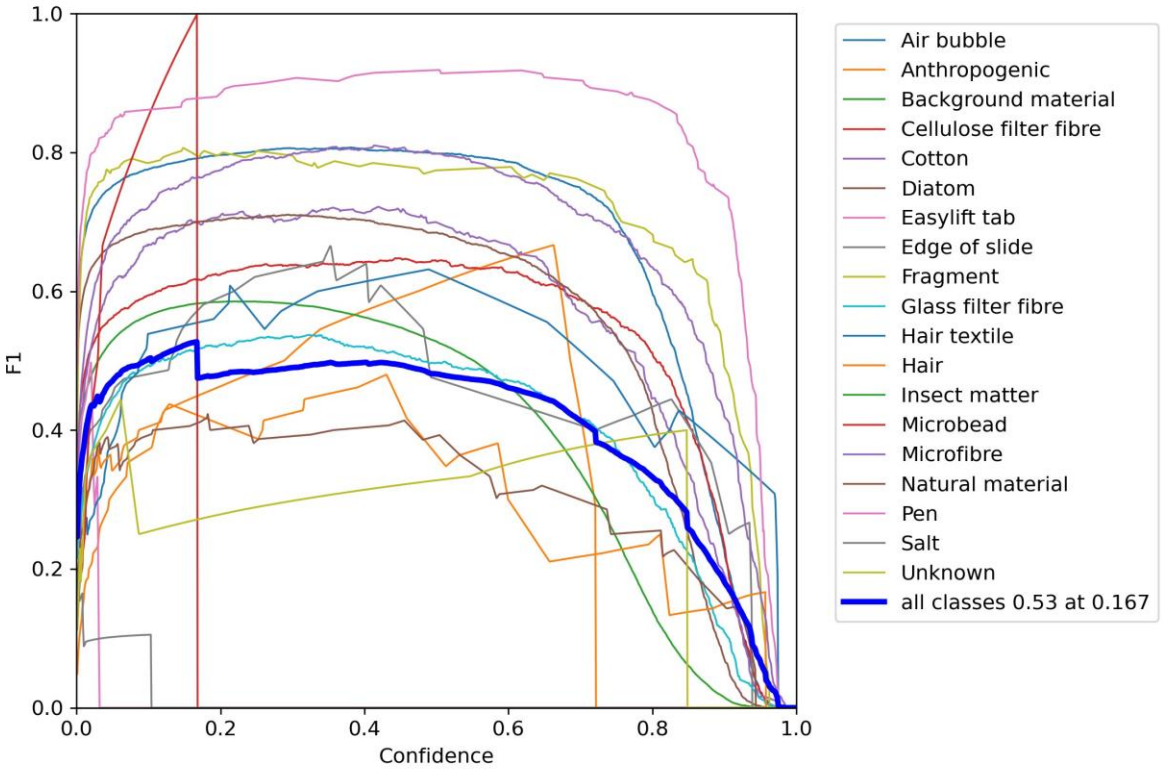

Figure 4.53 An F1-confidence curve to evaluate the model produced when trained with augmented images using YOLOv7 for 100 epochs.

Figure 4.54 shows a precision-recall curve for the model produced by training with YOLOv7 for 100 epochs with augmented images used in the training dataset. From this table it appears that the model was most successful at identifying microbeads with an area under the curve of 0.995, but as this is a very underrepresented class in the data set (only one instance) this does not fully demonstrate how well the model may or may not be able to identify microbeads. The dataset would need to be expanded to include more microbeads to be able to say with confidence how successful it was at identifying microbeads, as only one correct identification would be a 100% detection rate. Pen is then the next most successful identification with an area under the curve of 0.889 followed by microfibres with an area under the curve of 0.830, air bubbles with an area under the curve of 0.815 and fragments with an area under the curve of 0.791. The model was least successful at identifying insect matter with an area under the curve of 0.0, meaning no correct identifications were made for these classes. Overall, the model had an area under the curve of 0.542 indicating that the model has performed average in the overall classification of objects commonly found in

microplastic samples. But some classes are being correctly classified more than others.

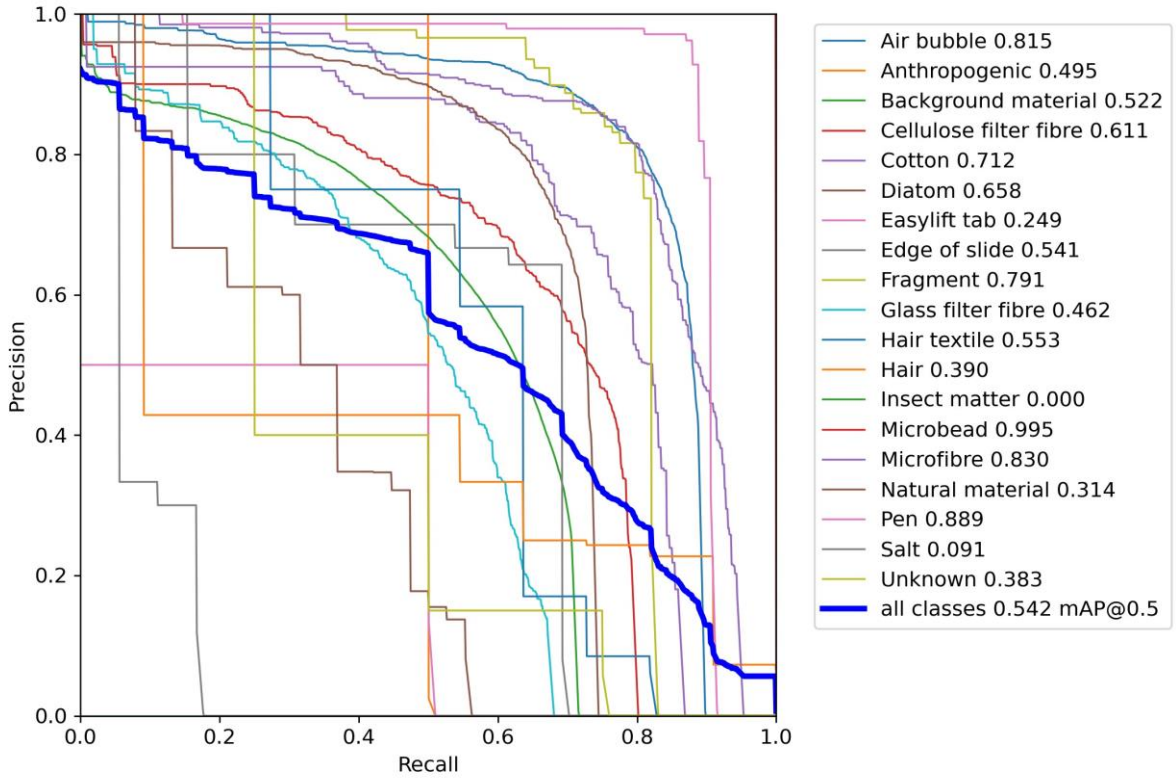

Figure 4.54 A Precision-Recall curve to evaluate the model when trained with augmented images using YOLOv7 for 100 epochs.

4.3.3. YOLOv8

4.3.3.1 YOLOv8 Training With 25 Epochs

Table 4.10 shows the metrics produced for each classification when trained with YOLOv8 for 25 epochs. The precision for all classes is 0.719 meaning that 71.9% of positive identifications were true positives. The recall is 0.376, meaning 37.6% of objects were correctly detected. For this model the precision and recall are closer to each other. The F1 Score for all classes is 0.494 this is a low overall F1 score. Microfibres and fragments have done well in this model with both having and F1 score over 0.700. Easylift® tab, insect matter, microbead, salt and unknown all have a recall of 0 meaning that this model was not able to identify any occurrence of these classes correctly. From the data in Table 4.10 the model is most successful at

identifying pen, air bubbles, microfibres and fragments. The most accurate bounding boxes were produced by pen, microfibres and fragments.

Table 4.10 A table to show the overall precision, recall, F1 Score, mAP50 (a metric to evaluate how successful an identification is when the Intersection Over Union (IOU) or the overlap between the predicted and actual bounding box is over 50% identification is successful) and mAP50-95 a metric to evaluate how successful an identification is when the IOU is 50-95%) when trained with YOLOv8 and 25 epochs.

Class	Precision	Recall	F1 Score	mAP50	mAP50-95
All	0.719	0.376	0.494	0.414	0.301
Air bubble	0.821	0.698	0.755	0.783	0.517
Anthropogenic	0.718	0.167	0.271	0.193	0.156
Background material	0.699	0.434	0.536	0.542	0.247
Cellulose filter fibre	0.636	0.498	0.559	0.553	0.355
Cotton	0.591	0.624	0.607	0.634	0.526
Diatom	0.791	0.539	0.641	0.653	0.403
Easylift tab	1	0	0	0	0
Edge of slide	0.498	0.385	0.434	0.478	0.298
Fragment	0.704	0.723	0.713	0.776	0.61
Glass filter fibre	0.606	0.42	0.496	0.472	0.277
Hair textile	0.383	0.273	0.319	0.327	0.301
Hair	0.374	0.727	0.494	0.521	0.428
Insect matter	1	0	0	0	0
Microbead	1	0	0	0	0
Microfibre	0.711	0.724	0.717	0.786	0.651
Natural material	0.228	0.105	0.122	0.123	0.104
Pen	0.901	0.828	0.863	0.885	0.739
Salt	1	0	0	0.0887	0.0627
Unknown	1	0	0	0.0515	0.0412

Figure 4.55 shows a confusion matrix produced when the dataset was trained with YOLOv8 for 25 epochs. Air bubble has a true positive identification rate of 73% (2041 identifications). The misidentifications for air bubble were, background material 6% (168 identifications) and cellulose filter fibre 1% (28 identifications). The model has a good reliability identifying air bubbles and those that were not identified (false negatives) could be due to

the fact that some air bubbles were very large or had part that were interrupted by other objects that may mean that the human manually tagging may have provided bounding boxes that the model would classify differently for example one large air bubble may have been given two boxes by the examiner and only one by the model or vice versa. There were no correct identifications for anthropogenic, the misidentifications for anthropogenic were cotton 17% (1 identification) and microfibre 50% (6 identifications), the misidentifications are understandable as both cotton and microfibres fall under the definition of anthropogenic as they are artificial. Background material had a true positive detection rate of 54% (25489 identifications) there were no misidentifications for this classification the remaining objects in the classification were not detected by the model. Cellulose filter fibres had a true positive detection rate of 56% (514 identifications). The misidentifications for cellulose filter fibres were air bubble 2% (18 identifications, background material 10% (92 identifications) and cotton 2% (18 identifications). Cotton had a true positive identification rate of 60% (149 identifications). The misidentifications for cotton were air bubble 1% (2 identifications), background material 2% (5 identifications), cellulose filter fibres 8% (20 identifications), hair 1% (2 identifications), microfibre 10% (25 identifications) and natural material 3% (7 identifications). Diatom had a true positive identification rate of 58% (1412 identifications) the only misidentifications for diatoms were background material 10% (243 identifications). This is likely because diatoms were often mixed in with the background material and would be difficult to separate in the bounding boxes. The diatoms were also quite easy to miss in samples with a high level of background material as the debris could obscure the diatoms. Easylift® tab had no correct identifications the misidentifications for this classification were background material and edge of slide 25% (2 identifications respectively). Both incorrect classifications are likely to appear in the vicinity of the Easylift® tab, indicating that the Easylift® tab classification needed better representation in the dataset to help avoid these misidentifications. The edge of slide classification had a true positive identification rate of 38% (5 identifications). The misidentifications were background material 8% (1 identification), cellulose filter fibre 15% (2 identifications), cotton 8% (1

identification) and pen 8% (identification). As with Easylift® tab, edge of slide is and underrepresented class and so to increase the model's ability to correctly identify this class its representation in the dataset should be increased. Fragments had a true positive identification rate of 69% (61 identifications). The misidentifications for fragments were, background material 15% (13 identifications), cotton, diatoms and pen are misclassified in 1% of cases (1 identification respectively). Overall, the model had done fairly well at identifying fragments, but the performance could be improved by increasing training time or increasing the number of fragments in the dataset. Glass filter fibres had a true positive identification rate of 49% (404 identifications). The misidentifications for glass filter fibres were air bubble 1% (8 identifications and cotton 18% (49 identifications). The misidentification for cotton is unexpected as they have different features being that one is a natural fibre, and one is synthetic. The only commonality between the two is that the cotton can be colourless which is why it may have been identified as glass filter fibres. The colourless cotton and glass filter fibres are also likely to appear in the same images as glass filter papers were predominantly used with the air samples which allowed the colourless cotton to be detected whereas when the cellulose filter fibres were used the colourless cotton could not be differentiated between the cellulose filter fibres. Hair textile had a true positive identification rate of 27% (3 identifications). The misidentifications for this classification were air bubble 9% (1 identification), cotton 18% (2 identifications) and microfibres 36% (4 identifications). The fact that more textile hairs are being identified as microfibres that hairs is an issue as it might falsely inflate the number of microplastics counted in a sample. Hair had a true positive identification rate of 55% (6 identifications). The misidentifications for this classification were cotton 9% (1 identification) and microfibres 36% (4 identifications). The fact that hair and hair textile were not confused for each other is a good sign, but as they are very small classes, if the representation were to increase, it is likely that the level of misidentification for each other would also increase. But this would potentially resolve the issue of being misidentified as a microfibre. Insect matter had no correct identifications, but there were misidentifications, cellulose filter fibre, cotton and pen were all identified in

33% of insect matter instances (1 identification respectively). However, as the class is so small and underrepresented the chance of a successful identification is low, and this classification needs to be increased. Microbeads also had no correct identifications 100% of microbeads were identified as fragments (1 identification), but, as this equates to only one identification this is not a reliable predictor in how the model will perform, although it is not likely to be able to identify microbeads well until their representation has been increased. Microfibres had a true positive identification rate of 74% (286 identifications). Microfibres were misidentified as air bubbles, background material, hair textile, hair and natural material 1% of the time (4 identifications respectively) and cotton 9% (35 identifications). Overall, the model has performed well in the identification of microfibres but there is still room for improvement. Natural material had a true positive identification rate of 13% (5 identifications). The misidentifications were, background material 24% (9 identifications), cotton 18% (7 identifications), diatom 5% (2 identifications and microfibres 8% (3 identifications). Pen had a true positive identification rate of 83% (96 identifications). The misidentifications for pen were air bubble 2% (2 identifications) and background material 10% (12 identifications). Salt had no correct identifications, salt had a 67% misidentification rate for background material (12 identifications), to resolve this more samples with high levels of salt need to be included in the dataset. Overall, the model has not performed well in the classification in all objects that may be present in samples. It has, however, performed fairly well in the identification of microplastics, with both fragments and microfibres correctly identified in nearly 70% of cases.

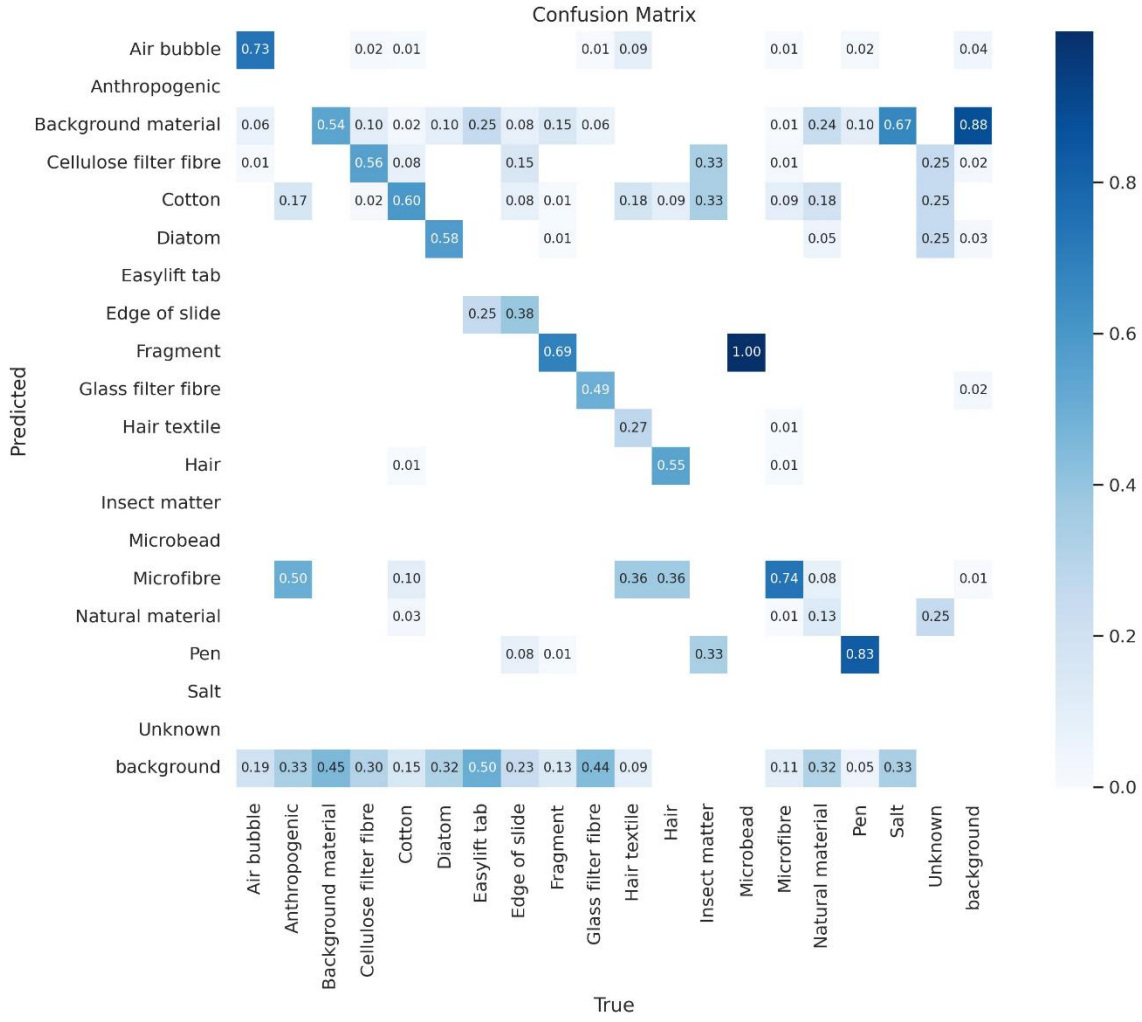

Figure 4.55 A confusion matrix to show how successful the algorithm was at correctly predicting each class when trained using YOLOv8 for 25 epochs.

Figure 4.56 shows a precision-confidence curve and Figure 4.57 shows a recall-confidence curve when the dataset was trained with YOLOv8 for 25 epochs. From these two graphs it can be seen that the model's overall precision is high with all classes being having a precision of 1 at a confidence level of 0.968, whereas the overall recall is relatively low for this model with all classes having a recall of 0.54 at a confidence of 0.0. However, some of the classes are performing far better than others which is bringing the average down. For instance, pen, air bubble and fragments have a good recall level for this model.

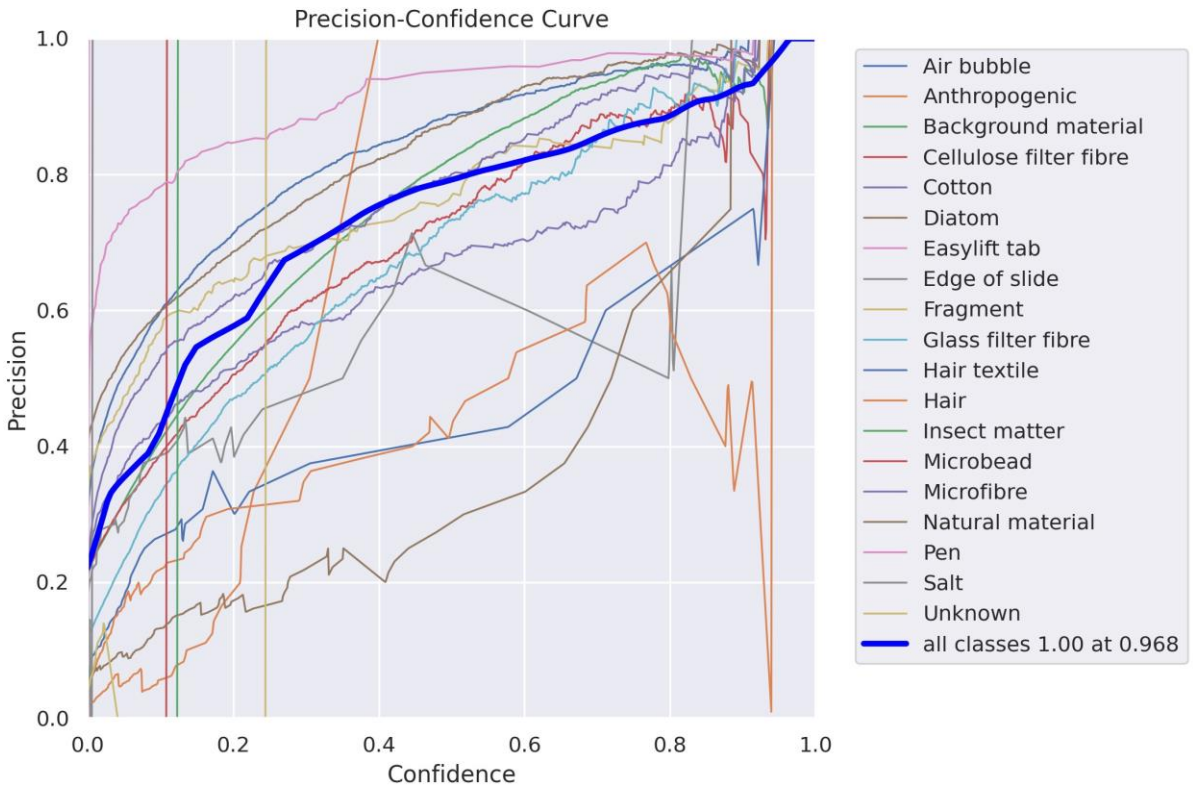

Figure 4.56 A precision-confidence curve to evaluate the model when trained using YOLOv8 for 25 epochs.

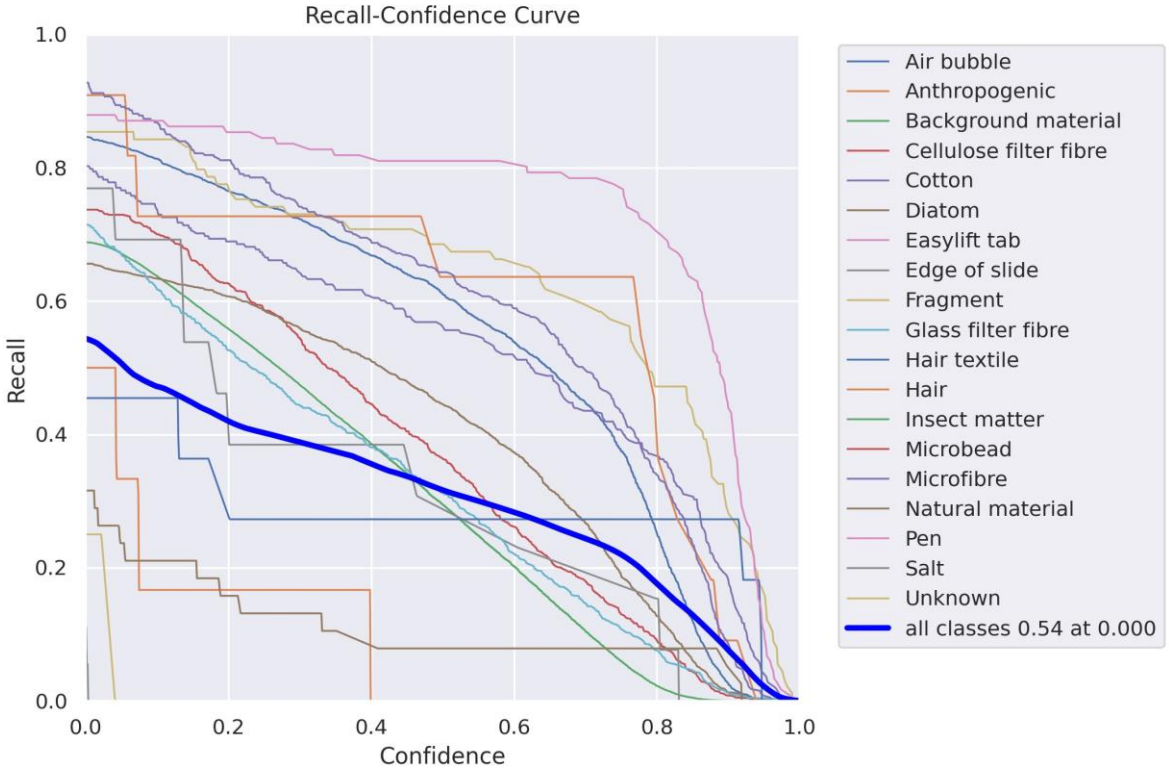

Figure 4.57 A recall-confidence curve to evaluate the model when trained using YOLOv8 for 25 epochs.

Figure 4.58 show a F1-confidence curve when the dataset was trained with YOLOv8 for 25 epochs. All classes are at 0.40 at a confidence of 0.337, after this point the F1 score begins to decrease. This average is, however, being brough down a few underperforming classes namely, natural material, hair, anthropogenic, unknown and hair textile. All the other classes are performing well above the average for all classes. The model overall performs best in the identification of pen, followed by air bubble, fragments, diatoms and microfibres.

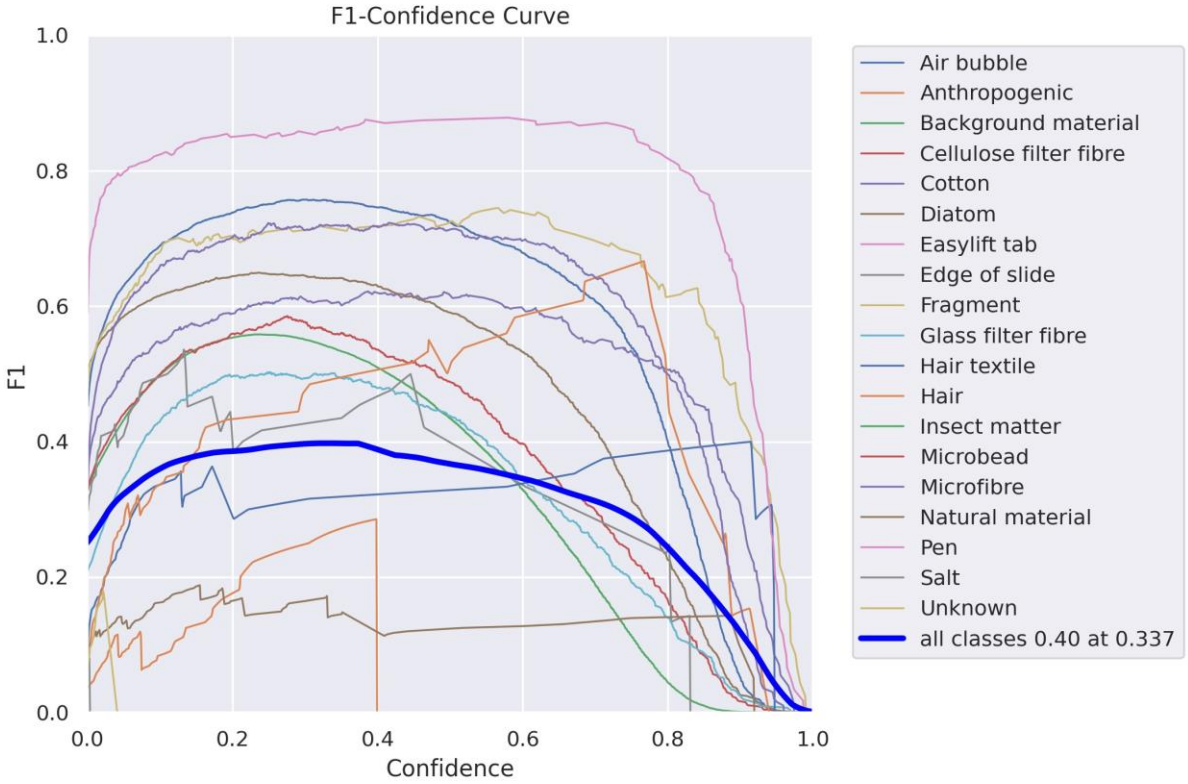

Figure 4.58 A F1-confidence curve to evaluate the model produced when trained using YOLOv8 for 25 epochs.

Figure 4.59 shows a precision-recall curve for the model produced by training with YOLOv8 for 25 epochs. The model was most successful at identifying pen with and area under the curve of 0.885, followed by microfibres with an area under the curve of 0.786, air bubbles with an area under the curve of 0.781 and fragments with an area under the curve of 0.776. The model was least successful at identifying, microbeads, and Easylift® tab with an area under the curve of 0.0 meaning no correct identifications were made for these classes. Overall, the model had an area under the curve of 0.414 indicating that the model has not performed well in the overall classification of objects commonly found in microplastic samples, but it has performed well in the detection of microplastic microfibres and fragments which is the main goal of this model.

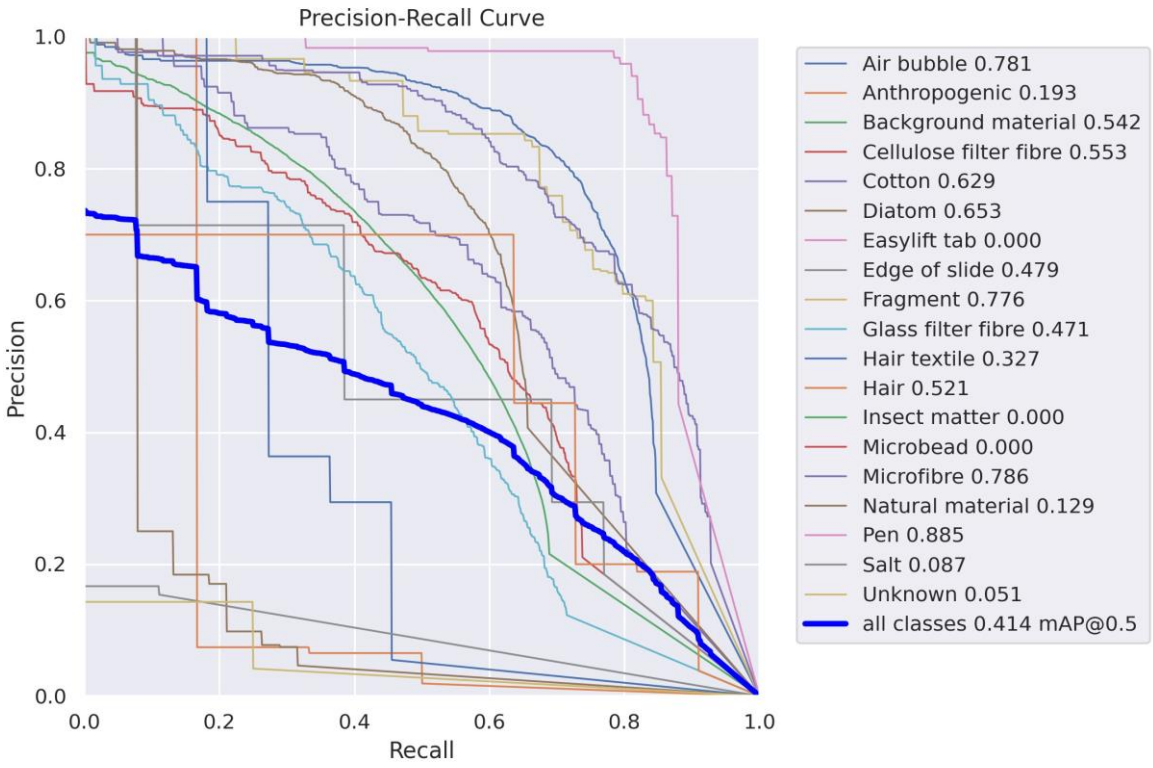

Figure 4.59 A Precision-Recall curve to evaluate the model when trained using YOLOv8 for 25 epochs.

4.3.3.2 YOLOv8 Training With 100 Epochs

Table 4.11 shows the metrics produced for each classification when trained with YOLOv8 for 100. The precision for all classes is 0.65 meaning that 65% of positive identifications were true positives. The recall is 0.528, meaning 52.8% of objects were correctly detected. For this model the precision and recall are closer to each other. The F1 Score for all classes is 0.583 this is still a low F1 score. Some classifications performed very well in this model with pen performing the best with a F1 score of 0.854, which is a very good result. Microfibres and fragments also performed fairly well in this model with both having an F1 score over 0.675. Pen, microfibre and fragments also produced the most accurate bounding boxes.

Table 4.11 A table to show the overall precision, recall, F1 Score, mAP50 (a metric to evaluate how successful an identification is when the Intersection Over Union (IOU) or the overlap between the predicted and actual bounding box is over 50% identification is successful) and mAP50-95 a metric to evaluate how successful an identification is when the IOU is 50-95%) when trained with YOLOv8 and 100 epochs.

Class	Precision	Recall	F1 Score	mAP50	mAP50-95
All	0.65	0.528	0.583	0.537	0.401
Air bubble	0.734	0.779	0.756	0.798	0.532
Anthropogenic	0.374	0.5	0.529	0.328	0.328
Background material	0.561	0.562	0.561	0.542	0.246
Cellulose filter fibre	0.458	0.667	0.543	0.559	0.353
Cotton	0.593	0.669	0.629	0.645	0.51
Diatom	0.71	0.63	0.668	0.668	0.419
Easylift tab	1	0	0	0.539	0.485
Edge of slide	0.581	0.615	0.598	0.642	0.486
Fragment	0.706	0.685	0.695	0.759	0.607
Glass filter fibre	0.47	0.588	0.522	0.516	0.294
Hair textile	0.527	0.455	0.488	0.374	0.32
Hair	0.463	0.727	0.566	0.495	0.443
Insect matter	1	0	0	0	0

Microbead	0.837	1	0.911	0.995	0.697
Microfibre	0.595	0.809	0.686	0.784	0.638
Natural material	0.262	0.234	0.247	0.21	0.145
Pen	0.847	0.862	0.854	0.907	0.76
Salt	1	0	0	0.15	0.086
Unknown	0.624	0.25	0.357	0.292	0.263

Figure 4.60 shows a confusion matrix produced when the dataset was trained with YOLOv8 for 100 epochs. Air bubble had a true positive identification rate of 76% (2125 identifications). The misidentifications for this classification are background material 7% (196 identifications) and cellulose filter paper 1% (28 identifications). The model has performed very well in detection of air bubbles. Anthropogenic had a true positive identification rate of 33% (2 identifications). The misidentifications were cotton 17% (1 identification) and microfibres 33% (2 identifications). The misidentifications could technically be classed as anthropogenic in origin as the anthropogenic class is any object that doesn't have a conclusive identification such as cotton but is thought to be anthropogenic in origin due to certain features such as the colour. Background material had a true positive identification rate of 56% (26433 identifications) there were no misidentifications for this classification. The false negative rate for background material is likely to always be a bit higher than the other classifications as it was so ubiquitous within each image, and it was a subjective opinion as to what was within each bounding box. Some bounding boxes contained many small bits of background material that the algorithm could identify individually, conversely the algorithm could be grouping background materials that had their own individual bounding box. Cellulose filter fibre had a true positive identification rate of 64% (587 identifications). The misidentifications for cellulose filter fibres were, air bubble 1% (9 identifications), background material 7% (64% identifications), cotton 1% (9 identifications) and microfibre 1% (9 identifications). Cotton has a true positive identification rate of 59% (146 identifications). The misidentifications were, background material 2% (5 identifications), cellulose filter fibre 13% (32 identifications), microfibre 11%

(27 identifications) and natural material 1% (2 identifications). Diatoms had a true positive identification rate of 61% (1485 identifications). The misidentification for this class was background material 11% (267 identifications). This misidentification is not surprising as background material and diatoms were both commonly occurring in the same spaces and so difficult to separate from each other when creating bounding boxes. Easylift® tab had no correct identifications, the misidentifications for this classification were background material and edge of slide 25% each (1 identification respectively). Both incorrect classifications are likely to appear in the vicinity of the Easylift® tab, indicating that the Easylift® tab classification needed better representation in the dataset to help avoid these misidentifications. Edge of slide had a true positive rate of 38% (5 identifications). The misidentifications were, background material 8% (1 identification), cellulose filter fibre 31% (4 identifications) and cotton 8% (1 identification). As with Easylift® tab, edge of slide is and underrepresented class and so to increase the model's ability to correctly identify this class its representation in the dataset should be increased. Fragments had a true positive rate of 64% (57 identifications). The misidentifications for this class were, background material 16% (14 identifications), cotton 1% (1 identification), diatom 2% (2 identifications), microfibre 1% (1 identification) and natural material 1% (1 identification). Glass filter fibres had a true positive identification rate of 57% (469 identifications), the only misidentification for this classification was background material 5% (41 identifications). This is likely because the glass filter fibres would be mixed in with the background material and difficult to separate from each other. Hair textile had a true positive rate of 27% (3 identifications). The misidentifications were air bubble 9% (1 identification), cotton 9% (1 identification) and microfibre 55% (6 identifications). Hair had a true positive identification rate of 55% (6 identifications). The misidentifications were cotton 18% (2 identifications) and microfibres 27% (3 identifications). As hair textile is being misidentified as a microfibre more frequently than hair, it demonstrates that they may share feature in common that makes the fibre look less like a hair, for instance the presence of dye. Insect matter had no correct identifications and was misidentified as background material and

cellulose filter fibres in 33% of instances (1 identification respectively). Microbeads had no correct identifications, 100% of microbeads were identified as fragments (1 identification), but, as this equates to only one identification this is not a reliable predictor in how the model will perform, although it is not likely to be able to identify microbeads well until their representation has been increased. Microfibres had a true positive identification rate of 76% (293 identifications). The misidentifications for this class were, air bubble, anthropogenic, background material, fragment and natural material 1% (3 identifications respectively), cellulose filter fibre 3% (11 identifications), cotton 6% (22 identifications) and hair 2% (7 identifications). The model has done well at identifying microfibres, however, there is still a lot of misclassifications both false positives and false negatives for the classification that would need to be improved. The issue could be resolved by increasing the representation of the underrepresented classes that are being misclassified as microfibres such as hair. Natural material had a true positive rate of 16% (6 identifications). The misidentifications for this classification were background material 18% (7 identifications), cellulose filter fibres 13% (5 identifications), cotton 11% (4 identifications), diatoms 8% (3 identifications) and natural material 5% (1 identification). Pen had a true positive identification rate of 85% (99 identifications). The misidentifications were, air bubble 2% (2 identifications), background material 8% (9 identifications) and natural material 1% (1 identification). The model has performed well in the identification of this classification. Salt has no correct identifications; the misidentification was background material 78% (14 identifications. To resolve this more samples with high levels of salt need to be included in the dataset. Overall, the model has not performed well in the classification in all objects that may be present in samples. It has, however, performed fairly well in the identification of microplastics, with both fragments and microfibres correctly identified in nearly 60% of cases.

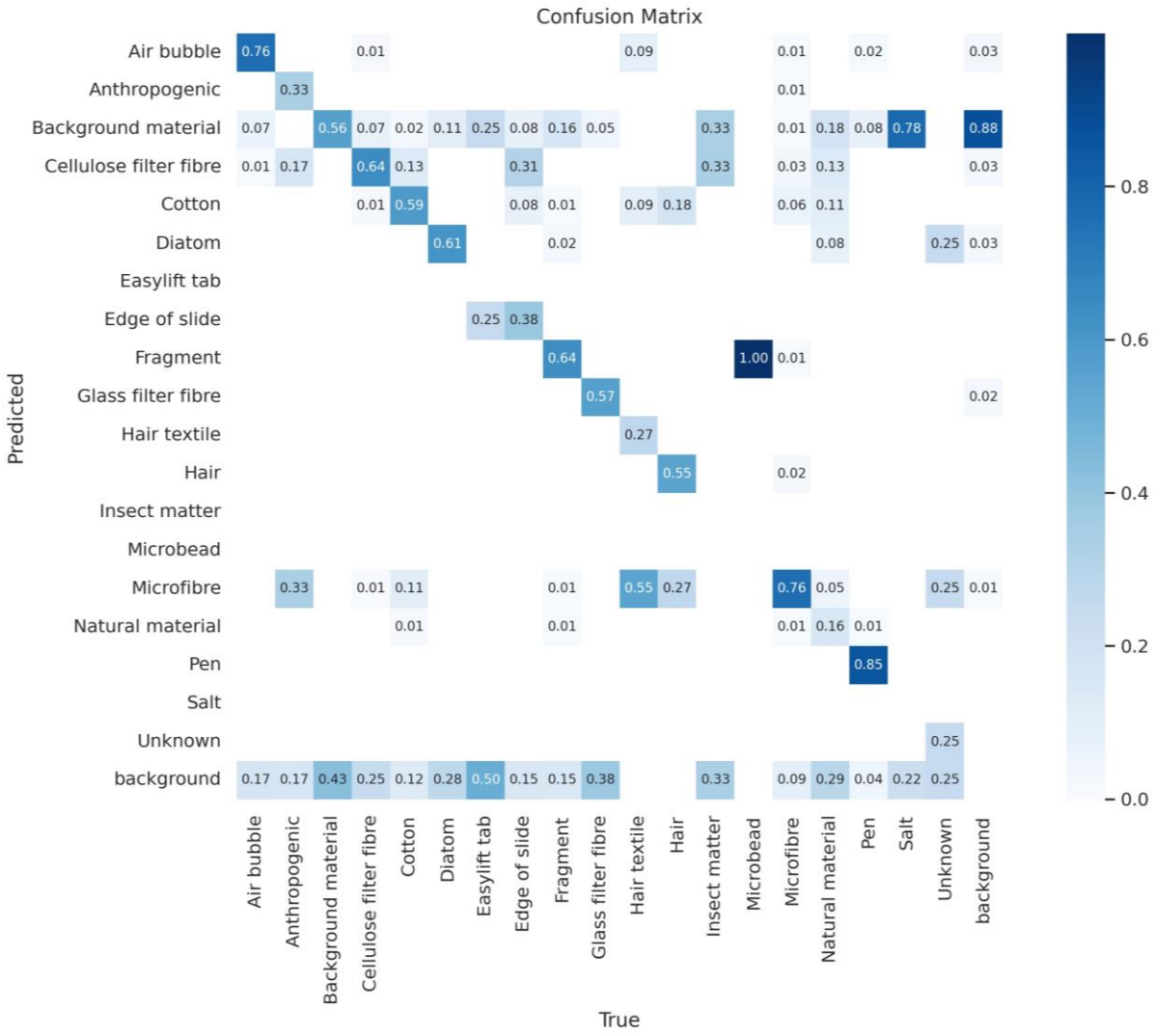

Figure 4.60 A confusion matrix to show how successful the algorithm was at correctly predicting each class when trained using YOLOv8 for 100 epochs.

Figure 4.61 shows a precision-confidence curve and Figure 4.62 shows a recall-confidence curve when the dataset was trained with YOLOv8 for 100 epochs. From these two graphs it can be seen that the model's overall precision is high with all classes having a precision of 1 at a confidence level of 0.993, whereas the overall recall is relatively low for this model with all classes having a recall of 0.63 at a confidence of 0.0. However, some of the classes are performing far better than others which is bringing the average down. For instance, pen, air bubble, microfibre and fragments have a good recall level for this model.

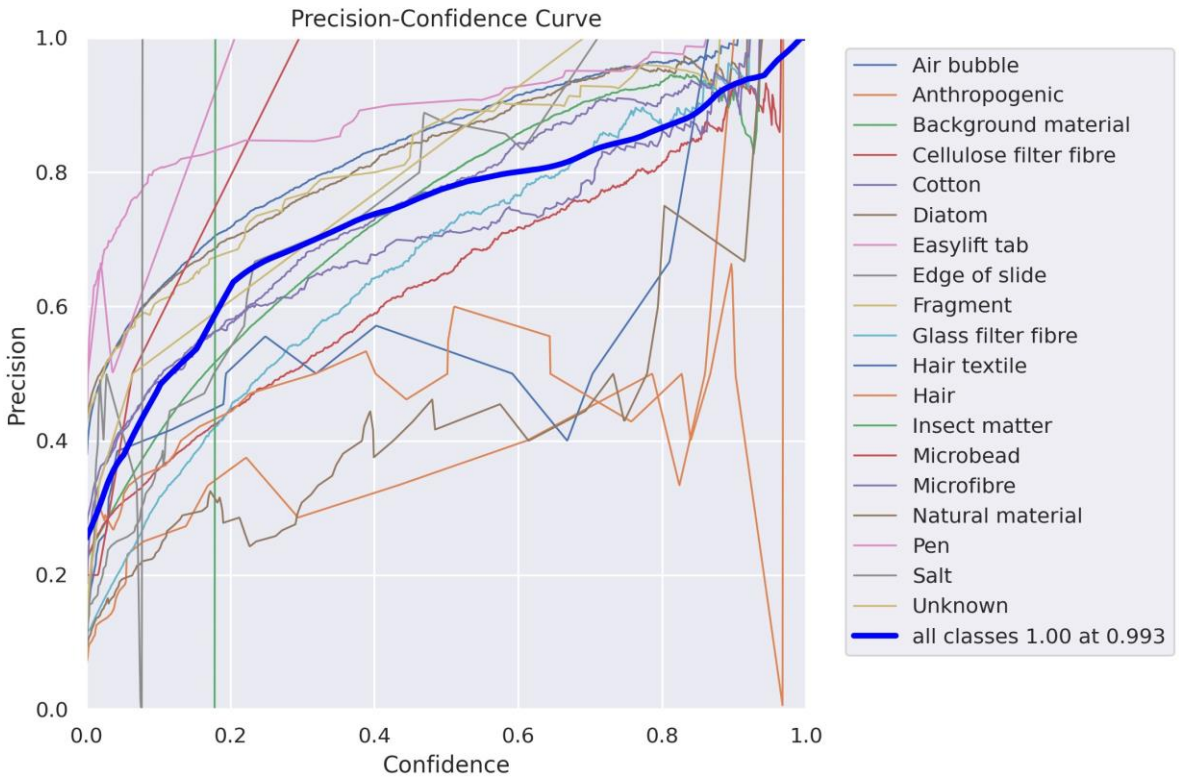

Figure 4.61 A precision-confidence curve to evaluate the model when trained using YOLOv8 for 100 epochs.

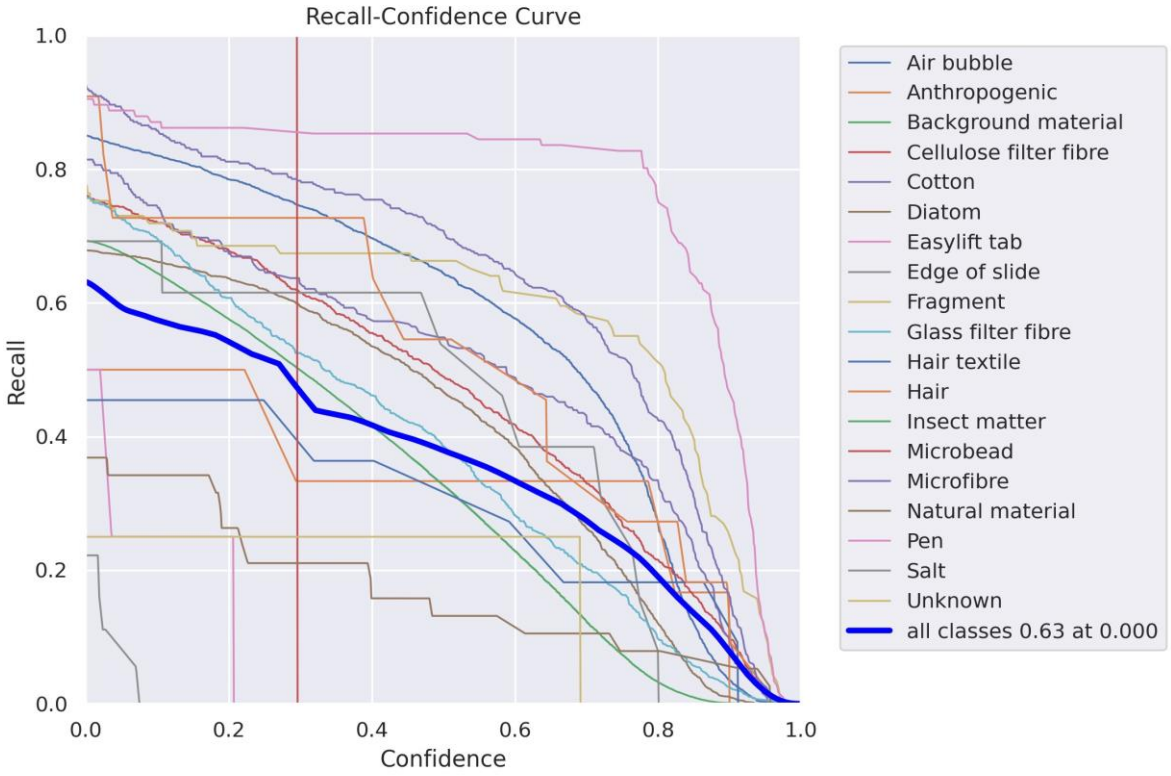

Figure 4.62 A recall-confidence curve to evaluate the model when trained using YOLOv8 for 100 epochs.

Figure 4.63 shows an F1-confidence curve when the dataset was trained with YOLOv8 for 100 epochs. All classes are at 0.51 at a confidence of 0.181, after this point the F1 score begins to decrease. This average is, however, being brought down a few underperforming classes, namely, natural material, hair, anthropogenic, unknown and hair textile. Most other classes are performing well above the average for all classes. The model overall performs best in the identification of pen, followed by air bubble, fragments, diatoms and microfibres.

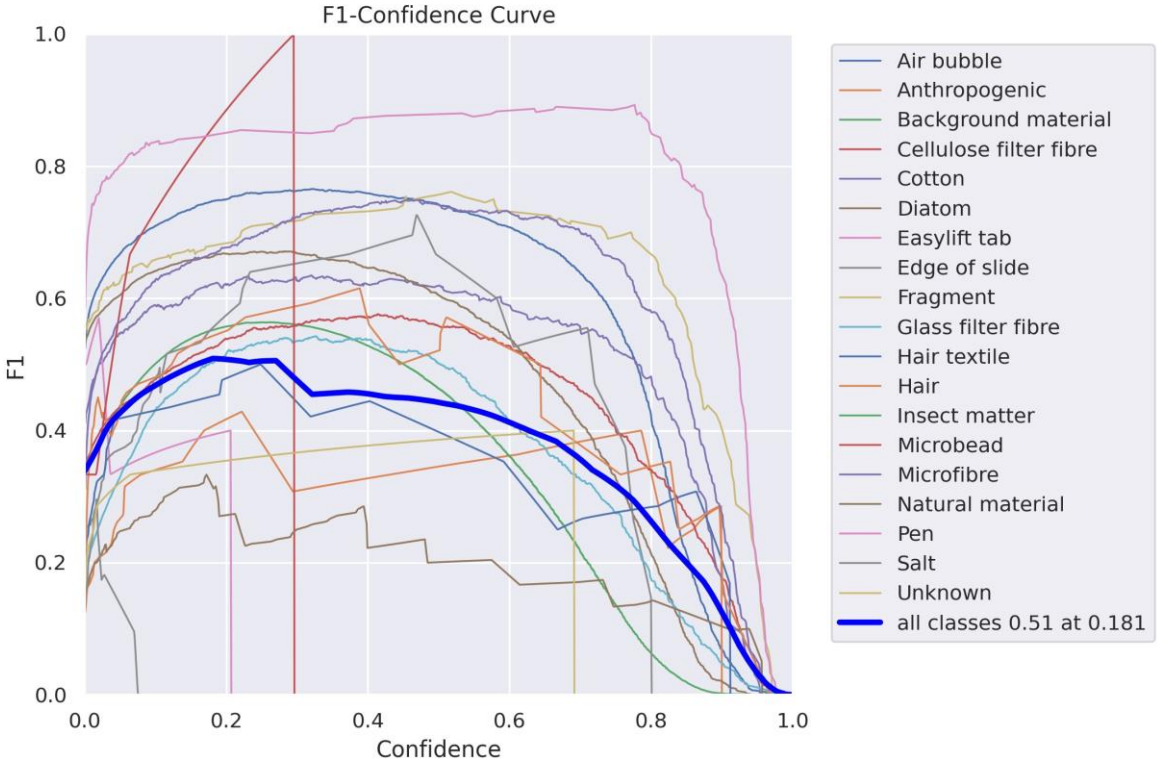

Figure 4.63 An F1-confidence curve to evaluate the model produced when trained using YOLOv8 for 100 epochs.

Figure 4.64 shows a precision-recall curve for the model produced by training with YOLOv8 for 100 epochs. From this table, it appears that the model was most successful at identifying microbeads with an area under the curve of 0.995, but as this is a very underrepresented class in the data set (only one instance), this does not fully demonstrate how well the model may or may not be able to identify microbeads. The dataset would need to be expanded to include more microbeads to be able to say with confidence how

successful it was at identifying microbeads, as only one correct identification would be a 100% detection rate. Pen is then the next most successful identification with an area under the curve of 0.907, followed by air bubbles with an area under the curve of 0.798, microfibres with an area under the curve of 0.784 and fragments with an area under the curve of 0.759. The model was least successful at identifying insect matter with an area under the curve of 0.0 meaning no correct identifications were made for these classes. Overall, the model had an area under the curve of 0.537 indicating that the model has not performed well in the overall classification of objects commonly found in microplastic samples, but it has performed well in the detection of microplastic microfibres and fragments which is the main goal of this model.

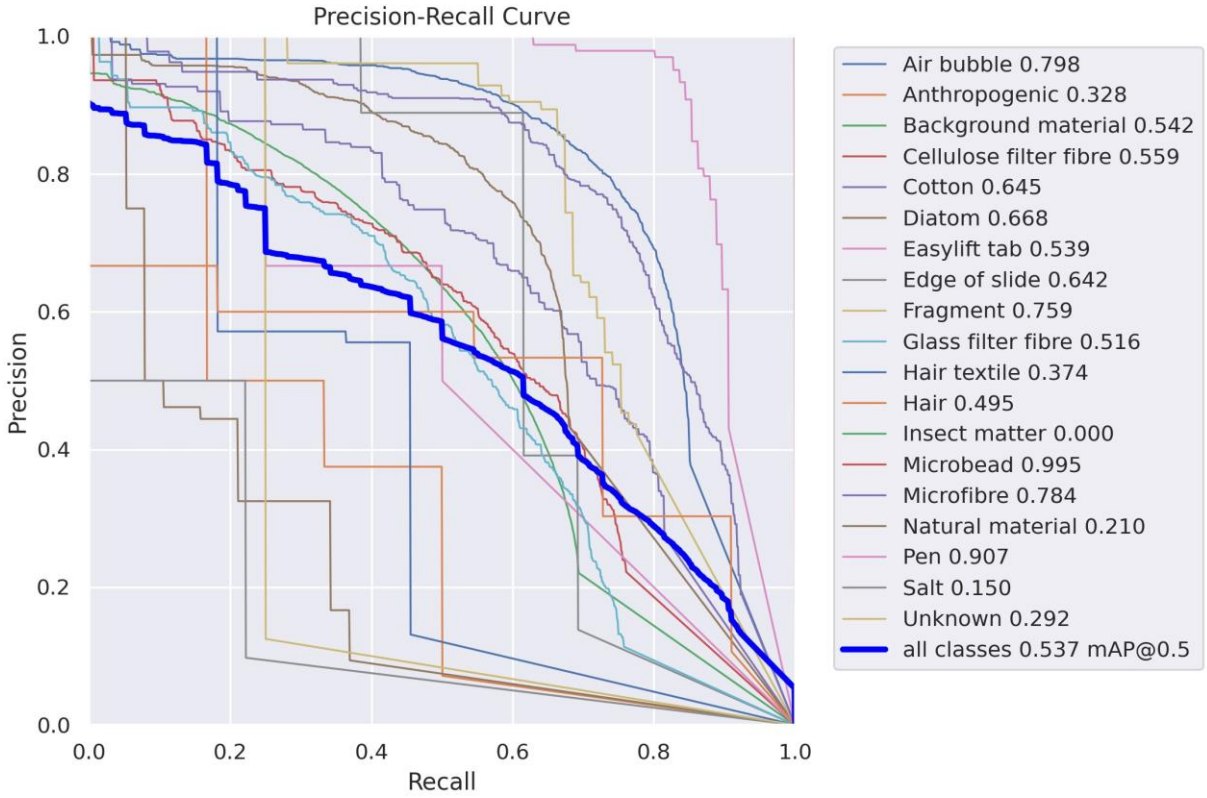

Figure 4.64 A Precision-Recall curve to evaluate the model when trained using YOLOv8 for 100 epochs.

4.3.3.3 YOLOv8 Training with Augmented Data and 100 Epochs

Table 4.12 shows the metrics produced for each classification when trained with YOLOv8 for 100 with augmented images in the training dataset. The precision for all classes is 0.675 meaning that 67.5% of positive identifications were true positives. The recall is 0.492, meaning 49.2% of objects were correctly detected. For this model the precision and recall are closer to each other. The F1 Score for all classes is 0.569 this is still a low F1 score. Some classifications performed very well in this model with pen performing the best with a F1 score of 0.867, which is a very good result. Microfibres and fragments also performed fairly well in this model with both having an F1 score over 0.7. Pen, microfibre and fragments also produced the most accurate bounding boxes.

Table 4.12 A table to show the overall precision, recall, F1 Score, mAP50 (a metric to evaluate how successful an identification is when the Intersection Over Union (IOU) or the overlap between the predicted and actual bounding box is over 50% identification is successful) and mAP50-95 a metric to evaluate how successful an identification is when the IOU is 50-95%) when trained with augmented images using YOLOv8 for 100 epochs.

Class	Precision	Recall	F1 Score	mAP50	mAP50-95
All	0.675	0.492	0.569	0.564	0.424
Air bubble	0.807	0.726	0.764	0.8	0.533
Anthropogenic	0.364	0.667	0.471	0.597	0.519
Background material	0.729	0.403	0.519	0.53	0.239
Cellulose filter fibre	0.62	0.559	0.588	0.572	0.363
Cotton	0.618	0.613	0.615	0.633	0.502
Diatom	0.18	0.517	0.267	0.647	0.4
Easylift tab	1	0	0	0.75	0.549
Edge of slide	0.656	0.589	0.621	0.571	0.388
Fragment	0.966	0.742	0.839	0.839	0.661
Glass filter fibre	0.634	0.396	0.488	0.435	0.252
Hair textile	0.496	0.364	0.420	0.424	0.407
Hair	0.529	0.636	0.578	0.617	0.569

Insect matter	0	0	0	0.0523	0.0157
Microbead	0.914	1	0.955	0.995	0.763
Microfibre	0.694	0.76	0.726	0.778	0.639
Natural material	0.451	0.259	0.329	0.241	0.181
Pen	0.87	0.864	0.867	0.899	0.763
Salt	1	0	0	0.0471	0.0291
Unknown	0.671	0.25	0.364	0.287	0.259

Figure 4.65 shows a confusion matrix produced when the dataset was trained with YOLOv8 for 100 epochs with augmented images used in the training dataset. Air bubbles had a true positive identification rate of 78% (2181 identifications). The misidentifications for this class were background material 4% (112 identifications) and cellulose filter fibres 1% (28 identifications). Anthropogenic had a true positive identification rate of 67% (3 identifications). The misidentifications were cotton 17% (1 identification) and microfibres 17% (1 identification). The misidentifications could technically be classed as anthropogenic in origin as the anthropogenic class is any object that doesn't have a conclusive identification such as cotton, but is thought to be anthropogenic in origin due to certain features such as the colour. Background material had a true positive identification rate of 53% (25017 identifications) there were no misidentifications for this classification. The false negative rate for background material is likely to always be higher than the other classifications as it was so ubiquitous within each image, and it was a subjective opinion as to what was within each bounding box. Some bounding boxes contained many small bits of background material that the algorithm could identify individually, conversely the algorithm could be grouping background materials that had their own individual bounding box. Cellulose filter fibre had a true positive identification rate of 62% (569 identifications). The misidentifications for cellulose filter fibres were, air bubble 1% (9 identifications), background material 8% (74% identifications), cotton 2% (18 identifications) and microfibre 1% (9 identifications). Cotton has a true positive identification rate of 65% (161 identifications). The misidentifications were, anthropogenic 1% (3 identifications), background

material 2% (5 identifications), cellulose filter fibre 8% (20 identifications), microfibre 10% (25 identifications) and natural material 2% (5 identifications). Diatoms had a true positive identification rate of 57% (1387 identifications), The misidentification for this classification was background material 9% (219 identifications). This misidentification is not surprising as background material and diatoms were both commonly occurring in the same spaces and so difficult to separate from each other when creating bounding boxes. Easylift® tab had no correct identifications, the misidentifications for this classification were background material 25% (1 identification) and edge of slide 50% (2 identifications). Both incorrect classifications are likely to appear in the vicinity of the Easylift® tab, indicating that the Easylift® tab classification needed better representation in the dataset to help avoid these misidentifications. Edge of slide had a true positive identification rate of 54% (7 identifications), the misidentifications for this class were background material and microfibre at 8% (1 identification respectively). As with Easylift® tab, edge of slide is and underrepresented class and so to increase the model's ability to correctly identify this class its representation in the dataset should be increased. Fragments had a true positive identification rate of 69% (61 identifications). The misidentifications for this class were, background material 16% (14 identifications), diatom 1% (1 identification), and microfibre 3% (3 identification). Glass filter fibres had a true positive identification rate of 47% (387 identifications). The misidentifications were background material 8% (33 identifications). This is likely because the glass filter fibres would be mixed in with the background material and difficult to separate from each other. Hair textile had a true positive rate of 36% (4 identifications). The misidentifications were air bubble 9% (1 identification), background material 9% (1 identification), microfibre 18% (2 identifications) and natural material 9% (1 identification). Hair had a true positive identification rate of 55% (6 identifications). The misidentifications were cotton 9% (1 identification) and microfibres 36% (4 identifications). As hair textile is being misidentified as a microfibre more frequently than hair, it demonstrates that they may share feature in common that makes the fibre look less like a hair, for instance the presence of dye. Insect matter had no correct identifications and was misidentified as insect matter and pen in 33% of instances (1 identification

respectively). Microbeads had a true positive identification rate of 100% (1 identification) but, as this equates to only one identification this is not a reliable predictor in how the model will perform, although it is not likely to be able to identify microbeads well until their representation has been increased. Microfibres had a true positive identification rate of 76% (294 identifications). The misidentifications for this classification were, anthropogenic, background material, diatoms, hair textile, hair, and natural material 1% (3 identifications respectively), cellulose filter fibre 2% (7 identifications), and cotton 7% (26 identifications). The model has done well at identifying microfibres, however, there is still a lot of misclassifications both false positives and false negatives for the classification that would need to be improved. The issue could be resolved by increasing the representation of the underrepresented classes that are being misclassified as microfibres such as hair. Natural material has a true positive identification rate of 26% (10 identifications). The misidentifications were background material 16% (6 identifications), cellulose filter fibres 8% (3 identifications), cotton 5% (2 identifications), diatom 11% (4 identifications), glass filter fibre 3% (1 identification) and microfibre 11 % (4 identifications). Pen had a true positive identification rate of 88% (102 identifications). The misidentifications were, air bubble 2% (2 identifications), background material 6% (7 identifications) and cellulose filter fibre 1% (1 identification). The model has performed well in the identification of this classification. Salt has no correct identifications; the misidentification was background material 61% (11 identifications). To resolve this more samples with high levels of salt need to be included in the dataset. Overall, the model has not performed well in the classification in all objects that may be present in samples. It has, however, performed fairly well in the identification of microplastics, with both fragments and microfibres correctly identified in nearly 70% of cases.

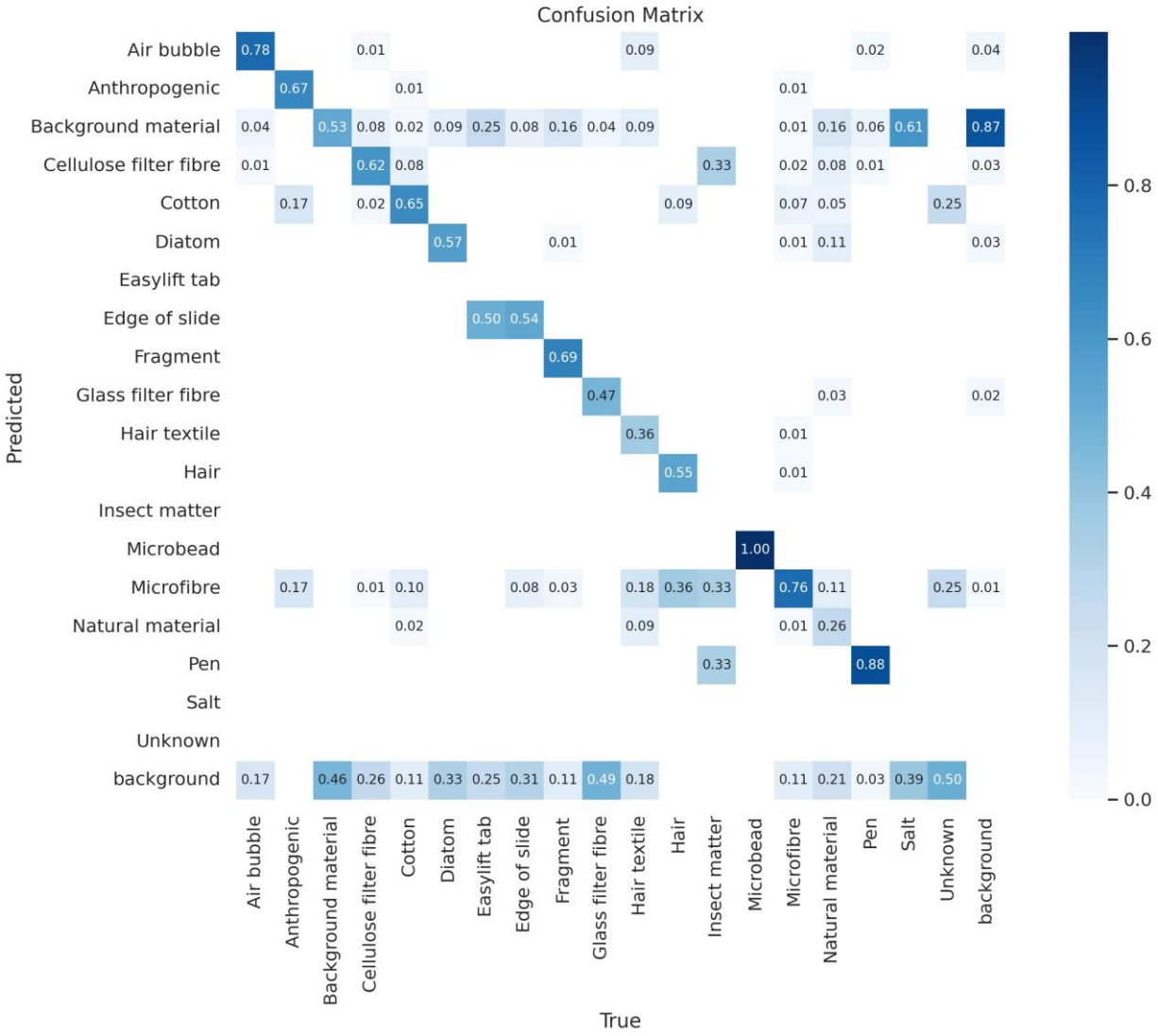

Figure 4.65 A confusion matrix to show how successful the algorithm was at correctly predicting each class when trained with augmented images using YOLOv8 for 100 epochs.

Figure 4.66 shows a precision-confidence curve and Figure 4.67 shows a recall-confidence curve when the dataset was trained with YOLOv8 for 100 epochs when augmented images were used in the training dataset. From these two graphs it can be seen that the model's overall precision is high with all classes being having a precision of 1 at a confidence level of 1.00, whereas the overall recall is relatively low for this model with all classes having a recall of 0.67 at a confidence of 0.0. However, some of the classes are performing far better than others which is bringing the average down. For instance, pen, air bubble, microfibre and fragments have a good recall level for this model.

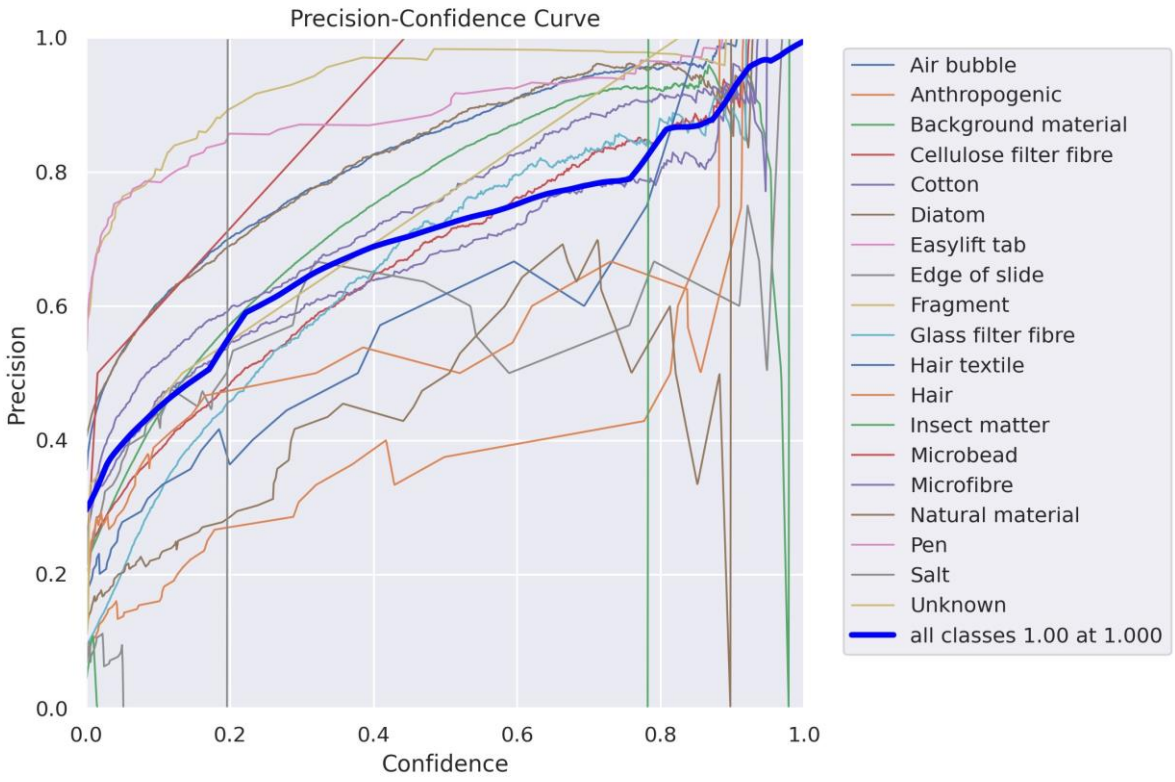

Figure 4.65 A precision-confidence curve to evaluate the model when trained with augmented images using YOLOv8 for 100 epochs.

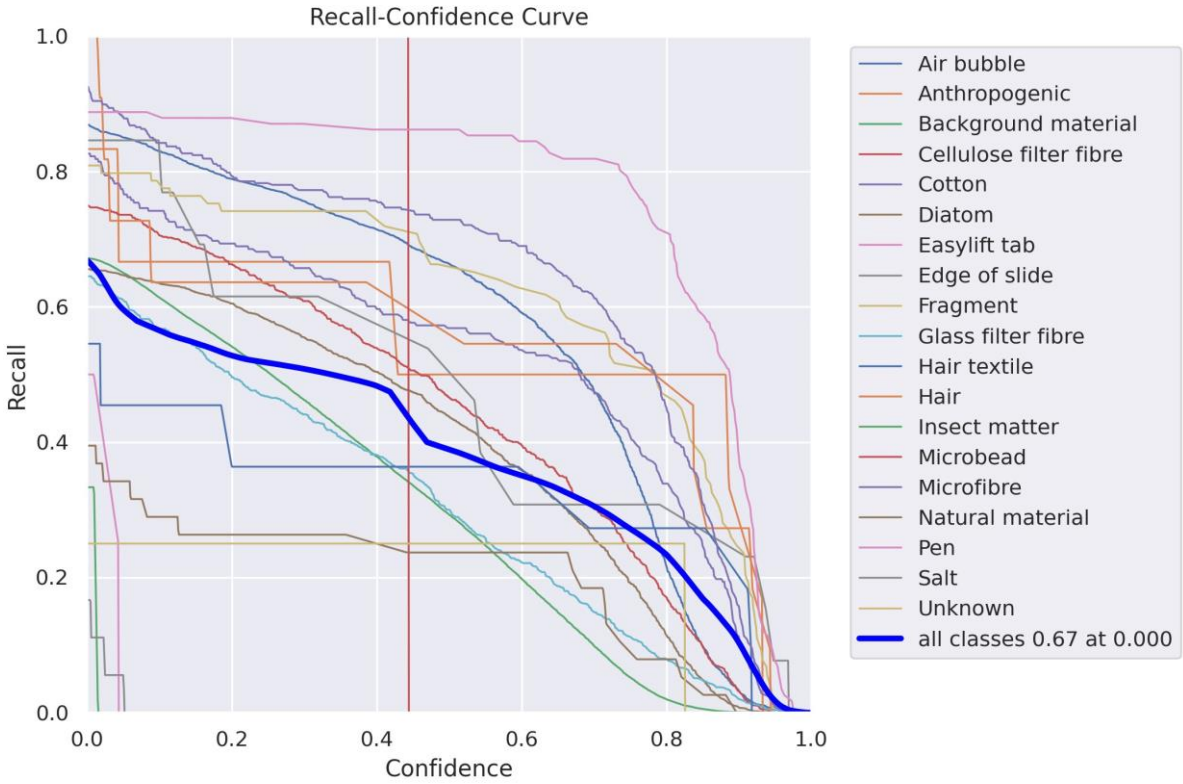

Figure 4.66 A recall-confidence curve to evaluate the model when trained with augmented images using YOLOv8 for 100 epochs.

Figure 4.68 show a F1-confidence curve when the dataset was trained with YOLOv8 for 100 epochs and augmented images used in the training dataset. All classes are at 0.51 at a confidence of 0.381, after this point the F1 score begins to decrease. This average is, however, being brough down a few underperforming classes namely, natural material and insect matter. Most other classes are performing well above the average for all classes. The model overall performs best in the identification of pen, followed by fragments, air bubble, diatoms and microfibres.

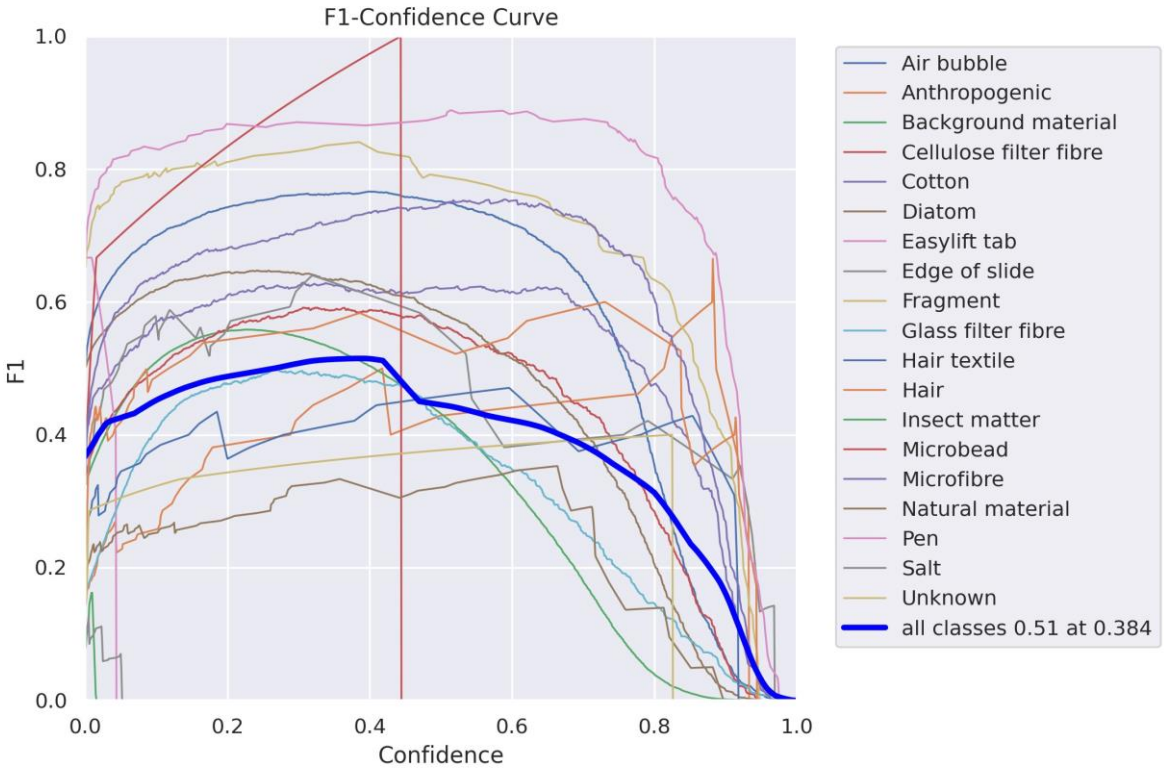

Figure 4.67 An F1-confidence curve to evaluate the model produced when trained with augmented images using YOLOv8 for 100 epochs.

Figure 4.69 shows a precision-recall curve for the model produced by training with YOLOv8 for 100 epochs and augmented images used in the training dataset. From this table it appears that the model was most successful at identifying microbeads with an area under the curve of 0.995, but as this is a very underrepresented class in the data set (only one instance) this does not fully demonstrate how well the model may or may not be able to identify microbeads. The dataset would need to be expanded to include more microbeads to be able to say with confidence how successful it was at identifying microbeads, as only one correct identification would be a 100% detection rate. Pen is then the next most successful identification with and area under the curve of 0.899, followed by fragments with an area under the curve of 0.839, air bubbles with an area under the curve of 0.800, microfibres with an area under the curve of 0.778. The model was least successful at identifying salt with an area under the curve of 0.047 and insect matter with an area under the curve of 0.052. Overall, the model had an area under the curve of 0.564, indicating that the model has not performed well in the overall classification of objects commonly found in microplastic samples, but it has performed well in the detection of microplastic microfibres and fragments, which is the main goal of this model.

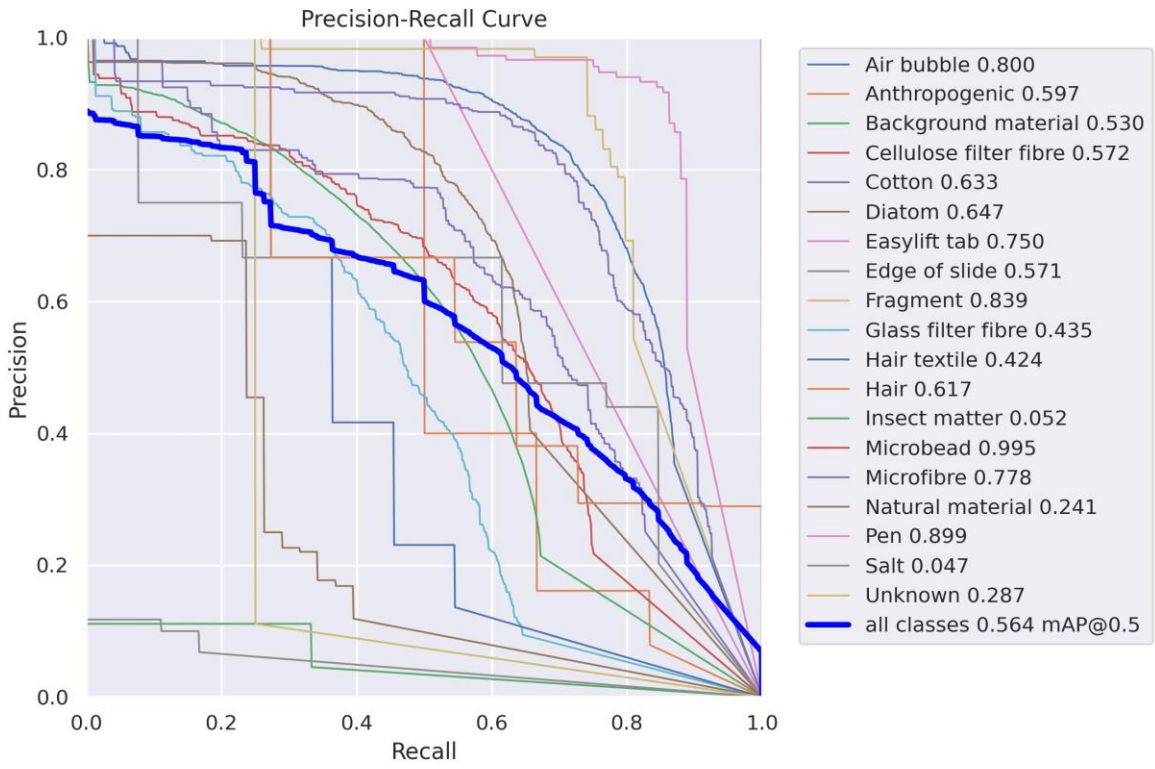

Figure 4.68 A Precision-Recall curve to evaluate the model when trained with augmented images using YOLOv8 for 100 epochs.

4.3.4 Comparison of The Different Models

Table 4.13 shows a series of metrics for all of the models produced in this chapter. From the results displayed, YOLOv5 performed the worst out of each of the three algorithms used, with YOLOv5 and 25 epochs producing the worst all-round results as the training can be seen to improve with the increased number of epochs. The high false negative rate indicates that the model is missing a lot of detections. This could be because YOLOv5 can struggle to detect small object or objects that have a complex shape (Talaat & ZainEldin, 2023). YOLOv7 with augmentation then appears to have performed the best with the highest recall and F1 score and is the strongest performer across all the metrics. It does, however, have a false discovery rate of 0.389, meaning 38.9% of discoveries are incorrect, which is quite high and is the largest false discovery rate of all the models tested. YOLOv8 has

the best mAP scores of all the algorithms tested this indicates that YOLOv8 may be better at generalising to unseen data compared to the other algorithms tested. From these metrics the best overall performer was YOLOv8 100 epochs with augmentation as it has a good balance between precision and recall, while YOLOv7 100 epochs with augmentation is the best model produced for detection as it has the highest recall at 0.56 and the best F1 score

Table 4.13 A table to compare each algorithms precision (positive predictive value), recall (True positive rate), F1 score, mAP50, mAP50-95, False discovery rate and false negative rate with the best algorithm for each metric highlighted green and the worst metric highlighted red.

Model	YOLOv5			YOLOv7			YOLOv8		
Epoch	25	100	100	25	100	100	25	100	100
Aug	No	No	Yes	No	No	Yes	No	No	Yes
Precision	0.68	0.787	0.728	0.843	0.715	0.611	0.715	0.65	0.675
Recall	0.108	0.196	0.217	0.332	0.463	0.56	0.376	0.528	0.492
F1 score	0.186	0.314	0.334	0.475	0.562	0.584	0.494	0.583	0.569
mAP50	0.0895	0.213	0.269	0.354	0.455	0.542	0.414	0.537	0.564
mAP50-95	0.0414	0.122	0.162	0.244	0.319	0.394	0.301	0.401	0.424
False discovery rate	0.32	0.213	0.272	0.157	0.285	0.389	0.285	0.35	0.325
False negative rate	0.892	0.804	0.783	0.668	0.537	0.44	0.624	0.472	0.508

In order to fully evaluate the model, it would need to be evaluated whether false positives were more detrimental that false negatives. For example, in cases of mammogram screenings a false negative would mean that cancer is missed, so it may be more beneficial to have a higher false positive rate to ensure that no cancer is missed, but this leaves the potential of exposing patients to harmful unnecessary treatments if the false positive is not detected (Bagchi *et al.*, 2019). In the case of this model the effects would not be as detrimental, but nonetheless needs to be considered, as a false negative would mean that microplastics are potentially being missed providing an under representation of the population of microplastics in a given environment. But a false positive could over inflate the microplastic population, however if results have to be examined by a researcher through confirmatory analysis such as Raman or FTIR false positives should be detected and can then be removed from the total of microplastics found. Across all three algorithms the models with only 25 epochs performed the

worst as most metric tended to improve for the 100 epoch models, this demonstrates that for this data training for 25 epochs is not enough training time to produce a successful model. Some of the metrics have decreased going from 100 epoch to 100 epoch and augmented images, this could be due to the fact that augmentation can cause overfitting (Wong, Gatt & Stamatescu, 2016) where after a certain point robust training will adversely affect the model's performance due to overfitting leading to the model's accuracy decreasing (Rebuffi *et al.*, 2021). Overfitting, however, can also be caused by the presence of 'noise' in the dataset, limited training data size and complex classifiers (Ying, 2019). There are ways to resolve this issue, such as early stopping, where accuracy is observed at the end of every epoch find the perfect balance between overfitting and underfitting at the point accuracy starts to decrease training is stopped (Büttner *et al.*, 2023). Network-reduction/noise reduction, reducing the number of final classifiers can help to reduce noise and classifier complexity, increasing the dataset particularly underrepresented classes can also help to prevent overfitting (Ying, 2019). Augmenting images can provide a benefit to the models' performance as it is a useful method for reducing errors by creating a more comprehensive dataset (Shorten & Khoshgoftaar, 2019). For instance, Jaipuria *et al.* (2020) found that synthetic augmented images in the training dataset over three different computer vision tasks provided a significant improvement in cross-dataset generalisation performance. Another potential explanation for the augmented models performing slightly worse than the non-augmented models is that using augmented images has the potential to distort the training images, leading to a discrepancy between the training images and the testing images (Merchant, Zoph & Cubuk, 2020).

Table 4.14 shows the true positive rate for each model for each class, YOLOv7 with 100 epochs despite not having any of the best performing metrics in Table 4.13, demonstrates the best overall correct identifications over multiple classes. However, this does not include microfibres and fragments which was successfully identified the most by YOLOv7 with 100 epochs and augmented images. Although, YOLOv7 100 epochs is only a little bit lower than YOLOv7 with augmented images. Once again YOLOv5

has performed the worse across all the models tested, with some instances it is performing far worse than the other algorithms, for example YOLOv5 25 epochs had a correct identification rate of 17% for pen while YOLOv7 25 epoch had a correct identification rate of 90%. YOLOv5 also performed poorly in the identification of microfibres and fragments indicating that it is not the most appropriate algorithm to apply to microplastic identification. YOLOv8 has performed fairly well in the identification of microplastics and materials likely to appear in environmental samples and has performed the best in the identification of anthropogenic material, hair and microbeads, but, as this equates to only one identification this is not a reliable predictor in how the model will perform, although it is not likely to be able to identify microbeads well until their representation has been increased. This is backed up by literature as in a study detecting plastic bottles in a recycling plant, YOLOv8 despite having more parameters and needing a longer computation time outperformed YOLOv5 in accurate identifications (Matta *et al.*, 2024). Pen has been successfully identified in both YOLOv7 and YOLOv8, this means that analysts are safe to annotate the samples without much risk that it will result in misidentification of microplastics, this is a very useful ability, as it means that potential microplastics can be marked and numbered without consequence for identifications. All algorithms were unable to identify, Easylift® tab, insect matter and salt, this indicates that these classes need to have more representation within the dataset. For example, the images used in this chapter were all from the upper Hudson where salt levels were lower and so not as present in the images generated, adding more images to the dataset from the lower Hudson River could improve the detection rate of salt.

Table 4.14 A table to show the true positive rate for each model for each class with 1.00 being 100% and 0 being no correct identifications (0 is represented with -).

Model	YOLOv5			YOLOv7			YOLOv8		
Epoch	25	100	100	25	100	100	25	100	100
Aug	No	No	Yes	No	No	Yes	No	No	Yes
Air bubble	0.25	0.54	0.62	0.82	0.82	0.81	0.73	0.76	0.78
Anthropogenic	-	-	-	-	0.50	0.40	-	0.33	0.67
Background material	0.41	0.49	0.51	0.56	0.62	0.57	0.54	0.56	0.53
Cellulose filter paper	0.01	0.24	0.33	0.63	0.67	0.66	0.56	0.64	0.62
Cotton	0.01	0.29	0.33	0.57	0.73	0.70	0.60	0.59	0.65
Diatom	0.04	0.30	0.40	0.70	0.73	0.67	0.58	0.61	0.57
Easylift® tab	-	-	-	-	-	-	-	-	-
Edge of slide	-	-	-	-	0.64	0.64	0.38	0.38	0.54
Fragment	0.08	0.24	0.38	0.81	0.80	0.81	0.69	0.64	0.69
Glass filter fibre	-	0.20	0.34	0.61	0.64	0.50	0.49	0.57	0.47
Hair textile	-	-	-	0.17	0.67	0.50	0.27	0.27	0.36
Hair	-	-	-	-	0.50	0.42	0.55	0.55	0.55
Insect matter	-	-	-	-	-	-	-	-	-
Microbead	-	-	-	-	-	-	-	-	1.00
Microfibre	0.16	0.44	0.52	0.68	0.74	0.79	0.74	0.76	0.76
Natural material	-	-	-	0.19	0.43	0.46	0.13	0.16	0.26
Pen	0.17	0.49	0.62	0.90	0.94	0.94	0.83	0.85	0.88
Salt	-	-	-	-	-	-	-	-	-
Unknown	-	-	-	-	-	0.50	-	0.25	-

Figures 4.70 and 4.71 show heatmaps for the distribution of false positives and false negatives for microfibres and fragments across all models. In Figure 4.79, the classification that is most often confused with microfibres is

cotton, with a high number of cotton being identified as microfibres (false positives) and microfibres being identified as cotton (false negatives). YOLOv7 had the fewest number of false positives for cotton compared to the other algorithms, with YOLOv5 having the highest number of false positives. However, YOLOv7 had a higher level of false negatives and YOLOv5 having the lowest level of false negatives. This means that the model is more likely to falsely identify microfibres as something else but more likely to falsely identify other classes as microfibres. Overall, there are several different false positives and false negatives for microfibres with varying degrees of occurrence. Fragments had very few false positives across all models with the most common false positive being pen, but this false positive of pen only occurs in YOLOv5 and not the other two algorithms investigated. Fragments had a higher number of false negatives than false positives, with the most common false negatives being background material. YOLOv7 had the fewest number of false negatives than the other algorithms, with YOLOv5 having the most false negatives. Fragments have a few false negatives that would not normally be considered visually similar, namely microfibres and cotton. These false negatives are likely to have occurred due to their colouration as the majority of fragments in the dataset are blue, which is a common colour for both microfibres and cotton.

Figure 4.69 Heat maps to show the distribution of false positives (left) and false negatives (right) for microfibres across all models.

Figure 4.70 Heat maps to show the distribution of false positives (left) and false negatives (right) for fragments across all models.

4.3.4.1 Evaluating the Dataset

The 3102 images and annotations were split into training, validation, and test set with a 70% (2171), 20% (621), 10% (310) split. A second dataset was created by randomly augmenting the training images, the augmentations used were flipped horizontal and vertical, 90° rotate clockwise, counterclockwise and upside down and an up to 4% blur was applied this bought the number of training images to 6504. While the number of images could be considered fairly large, there is an imbalance between the different classifications used to annotate the dataset, as some classes are far more common than others. When a model has unbalanced data, using accuracy as a metric to evaluate the model is unreliable as it will provide and overoptimistic estimation of the model's ability to classify minority classes (Chicco & Jurman, 2020). Some of the imbalances in the dataset could be improved by increasing the number of images used in the dataset. For example, the images used in this dataset were all predominantly from the upper Hudson where salt levels were lower and so not as present in the images generated, adding more images to the dataset from the lower Hudson River could improve the detection rate of salt as there will be a natural increase in the presence of salt in the images. For other classes increasing the representation is not as simple, for example the presence of insect matter and microbeads is a random addition to the samples that is not more likely to be found in certain samples more than others. Due to this, it is difficult to add more representation to the dataset with genuine environmental samples; it could be increased by manufacturing images. This would potentially mean the images used are not representative environmental samples, which could mean they are not appropriate for the training dataset as environmental samples would have natural weathering and debris that could mean that they would not be correctly identified. Another potential solution would be to consolidate some classes together, for example, into microplastic or not microplastic or classifying diatoms, insect material, etc., into natural material. Doing this would increase the representation in each class and reduce the number of potential different classification outcomes. It would then mean, however, that it becomes

difficult to see what the potential misidentifications are allowing the dataset to be altered to try and resolve the misidentifications. Augmentation could be further applied to these images to increase the representation of these classes, but this would also come with potential drawbacks for the dataset. For instance, as there are only a small number of microbeads in the dataset augmentation could be used to increase its representation, but these new images would potentially still not be fully representative of any microbead that the model could encounter as it will not be representative in terms of the potential, size, colour and degree of weathering and biofouling that could be encountered. A lot of the images in the dataset are also overcrowded. Object overcrowding is a common issue with microscope images used in machine learning as the images often contain a large number of items of interest overlapping each other this is very true with microplastic samples particularly microfibres. This overcrowding can cause a barrier to automatic detection and segmentation of individual objects (Zinchuk, Grossenbacher-Zinchuk, 2020). This would be difficult to resolve as the intended goal of the model is to be used to detect microplastics within environmental samples, these samples are also likely to be heavily overcrowded, meaning that the model would need to be able to cope with overcrowding in the images in order to be an effective method of automated detection of microplastics. The vast majority of the water samples used in the dataset are from the upper Hudson River meaning that there is a larger representation of freshwater samples meaning that the system may not be appropriate for use on saltwater samples as there will be different materials present, for example the diatoms encountered in freshwater will be different to the diatoms encountered in saltwater. There is a good representation of air samples within the dataset, but as with the water, the vast majority of the air samples used in the dataset are from the upper Hudson River, and so there may be differences in the materials encountered in different environments. But as there is a lower level of background material in the air samples it should still be able to cope with air samples from different environments. None of the soil samples were in the dataset used as they were taken after training started, this means that the models produced are unlikely to perform well on soil samples, and these samples would need to be incorporated into the dataset. The images in this

dataset are also all on the same medium, mounted on a glass slide with Easylift®, and so the models may not perform well on different types of samples for example those still on filter paper, this could be investigated by testing the models on images that are not mounted with Easylift® and by adding different images of samples on different mediums into the dataset. The highest priority should be increasing the representation of microbeads and plastic film in the data set as these are severely underrepresented and are two types of microplastic an automated method of detection for microplastics should be able to identify. Then other classes, such as hair and hair textile, should be increased as these are often confused for microfibres, so a better representation would hopefully resolve this issue. After which the next priority would be to increase the representation of classes such as salt and sand which are either poorly represented or absent from the dataset this could be done by including more saltwater and soil/sediment samples into the data set, this would also naturally increase the representation of the different types of diatoms that can be encountered in different environments.

4.4 Conclusion

The aim of this chapter was to generate a comprehensive dataset using samples taken from the Hudson River and to train and test the dataset with multiple algorithms to determine how accurate the identifications produced are and which algorithm performs the best. This was achieved by collecting images from samples of the Hudson River, air, water and soil. A subsection of 3102 of these images formed that dataset that was annotated and used to train and test different models. Three different algorithms were investigated, YOLOv5, YOLOv7 and YOLOv8, each algorithm was tested with 25 epochs, 100 epochs and 100 epochs with augmented images used in the training data.

It was found that YOLOv5 performed the worst out of all algorithms investigated, meaning it is not suitable for use in microplastic samples. YOLOv7 with 100 epochs had the best all-round correct identification rate, but YOLOv7 with 100 epochs and augmentation had the highest identification rate for microfibres and fragments. YOLOv8 performed well overall and had a good level of identification comparable with YOLOv7's but

did not have the highest level of correct identifications for most classes with the exception of anthropogenic material, hair and microbeads. But, as microbeads equates to only one identification this is not a reliable predictor in how the model will perform, and it is not likely to be able to identify microbeads well until their representation has been increased. YOLOv7 with augmentation had the highest recall (0.56) and F1 score (0.584). It does, however, have a false discovery rate of 0.389, meaning 38.9% of discoveries are incorrect. YOLOv7 performed well in the metrics shown in Table 4.13 but did not have the best performance in any of the metrics being observed, while YOLOv5, with 25 epochs, performed the worst out of all models being investigated. For all algorithms the 25 epochs model performed the worst, indicating that it is not enough epochs to successfully train the model to identify microplastics. The category with 100 epochs and augmented images performed well but there would often be a decrease in successful identifications and metrics when compared to just the 100 epochs category, this could be due to overfitting of the data. Overall YOLOv7 with 100 epochs performs the best in the identification of all objects found in microplastic samples.

The most successful class identified is pen with the highest identification rate of 94% being achieved by YOLOv7 100 epochs with and without augmented images. All models were unable to identify, Easylift® tab, insect matter and salt, this indicates that these classes need to have more representation within the dataset.

4.5 Further work

Due to the findings of this study, there have been several areas identified that need further investigation and improvement to further understand the data within this study. More images should be added to the dataset to increase the representation of different classifications and different sample types in the dataset, this would improve the different model's ability to be used to accurately identify microplastics in environmental samples. The models should also be tested with samples of different backgrounds, such as on filter papers, to test its performance when the sample is not mounted in

Easylift®. The classifiers could also be altered to reduce the number of classifications and reduce noise in the algorithms as this may increase performance. The presence of microbeads in the dataset needs to be increased as it is currently a very small class but is a commonly found microplastics and so the model needs to be able to successfully locate and identify microbeads to be considered a good method of quantifying microplastics in samples.

There should also be further investigation into the addition of augmented images in the dataset, for example by employing early stopping to find the point where the model performs its best and before performance drops stopping the training to prevent overfitting. Other algorithms should also be investigated to determine if they perform better than the YOLO algorithms investigated in this chapter.

Chapter 5 Conclusion

5.1 Overview of Key Findings

This thesis aims to develop a standardised method of characterising and quantifying microplastics in environmental samples, taken from the Hudson River. Air, water and soil samples were taken every three miles along the course of the river from the 'Tears of the Clouds' to 'Ambrose light', for a total of 447 samples: 227 water, 163 air and 57 soil samples. Additional samples were taken around three wastewater treatment plants on the Hudson River: Hudson River WWTP, East River WWTP and Yonkers WWTP. In this study, 27 water samples were taken for each WWTP. Surface, middle and bottom water samples were taken every half mile from 2 miles north of the WWTP to 2 miles South of the WWTP. The use of Easylift® was investigated as a method of retrieval from different filter paper and filter combinations. In addition, a study was undertaken to determine whether the inclusion of Polarised light microscopy (PLM) is beneficial in the search process. The use of three machine learning algorithms was also investigated to determine its accuracy in detecting microplastics. Figure 5.1 shows a flow chart with the aim and key findings of each Chapter.

A seeded study was employed to investigate if microfibres are lost in the process of filtering the microfibers from a water sample and whether the non-birefringent forensic tape lift, Easylift®, was a suitable method of retrieval of microfibres from the surface of filter papers. This study was undertaken to try to produce a method that maximises the retrieval of microfibres from water samples and to give an indication of potentially how many microfibres may have been lost to the filtration and extraction process. Two filtration methods and two filter papers were investigated: a Buchner funnel and a glass frit, and cellulose filter papers and glass microfibre filter papers. The use of Easylift® was then investigated as a method of collection of microfibres from the surfaces of the two filter papers investigated. This determined the optimum method for minimal loss of microfibres when filtering water samples and so that potential loss rates would be known. The filtering process was found to result in a loss of microfibres, with a mean loss of 7.97% of

microfibres lost over all category combinations investigated, with glass filter paper used with a Buchner funnel resulting in the most microfibres lost (87.36% retrieval rate) and cellulose filter paper with the glass frit resulted in the least amount of loss of microfibres (94.03% retrieval rate). Easylift® was found to be an effective method of collecting microfibres from the surface of filter papers, with a mean loss of 3.75% microfibres across all categories investigated. The combination with the overall best retrieval rate was cellulose filter paper used with the glass frit with an overall retrieval rate of 93.24%. The glass filter paper with the Buchner filtration combination performed the worst with an overall retrieval rate of 79.65%.

The use of the addition of PLM into the search process was investigated to determine if its use would result in the detection of additional anthropogenic materials that were missed in the preliminary search with stereomicroscopy. The majority of research currently uses stereomicroscopes to detect anthropogenic materials within their samples, and then a confirmatory method such as FTIR or Raman spectroscopy is used. This investigation aimed to determine if anthropogenic materials are being missed by stereomicroscopy, and if there are any features that make the anthropogenic material more likely to be missed. PLM was found to be a beneficial addition to the search process as it was able to examine the sample under crossed polars, allowing birefringence to be observed. In the study, 1331 anthropogenic materials were detected using the stereomicroscope; the addition of PLM found an additional 549 particulates over the 244 sample slides subsection used in this study. A significant number of the anthropogenic materials found with PLM were colourless, 371 (67% of those found by PLM). While stereomicroscopy found 285 colourless anthropogenic materials (21% of those found by stereomicroscopy).

One of the biggest challenges to microplastic research is how time-consuming and expensive it is to process samples. The use of machine learning to automate the detection of microplastics and other anthropogenic materials has the potential to substantially decrease the time it takes to process samples, allowing more research to be completed in a smaller amount of time. 3102 images from the Hudson River samples were split into

training, validation, and test set with a 70% (2171), 20% (621), 10% (310) split. A second dataset was created by randomly augmenting the training images; the augmentations used were flipped horizontally and vertically, 90° rotated clockwise, counterclockwise and upside down and up to 4% blur was applied. This brought the number of training images to 6504. The training was undertaken with YOLOv5, YOLOv7 and YOLOv8 three times each, once with 25 epochs, once with 100 epochs and once with the augmented training set with 100 epochs. YOLOv5 performed the worst out of all algorithms investigated, with most classes having a classification rate under 50%, meaning it is not suitable for use with the microplastic samples used in this study. YOLOv7, with 100 epochs, while not having the highest precision and recall, had the best all-around correct identification rate for each class, including microfibres and fragments. YOLOv7 with augmented images had the best F1 score of 0.584. The most successful class identified was pen with the highest identification rate of 94% being achieved by YOLOv7 100 epochs with and without augmented images.

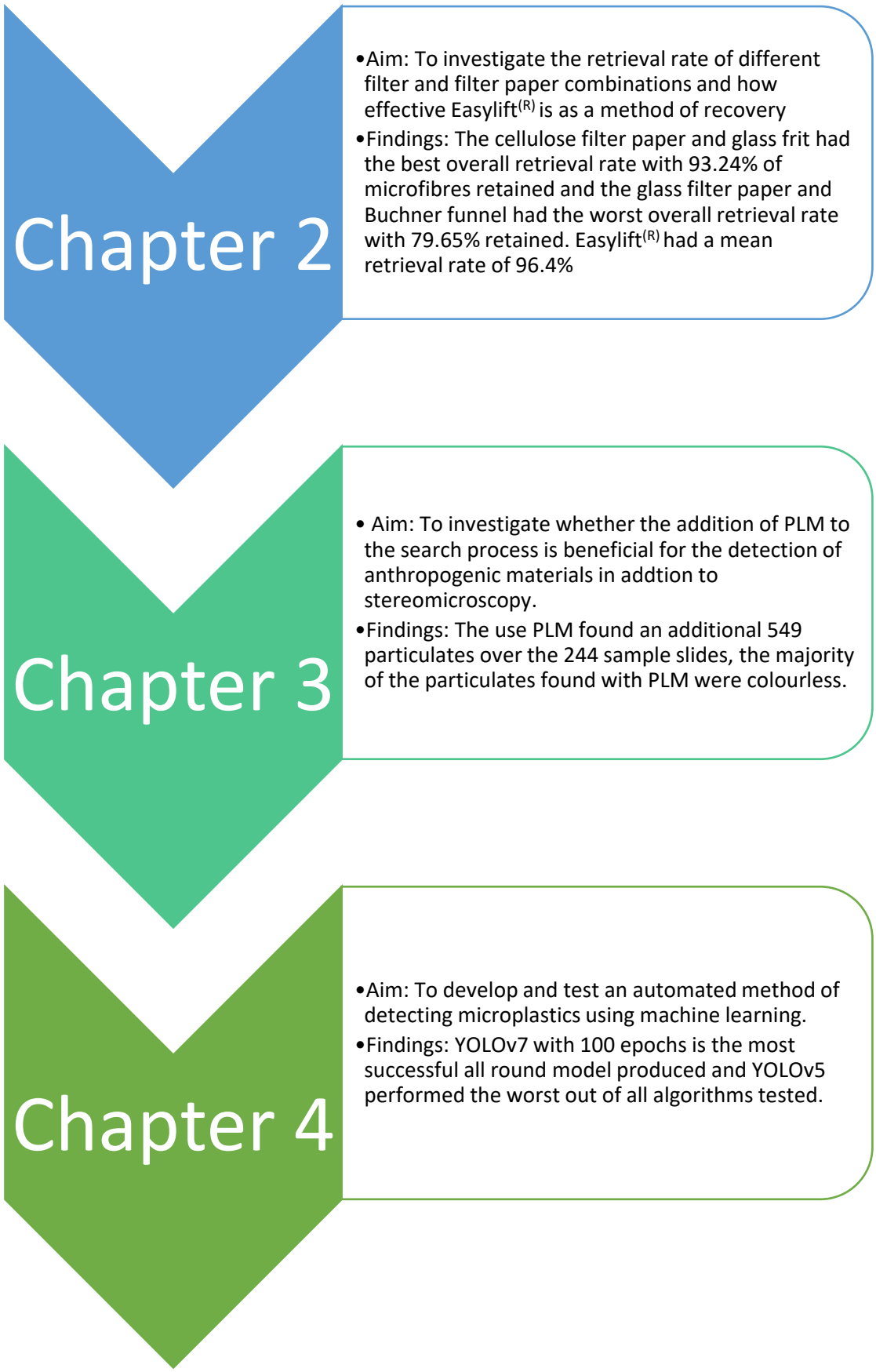

Figure 5.1 A Flow chart showing the aims and key findings for each chapter.

5.1.1 Key Findings for Chapter 2: Improved Method for the Retrieval of Microplastics from Water Samples Using a Forensic Fibre Recovery Approach

5.1.1.1 Objectives

The objectives of Chapter 2 were as follows:

Objective 1: To investigate and evaluate the different properties of Easylift® to allow the analysis of microplastics.

Objective 2: To determine if microfibres are being lost during the filtration of water samples.

Objective 3: If so, determine if the filter paper type or funnel used impacts on the amount microfibres lost through filtration.

Objective 4: to determine the efficacy of Easylift® as a method for retrieving microfibres from the surface of two different filter papers.

5.1.1.2 Chapter Summary

Two different filter papers (Glass filter paper and cellulose filter paper) were tested with two filter funnel types (Buchner funnel and glass frit). 10 litres of tap water seeded with approximately 200 fluorescent microfibres was filtered with each filter and funnel combination three times. The fibres were counted before they were added to the water, then the number of fibres caught by the filter was counted again to see if any were lost in the filtering process. The filter paper was then tape lifted with a piece of Easylift® tape, to retrieve the microfibres. Once tape lifted the number of fibres was once again counted to determine Easylift®'s retrieval rate and the overall percentage of microfibres lost during the filtration and collections steps.

5.1.1.3 Key Findings

The key findings of this chapter were that:

1. Easylift® is compatible with a number of techniques in situ, including PLM, confocal Raman and microspectrophotometry.
2. It is possible to dissect and remove the microplastics from the Easylift® tape lift allowing it to be analysed with a variety of alternative techniques including Fourier transform infra-red spectroscopy (FTIR).
3. Microfibres were found to be lost during the filtration process with an average of 7.97% of microfibres lost over all combinations investigated with glass filter paper and a Buchner funnel resulting in the most loss and cellulose filter paper with a glass frit resulting in the least loss.
4. Filter type and funnel type were not found to produce a significant interaction effect on the rate of microfibre recovery post-filtration (P = 0.218).
5. The optimal funnel and filter combination for Easylift® recovery was found to be cellulose filter paper with glass frit, as it had a mean fibre recovery rate from the filter paper with Easylift® of 99.16%, a standard deviation of 0.96% points, and an overall recovery rate of 93.24%.
6. A statistically significant difference was found when comparing the recovery of the glass filter paper and glass frit funnel combination (m = 96.55%, sn-1 = 1.71) with the glass filter paper with the ceramic funnel (m = 91.21%, sn-1 = 2.03) with an adjusted p value of 0.006.
7. A statistically significant difference was found when comparing the ceramic funnel and cellulose filter combination, (m = 98.54%, sn-1 = 1.25) with the ceramic funnel with the glass filter paper (m = 91.21%, sn-1 = 2.03) with an adjusted p value of 0.001.
8. The glass filter paper with the Buchner filter combination resulted in the lowest retrieval rate (91.21% with a standard deviation of 2.03%).
9. The water content of the filter paper was also not found to affect the rate at which tape lifting can recover microfibres from the filters used when looking at the range of water contents observed in this study

prior to tape lifting. However, it was observed that when the filter paper was very wet the tackiness of the tape lift was affected, and when the filter was dry, more background fibres from the filter were retrieved.

5.1.1.4 Recommendations

From the findings outlined above the following recommendations are made.

1. Based on the observed retrieval rates, using a cellulose filter paper and a Buchner funnel had the lowest rates of losing microfibres and so is the best method for maximum retrieval. Although thought should also be put into the study design when selecting filter paper. For example, if any anthropogenic material such as cotton is being investigated then a cellulose filter paper may not be appropriate. In these instances, the possible loss of microfibres should be considered in the interpretation.
2. The use of Easylift® in microplastic research allows for the quick and easy retrieval of microfibres from the filter paper with a high retrieval rate. Easylift® also prevents any contamination to the sample after tape lifting and allows the sample to be stored for long periods of time.
3. An investigation into Easylift®'s retrieval rates with other forms of microplastics for instance fragments and microbeads should be conducted.
4. An investigation into Easylift®'s retrieval rates with other sample mediums should also be conducted for example soils and sediment samples.
5. An investigation into Easylift®'s performance with environmental samples that may contain materials such as debris, salt etc should be investigated.

5.1.2 Key Findings for Chapter 3: Development of an improved method of processing microplastic samples – Easylift® field trial and the addition of polarised light microscopy for the detection of microplastics

5.1.2.1 Objectives

The objectives of Chapter 3 are as follows:

Objective 1: To build on the evaluation of the use of Easylift® from Chapter 2, during a field trial.

Objective 2: To determine if there is a benefit to adding PLM to the process of searching for microplastics with stereomicroscopy, or as a standalone technique.

Objective 3: To investigate whether certain characteristics, e.g., colour, microplastic type or size, influences whether they are found with stereomicroscopy or PLM.

5.1.2.2 Chapter Summary

528 samples were taken across the whole Hudson River expedition, these samples were used as the first field trial of Easylift®, to determine if there were any problems that arose during its use with environmental samples both for retrieval and analysis. 244 sample slides out of 528 samples were searched with stereomicroscopy at a x30 magnification for any potential anthropogenic material. Anything of potential interest was marked on the surface of the tape lift with a pen. After the search with the stereomicroscope the sample was examined by the same examiner with a Polarised light microscope, the samples that were marked during the first stage were analysed first to determine if they were anthropogenic in origin or natural. The entire slide was then searched again at x40 under crossed polars, this allows any interference colours to be observed, making plastic materials more visible. The slide was then searched again under plane polarised light at x100 to search for smaller microplastics that may have been missed.

5.1.2.3 Key Findings

The key findings of Chapter 3 were that:

1. Easylift® was found to be an effective method for retrieving microplastics from filter papers in a field study. It was used on over 500 samples encompassing, air, water, and soil samples.
2. During the field trial a small number of particulates remained on the filter, these particulates could be retrieved with tweezers and placed underneath an Easylift® tape.
3. The addition of PLM after stereomicroscopy found an additional 549 to the 1331 particulates found by stereomicroscopy over the 244 sample slides subsection used in this study.
4. A logistical regression found that there was a significant relationship found between the particulate being colourless and what method it was found by (P value = 8.8×10^{-8}). With 67% of the additional 549 found being colourless.
5. Width was not shown to have an impact on the method of detection, however, there are several other factors which may be playing a role in this finding.
6. By further categorising microfibres to include cross-sectional shape, birefringence, sign of elongation and presence of delusterant, a more accurate estimation of the level of microplastic pollution, and information about potential sources of microplastic contamination, can be achieved.

5.1.2.4 Recommendations.

From the findings outlined above the following recommendations are:

1. Easylift® should be used to collect anthropogenic particulates from filter papers as this puts the particulate into a field where it is protected from contamination and allows the sample to be observed under crossed-polars on a PLM.

2. PLM should be added to the search process as it allows more features to be observed such as birefringence allowing colourless microplastics to be more easily detected.
3. A study should be undertaken to investigate if when PLM is used first followed by stereomicroscopy, the second search should be done with stereomicroscopy to determine if it detects any additional anthropogenic particulates missed by PLM. If this is found to be the case, then a two stage-search is recommended if not then the use of stereomicroscopy can be removed from the search process.
4. A study should be done with different examiners to see if there is any intra-variation between what is found in the samples and if experience has an impact on what is identified as an anthropogenic material.

5.1.3 Key Findings from Chapter 4:

5.1.3.1 Objectives

The objectives of this Chapter are as follows:

Objective 1: To generate a comprehensive dataset using samples taken from the Hudson River

Objective 2: To create an annotation system to classify objects in the dataset.

Objective 3: To train and test the dataset with YOLOv5, YOLOv7 and YOLOv8 with varying levels of epoch and augmentation in the dataset to determine how accurate the detections produced are.

5.1.3.2 Chapter Summary

During the analysis of the 528 samples taken from the Hudson River 13,992 images were taken, these comprised of 8927 images from water samples from a saltwater environment to the source of the Hudson River. 3742 images taken from air samples; 330 images taken from soil samples. A further 746 images were taken of known textile fibres mounted with Easylift®.

Of the 13992 images taken 3102 images were annotated using the Computer Vision Annotation Tool (CVAT), for 21 classifications; air bubble, background material, sand, cellulose filter fibre, cotton, diatom, Easylift® tab, film, edge of slide, fragment, glass filter fibre, hair textile, hair, insect matter, microbead, microfibre, natural material, pen, salt and unknown. These images were then split into training, validation, and test set with a 70% (2171), 20% (621), 10% (310) split. A second dataset was created by randomly augmenting the training images, the augmentations used were flipped horizontal and vertical, 90° rotate clockwise, counterclockwise and upside down and an up to 4% blur was applied this bought the number of training images to 6504. Training was undertaken with YOLOv5, YOLOv7 and YOLOv8 three times each: once with 25 epochs, once with 100 epochs and once with the augmented training set with 100 epochs.

5.1.3.3 Key Findings

The key findings of Chapter 4 were that:

1. YOLOv5 performed the worst in the overall identification of microplastic samples with a mean F1 score of 0.278. YOLOv5 also had the lowest mAP50 with a mean of 0.191, meaning that it generated inaccurate bounding boxes.
2. YOLOv7 100 epochs had the best all round correct identification rate for each class including microfibres and fragments. However, YOLOv7 with augmented images had the best F1 score of 0.584.
3. 25 epochs performed the worst for all models produced.
4. The performance of the models with augmentation decreased compared to the 100 epochs with no augmentation category.
5. The most successful class identified was pen with the highest identification rate of 94% being achieved by YOLOv7 100 epochs with and without augmented images.
6. All models were unable to identify Easylift® tab, insect matter and salt, this indicates that these classes need to have more representation within the dataset.

5.1.3.4 Recommendations

From the findings outlined above the following recommendations can be made.

1. More images should be added to the dataset to increase the representation of different classifications particularly the underrepresented classes such as salt, hair, microbeads and sand. Different sample types should also be better represented in the dataset in particular saltwater images and soil/ sediment samples.
2. There should also be further investigation into the addition of augmented images in the dataset, for example by employing early stopping to cease training when the model has reached the optimum number of epochs before performance decreases.
3. Other algorithms should also be investigated, including Random Forest and K-nearest neighbour.

5.2 Implications of findings.

The findings of this thesis have provided a new approach to collecting and storing microplastic samples from filter papers. The ability to store samples without fear of contamination or loss, allows samples to be quickly obtained in the field, it also facilitates inter laboratory studies, by allowing the samples to be easily sent to different facilities allowing results to be validated by other researchers creating more reliable data. The ability to store samples long-term also allows the samples to be re-analysed as new techniques emerge. In addition, knowing the potential rates of loss of microplastics from different commonly used filtration methods allows researchers to choose the most appropriate method for the equipment available and make adjustments to the overall microplastic population to account for the potential losses caused through filtration. In addition, In addition, this thesis compared the more commonly used stereomicroscopy with polarised light microscopy. The findings of which demonstrated that stereomicroscopy misses a large number of microplastics, predominantly colourless microplastics. With this information, researchers will be able to better inform the research design to

maximise the detection of microplastics that may be missed if stereomicroscopy is used alone. Finally, the development of a wide dataset of microplastic images and development of an automated machine learning method of detecting and characterising microplastics will have wide positive effects on microplastic research by speeding up analysis times. The findings of chapter 5 will help to continue the advancement of this goal and help inform the next phase of development.

5.3 Further Work

The study in Chapter 3 should be replicated, using PLM as the initial method of searching followed by stereomicroscopy. This would conclusively determine if the use of PLM results in more anthropogenic materials being identified or whether the action of a second search is what is responsible for finding further particulates. This study should be done by the same examiner to ensure comparable results to the previous study; this should be done on new samples so that there is no bias about what is expected on the slides. This study could be repeated with different examiners to see if there are any intra-examiner differences in what is detected on the slides, as the identification of anthropogenic materials can be subjective, meaning what one examiner identifies as anthropogenic, another may not. This could help to inform a standardised method of identifying anthropogenic materials that could be applied to future research. A double-blind study could also be conducted where it is known exactly what is on each slide, and a separate examiner with no knowledge of what is present on the slide searches it. This study would need to run both with stereomicroscopy used first, followed by PLM, and using PLM first, followed by stereomicroscopy. This would allow the determination of how accurate the two methods are and if there is a common particulate type that is missed by both methods. The effect of size on the rate of detection also needs to be investigated further as it was not possible to accurately ascertain from the data used in this study as often it was not possible to accurately measure the length due to the presence of background material obscuring part of the particulate or in the case of very

long microfibres, excessive twisting and overlaying made measuring the length impossible. This could be done in a laboratory simulation similar to the study conducted in Chapter two, by including samples of known size ranges to see if certain size ranges are missed more than others. An investigation also needs to be carried out to determine if Easylift® has a limit of extraction, by testing it with smaller size fraction down to the nanoplastic range, this would allow the determination of whether Easylift® is able to extract small particulates, which would explain their absence in the sample slide if this was found to be the case. In addition, the extraction rate of Easylift® with other microplastic types such as microbeads and fragments should be investigated.

Due to the findings of Chapter 4, there have been several areas identified that need further investigation and improvement to further understand the data within this study. Firstly, more images should be tagged and added to the dataset to increase the representation of different classifications; the classes that need better representation are sand, microbeads, insect materials, hair, hair textile, Easylift® tab, edge of the slide, microfibres and fragments. Different sample types also need to be incorporated in the dataset, such as saltwater, soil, sediment and freshwater, from different bodies of water for example lakes. This would improve the different models' ability to be used to accurately identify microplastics in environmental samples. The models produced should also be tested with samples of different backgrounds, such as those left on filter papers, to test its performance when the sample is not mounted in Easylift®. Additional algorithms could also be investigated as an alternative to those used in this thesis, algorithms that could be investigated include Random Forrest and K-Nearest Neighbour. Further research could also be done with the algorithms investigated, by changing parameters and confidence levels to find the optimum setting for successful detection. Then number of epochs employed could also be altered to find the optimum number of epochs before overfitting occurs and performance decreases. Augmentation of the images to generate more data should also be further investigated for example altering the blur

further, colour manipulation and flipping or altering the orientation further could allow a greater level of detection being achieved. The split of the training, testing and validation set could also be altered to determine if there more or less images in the training dataset has an impact on detection rates.

References

ABAS, S. M., ABDULAZEEZ, A. M. & ZEEBAREE, D. Q. (2022). A YOLO and convolutional neural network for the detection and classification of leukocytes in leukaemia. *Indonesian Journal of electrical engineering and computer science*. 25 (1). pp. 200-213. (Online). Available from: http://doi.org/10.11591/ijeecs.v25.i1.pp200-213. [Accessed: 16/01/2023].

ABDULLAH, M. (2023). YOLO working principle, difference between its different variants and versions. *Medium*. Available at: https://medium.com/@muhabd51/yolo-working-principle-difference-between-its-ddifferent-variants-and-versions-95b8ad7b95ab#:~:text=The%20main%20difference%20between%20the,but%20they%20are%20also%20faster. [Accessed: 15/05/2024].

AHMAD, I., BASHERI. M., IQBAL, M. J. & RAHIM, A. (2018). Performance comparison of support vector machine, random forest, and extreme learning for intrusion detection. *IEEE Access*. 6. pp. 33789-33795. (Online). Available from: https://ieeexplore.ieee.org/document/8369054. [Accessed: 19/02/2021].

AHMAD, M., CHEN, J., KHAN, M. T., YU, Q., PHAIRUANG, W., FURUUCHI, M., ALI, S. W., NAWAB, A. & PANYAMETHEEKUL, S. (2023). Sources, analysis and health implications of atmospheric microplastics. *Emerging Contaminants*. 9 (3). pp. 100233. (Online). Available from: https://doi.org/10.1016/j.emcon.2023.100233. [Accessed: 05/06/2024].

ALAVA, J. J., KAZMIRUK, T. N., DOUGLAS, T., SCHUERHOLZ, G., HEATH, B., FLEMMING, S. A., BENDALL, L. & DREVER, M. C. (2021). Occurrence and size distribution of microplastics in mudflat sediments of the Cowichan-Koksilah Estuary, Canada: A baseline for plastic particles contamination in an anthropogenic-influenced estuary. *Marine Pollution Bulletin*. 173. pp. 113033. (Online). Available from: https://doi.org/10.1016/j.marpolbul.2021.113033. [Accessed: 10/06/2025].

ALBERGHINI, L., TRUANT, A., SANTONICOLA, S., COLAVITA, G. & GIACCONE, V. (2023). Microplastics in fish and fishery products and risk for human health: A review. *International Journal of Environmental Research and Public Health*. 20 (1). (Online). Available from: https://doi.org/10.3390/ijerph20010789. [Accessed: 28/06/2023].

ALLEN, S., ALLEN, D., PHOENIX, V. R., LE ROUX, G., DURANTEZ, P., SIMONNEAU. A., BINET, S. & GALOP, D. (2019). Atmospheric transport and deposition of microplastics in a remote mountain catchment. *Nature Geoscience*. 12 (5). pp. 339-344. (Online). Available from: https://www.nature.com/articles/s41561-019-0335-5. [Accessed: 06/03/2020].

ANDERSON, T. L., VEGA, B. & KOVSCEK, A. R. (2020). Multimodal imaging and machine learning to enhance microscope images of shale. *Computers and Geosciences*. 145. pp. 104934. (Online). Available from: https://doi.org/10.1016/j.cageo.2020.104593. [Accessed: 11/01/2023].

ANDRADY, A. L. (2011). Microplastics in the marine environment. *Marine Pollution Bulletin*. 62 (8). pp. 1596-1605. (Online). Available from: https://doi.org/10.1016/j.marpolbul.2011.05.030. [Accessed: 01/12/2017].

ARAUJO. C. F., NOLASCO, M. M., RIBEIRO, A. M. P. & RIBEIRO-CLARO, P. J. A. (2018). Identification of microplastics using Raman spectroscopy: Latest developments and future prospects. *Water Research*. 142. pp. 426-440.

ARIAS-VILLAMIZAR, C. A. & VÁZQUEZ-MORILLAS, A. (2018). Degradation of conventional and oxydegradable high-density polyethylene in tropical aqueous and outdoor environments. *Revista internacional de contaminacion ambiental*. 34 (1). pp. 137-147. (Online). Available from: https://www.revistascca.unam.mx/rica/index.php/rica/article/view/RICA.2018.34.01.12/46744. [Accessed: 14/09/2018].

ASADI, A., VERMA, A., YANG, K. & MEJABI, B. (2017). Wastewater treatment aeration process optimisation: A data mining approach. *Journal of*

environmental Management. 203. pp. 630-639. (Online). Available from: http://dx.doi.org/10.1016/j.jenvman.2016.07.047. [Accessed: 23/04/2024].

BAGAEV, A., MIZYUK, A., KHATMULLINA, L. & CHUBARENKO, I. (2017). Anthropogenic fibres in the Baltic Sea water column: Field data, laboratory and numerical testing of their motion. *Science of the Total Environment*. 599-600. pp. 560-571. (Online). Available from: http://dx.doi.org/10.1016/j.scitotenv.2017.04.185. [Accessed: 1/12/2017].

BAGCHI, S., TAY, K. G., HUONG, A. & DEBNATH, S. K. (2019). Image processing and machine learning techniques used in computer-aided detection system for mammogram screening – A review. *International Journal of Electrical and Computer Engineering.* 10 (3). pp. 2336-2348. (Online). Available from: http://ijece.iaescore.com/index.php/IJECE. [Accessed: 15/02/2024].

BAKIR, A., MCGORAN, A. R., SILBURN, B., RUSSELL, J., NEL, H., LUSHER, A. L., AMOS, R., SHADRACK, R. S., ARNOLD, S. J., CASTILLO, C., URBINA, J. F., BARRIENTOS, E., SANCHEZ, H., PILLAY, K., HUMAN, L., SWARTBOOI, T., CORDOVA, M. R., SANI, S. Y., WIJESINGHE, T. W.A. W., AMARATHUNGA, A. A. D., GUNASEKARA, J., SOMASIRI, S., MAHATANTILA, K., LIYANAGE, S., MÜLLER, M., HEE, Y., ONDA, D. F., JANSAR, K. M., SHIRA, Z., AMIR, H. & MAYES, A. G. (2024). Creation of an international laboratory network towards global microplastics monitoring harmonisation. *Scientific Reports*. 14 (1). pp. 12714. (Online). Available from: https://doi.org/10.1038/s41598-024-62176-y. [Accessed: 09/06/2024].

BALAS, C., BORAS, C., CHOUSOS, C., KAMINAKIS, N., KORTSALIOUDAKIS, N., ROSSOS, C., TSAPRAS, A. & TSIAOUSIS, C. (2023). A novel, multimodal throughput screening microscope platform for automating the analysis of a vast population of forensic traces. *IEEE international workshop on technologies for defence and security*. Rome: Italy (Online). Available from: https://ieeexplore.ieee.org/document/10380856/authors#authors. [Accessed: 15/05/2024].

BANIK, P., ANISUZZAMAN, M., BHATTACHARJEE, S., MARSHALL, D. J., YU, J., NUR, A. U., JOLLY, Y. N., AL-MAMUN, M., PARAY, B. A., BAPPY, M. M. M., BHUIYAN, T. & HOSSAIN, M. B. (2024). Quantification, characterization and risk assessment of microplastics from five major estuaries along the northern Bay of Bengal coast. *Environmental Pollution*. 342. pp. 123036. (Online). Available from: https://doi.org/10.1016/j.envpol.2023.123036. [Accessed: 27/03/2024].

BANK, M. S. & HANSSON, S. V. (2019). The plastic cycle: a novel and holistic paradigm for the Anthropocene. *Environmental Science and Technology*. 53 (13). pp. 7177-7179. (Online). Available from: https://pubs.acs.org/doi/10.1021/acs.est.9b02942. [Accessed: 06/03/2020].

BARROWS, A. P. W., NEUMANN, C. A., BERGER, M. L. & SHAW, S. D. (2017). Grab vs. neuston two net: a microplastic sampling performance comparison and possible advances in the field. *Analytical Methods*. 9 (9). pp. 1446-1453. (Online). Available from: http://xlink.rsc.org/?DOI=C6AY02387H. [Accessed: 20/20/2018].

BARTHELME, S. (2020). imager: Image Processing Library Based on 'CImg'. R package version 0.42.1. https://CRAN.R-project.org/package=imager. [Accessed: 30/03/2020].

BAYO, J., OLMOS, S. & LÓPEZ-CASTELLANOS, J. (2020). Microplastics in an urban wastewater treatment plant: The influence of physicochemical parameters and environmental factors. *Chemosphere*. 238. pp. 124593. (Online). Available from: https://doi.org/10.1016/j.chemosphere.2019.124593. [Accessed: 50/08/2021].

BEANS, C. (2023). Are microplastics spreading infectious disease? *Proceedings of the National Academy of Sciences of the United States of America.* 120 (3). pp. 1-5. (Online). Available from: https://doi.org/10.1073/pnas.2311253120. [Accessed: 07/08/2023].

BELEITES, C. & SERGO, V. (2020) `hyperSpec: a package to handle hyperspectral data sets in R', R package version 0.99-20200213. https://github.com/cbeleites/hyperSpec. [Accessed: 30/03/2020].

BELL, J. P. & DUMBLETON, J. H. (1971). Changes in the structure of Wet-spun acrylic fibres during processing. *Textile Research Journal*. 41 (3). pp. 196-203. (Online). Available from: https://doi.org/10.1177/004051757104100302. [Accessed: 16/09/2022].

BENEZETH, Y., JODOIN, P. M., EMILE, B., LAURENT, H. & ROSENBERGER, C. (2010). Comparative study of background subtraction algorithms. *Journal of electronic Imaging, Society of Photo-optical Instrumentation Engineers*. (3). pp. 1-12. (Online). Available from: https://hal.inria.fr/inria-00545478. [Accessed: 09/12/2020].

BERGFJORD, C. & HOLST, B. (2010). A procedure for identifying textile bast fibres using microscopy: Flax, nettle/ramie, hemp and jute. *Ultramicroscopy*. 110 (9). pp. 1192-1197. (Online). Available from: http://dx.doi.org/10.1016/j.ultramic.2010.04.014. [Accessed: 12/09/2022].

BERGMANN, M., MÜTZEL, S., PRIMPKE, S., TEKMAN, M. B., TRACHSEL, J. & GERDTS, G. (2019). White and wonderful? Microplastics prevail in snow from the Alps to the Artic. *Science Advances*. 5 (8). pp. 1-11. (Online). Available from: https://www.science.org/doi/10.1126/sciadv.aax1157. [Accessed: 12/03/2020].

BESSELING, E., WANG, B., LÜRLING, M. & KOELMANS, A. A. (2014). Nanoplastic affects growth of S. Obliquus and reproduction of D.magna. *Environmental Science and Technology*. 48 (20). pp. 12336-12343. (Online). Available from: http://www.dx.doi.org/10.1021/es503001d. [Accessed: 13/11/2019].

BEWES, J., LOW. A., MORPHETT, A., PATE, F. D. & HENEBERG, M. (2019). Artificial intelligence for sex determinisation of skeletal remains: Application of a deep learning artificial neural network to human skulls. *Journal of Forensic and Legal Medicine*. 62 (January). pp. 40-43. (Online).

Available from: https://doi.org/10.1016/j.jflm.2019.01.004. [Accessed: 27/20/2019].

BHARADIYA, J. P. (2023). Convolutional Neural Networks for Image Classification. *International Journal of Innovative Science and Research Technology*. 8 (5). pp. 673-677. (Online). Available from: https://www.researchgate.net/profile/Jasmin-Bharadiya-4/publication/370944952_Convolutional_Neural_Networks_for_Image_Classification/links/646b960b7b575d49292a0be3/Convolutional-Neural-Networks-for-Image-Classification.pdf. [Accessed: 14/05/2024].

BHAT, M. A. & JANASZEK, A. (2024). Delving into river health: unveiling microplastic intrusion and heavy metal contamination in freshwater. *Discover Environment*. 2 (61). (Online). Available from: https://doi.org/10.1007/s44274-024-00101-w. [Accessed: 09/06/2024].

BHATIA, N. & VANDANA, A. (2010). Survey of Nearest Neighbour Techniques. *International Journal of Computer Science and Information Security*. 8 (2). pp. 302-305. (Online). Available from: http://arxiv.org/abs/1007.0085. [Accessed: 19/20/2021].

BIERMANN T. W. & WIGGINS K. (2018). 'Colour analysis of fibres' in Robertson, J., Roux, C. and Wiggins, K. (eds*). Forensic Examination of Fibres*. Third edition. Boca Raton: CRC Press.

BIJKER, I. (2023). *AUAS develop teaching package for international SHUTTLE project with the compliments of the European Commission.* Available from: https://www.amsterdamuas.com/content/news/news/2023/01/auas-develops-teaching-package-for-international-shuttle-project.html. [Accessed: 23/03/2023].

BISWAS, S. & BISWAS, D. (2021). Deep learning based asbestos fibre detection. *IEEE Applied imagery pattern recognition workshop (AIPR)*. Washington DC. 12-14th October. (Online). Available from: https://ieeexplore.ieee.org/abstract/document/9762114. [Accessed: 30/01/2023].

BLAIR, R. M., WALDRON, S. & GAUCHOTTE-LINDSAY, C. (2019). Average daily flow of microplastics through a tertiary wastewater treatment plant over a ten-month period. *Water Research*. (Online). 163. pp. 114909. Available from: https://doi.org/10.1016/j.watres.2019.114909. [Accessed 10/08/2021].

BLAIR, R. M., WALDRON, S., PHOENIX, V. & GAUCHOTTE-LINDSAY, C. (2017). Micro- and nanoplastic pollution of freshwater and wastewater treatment systems. *Springer Science Reviews*. 5 (1). pp. 19-30. (Online). Available from: https://doi.org/10.1007/s40362-017-0044-7. [Accessed: 14/09/2018].

BLETTLER, M. C. M., ABRIAL, E., KHAN, F. R., SIVRI, N. & ESPINOLA, L. A. (2018). Freshwater plastic pollution: Recognising research biases and identifying knowledge gaps. *Water Research*. 143. pp. 416-424. (Online). Available from: https://doi.org/10.1016/j.watres.2018.06.015. [Accessed: 06/09/2018].

BOTTERELL, Z. L. R., BEAUMONT, N., DORRINGTON, T., STEINKE, M., THOMPSON, R. C. & LINDEQUE, P. K. (2019). Bioavailability and effects of microplastics on marine zooplankton: A review. *Environmental Pollution*. 245. pp. 98-110. (Online). Available from: https://doi.org/10.1016/j.envpol.2018.10.065. [Accessed: 05/08/2023].

BOUCHER, J. & FRIOT, D. (2017). *Primary microplastics in the ocean: A Global Evaluation of Sources*. Switzerland: IUCN. pp. 1-44. (Online). Available from: https://www.iucn.org/content/primary-microplastics-oceans. [Accessed: 21/20/2020].

BRADLEY, A. P. (1997). The use if the area under the ROC curve in the evaluation of machine learning algorithms. *Pattern Recognition*. 30 (7). pp. 1145-1159. (Online). Available from: https://doi.org/10.1016/S0031-3203(96)00142-2. [Accessed: 08/02/2023].

BRINSKO, K. M., SPARENGE, S. & KING, M. (2016). The effects of environmental exposure on the optical, physical and chemical properties of manufactured fibres of natural origin. *Journal of Forensic science*. 61 (5). pp.

1215-1227. (Online). Available from: https://doi.org/10.1111/1556-4029.13140. [Accessed: 29/11/2018].

BROWNE, M. A., CRUMP, P., NIVEN, S. J., TEUTEN, E., TONKIN, A., GALLOWAY, T. & THOMPSON, R. (2011). Accumulation of microplastic on shorelines worldwide: sources and sinks. *Environmental Sciences & Technology*. 45 (21). pp. 9175-9179. (Online). Available from: https://doi.org/10.1021/es201811s. [Accessed: 02/03/2018].

BROWNLEE, C., HELLIWELL, K. E., MEEDA, Y., MCLACHLAN, D., MURPHY, E. A. & WHEELER, G. L. (2022). Regulation and integration of membrane transport in marine diatoms. *Seminars in cell and developmental biology*. (March). pp. 1-11. (Online). Available from: https://doi.org/10.1016/j.semcdb.2022.03.006. [Accessed: 19/08/2022].

BUHL, N. (2024). YOLO Object Detection Explained: Evolution, Algorithm, and Applications. *Encord*. Available from: https://encord.com/blog/yolo-object-detection-guide/. [Accessed: 05/08/2025].

BÜNGENER, L., SCHÄFFER, S. M., SCWARZ, A. 7 SCHWALB, A. (2024). Microplastics in a small river: Occurrence and influencing factors along the river Oker, Northan Germany. *Journal of Contaminant Hydrology*. 264. pp. 104366. (Online). Available from: https://doi.org/10.1016/j.jconhyd.2024.104366. [Accessed: 09/06/2024].

BURNS, E. E. & BOXALL, B. A. (2018) Microplastics in the aquatic environment: Evidence for or against adverse impacts and major knowledge gaps. *Environmental Toxicology and Chemistry*. 37 (18). pp. 2776-2796. (Online). Available from: https://doi.org/10.1002/etc.4268. [Accessed: 30/01/2020].

BÜTTNER, M., SCHNEIDER, L., KRASOWKI, A., KROIS, J., FELDBERG, B. & SCHWENDICKE, F. (2023). Impact of noisy labels on dental deep learning- Calculus detection on bitewing radiographs. *Journal of clinical medicine*. 12. (Online) Available from: https://doi.org/10.3390/jcm12093058. [Accessed: 17/02/2024].

BUZZINI, P. & MASSONNET, G. (2015). The analysis of coloured acrylic, cotton, and wool textile fibres using micro-raman spectroscopy. Part 2: Comparison with the traditional methods of fiber examination. *Journal of Forensic Science*. 60 (3). pp. 712-720. (Online). Available from: https://doi.org/10.1111/1556-4029.12654. [Accessed: 28/11/2018].

CAI, L., WANG, J., PENG, J., TAN, Z., ZHAN, Z., TAN, X. & CHEN, QIUQIANG. (2017). Characteristic of microplastics in the atmospheric fallout from Dongguan city, China: preliminary research and first evidence. *Environmental Science and Pollution Research*. 24 (32). pp. 24928-24935. (Online). Available from: https://link.springer.com/article/10.1007/s11356-017-0116-x. [Accessed: 03/01/2019].

CARBERY, M., O'CONNOR, W. & THAVAMANI, P. (2018). Trophic transfer of microplastics and mixed contaminants in the marine food web and implication for human health. *Environmental International*. 115. pp. 400-409. (Online). Available from: https://doi.org/10.1016/j.envint.2018.03.007. [Accessed: 02/01/2019].

CARR, D., CRUTHERS, N., SMITH, C. & MYERS, T. (2008). Identification of selected vegetable textile fibres. *Studies in Conversation*. 53. pp. 75-87. (Online). Available from: http://dx.doi.org/10.1179/sic.2008.53.Supplement-2.75. [Accessed: 24/09/2022].

CARR, S. A., LIU, J. & TESORO, A. G. (2024). Transport and fate of microplastic particles in wastewater treatment plants. *Water Research*. 91. pp. 174-182. (Online). Available from: http://dx.doi.org/10.1016/j.watres.2016.01.002. [Accessed:23/04/2024].

CARSON, H. S., NERHEIM, M. S., CARROLL, K. A. & ERIKSEN, M. (2013). The plastic-associated microorganisms of the North Pacific Gyre. *Marine Pollution Bulletin*. 75 (1-2). pp. 126-132. (Online). Available from: http://dx.doi.org/10.1016/j.marpolbul.2013.07.054. [Accessed: 31/01/2018].

CARUANA, R. & NUCULESCU-MIZIL, A. (2006). An empirical comparison of supervised learning algorithms. *ACM international conference on machine*

learning. Pittsburgh. pp. 161-168. (Online). Available from: https://doi.org/10.1145/1143844.1143865. [Accessed: 01/09/2022].

CASSIDY, P. E. & AMINABHAVI, T. M. (1981). Enhanced Environmental Degradation of Plastics. *Journal of Macromolecular Science, Part C*. 21 (1). pp. 89-133. (Online). Available from: https://doi.org/10.1080/00222358108080926. [Accessed: 23/09/2022].

CHANDRAMOHAN, D. & MARIMUTHU, K. (2011). A review on natural fibres. *International Journal of Research and Reviews in Applied Science*. 8 (2). pp. 194-206. (Online). Available from: https://kompozit.org.tr/wp-content/uploads/2020/01/A_REVIEW_ON_NATURAL_FIBERS.pdf. [Accessed: 23/09/2022].

CHAUDHURI, S. K. (2018). Structure and properties of carpet fibres and yarns. In: Goswami (Ed). *Advances in carpet manufacture*. Second edition. Duxford: Woodhead publishing. (Online). Available from: https://doi.org/10.1016/B978-0-08-101131-7.00002-2. [Accessed: 26/09/2022].

CHEN, G., LI, Y. & WANG, J. (2023). Chapter 8- Human health effects of airborne microplastics. *Comprehensive Analytical Chemistry*. (ed. Wang, J). Volume 100. (Online). Available from: https://doi.org/10.1016/bs.coac.2022.07.008. [Accessed 28/06/2023].

CHEN, Q., REISSER, J., CUNSOLO, S., KWADIJK, C., KOTTERMAN, M., PROIETTI, M., SLAT, B., FERRARI, F. F., SCHWARZ, A., LEVIVIER, A., YIN, D., HOLLERT, H. & KOELMANS, A. A. (2018). Pollutants in plastics within the North Pacific subtropical gyre. *Environmental Science & Technology*. 52. pp. 446-456. (Online). Available from: https://pubs.acs.org/doi/10.1021/acs.est.7b04682. [Accessed: 02/01/2019].

CHEN, S. Y. C., YOO, S. & FANG, Y, L. (2022). Quantum long short-term memory. *IEEE International Conference on Acoustics, Speech and Signal Processing (ICASSP).* Singapore. pp. 8622-8626. (Online). Available from: https://ieeexplore.ieee.org/abstract/document/9747369?casa_token=qV2bK3S5y-EAAAAA:M5ti1VPQxx-a-

AFI1Cme2RwC4hFDT_EYjYCFrYV_cTsf6S3WYgswg-MfmxqVX6jFQIR8aDel. [Accessed: 16/05/2014].

CHEN, X., XIONG, X., JIANG, X., SHI, H. & WU, C. (2019). Sinking of floating plastic debris caused by biofilm development in a freshwater lake. *Chemosphere*. 222. pp. 856-864. (Online). Available from: https://doi.org/10.1016/j.chemosphere.2019.02.015. [Accessed: 05/04/2024].

CHEN, Y., ZOU, C., MASTALERZ, M., HU, S., GASAWAY, C. & TAO, X. (2015). Applications of Micro-Fourier Transform Infrared Spectroscopy (FTIR) in the Geological sciences – A review. *International Journal of Molecular Sciences*. 16 (12). pp. 30223-30250. (Online). Available from: https://www.mdpi.com/1422-0067/16/12/26227. [Accessed: 02/10/2022].

CHENG, Z. & ZHANG, F. (2020). Flower end-to-end detection based on YOLOv4 using a mobile device. *Wireless Communications and mobile computing*. (Online). Available from: https://www.hindawi.com/journals/wcmc/2020/8870649/. [Accessed: 26/02/2024].

CHICCO, D. & JURMAN, G. (2020). The advantages of the Mathews correlation coefficient (MCC) over F1 score and accuracy in binary classification evaluation. *BMC Genomics*. 21 (6). (Online). Available from: https://doi.org/10.1186/s12864-019-6413-7. [Accessed: 06/01/2024].

CHOUCHENE, K., PINTO DE COSTA, J., CHAMKHA, M., KSIBI, M. & SAYADI, S. (2023). Effects of microplastics' physical and chemical properties on aquatic organisms: State-of-the-art and future research trends. *Trends in Analytical Chemistry*. 166. pp.117192. (Online). Available from: https://doi.org/10.1016/j.trac.2023.117192. [Accessed: 05/08/2023].

CHRISTIN, S., HERVET, É. & LECOMTE, N. (2019). Applications for deep learning in ecology. *Methods in ecology and evolution*. 10. pp. 1632-1644. (Online). Available from: https://doi.org/10.1111/2041-210X.13256. [Accessed: 15/05/2024].

CHU, F., ANEX, D. S., JOINES, A. D. & HART, B. R. (2020). Automated analysis of scanning electron microscopic images for assessment of hair

damage. *Royal Society open science*. 7 (1). pp. 1-12. (Online). Available from: http://dx.doi.org/10.1098/rsos.191438. [Accessed: 20/01/2023].

CLAESSENS, M., DE MESTER, S., VAN LANDUYT, L., DE CLERCK, K. & JANSSEN, C. R. (2011). Occurrence and distribution of microplastics in marine sediments along the Belgian coast. *Marine Pollution Bulletin*. 62 (10). pp. 2199-2204. (Online). Available from: http://dx.doi.org/10.1016/j.marpolbul.2011.06.030. [Accessed: 09/03/2019].

COHEN, J. (1969). *Statistical power analysis for the behavioural sciences*. New York: Academic Press.

COHEN, J. (1988). *Statistical power analysis for the behavioural sciences*. 2nd edn. Hillsdale: Lawrence Erlbaum Associates.

COLE, M., LINDEQUE, P., FILEMAN, E., HALSBAND, C. & GALLOWAY, T. S. (2015). The Impact of Polystyrene microplastics on feeding, function and fecundity in the marine copepod Calanus Gelgolandicus. *Environmental Science and Technology*. 49 (2). pp.1130-1137. (Online). Available from: https://doi.org/10.1021/es504525u. [Accessed: 26/03/2018].

COLE, M., LINDEQUE, P., HALSBAND, C. & GALLOWAY, T. S. (2011). Microplastics as contaminants in the marine environment: A review. *Marine Pollution Bulletin*. 62 (12). pp. 2588-2597. (Online). Available from: https://doi.org/10.1016/j.marpolbul.2011.09.025. [Accessed: 01/12/2017].

CORDOVA, M. R., HADI, T. A. & PRAYUDHA, B. (2018). Occurrence and abundance of microplastics in coral reef sediment: a case study in Sekotong, Lombok-Indonesia. *AES Bioflux*. 10 (1). pp. 23-29. (Online). Available from: https://api.semanticscholar.org/CorpusID:203599586. [Accessed: 04/11/2019].

COSTA, F. M., IVAR DO SUL, J. A., SILVA-CAVALCANTI, J. S., ARAÚJO, C. B., SPENGLER, Â. & TOURINHO, P. S. (2010). On the importance of size of plastic fragments and pellets on the strandline: A snapshot of a Brazilian beach. *Environmental Monitoring and Assessment*. 168 (1-4). pp. 299-304. (Online). Available from: https://doi.org/10.1007/s10661-009-1113-4. [Accessed: 09/03/2018].

COX, G., HAWES, C. R., VAN DER LUBBE, L. & JUNIPER, B. E. (1987). High-voltage electron microscopy of whole, critical-point dried plant cells. *Protoplasma*. 140 (2-3). pp. 173-186. (Online). Available from: https://doi.org/10.1007/BF01273727. [Accessed: 12/09/2022].

CRAIG, J. P., KNUDSEN, J. P. & HOLLAND, V. F. (1962). Characterisation of acrylic fibre structure. *Textile Research Journal*. 32 (6). pp. 435-448. (Online). Available from: https://doi.org/10.1177/004051756203200601. [Accessed: 13/09/2022].

CRAWFORD, C. B. & QUINN, B. (2017). Microplastic Separation techniques. In: CRAWFORD, C. B. & QUINN, B. (Eds). *Microplastic pollutants*. Amsterdam: Elsevier.

CUBAYNES, H. C. & FRETWELL, P. T. (2022). Whales from space dataset, an annotated satellite image dataset of whales for training machine learning models. *Scientific data*. 9. pp. 1-8. (Online). Available from: https://doi.org/10.1038/s41597-022-01377-4. [Accessed: 30/08/2022].

CUNNINGHAM, E. M., SEIJO, N. R., ALTIERI, K. E., AUDH, R. R., BURGER, J. M., BORNMAN, T. G., FAWCETT, S., GWINNETT, C. M. B., OSBORNE, A. O. & WOODALL. L. C. (2022). The transport and fate of microplastic fibres in the Antarctic: The role of multiple global processes. *Frontiers in Marine Science*. 9. pp. 1056081. (Online). Available from: https://doi.org/10.3389/fmars.2022.1056081. [Accessed: 23/11/2022].

DAKKA, W., IPEIROTIS, P. & SACCO, G. M. (2009). 7 Taxonomy design. In: Sacco, G. M. & Tzitzikas, Y (Eds). *Dynamic Taxonomies and Faceted Search: Theory, Practice, and Experience*. Heidelberg: Springer.

DAM, N. L., VAN DER BORG, G., VAN RAAMSDONK, L. W. D., ZHENG, R., SCHMITT, E., HEDEMANN, J. B. G.M., RUIS, S., VAN BEMMEL, G. & MEIJER, N. (2024). Determination of microplastics in reared black soldier fly larvae (Hermetia illucens) using polarised light optical microscopy. *Journal of insects as food and feed.* (Online). Available from: https://brill.com/view/journals/jiff/aop/article-10.1163-23524588-00001298/article-10.1163-23524588-00001298.xml. [Accessed: 16/04/2025].

DAS, D. K., GHOSH, M., PAL, M. & CHAKRABORTY, C. (2013). Machine learning approach for automated screening of malaria parasite using light microscopic images. *Micron*. 45. pp. 97-106. (Online). Available from: http://dx.doi.org/10.1016/j.micron.2012.11.002. [Accessed: 13/01/2023].

DAVIDSON, R. (2009). Reliable inference for the Gini index. *Journal of Econometrics*. 150 (1). pp. 30-40. (Online). Available from: http://dx.doi.org/10.1016/j.jeconom.2008.11.004. [Accessed: 16/20/2021].

DE HAAN, H. (1993). Solar UV-light penetration and photodegradation of humic substances in peaty lake water. *Limnology and Oceanography*. 38 (5). 1072-1076. (Online). Available from: https://aslopubs.onlinelibrary.wiley.com/doi/pdf/10.4319/lo.1993.38.5.1072. [Accessed: 17/01/2018].

DE ROSARIO-MARTINEZ, H. (2015). phia: Post-Hoc Interaction Analysis. R package version 0.2-1. https://CRAN.R-project.org/package=phia. [Accessed: 24/07/2019].

DE WAEL, K. & LEPOT, L. (2012). Dichroism measurements in forensic fibre examination Part 5—Pigmented fibres. *Science & Justice*. 52 (3). pp. 161–167. (Online). Available from: https://doi.org/10.1016/j.scijus.2011.10.002. [Accessed: 29/11/2018].

DE WAEL, K. (2021). Microscopy in forensic fibre examinations a practical photo atlas and training tool. *Cobalt blue publishing*. (Online). Available from: https://www.cobaltbluecoaching.be/fibre-microscopy-atlas. [Accessed: 11/06/2024].

DE WAEL, K., GASON, F. C. S. J. & BAES, C. A. V. (2008). Selection of an adhesive tape suitable for forensic fiber sampling. *Journal of Forensic Science*. 53 (1). pp. 168-171.

DEEDRICK, D. W. & KOCH, S. L. (2004). Microscopy of hair part 1: A practical guide and manual for human hairs. *Federal Bureau of Investigation*. 6 (1). pp. 1-44. (Online). Available from: https://archives.fbi.gov/archives/about-us/lab/forensic-science-

communications/fsc/jan2004/research/2004_01_research01b.htm. [Accessed: 04/10/2022].

DELL'ANNA, R., LAZZERI, P., FRISANCO, M., MONTI, F., CAMPEGGI, F. M., GOTTARDINI, BERSANI, M. (2009). Pollen discrimination and classification by Fourier transform infrared (FT-IR) microspectroscopy and machine learning. *Analytical and Bioanalytical Chemistry*. 394 (5). pp. 1443-1452. (Online). Available from: https://link.springer.com/article/10.1007/s00216-009-2794-9. [Accessed: 10/01/2023].

DING Y., SHA, C. & WANG, T. (2025). Seasonal dynamics of microplastics in the central south China Sea: Abundance, sources, influencing factors, and ecological risks. *Journal of environmental chemical engineering*. 13. (Online). Available from: https://doi.org/10.1016/j.jece.2025.115937. [Accessed: 16/04/2025].

DOWARAH, K., PATCHAIYAPPAN, A., THIRUNAVUKKARASU, C., JAYAKUMAR, S. & DEVIPRIYA, S. P. (2020). Quantification of microplastics using Nile Red in two bivalve *Perna viridia* and *Meretrix meretrix* from three estuaries in Pondicherry, India and microplastics uptake by local communities through bivalve diet. *Marine Pollution Bulletin*.153. pp. 110982. (Online). Available from: https://doi.org/10.1016/j.marpolbul.2020.110982. [Accessed: 17/02/2023].

DRIS, R., GASPERI, J., ROCHER, V., SAAD, M., RENAULT, N. & TASSIN, B. (2015a). Microplastic contamination in an urban area: a study in Greater Paris. *Environmental chemistry*. 12 (5). pp. 592-599. (Online). Available from: http://dx.doi.org/10.1071/EN14167. [Accessed: 01/10/2018]/

DRIS, R., GASPERI, J., SAAD, M., MIRANDE, C. & TASSIN, B. (2016). Synthetic fibres in atmospheric fallout: A source of microplastics in the environment? *Marine Pollution Bulletin*.104 (1-2). pp. 290-293. (Online). Available from: http://dx.doi.org/10.1016/j.marpolbul.2016.01.006. [Accessed: 08/02/2018].

DRIS, R., IMHOF, H., SANCHEZ, W., GASPERI, J., GALGANI, F., TASSIN, B. & LAFORSCH, C. (2015b). Beyond the ocean: contamination of freshwater ecosystems with (micro-) plastic particles. *Environmental chemistry*. 12 (5). pp. 539-550. (Online). Available from: http://dx.doi.org/10.1071/EN14172. [Accessed: 29/01/2018].

DWYER, B. & NELSON. (2022). Roboflow (Version 1.0). [Software]. Available from: https://roboflow.com. [Accessed: 12/09/2023.

DYACHENKO, A., MITCHELL, J. & ARSEM, N. (2017). Extraction and identification of microplastic particles from secondary wastewater treatment plant (WWTP) effluent. *Analytical Methods*. 9 (9). pp. 1412-1418. (Online). Available from: https://doi.org/10.1039/C6AY02397E. [Accessed: 04/11/2019].

EBERE, E. C., WIRNKOR, V. A., NGOZI, V. E. & CHUKWUEMEKA, I. S. (2019). Macrodebris and microplastics pollution in Nigeria: first report on abundance distribution and composition. *Preprints*. pp. 1-19. Available at: https://www.preprints.org/manuscript/201908.0255/v1. [Accessed: 06/09/2019].

EFFENDI, A., RAMADHAN, N. H. & HIDAYAT, A. (2023). Image-based quality identification of black soybean (Glycine soja) using convolution neural network. *Industria: Jurnal Teknologi dan Manajemen Agroindustri*. 12 (1). pp. 73-88. (Online). Available from: https://www.cabidigitallibrary.org/doi/full/10.5555/20230400119. [Accessed: 16/05/2024].

EGMONT-PETERSON, M., RIDDER, D. & HANDELS, H. (2002). Image processing with neural networks – a review. *Pattern Recognition*. 35 (10). pp. 2279-2301. (Online). Available from: https://doi.org/10.1016/S0031-3203(01)00178-9. [Accessed: 11/11/2020].

ERIKSEN, M., MASON, S., WILSON, S., BOX, C., ZELLERS, A., EDWARDS, W., FARLEY, H. & AMATO, S. (2013). Microplastic pollution in the surface waters of the Laurentian Great lakes. *Marine Pollution Bulletin*.

77 (1-2). pp. 177-182. (Online). Available from: http://dx.doi.org/10.1016/j.marpolbul.2013.10.007. [Accessed: 29/01/2018].

ERNI-CASSOLA, G., GIBSON, M. I., THOMPSON, R. C. & CHRISTIE-OLEZA, J. A. (2017). Lost, but found with Nile Red: A Novel method for detecting and quantifying small microplastics (1mm to 20 μm) in environmental samples. *Environmental Science and Technology*. 51 (23). pp. 13641-13648. (Online). Available from: https://doi.org/10.1021/acs.est.7b04512. [Accessed: 17/02/2023].

EVANGELIOU, N., GRYTHE, H., KLIMONT, Z., HEYES, C., ECKHARDT, S., LOPEZ-APARICIO, S. & STOHL, A. (2020). Atmospheric transport is a major pathway of microplastics to remote regions. *Nature Communications*. 11 (1). pp. 1-11. (Online). Available from: https://doi.org/10.1038/s41467-020-17201-9 | www.nature.com/naturecommunications. [Accessed: 29/20/2020].

FANG, Y., GUO, X., CHEN, K., ZHOU, Z. & YE, Q. (2021). Accurate and automated detection of surface knots on sawn timbers suing YOLO-V5 model. *BioResources*. 16 (3). pp. 5390-5406. (Online). Available from: https://bioresources.cnr.ncsu.edu/resources/accurate-and-automated-detection-of-surface-knots-on-sawn-timbers-using-yolo-v5-model/. [Accessed: 26/02/2024].

FARAH, S., KUNDURU, K. R., TSACH, T., BENTOLILA, A. & DOMB, A. J. (2015). Forensic Comparison of Synthetic fibres. *Polymers for Advanced Technologies*. 26 (7). pp. 785-796. (Online). Available from: https://doi.org/10.1002/pat.3540. [Accessed: 17/06/2021].

FARRELL, P. & NELSON, K. (2013). Tropic level transfer of microplastic: Mytilus edulis (L). to Carcinus maenas (L). *Environmental pollution*. 117. pp. 1-3. (Online). Available from: http://dx.doi.org/10.1016/j.envpol.2013.01.046. [Accessed: 08/02/2018].

FAURE, F., DEMARS, C., WIESER, O., KUNZ, M. & ALENCASTRO, L. F. (2015). Plastic pollution in Swiss surface waters: nature and concentrations, interactions with pollutants. *Environmental Chemistry*. 12 (5). pp. 582-591.

(Online). Available from: http://dx.doi.org/10.1071/EN14218. [Accessed: 18/04/2018].

FAWCETT, T. (2006). An introduction to ROC analysis. *Pattern recognition letters.* 27 (8). pp. 861-874. (Online). Available from: https://doi.org/10.1016/j.patrec.2005.10.010. [Accessed: 08/20/2023].

FENDALL, L. & SEWELL, M. (2009). Contributing to marine pollution by washing your face: Microplastics in facial cleansers. *Marine Pollution Bulletin*. 58 (8). pp. 1225-1228. (Online). Available from: http://dx.doi.org/10.1016/j.marpolbul.2009.04.025. [Accessed: 25/01/2018].

FIELD, A., MILES, J. & FIELD, Z. (2012). *Discovering Statistics Using R*. London: SAGE.

FOURNIER, E., LEVEQUE, M., RUIZ, P., RATEL, J., DURIF, C., CHALANCON, S., AMIARD, F., EDELY, M., BEZIRARD, V., GAULTIER, E., LAMAS, B., HOUDEAU, E., LAGARDE, F., ENGEL, E., ETIENNE-MESMIN, L., BLANQUET-DIOT, S. & MERCIER-BONIN, M. (2023). Microplastics: What happens in the human digestive tract? First evidence in adults using in vitro gut models. *Journal of Hazardous Materials.* 442. (Online). Available from: https://doi.org/10.1016/j.jhazmat.2022.130010. [Accessed: 28/06/2023].

FOX, J. & WEISBERG, S. (2011). An {R} Companion to Applied Regression. Second edition. Thousand Oaks: Sage. Available from: http://socserv.socsci.mcmaster.ca/jfox/Books/Companion. (Accessed 14 May 2018).

FOX, J. & WEISBERG, S. (2019). An R Companion to Applied Regression. Third edition. Thousand Oaks: Sage. Available from: http://tinyurl.com/carbook. (Accessed 12th July 2019).

FREE, C. M., JENSEN. O. P., MASON, S. A., ERIKSEN, M., WILLIAMSON, N. J. & BOLDGIV. B. (2014). High-levels of microplastic pollution in a large, remote, mountain lake. *Marine Pollution Bulletin*. 85 (1). pp. 156-163. (Online). Available from: http://dx.doi.org/10.1016/j.marpolbul.2014.06.001. [Accessed: 25/01/2018].

FRÈRE, L., PAUL-PONT, I., MOREAU, J., SOUDANT, P., LAMBERT, C., HUVET, A. & RINNERT, E. (2016). A semi-automated Raman micro-spectroscopy method for morphological and chemical characterisations of microplastic litter. *Marine Pollution Bulletin*. 113 (1-2). pp. 461-468. (Online). Available from: http://dx.doi.org/10.1016/j.marpolbul.2016.10.051. [Accessed: 08/01/2019].

FU, W., MIN, J., JIANG, W., LI, Y. & ZHANG, W. (2020). Separation, characterisation and identification of microplastics and nanoplastics in the environment. *Science of the Total Environment*. 721. pp. 137561. (Online). Available from: https://doi.org/10.1016/j.scitotenv.2020.137561. [Accessed: 02/10/2020].

GALLOWAY, T., COLE, M. & LEWIS, C. (2017). Interactions of microplastic debris throughout the marine ecosystem. *Nature Ecology and Evolution*. 1 (5). pp. 1-8. (Online). Available from: https://www.nature.com/articles/s41559-017-0116. [Accessed: 26/03/2018].

GALVÃO, L. S., FERREIRA, R. R., FERNANDES, E. M. S., CORRERIA, C. A., VALERA, T. S., DOS SANTOS ROSA, D. & WIEBECK, H. (2023). Analysis of selective fluorescence for the characterisation of microplastic fibres: Use of a Nile red-based analytical method to compare between natural and synthetic fibres. *Journal of hazardous materials*. 443. pp. 130217. (Online). Available from: https://doi.org/10.1016/j.jhazmat.2022.130217. [Accessed: 17/02/2023].

GAO, L., XIONG, X., CHEN, C., LUO, P., LI, J., GAO, X. & HUANG, L. (2023). The male reproductive toxicity after nanoplastics and microplastics exposure: Sperm quality and changes of different cells in testis. *Ecotoxicological and Environmental Safety*. 267. pp. 115618. (Online). Available from: https://doi.org/10.1016/j.ecoenv.2023.115618. [Accessed: 07/06/2024].

GAUEN, K., DAILEY, R., LAIMAN, J., Z1, Y., ASOKAN, N., LU, Y. H., THIRUVATHUKAL, G. K., SHYU, M. L. & CHEN, S. C. (2017). Comparison of Visual Datasets for Machine Learning. *2017 IEEE International Conference on Information Reuse and Integration (IRI)*. pp. 346-355.

(Online). Available from: https://ieeexplore.ieee.org/abstract/document/8102956/citations#citations. [Accessed: 19/07/2022].

GÉRON, A. (2019). *Hands-on Machine learning with Scikit-Learn, Keras and TensorFlow concepts, tools and techniques to build intelligent systems.* Second edition. Sebastopo: O'Reilly Media Inc.

GHOSAL, S. & SARKAR, K. (2020). Rice leaf diseases classification using CNN with transfer learning. *IEEE Calcutta Conference (CALCON).* Kolkata: India. (Online). Available from: https://ieeexplore.ieee.org/abstract/document/9106423. [Accessed: 16/05/2024].

GIARDINO, M., BALESTRA, V., JANNER, D. & BELLOPEDE. (2023). Automated method for routine microplastic detection and quantification. *Science of the Total Environment*. 859. pp. 160036. (Online). Available from: http://dx.doi.org/10.1016/j.scitotenv.2022.160036. [Accessed: 18/06/2024].

GIECHASKIEL, B., GRIGORATOS, T., MATHISSEN, M., QUIK, J., TROMP, P., GUSTAFSSON, M., FRANCO, V. & DILARA, P. (2024). Contribution of road vehicle tyre wear to microplastic and ambient air pollution. *Sustainability*. 16 (522). (Online). Available from: https://doi.org/10.3390/su16020522. [Accessed: 03/03/2024].

GONÇALVES, A. B., SOUZA, J. S., GONÇALVES DA SILVA, G., CEREDA, M. P., POTT, A., NAKA, M. H. & PISTORI, H. (2016). Feature extraction and machine learning for the classification of Brazilian savannah pollen grains. *PLoS ONE*. 11 (6). pp. 1-20. (Online). Available from: https://doi.org/10.1371/journal.pone.0157044. [Accessed: 06/01/2023].

GORDON, S. (2009). Identifying plant fibres in textiles: the case of cotton. In: HOUCK, M. (Ed). *Identification of textile fibres*. Cambridge: Woodhead Publishing Limited.

GORSKI, A. MCCRONE, W. C. (1998). Birefringence of fibres. *Microscope*. 46 (1). pp. 3-16.

GRIEVE, M. (1983). The use of melting point and refractive index determination to compare colourless polyester fibres. *Forensic Science International*. 22. pp. 31-48.

GRIEVE, M., BIERMANN, T. & SCHAUB, K. (2005). The individuality of fibres used to provide forensic evidence – not all blue polyesters are the same. *Science and justice*. 45 (1). pp. 13-28. (Online). Available from: https://doi.org/10.1016/S1355-0306(05)71616-6. [Accessed: 28/11/2018].

GRIEVE, M., ROUX, C., WIGGINS, K. G., CHAMPOD, C. & TARONI, F. (2018). Interpretation of fibre evidence. Ins: Robertson, J., Roux, C. & Wiggins, K. G. (eds). *Forensic examination of fibres*. Third edition. Boca Raton: CRC Press.

GWINNETT, C. & JACKSON, A. R. W. (2013). A Novel Tape Lifting System for the Retrieval of Trace Evidence from Crime Scenes. [Online]. *International Labmate*. (October/November). pp. 58-59. Available from: https://www.envirotech-online.com/article/microscopy-and-microtechniques/4/staffordshire-university/a-novel-tape-lifting-system-for-the-retrieval-of-trace-evidence-from-crime-scenes/1516. [Accessed: 11/04/18].

GWINNETT, M. B., OSBORNE, A. O. & JACKSON, A. R. W. (2021). The application of tape lifting for microplastic pollution monitoring. *Environmental Advances*. 5. pp. 100066. (Online). Available from: https://doi.org/10.1016/j.envadv.2021.100066. [Accessed: 26/06/21].

HABIB, R. Z., THIEMANN, T. & AL KENDI, R. (2020). Microplastics in wastewater treatment plants- A review. *Journal of Water Resource and Protection*. 12. pp. 1-35. (Online). Available from: https://doi.org/10.4236/jwarp.2020.121001. [Accessed: 17/01/2020].

HARRISON, J. P., HOELLEIN, T J., SAPP, M., TAGG, A. S., JU-NAM, Y. & OJEDA, J. J. (2018). Microplastic-Associated Biofilm: A Comparison of Freshwater and Marine Environments. In: Wagner, M. & Lambert, S. (Eds). *Freshwater Microplastics: Emerging Environmental Contaminants?* The Handbook of Environmental Chemistry volume 58. Cham: Springer

International Publishing. (Online). Available from: http://link.springer.com/10.1007/978-3-319-61615-5. [Accessed: 26/01/2018].

HARTMANN, N. B., HÜFFER, T., THOMPSON, R. C., HASSELLÖV, M., VERSCHOOR, A., DAUGAARD, A. E., RIST, S., KARLSSON, T., BRENNHOLT, N., COLE, M., HERRLING, M. P., HESS, M. C., IVLEVE, N. P., LUSHER, A. L. & WAGNER, M. (2019). Are we speaking the same language? Recommendations for a definition and categorization framework for plastic debris. *Environmental Science and Technology*. 53 (3). pp. 1039-1047. (Online). Available from: https://doi.org/10.1021/acs.est.8b05297. [Accessed: 02/05/2019].

HAQUE, A., HOLSEN, T. M. & BAKI, A. B. M. (2024). Distribution and risk assessment of microplastic pollution in a rural river system near a wastewater treatment plant, hydro-dam, and river confluence. *Scientific Reports*. 14. (Online). Available from: https://doi.org/10.1038/s41598-024-56730-x. [Accessed: 08/05/2024].

HENDERSON, P., ISLAM, R., BACHMAN, P., PINEAU, J., PRECUP, D. & MEGER, D. (2017). Deep reinforcement learning that matters. *The AAAI conference on artificial intelligence*. New Orleans. 2-7th February. Association for the Advancement of Artificial Intelligence.

HIDALGO-RUZ.V., GUTOW, L., THOMPSON, R. C. & THIEL, M. (2012). Microplastics in the marine environment: A review of the methods used for identification and quantification. *Environmental Science & Technology*. 46. pp. 3060-3075. (Online). Available from: http://www.ncbi.nlm.nih.gov/pubmed/22321064%5Cnhttp://pubs.acs.org/doi/abs/10.1021/es2031505%5Cnhttp://www.ncbi.nlm.nih.gov/pubmed/22321064. [Accessed: 01/12/2017].

HIMAMI, Z. R., BUSTAMAM, A. & ANKI, P. (2021). Deep learning in image classification using dense networks and residual networks for pathologic myopia selection. *International Conference on Artificial Intelligence and Big Data Analytics*. Bandung: Indonesia. pp. 1-6. (Online). Available from: https://ieeexplore.ieee.org/abstract/document/9689744?casa_token=R1tgBdj

7WsgAAAAA:cUEYiEhaCzR07U9OV7fKcCFH2Ok1emCdIufR0AwCdaHoZOI7H2sMLym9cGRCNy2VxCsSy9vm. [Accessed: 16/05/2024].

HOLME, I (1999). Adhesion to textile fibres and fabrics. *International journal of Adhesion and Adhesives*. 19 (6). pp. 455-463. (Online). Available from: https://doi.org/10.1016/S0143-7496(99)00025-1. [Accessed: 13/09/2023].

HORTON, A. A., SVENDSEN, C., WILLIAMS, R. J., SPURGEON, D. J. & LAHIVE, E. (2017). Large microplastic particles in sediments of tributaries of the River Thames, UK – Abundance, sources and methods for effective quantification. *Marine Pollution Bulletin*. 114 (1). pp. 218-226. (Online). Available from: http://dx.doi.org/10.1016/j.marpolbul.2016.09.004. [Accessed: 30/01/2018].

HORTON, A. A., VIJVER, M. G., LAHIVE, E., SPURGEON, D. J., SVENDSEN, C., HEUTINK, R., BODEGOM, P. M. & BAAS, J. (2018). Acute toxicity of organic pesticides to Daphnia magna is unchanged by co-exposure to polystyrene microplastics. *Ecotoxicity and Environmental Safety*. 166 (June). pp. 26-34. (Online). Available from: https://doi.org/10.1016/j.ecoenv.2018.09.052. [Accessed: 13/12/2018].

HUANG, J., HE, H., LV, R., ZHANG, G., ZHOU, Z. & WANG, X. (2022). Non-destructive detection and classification of textile fibres based on hyperspectral imaging and 1D-CNN. *Analytica Chimica Acta*. 1224. pp. 340238. (Online). Available from: https://doi.org/10.1016/j.aca.2022.340238. [Accessed: 14/02/2023].

HUFENUS, R., YAN, Y., DAUNER, M. & KIKUTANI, T. (2020). Melt-spun fibers for textile applications. *Materials*. 13 (19). pp. 1-32. (Online). Available from: https://doi.org/10.3390/ma13194298. [Accessed: 13/09/2022].

IEAMSAARD, J., CHAROENSOOK, S. N. & YAMMEN, S. (2021). Deep learning-based Face mask detection using YOLOv5. *9th International Electrical Engineering Congress (iEECON).* Pattaya: Thailand. pp. 428-431. (Online). Available from: https://ieeexplore.ieee.org/abstract/document/9440346?casa_token=szSsPceV7jkAAAAA:D_8FU1OR3Hq9OsLjSCy01V-

AVq0RmOmw1pTRt6AFnM0DJQ-fo4yWr_1htrZUWwOtOXdFAME0. [Accessed: 16/05/2024].

IKADA, E. (1999). Electron Microscope Observation of Biodegradation of Polymers. *Journal of Environmental Polymer Degradation*. 7 (4). pp. 197-201. (Online). Available from: https://link.springer.com/article/10.1023/A:1022882732403. [Accessed: 01/12/2017].

ISO 472. (2013). *International Organization for Standardization. Plastics – Vocabulary*. [Online]. Available from: https://www.iso.org/obp/ui/#iso:std:iso:472:ed-4:v1:en. [Accessed: 03/05/2019].

JACKSON, A. R. W. & GWINNETT, C. (2013). Easylift: A Novel Tape System. *Forensic Science Society*. 73. pp. 22-23.

JACKSON, A. R. W. & GWINNETT, C. M. B. (2006). *Improved apparatus and methods for the optical examination of birefringent specimens*. UK Intellectual Property Office Patent no. GB 2467810 B. Available at: https://patents.google.com/patent/US8961727B2/en [Accessed: 06/12/19].

JACKSON, A. R. W., OSBORNE, A. O., GWINNETT, C. M. B. (2021), *Microplastic pollution isolation - a forensic science approach*, Mendeley Data, v1, http://dx.doi.org/10.17632/jzppg7h8j4.1.

JAHANDARI, A. (2023). Microplastics in the urban atmosphere: Sources, occurrences, distribution and potential health implications. *Journal of Hazardous Materials Advances*. 12. pp. 100346. (Online). Available from: https://doi.org/10.1016/j.hazadv.2023.100346. [Accessed: 05/06/2024].

JAIPURIA, N., ZHANG, X., BHASIN, R. ARAFA, M., CHAKRAVARTY, P., SHRIVASTAVA, S., MANGLANI, S. & MURALI, V. N. (2020). Deflating dataset bias using synthetic data augmentation. *IEEE Computer Society Conference on Computer Vision and Pattern Recognition Workshops*. (Online). Available from: https://openaccess.thecvf.com/content_CVPRW_2020/html/w45/Jaipuria_De

flating_Dataset_Bias_Using_Synthetic_Data_Augmentation_CVPRW_2020_paper.html. [Accessed: 17/02/2024].

JEON, M. S., KIM, J. W., HAN, Y. B., JEONG, M. H., KIM, H. R., KIM, H. S., PARK, Y. J. & CHUNG, K. H. (2023). Polystyrene microplastic particles induce autophagic cell death in BEAS-2B human bronchial epithelial cells. *Environmental Toxicology*. 38 (2). pp.359-367. (Online). Available from: https://doi.org/10.1002/tox.23705. [Accessed: 16/07/2023].

JIA, W., KARAPETROVA, A., ZHANG, M., XU, L., LI, K., HUANG, M., WAMG, J. & HUANG, Y. (2022). Automated identification and quantification of invisible microplastics in agricultural soils. *Science of the Total environment*. 844. pp. 156853. (Online). Available from: http://dx.doi.org/10.1016/j.scitotenv.2022.156853. [Available from: 18/06/2024].

JOCHER, G., CHAURASIA, A., STOKEN, A., BOROVEC, J., NANOCODE012., KWON, Y., MICHAEL, K., TAOXIE., FANG, J., IMYHXY., LORNA., ZENG, Y., WONG, C., V, A., MONTES, D., WANG, Z., FATI, C., NADAR, J., LAUGHING., UNGLVKITDE., SONCK, V., TKIANAI., YXNONG., SKALSKI, P., HOGAN, A., NAIR, D., STROBEL, M. & JAIN, M. (2022). ultralytics/yolov5: v7.0 - YOLOv5 SOTA Realtime Instance Segmentation. [Software]. DOI: DOI: 10.5281/zenodo.7347926. Available from: https://ultralytics.com/yolov5. [Accessed: 12/09/2023].

JOHRI, M. C. (1979). Identification of some synthetic fibres by their birefringence. *Journal of Forensic Science*. 24 (3). pp. 692-697.

JONES, J. & COYLE, T. (2011). Synthetic flock fibres: A population and target fibre study. *Science and Justice*. 51 (2). pp. 68-71. (Online). Available from: https://doi.org/10.1016/j.scijus.2010.10.004. [Accessed: 05/12/2019].

JORDAN, M. I. & MITCHELL, T. M. (2015). Machine learning: Trends, perspective, and prospects. *Science*. 349 (6245). pp. 255-260. [Online). Available from: https://doi.org/10.1126/science.aaa8415. [Accessed: 09/06/2024].

JOUCHER, G., CHAURASIA, A. & QIU, J. (2023). Ultralytics YOLOv8 Version 8.0.0. [Software]. Available from: https://github.com/ultralytics/ultralytics. [Accessed: 30/09/2023].

JUNG, H. K. & CHOI, G. S. (2022). Improved YOLOv5: Efficient object detection using drone images under various conditions. *Applied Sciences*. 12 (14). (Online). Available from: https://doi.org/10.3390/app12147255. [Accessed: 14/3/2024].

KALČÍKOVÁ, G. (2023). Beyond ingestion: Adhesion of microplastics to aquatic organisms. *Aquatic Toxicology*. 258. pp.106480. (Online). Available from: https://doi.org/10.1016/j.aquatox.2023.106480. [Accessed: 07/06/2024].

KANG, H., PARK, S., LEE, B., AHN, J. & KIM, S. (2020). Modification of a Nile Red staining Method for microplastic analysis: A Nile Red plate method. *Water*. 12 (11). pp. 3251. (Online). Available from: https://doi.org/10.3390/w12113251. [Accessed: 28/02/2023].

KANG, J. H., KWON, O. Y., LEE, K. W., SONG, Y. K. & SHIM, W. J. (2015). Marine neustonic microplastics around the south-eastern coast of Korea. *Marine Pollution Bulletin*. 96 (1-2). pp. 304-312. (Online). Available from: http://dx.doi.org/10.1016/j.marpolbul.2015.04.054. [Accessed: 25/01/2018].

KANHAI, L. D. K., GÅRDFELT, K., LYASHEVSKA, O., HASSELLÖV, M., THOMPSON, R. C. & O'CONNOR, I. (2018). Microplastics in sib-surface waters of the artic central basin. *Marine Pollution Bulletin*. pp. 8-18. (Online). Available from: https://doi.org/10.1016/j.marpolbul.2018.03.011. [Accessed: 04/11/2019].

KAPP, K. J. & YEATMAN, E. (2018). Microplastics hotspots in the snake and lower Columbia rivers: A journey from the greater Yellowstone ecosystem to the Pacific Ocean. Environmental Pollution. 241. pp. 1082-1090. (Online). Available from: https://doi.org/10.1016/j.envpol.2018.06.033. [Accessed: 31/03/2022].

KARAMI, A., GOLIESKARDI, A., HO, Y. B., LARAT, V. SALAMATINIA, B. (2017). Microplastics in eviscerated flesh and excised organs of dried fish.

Scientific Reports. 7 (1). pp. 1-9. (Online). Available from: http://dx.doi.org/10.1038/s41598-017-05828-6. [Accessed: 26/03/2018].

KASETTY, S., RAMMANOHAR, M. & RAGAVENDRA, R. T. (2010). Dental cementum in age estimation: A polarised light and stereomicroscopic study. *Journal of Forensic Science*. 55 (3). pp. 779-783. (Online). Available from: https://doi.org/10.1111/j.1556-4029.2010.01363.x. [Accessed: 06/07/2022].

KERKHOFF, K., CESCUTTI, G., KRUSE, L. & MÜSSIG, J. (2009). Development of DNA-analytical method for the identification of animal hair fibres in textiles. *Textile Research Journal*. 79 (1). pp. 69-75.

KESWANI, A., OLIVER, D. M., GUTIERREZM, T. & QUILLIAM, R. S. (2016). Microbial hitchhikers on marine plastic debris: human exposure risks at bathing waters and beach environments. *Marine Environmental Research*. 118. pp. 10-19. (Online). Available from: http://dx.doi.org/10.1016/j.marenvres.2016.04.006. [Accessed: 18/09/2018].

KHAN, N. M. & AHMED, M. M. (2019). Snow detection using in vehicle video camera with texture-based image features utilising K-nearest neighbor, support vector machine and random forest. *Transportation Research Record*. 1 (12). pp. 221-232. (Online). Available from: https://doi.org/10.1177/0361198119842105. [Accessed: 19/02/2021].

KIRKBRIDE, K. P. & TUNGOL, M. W. (1999). Infrared Microspectroscopy of fibres. in: Robertson, J. and Grieve, M. (eds). *Forensic Examination of Fibres*. Second edition. London: Taylor and Francis.

KLIEN, M. & FISCHER, E. K. (2019). Microplastic abundance in atmospheric deposition within the Metropolitan area of Hamburg, Germany. *Science of the Total Environment*. 685. pp. 96-103. (Online). Available from: https://doi.org/10.1016/j.scitotenv.2019.05.405. [Accessed: 10/03/2020].

KOIRALA, A., JHA, M., BODAPATI, S., MISHRA, A., CHETTY, G., SAHU, P. K., MOHANTY, S., PADHAN, T. K., MATTOO, J. & HUKKOO, A. (2022). Deep learning for Real time malaria parasite detection and counting using YOLO-mp. *1EEE Access* 10. pp. 102157-102172. (Online). Available from: https://ieeexplore.ieee.org/document/9896857. [Accessed: 16/01/2023].

KOLE, P. J., LÖHR, A. J., VAN BELLEGHEM, F. G. A. J. & RAGAS, A. M. J. (2017). Wear and tear of tyres: A stealthy source of microplastics in the environment. *International Journal of Environmental Research and Public Health*. 14 (10).

KORALTAN, I., MAVRUK, S & GÜVEN, O. (2022). Effect of biological and environmental factors on microplastic ingestion of commercial fish species. *Chemosphere*. 303. pp. 135101. (Online). Available from: https://doi.org/10.1016/j.chemosphere.2022.135101. [Accessed: 13/08/2023].

KOUROU, K., EXARCHOS, T. P., EXARCHOS, K. P., KARAMOUZIS, M. V. & FOTIADIS, D. I. (2015). Machine learning application in cancer prognosis and prediction. *Computational and Structural Biotechnology Journal*. 13. pp. 8-17. (Online). Available from: http://dx.doi.org/10.1016/j.csbj.2014.11.005. [Accessed: 17/01/2023].

KROES, A. D. A. & FINLEY, J. R. (2023). Demystifying omega squared: Practical guidance for effect size in common analysis variance designs. *Psychological Methods*. (Online). Available from: https://doi.org/10.1037/met0000581. [Accessed: 16/06/2024].

KUBAT, M., HOLTE, R. C. & MATWIN, S. (1998). Machine learning for the detection of oil spills in satellite radar images. *Machine Learning*. 30 (2-3). pp. 195-215. (Online). Available from: https://link.springer.com/article/10.1023/A:1007452223027. [Accessed: 22/08/2018].

LAHENS, L., STRADY, E., KIEU-LE, T. C., DRIS, R., BOUKERMA, K., RINNERT, E., GASPERI, J. & TASSIN, B. (2018). Macroplastic and microplastic contamination assessment of a tropical river (Saigon River, Vietnam) traversed by a developing megacity. *Environmental Pollution*. 236. pp. 661-671. (Online). Available from: https://doi.org/10.1016/j.envpol.2018.02.005. [Accessed: 18/09/2018].

LAJU, R. L., JAYANTHI, M. JEYASANTA, K. I., PATTERSON, J., ASIR, N. G. G., SATHISH, N. N. & EDWARD, J. K. (2022). Spatial and vertical

distribution of microplastics and their ecological risk in an Indian freshwater lake ecosystem. *Science of the Total Environment*. pp. 153337. (Online). Available from: http://dx.doi.org/10.1016/j.scitotenv.2022.153337. [Accessed: 10/05/2022].

LANGDON, S., MAYNARD, P., ROBERTSON, J. & ROUX, C. (2003). An evaluation on the Maxcan fibre finder version 3.3 on cotton fibres. *Forensic Science International*. 135 (2). pp. 137-145. (Online). Available from: https://doi.org/10.1016/S0379-0738(03)00180-4. [Accessed: 08/01/2019].

LEADS, R. R. & WEINSTEIN, J. E. (2019). Occurrence of tire wear particles and other microplastics within the tributaries of the Charleston Harbour Estuary, South Carolina, USA. *Marine Pollution Bulletin*. 145. pp. 569-582. (Online). Available from: https://doi.org/10.1016/j.marpolbul.2019.06.061. [Accessed: 29/09/2020].

LECHNER, A., KECKEIS, H., LUMBERGER-LOISL, F., ZENS, B., KRUSH, R., TRITTHART, M., GLAS, M. & SCHLUDERMANN, E. (2014). The Danube so colourful: a potpourri of plastic litter outnumbers fish larvae in Europe's second largest river. *Environmental pollution*. pp. 177-181. (Online). Available from: http://dx.doi.org/10.1016/j.envpol.2014.02.006. [Accessed: 18/09/2018].

LECUN, Y., BENGIO, Y. & HINTON, G. (2015). Deep learning. *Nature*. 521. pp. 436-444. (Online). Available from: https://www.nature.com/articles/nature14539. [Accessed: 01/09/2022].

LEE, C. S., ROBINSON, J. & CHONG, M. F. (2014). A review on application of flocculants in wastewater treatment. *Process Safety and Environmental Protection*. 92 (6). pp. 489-508. (Online). Available from: http://dx.doi.org/10.1016/j.psep.2014.04.010. [Accessed: 23/04/2024].

LEE, S. & LEE, D. (2018). Improved prediction of harmful agal blooms in four major South Korea's Rivers using deep learning models. *International Journal of Environmental Research and Public Health.* 15 (7). (Online). Available from: https://doi.org/10.3390/ijerph15071322. [Accessed: 17/05/2024].

LEI, L., WU, S., LU, S., LIU, M., SONG, Y., FU, Z., SHI, H., RALEY-SUSMAN, K. M. & HE, D. (2018). Microplastics particles cause intestinal damage and other adverse effects in zebrafish Danio rerio and nematode Caenorhabditis elegans. *Science of the Total Environment*. 619-620. pp. 1-8. (Online). Available from: https://doi.org/10.1016/j.scitotenv.2017.11.103. [Accessed: 03/01/2019].

LENZ, R., ENDERS, K., STEDSON, C. A., MACKENZIE, D. M. A. & NIELSEN, T. G. (2015). A critical assessment of visual identification of marine microplastic using Raman spectroscopy for analysis improvement. *Marine Pollution Bulletin*. 100 (1). pp. 82-91. (Online). Available from: http://dx.doi.org/10.1016/j.marpolbul.2015.09.026. [Accessed: 08/20/2018].

LEPOT, L., DE WAEL, K., GASON, F. & GILBERT, B. (2008). Application of Raman spectroscopy to forensic fibre cases. *Science & Justice*. 48 (3). pp. 109-117. (Online). Available from: https://doi.org/10.1016/j.scijus.2007.09.013. [Accessed: 03/01/2019].

LESLIE, H. A., BRANDSMA, S. H., VAN VELZEN, M. J. M. & VETHAAK, A. D. (2017), Microplastics en route: Field measurements in the Dutch river delta and Amsterdam canals, wastewater treatment plants, North Sea sediments and biota. *Environmental International*. 101. pp. 133-142. (Online). Available from: http://dx.doi.org/10.1016/j.envint.2017.01.018. [Accessed: 30/01/2018].

LI, J., JONG, M. C., HU, H., GIN, K. Y. H. & HE, Y. (2024a). Size-dependant effects of microplastics on intestinal microbiome for *Perna viridis*. *Journal of Hazardous Materials*. 474. pp. 134658. (Online). Available from: https://doi.org/10.1016/j.jhazmat.2024.134658. [Accessed: 09/06/2024].

LI, Y., XIE, S., CHEN, X., DOLLÁR, P., HE, K. & GIRSHICK, R. (2021) Benchmarking detection transfer learning with vision transformers. *Computer vision and pattern recognition*. (Online). Available from: https://doi.org/10.48550/arXiv.2111.11429. [Accessed: 16/05/2024].

LI, Z., ZHENG, Y., MAIMAITI, Z., FU, J., YANG, F., LI, Z. Y., SHI, Y., HAO, L. B., CHEN, J. Y. & XU, C. (2024b). Identification and analysis of microplastics in human lower limb joints. *Journal of Hazardous Materials*.

461. pp. 132640. (Online). Available from: https://doi.org/10.1016/j.jhazmat.2023.132640. [Accessed: 09/06/2024].

LIANG, B., DENG, Y., ZHONG, Y., CHEN, X., HUANGM Y. LI, Z., HUANG, X. YABG, X., DU, J., YE, R., XIAN, H., FENG, Y., BAI, R., FAN, B., YANG, X. & HUANG, Z. (2024). Gastrointestinal incomplete degradation exacerbates neurotoxic effects of PLA microplastics via oligomer nanoplastics formation. *Advanced Science*. pp. 2401009. (Online). Available from: https://doi.org/10.1002/advs.202401009. [Accessed: 09/06/2024].

LIBBRECHT, M. W. & NOBLE, W. S. (2015). Machine learning application on genetics and genomics. *Nature Reviews Genetics*. 16 (6). pp. 321-332. (Online). Available from: https://www.nature.com/articles/nrg3920. [Accessed: 17/01/2023].

LIU, K., WU, T., WANG, X., SONG, Z., ZONG, C., WEI, N. & LI, D. (2019). Consistent transport of terrestrial microplastics to the ocean through atmosphere. *Environmental Science Technology*. 53 (18). pp. 10612-10619. (Online). Available from: https://doi.org/10.1021/acs.est.9b03427. [Accessed: 12/03/2020].

LIU, L., XU, K., ZHANG, B., YE, Y., ZHANGE, Q. & JIANG, W. (2021c). Cellular internalisation and release of polystyrene microplastics and nanoplastics. *Science of the total environment*. 779. pp. 146523. (Online). Available from: https://doi.org/10.1016/j.scitotenv.2021.146523. [Accessed: 24/05/2024].

LIU, S., WANG, C., YANG, Y., DU, Z., LI, L., ZHANG, M., NI, S., YUE, Z., YANG, K., WANG, Y., LI, X., YANG, Y., QIN, Y., LI, J., YANG, Y. & ZHANG, M. (2024). Microplastics in three types of human arteries detected by pyrolysis-gas chromatography/mass spectrometry (Py-GC/MS). *Journal of Hazardous Materials*. 469. pp. 133855. (Online). Available from: https://doi.org/10.1016/j.jhazmat.2024.133855. [Accessed: 09/06/2024].

LIU, Y., GAO, F., LI, Z., DING, H., ZHANG, D., FENG, L. & LI, X. (2021a). An optimised procedure for extraction and identification of microplastics in marine sediment. *Marine Pollution Bulletin*. 165 (February). pp. 112130.

(Online). Available from: https://doi.org/10.1016/j.marpolbul.2021.112130. [Accessed: 28/02/2023].

LIU, Y., LIU, W., YANG, X., WANG, J., LIN, H. & YANG, Y. (2021b). microplastics are a hotspot for antibiotic resistance genes: Progress and perspective. *Science of the Total Environment*. 773 (1). pp. 145643. (Online). Available from: https://doi.org/10.1016/j.scitotenv.2021.145643. [Accessed: 13/08/2023].

LLOYD, S., MOHSENI, M. & REBENTROST, P. (2013). Quantum algorithms for supervised and unsupervised machine learning. *arxiv.org*. [Online]. (November). Available from: https://arxiv.org/abs/1307.0411. [Accessed: 11/02/2019].

LOBELLE, D. & CUNLIFFE, M. (2011). Early microbial biofilm formation on marine plastic debris. *Marine Pollution Bulletin*. 62 (1). pp. 197-200. (Online). Available from: https://doi.org/10.1016/j.marpolbul.2010.10.013. [Accessed: 31/01/2018].

LONG, Y., XIA, G. S., LI, S., YANG, W., YANG, M. Y., ZHU, X. X., ZHANG, L. & LI, D. (2021). On creating benchmark dataset for aerial image interpretation: Reviews, guidances, and million-AID. *IEEE Journal of Selected Topics in Applied Earth Observations and Remote Sensing*. 14. pp. 4205-4230. (Online). Available from: https://ieeexplore.ieee.org/document/9393553. [Accessed: 27/07/2022].

LONG, Z., PAN, Z., WANG, W., REN, J., YU, X., LIN, L., LIN, H., CHEN, H. & JIN, X. (2019). Microplastic abundance, characteristics, and removal in wastewater treatment plants in a coastal city in China. *Water Research*. 155. pp. 255-265. (Online). Available from: https://doi.org/10.1016/j.watres.2019.02.028. [Accessed: 21/01/2022].

LORENZO-NAVARRO, J., CASTRILLÓN- SANTANA, M., SÁNCHEZ-NIELSEN, E., ZARCO, B., HERRERA, A., MARTÍNEZ, I. & GÓMEZ, M. (2021). Deep learning approach for automatic microplastics counting and classification. *Science of the Total Environment*. 765. pp. 142728. (Online).

Available from: https://doi.org/10.1016/j.scitotenv.2020.142728. [Accessed: 30/01/2023].

LORENZO-NAVARRO, J., CASTRILLÓ-SANTANA, M., GÓMEZ, M., HERRERA, A. & MARÍN-REVES, P. A. (2018). Automatic counting and classification of microplastic particles. *Proceedings of 7th international conference on pattern recognition applications and methods*. Portugal, January 16th-18th 2018. Portugal: Science and Technology Publications, Lda. (Online). Available from: https://www.semanticscholar.org/paper/Automatic-Counting-and-Classification-of-Particles-Lorenzo-Navarro-Santana/8abc9e78590ee966781f983b2448723fe054d26f. [Accessed: 29/11/2018].

LORENZO-NAVARRO, J., CASTRILLÓ-SANTANA, M., SANESARTI, E., MARSICO, M., MARTÍNEZ, I., RAYMOND, E., GÓMEZ, M. & HERRERA, A. (2020). SMACC: A system for microplastics automatic counting and classification. *IEEE Access*. 8. pp. 25249-25261. (Online). Available from: https://ieeexplore.ieee.org/abstract/document/8976153. [Accessed: 18/06/2024].

LUO, Y., ZHANG, X., ZHANG, Z., NAIDU, R. & FANG, C. (2022). Dual-principal component analysis of the Raman spectrum matrix to automatically identify and visualise microplastics and nanoplastics. *Analytical Chemistry*. 94. pp. 3150-3157. (Online). Available from: https://doi.org/10.1021/acs.analchem.1c04498. [Accessed: 31/03/2023].

LUSHER, A. L., BURKE, A., O'CONNOR, I. & OFFICER, R. (2014). Microplastic pollution in the Northeast Atlantic Ocean: Validated and opportunistic sampling. *Marine pollution bulletin*. 88 (1-2). pp. 325-333. (Online). Available from: http://dx.doi.org/10.1016/j.marpolbul.2014.08.023. [Accessed: 04/11/2019].

LUSHER, A. L., HERNANDEZ-MILAN, G., O'BRIEN, J., BERROW, S., O'CONNOR, I. & OFFICER, R. (2015). Microplastic and macroplastic ingestion by deep diving, oceanic cetacean: The True's beaked whale Mesoplodon mirus. 199. pp. 185-191. (Online). Available from: http://dx.doi.org/10.1016/j.envpol.2015.01.023. [Accessed: 04/11/2019].

LUSHER, A. L., WELDEN, N. A., SOBRAL, P. & COLE, M. (2017). Sampling, isolating and identifying microplastics ingested by fish and invertebrates. *Analytical methods*. 9 (9). pp. 1346-1360. (Online). Available from: https://doi.org/10.1039/C6AY02415G. [Accessed: 20/04/2021].

LV, L., QU, J., YU., CHEN, Z., ZHOU, C., HONG, P., SUN, S. LI, C. (2019b). A simple method for detecting and quantifying microplastics utilising fluorescent dyes – Safranine T, fluorescein isophosphate, Nile red based on thermal expansion and contraction property. *Environmental Pollution*. 255. pp. 113283. Available from: https://www.sciencedirect.com/science/article/pii/S0269749119329562. [Accessed: 04/09/2020].

LV, X., DONG, Q., ZUO, Z., LIU, Y., HUANG, X. & WU, W. M. (2019a). Microplastics in a municipal wastewater treatment plant: Fate, dynamic distribution, removal efficiencies, and control strategies. *Journal of Cleaner Production*. 255. pp. 579-586. (Online). Available from: https://doi.org/10.1016/j.jclepro.2019.03.321. [Accessed: 11/08/2021].

MAES, T., JESSOP, R., WELLNER, N., HAUPT, K. & MAYES, A. G. (2017). A rapid-screening approach to detect and quantify microplastics based on fluorescent tagging with Nile red. *Scientific Reports*. 7 (February). pp. 44501. (Online). Available from: http://dx.doi.org/10.1038/srep44501. [Accessed: 16/02/2023].

MAGNI, S., BINELLI, A., PITTURA, L., GIACOMO AVIO, C., DELLA TORRE, C., PARENTI, C. C., GORBI, S. & REGOLI, F. (2019). The fate of microplastics in an Italian Wastewater Treatment Plant. *Science of the Total Environment*. 652. pp. 602-610. (Online). Available from: https://doi.org/10.1016/j.scitotenv.2018.10.269. [Accessed: 11/08/2021].

MAGNUSSON, K. & NORÉN, F. (2014). Screening of Microplastic Particles in and Downstream a Wastewater Treatment Plant. *IVL Swedish Environmental Research Institute*. Report Number C55.

MASSARELLI, C., CAMPANALE, C. & URICCHIO, V. F. (2021). Handy open-source application based on computer vision and machine learning

algorithms to count and classify microplastics. *Water*. 13 (15). (Online). Available from: https://doi.org/10.3390/w13152104. [Accessed: 08/06/2024].

MATTA, V. D., MUDUNURI, K. A. V. R. R., BABA, B. C. S. N. L. S. S., KIRAN, K. B., VEENADHARI, C. H. L. & PRASANTHI, B. V. (2024). Single use plastic bottle recognition and classification using YOLO V5 and V8 architectures. In: PAREEK, P., GUPTA, N., REIS, M.J.C.S. (eds). *Cognitive Computing and Cyber Physical Systems*. Volume 537. Cham: Springer. (Online). Available from: https://doi.org/10.1007/978-3-031-48891-7_8. [Accessed: 19/06/2024].

MCCRONE, W. C. (1994). Polarized light microscopy in conservation: A personal perspective. *Journal of the American Institute for Conservation*. 33 (2). pp. 101-114. (Online). Available from: http://dx.doi.org/10.1179/019713694806124757. [Accessed: 06/07/2022].

MCDERMID, K. & MCMULLEN, T. (2004). Quantitative analysis of small-plastic debris on beaches in the Hawaiian archipelago. *Marine Pollution Bulletin*. 48 (7-8). P. 790-794. (Online). Available from: https://doi.org/10.1016/j.marpolbul.2003.10.017. [Accessed: 05/03/2018].

MERCHANT, A., ZOPH, B. & CUBUK, E. (2020). Does data augmentation benefit from split batchnorms. *arXiv.* (Online) Available from: https://doi.org/10.48550/arXiv.2010.07810. [Accessed: 25/02/2024].

MIA, S. M., ISLAM, A. R. M. T., ALI, M. M., SIDDIQUE, M. A. B., PAL, S. C., IDRIS, A. M. & SENAPATHI, V. (2024). Microplastics in sediment and surface water from an island ecosystem in Bay of Bengal. *Regional studies in Marine science*. 69. pp. 103332. (Online). Available from: https://doi.org/10.1016/j.rsma.2023.103332. [Accessed: 13/06/2025].

MILLER, R. Z. & GWINNETT, C. (2021). Are we contaminating our samples? A preliminary study to investigate procedural contamination during field sampling and processing for microplastic and anthropogenic microparticles. *Marine Pollution Bulletin*. 173 (Part B). (Online). Available from: https://doi.org/10.1016/j.marpolbul.2021.113095. [Accessed: 05/04/2023].

MILLER, R. Z., WATTS, A. J. R., WINSLOW, B. O., GALLOWAY, T. S. & BARROWS, A. P. W. (2017). Mountains to the sea: River study of plastic and non-plastic microfiber pollution in the northeast USA. *Marine Pollution Bulletin*. 124 (1). pp.245-251. (Online). Available from: http://dx.doi.org/10.1016/j.marpolbul.2017.07.028. [Accessed: 20/20/2018].

MILLER, R. Z., WINDSLOW, B., KAPP, K. OSBORNE, A. & GWINNETT, C. (2024). Microplastic and anthropogenic microfibre pollution in the surface waters of the East River and Long Island Sound, USA. *Regional Studies in Marine Science*. 70. pp. 103360. (Online). Available from: https://doi.org/10.1016/j.rsma.2023.103360. [Accessed: 02/04/2024].

MINTENIG, S. M., INT-VEEN, I., LÖDER, M. G. J., PRIMKE, S. & GERDTS, G. (2017). Identification of microplastic in effluents of wastewater treatment plants using focal plane array-based micro-Fourier-transform infrared imaging. *Water Research*. 108. pp.365-372. (Online). Available from: http://dx.doi.org/10.1016/j.watres.2016.11.015. [Accessed: 11/08/2021].

MISRA, S., LU, F. M., SPRUIELL, J. E., RICHESON, G. C. (1995). Influence of molecular weight distribution on the structure and properties of melt-spun polypropylene filaments. *Journal of applied polymer science*. 56 (12). pp. 1761-1779. (Online). Available from: https://doi.org/10.1002/app.1995.070561307. [Accessed: 15/09/2022].

MORDKOFF, J. T. (2019). A simple method for removing bias from a popular measure of standardised effect size: adjusted partial eta squared. *Advances in methods and Practices in Psychological Science.* 2 (3). pp. 228-232. (Online). Available from: https://doi.org/10.1177/2515245919855053. [Accessed: 16/06/2024].

MUHTADI, M., LEIDONALD, R., RTAHMAWATI, A. MERDANGGA, T. D. T., NURHAMIYA, Y. & CORDOVA, M. R. (2025). Spatial and temporal distribution of microplastics in the Belawan Esturary, Indonesia. *Egyption Journal of Aquatic Research*. 51 (2). (Online). Available from: https://doi.org/10.1016/j.ejar.2025.03.004. [Accessed: 23/06/2025].

MURPHY, F., EWINS, C., CARBONNIER, F. & QUINN, B. (2016). Wastewater treatment works (WwTW) as a source of microplastics in the Aquatic Environment. *Environmental Science and technology*. 50 (11). pp. 5800-5808. (Online). Available from: https://doi.org/10.1021/acs.est.5b05416. [Accessed: 08/02/2018].

MUTHU, S. S., LI, Y., HU, J. Y. & MOK, P. Y. (2012). Quantification of environmental impact and ecological sustainability for textile fibres. *Ecological Indicators*. 13 (1). pp. 66-74. (Online). Available from: https://doi.org/10.1016/j.ecolind.2011.05.008. [Accessed: 21/09/2022].

MUTLU, T., ERYAŞAR, A. R., KARAOĞLU, K., VESKE, E. & GEDIK, K. (2025). Microplastic pollution in Gulf of Bandırma, sea of Marmara: biota and sediment. *Marine pollution bulletin*. 213. pp. 117667. (Online). Available from: https://doi.org/10.1016/j.marpolbul.2025.117667. [Accessed:16/04/2025].

NANDIYANTO, A. B. D., OKTIANI, R. & RAGADHITA, R. (2019). How to read and interpret FTIR spectroscope of organic material. *Indonesian Journal of Science & Technology*. 4 (1). pp. 97-118. (Online). Available from: https://ejournal.kjpupi.id/index.php/ijost/article/view/189/180. [Accessed: 27/03/2024].

NAPPER, I. E. & THOMPSON, R. C. (2016). Release of synthetic microplastic plastic fibres from domestic washing machines: Effects of fabric type and washing conditions. *Marine Pollution Bulletin*. 112 (1-2). pp. 39-45. (Online). Available from: http://dx.doi.org/10.1016/j.marpolbul.2016.09.025. [Accessed: 05/03/2020].

NAPPER, I. E., BAROTH, A., BARRETT, A. C., BHOLA, S., CHOWDHURY, G. W., DAVIES, B. F.R., DUNCAN, E. M., KUMAR, S., NELMS, S.E., NILOY, M. N. H., NISHAT, B., MADDALENE, T., THOMPSON, R. C. & KOLDEWEY, H. (2021). The abundance and characteristics of microplastic in surface water in the transboundary Ganges River. *Environmental Pollution*. 274. pp. 116348. (Online). Available from: https://doi.org/10.1016/j.envpol.2020.116348. [Accessed: 21/07/2022].

NARKHEDE, S. (2018). Understanding AUC-ROC curve. *Towards data science*. 26 (1). pp. 220-227.

NASERI, A. S. & ALI, N. H. M. (2022). Detection of drones with TOLOv4 deep learning algorithm. *International Journal of Nonlinear Analytical Applications*. 13 (January). pp. 2709-2722. (Online). Available from: http://dx.doi.org/10.22075/ijnaa.2022.27556.3648. [Accessed: 01/09/2022].

NAYAK, R. K., PADHYE, R. & FERGUSSON, S. (2012). Identification of natural textile fibres. In: Kozłowski, M. (Ed). *Handbook of Natural Fibres*. Volume 2. Cambridge: Woodhead Publishing. (Online). Available from: http://dx.doi.org/10.1533/9780857095503.1.314. [Accessed: 06/12/2019].

NAYAK, R., HOUSHYAR, S., KHANDUAL, A., PADHYE, R. & FERGUSSON, S. (2020). Identification of natural textile fibres. In KOZLOWSKI, R. M. & MACKIEWICZ-TARACZYK, M. (Eds). *Handbook of Natural fibres*. Second edition. Duxford: Woodhead Publishing. (Online). Available from: https://doi.org/10.1016/B978-0-12-818398-4.00016-5. [Accessed: 23/09/2022].

NEL, H. A., DALU, T. & WASSERMAN, R. J. (2018). Sinks and sources: Assessing microplastic abundance in river sediments and deposit feeders in an Austral temperate urban river system. *Science of the total environment*. 612. pp. 950-956. (Online). Available from: http://dx.doi.org/10.1016/j.scitotenv.2017.08.298. [Accessed: 06/09/2018].

NELMS, S. E., GALLOWAY, T. S., GODLEY, B. J., JARVIS, D. S. & LINDEQUE, P. K. (2018). Investigating microplastic trophic transfer in marine top predators. *Environmental Pollution*. 238. pp. 999-1007. (Online). Available from: https://doi.org/10.1016/j.envpol.2018.02.016. [Accessed: 06/09/2018].

NELSON, J. (2021). What is YOLO? The ultimate guide. *Roboflow*. Available from: https://blog.roboflow.com/guide-to-yolo-models/. [Accessed: 15/05/2024].

NEUPANE, S., PYAKUREL, M., SINHA, K., SHARMA, B. & PRAKASH, A. (2024). GraphoMatch: Forensic handwriting analysis using machine learning.

International journal of science and research archive. 11 (02). pp. 1526-1537. (Online). Available from: https://doi.org/10.30574/ijsra.2024.11.2.0643. [Accessed: 15/05/2024].

NG, W., MINASNY, B. & MCBRATNEY, A. (2020). Convolutional neural network for soil microplastic contamination using infrared spectroscopy. *Science of the Total Environment*. 702. pp. 134723. Available from: https://doi.org/10.1016/j.scitotenv.2019.134723. (Accessed 06/08/2021).

NGO, V. M., MCKEEVER, S. & THORPE, C. (2023). Identifying online child sexual texts in dark web through machine learning and deep learning algorithms. *APWG.Eu Technical summit and researcher sync-up (APWG.EU-Tech 2023).* pp. 1-6. (Online). Available from: https://doi.org/10.21427/WFN5-RT72. [Accessed: 15/05/2024].

NIZZETTO, L., BUSSI, G., FUTTER, M. N., BUTTERFIELD, D. & WHITEHEAD, P. G. (2016). A theoretical assessment of microplastic transport in river catchments and their retention by soils and river sediments. *Environmental Science: Processes and Impacts*. 18 (8). pp. 1050-1059. (Online). Available from: https://pubs.rsc.org/en/content/articlelanding/2016/em/c6em00206d. [Accessed: 21/11/2019].

NOBLE, W. S. (2006). What is a support vector machine? *Nature Biotechnology*. 24 (12). pp. 1565-1567. (Online). Available from: https://www.nature.com/articles/nbt1206-1565. [Accessed: 18/02/2021].

NOI, P. T. & KAPPAS, M. (2017). Comparison of Random Forest, K-Nearest Neighbor and Support Vector Machine classifiers for land cover classification using sentiner-2 imagery. *Sensors*. 18 (1). pp. 1-20.

NORÉN, F. (2007). Small plastic particles in costal Swedish waters. *N-research*. pp. 1-11.

NUELLE, M. T., DEKIFF, J. H., REMY, D. R. & FRIES, E. (2014). A new analytical approach for monitoring microplastics in marine sediments. *Environmental Pollution*. 184. pp. 161-169. (Online). Available from: http://dx.doi.org/10.1016/j.envpol.2013.07.027. [Accessed: 08/02/2018].

NURMAINI, S., PACHMATULLAH, M. N., SANIF, R., AGUSTIANSYAH, P., SASTRADINATA, I., LEGIRAN, L., DARMAWAHYNI, A., SAPITRI, A. I., ISLAMI, A., FIRDAUS, F., TUTUKO, B. & LUBIS, N. M. E. R. (2023). Real time mobile AI-assisted cervicography interpretation system. *Informatics in Medicine Unlocked.* 42 (July). pp. 101360. (Online), Available from: https://doi.org/10.1016/j.imu.2023.101360. [Accessed: 30/10/2023].

O'BRIEN, S., RAUERT, C., RIBERIO, F., OKOFFO, E. D., BURROWS, S. D., O'BREIN, J. W., WANG, X., WRIGHT, S. & THOMAS, K. V. (2023). There's something in the air: A review of sources, prevalence and behaviour of microplastics in the atmosphere. *Science of the Total Environment*. 874. pp. 162193. (Online). Available from: http://dx.doi.org/10.1016/j.scitotenv.2023.162193. [Accessed: 05/06/2024].

O'BRINE, T. & THOMPSON, R. C. (2010). Degradation of plastic carrier bags in the marine environment. Marine Pollution Bulletin. 60 (12). pp. 2279-2283. (Online). Available from: https://doi.org/10.1016/j.marpolbul.2010.08.005. [Accessed: 16/01/2018].

O'SHEA, K. & NASH, R. (2015). An introduction to convolutional neural networks. *ArXiv preprint*. (Online). Available from: https://arxiv.org/abs/1511.08458. [Accessed: 14/02/2023].

PADILLA, R., NETTO, S. L. & DA SILVA, E. A. B. (2020). A survey on performance metrics for object-detection algorithms. *International conference on systems, signals, and image processing.* July. (Online). Available from: https://ieeexplore.ieee.org/abstract/document/9145130. [Accessed: 20/10/2023].

PADMANABAN, K. R. A. & PARTHIBAN, G. (2016). Applying machine learning techniques for predicting the risk of chronic kidney disease. *Indian Journal of Science and Technology*. 9 (29). pp. 1-6.

PAL, M. (2005). Random forest classifier for remote sensing classification. *International Journal of Remote Sensing*. 26 (1). pp. 217-222. (Online). Available from: https://doi.org/10.1080/01431160412331269698. [Accessed: 16/02/2021].

PALENIK, C. S., BECKERT, J. C. AND PALENIK, S. (2016). Microspectrophotomerty of fibers: Advances in analysis and interpretation. National Criminal Justice Reference Service, U. S. Department of Justice.

PALENIK, S. J. (1992). Microscopical examination of fibres. In: Roberston, J., Roux, C. & Wiggins, K.G. (Eds). *Forensic examination of fibres*. Second edition. London: Taylor & Francis Ltd.

PALENIK, S. J. (1999). Microscopical examination of fibres. In: ROBERTSON, J., ROUX, C. & WIGGINS, K. G. (Eds). *Forensic examination of fibres*. Second edition. London: Taylor Francis Ltd.

PALENIK, S. J. (2018). Microscopic examination of fibres. In: Robertson, J., Roux, C. and Wiggins, K. (eds). *Forensic Examination of Fibres*. Third edition. Boca Raton: CRC Press.

PARKER, B. W., BECKINHAM, B. A., INGRAM, B. C., BALLENGER, J. C., WEINSTEIN, J. E. & SANCHO, G. (2020). Microplastics and tire wear particle occurrence in fishes from an urban estuary: influence of feeding characteristics on exposure risk. *Marine Pollution Bulletin*. 160. pp. 111539. Online. Available from: https://www.sciencedirect.com/science/article/pii/S0025326X20306573. [Accessed: 21/09/2020].

PARKS, D. H. & FELS, S. S. (2008). Evaluation of background subtraction algorithms with post-processing. *IEEE 5th International Conference on Advanced Video and Signal Based Surveillance*. Unites States.1st-3rd September. (Online). Available from: https://ieeexplore.ieee.org/document/4730412. [Accessed: 14/12/2020].

PAULLADA, A., RAJI, I. D., BENDER, E. M., DENTON, E. & HANNA, A. (2021). Data and its (dis)contents: a survey of dataset development and use in machine learning research. *Patterns*. 2 (11). pp. 100336 (online). Available from: https://doi.org/10.1016/j.patter.2021.100336. [Accessed: 19/07/2022].

PAULSSON, N. & STOCKASSA, B. (1999). A real-time colour image processing system for forensic fibre investigations. *Forensic Science*

International. 103 (1). pp. 37-59. (Online). Available from: https://doi.org/10.1016/S0379-0738(99)00046-8. [Accessed: 29/11/2018].

PELLONDO'U, P. T. E. A., TOYA, R. A. & NOVELYN, S. (2023). Identification of diatoms in the upstream, middle and downstream Ciliwung River as a diagnostic tool for drowning. *International journal of tropical disease and health*. 44 (2). pp. 29-48. (Online). Available from: https://doi.org/10.9734/ijtdh/2023/v44i21388. [Accessed: 21/03/2023].

PENA, E. A & SLATE, E. H. (2019). gvlma: Global Validation of Linear Models Assumptions. R package version 1.0.0.3. https://CRAN.R-project.org/package=gvlma. [Accessed: 12/07/2019).

PerkinElmer. (2023). *Spotlight 400 FT-IR Imaging System.* Available at: https://www.citethemrightonline.com/sourcetype?docid=b-9781350927964&tocid=b-9781350927964-34. [Accessed: 28/02/2023].

PETERS, C. A. & BRATTON, S. P. (2016). Urbanisation is a major influence on microplastic ingestion by sunfish in the Brazos River Basin, Central Texas, USA. *Environmental Pollution*. 210. pp. 380-387. (Online). Available from: http://dx.doi.org/10.1016/j.envpol.2016.01.018. [Accessed: 18/09/2018].

POLI, V., LITTI, L. & LAVAGNOLO, M. C. (2024). Microplastic pollution in the North-East Atlantic Ocean surface water: How the sampling approach influences the extent of the issue. *Science of the Total Environment*. 947. pp. 174561. (Online). Available from: https://doi.org/10.1016/j.scitotenv.2024.174561. [Accessed: 17/04/2025].

PRATA, J. C. (2018). Microplastics in wastewater: state of the knowledge on sources, fate and solutions. *Marine pollution Bulletin*. 129. (1). pp. 262-265. (Online). Available from: https://doi.org/10.1016/j.marpolbul.2018.02.046. [Accessed: 18/09/2018].

PRATA, J. C., CASTRO, J. L., DA COSTA, J. P., DUARTE, A. C., CERQUEIRA, M. & ROCHA-SANTOS, T. (2020a). An easy method for processing and identification of natural and synthetic microfibres and microplastics in indoor and outdoor air. *MethodsX*. 7. pp. 100763. (Online).

Available from: https://www.sciencedirect.com/science/article/pii/S2215016119303383. [Accessed: 08/04/2021].

PRATA, J. C., PAÇO, A., REIS, V., DA COSTA, J. P., FERNANDES, A. J. S., DA COSTA, F. M., DUARTE, A. C. & ROCHA-SANTOS, T. (2020b). Identification of microplastics in white wines capped with polyethylene stoppers using micro-Raman spectroscopy. *Food chemistry*. 331 (Dec). pp. 127323. (Online). Available from: https://www.sciencedirect.com/science/article/pii/S0308814620311857. [Accessed: 13/04/2021].

PRIMPKE, S., CROSS, R. K., MINTENIG, S. M., SIMON, M., VIANELLO, A., GERDTS, G. & VOLLERTSEN, J. (2020). Towards the systematic identification of microplastics in the environment: Evaluation of a new independent software tool (simple) for spectroscopic analysis. *Applied Spectroscopy*. 74 (9). pp. 1127-1138. (Online). Available from: https://doi.org/10.1177/0003702820917760. [Accessed: 04/03/2023].

PRIMPKE, S., LORENZ, C., RASCHER-FRIESENHAUSEN, R. & GERDTS, G. (2017). An automated approach for microplastic analysis using focal plane array (FPA) FTIR microscopy and image analysis. *Analytical Methods*. 9 (9). pp. 1499-1511. (Online). Available from: https://pubs.rsc.org/en/content/articlehtml/2017/ay/c6ay02476a. [Accessed: 30/11/2018].

QIN, Y., QU, M., KASCHTA, J. & SCHUBERT, D. W. (2018). Comparing recycled and virgin poly (ethylene terephthalate) melt-spun fibres. *Polymer Testing*. 72. pp. 364-371. (Online). Available from: https://doi.org/10.1016/j.polymertesting.2018.10.028. [Accessed: 15/09/2022].

R Core Team (2018). R: A language and environment for statistical computing. R Foundation for Statistical Computing, Vienna, Austria, https://www.R-project.org/ [Accessed: 12/07/2019].

R Core Team (2020). R: A language and environment for statistical computing. R Foundation for Statistical Computing, Vienna, Austria. URL https://www.R-project.org/ [Accessed:30/03/2020].

RADJA, A., HORSLEY, E. M., LAVRENTOVICH, M. O. & SWEENEY, A. M. (2019). Pollen cell wall patterns form from modulated phases. *Cell*. 176 (4). pp. 856-868.

RAILEANU, L. E. & STOFFEL, K. (2004). Theoretical comparison between the Gini Index and Information Gain Criteria. *Annals of Mathematics and Artificial Intelligence*. 41 (1). pp. 77-93. (Online). Available from: https://doi.org/10.1023/B:AMAI.0000018580.96245.c6. [Accessed: 16/02/2021].

RAJAGOPALAN, B. & LALL, U. (1999). A K-nearest-neighbour simulator for daily precipitation and other weather variables. *Water Resources Research*. 35 (10). pp. 3089-3101. (Online). Available from: https://doi.org/10.1029/1999WR900028. [Accessed: 21/07/2022].

RAJALA, K., GRÖNFORS, O., HESAMPOUR, M. & MIKOLA, A. (2020). Removal of microplastics from secondary wastewater treatment plant effluent by coagulation/flocculation with iron, aluminium, and polyamine-based chemicals. *Water Research*. 183. pp. 116045. (Online). Available from: https://doi.org/10.1016/j.watres.2020.116045. [Accessed: 17/08/2020].

REBUFFI, S. A., GOWAL, S., CALIAN, D., STIMBERG, F., WILES, O. & MANN, T. (2021). Data augmentation can improve robustness. *Advances in neural information processing systems*. 36. pp. 29935-29948. (Online). Available from: https://proceedings.neurips.cc/paper/2021/hash/fb4c48608ce8825b558ccf07169a3421-Abstract.html. [Accessed: 15/02/2024].

REDMON, J., DIVVALA, S., GIRSHICK, R. & FARHADI, A. (2016). You Only Look Once: Unified, Real-Time Object Detection. *Proceedings of the IEEE Conference on Computer Vision and Pattern Recognition (CVPR)*. (June). pp. 779-788. (Online). Available from: https://www.cv-

foundation.org/openaccess/content_cvpr_2016/html/Redmon_You_Only_Look_CVPR_2016_paper.html. [Accessed: 02/02/2023].

REFFNER, J. A., KAMMRATH, B. W. & KAPLAN, S. (2020). A More efficient method for synthetic textile fibre analysis using polarised light microscopy. *Journal of Forensic Science*. 65 (3). pp. 744-750. (Online). Available from: https://doi.org/10.1111/1556-4029.14252. [Accessed: 25/06/2020].

REVI, V., KASODARIYA, S., TALAPATRA, A., PILANIA, G. & ALANKAR, A. (2021). Machine learning elastic constituents of multi-component alloys. *Computational materials science*. 198. pp. 110671. (Online). Available from: https://doi.org/10.1016/j.commatsci.2021.110671. [Accessed: 16/05/2024].

RICHARDSON, J. T. E. (2011). Eta squared and partial eta squared as measurements of effect size in educational research. *Educational Research Review*. 6. pp. 135-147.

RÍOS, J. M., TESITORE, G. & TEIXERIRA DE MELLO, F. (2022). Does color play a predominant role in the intake of microplastic fragments by freshwater fish: an experimental approach with *Psalidodon eigenmanniorum*. Environmental Science and Pollution Research. 29. pp. 49457-49464. (Online). Available from: https://doi.org/10.1007/s11356-022-20913-8. [Accessed: 05/08/2023].

RIVERS, M. L., GWINNETT, C. & WOODALL, L. C. (2019). Quantification is more than counting: Actions required to accurately quantify, and report isolated marine microplastics. *Marine Pollution Bulletin*. 139 (Aug). pp. 100-104. (Online). Available from: https://doi.org/10.1016/j.marpolbul.2018.12.024. [Accessed: 08/01/2019].

ROBERSTON, J. & GRIEVE, M. (1999). *Forensic Examination of Fibres*. London: Taylor and Francis

ROBERTSON, J. & ROUX, C. (2016). Fiber: Protocols for examination. In: Houck, M. M. (Ed). Materials Analysis in Forensic science. London: Academic Press.

ROBERTSON, J. & ROUX, C. (2017). From crime scene to laboratory. In: Robertson, J., Roux, C. & Wiggins, K. G. (eds). *Forensic Examination of Fibres*. Third edition. Boca Raton: CRC Press.

ROBERTSON, J. & ROUX, C. (2018), From Crime Scene to Laboratory. In: Robertson, J., Roux, C. and Wiggins, K. (eds), *Forensic Examination of Fibres*. Third edition. Boca Raton: CRC Press

RODRÍGUEZ-HERNÁNDEZ, M. M., PRUNEDA, R. E. & RODRÍGUEZ-DÍAZ, J. M. (2021). Development in the resolution of mathematical problems in primary school education. *Mathematics*. 9 (10). pp. 1-14.

ROSSO, B., SCOTTO, F., HALLANGER, I. G., LAROSE, C., GALLET, J. C., SPOLAOR, A., BRAVO, B., BARBANTE, C., GAMBARO, A. & CORAMI, F. (2024). Characteristics and quantification of small microplastics (<100 µm) in seasonal Svalbard snow on glaciers and lands. *Journal of Hazardous Materials*. 467. pp. 133723. (Online). Available from: https://doi.org/10.1016/j.jhazmat.2024.133723. [Accessed: 27/03/2024].

ROSTRON, P., GABER, S. & GABER, D. (2026). Raman Spectroscopy, Review. *International journal of engineering and technical Research*. 6 (1). pp. 50-64. (Online). Available from: https://www.researchgate.net/profile/Paul-Rostron/publication/309179824_Raman_Spectroscopy_a_review/links/580329fe08ae23fd1b673f34/Raman-Spectroscopy-a-review.pdf. [Accessed: 08/04/2024].

RStudio (N.D). https://www.rstudio.com/products/rstudio/. (Accessed: 12th July 2019).

SAEED, T., AL-JANDAL, N., AL-MUTAIRI. & TAQI, H. (2020). Microplastics in Kuwait marine environment: Results of first survey. *Marine Pollution Bulletin*. 152. pp. 110880. (Online). Available from: https://doi.org/10.1016/j.marpolbul.2019.110880. [Accessed: 06/02/2020].

SCHER, S. & MESSORI, G. (2018). Predicting weather forecast uncertainty with machine learning. *Journal of the Royal Meteorological Society*. 144

(717). pp. 2830-2841. (Online). Available from: https://doi.org/10.1002/qj.3410. [Accessed: 17/01/2023].

SCHNEIDER, M., STRACKE, F., HANSEN, S. & SCHAEFER, U. F. (2009). Nanoparticles and their interactions with the dermal barrier. *Dermo-Endocrinology*. 1 (4). pp. 197-206. (Online). Available from: https://doi.org/10.4161/derm.1.4.9501. [Accessed: 16/07/2023].

SCHRAUFNAGEL, D. (2020). The health effects of ultrafine particles. *Experimental and Molecular Medicine*. 52 (3). pp. 311-317. (Online). Available from: https://doi.org/10.1038/s12276-020-0403-3. [Accessed: 58/07/2023].

SCZOSTAK, A. (2009). Cotton linters: an alternative cellulosic raw material. *Macromolecular Symposia*. 280 (1). pp. 45-53. (Online). Available from: https://doi.org/10.1002/masy.200950606. [Accessed: 06/01/2024].

SEELEY, M. E., HALE, R. C., ZWOLLO, P., VOGELBEIN, W., VERRY, G. & WARGO, A. R. (2023). Microplastics exacerbate virus-mediated mortality in fish. *Science of the total Environment*. 866. pp. 161191. (Online). Available from: http://dx.doi.org/10.1016/j.scitotenv.2022.161191. [Accessed: 13/08/2023].

SEKACHEV, B., MANOVICH, N., ZHILTSOV, M., ZHAVORONKOV, A., KALININ, D., HOFF, B., TOSMANOV., KRUCHININ, D., ZANKEVICH, A., SIDVEV, D., MARKELOV, M., JOHANNES222., CHENUET, M., A-ANDRE., TELENACHOS., MELNIKOV, A., KIM, J., ILOUZ, L., GLAZOV, N., PRIYA4607., TEHRANI, R., JEONG, S., SKUBRIEV, V., YONEKURA, S., TRUONG, V., ZLIANG7., LIZMING. & TRUONG, T. (2020). Opencv/cvat. [Software]. DOI: 10.5281/zenodo.3497105. Available from: https://github.com/opencv/cvat. [Accessed: 21/07/2021].

SERMIER, F. M., MASSONNET, G. BUZZINI, P., FORTINI, A., GASON, F., DE WAEL, K. & ROVAS, P. (2006). A comparison of sufficiency of manual and automatic fibre search with the Maxcan fibre finder. *Forensic Science international*. 160 (2-3). pp. 102-108. (Online). Available from: https://pubmed.ncbi.nlm.nih.gov/16216460/. [Accessed: 08/01/2019].

SHAFIEE, M. J., CHYWL, B., LI, F. & WONG, A. (2017). Fast YOLO: A fast you only look once system for real-time embedded object detection in video. *arXiv*. (Online). Available from: https://arxiv.org/abs/1709.05943. [Accessed: 02/02/2023].

SHAH, A. A., HASAN, F., HAMEED, A. & AHMED, S. (2008). Biological degradation of plastics: A comprehensive review. Biotechnology Advances. 26 (3). P. 246-265. (Online). Available from: https://doi.org/10.1016/j.biotechadv.2007.12.005. [Accessed: 01/12/2017].

SHAHI, N. K., MAENG, M., KIM, D. & DOCKKO, S. (2020). Removal behaviour of microplastics using alum coagulant and its enhancement using polyamine-coated sand. *Process Safety and Environmental Protection*. 141. pp. 9-17. (Online). Available from: https://doi.org/10.1016/j.psep.2020.05.020. [Accessed: 17/08/2020].

SHAHINFAR, S., MEEK, P. & FALZONE, G. (2020). "How many images do I need?" Understanding how sample size per class affects deep learning model performance metrics for balanced designs in autonomous wildlife monitoring. *Ecological informatics*. 57 (12). pp. 101085. (Online). Available from: https://doi.org/10.1016/j.ecoinf.2020.101085. [Accessed: 07/10/2023].

SHIM, W. J., HONG, S. H. & EO EO, S. (2017). Identification methods in microplastic analysis: a review. *Analytical methods*. 9 (9). pp. 1384-1391. (Online). Available from: https://doi.org/10.1039/C6AY02558G. [Accessed: 12/04/2021].

SHIM, W. J., SONG, Y. K., HONG, S. H. & JANG, M. (2016). Identification and quantification of microplastics using Nile Red staining. *Marine Pollution Bulletin*. 113 (1-2). pp. 469-476.

SHISHKIN, I. E. & GREKOV, A. N. (2023). Classification of microplastics and microorganisms in marine environment. *International Russian Smart Industry Conference*. Sochi. Russia. (Online). Available from: https://ieeexplore.ieee.org/abstract/document/10110736. [Accessed: 18/06/2024].

SHORTEN, C. & KHOSHGOFTAAR, T. (2019). A survey on image data augmentation for deep learning. *Journal of big data*. 6 (1). (Online). Available from: https://doi.org/10.1186/s40537-019-0197-0. [Accessed: 25/02/2024].

SHRUTI, V. C., PÈREZ-GUEVARA, F., ROY, P. D. & KUTRALAM-MUNIASAMY, G. (2022). Analysing microplastics with Nile Red: Emerging trends, challenges and prospects. *Journal of hazardous materials*. 423. pp. 12717. (Online). Available from: https://doi.org/10.1016/j.jhazmat.2021.127171. [Accessed: 16/02/2023].

SHUTTLE. (2022). *Final Public SHUTTLE Workshop*. https://www.shuttle-pcp.eu/the-report-on-the-shuttle-public-workshop-is-now-available/. [Accessed: 23/03/2023].

SIERRA, I., CHIALANZA, M. R., FACCIO, R., CARRIZOM, D., FORNARO, L. & PÉREZ-PARADA, A. (2019). Identification of microplastics in wastewater samples by means of polarised light optical microscopy. *Environmental Science and pollution Research*. 27 (7). pp. 7409-7419. (Online). Available from: https://doi.org/10.1007/s11356-019-07011-y. [Accessed: 19/04/2021].

SINGH, B. & SHARMA, N. (2008). Mechanistic implications of plastic degradation. *Polymer Degradation and Stability*. 93. pp. 561-584. (Online). Available from: https://doi.org/10.1016/j.polymdegradstab.2007.11.008. [Accessed: 16/01/2018].

SOININEN, T., UURASJÄRVI, E., HÄMÄLÄININ, L., HUUSARI, N., FEODOROFF, J., MOSHNIKOFF, J., NIIRANEN, E., FEODOROFF, P., MUSTONEN, T. & KOISTINEN, A. (2024). Microplastics in Artic waters of the Finnish Sámi area. *Science of the Total Environment*. 940. pp. 173666. (Online). Available from: https://doi.org/10.1016/j.scitotenv.2024.173666. [Accessed: 08/05/2025].

SOLAWETZ, J. (2020). What is YOLOv5: A guide for beginners. *Roboflow blogs*. Available from: https://blog.roboflow.com/yolov5-improvements-and-evaluation/. [Accessed:15/05/2024].

SOLAWETZ, J. & FRANCESCO (2024). What is YOLOv8? A complete guide. *Roboflow blogs*. Available from: https://blog.roboflow.com/whats-new-in-yolov8/. [Accessed: 05/08/2024].

SOLAWETZ, J. (2024). What is YOLOv7? A complete guide. *Roboflow blogs*. Available from: https://blog.roboflow.com/yolov7-breakdown/. [Accessed: 15/5/2024].

SONG, Y. K., HONG, S. H., JANG, M., HAN, G. M., RANI, M., LEE, J. & SHIM, W. J. (2015). A comparison of microscopic and spectroscopic identification methods for analysis of microplastics in environmental samples. *Marine Pollution Bulletin*. 93 (1-2). pp. 202-209. (Online). Available from: http://dx.doi.org/10.1016/j.marpolbul.2015.01.015. [Accessed: 19/12/2017].

SONKA, M., HLAVAC, V. & BOYLE, R. (2014). *Image processing, analysis, and machine vision*. Fourth Edition. Boston: CENGAGE Learning.

STANTON, T., JOHNSON, M., NATHANAIL, P., MACNAUGHTAN, W. & GOMES, R. L. (2019). Freshwater and airborne textile fibre population are dominated by 'natural', not microplastic, fibres. *Science of the Total Environment*. 666. pp. 377-389. (Online). Available from: https://doi.org/10.1016/j.scitotenv.2019.02.278. [Accessed: 12/03/2020].

STANTON, T., STANES, E., GWINNETT, C., LEI, X., CAUILAN, M., RAMOS, M., SALLACH, J. B., HARRISON, E., OSBORNE, A., SANDERS, C. H., BAYNES, E., LAW, A., JOHNSON, M., RYVES, D. B., SHERIDAN, K. J., BLACKBURN, R. S. & MCKAY, D. (2023). Shedding off-the-grid: The role of garment manufacturing and textile care in global microfibre pollution. *Journal of Cleaner Production*. 428. (Online). Available from: https://doi.org/10.1016/j.jclepro.2023.139391. [Accessed: 05/12/2023].

STEER, M., COLE, M., THOMPSON, R. C. & LINDEEQUE, P. K. (2017). Microplastic ingestion in fish larvae in the western English Channel. *Environmental pollution*. 226. pp. 250-259. (Online). Available from: http://dx.doi.org/10.1016/j.envpol.2017.03.062. [Accessed: 22/08/2023].

STEPANOVIĆ, S., ĆIRKOVIĆ, I. C., RANIN, L. & ŠVABIĆ-VLAHOVIĆ, M. (2004). Biofilm formation by Salmonella spp. and Listeria monocytogenes on

plastic surface. *Letters in Applied Microbiology*. 38 (5). pp. 428-432. (Online). Available from: https://pubmed.ncbi.nlm.nih.gov/15059216/. [Accessed: 31/01/2018].

STOCK, F., NARAYANA, V. K. B., SCHERER, C., LÖDER, M. G. J., BRENNHOLT, N., LAFORSCH, C. & REIFFERSCHEID, G. (2022). Pitfalls and Limitations in Microplastic Analyses. In: STOCK, F., REIFFERSCHEID, G., BRENNHOLT, N., KOSTIANAIA, E. (eds). *Plastics in the aquatic environment – Part I Current status and challenges*. The Handbook of Environmental chemistry. Volume 111. Cham: Springer.

STOEFFLER, S. F. (1996). A Flowchart System for the Identification of Common Synthetic Fibres by Polarised Light Microscopy. *Journal of Forensic Science*. 41 (2). pp. 297-299. (Online). Available from: https://www.semanticscholar.org/paper/A-Flowchart-System-for-the-Identification-of-Common-Stoeffler/d6528efbf82d3e5b7cdd8bbff874226d04f59a3d. [Accessed: 28/11/2018].

STONE, C., WINDSOR, F. M., MUNDAY, M. & DURANCE, I. (2020). Natural or synthetic – how global trends in textile usage threaten freshwater environments. *Science of the total environment*. 718. pp. 134689. (Online). Available from: https://doi.org/10.1016/j.scitotenv.2019.134689. [Accessed: 30/05/2023].

STUER, N. (2016). Easylift®: A novel tape lifting system for forensic evidence, Un-published internship report.

STURM, M. T., MYERS, E., SCHOBER, D., KORZIN, A. & SCHUHEN, K. S. (2023). Development of an inexpensive and comparable microplastic detection method using fluorescent staining with novel Nile Red-derivatives. *Analytica*. 4 (1). (Online). Available from: https://doi.org/10.3390/analytica4010004. [Accessed: 17/02/2023].

SUMMERSCALES, J. & GWINNETT, C. (2017). Forensic Identification of Bast Fibres.in Dipa Ray (editor). *Biocomposites for High-Performance*

Applications: Current Barriers and Future Needs Towards Industrial Development. Duxford: Woodhead Publishing.

SUN, J., DAI, X., WANG, Q., VAN LOOSDRECHT, M. C. M. & NI, B, J. (2019). Microplastics in wastewater treatment plants: Detection, occurrence and removal. *Water Research*. 152. pp. 21-37. (Online). Available from: https://doi.org/10.1016/j.watres.2018.12.050. [Accessed: 11/08/2021].

SUN, Y., LI, Y., DUAN, Z., MING, H. & ZHANG, Y. (2023). PBA-YOLOv7: An object detection method based on an improved YOLOv7 network. *Applied Sciences*. 13. (Online). Available from: https://doi.org/10.3390/app131810436. [Accessed: 01/03/2024].

SUSAN, S., KUMAR, A. (2021). The balancing trick: Optimised sampling of imbalanced datasets – a brief survey of the recent state of the art. *Engineering Reports*. 3 (4). pp. 1-24. (Online). Available from: https://doi.org/10.1002/eng2.12298. [Accessed: 16/05/2024].

TAGG, A. S., SAPP, M., HARRISON, J. P. & OJEDA, J. J. (2015). Identification and quantification of microplastics in wastewater using focal plane array-based reflectance micro-FTIR imaging. *Analytical Chemistry*. 87 (12). pp. 6032-6040. (Online). Available from: https://doi.org/10.1021/acs.analchem.5b00495. [Accessed: 18/03/2020].

TALAAT, F. M. & ZAINELDIN, H. (2023). An improved fire detection approach based on YOLO-v8 for smart cities. *Neural computing and applications*. 35 (28). pp. 20939-20954. (Online). Available from: https://doi.org/10.1007/s00521-023-08809-1. [Accessed: 01/03/2024].

TALVITIE, J., MIKOLA, A., SETÄLÄ, O., HEINONEN, M. & ARTO, K. (2017). How well in microliter purified from wastewater? – A detailed study on the stepwise removal of microliter in a tertiary level wastewater treatment plant. *Water Research*. 109. pp. 164-172. (Online). Available from: http://dx.doi.org/10.1016/j.watres.2016.11.046. [Accessed: 18/09/2018].

TANG, Y., YAO, J., DONG, Z., HU, Z., WU, T. & ZHANG, Y. (2024). A highly accurate and semi-automated method for quantifying spherical microplastics based on digital slide scanners and image processing. *Environmental*

research. 250. pp. 118494. (Online). Available from: https://doi.org/10.1016/j.envres.2024.118494. [Accessed: 18/06/2024].

TAYLOR, M. A. (1990). *Technology of textile properties*. Third edition. London: Forbes publications

TEDESCO, M. C. & BROWNE, M. A. (2021). Identifying and measuring individual micrometre-sized fibres in environmental samples by light and confocal microscopes. *Chemical Engineering Journal*. 417 (March). pp. 129218. (Online). Available from: https://doi.org/10.1016/j.cej.2021.129218. [Accessed:22/08/2022).

TENDER, C. D., SCHLUNDT, L., DEVRIESE, L. I., MINCER, T. J., ZETTLER, E. R. & AMARAL-ZETTLER, L. A. (2017). A review of microscopy and comparative molecular-based methods to characterize "Plastisphere" communities. *Analytical Methods*. 9. pp. 2132-2143. (Online). Available from: https://doi.org/10.1039/C7AY00260B. [Accessed: 01/02/2018].

THOMPSON, R. C., MOORE, C. J., VOM SAAL, F. S. & SWAN, S. H. (2009). Plastics, the current environment and human health: current consensus and future trends. *Philosophical transactions of the royal society B: biological sciences*. 364. pp. 2153-2166.

THOMPSON, R. C., OLSEN, Y., MITCHEL, R. P., DAVIS, A., ROWLAND, S. J., MCGONIGLE, D. & RUSSEL, A. E. (2004). Lost at Sea: Where Is All the Plastic? *Science.* 304. pp. 838. (Online). Available from: http://www.sciencemag.org/cgi/doi/10.1126/science.1094559. [Accessed: 05/12/2017].

TOMAR, D. & AGARWAL, S. (2014). Feature selection based least square twin support vector machine for diagnosis of heart disease. *International Journal of Bio-science and Bio-technology*. 6 (2). pp. 69-82. (Online). Available from: https://www.researchgate.net/publication/262105416_Feature_Selection_based_Least_Square_Twin_Support_Vector_Machine_for_Diagnosis_of_Heart_Disease. [Accessed: 10/20/2023].

TURRA, A., MANZANO, A. B., DIAS, R. J. S., MAHIQUES, M. M., BARBOSA, L., BALTHAZAR-SILVA, D. & MOREIRA, F. (2014). Three-dimensional distribution of plastic pellets in sandy beaches: shifting paradigms. *Scientific Reports*. 4. pp. 1-7.

UETANI, K., KOGA, H. & NOGI, M. (2019). Estimation of the Intrinsic Birefringence of Cellulose Using Bacterial Cellulose Nanofiber Films. *ACS Macro Letters*. 8 (3). pp. 250-254

URBANEK, S. (2019). jpeg: Read and write JPEG images. R package version 0.1-8.1. https://CRAN.R-project.org/package=jpeg. (Accessed: 30th April 2020).

VAN CAUWENBERGHE, L., VANREUSEL, A., MEES, J. & JANSSEN, C. R. (2013). Microplastic pollution in deep-sea sediments. *Environmental Pollution*. pp. 495-499. (Online). Available from: https://doi.org/10.1016/j.envpol.2013.08.013. [Accessed: 04/12/2017].

VIRŠEK, M. K., PALATINUS, A., KOREN, Š., PETERLIN, M. & KRŽAN, A. (2016). Protocol for microplastics sampling on the sea surface and sample analysis. *Journal of visualised experiments*. (118). pp. 1-9.

VITHATABANDHU, P., LEELAKUN, P., YOTTIAM, A., DAMRONGSIRI, S., HAWANGCHU, Y., SUPAKATA, N., KANOKKANTAPONG, V. & SRITHONGOUTHAI, S. (2025). Impact of seasonal variations on microplastic accumulation and characteristics in sandy beaches of Sichang Island, the inner Gulf of Thailand. *Marine Pollution Bulletin*. 215. pp. 117936. (Online). Available from: https://doi.org/10.1016/j.marpolbul.2025.117936. [Accessed:16/04/2025].

WALKINSHAW, C., LINDEQUE, P., THOMPSON, R., TOLHURST, T. & COLE, M. (2020). Microplastics and seafood: lower trophic organisms at highest risk of contamination. *Ecotoxicology and Environmental Safety*. 190. pp. 110066. (Online). Available from: https://doi.org/10.1016/j.ecoenv.2019.110066. [Accessed: 13/01/2020].

WANG, C. Y., BOCHKOVSKIY, A. & LIAO, H. Y. M. (2022). YOLOv7: Trainable bag-of-freebies sets new state-of-the-art- for real-time object

detection. *CVPR*. (Online). Available from: https://openaccess.thecvf.com/content/CVPR2023/papers/Wang_YOLOv7_Trainable_Bag-of-Freebies_Sets_New_State-of-the-Art_for_Real-Time_Object_Detectors_CVPR_2023_paper.pdf. [Accessed: 30/09/2023].

WANG, F., WONG, C. S., CHEN, D., LU, X., WANG, F. & ZENG, E. Y. (2018). Interaction of toxic chemicals with microplastics: A critical review. *Water Research*. 139. P. 208-219. (Online). Available from: https://doi.org/10.1016/j.watres.2018.04.003. [Accessed: 02/01/2019].

WANG, W., NDUNGU, A. W., LI, Z. & WANG, J. (2017). Microplastics pollution in inland freshwaters of China: A case study in urban surface waters of Wuhan China. *Science of the Total Environment*. 575. pp. 1369-1374. (Online). Available from: http://dx.doi.org/10.1016/j.scitotenv.2016.09.213. [Accessed: 04/11/2019].

WANG, X., LI, Y., KROLL, A. & MITRANO, D. M. (2024). Differentiating microplastics from natural particles in aqueous suspensions using flow cytometry with machine learning. *Environmental Science and Technology*. 58. pp. 10204-10251. (Online). Available from: https://doi.org/10.1021/acs.est.4c00304. [Accessed: 18/06/2024].

WANG, Y., ZHANG, D., ZHANG, M., MU, J., DING, G., MAO, Z., CAO, Y., JIN, F., CONG, Y., WANG, L., ZHANG, W. & WANG, J. (2019). Effects of ingested polystyrene microplastics on brine shrimp, Artemia parthenogenetica. *Environmental Pollution*. 244. pp. 715-722. (Online). Available from: https://doi.org/10.1016/j.envpol.2018.10.024. [Accessed: 27/04/2021].

WARD, E., GORDON, M., HANSON, R. & JANTUNEN, L. M. (2024). Modelling the effects of shape on atmospheric microplastic fallout. *Atmospheric Environment*. 326. pp. 120458. (Online). Available from: https://doi.org/10.1016/j.atmosenv.2024.120458. [Accessed: 03/04/2024].

WELLER, H. (2019a). countcolors: Locates and Counts Pixels Within Color Range(s) in Images. R package version 0.9.1. https://CRAN.R-project.org/package=countcolors. (Accessed: 30th April 2020).

WELLER, H. (2019b). colordistance: Distance Metrics for Image Color Similarity. R package version 1.1.0. https://CRAN.R-project.org/package=colordistance. (Accessed: 30th April 2020).

WETZER, E. & LOHNINGER, H. (2018). Image processing using colour space models for forensic fibre detection. *IFAC-PapersOnLine*. 51 (2). pp. 445-450. (Online). Available from: https://doi.org/10.1016/j.ifacol.2018.03.076. [Accessed: 09/11/2018].

WIGGINS, K. (2018). Ropes and Cordages. In: Robertson, J., Roux, C. and Wiggins, K. (eds), *Forensic Examination of Fibres*. Third edition. Boca Raton: CRC Press

WIGGINS, K. G., TURNER, Y. J. & MILES, J. H. (1999). The use of the Foster & Freeman Fx5 fibre finder in forensic textile examinations. *Science and Justice*. 39 (1). pp. 19-25. (Online). Available from: https://doi.org/10.1016/S1355-0306(99)72010-1. [Accessed: 08/01/2019].

WOLFF, S., KERPEN, J., PREDIGER, J., BARKMANN, L. & MÜLLER, L. (2019). Determination of the microplastics emission in the effluent of a municipal wastewater treatment plant using Raman microspectroscopy. *Water Research X*. 2. pp. 100014.

WONG, S. C., GATT, A. & STAMATESCU, V. (2016). Understanding data augmentation for classification when to warp? *International Conference on Digital Image Computing: Techniques and Applications (DICTA).* Gold coast: Australia. (Online). Available from: https://ieeexplore.ieee.org/abstract/document/7797091. [Accessed 16/02/2024].

WOODALL, L. C., GWINNETT, C., PACKER, M., THOMPSON, R. C., ROBINSON, L. F. & PATERSON, L. J. (2015). Using a forensic science approach to minimize environmental contamination and to identify microfibres in marine sediments. *Marine pollution Bulletin*. 95 (1). pp. 40-46. (Online). Available from: http://dx.doi.org/10.1016/j.marpolbul.2015.04.044. [Accessed: 17/01/2018].

WOODALL, L. C., SANCHEZ-VIDAL, A., CANALS, M., PATTERSON, G. L. J., COPPOCK, R., SLEIGHT, V., CALAFAT, A., ROGERS, A. D., NARAYANASWAMY, B. E. & THOMPSON, R. C. (2014). The deep sea is a major sink for microplastic debris. *Royal society open science.* 1 (4). pp. 140317. (Online). Available from: http://dx.doi.org/10.1098/rsos.140317. [Accessed: 10/04/2018].

WOODWARD, L. A. (1967). General introduction. In: SYMANSKI, H. A. (Ed). *Raman spectroscopy: Theory and Practice*. New York: Plenum Press.

WOŹNIAK, P., WYRZYKOWSKI, L. & BELOKUROV, V. (2012). Classification of variable objects in massive sky monitoring surveys. In: WAY, M. J., SCARGLE, J. D., ALI, K. M. & SRIVASTAVA, A. V. (Eds). *Advances in Machine Learning and Data Mining for Astronomy*. Boca Raton: CRC Press.

WRIGHT, S. L., ULKE, J., FONT, A., CHAN, K. L. A. & KELLY, F. J. (2020). Atmospheric microplastic deposition in an urban environment and an evaluation of transport. *Environmental International*. 136. pp. 105411. (Online). Available from: https://doi.org/10.1016/j.envint.2019.105411. [Accessed: 10/20/2020].

WRIGHT, S., THOMPSON, R. & GALLOWAY, T. (2013). The physical impacts of microplastics on marine organisms: a review. *Environmental Pollution*. 178. pp. 483-492. (Online). Available from: http://dx.doi.org/10.1016/j.envpol.2013.02.031. [Accessed: 01/12/2017].

WU, F., REDING, L., STARKENBURG, M., LEISTENSCHNEIDER, C., PRIMPKE, S., VIANELLO, A., ZONNEVELD, K. A. F. HUSERBEÅTEN, M. B. O., VERSTEEGH, G. J. M. & GERDTS, G. (2024). Spatial distribution of small microplastics in the Norwegian Coastal Current. *Science of the Total Environment*. 942. pp. 173808. (Online). Available from: https://doi.org/10.1016/j.scitotenv.2024.173808. [Accessed: 10/06/2025].

XI, I. L., ZHAO, Y., WANG, R., CHANG, M., PURKAYASTHA, S., CHANG, K., HUANG, R. Y., SILVA, A. C., VALLIÈRES, M., HABIBOLLAHI, P., FAN, Y., ZOU, B., GADE, T., ZHANG, P. J., SOULEN, M. C., ZHANG, Z., BAI, Z.

Z. & STARVROPOULOS, S. W. (2020). Deep learning to distinguish benign from malignant renal lesions based on routine MR imaging. *Clinical Cancer Research*. 26 (8). pp. 1944-1952. (Online). Available from: https://doi.org/10.1158/1078-0432.CCR-19-0374. [Accessed: 16/05/2024].

XIE, J., GOWEN, A. & XU, J. (2024). Development of a YOLO-Guided automated microplastic detection workflow. *Social Science Research Network SSRN*. (Online). Available from: http://dx.doi.org/10.2139/ssrn.4846421. [Accessed: 18/06/2024].

XU, B., POURDEYHIMI, B. & SOBUS, J. (1993). Fiber Cross-sectional shape analysis using image processing techniques. *Textile Research Journal*. 63 (12). pp. 717-730.

XU, J., THOMAS, K. V., LUO, Z. & GOWEN, A. A. (2019). FTIR and Raman imaging for microplastics analysis: State of the art, challenges and prospects. *Trends in analytical chemistry*. 119. pp. 115629. (Online). Available from: https://doi.org/10.1016/j.trac.2019.115629. [Accessed: 02/04/2024].

XU, L., BAI, X., LI, K., ZHANG, G., ZHANG, M., HU, M., HUANG, Y. (2024). Human exposure to ambient atmospheric microplastics in a megacity: spatiotemporal variation and associate microorganism related health risk. *Environmental science and Technology*. 58 (8). pp. 3702-3713. (Online). Available from: https://doi.org/10.1021/acs.est.3c09271. [Accessed: 03/04/2024].

XU, M., YOON, S., FUENTES, A. % PARK, D. S. (2023). A comprehensive survey of image annotation techniques for deep learning. *Pattern Recognition*. 137. pp. 109347. (Online). Available from: https://doi.org/10.1016/j.patcog.2023.109347. [Accessed: 17/05/2024].

XU, Y. & GOODACRE, R. (2018). On Splitting Training and Validation Set: A Comparative, Study of Cross-Validation, Bootstrap and Systematic Sampling for Estimating the Generalisation Performance of Supervised Learning. (Online). Available from: https://doi.org/10.1007/s41664-018-0068-2. [Accessed: 17/10/2020].

YADAV, S., KATARIA, N., KHYALIA, P., ROSE, P. K., MUKHERJEE, S., SABHERWAL, H., CHAI, W. S., RAJENDRAN, S., JIANG, J. & KHOO, K. S. (2023). Recent analytical techniques and potential eco-toxicological impacts of textile fibrous microplastics (FMPs) and associated contaminates: a review. *Chemosphere*. 326. pp. 138495. (Online). Available from: https://doi.org/10.1016/j.chemosphere.2023.138495. [Accessed: 31/05/2023].

YANG, G., WANG, J., NIE, Z., YANG, H. & YU, S. (2023a). A lightweight YOLOv8 tomato detection algorithm combining feature enhancement and attention. *Agronomy*. 13 (7). (Online). Available from: https://doi.org/10.3390/agronomy13071824. [Accessed: 01/03/2024].

YANG, J., MONNOT, M., ASIA, L., WONG-WAH-CHUNG, P., DOUMENQ, P. & MOULIN, P. (2023c). *Water research*. 232. pp. 119711. (Online). Available from: https://doi.org/10.1016/j.watres.2023.119711. [Accessed: 08/05/2025].

YANG, P., BURNS, G. R., GUO, J., LUK, T. S. & VAWTER, A. (2012). Femtosecond laser-pulse-induced birefringence in optically isotropic glass. *Journal of applied Physics*. 95 (10). pp. 5280-5283. (Online). Available from: http://dx.doi.org/10.1063/1.1707231. [Accessed: 04/11/2019].

YANG, Y., XIE, E., DU, Z., HAN, Z., LI, L., ZHAO, R., QIN, Y., XUE, M., LI, F., HUA, K. & YANG, X. (2023b). Detection of various microplastics in patents undergoing cardiac surgery. *Environmental Science and Technology*. 57 (30). pp. 10911-10918. (Online). Available from: https://doi.org/10.1021/acs.est.2c07179. [Accessed: 05/05/2014].

YIN, L., WEN, X., HUANG, D., ZHOU, Z., XIAO, R., DU, L., SU, H., HONG, W., TIAN, Q., TANG, Z. & GAO, L. (2022). Abundance, characteristics, and distribution of microplastics in the Xianjiang river, China. *Gindwana Research*. 107. pp. 123-133. (Online). Available from: https://doi.org/10.1016/j.gr.2022.01.019. [Accessed: 10/05/2022].

YING, X. (2019). An overview of overfitting and its solutions. *Journal of physics: Conference series*. 1168 (2). pp. 022022. (Online). Available from:

https://iopscience.iop.org/article/10.1088/1742-6596/1168/2/022022/meta. [Accessed: 17/02/2024].

YU, Y., WANG, C., FU, Q., KOW, R., HUANG, F., YANG, B., YANG, T. & GAO, M. (2023). Techniques and challenges of image segmentation: a review. *Electronics*. 12 (5). pp. 103390. (Online). Available from: https://doi.org/10.3390/electronics12051199. [Accessed: 14/05/2024].

ZAKI, M. R. M., YING, P. X., ZAINUDDIN, A. H., RAZAK, M. R. & ARIS, A. Z. (2021). Occurrence, abundance, and distribution of microplastics pollution: evidence in surface tropical water of Klang River estuary, Malaysia. *Environmental Geochemistry and Health*. 43 (9). pp. 3733-3748. (Online). Available from: https://doi.org/10.1007/s10653-021-00872-8. [Accessed: 06/07/2022].

ZANERO, S. & SAVARESI, S. (2004). Unsupervised learning techniques for an intrusion detection system. *Proceedings of the ACM symposium in Applied computing.* Cyprus. (Online). Available from: https://doi.org/10.1145/967900.967988. [Accessed: 18/02/2019].

ZETTLER, E. R., MINCER, T. J. & AMARAL-ZETTER, L. A. (2013). Life in the “Plastisphere”: Microbial communities on plastic marine debris. *Environmental Science and Technology*. 47 (13). pp. 7137-7146.

ZHANG, D., WU, C., LIU, Y., LI, W., LI, S., PENG, S., KANG, L., ULLAH, S., GONG, Z., LI, Z., DING, D., JIN, Z. & HUANG, H. (2024). Microplastics are detected in human gallstones and have the ability to form large cholesterol-microplastic heteroaggregates. *Journal of Hazardous Materials*. 467. pp. 133631. (Online). Available from: https://doi.org/10.1016/j.jhazmat.2024.133631. [Accessed: 09/06/2024].

ZHANG, L., XU, B., WEI, Z., LIANG, X., CHEN, Y., RU, X., ZHANG, Q. & ZHONG, S. (2025). Atmospheric Microplastic Deposition in Guilin Karst Wetlands: Sources and Agricultural Impact. *Atmospheric Pollution*. (Online). Available from https://doi.org/10.1016/j.apr.2025.102537. [Accessed:16/04/2025].

ZHANG, M., LIU, T., ZHANG, L., HUA, Z., GUO, Z., DONG, J., TAN, Q., XIE, Y., YIN, X., PAN, G. & SUN, W. (2024). Assessment of microplastic exposure in naval lavage fluid and the influence of face masks. *Journal of hazardous materials*. 480. pp. 136069. (Online). Available from: https://doi.org/10.1016/j.jhazmat.2024.136069. [Accessed: 17/04/2025].

ZHANG, Y., LU, J., WU, J., WANG, J. & LUO, Y. (2020). Potential risks of microplastics combined with superbugs: Enrichment of antibiotic resistant bacteria on the surface of microplastics in mariculture system. *Ecotoxicology and Environmental safety*. 187. pp. 109852. (Online). Available from: https://doi.org/10.1016/j.ecoenv.2019.109852. [Accessed: 13/08/2023].

ZHAO, Q., ZHU, L., WENG, J., CAO, Y., JIANG, H & ZHANG, Z. (2023). Detection and characterisation of microplastics in the human testis and semen. *Science of the Total Environment*. 877. pp. 162713. (Online). Available from: http://dx.doi.org/10.1016/j.scitotenv.2023.162713. [Accessed: 07/06/2024].

ZHOU, C., KUTTAL, S. K. & AJMED, I. (2018). What makes a good developer? An empirical study of developers' technical and social competencies. *Proceedings of IEEE Symposium on Visual Languages and Human-Centric Computing.* Lisbon. 1-04 October. (Online). Available from: https://ieeexplore.ieee.org/abstract/document/8506577. [Accessed: 28/09/2022].

ZHOU, Y., CAO, Y., HUANG, J., DENG, K., MA, K., ZHANG, T., CHEN, L., ZHANG, J. & HUANG, P. (2020). Research advances in forensic diatom testing. *Forensic science research*. 5 (2). pp. 98-105. (Online). Available from: https://ieeexplore.ieee.org/document/8506577. [Accessed: 28/09/2022].

ZHU, L., ZHU, J., ZUO, R., XU, Q., QIAN, Y. & AN, L. (2023). Identification of microplastics in human placenta using laser direct infrared spectroscopy. *Science of the Total Environment.* 856. pp. 159060. (Online). Available from: http://dx.doi.org/10.1016/j.scitotenv.2022.159060. [Accessed: 07/06/2024].

ZIABICKI, A. (1976). *Fundamentals of fibre formation: the science of fibre spinning and drawing*. Hoboken: John Wiley & Sons.

ZIAJAHROMI, S., NEALE, P. A., RINTOUL, L. & LEUSCH, F. D. L. (2017). Wastewater treatment plants as a pathway for microplastics: Development of a new approach to sample wastewater-based microplastics. *Water Research*. 112. pp. 93-99. (Online). Available from: http://dx.doi.org/10.1016/j.watres.2017.01.042. [Accessed: 18/09/2018].

ZINCHUK, V. & GROSSENBACHER-ZINCHUK, O. (2020). Machine learning for analysis of microscopy images: A practical guide. *Current protocols in cell biology*. 86 (1). pp. 1-14. (Online). Available from: https://doi.org/10.1002/cpcb.101. [Accessed: 16/01/2023].

Appendix

Appendix A – Supplementary Resources

Appendix A.1 – R Code

Figure 3.9 code

```
boxplot(Widths_csv$Stereo, Widths_csv$PLM, main = "A boxplot to show approximate width of microplasics in ?m", names = "Stereomicroscope", "Polarised light microscope", ylab = "Width of microplastics (?m)")")
```

Logistic regression code

```
 sapply (LRdata,function(x) sum(is.na(x)))

data <- subset(LRdata, select=c(1,6,7,8,10,16))

data[data$`MP type` == "blue",]$'MP type' <- "Fibre"

data[data$`MP type` == "Blue",]$'MP type' <- "Fibre"

data[data$Delusterant == "N",]$'Delusterant' <- "N/A"

data[data$Delusterant == "L",]$'Delusterant' <- "Low"

data[data$Delusterant == "M",]$'Delusterant' <- "Medium"

data[data$Delusterant == "H",]$'Delusterant' <- "High"
```

```
data[data$`cross sectional shape` == "Hair (animal)",]$'cross sectional shape' <-
"Cylindrical"

data[data$Identification == "Hair (Human)",]$'Identification' <- "Hair"

data[data$Identification == "Hair (Animal)",]$'Identification' <- "Hair"

data[data$Identification == "Hair (Textile)",]$'Identification' <- "Hair"

data[data$Colour == "Purple",]$'Colour' <- "Pink"

data[data$Colour == "Grey",]$'Colour' <- "Black"

data[data$Colour == "Orange",]$'Colour' <- "Yellow"

data$Method <- as.factor(data$Method)

data$`MP type` <- as.factor(data$`MP type`)

data$Colour <- as.factor(data$Colour)

data$`cross sectional shape` <- as.factor(data$`cross sectional shape`)

data$Delusterant <- as.factor(data$Delusterant)

data$Identification <- as.factor(data$Identification)

str(data)

Logistics <- glm(Method ~ ., data = data, family= "binomial")

summary(Logistics)

Call:

  glm(formula = Method ~ ., family = "binomial", data = data)

ll.nul <-Logistics$null.deviance/-2

ll.proposed <-Logistics$deviance/-2

pseudo r2

(ll.nul - ll.proposed)/ll.nul

0.1950978

1- pchisq(2*(ll.proposed - ll.nul), df=(length(Logistics$coefficients)-1))
```

```
[1] 0
```

```
predicted.dataAllC <- data.frame(probability.of.Method=Logistics$fitted.values, Method=
data$Method)
```

```
predicted.dataAllC <- predicted.dataAllC[order(predicted.dataAllC$probability.of.Method,
decreasing = FALSE),]
```

```
predicted.dataAllC$rank <- 1:nrow(predicted.dataAllC)
```

Figure 3.10 code

```
ggplot(data = predicted.dataAllC, aes(x=rank, y=probability.of.Method)) +
geom_point(aes(colour=Method), alpha=1, shape=4, stroke=2) + xlab("Index") +
ylab("Predicted probability of being detected with Stereomicroscopy")
```

Appendix A.2 Standard operating procedure of the use of Easylift®

1. Easylift®.

Easylift® was developed at Staffordshire University as a method of retrieval of forensic fibres from crime scenes. As the tape is non-Birefringent it allows the fibres to be analysed with a polarised light microscope in situ, preventing contamination and loss of samples. Easylift® has also been applied to retrieval of microplastics from filter paper to maximise sample retrieval and protect the samples from any further contamination.

2. Filter paper selection.

Easylift® is suitable for use on microfibre filter paper such as cellulose or glass filter papers, it is not suitable for use on membrane filter papers as it will rip the filter paper when lifted.

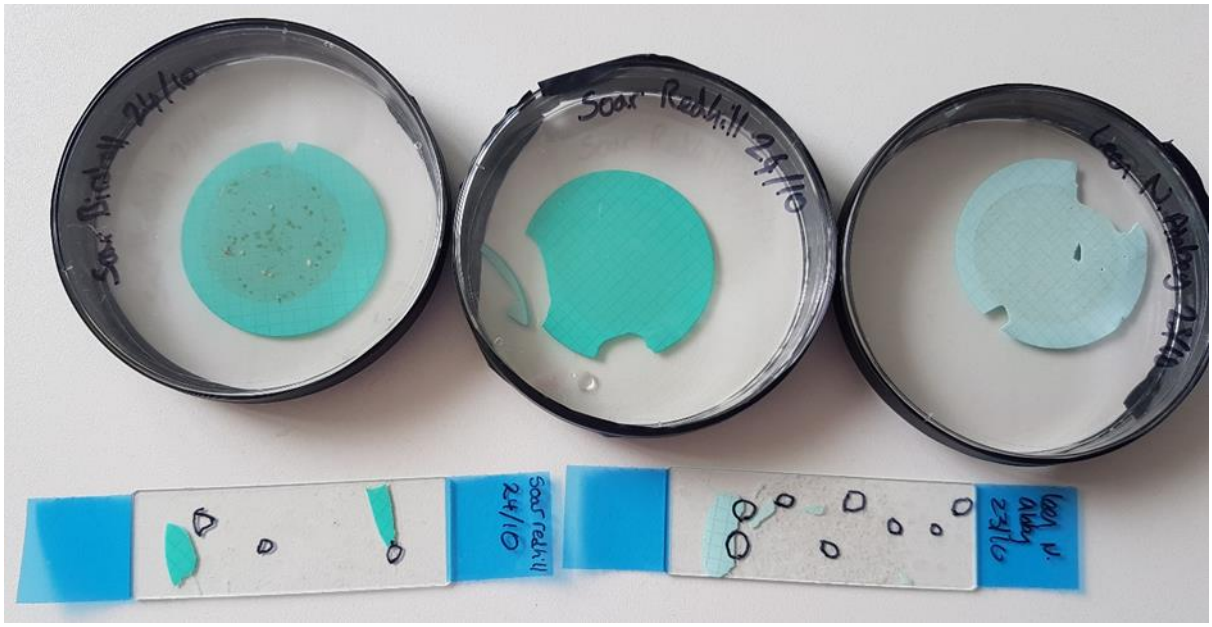

Figure A.1 from left to right: Nitrocellulose filter paper that has been filtered dry and tape lifted with Easylift®, damp filter paper after Easylift®, dry filter paper after Easylift®, and examples of the Easylift®, tape after retrieval of microplastics.

3. <u>Preparation of filter paper.</u>

Easylift® is most effective at retrieving microplastic samples whilst recovering a minimal number of fibres from the filter paper when it is tape lifted immediately or soon after filtration of the sample so that the filter paper is slightly damp. If the filter paper is dry during recovery, it will retrieve a large number of filter paper fibres, potentially masking any potential microplastics.

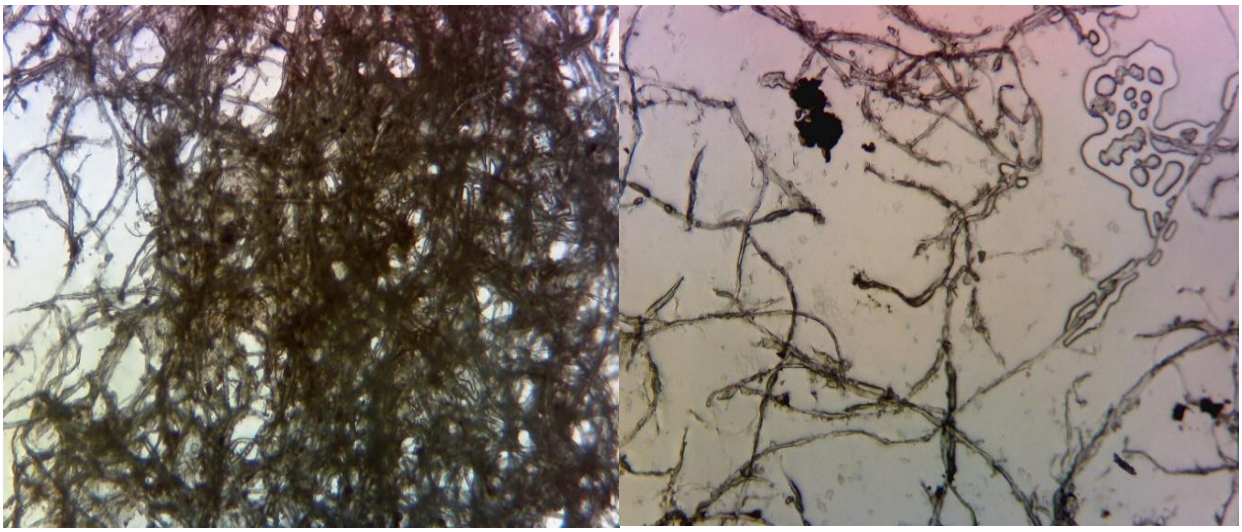

Figure A.2 An example of an overloaded Easylift® tape retrieved when the filter paper was dry (left) and an example of a tape taken whilst the filter paper was damp (right).

4. Retrieval of microplastics from the filter paper.

Before using Easylift® observe the tape under the microscope to ensure that there is no contamination on the tape.

Carefully peel the back of off the Easylift® by holding on to one of the blue tabs at either end of the tape and carefully pulling it away from the protective backing. Once removed hold each end of the tape pulling it taught, gently place Easylift® on one side of the filter paper and press on the tape where it is over the filter paper to ensure good adhesion, then lift the tape and place it down again so that there is a small overlap with the previous area tape lifted. This is repeated until the entire surface of the filter paper has been tape lifted by Easylift® maximising recovery of any microplastics present on the surface. If the filter paper is particularly laden with debris or microplastics it may be beneficial to use multiple tapes of Easylift® to prevent the tape from becoming overloaded and making later analysis easier. Once you have finished tape lifting from the filter paper the Easylift® can then adhere to a clean glass microscope slide for storage and analysis. The sample name can be written on the blue tabs and you can mark on the slide where fibres of interest are with a marker pen.

Figure A.3 A completed Easylift® tape lift with microplastics marked onto the tape.

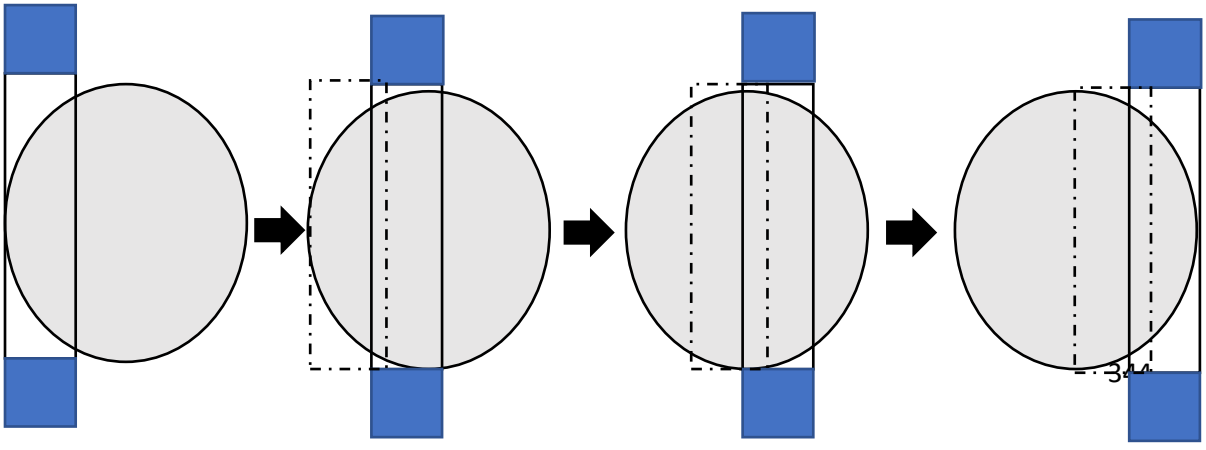

Figure A.4 A diagram to show how to effectively tape lift the entire surface of the filter paper, with the previous location of Easylift® demonstrated by the dashed lines.

5. Use of a mounting agent.

A mounting agent such as DEPEX can be used alongside Easylift® to ensure good adhesion of the tape to the microscope slide, this is particularly useful in situations where there is a lot of debris and background material on the surface of Easylift® which may affect its adhesion to the slide. Apply mounting agent to the microscope slide and spread it across the surface of the slide to ensure even coverage, after this apply Easylift® on top of the mounting agent and press down spreading the mounting agent out further and removing any air bubbles that may be present, leave the mounting agent to dry for 24 hours.

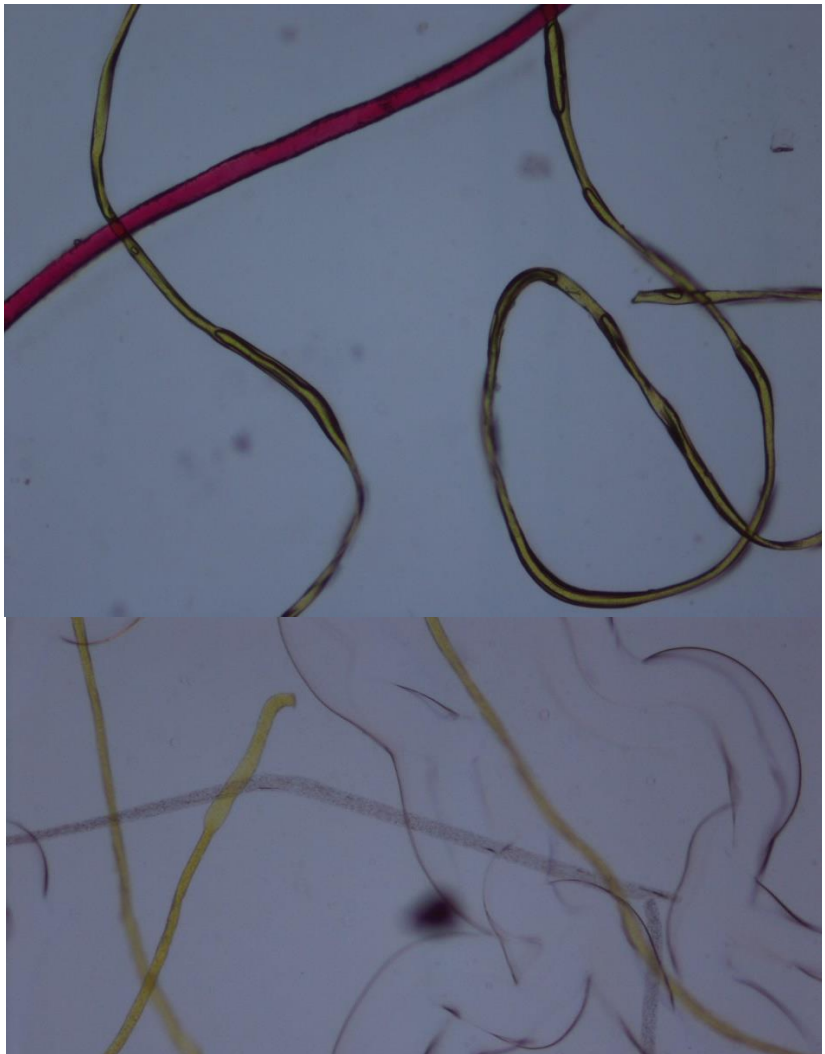

Appendix A.3 – Additional Tables and Figures.

Chapter 2

Table A.1 full results from the piolet study in chapter 2 N= number.

Sample	N fibres used	N fibres retrieved by filter paper	% fibres recovered by filter paper	N fibres retrieved by Easylift®	% fibres retrieved by Easylift®	Overall % recovered
1	/	55	/	51	92.7	/
2	25	24	96	24	96	96
3	26	14	54	13	92.9	50
4	25	25	100	25	100	100
5	25	21	84	21	100	84
6	25	17	68	17	100	68
7	25	25	100	24	96	96
8	25	22	88	22	100	88
9	25	20	80	20	100	80
10	25	21	84	21	100	84
11	25	17	68	17	100	68
12	25	17	68	17	100	68
13	25	25	100	25	100	100
14	25	19	76	19	100	76
15	25	25	100	25	100	100
Overall			78		99	76

Table A.2 A table to show the amount of moisture cellulose filter paper and glass filter paper contain after being left in a 105°C oven for 16 hours.

	Cellulose			Glass		
	before	after	difference	before	after	difference
1	0.6848	0.6673	0.0175	0.1929	0.1932	0.003
2	0.6713	0.6583	0.013	0.1928	0.1913	0.0015
3	0.6724	0.6583	0.0141	0.1975	0.1932	0.0043
4	0.667	0.6508	0.0162	0.1907	0.1908	0.0001
5	0.6886	0.6767	0.0119	0.1901	0.188	0.0021
6	0.6536	0.6386	0.015	0.1926	0.1932	0.006
7	0.6792	0.668	0.0112	0.1951	0.1949	0.0004
8	0.6598	0.6474	0.0124	0.1921	0.1921	0
9	0.6915	0.6792	0.0123	0.1934	0.1926	0.0008
10	0.6679	0.6566	0.0113	0.1921	0.192	0.0001
11	0.6825	0.6692	0.0133	0.1916	0.191	0.0006
12	0.6579	0.6503	0.0076	0.1895	0.1893	0.0002
13	0.6889	0.6824	0.0065	0.1888	0.1885	0.0003
14	0.6789	0.6701	0.0088	0.1885	0.1893	0.0008

15	0.6704	0.6563	0.141	0.1891	0.1886	0.0004
16	0.6898	0.687	0.0028	0.1912	0.1915	0.0003
17	0.6755	0.6685	0.007	0.1905	0.1903	0.0002
18	0.671	0.657	0.014	0.1934	0.1921	0.0013
19	0.6619	0.6478	0.0141	0.1911	0.1909	0.0002
20	0.6798	0.6646	0.0152	0.1894	0.1899	0.0005

Table A.3 Full results for main study of Chapter 2 N= number.

Sample	N fibres used	N fibres on the filter paper	% of fibres recovered by the filter paper	N fibres retrieved from the filter paper with Easylift®	% fibres recovered from the filter paper with Easylift®	Overall % recovered
Condition Cellulose filter paper and Buchner filtration						
1	192	175	91.1	175	98.9	88.5
2	239	221	92.5	220	99.5	92.1
3	198	188	95.0	186	98.9	93.9
Total			92.9		99.1	91.5
Condition Glass filter paper with Buchner filtration						
1	394	362	91.9	322	89.0	81.7
2	121	98	81.0	90	91.8	74.4
3	204	182	89.2	169	92.9	82.8
Total			89.3		90.5	80.8
Condition Cellulose filter paper with Glass frit						
1	171	159	93.0	156	98.1	91.2
2	164	157	95.7	156	99.4	95.1
3	181	169	93.4	169	100	93.4
Total			94.0		99.2	93.2
Condition Glass filter paper with Glass frit						
1	182	164	90.1	156	95.1	86.2
2	202	193	95.5	190	98.5	94.5
3	159	153	96.2	147	96.1	92.5
Total			93.9		96.7	90.8

A)

Filter type and funnel type	W	p
Cellulose and Ceramic	0.92547	0.4719
Glass fibre and Ceramic	0.92933	0.4861
Cellulose and Glass	0.96602	0.6459
Glass fibre and Glass	0.94335	0.5410

B)

Filter type and funnel type	W	p
Cellulose and Ceramic	0.97003	0.6677
Glass fibre and Ceramic	0.91997	0.4522
Cellulose and Glass	0.85337	0.2495
Glass fibre and Glass	0.83246	0.1946

Figure A.6 The results of the Shapiro wilks tests conducted on each of the four subsets of the recovered-on tape lift (A) and recovered on filter (B) unique level combinations of filter type and funnel type. Produced by Professor Andrew Jackson.

```
Levene's Test for Homogeneity of Variance (center = median)
      Df F value Pr(>F)
group  3  0.5907 0.6382
       8
```

Figure A.7 the results of the Levene's test for homogeneity of Variance for the data from Chapter 2. Produced by Professor Andrew Jackson.

Chapter 3

Table A.4 A table to show the full data used in Chapter 3, to show the results after stereomicroscopy, after PLM the increase and how many misidentifications there were per sample.

Found by Stereomicroscopy	Found by PLM	Difference	Misidentifications
4	10	6	1
1	3	4	3
3	10	7	1
7	12	5	2
4	5	1	0
3	7	4	3
7	11	4	4
3	7	4	6
3	5	2	1
4	8	4	1
0	0	0	6
3	5	2	2
7	7	0	7
2	4	2	4
9	11	2	5
3	6	3	2
3	5	3	4
3	6	3	2
3	7	4	2
8	10	2	2
10	11	1	4
3	5	2	0
8	10	2	1
5	7	2	3
6	8	2	2
4	4	0	2
3	4	1	0
11	15	4	3
17	20	3	1
11	12	1	7
8	10	2	4
6	7	1	5
4	5	1	2
5	7	2	2
10	10	0	2
1	2	1	6
5	7	2	2
2	4	2	1

8	9	1	5
2	6	4	1
12	12	1	1
10	12	2	7
11	13	2	4
8	9	1	2
1	2	1	6
4	4	0	0
5	5	0	3
6	7	1	2
8	8	0	1
6	7	1	1
3	3	0	4
5	9	4	2
5	5	0	0
2	4	2	1
15	16	1	0
11	11	0	4
8	9	1	3
3	4	1	9
6	7	1	6
7	11	4	4
12	12	0	5
7	7	0	1
12	14	2	4
6	8	2	4
11	11	0	4
21	23	2	5
4	5	1	0
2	5	3	1
7	7	0	0
7	8	1	1
6	6	0	3
8	9	1	5
8	10	2	7
4	4	0	4
6	6	0	1
4	5	1	2
12	14	2	3
10	12	2	2
3	4	1	7
5	6	1	2
4	5	1	4
7	7	0	8
12	14	2	3
5	7	2	0

1	8	7	1
5	6	1	2
4	4	0	4
4	7	3	0
4	9	5	3
6	7	1	5
4	4	0	1
3	4	1	5
8	10	2	9
3	9	6	21
5	6	1	20
3	5	2	13
12	16	4	1
6	10	4	2
3	6	3	25
7	10	3	30
6	6	0	25
7	11	4	6
4	8	4	0
3	5	2	35
3	5	2	42
3	4	1	28
13	17	4	4
3	6	3	6
4	6	2	32
3	3	0	37
3	8	5	26
5	8	3	3
5	7	2	4
3	5	2	37
6	11	5	3
3	7	4	1
6	7	1	35
4	4	0	32
1	5	4	35
7	12	5	3
3	6	3	6
1	1	0	38
8	10	2	50
5	7	2	2
10	19	9	4
2	3	1	38
2	3	1	36
4	8	4	1
6	9	3	1
6	6	0	29

3	6	3	28
3	7	4	30
5	8	3	2
6	9	3	2
3	4	1	12
5	6	1	24
5	7	2	27
6	9	3	0
3	5	2	3
7	7	0	6
6	8	2	4
8	10	2	30
3	8	5	0
9	13	4	10
7	9	2	3
11	14	3	10
8	8	0	7
4	7	3	3
4	8	4	0
6	7	1	4
3	6	3	1
0	2	0	2
7	9	2	2
4	9	5	0
5	5	0	3
6	6	0	7
9	10	1	4
6	14	8	0
3	11	8	6
9	9	0	3
9	10	1	6
4	5	1	13
2	9	7	1
2	8	6	1
3	4	1	1
4	4	0	1
5	5	0	2
2	10	8	2
1	8	7	0
5	5	0	1
6	7	1	1
6	7	1	3
4	12	8	1
4	13	9	0
7	9	2	27
5	6	1	44

2	4	2	43
1	13	12	0
4	9	5	3
5	9	4	33
6	8	2	40
3	6	3	44
4	13	9	0
7	14	7	1
6	7	1	4
11	12	1	7
4	6	2	5
0	4	4	0
10	15	5	6
10	11	1	6
5	6	1	9
6	7	1	2
7	16	9	1
3	7	4	1
1	1	0	3
7	10	3	6
3	5	2	2
7	16	9	0
11	16	5	2
4	6	2	2
9	11	3	1
3	6	3	0
1	6	5	1
2	5	3	1
5	5	0	2
2	3	1	7
6	7	1	3
1	6	5	1
3	9	6	0
5	5	0	2
2	3	1	1
6	6	0	4
5	15	10	1
6	10	4	0
11	11	0	4
9	10	1	1
4	5	1	8
4	7	3	8
6	7	1	3
12	12	0	7
4	7	3	4
1	2	1	3

14	15	1	2
6	8	2	47
8	10	2	55
7	7	0	27
4	4	0	1
4	4	0	3
8	10	2	3
15	15	0	7
7	9	2	4
6	6	0	8
8	8	0	7
4	5	1	10
3	3	0	4
3	3	0	9
1	1	0	4
2	3	1	3
4	4	0	2
5	6	1	16
4	4	0	3
6	7	1	14
3	3	0	9
3	4	1	5

Table A.5 A table to show the full characterisation of results found by stereomicroscopy.

Sample type	MP type	Colour	cross sectional shape	Deluster ant	Other inclusions	Width µm	Length µm	sign of elongation	Birefringence	Identification
W	Fibre	Black	Ribbon	N	N					Cotton
W	Fibre	Blue	Ribbon	N	N					Cotton
W	fibre	colourless	Cylindrical	N	N					Hair (Human)
W	fibre	colourless	Ribbon	N	N					Cotton
W	fibre	blue	Ribbon	N	N					Cotton
W	fibre	colourless	Cylindrical	N	N	10.68	801	N		Synthetic
W	fibre	red	Ribbon	N	N					Cotton
W	fibre	colourless	Ribbon	N	N					Cotton
W	fibre	blue	Cylindrical	N	N					Anthropogenic
W	fibre	colourless	Cylindrical	N	N					Hair (Textile)
W	fibre	colourless	Cylindrical	N	N					Hair
W	fibre	colourless	Cylindrical	N	N	10.68	747.6	P	0.034	Polypropylene
W	fibre	pink	Ribbon	N	N					Cotton
W	fibre	blue	Ribbon	N	N					Cotton
W	fibre	blue	Ribbon	N	N					Cotton
W	fibre	blue	Cylindrical	N	N	8.01		P	0.099	Polyester
W	fibre	black	Ribbon	N	N					Cotton
W	fibre	blue	Ribbon	N	N					Cotton
W	fibre	blue	Irregular	N	N	8.01	1473.84	P	0.081	Nylon
W	fibre	colourless/blue	Multilobal	N	N	10.68	995.1	P	>0.34	Synthetic

W	fibre	blue	Ribbon	N	N					Cotton
W	fibre	blue	Ribbon	N	N					Cotton
W	fibre	blue	Ribbon	N	N					Cotton
W	fibre	black	Ribbon	N	N					Cotton
W	fibre	blue	Cylindrical	L	N	12.015	1372.38	P	0.166	Polyester
W	fibre	blue	Cylindrical	N	N	8.01		P	0.097	Polyester
W	fibre	blue	Cylindrical	N	N					Hair (Textile)
W	fibre	red	Cylindrical	N	N	18.69	280	P	0.037	Polypropylene
W	fibre	red	Ribbon	N	N					Cotton
W	fibre	blue	Ribbon	N	N					Cotton
W	fibre	colourless	Trilobal	N	N	12.015	389.82	P	0.081	Synthetic
W	fibre	blue	Ribbon	N	N					Cotton
W	fibre	orange	Ribbon	N	N					Cotton
W	fibre	blue	Ribbon	N	N					Cotton
W	fibre	colourless	Cylindrical	N	N					Hair
W	fibre	blue	Ribbon	N	N					Cotton
W	fibre	blue	Ribbon	N	N					Cotton
W	fibre	blue	Ribbon	N	N					Cotton
W	fibre	blue	Ribbon	N	N					Cotton
W	fibre	blue	Ribbon	N	N					Cotton
W	fibre	blue	Ribbon	N	N					Cotton
W	fragment	blue		N	N					Synthetic
W	fragment	colourless		N	N					Synthetic
W	fibre	black	Ribbon	N	N					Cotton
W	fibre	black	Ribbon	N	N					Cotton
W	fibre	black	Ribbon	N	N					Cotton
W	fibre	blue	Ribbon	N	N					Cotton
W	fibre	blue	Ribbon	N	N					Cotton
W	fragment	blue		N	N					Polypropylene
W	fragment	blue		N	N					Synthetic
W	fibre	blue	Ribbon	N	N					Cotton
W	fibre	blue	Cylindrical	N	N	8.01	814.35		0.087	Synthetic
W	fibre	blue	Ribbon	N	N					Cotton
W	fibre	blue	Cylindrical	N	N	13.35	293.7			Synthetic
W	fibre	blue	Ribbon	N	N					Cotton
W	fibre	blue	Cylindrical	N	N	8.01		P	0.099	Polyester
W	fibre	blue	Ribbon	N	N					Cotton
W	fibre	blue	Ribbon	N	N					Cotton
W	fibre	colourless	Cylindrical/Irregular	N	N	9.88	1617.85			UNKN
W	fibre	colourless	Ribbon	N	N					Cotton
W	fibre	blue	Ribbon	N	N					Cotton
W	fibre	blue	Ribbon	N	N					Cotton
W	fibre	blue	Ribbon	N	N					Cotton
W	fibre	red	Ribbon	N	N					Cotton
W	fibre	black	Ribbon	N	N					Cotton
W	fibre	colourless	Irregular	N	N	86.45	2754.05	P	>0.036	Synthetic

W	fibre	blue	Ribbon	N	N					Cotton
W	fragment	red		N	N					Synthetic
W	fibre	blue	Ribbon	N	N					Cotton
W	fibre	blue	Ribbon	N	N					Cotton
W	fibre	red	Ribbon	N	N					Cotton
W	fibre	red	Cylindrical	N	N	9.88	988	P	0.061	Nylon
W	fibre	black	Ribbon	N	N					Cotton
W	fibre	blue	Ribbon	N	N					Cotton
W	fragment	red		N	N					Synthetic
W	fibre	blue	Cylindrical	N	N					Hair (Textile)
W	fibre	blue	Ribbon	N	N					Cotton
W	fibre	blue	Ribbon	N	N					Cotton
W	fibre	red	Ribbon	N	N					Cotton
W	fibre	blue	Ribbon	N	N					Cotton
W	fibre	blue	Ribbon	N	N					Cotton
W	fibre	blue	Ribbon	N	N					Cotton
W	fibre	colourless	Ribbon	N	N					Cotton
W	fibre	blue	Ribbon	N	N					Cotton
W	fibre	yellow	Irregular	N	stripes	32.11	923.78		>0.098	Polyester
W	fibre	blue	Ribbon	N	N					Cotton
W	fibre	colourless/blue	Cylindrical	N	N	7.41	382.85	P	0.094	Polyester
W	fibre	brown	Cylindrical	N	N					Hair (Human)
W	fibre	blue	Ribbon	N	N					Cotton
W	fibre	blue	Ribbon	N	N					Cotton
W	fibre	blue	Ribbon	N	N					Cotton
W	fibre	colourless	multilobed	N	N	17.29	864.5	P		Synthetic
W	fibre	Colourless/blue	Ribbon	N	N					Cotton
W	fibre	blue	Ribbon	N	N					Cotton
W	fibre	Colourless/blue	Ribbon	N	N					Cotton
W	fibre	blue	Cylindrical	N	N	7.41	284.05	P	0.148	Polyester
W	fibre	colourless	Hair (animal)	N	N					Hair (Textile)
W	fibre	blue	Ribbon	N	N					Cotton
W	fragment	blue		N	N					Synthetic
W	fibre	black	Ribbon	N	N					Cotton
W	fibre	blue	Cylindrical	N	N					Hair (Textile)
W	fibre	black	Ribbon	N	N					Cotton
W	fibre	blue	Ribbon	N	N					Cotton
W	fibre	colourless	Cylindrical	M	N	10.68	234.65	P	0.051	Polyethylene/ Nylon
W	fibre	Colourless/blue	Bilobal	N	N	12.35		P	0.049	Polyethylene/ Nylon
W	fibre	blue	Ribbon	N	N					Cotton
W	fibre	blue	Ribbon	N	N					Cotton
W	fibre	black	Ribbon	N	N					Cotton
W	fragment	colourless		N	N					Synthetic
W	fibre	blue	Ribbon	N	N					Cotton
W	fragment	blue		N	N					Nylon
W	fibre	red	Ribbon	N	N					Cotton

W	fibre	blue	Ribbon	N	N					Cotton
W	fibre	black	Ribbon	N	N					Cotton
W	fibre	blue	Ribbon	N	N					Cotton
W	fibre	blue	Ribbon	N	N					Cotton
W	fibre	red	Ribbon	N	N					Cotton
W	fibre	blue	Ribbon	N	N					Cotton
W	fibre	blue	Ribbon	N	N					Cotton
W	fragment	red		N	N					Polyester
W	fibre	red	Ribbon	N	N					Cotton
W	fibre	blue	Ribbon	N	N					Cotton
W	fragment	red		N	N					Synthetic
W	fibre	blue	Cylindrical	L	N	9.88	691.9	P	0.081	Synthetic
W	fibre	blue	Cylindrical	L	N	9.88	1642.55	P	0.091	Polyester
W	fibre	black	Ribbon	N	N					Cotton
W	fibre	black	Cylindrical	N	N	12.35	518.7			Synthetic
W	fibre	blue	Ribbon	N	N					Cotton
W	fibre	blue	Ribbon	N	N					Cotton
W	fibre	blue	Ribbon	N	N					Cotton
W	fibre	blue	Cylindrical	L	N	9.88		P	0.091	Polyester
W	fibre	blue	Ribbon	N	N					Cotton
W	fibre	red	Cylindrical	L	N	14.82	2754.05	P	0.101	Polyester
W	fibre	black	Ribbon	N	N					Cotton
W	fibre	blue	Ribbon	N	N					Cotton
W	fibre	blue	Ribbon	N	N	2.47				Cotton
W	fibre	blue	Ribbon	N	N					Cotton
W	fibre	red	Ribbon	N	N					Cotton
W	fragment	blue		N	N					Synthetic
W	fibre	blue	Ribbon	N	N					Cotton
W	fibre	blue	Ribbon	N	N					Cotton
W	fragment	blue		N	N					Synthetic
W	fibre	red	Cylindrical	L	N	7.41	370.5	P	0.094	Polyester
W	fibre	blue	Ribbon	N	N					Cotton
W	fibre	blue	Ribbon	N	N					Cotton
W	fibre	blue	Ribbon	N	N					Cotton
W	fragment	blue		N	N					Synthetic
W	fibre	blue	Cylindrical	L	N	7.41		P	0.148	Polyester
W	fragment	blue		N	N					Synthetic
W	fibre	grey	Ribbon	N	N					Cotton
W	fibre	blue	Ribbon	N	N					Cotton
W	fibre	blue	Cylindrical	L	N	7.41	1778.4	P	0.094	Polyester
W	fibre	blue	Ribbon	N	N					Cotton
W	fragment	yellow/red/blue		N	N					Synthetic
W	fibre	blue	Ribbon	N	N					Cotton
W	fibre	blue	Ribbon	N	N					Cotton
W	fragment	blue		N	N					Synthetic
W	fibre	blue	Ribbon	N	N					Cotton

W	fibre	red	Ribbon	N	N					Cotton
W	microbead	blue		N	N					Polyester
W	fragment	red		N	N					Synthetic
W	fibre	black	Ribbon	N	N					Cotton
W	fibre	black	Ribbon	N	N					Cotton
W	fibre	black	Irregular	N	N	12.35				Synthetic
W	fibre	red	Ribbon	N	N					Cotton
W	fragment	blue		N	N					Polypropylene
W	fibre	blue	Ribbon	N	N					Cotton
W	fibre	blue	Ribbon	N	N					Cotton
W	fibre	blue	Ribbon	N	N					Cotton
W	fibre	blue	Ribbon	N	N					Cotton
W	fibre	blue	Ribbon	N	N					Cotton
W	fragment	blue		N	N					Synthetic
W	fragment	blue		N	N					Synthetic
W	fibre	black	Ribbon	N	N					Cotton
W	fibre	blue	Ribbon	N	N					Cotton
W	fibre	blue	Cylindrical	N	N	14.82	135.85	P	0.168	Polyester
W	fibre	blue	Ribbon	N	N					Cotton
W	fibre	black	Irregular	N	N	19.78	2272.4	P	0.051	Polyethylene/ Nylon
W	fibre	blue	Bilobal	N	N	9.88	518.7	P	0.085	Synthetic
W	fibre	blue	Ribbon	N	N					Cotton
W	fibre	blue	Cylindrical	L	N	7.41		P	0.148	Polyester
W	fibre	blue	Cylindrical	N	N	9.88		P	0.096	Polyester
W	fragment	blue		N	N					Synthetic
W	fibre	blue	Ribbon	N	N					Cotton
W	fibre	colourless	Cylindrical	N	N	16.055	980.58	N	0.004	Acrylic
W	fibre	blue	Ribbon	N	N					Cotton
W	fibre	blue	Cylindrical	H	N	12.35		P	0.065	Nylon
W	fibre	red	Ribbon	N	N					Cotton
W	fibre	blue	Ribbon	N	N					Cotton
W	fragment	blue		N	N					Synthetic
W	fibre	blue	Ribbon	N	N					Cotton
W	fragment	blue		N	N					Synthetic
W	fibre	red	Cylindrical	N	N	14.82	741	P	0.067	Nylon
W	fibre	blue	Ribbon	N	N					Synthetic
W	fibre	colourless	Cylindrical	N	N					Hair (Human)
W	fibre	blue	Ribbon	N	N					Cotton
W	fragment	blue		N	N					Synthetic
W	fibre	blue	Ribbon	N	N					Cotton
W	fibre	blue	Ribbon	N	N					Cotton
W	fibre	blue	Cylindrical	N	N	9.88	531.05	P	0.096	Polyester
W	fibre	blue	Ribbon	N	N					Cotton
W	fibre	red	Ribbon	N	N					Cotton
W	fibre	red	Cylindrical	L	N					Synthetic
W	fibre	blue	Ribbon	N	N					Cotton

W	fibre	colourless	Cylindrical	N	N	12.35	904.02	P	0.161	Polyester
W	fibre	red	Cylindrical	N	N					Hair (Textile)
W	fibre	red	Ribbon	N	N					Cotton
W	fibre	black	flat	N	N	14.82	449.54	P		Polyester
W	fibre	colourless	Cylindrical	L	N	9.88		P	0.151	Polyester
W	fibre	blue	Cylindrical	L	N	9.88	308.75	P	0.081	Polyester
W	fibre	blue	Ribbon	N	N					Cotton
W	fibre	red	Ribbon	N	N					Cotton
W	fibre	blue	Cylindrical	L	N	12.35	592.8	P	0.052	Nylon
W	fibre	blue	Ribbon	N	N					Cotton
W	fibre	red	Multilobal	N	N	7.41		P		Synthetic
W	fibre	blue	Ribbon	N	N					Cotton
W	fibre	blue	Ribbon	N	N					Cotton
W	fragment	blue		N	N					Synthetic
W	fibre	blue	Ribbon	N	N					Cotton
W	fibre	red	Ribbon	N	N					Cotton
W	fibre	blue	Ribbon	N	N					Cotton
W	fragment	blue		N	N					Synthetic
W	fibre	red	Bilobal	N	N	13.59	696.54	P	0.151	Polyester
W	fibre	pink	flat	N	N	9.88		P	0.101	Polyester
W	fibre	red	Ribbon	N	N					Cotton
W	fibre	blue	Ribbon	N	N					Cotton
W	fibre	blue	Ribbon	N	N					Cotton
W	fibre	red	Ribbon	N	N					Cotton
W	fibre	blue	Ribbon	N	N					Cotton
W	fibre	blue	Ribbon	N	N					Cotton
W	fibre	black	Ribbon	N	N					Cotton
W	fragment	blue		N	N					Synthetic
W	fibre	blue	Ribbon	N	N					Cotton
W	fibre	Colourless/res	Bilobal	N	N	12.35		P	0.161	Polyester
W	fibre	blue	Ribbon	N	N					Cotton
W	fibre	red	Ribbon	N	N					Cotton
W	fibre	blue	Cylindrical	N	N	2.47		P		Synthetic
W	fragment	blue		N	N					Synthetic
W	fibre	blue	Ribbon	N	N					Cotton
W	fibre	black	Trilobal	N	N	19.76	370.5	P	0.025	Polypropylene
W	fibre	blue	Ribbon	N	N	27.17	580.45	P		Nylon
W	fragment	red		N	N					Cotton
W	fibre	blue	Ribbon	N	N					Synthetic
W	fibre	red	Ribbon	N	N					Cotton
W	fibre	blue	Ribbon	N	N					Cotton
W	fibre	blue	Ribbon	N	N					Cotton
W	fragment	blue		N	N					Synthetic
W	fibre	black	Cylindrical	N	N	17.29				Synthetic
W	fibre	black	Ribbon	N	N					Cotton
W	fragment	colourless		N	N					Synthetic

W	fibre	colourless	Cylindrical	L	N	12.35		P	0.069	Nylon
W	fragment	colourless		N	N					Synthetic
W	fibre	blue	Cylindrical	L	N	9.88		P	0.172	Polyester
W	fibre	red	Ribbon	N	N					Cotton
W	fibre	red	Ribbon	N	N					Cotton
W	fragment	blue		N	N					Polypropylene
W	fibre	blue	Cylindrical	H	N	14.82	1109	P	0.094	Polyester
W	fibre	blue	Ribbon	L	N	27.17	543.4	P		Synthetic
W	fibre	blue	Ribbon	N	N					Cotton
W	fibre	blue	Ribbon	N	N					Cotton
W	fibre	red	Ribbon	N	N					Cotton
W	fibre	blue	Ribbon	N	N					Cotton
W	fibre	colourless/blue	Multilobal	N	N	12.35		P	0.148	Polyester
W	fibre	blue	Ribbon	N	N					Cotton
W	fibre	blue	Ribbon	N	N					Cotton
W	fragment	blue		N	N					Synthetic
W	fragment	grey		N	N					Synthetic
W	fibre	blue	Ribbon	N	N					Cotton
W	fibre	blue	Ribbon	N	N					Cotton
W	fibre	blue	Ribbon	N	N					Cotton
W	fibre	blue	Ribbon	N	N					Cotton
W	fibre	blue	Ribbon	N	N					Cotton
W	fibre	blue	Ribbon	N	N					Cotton
W	fibre	red	Ribbon	N	N					Cotton
W	fibre	blue	Ribbon	N	N					Cotton
W	fibre	colourless	Cylindrical	N	N	12.35		N	0.005	Acrylic
W	fibre	blue	Ribbon	N	N					Cotton
W	fibre	blue	Ribbon	N	N					Cotton
W	fibre	blue	Bilobal	N	N	14.82	778	P		Synthetic
W	fragment	blue		N	N					Synthetic
W	fibre	red	Ribbon	N	N					Cotton
W	fibre	blue	Ribbon	N	N					Cotton
W	fragment	blue		N	N					Synthetic
W	fibre	blue	Ribbon	N	N					Cotton
W	fibre	colourless	Cylindrical	L	N	14.82	1106.56	P	0.172	Polyester
W	fragment	colourless		N	N					Synthetic
W	fibre	blue	Ribbon	N	N					Cotton
W	fibre	blue	Multilobal	N	N	13.59	1407.9	P		Nylon
W	fibre	blue	Ribbon	N	N					Cotton
W	fibre	red	Ribbon	N	N					Cotton
W	fibre	blue	Ribbon	N	N					Cotton
W	fibre	blue	Ribbon	N	N					Cotton
W	fibre	blue	Ribbon	N	N					Cotton
W	fibre	blue	Ribbon	N	N					Cotton
W	fibre	blue	Cylindrical	M	N	11.115		P	0.098	Polyester
W	fragment	blue		N	N					Synthetic

W	fragment	blue		N	N					UNKN
W	fibre	red/colourless	Irregular	N	N					Anthropogenic
W	fibre	red	Ribbon	N	N					Cotton
W	fibre	colourless	Ribbon	N	N	14.82		P		Anthropogenic
W	fibre	colourless	Cylindrical	M	N	13.585		P	0.177	Polyester
W	fibre	red	Ribbon	N	N					Cotton
W	fragment	blue		N	N					Synthetic
W	fragment	red		N	N					Synthetic
W	fibre	grey	Cylindrical	L	N	9.88		P	0.151	Polyester
W	fibre	black	Cylindrical	N	N	19.76	412.49	P	0.051	Polyethylene
W	fibre	blue	Cylindrical	N	N	14.82	269.23			Polypropylene
W	fibre	blue	Ribbon	N	N					Cotton
W	fibre	colourless	Cylindrical	N	N					Hair
W	fragment	colourless		N	N					Synthetic
W	fibre	colourless	Irregular	N	N	12.35		P	0.064	Nylon
W	fibre	red	Ribbon	N	N					Cotton
W	fibre	blue	Ribbon	N	N					Cotton
W	fibre	colourless	Irregular	N	N	22.23		P	0.016	Anthropogenic
W	fibre	black	Ribbon	N	N					Cotton
W	fibre	colourless		N	N					Hair
W	fragment	colourless		N	N					Synthetic
W	fibre	blue	Ribbon	N	N					Cotton
W	fibre	blue	Ribbon	N	N					Cotton
W	fibre	brown	Cylindrical	N	N					Hair
W	fibre	brown	Cylindrical	H	N	14.82		P	0.074	Synthetic
W	fragment	red		N	N					Synthetic
W	fibre	blue	Bilobal	N	N	12.35	741	P	0.163	Polyester
W	fragment	blue		N	N					UNKN
W	fibre	blue	Cylindrical	L	N	12.35		P	0.148	Polyester
W	fibre	red	Ribbon	N	N					Cotton
W	fibre	red	Ribbon	N	N					Cotton
W	fragment	blue		N	N					Polypropylene
W	fibre	blue	Ribbon	N	N					Cotton
W	fibre	red	Ribbon	N	N					Cotton
W	fragment	blue		N	N					Polypropylene
W	fibre	blue	Cylindrical	N	N	4.94				Nylon
W	fragment	blue		N	N					Polypropylene
W	fibre	blue	Ribbon	N	N					Cotton
W	fibre	red	Ribbon	N	N					Cotton
W	fragment	blue		N	N					Polypropylene
W	fibre	blue	Ribbon	N	N					Cotton
W	fibre	blue	Ribbon	N	N					Cotton
W	fibre	blue	Cylindrical	L	N	9.88	396.2	P	0.162	Polyester
W	fibre	colourless	Cylindrical	N	N	11.12	444.6	N	0.006	Acrylic
W	fragment	red		N	N					Synthetic
W	fibre	blue	Ribbon	N	N					Cotton

W	fibre	red/colourless	Multilobal	N	N	12.35		P	0.101	Polyester
W	fibre	blue	Ribbon	N	N					Cotton
W	fibre	blue	Ribbon	N	N					Cotton
W	fragment	blue		N	N					Synthetic
W	fragment	blue		N	N					Synthetic
W	fibre	blue	Ribbon	N	N					Cotton
W	fragment	blue		N	N					Synthetic
W	fibre	blue	Ribbon	N	N					Cotton
W	fibre	colourless	Cylindrical	N	N					Hair
W	fragment	blue		N	N					Polypropylene
W	fibre	blue	Ribbon	N	N					Cotton
W	fibre	blue	Cylindrical	L	N	7.41		P	0.148	Polyester
W	fibre	blue	Ribbon	N	N					Cotton
W	fragment	blue		N	N					Synthetic
W	fragment	blue		N	N					Synthetic
W	fragment	blue		N	N					Polypropylene
W	fragment	blue		N	N					Synthetic
W	fragment	blue		N	N					Polypropylene
W	fibre	red	Ribbon	N	N					Cotton
W	fragment	blue		N	N					Synthetic
W	fragment	blue		N	N					Synthetic
W	fragment	blue		N	N					Polypropylene
W	fragment	blue		N	N					Polypropylene
W	fragment	blue		N	N					Polypropylene
W	fibre	blue	Ribbon	N	N					Cotton
W	fibre	blue	Ribbon	N	N					Cotton
W	fragment	blue		N	N					Polypropylene
W	fragment	blue		N	N					Polypropylene
W	fragment	blue		N	N					Polypropylene
W	fragment	blue		N	N					Polypropylene
W	fragment	blue		N	N					Polypropylene
W	fibre	blue	Ribbon	N	N					Cotton
W	fragment	blue		N	N					Synthetic
W	fibre	brown/colourless	Cylindrical	N	N					Hair (Animal)
W	fragment	blue		N	N					Polypropylene
W	fibre	colourless	Irregular	N	N	3.705	128.44	P	0.175	Polyester
W	fragment	blue		N	N					Polypropylene
W	fragment	blue		N	N					Polypropylene
W	fragment	blue		N	N					Synthetic
W	fragment	blue		N	N					Synthetic
W	fibre	blue	Ribbon	N	N					Cotton
W	fragment	blue		N	N					Polypropylene
W	fragment	colourless		N	N					Synthetic
W	fragment	blue		N	N					Synthetic
W	fibre	colourless	Cylindrical	N	N					Hair
W	fragment	blue		N	N					Polypropylene

W	fragment	blue		N	N					Synthetic
W	fragment	blue		N	N					Polypropylene
W	fragment	blue		N	N					Polypropylene
W	fibre	blue	Ribbon	N	N					Cotton
W	fibre	blue	Trilobal	N	N	11.115		P	0.034	Polypropylene
W	fibre	black	Cylindrical	N	N					Hair
W	fibre	black	Cylindrical	N	N					Hair
W	fibre	blue	Ribbon	N	N					Cotton
W	fragment	blue		N	N					Synthetic
W	fibre	blue	Ribbon	N	N					Cotton
W	fragment	blue		N	N					Synthetic
W	fragment	blue		N	N					Polypropylene
W	fibre	blue	Ribbon	N	N					Cotton
W	fragment	blue		N	N					Polypropylene
W	fibre	blue	Ribbon	N	N					Cotton
W	fibre	blue	Ribbon	N	N					Cotton
W	fibre	blue	Ribbon	N	N					Cotton
W	fibre	blue	Ribbon	N	N					Cotton
W	fibre	blue	Ribbon	N	N					Cotton
W	fragment	blue		N	N					Polypropylene
W	fibre	colourless	Cylindrical	N	N	8.645		P	0.098	Polyester
W	fragment	blue		N	N					UNKN
W	fibre	blue	Ribbon	N	N					Cotton
W	fibre	blue	Ribbon	N	N					Cotton
W	fibre	blue	Cylindrical	N	N					Hair (Textile)
W	fibre	blue	Cylindrical	M	N	7.41		P	0.162	Polyester
W	fragment	blue		N	N					Polypropylene
W	fibre	blue	Ribbon	N	N					Cotton
W	fragment	blue		N	N					Polypropylene
W	fibre	blue	Cylindrical	N	N	9.88	654.55	P		Nylon
W	fragment	blue		N	N					Polypropylene
W	fibre	blue	Ribbon	N	N					Cotton
W	fragment	blue		N	N					Polypropylene
W	fragment	blue		N	N					Synthetic
W	fibre	red	Cylindrical	N	N					Hair (Textile)
W	fragment	blue		N	N					Synthetic
W	fibre	blue	Ribbon	N	N					Cotton
W	fibre	blue	Ribbon	N	N					Cotton
W	fragment	blue		N	N					Synthetic
W	fibre	blue	Bilobal	M	N	12.35	424.84			Synthetic
W	fibre	blue	Ribbon	N	N					Cotton
W	fibre	colourless	Cylindrical	N	N	14.82		P	0.159	Polyester
W	fibre	colourless	Bilobal	M	N	9.88				Synthetic
W	fibre	blue	Ribbon	N	N					Cotton
W	fibre	blue	Ribbon	N	N					Cotton
W	fragment	blue		N	N					Polypropylene

W	fragment	blue		N	N					Synthetic
W	fibre	colourless	Cylindrical	N	N					Hair
W	fibre	blue	Ribbon	N	N					Cotton
W	fragment	blue		N	N					Polypropylene
W	fibre	colourless	Cylindrical	N	N					Hair (Textile)
W	fragment	blue		N	N					Synthetic
W	fibre	colourless	Cylindrical	N	Cross hatching					Anthropogenic
W	fragment	blue		N	N					Synthetic
W	fragment	blue		N	N					Synthetic
W	fibre	blue	Cylindrical	N	N	11.115				Synthetic
W	fragment	blue		N	N					Synthetic
W	fibre	blue	delta	N	N	19.76		P	0.099	Polyester
W	fibre	colourless	Cylindrical	N	N					Hair
W	fibre	blue	Ribbon	N	N					Cotton
W	fragment	blue		N	N					Polypropylene
W	fragment	blue		N	N					Synthetic
W	fragment	blue		N	N					Polypropylene
W	fibre	red	Irregular	N	N					Nylon
W	fragment	blue		N	N					Synthetic
W	fibre	black	Square	N	N	24.7		P	0.032	Polypropylene
W	fragment	blue		N	N					Synthetic
W	fibre	blue	Ribbon	N	N					Cotton
W	fragment	blue		N	N					Polypropylene
W	fragment	blue		N	N					Synthetic
W	fibre	blue	Ribbon	N	N					Cotton
W	fibre	blue	Ribbon	N	N					Cotton
W	fibre	blue	Ribbon	N	N					Cotton
W	fragment	blue		N	N					Polypropylene
W	fibre	blue	Ribbon	N	N					Cotton
W	fibre	blue	Ribbon	N	N					Cotton
W	fibre	red	Cylindrical	N	N					Hair
W	fragment	blue		N	N					Synthetic
W	fragment	blue		N	N					Polypropylene
W	fibre	blue	Ribbon	N	N					Cotton
W	fibre	blue	Cylindrical	L	N	9.88		P	0.148	Polyester
W	fibre	blue	Ribbon	N	N					Cotton
W	fibre	blue	Cylindrical	N	N					Hair (Textile)
W	fragment	blue		N	N					Synthetic
W	fragment	blue		N	N					Synthetic
W	fibre	black	Ribbon	N	N					Cotton
W	fragment	blue		N	N					Synthetic
W	fragment	blue		N	N					Synthetic
W	fibre	blue	Ribbon	N	N					Cotton
W	fragment	blue		N	N					Polypropylene
W	fragment	blue		N	N					Synthetic
W	fragment	blue		N	N					Synthetic

W	fibre	blue	Ribbon	N	N					Cotton
W	fragment	blue		N	N					Synthetic
W	fibre	red	Ribbon	N	N					Cotton
W	fibre	blue	Ribbon	N	N					Cotton
W	fibre	blue	Ribbon	N	N					Cotton
W	fibre	blue	Ribbon	N	N					Cotton
W	fibre	blue	Cylindrical	N	N					Hair
W	fragment	blue		N	N					Synthetic
W	fragment	blue		N	N					Synthetic
W	fibre	blue	Ribbon	N	N					Cotton
W	fibre	blue	Cylindrical	N	N	12.7		P	0.177	Polyester
W	fibre	blue	Cylindrical	N	N	10.16		P	0.059	Nylon
W	fibre	colourless	Irregular	N	N	15.24		P		Synthetic
W	fragment	red		N	N	200.66	215.9			Synthetic
W	fibre	blue	delta	L	N	13.97		P	0.103	Polyester
W	fibre	blue	Ribbon	N	N					Cotton
W	fibre	blue	Irregular	L	N	10.16		P	0.059	Nylon
W	fibre	colourless	Cylindrical	N	N	10.16		P	0.098	Polyester
W	fibre	blue	Cylindrical	L	N	10.16		P	0.093	Polyester
W	fragment	blue		N	N	27.94	132.08	N		Polypropylene
W	fibre	black	Ribbon	N	N					Cotton
W	fragment	yellow		N	N	43.18	86.36			Synthetic
W	fibre	blue	Ribbon	N	N					Cotton
W	fibre	blue	Cylindrical	L	fisheyes	10.16		P	0.098	Polyester
W	fibre	blue	delta	L	N	10.16		P	0.103	Polyester
W	fibre	blue	Ribbon	N	N					Cotton
W	fibre	blue	Ribbon	N	N					Cotton
W	fragment	blue		N	N	160.02	170.18			Polypropylene
W	fibre	black	Cylindrical	L	fisheyes	7.62		P	0.151	Polyester
W	fibre	blue	Ribbon	N	N					Cotton
W	fibre	colourless	Ribbon	N	blue substance					Cotton
W	fibre	blue	delta	L	N	7.65		P	0.098	Polyester
W	fibre	blue	delta	N	N	7.65		P	0.098	Polyester
W	fibre	blue	delta	N	N	7.65		P	0.105	Polyester
W	fibre	colourless	Ribbon	N	N	10.16		P	0.034	Polypropylene
W	fibre	blue	Ribbon	N	N					Cotton
W	fibre	blue	Ribbon	N	N					Cotton
W	fibre	blue	Ribbon	N	N					Cotton
W	fibre	blue	Cylindrical	N	N	7.62		P	0.144	Polyester
W	fibre	red	Bilobal	N	N	15.24		P		Synthetic
W	fibre	blue	Ribbon	N	N					Cotton
W	fibre	blue	Ribbon	N	N					Cotton
W	fibre	blue	delta	N	voids	7.62		P	0.104	Polyester
W	fibre	colourless	Cylindrical	L	fisheyes	12.8		P	0.176	Polyester
W	fibre	blue	Ribbon	N	N					Cotton
W	fibre	colourless	delta	N	N	12.7		P	0.098	Polyester

W	fibre	blue	Ribbon	N	N					Cotton
W	fibre	black	Cylindrical	N	N	10.16				Hair
W	fibre	blue	Cylindrical	N	N	7.62		P	0.171	Polyester
W	fibre	blue	Ribbon	N	N					Cotton
W	fibre	blue	delta	L	N	12.7		P	0.055	Polyethylene/ Nylon
W	fibre	blue	delta	L	N	7.62		P	0.171	Polyester
W	fibre	blue	delta	N	N	7.62		P	0.151	Polyester
W	fibre	red	Cylindrical	N	N	10.16		P	0.098	Polyester
W	fibre	colourless	Cylindrical	N	N					Hair
W	fibre	colourless	Cylindrical	L	crosshatch	10.16		p	0.177	Polyester
W	fibre	blue	Ribbon	N	N					Cotton
W	fibre	red	Ribbon	N	N					Cotton
W	fragment	blue		N	N	142.24	289.56			Synthetic
W	fibre	blue	Ribbon	N	N					Cotton
W	fibre	blue	Ribbon	N	N					Cotton
W	fibre	blue	Ribbon	N	N					Cotton
W	fragment	blue		N	N	370.84	1079.5			Synthetic
W	fibre	blue	Ribbon	N	N					Cotton
W	fragment	blue		N	N	multiple small fragments				Synthetic
W	fragment	blue	delta	N	N	15.24		P	0.177	Polyester
W	fibre	blue	Ribbon	N	N					Cotton
W	fibre	colourless	delta	N	N	10.16		P	0.103	Polyester
W	fibre	blue	Ribbon	N	N					Cotton
W	fibre	colourless	Cylindrical	L	N	10.16		P	0.177	Polyester
W	fibre	blue	Ribbon	N	N					Cotton
W	fibre	blue	Ribbon	N	N					Cotton
W	fibre	black	Ribbon	N	N					Cotton
W	fibre	blue	Ribbon	N	N					Cotton
W	fibre	colourless	Cylindrical	N	N	7.62		P		Hair (Textile)
W	fibre	blue	Ribbon	N	N					Cotton
W	fibre	colourless	Cylindrical	L	N	12.7		P	0.142	Polyester
W	fragment	blue		N	N	111.76	160.02			Synthetic
W	fragment	blue		N	N	33.02	116.84			Synthetic
W	fibre	red	Ribbon	N	N					Cotton
W	fibre	blue	Ribbon	N	N					Cotton
W	fragment	blue		N	N	134.62	350.52			UNKN
W	fibre	blue	Ribbon	N	N					Cotton
W	fibre	blue	delta	N	N	11.43		P	0.061	Nylon
W	fibre	blue	delta	N	N	7.62		P	0.151	Polyester
W	fibre	blue	Ribbon	N	N					Cotton
W	fibre	colourless	delta	N	N	7.62		P	0.098	Polyester
W	fibre	colourless	delta	N	N	10.16		P	0.098	Polyester
W	fibre	blue	Cylindrical	L	N	12.7		P	0.047	Nylon
W	fibre	blue	Ribbon	N	N					Cotton
W	fibre	brown	Cylindrical	L	N	10.16		P	0.167	Polyester
W	fibre	red	Ribbon	N	N					Cotton

W	fibre	blue	Ribbon	N	N					Cotton
W	fibre	blue	Cylindrical	N	N	7.62		P	0.157	Polyester
W	fibre	blue	Ribbon	N	N					Cotton
W	fibre	blue	delta	N	N	10.16		P	0.098	Polyester
W	fibre	blue	Ribbon	N	N					Cotton
W	fibre	blue	Square	N	N	17.78		P	0.163	Polyester
W	fibre	blue	Ribbon	N	N					Cotton
W	fibre	black	Cylindrical	L	N	10.16		P	0.177	Polyester
W	fibre	blue	delta	N	N	10.16		P	0.147	Polyester
W	fibre	blue	delta	N	N	10.16		P	0.103	Polyester
W	fibre	blue	Ribbon	N	N					Cotton
W	fibre	blue	Ribbon	N	N					Cotton
W	fibre	blue	Ribbon	N	N					Cotton
W	fibre	blue	Cylindrical	N	N	10.16		P	0.098	Polyester
W	fibre	blue	Ribbon	N	N					Cotton
W	fibre	blue	delta	L	N	7.62		P	0.157	Polyester
W	fibre	blue	Ribbon	N	N					Cotton
W	fibre	blue	delta	N	N	8.89		P	0.101	Polyester
W	fragment	blue		N	N	215.9	368.3			Synthetic
W	fibre	blue	Ribbon	N	N					Cotton
W	fragment	blue		N	N	99.06	170.18			Polypropylene
W	fibre	red	Ribbon	N	N					Cotton
W	fibre	black	Ribbon	N	N					Cotton
W	fibre	blue	Ribbon	N	N					Cotton
W	fibre	blue	Ribbon	N	N					Cotton
W	film	pink		N	N	152.4	236.22			Natural
W	fibre	red	Ribbon	N	N					Cotton
W	fibre	red	Ribbon	N	N					Cotton
W	fibre	blue	Ribbon	N	N					Cotton
W	fragment	red		N	N	91.44	129.54			Synthetic
W	fibre	colourless	Cylindrical	N	N	10.16		N	0.009	Acrylic
W	fibre	blue	delta	N	N	7.62		P	0.157	Polyester
W	fibre	blue	Ribbon	N	N					Cotton
W	fibre	colourless	delta	M	N	10.16		P	0.103	Polyester
W	fibre	blue	Ribbon	N	N					Cotton
W	fibre	red	Ribbon	N	N					Cotton
W	fragment	blue		N	N	81.28	109.22			Polypropylene
W	fibre	red	Cylindrical	L	N	19.05		P	0.142	Polyester
W	fibre	colourless	delta	N	N	10.16		P	0.103	Polyester
W	fibre	blue	Cylindrical	M	N	7.62		P	0.151	Polyester
W	fragment	blue		N	N	35.56	162.56			Polypropylene
W	fragment	blue		N	N	71.12	86.36			Synthetic
W	fibre	blue	Square	L	N	22.86		P	0.061	Nylon
W	fibre	blue	delta	N	N	10.16		P	0.157	Polyester
W	fibre	blue	delta	L	N	10.16		P	0.098	Polyester
W	fibre	blue	Ribbon	N	N					Cotton

W	fibre	blue	delta	N	N	7.62		P	0.144	Polyester
W	fibre	blue	Ribbon	N	N					Cotton
W	fibre	colourless	Irregular	L	N	10.16		P	0.147	Polyester
W	fibre	blue	Irregular	N	N	10.16		P	0.157	Polyester
W	fibre	blue	Cylindrical	N	N	7.62		P	0.177	Polyester
W	fibre	colourless	Cylindrical	H	N	10.16		P	0.147	Polyester
W	fibre	blue	Ribbon	N	N					Cotton
W	fibre	colourless	Cylindrical	N	N	30.48				Hair
W	fibre	blue	Ribbon	N	N					Cotton
W	fragment	red		N	N	101.6	434.34			Synthetic
W	fibre	blue	Irregular	N	N	10.16		P	0.096	Polyester
W	fibre	blue	Ribbon	N	N					Cotton
W	fibre	red	Ribbon	N	N					Cotton
W	fibre	blue	delta	N	N	10.16		P	0.064	Nylon
W	fibre	colourless	Cylindrical	N	N	10.16		P	0.032	Polypropylene
W	fibre	colourless	Cylindrical	L	N	12.7		P	0.173	Polyester
W	fibre	colourless	Cylindrical	N	N					Hair
W	fibre	blue	Ribbon	N	N					Cotton
W	fibre	blue	Irregular	L	N	7.62		P	0.177	Polyester
W	fibre	blue	Irregular	N	N	10.16		P	0.098	Polyester
W	fibre	blue	Irregular	L	N	10.16		P	0.177	Polyester
W	fibre	brown	Cylindrical	N	N	33.02				Hair
W	fibre	blue	Ribbon	N	N					Cotton
W	fibre	blue	Ribbon	N	N					Cotton
W	fibre	blue	delta	N	N	7.62		P	0.144	Polyester
W	fibre	colourless	Cylindrical	N	N	10.16		P	0.157	Polyester
W	fibre	red	Ribbon	N	N					Cotton
W	fibre	blue	Ribbon	N	N					Cotton
W	fibre	blue	Ribbon	N	N					Cotton
W	fibre	blue	Ribbon	N	N					Cotton
W	fibre	black	Ribbon	N	N					Cotton
W	fibre	blue	Ribbon	N	N					Cotton
W	fibre	blue	Ribbon	N	N					Cotton
W	fragment	blue		N	N	76.2	139.7			UNKN
W	fibre	blue	Ribbon	N	N					Cotton
W	fibre	red	Ribbon	N	N					Cotton
W	fragment	blue		N	N	30.48	91.44			Synthetic
W	fibre	colourless	Cylindrical	L	N	12.7		P	0.15	Polyester
W	fibre	red	Bilobal	N	N	10.16		P	0.059	Nylon
W	fibre	blue	Ribbon	N	N					Cotton
W	fibre	blue	Ribbon	N	N					Cotton
W	fibre	colourless	Cylindrical	N	N	12.7		P	0.098	Polyester
W	fibre	blue	Ribbon	N	N					Cotton
W	fibre	blue	Cylindrical	L	N	12.7		P	0.157	Polyester
W	fibre	blue	Ribbon	N	N					Cotton
W	fibre	blue	Ribbon	N	N					Cotton

W	fibre	blue	Ribbon	N	N					Cotton
W	fibre	black	Cylindrical	M	N	17.78		P	0.149	Polyester
W	fibre	colourless	Cylindrical	M	N	22.86		P	>0.175	Polyester
W	fibre	blue	Ribbon	N	N					Cotton
W	fibre	colourless	Cylindrical	N	N	10.16		P	0.177	Polyester
W	fibre	brown	Cylindrical	N	N					Hair (Textile)
W	fibre	blue	Ribbon	N	N					Cotton
W	fibre	blue	Ribbon	N	N					Cotton
W	fibre	blue	Cylindrical	N	N	12.7		P	0.141	Polyester
W	fibre	colourless	Cylindrical	M	N	10.12		P	0.187	Polyester
W	fibre	blue	Ribbon	N	N					Cotton
W	fibre	blue	Ribbon	N	N					Cotton
W	fibre	colourless	Cylindrical	N	N	25.4				Hair
W	fragment	blue		N	N	50.8	195.58			Polyester
W	fragment	red		N	N	45.72	218.44			Synthetic
W	fibre	blue	Ribbon	N	N					Cotton
W	fibre	red	Cylindrical	M	N	6.35		P	0.173	Polyester
W	fibre	blue	Cylindrical	N	N	10.16		P	0.196	Polyester
W	fibre	blue	Ribbon	N	N					Cotton
W	fibre	colourless	Irregular	L	N	10.16		P	0.095	Polyester
W	fibre	blue	Ribbon	N	N					Cotton
W	fibre	red	Ribbon	N	N					Cotton
W	fragment	colourless		N	N	33.02	33.02			Synthetic
W	fibre	colourless	Cylindrical	N	N	12.7		P	0.161	Polyester
W	fibre	blue	delta	L	N	7.62		P	0.144	Polyester
W	fibre	blue	Ribbon	N	N					Cotton
W	fibre	colourless	delta	L	N	11.43		P	0.161	Polyester
W	fibre	blue	Ribbon	N	N					Cotton
W	fibre	blue	Ribbon	N	N					Cotton
W	fibre	blue	Ribbon	N	N					Cotton
W	fibre	colourless	Irregular	L	N	10.16		P	0.177	Polyester
W	fibre	blue	Ribbon	N	N					Cotton
W	fibre	blue	Cylindrical	N	N	12.7		P	0.146	Polyester
W	fibre	red	Ribbon	N	N					Cotton
W	fibre	blue	Ribbon	N	N					Cotton
W	fibre	red	Ribbon	N	N					Cotton
W	fibre	blue	Ribbon	N	N					Cotton
W	fibre	red	Ribbon	N	N					Cotton
W	fragment	blue		N	N	30.48	66.04			Synthetic
W	fibre	blue	Ribbon	N	N					Cotton
W	fibre	red	Ribbon	N	N					Cotton
W	fibre	blue	Multilobal	H	N	15.24				Synthetic
W	fibre	blue	Ribbon	N	N					Cotton
W	fibre	blue	Ribbon	N	N					Cotton
W	fibre	blue	Ribbon	N	N					Cotton
W	fibre	blue	Ribbon	N	N					Cotton

W	fibre	blue	Ribbon	N	N					Cotton
W	fibre	colourless	Cylindrical	M	N	13.97		P	0.175	Polyester
W	fragment	blue		N	N	45.72	60.96			Synthetic
W	fibre	blue	Ribbon	N	N					Cotton
W	fibre	black	Ribbon	N	N					Cotton
W	fibre	blue	Ribbon	N	N					Cotton
W	fibre	red	Ribbon	N	N					Cotton
W	fibre	blue	Ribbon	N	N					Cotton
W	fragment	blue		N	N	127	170.18			UNKN
W	fibre	blue	Ribbon	N	N					Cotton
W	fibre	blue	Ribbon	N	N					Cotton
W	fibre	blue	Ribbon	N	N					Cotton
W	fibre	blue	Ribbon	N	N					Cotton
W	fibre	blue	Ribbon	N	N					Cotton
W	fibre	colourless	Cylindrical	L	N	11.43		P	0.175	Polyester
W	fibre	blue	Cylindrical	M	N	7.62		P	0.144	Polyester
W	fibre	blue	Ribbon	N	N					Cotton
W	fibre	blue	Ribbon	N	N					Cotton
W	fibre	blue	Ribbon	N	N					Cotton
W	fibre	blue	delta	L	N	7.62		P	0.171	Polyester
W	fibre	black	Multilobal	N	N	15.24		P		Synthetic
W	fibre	colourless	Cylindrical	N	N	10.16		P	0.187	Polyester
W	fibre	blue	delta	N	N	10.16		P	0.103	Polyester
W	fibre	blue	Cylindrical	N	N	7.62		P	0.151	Polyester
W	fibre	blue	Ribbon	N	N					Cotton
W	fibre	colourless	delta	L	N	10.16		P	0.143	Polyester
W	fibre	blue/colourless	Irregular	N	N	11.43		P	0.103	Polyester
W	fibre	blue	Ribbon	N	N					Cotton
W	fibre	blue	Ribbon	N	N					Cotton
W	fibre	blue	Ribbon	N	N					Cotton
W	fibre	colourless	Cylindrical	L	N	12.7		P	0.142	Polyester
W	fibre	blue	Cylindrical	N	N	7.62		P	0.151	Polyester
W	fibre	blue	Ribbon	N	N					Cotton
W	fibre	colourless	Cylindrical	N	fisheyes	24.13		P	>0.166	Polyester
W	fibre	blue	Cylindrical	L	N	10.16		P	0.059	Nylon
W	fibre	blue	Cylindrical	L	N	7.62		P	0.157	Polyester
W	fibre	red	Ribbon	N	N					Cotton
W	fibre	blue	Ribbon	N	N					Cotton
W	fibre	blue	Cylindrical	N	N	10.16		P	0.098	Polyester
W	fibre	blue	delta	N	N	7.62		P	0.144	Polyester
W	fibre	blue	Ribbon	N	N					Cotton
W	fibre	colourless	delta	N	N	7.62		P	0.164	Polyester
W	fibre	blue	delta	L	N	10.16		P	0.103	Polyester
W	fibre	blue	Ribbon	N	N					Cotton
W	fibre	blue	Multilobal/tape	N	N	15.24		P		Synthetic
W	fragment	red		N	N	119.38	381			Synthetic

W	fibre	red	Ribbon	N	N					Cotton
W	fragment	orange		N	N	96.52	330.2			Synthetic
W	fibre	blue	delta	L	N	7.62			0.144	Polyester
W	fibre	blue	Ribbon	N	N					Cotton
W	fibre	blue	Ribbon	N	N					Cotton
W	fibre	colourless	Cylindrical	N	N	22.86		P	0.175	Polyester
W	fibre	blue	Ribbon	N	N					Cotton
W	fibre	blue	Ribbon	N	N					Cotton
W	fibre	blue	Ribbon	N	N					Cotton
W	fragment	blue		N	N	68.58	104.14			Synthetic
W	fibre	blue	Ribbon	N	N					Cotton
W	fibre	blue	Ribbon	N	N					Cotton
W	fibre	blue	Ribbon	N	N					Cotton
W	fibre	red	Ribbon	N	N					Cotton
W	fibre	red	Ribbon	N	N					Cotton
W	fibre	blue	Ribbon	N	N					Cotton
W	fibre	blue	Ribbon	N	N					Cotton
W	fibre	blue	Ribbon	N	N					Cotton
W	fibre	blue	Ribbon	N	N					Cotton
W	fragment	blue		N	N	35.56	200.66			Nylon
W	fibre	red	Ribbon	N	N					Cotton
W	fragment	blue		N	N	76.2	86.36			Synthetic
W	fibre	blue	Ribbon	N	N					Cotton
W	fibre	blue	Ribbon	N	N					Cotton
W	fibre	blue	Ribbon	N	N					Cotton
W	fibre	blue	Ribbon	N	N					Cotton
W	fibre	blue	Ribbon	N	N					Cotton
W	fibre	colourless	Cylindrical	N	fisheyes	30.48		P	>0.131	Polyester
W	fibre	black	Cylindrical	L	N	12.7		P	0.094	Polyester
W	fibre	blue	Ribbon	N	N					Cotton
W	fibre	blue	Ribbon	N	N					Cotton
W	fibre	blue	Ribbon	N	N					Cotton
W	fibre	blue	Ribbon	N	N					Cotton
W	fibre	blue	Ribbon	N	N					Cotton
W	fibre	blue	Ribbon	N	N					Cotton
W	fibre	blue	Ribbon	N	N					Cotton
W	fibre	black	Cylindrical	H	N	25.4		P		Synthetic
W	fibre	blue	Multilobal/tape	N	N	12.7		P		Synthetic
W	fibre	blue	Ribbon	N	N					Cotton
W	fibre	blue	Ribbon	N	N					Cotton
W	fibre	blue	Ribbon	N	N					Cotton
W	fibre	blue	Cylindrical	L	N	7.62		P	0.104	Polyester
W	fragment	blue		N	N	76.2	584.2			Synthetic
W	fibre	colourless	Cylindrical	L	N	10.16		P	0.172	Polyester
W	fibre	colourless	Cylindrical	N	N	15.24		N	0.006	Acrylic
W	fibre	colourless	Cylindrical	L	fisheyes	35.56		P	0.031	Polypropylene

W	fibre	blue	Ribbon	N	N					Cotton
W	fragment	blue		N	N	35.56	218.44			Synthetic
W	fibre	blue	Irregular	L	N	10.16		P	0.167	Polyester
W	fibre	blue	Ribbon	N	N					Cotton
W	fibre	blue	Irregular	L	N	15.24		P	0.51	Nylon
W	fibre	blue	Ribbon	N	N					Cotton
W	fibre	blue	Cylindrical	N	N	10.16		P	0.163	Polyester
W	fibre	blue	Ribbon	N	N					Cotton
W	fibre	blue	Ribbon	N	N					Cotton
W	fibre	black	Ribbon	N	N					Cotton
W	fibre	red	Ribbon	N	N					Cotton
W	fibre	blue	Ribbon	N	N					Cotton
W	fibre	blue	Ribbon	N	N					Cotton
W	fibre	blue	Ribbon	N	N					Cotton
W	fibre	colourless	Cylindrical	L	N	10.16		P	0.196	Polyester
W	fibre	blue	Ribbon	N	N					Cotton
W	fibre	black	Ribbon	N	N					Cotton
W	fibre	blue	Ribbon	N	N					Cotton
W	fibre	blue	Ribbon	N	N					Cotton
W	fibre	colourless	Cylindrical	N	N					Hair
W	fragment	red		N	N	62.5	193.04			UNKN
W	fragment	red		N	N	101.6	180.34			UNKN
W	fibre	black	Cylindrical	N	N	33.02				Synthetic
W	fibre	colourless	Cylindrical	N	fisheyes	22.86		P	>0.175	Synthetic
W	fibre	blue	Cylindrical	N	N	15.24		P		Synthetic
W	fibre	blue	Ribbon	N	N					Cotton
W	fibre	colourless	Cylindrical	N	N					Hair
W	fibre	blue	Ribbon	N	N					Cotton
W	fibre	red	Ribbon	N	N					Cotton
W	fibre	blue	Ribbon	N	N					Cotton
W	fibre	red	Ribbon	N	N					Cotton
W	fragment	blue		N	N	40.64	104.14			Synthetic
W	fibre	black	Ribbon	N	N					Cotton
W	fibre	blue	Ribbon	N	N					Cotton
W	fibre	blue	Cylindrical	L	N	7.62		P	0.151	Polyester
W	fibre	blue	Ribbon	N	N					Cotton
W	fibre	colourless	Cylindrical	N	N	11.43		P	0.201	Synthetic
W	fibre	red	Cylindrical	N	N	22.66		P	>0.176	Synthetic
W	fragment	blue		N	N	119.38	180.34			Synthetic
W	fibre	blue	Ribbon	N	N					Cotton
W	fibre	colourless	Cylindrical	N	N					Hair
W	fibre	colourless	Cylindrical	L	N	15.24		P	0.059	Nylon
W	fibre	blue	Ribbon	N	N					Cotton
W	fibre	blue	Ribbon	N	N					Cotton
W	fibre	blue	Ribbon	N	N					Cotton
W	fibre	blue	Ribbon	N	N					Cotton

W	fibre	blue	Ribbon	N	N					Cotton
W	fibre	colourless	Cylindrical	N	N					Cotton
W	fibre	red	Ribbon	N	N					Cotton
W	fibre	blue	Ribbon	N	N					Cotton
W	fibre	blue	Ribbon	N	N					Cotton
W	fibre	blue	Ribbon	N	N					Cotton
W	fibre	blue	Ribbon	N	N					Cotton
W	fibre	black	Ribbon	N	N					Cotton
W	fibre	blue	Ribbon	N	N					Cotton
W	fibre	blue	Ribbon	N	N					Cotton
W	fibre	blue	Ribbon	N	N					Cotton
W	fragment	colourless		N	N	342.9	508			Synthetic
W	fibre	blue	Ribbon	N	N					Cotton
W	fibre	blue	Ribbon	N	N					Cotton
W	fibre	black	Irregular	M	N	15.24		P	0.066	Nylon
W	fibre	blue	Ribbon	N	N					Cotton
W	fibre	black	Ribbon	N	N					Cotton
W	fibre	blue	Ribbon	N	N					Cotton
W	fibre	green	Cylindrical	N	N					Hair
W	fibre	colourless	Cylindrical	L	N	10.16		P	0.167	Polyester
W	fibre	blue	Ribbon	N	N					Cotton
W	fibre	blue	Ribbon	N	N					Cotton
W	fibre	red	Bilobal	L	fisheyes	12.7		P	0.062	Nylon
W	fibre	blue	Ribbon	N	N					Cotton
W	fibre	blue	Ribbon	N	N					Cotton
W	fibre	colourless	Cylindrical	M	N	12.7		P	0.177	Polyester
W	fibre	colourless	Cylindrical	N	N					Hair
W	fibre	colourless	Cylindrical	N	N					Hair
W	fibre	blue	Ribbon	N	N					Cotton
W	fibre	blue	Ribbon	N	N					Cotton
W	fibre	blue	Cylindrical	N	N	22.86		P	>0.175	Polyester
W	fibre	blue	Ribbon	N	N					Cotton
W	fibre	blue	Ribbon	N	N					Cotton
W	fibre	blue	Ribbon	N	N					Cotton
W	fibre	red	Ribbon	N	N					Cotton
W	fibre	red	Ribbon	N	N					Cotton
W	fibre	black	Ribbon	N	N					Cotton
W	fibre	blue	Ribbon	N	N					Cotton
W	fibre	black	Cylindrical	L	N	12.7		P	0.098	Polyester
W	fibre	blue	Ribbon	N	N					Cotton
W	fragment	red		N	N	33.02	134.62			Synthetic
W	fibre	blue	Ribbon	N	N					Cotton
W	fibre	colourless	Cylindrical	L	N	10.16		P	0.181	Polyester
W	fibre	blue	Ribbon	N	N					Cotton
W	fibre	blue	Ribbon	N	N					Cotton
W	fibre	colourless	Cylindrical	M	N	25.4		P	0.143	Polyester

W	blue	blue	Irregular	N	N	25.4		P		Synthetic
W	fibre	blue	Ribbon	N	N					Cotton
W	fibre	blue	Ribbon	N	N					Cotton
W	fibre	blue	Ribbon	N	N					Cotton
W	fibre	blue	Ribbon	N	N					Cotton
W	fibre	blue	Ribbon	N	N					Cotton
W	fibre	red	Ribbon	N	N					Cotton
W	fibre	red	Ribbon	N	N					Cotton
W	fragment	blue/pink		N	N	116.84	190.5			Synthetic
W	fibre	black	Ribbon	N	N					Cotton
W	fibre	blue	Ribbon	N	N					Cotton
W	fibre	colourless	Cylindrical	L	N	10.16		P	0.167	Polyester
W	fibre	blue	Ribbon	N	N					Cotton
W	fragment	blue		N	N	91.44	149.86			Synthetic
W	fragment	blue		N	N	25.4	205.74			Synthetic
W	fibre	blue	Ribbon	N	N					Cotton
W	fibre	blue	Ribbon	N	N					Cotton
W	fibre	blue	Cylindrical	M	N	12.7		P		Synthetic
W	fibre	black	Cylindrical	H	N	12.7		P	0.141	Polyester
W	fibre	black	Multilobal/tape	N	N	12.7		P		Synthetic
W	fibre	red	Ribbon	N	N					Cotton
W	fibre	black	Cylindrical	M	fisheyes	10.16		P		Synthetic
W	fibre	colourless	Cylindrical	M	N	15.23		P	0.164	Polyester
W	fibre	blue	Ribbon	N	N					Cotton
W	fibre	colourless	Cylindrical	L	N	25.4		P	>0.158	Polyester
W	fibre	blue	Cylindrical	N	N	7.62		P	0.144	Polyester
W	fibre	blue	Cylindrical	L	N	7.62		P	0.144	Polyester
W	fibre	blue	Cylindrical	N	N	7.62		P	0.157	Polyester
W	fibre	colourless	Cylindrical	N	N	10.16		P	0.196	Synthetic
W	fibre	blue	Ribbon	N	N					Cotton
W	fibre	blue	Ribbon	N	N					Cotton
W	fibre	colourless	Cylindrical	L	N	10.16		P	0.177	Polyester
W	fibre	blue	Cylindrical	N	N	7.62		P	0.144	Polyester
W	fibre	blue	Cylindrical	N	N	10.16		P	0.098	Polyester
W	fibre	blue	Cylindrical	N	N	7.62		P	0.157	Polyester
W	fibre	blue	Ribbon	N	N					Cotton
W	fibre	blue	Ribbon	N	N					Cotton
W	fibre	colourless	Cylindrical	N	N					Hair
W	fibre	blue	Ribbon	N	N					Cotton
W	fibre	blue	Ribbon	N	N					Cotton
W	fibre	blue	Ribbon	N	N					Cotton
W	fibre	blue	Cylindrical	L	N	7.62		P	0.151	Polyester
W	fibre	blue	Ribbon	N	N					Cotton
W	fibre	blue	Ribbon	N	N					Cotton
W	fragment	red		N	N	76.2	134.62			Synthetic
W	fibre	blue	Ribbon	N	N					Cotton

W	fibre	blue	Ribbon	N	N					Cotton
W	fibre	blue	Ribbon	N	N					Cotton
W	fibre	blue	Ribbon	N	N					Cotton
W	fibre	colourless	Cylindrical	M	fisheyes	25.4		P	0.156	Polyester
W	fibre	blue	Ribbon	N	N					Cotton
W	fibre	colourless	Cylindrical	N	N					Hair
W	fragment	yellow		N	N	101.6	210.82			Synthetic
W	fibre	blue	Ribbon	N	N					Cotton
W	fibre	colourless	Cylindrical	H	N	12.7		P	0.173	Polyester
W	fibre	colourless	Cylindrical	M	N	12.7		P	0.173	Polyester
W	fibre	blue	Ribbon	N	N					Cotton
W	fibre	blue	Ribbon	N	N					Cotton
W	fibre	black	Ribbon	N	N					Cotton
W	fibre	blue	Cylindrical	L	N	10.16		P	0.138	Polyester
W	fibre	blue	Ribbon	N	N					Cotton
W	fibre	blue	Ribbon	N	N					Cotton
W	fibre	blue	Ribbon	N	N					Cotton
W	fibre	purple/grey	Bilobal	N	fisheyes	10.16		P		Synthetic
W	fibre	blue	Ribbon	N	N					Cotton
W	fibre	black	Cylindrical	M	N	10.16		P	0.177	Polyester
W	fibre	blue	Ribbon	N	N					Cotton
W	fibre	red	Ribbon	N	N					Cotton
W	fibre	blue	Cylindrical	L	N	5.06		P		Synthetic
W	fibre	blue	Ribbon	N	N					Cotton
W	fibre	blue	Ribbon	N	N					Cotton
W	fibre	blue	Ribbon	N	N					Cotton
W	fibre	red	Ribbon	N	N					Cotton
W	fibre	colourless	Cylindrical	L	N	10.16		P	0.157	Polyester
W	fibre	blue	Cylindrical	N	N					Hair
W	fibre	blue	Ribbon	N	N					Cotton
W	fibre	black	Cylindrical	N	N	53.34		P	0.045	Nylon
W	fibre	blue	Ribbon	N	N					Cotton
W	fibre	blue	Ribbon	N	N					Cotton
W	fibre	blue	Ribbon	N	N					Cotton
W	fibre	blue	Ribbon	N	N					Cotton
W	fibre	blue	Ribbon	N	N					Cotton
W	fibre	blue	Cylindrical	N	N					Hair
W	fibre	colourless	Cylindrical	L	N	7.62		P	0.184	Polyester
W	fibre	blue	Ribbon	N	N					Cotton
W	fibre	blue	Ribbon	N	N					Cotton
W	fibre	blue	Ribbon	N	N					Cotton
W	fibre	blue	Ribbon	N	N					Cotton
W	fibre	blue	Ribbon	N	N					Cotton
W	fibre	blue	Ribbon	N	N					Cotton
W	fibre	blue	Cylindrical	L	N	7.62		P	0.091	Polyester
W	fibre	blue	Ribbon	N	N					Cotton

W	fibre	colourless	Irregular	N	fisheyes	12.7		P	0.165	Polyester
W	fibre	colourless	Bilobal	H	N	15.24		P	0.035	Polypropylene
W	fibre	blue	Ribbon	N	N					Cotton
W	fibre	blue	Ribbon	N	N					Cotton
W	fibre	colourless	Irregular	N	N	15.24		P	0.043	Nylon
W	fibre	red	Cylindrical	L	N	7.62		P	0.144	Polyester
W	fragment	blue		N	N	73.66	134.62			Synthetic
W	fibre	black	Ribbon	N	N					Cotton
W	fragment	red		N	N	45.72	81.28			Synthetic
W	fibre	blue	Ribbon	N	N					Cotton
W	fibre	red	Cylindrical	N	N	10.16		P	0.147	Polyester
W	fibre	blue	Ribbon	N	N					Cotton
W	fibre	blue	Ribbon	N	N					Cotton
W	fragment	red		N	N	58.42	60.96			Synthetic
W	fibre	black	Cylindrical	H	N	16.51				Nylon
W	fibre	blue	Ribbon	N	N					Cotton
W	fibre	blue	Cylindrical	L	N	7.62		P	0.144	Polyester
W	fibre	blue	Ribbon	N	N					Cotton
W	fibre	blue	Ribbon	N	N					Cotton
W	fibre	blue	Ribbon	N	N					Cotton
W	fibre	blue	Ribbon	N	N					Cotton
W	fibre	blue	Ribbon	N	N					Cotton
W	fibre	blue	Ribbon	N	N					Cotton
W	fibre	blue	Ribbon	N	N					Cotton
W	fibre	black	Cylindrical	L	N	7.62		P		Synthetic
W	fibre	black	delta	L	N	20.32		P	0.044	Nylon
W	fibre	blue	Ribbon	N	N					Cotton
W	fibre	blue	Ribbon	N	N					Cotton
W	fragment	colourless		N	N	203.2	368.3			Synthetic
W	fibre	blue	Ribbon	N	N					Cotton
W	fibre	green	Ribbon	N	N					Cotton
W	fibre	blue	Ribbon	N	N					Cotton
W	fibre	blue	Ribbon	N	N					Cotton
W	fibre	blue	Ribbon	N	N					Cotton
W	fibre	blue	Ribbon	N	N					Cotton
W	fibre	blue	Ribbon	N	N					Cotton
A	fibre	blue	Ribbon	N	N					Cotton
A	fibre	colourless	Ribbon	N	N					Cotton
A	fibre	colourless	Ribbon	N	N					Cotton
A	fibre	red	Ribbon	N	N					Cotton
A	fibre	colourless	Ribbon	N	N					Cotton
A	fibre	colourless	Ribbon	N	N					Cotton
A	fibre	blue	Ribbon	N	N					Cotton
A	fibre	colourless	Ribbon	N	N					Cotton
A	fibre	colourless	Ribbon	N	N					Cotton
A	fibre	red	Cylindrical	M	N	10.2	803.25	P	0.167	Polyester

A	fibre	pink	Ribbon	N	N					Cotton
A	fibre	blue	Cylindrical	N	N	12.75		P	0.145	Polyester
A	fibre	colourless	Cylindrical	M	N	15.3		P	0.098	Polyester
A	fibre	blue	Ribbon	N	N					Cotton
A	fibre	red	Ribbon	N	N					Cotton
A	fibre	blue	Ribbon	N	N					Cotton
A	fibre	blue	Ribbon	N	N					Cotton
A	fibre	red	Ribbon	N	N					Cotton
A	fibre	colourless	Cylindrical	N	fisheyes	10.2		P	0.166	Polyester
A	fibre	colourless	Ribbon	N	N					Cotton
A	fibre	colourless	Ribbon	N	N					Cotton
A	fibre	colourless	Ribbon	N	N					Cotton
A	fibre	blue	Ribbon	N	N					Cotton
A	fibre	blue	Ribbon	N	N					Cotton
A	fibre	red	Ribbon	N	N					Cotton
A	fibre	yellow	Multilobal	N	voids	10.2				UNKN
A	fibre	red	Cylindrical	M	N	12.75		P	0.184	Polyester
A	fibre	blue	Ribbon	N	N					Cotton
A	fibre	colourless	Ribbon	N	N					Cotton
A	fibre	red	Ribbon	N	N					Cotton
A	fibre	colourless	Ribbon	N	N					Cotton
A	fibre	colourless	Ribbon	N	N					Cotton
A	fibre	blue	Ribbon	N	N					Cotton
A	fibre	colourless	Ribbon	N	N					Cotton
A	fibre	blue	Cylindrical	L	N	11.48		P	0.166	Polyester
A	fragment	blue		N	N	53.55	214.2			Polypropylene
A	fibre	black	Cylindrical	H	N	17.85		P	0.148	Polyester
A	fibre	blue	Ribbon	N	N					Cotton
A	fibre	blue	Ribbon	N	N					Cotton
A	fibre	colourless	Ribbon	N	N					Cotton
A	fragment	yellow		N	N	68.85	163.2			Synthetic
A	fibre	blue	Ribbon	N	N					Cotton
A	fibre	blue	Ribbon	N	N					Cotton
A	fibre	blue	Ribbon	N	N					Cotton
A	fibre	colourless	Ribbon	N	N					Cotton
A	fibre	blue	Ribbon	N	N					Cotton
A	fibre	colourless	Ribbon	N	N					Cotton
A	fibre	colourless	Ribbon	N	N					Cotton
A	fibre	colourless	Ribbon	N	N					Cotton
A	fibre	colourless	Ribbon	N	N					Cotton
A	fibre	colourless	Ribbon	N	N					Cotton
A	fibre	blue	Cylindrical	M	N	7.65		P	0.104	Polyester
A	fibre	colourless	Ribbon	N	N					Cotton
A	fibre	colourless	Ribbon	N	N					Cotton
A	fibre	colourless	Ribbon	N	N					Cotton
A	fibre	colourless	Ribbon	N	N					Cotton

A	fibre	colourless	Ribbon	N	N					Cotton
A	fibre	blue	Ribbon	N	N					Cotton
A	fibre	colourless	Ribbon	N	N					Cotton
A	fibre	colourless	Ribbon	N	N					Cotton
A	fibre	colourless	Ribbon	N	N					Cotton
A	fibre	colourless	Ribbon	N	N					Cotton
A	fibre	red	Ribbon	N	N					Cotton
A	fibre	colourless	Ribbon	N	N					Cotton
A	fibre	colourless	Ribbon	N	N					Cotton
A	fibre	colourless	Cylindrical	M	fish eyes	22.86		P	0.175	Polyester
A	fibre	colourless	Ribbon	N	N					Cotton
A	fibre	colourless	Ribbon	N	N					Cotton
A	fragment	yellow		N	N	30.48	91.44			Synthetic
A	fibre	colourless	Ribbon	N	N					Cotton
A	fibre	colourless	Cylindrical	N	N	27.94				Hair
A	fibre	colourless	Ribbon	N	N					Cotton
A	fibre	colourless	Ribbon	N	N					Cotton
A	fibre	colourless	Ribbon	N	N					Cotton
A	fibre	blue	Irregular	N	N	12.7				Synthetic
A	fibre	blue	Cylindrical	L	N	7.62		P	0.144	Polyester
A	fibre	colourless	Ribbon	N	N					Cotton
A	fibre	colourless	Bilobal	N	N	20.32		P	>0.263	Synthetic
A	fibre	blue	Ribbon	N	N					Cotton
A	fibre	blue	Ribbon	N	N					Cotton
A	fibre	blue	Irregular	N	cross-hatch	12.7		P		Synthetic
A	fibre	blue	Cylindrical	N	N	10.16		P	0.098	Polyester
A	fibre	blue	delta	N	N	10.16		P	0.093	Polyester
A	fibre	blue	Ribbon	N	N					Cotton
A	fibre	blue	Ribbon	N	N					Cotton
A	fragment	blue		N	N	55.88	134.62			Polypropylene
A	fibre	red	Ribbon	N	N					Cotton
A	fibre	red	Irregular	N	N	30.48	223.52	P	>0.131	Polyester
A	fibre	red	Ribbon	N	N					Cotton
A	fibre	grey	Cylindrical	N	N	17.78				Hair
A	fibre	red	Ribbon	N	N					Cotton
A	fibre	blue	Ribbon	N	N					Cotton
A	fibre	colourless	Ribbon	N	N					Cotton
A	fibre	colourless	Ribbon	N	N					Cotton
A	fibre	blue	Ribbon	N	N					Cotton
A	fibre	blue	Ribbon	N	N					Cotton
A	fibre	red	Ribbon	N	N					Cotton
A	fibre	blue	Ribbon	N	N					Cotton
A	fibre	colourless	Ribbon	N	N					Cotton
A	fibre	green	Ribbon	N	N					Cotton
A	fibre	colourless	Ribbon	N	N					Cotton
A	fibre	colourless	Ribbon	N	N					Cotton

A	fibre	black	Ribbon	N	N					Cotton
A	fibre	blue	Ribbon	N	N					Cotton
A	fibre	colourless	Ribbon	N	N					Cotton
A	fibre	colourless	Ribbon	N	N					Cotton
A	fibre	colourless	Ribbon	N	N					Cotton
A	fibre	red	Cylindrical	L	N	7.62		P	0.104	Polyester
A	fibre	blue	Ribbon	N	N					Cotton
A	fragment	red		N	N	48.26	96.52			Synthetic
A	fibre	blue	Ribbon	N	N					Cotton
A	fibre	colourless	Ribbon	N	N					Cotton
A	fibre	red	Ribbon	N	N					Cotton
A	fibre	blue	Ribbon	N	N					Cotton
A	fibre	colourless	Ribbon	N	N					Cotton
A	fibre	blue	Cylindrical	L	N	10.16		P	0.059	Nylon
A	fibre	blue	Cylindrical	N	N	10.16		P	0.099	Polyester
A	fibre	blue	Multilobal	N	N	13.97		P		Synthetic
A	fibre	blue	Ribbon	N	N					Cotton
A	fibre	blue	Ribbon	N	N					Cotton
A	fibre	colourless	Ribbon	N	N					Cotton
A	fibre	colourless	Ribbon	N	N					Cotton
A	fibre	blue	Ribbon	N	N					Cotton
A	fibre	colourless	Ribbon	N	N					Cotton
A	fibre	red	Multilobal	N	N	10.16		P		Synthetic
A	fibre	blue	Ribbon	N	N					Cotton
A	fibre	purple	Ribbon	N	N					Cotton
A	fibre	colourless	Ribbon	N	N					Cotton
A	fibre	colourless	Ribbon	N	N					Cotton
A	fibre	colourless	Ribbon	N	N					Cotton
A	fibre	blue	Ribbon	N	N					Cotton
A	fibre	colourless	Ribbon	N	N					Cotton
A	fibre	blue	Ribbon	N	N					Cotton
A	fibre	blue	Ribbon	N	N					Cotton
A	fibre	blue	Ribbon	N	N					Cotton
A	fibre	blue	Ribbon	N	N					Cotton
A	fibre	red	Ribbon	N	N					Cotton
A	fibre	red	Cylindrical	L	N	16.54		P	0.175	Polyester
A	fibre	colourless	Ribbon	N	N					Cotton
A	fibre	colourless	Ribbon	N	N					Cotton
A	fibre	colourless	Ribbon	N	N					Cotton
A	fibre	colourless	Ribbon	N	N					Cotton
A	fibre	blue	Cylindrical	L	N	10.16		P	0.177	Polyester
A	fibre	colourless	Ribbon	N	N					Cotton
A	fibre	blue	Ribbon	N	N					Cotton
A	fibre	blue	Cylindrical	M	fish eyes	10.16		P	0.175	Polyester
A	fibre	colourless	Ribbon	N	N					Cotton
A	fibre	red	Ribbon	N	N					Cotton

A	fibre	colourless	Ribbon	N	N					Cotton
A	fibre	colourless	Ribbon	N	N					Cotton
A	fibre	colourless	Ribbon	N	N					Cotton
A	fibre	blue	Ribbon	N	N					Cotton
A	fibre	blue	Ribbon	N	N					Cotton
A	fibre	colourless	Ribbon	N	N					Cotton
A	fibre	colourless	Ribbon	N	N					Cotton
A	fibre	colourless	Ribbon	N	N					Cotton
A	fibre	colourless	Ribbon	N	N					Cotton
A	fibre	blue	Ribbon	L	N	15.24		P	0.033	Polypropylene
A	fibre	colourless	Irregular	M	N	17.78		P	0.056	Nylon
A	fibre	red	Ribbon	N	N					Cotton
A	fibre	blue	Ribbon	N	N					Cotton
A	fibre	black	Ribbon	N	N					Cotton
A	fragment	blue		N	degraded	154.96	144.78			Synthetic
A	fibre	colourless	Ribbon	N	N					Cotton
A	fibre	blue	Ribbon	N	N					Cotton
A	fibre	colourless	Cylindrical	H	N	12.7		P	0.173	Polyester
A	fibre	colourless	Ribbon	N	N					Cotton
A	fibre	red	Ribbon	N	N					Cotton
A	fibre	blue	Ribbon	N	N					Cotton
A	fibre	colourless	Ribbon	N	N					Cotton
A	fibre	colourless	Ribbon	N	N					Cotton
A	fibre	colourless	Ribbon	N	N					Cotton
A	fibre	colourless	Ribbon	N	N					Cotton
A	fibre	colourless	Ribbon	N	N					Cotton
A	fibre	colourless	Ribbon	N	N					Cotton
A	fibre	colourless	Ribbon	N	N					Cotton
A	fibre	blue	Cylindrical	L	N	7.62		P	0.144	Polyester
A	fibre	colourless	Ribbon	N	N					Cotton
A	fibre	blue	Ribbon	N	N					Cotton
A	fibre	colourless	Ribbon	N	N					Cotton
A	fibre	colourless	Ribbon	N	N					Cotton
A	fragment	blue		N	N	30.48	96.52			Polypropylene
A	fibre	blue	Cylindrical	L	N	7.62		P	0.157	Polyester
A	fibre	blue	Ribbon	N	N					Cotton
A	fibre	blue	Ribbon	N	N					Cotton
A	fibre	colourless	Ribbon	N	N					Cotton
A	fibre	colourless	Ribbon	N	N					Cotton
A	fibre	blue	Ribbon	N	N					Cotton
A	fibre	blue	Ribbon	N	N					Cotton
A	fibre	colourless	Ribbon	N	N					Cotton
A	fibre	colourless	Ribbon	N	N					Cotton
A	fibre	blue	Ribbon	N	N					Cotton
A	fibre	blue	Ribbon	N	N					Cotton

A	fibre	colourless	Ribbon	N	N					Cotton
A	fragment	red		N	N	71.12	160.02			Synthetic
A	fibre	blue	Ribbon	N	N					Cotton
A	fibre	blue	Ribbon	N	N					Cotton
A	fibre	colourless	Ribbon	N	N					Cotton
A	fibre	colourless	Ribbon	N	N					Cotton
A	fibre	colourless	Ribbon	N	N					Cotton
A	fibre	blue	Ribbon	N	N					Cotton
A	fibre	blue	Ribbon	N	N					Cotton
A	fibre	brown	Irregular	H	N	25.4		P		Synthetic
A	fibre	colourless	Ribbon	N	N					Cotton
A	fibre	colourless	Ribbon	N	N					Cotton
A	fibre	colourless	Ribbon	N	N					Cotton
A	fibre	colourless	Ribbon	N	N					Cotton
A	fibre	colourless	Ribbon	N	N					Cotton
A	fibre	blue	Ribbon	N	N					Cotton
A	fibre	blue	Ribbon	N	N					Cotton
A	fibre	blue	Cylindrical	L	N	7.62		P	0.144	Polyester
A	fibre	black/blue	Bilobal	L	bicomponent	10.16		P	0.092/0.157	Polyester
A	fibre	blue	Ribbon	N	N					Cotton
A	fibre	blue	Multilobal/tape	N	N	20.32		P	0.054	Nylon
A	fibre	colourless	Ribbon	N	N					Cotton
A	fibre	colourless	Ribbon	N	N					Cotton
A	fibre	colourless	Ribbon	N	N					Cotton
A	fibre	colourless	Ribbon	N	N					Cotton
A	fibre	blue	Ribbon	N	N					Cotton
A	fibre	red	Ribbon	N	N					Cotton
A	fibre	blue	Ribbon	N	N					Cotton
A	fibre	blue	Ribbon	N	N					Cotton
A	fibre	colourless	Ribbon	N	N					Cotton
A	fibre	colourless	Ribbon	N	N					Cotton
A	fibre	blue	Cylindrical	L	N	10.16		P	0.177	Polyester
A	fibre	colourless	Cylindrical	L	N	10.16		P	0.172	Polyester
A	fibre	colourless	Irregular	L	N	15.24		P	0.181	Polyester
A	fibre	colourless	Bilobal	N	N	17.78		N	0.009	Acrylic
A	fibre	colourless	Ribbon	N	N	58.42		P		Synthetic
A	fibre	colourless	Ribbon	N	N					Cotton
A	fragment	blue		N	N	99.6	104.14			Synthetic
A	fibre	blue	Irregular	L	N	5.06		P	0.168	Polyester
A	fibre	colourless	Ribbon	N	N					Cotton
A	fibre	colourless	Ribbon	N	N					Cotton
A	fragment	red		N	N	76.2	91.44			Synthetic
A	fragment	red		N	N	96.52	233.68			Synthetic
A	fibre	colourless	Ribbon	N	N					Cotton
A	fibre	blue	Ribbon	N	N					Cotton
A	fibre	blue	Square	M	N	30.48		P	0.106	Polyester

A	fibre	colourless	Ribbon	N	N					Cotton
A	fibre	colourless	Ribbon	N	N					Cotton
A	fibre	black	Cylindrical	N	N	7.62		P	0.144	Polyester
A	fibre	colourless	Ribbon	N	N					Cotton
A	fibre	colourless	Ribbon	N	N					Cotton
A	fibre	blue	Ribbon	N	N					Cotton
A	fragment	red		N	N	99.06	167.64			Synthetic
A	fragment	pink/red/blue		N	N	48.26	134.62			Synthetic
A	fibre	colourless	Ribbon	N	N					Cotton
A	fibre	colourless	Ribbon	N	N					Cotton
A	fibre	colourless	Ribbon	N	degraded	38.01		P		Polyester
A	fibre	colourless	Ribbon	N	N					Cotton
A	fibre	blue	Ribbon	N	N					Cotton
A	fibre	blue	Ribbon	N	N					Cotton
A	fibre	colourless	Ribbon	N	N					Cotton
A	fibre	colourless	Ribbon	N	N					Cotton
A	fibre	blue	Cylindrical	L	N	11.43		P	0.175	Polyester
A	fibre	colourless	Ribbon	N	N					Cotton
A	fibre	colourless	Ribbon	N	N					Cotton
A	fibre	blue	Ribbon	N	N					Cotton
A	fragment	blue		N	N	40.64	50.8			Synthetic
A	fibre	colourless	Ribbon	N	N					Cotton
A	fibre	blue	Ribbon	N	N					Cotton
A	fibre	colourless	Ribbon	N	N					Cotton
A	fibre	red	Irregular	N	crosshatch	17.78				Anthropogenic
A	fibre	blue	Ribbon	N	N					Cotton
A	fibre	colourless	Ribbon	N	N					Cotton
A	fibre	colourless	Ribbon	N	N					Cotton
A	fibre	colourless	Ribbon	N	N					Cotton
A	fibre	blue	Ribbon	N	N					Cotton
A	fibre	blue	Ribbon	N	N					Cotton
A	fibre	colourless	Ribbon	N	N					Cotton
A	fibre	blue	Ribbon	N	N					Cotton
A	fibre	colourless	Ribbon	N	N					Cotton
A	fibre	blue	Ribbon	N	N					Cotton
A	fibre	colourless	Ribbon	N	N					Cotton
A	fibre	blue	Ribbon	N	N					Cotton
A	fibre	blue	Ribbon	N	N					Cotton
A	fibre	blue	Ribbon	N	N					Cotton
A	fibre	blue	Ribbon	N	N					Cotton
A	fibre	blue	Ribbon	N	N					Cotton
A	fibre	colourless	Ribbon	N	N					Cotton
A	fibre	blue	Ribbon	N	N					Cotton
A	fibre	colourless	Ribbon	N	N					Cotton
A	fibre	colourless	Ribbon	N	N					Cotton
A	fibre	colourless	Ribbon	N	N					Cotton

A	fragment	red		N	N	58.42	157.48			Synthetic
A	fibre	red	Ribbon	N	N					Cotton
A	fibre	colourless	Cylindrical	N	N	2.54		P		Synthetic
A	fibre	blue	Ribbon	N	N					Cotton
A	fibre	blue	Ribbon	N	N					Cotton
A	fibre	colourless	Ribbon	N	N					Cotton
A	fibre	colourless	Ribbon	N	N					Cotton
A	fibre	colourless	Ribbon	N	N					Cotton
A	fibre	colourless	Ribbon	N	N					Cotton
A	fibre	black	Cylindrical	H	N	30.48		P		Synthetic
A	fibre	blue	Ribbon	N	N					Cotton
A	fibre	blue	Ribbon	N	N					Cotton
A	fibre	blue	Cylindrical	L	N	7.62		P	0.144	Polyester
A	fibre	blue	Ribbon	N	N					Cotton
A	fibre	colourless	Ribbon	N	N					Cotton
A	fibre	colourless	Ribbon	N	N					Cotton
A	fibre	black	Ribbon	N	N					Cotton
A	fibre	colourless	Ribbon	N	N					Cotton
A	fibre	blue	Ribbon	N	N					Cotton
A	fibre	black	Cylindrical	H	N	10.16		P	0.148	Polyester
A	fibre	blue	Ribbon	N	N					Cotton
A	fibre	blue	Ribbon	N	N					Cotton
A	fibre	colourless	Ribbon	N	N					Cotton

Table A.6 a table to show the full characterisation of results found by polarised light microscopy.

Sample type	MP type	Colour	cross sectional shape	Delusterant	Other inclusions	Width µm	Length µm	sign of elongation	Birefringence	Identification
W	fibre	colourless	ribbon	N	N					Cotton
W	fibre	colourless	ribbon	N	N					Cotton
W	film	colourless		N	N					Synthetic
W	fibre	Blue	ribbon	N	N					Cotton
W	fibre	colourless	cylindrical	N	N	9.32	1258.2	P	0.064	Nylon
W	fibre	colourless	cylindrical	N	N					Hair
W	fragment	pink		N	N	5.34				UNKN
W	Fibre	yellow	ribbon	N	N					Cotton
W	fragment	Blue		N	N					Polyethylene
W	Fibre	Blue	ribbon	N	N					Cotton
W	fragment	red		N	N					Synthetic
W	Fibre	Blue	ribbon	N	N					Cotton
W	fragment	Blue		N	N					Synthetic
W	fibre	colourless	cylindrical	N	N	18.69	720.9	P	0.025	Synthetic
W	fibre	Blue	ribbon	N	N					Cotton
W	fibre	Blue	ribbon	N	N					Cotton
W	fragment	pink		N	N					Nylon
W	fibre	Blue	ribbon	N	N					Cotton
W	fragment	Blue		N	N					Synthetic

W	fibre	colourless	cylindrical	N	N	13.35	1070.67		0.097	Polyester (PCDT)
W	fibre	Blue	ribbon	N	N					Cotton
W	fragment	orange		N	N					Synthetic
W	fibre	colourless	cylindrical	N	stripes	32.04	432.54	P		UNKN
W	fibre	Blue	cylindrical	N	N	9.345	809.01	P	0.096	Polyester (PCDT)
W	fibre	colourless	cylindrical	L	N	10.67	1148.1	P	0.182	Polyester (PET)
W	fibre	Blue	ribbon	N	N					Cotton
W	fibre	red	ribbon	N	N					Cotton
W	fibre	Blue	ribbon	N	N					Cotton
W	fragment	red		N	N					Synthetic
W	fragment	red		N	N					Nylon
W	fibre	Blue	ribbon	N	N					Cotton
W	fibre	colourless	cylindrical	N	N					Hair (Textile)
W	fibre	Blue	ribbon	N	N					Cotton
W	fragment	red		N	N					Synthetic
W	fibre	Blue	cylindrical	N	N					Hair (Textile)
W	fragment	red		N	N					Synthetic
W	fragment	red		N	N					Nylon
W	fragment	red		N	N					Nylon
W	fibre	Blue	ribbon	N	N					Cotton
W	fibre	Blue	ribbon	N	N					Cotton
W	fibre	colourless	cylindrical	N	N	16.02	854.4	P	0.034	Polypropylene
W	fibre	Blue	ribbon	N	N					Cotton
W	fibre	colourless	bilobal	N	N	40.05	1388.4	P	>0.158	Synthetic
W	fibre	colourless	cylindrical	N	N	10.68	1043.97	P	0.051	Polyethylene/Nylon
W	fibre	blue	irregular	N	N					UNKN
W	fibre	blue	irregular	N	N					UNKN
W	fibre	colourless	bilobal	N	N	14.82	1971.06	P	>0.212	Nylon
W	fragment	red		N	N					Synthetic
W	fragment	red		N	N					Synthetic
W	fragment	blue		N	N					Nylon
W	fibre	colourless	cylindrical	N	N	12.35	1654.9	P	0.049	nylon
W	fragment	blue		N	N					Synthetic
W	fragment	blue		N	N					Polyester
W	fibre	red	ribbon	N	N					Cotton
W	fibre	colourless	cylindrical	N	N	3.705	1133.73	P	0.094	polyester (PCDT)
W	fibre	red	ribbon	N	N					Cotton
W	fibre	blue	ribbon	N	N					Cotton
W	fragment	blue		N	N					Synthetic
W	fibre	colourless	cylindrical	L	N	7.51		P	0.049	nylon
W	fibre	colourless	cylindrical	L	N	7.51		P	0.049	nylon
W	fibre	colourless	ribbon	N	N	12.35	343.33		0.091	Synthetic
W	fibre	colourless	cylindrical	N	N	34.58	259.35		0.032	Polypropylene
W	fibre	colourless	cylindrical	N	N	19.76	741	P	0.02	Anthropogenic
W	fibre	blue	ribbon	N	N					Cotton
W	fibre	colourless	cylindrical	N	N	7.41	852.15			Synthetic

W	fibre	blue	ribbon	N	N					Cotton
W	fibre	blue	cylindrical	N	N	7.41	247	P	0.147	Polyester (PET)
W	fibre	colourless/blue	multilobal	N	N	12.35	1037	P		Synthetic
W	fibre	colourless	bilobal	N	N	17.29	666.9	N	0.005	acrylic
W	fragment	colourless		N	N					Synthetic
W	fibre	red	ribbon	N	N					Cotton
W	fibre	colourless	cylindrical	L	N	9.88		P	0.091	Nylon
W	fibre	colourless	cylindrical	L	N	8.65	2717	P	0.098	Polyester (PCDT)
W	fibre	blue	ribbon	N	N					Cotton
W	fibre	colourless	cylindrical	H	N	9.88	790.4	P	0.091	Synthetic
W	fragment	red		N	N					Synthetic
W	fibre	red	ribbon	N	N					Cotton
W	fibre	colourless	cylindrical	H	N	12.35	666.9	P	0.089	Synthetic
W	fibre	colourless	bilobal	N	N	11.115	1803.1	P	0.161	Polyester
W	fibre	colourless	cylindrical	L	N	19.76	741	P	0.051	polyethylene/nylon
W	Fibre	colourless	cylindrical	N	N	8.645	913.9	P	0.104	Polyester
W	fibre	blue	ribbon	N	N					Cotton
W	fibre	red	ribbon	N	N					Cotton
W	fragment	blue		N	N					Synthetic
W	fibre	colourless	cylindrical	N	N	22.23	1173.25	P	0.029	polypropylene
W	fibre	colourless	cylindrical	N	N	2.47	2185.95	P		Synthetic
W	fragment	red		N	N					Nylon
W	fibre	blue	ribbon	N	N					Cotton
W	fibre	colourless	cylindrical	N	N	12.35	728.65	P	0.151	Polyester
W	fibre	red	ribbon	N	N					Cotton
W	fibre	colourless	multilobal	N	N	24.7	4199	P	>0.128	Polyester
W	fibre	colourless	cylindrical	N	N	9.88		P		Synthetic
W	fibre	colourless	cylindrical	N	N	16.055	617.5	N	0.004	acrylic
W	fibre	blue	ribbon	N	N					Cotton
W	microbead	blue		N	N					Synthetic
W	fibre	blue	ribbon	N	N					Cotton
W	fibre	colourless	circular	N	N					Hair (Textile)
W	fibre	colourless	cylindrical	L	N	12.35		N	0.001	acrylic
W	fibre	colourless	cylindrical	N	N	17.29		P	0.052	polyethylene/nylon
W	fibre	colourless	cylindrical	N	N	29.64		P	0.052	Nylon
W	fragment	blue								Synthetic
W	fibre	colourless	cylindrical	L	N	11.115	1407.9	P	0.161	Polyester
W	fibre	colourless	cylindrical	L	N	11.115	889.2	P	0.061	nylon
W	fibre	colourless	cylindrical	N	N					Hair (Textile)
W	fibre	colourless	cylindrical	N	N					Hair (Textile)
W	fibre	colourless	cylindrical	H	N	7.41		P	0.175	Polyester
W	fibre	colourless	cylindrical	L	N	12.35		P	0.174	Polyester
W	fibre	colourless	cylindrical	M	N	9.88		P	0.151	Polyester
W	fibre	black	ribbon	N	N					Cotton
W	fibre	blue	ribbon	N	N					Cotton
W	fibre	blue	ribbon	N	N					Cotton

W	fibre	blue	cylindrical	L	N	7.41	543.4			Polyester
W	fragment	blue		N	N					Synthetic
W	fragment	blue		N	N					Polypropylene
W	fragment	blue		N	N					Synthetic
W	fragment	blue		N	N					polypropylene
W	fragment	blue		N	N					polypropylene
W	fibre	blue	ribbon	N	N					Cotton
W	fibre	blue	ribbon	N	N					Cotton
W	fibre	colourless	multilobal	N	N	9.88				Synthetic
W	fragment	blue		N	N					polypropylene
W	fibre	colourless	cylindrical	L	N	4.94		P	0.06	nylon
W	fibre	red/colourless	cylindrical	L	N	9.88	414.96	P	0.098	Polyester
W	fibre	blue	ribbon	N	N					Cotton
W	microbead	colourless		N	N					Synthetic
W	fibre	colourless	trilobal	N	N	2.47		P	0.163	Polyester
W	fragment	colourless		N	N					Synthetic
W	fibre	colourless	cylindrical	N	N					Hair
W	fibre	colourless	cylindrical	M	N	7.41	494	P	0.148	Polyester
W	fibre	colourless	cylindrical	L	N	7.41		P	0.094	Polyester
W	fragment	blue		N	N					Synthetic
W	fibre	blue	ribbon	N	N					Cotton
W	fragment	blue		N	N					Synthetic
W	fibre	red	ribbon	N	N					Cotton
W	fibre	blue	ribbon	N	N					Cotton
W	fragment	blue		N	N					Synthetic
W	fibre	colourless	cylindrical	L	N	14.82		N	0.001	acrylic
W	fibre	blue	ribbon	N	N					Cotton
W	fibre	blue	cylindrical	N	N	14.82		P	0.101	polyester
W	fibre	colourless	cylindrical	M	N	10.16		P	0.177	Polyester (PET)
W	fibre	blue	cylindrical	N	N	10.16		P	0.064	nylon
W	fibre	colourless	cylindrical	N	N	12.7		P	0.177	Polyester (PET)
W	fibre	blue	ribbon	N	N					Cotton
W	fibre	blue	ribbon	N	N					Cotton
W	fragment	blue		N	N	38.1	121.92	N		Synthetic
W	fibre	colourless	cylindrical	N	N	12.7		N	0.005	acrylic
W	fibre	blue	cylindrical	N	N	8.89		P	0.101	Polyester
W	fibre	blue	cylindrical	N	N	8.89		P	0.101	Polyester
W	fibre	colourless	cylindrical	L	N	12.8		P	0.18	Polyester
W	fibre	blue	irregular	N	N	10.16		P		Synthetic
W	fibre	blue	ribbon	N	N					Cotton
W	fibre	red	delta	L	N	6.35		P	0.173	polyester
W	fibre	colourless	delta	L	N	10.16		P	0.103	polyester
W	fragment	blue		N	N	25.4	27.94			Synthetic
W	fibre	blue	cylindrical	L	N	10.16	205.74	P	0.063	nylon
W	fibre	colourless	cylindrical	N	N	7.62		P	0.157	Polyester
W	fibre	blue	cylindrical	N	N	8.89		P	0.101	polyester

W	fibre	colourless	cylindrical	N	N	17.78		P		Hair
W	fragment	blue		N	N	53.34	134.62			Polyvinyl Chloride
W	fragment	blue		N	N	152.4	312.42			Natural
W	fibre	blue	delta	N	N	7.62		P	0.177	Polyester
W	fibre	blue	ribbon	N	N					Cotton
W	fibre	colourless	cylindrical	L	N	10.16		P	0.188	Polyester
W	fragment	blue		N	N	78.74	205.74			Synthetic
W	fragment	red		N	N	10.16	15.24	P		Synthetic
W	fibre	colourless	delta	N	N	10.16		P	0.094	polyester (PCDT)
W	fibre	colourless	ribbon	L	N	7.62		P	0.105	polyester
W	fibre	colourless	cylindrical	N	N	10.16		P	0.049	nylon
W	fibre	blue	ribbon	N	N					Cotton
W	fibre	colourless	irregular	N	N	15.24		P	0.052	Polyethylene
W	fibre	blue	delta	L	N	7.62		P	0.144	Polyester
W	fibre	colourless	cylindrical	L	N	10.16		P	0.177	Polyester
W	fibre	colourless	cylindrical	N	N					Hair (Textile)
W	fibre	colourless	irregular	N	N	10.16		P	0.147	Polyester
W	fragment	red		N	N	55.88	55.88			Synthetic
W	fragment	blue		N	N	38.1	48.26			Synthetic
W	fibre	blue	ribbon	N	N					Cotton
W	fragment	blue		N	N	241.3	264.16			Synthetic
W	fibre	blue	ribbon	N	N					Cotton
W	fibre	colourless	cylindrical	N	N					Hair (Textile)
W	fragment	orange		N	N	25.4	35.56			Synthetic
W	fibre	colourless	delta	L	N	10.16		P	0.167	Polyester
W	fibre	blue	ribbon	N	N					Cotton
W	fibre	blue	ribbon	N	N					Cotton
W	fibre	colourless	cylindrical	M	N	13.97		P	0.175	Polyester
W	fibre	blue	irregular	L	N	13.97		P	0.032	polypropylene
W	fibre	red	cylindrical	L	N	10.16		P	0.004	acrylic
W	fragment	blue		N	N	10.16	15.25	P		Synthetic
W	fibre	blue	cylindrical	N	N	7.62		P	0.144	Polyester
W	fragment	blue		N	N	119.38	119.38			Synthetic
W	fibre	blue	cylindrical	N	N	7.62		P	0.183	polyester
W	fibre	blue	ribbon	N	N					Cotton
W	fibre	blue	delta	N	N	10.16		P	0.098	polyester
W	fibre	blue/colourless	multilobal/tape	L	N	17.78		P		Synthetic
W	fibre	blue	ribbon	N	N					Cotton
W	fibre	blue	delta	N	N	10.16		P	0.098	polyester
W	fragment	blue		N	N	91.44	142.24			Synthetic
W	fibre	colourless	delta	M	N	12.7		P	0.102	polyester
W	fibre	blue	cylindrical	L	N	7.62		P	0.171	polyester
W	fibre	colourless	delta	N	N	12.7		P	0.047	nylon
W	fibre	blue	irregular	L	N	7.62		P	0.151	polyester
W	fibre	blue	ribbon	N	N					Cotton
W	fibre	colourless	cylindrical	N	crosshatch	13.97		P	0.100	polyester

W	fibre	red	ribbon	N	N					Cotton
W	fibre	colourless	cylindrical	N	N	10.16		P	0.059	nylon
W	fibre	blue	ribbon	N	N					Cotton
W	fragment	blue		N	N	35.67	33.02			Synthetic
W	fibre	blue	ribbon	N	N					Cotton
W	fibre	blue	ribbon	N	N					Cotton
W	fibre	colourless	delta	L	N	10.16		P	0.108	polyester
W	fibre	blue	ribbon	N	N					Cotton
W	fibre	blue	ribbon	N	N					Cotton
W	fibre	colourless	delta	L	N	10.16		P	0.147	polyester
W	fibre	red	cylindrical	M	N	7.62		P	0.144	Polyester
W	fibre	colourless	ribbon	N	N	15.24		P	0.151	Polyester
W	fibre	colourless	cylindrical	N	N	20.32		N	0.003	acrylic
W	fibre	blue	delta	N	N	10.16		P	0.093	polyester
W	fibre	blue	ribbon	N	N					Cotton
W	fibre	blue	ribbon	N	N					Cotton
W	fibre	colourless	cylindrical	N	N	10.16		P	0.064	nylon
W	fibre	blue	ribbon	N	N					Cotton
W	fibre	colourless	cylindrical	L	fisheyes	10.16		P	0.167	polyester
W	fibre	colourless	cylindrical	N	N	27.94	83.82	P		synthetic
W	fibre	blue	ribbon	N	N					Cotton
W	fibre	red	cylindrical	L	N	7.62		P	0.144	polyester
W	fibre	colourless	cylindrical	N	N	10.16		P	0.246	synthetic
W	fibre	blue	ribbon	N	N					Cotton
W	fibre	red	ribbon	N	N					Cotton
W	fibre	red	ribbon	N	N					Cotton
W	fibre	colourless	cylindrical	N	N	22.86		P	0.048	nylon
W	fibre	blue	ribbon	N	N					Cotton
W	fibre	red	cylindrical	L	N	12.7		P	0.154	polyester
W	fibre	red	ribbon	N	N					Cotton
W	fibre	blue	cylindrical	L	N	7.62		P	0.144	polyester
W	fibre	blue	ribbon	N	N					Cotton
W	fragment	blue		N	N	58.42	134.62			Synthetic
W	fibre	colourless	multilobal/tape	N	N	48.26		P		synthetic
W	fibre	colourless	square	L	N	25.4		P	0.098	polyester
W	fibre	colourless	cylindrical	L	N	10.16		P	0.146	polyester
W	fibre	colourless	cylindrical	N	N	10.16		P	0.148	polyester
W	fragment	blue		N	N	12.7	12.7			Synthetic
W	fibre	blue	cylindrical	N	N	5.06		P	0.099	polyester
W	fibre	colourless	cylindrical	N	N					Hair
W	fibre	colourless	irregular	N	N	5.06		P	0.167	polyester
W	fibre	black	cylindrical	L	N	10.16		P	0.167	polyester
W	fibre	blue	ribbon	N	N					Cotton
W	fibre	colourless	cylindrical	L	N	15.24		N	0.007	acrylic
W	fibre	blue	irregular	N	N	10.12		P	0.177	polyester
W	fibre	blue	ribbon	N	N					Cotton

W	fibre	red	ribbon	N	N					Cotton
W	fibre	colourless	cylindrical	M	fisheyes	12.7		P	0.177	polyester
W	fibre	blue	cylindrical	L	N	7.62		P	0.157	polyester
W	fibre	colourless	cylindrical	N	fisheyes	10.16		P	0.182	polyester
W	fibre	colourless	irregular	N	N	12.7		P	0.106	polyester
W	fibre	blue	delta	L	N	10.16		P	0.138	polyester
W	fibre	colourless	cylindrical	N	N	10.16		P	0.157	polyester
W	fibre	colourless	cylindrical	L	N	10.16		P	0.196	synthetic
W	fibre	colourless	irregular	M	fisheyes	15.24		P	0.105	polyester
W	fibre	colourless	cylindrical	L	N	10.16		P	0.221	synthetic
W	fibre	blue	ribbon	N	N					Cotton
W	fragment	blue		N	N	40.64	180.34			Synthetic
W	fibre	blue	delta	L	N	7.62		P	0.183	Polyester
W	fibre	colourless	cylindrical	L	N	6.35		P	0.173	polyester
W	fibre	blue	ribbon	N	N					Cotton
W	fibre	red	ribbon	N	N					Cotton
W	fibre	blue	cylindrical	L	N	7.62		P	0.144	polyester
W	fibre	colourless	delta	N	N	10.16		P	0.108	polyester
W	fibre	colourless	irregular	L	N	12.7		P	0.216	synthetic
W	fibre	colourless	cylindrical	N	N	10.16		P	0.177	polyester
W	fibre	blue	ribbon	N	N					Cotton
A	fibre	colourless	cylindrical	L	N	7.65		P	0.098	polyester
A	fibre	red	ribbon	N	N					Cotton
A	fibre	colourless	ribbon	N	N					Cotton
A	fibre	colourless	cylindrical	N	N	43.35	135.15	P	0.025	polypropylene
A	fibre	colourless	ribbon	N	N					Cotton
A	fibre	colourless	ribbon	N	N					Cotton
A	fibre	colourless	cylindrical	M	N	15.3		P	0.154	polyester
A	fibre	colourless	ribbon	N	N					Cotton
A	fibre	colourless	ribbon	N	N					Cotton
A	fibre	blue	ribbon	N	N					Cotton
A	fibre	blue	cylindrical	N	N	12.75		P	0.156	polyester
A	fibre	colourless	ribbon	N	N					Cotton
A	fibre	colourless	ribbon	N	N					Cotton
A	fibre	colourless	ribbon	N	N					Cotton
A	fibre	blue	irregular	L	N	10.2		P	0.066	nylon
A	fibre	colourless	ribbon	N	N					Cotton
A	fibre	pink	ribbon	N	N					Cotton
A	fibre	colourless	ribbon	N	N					Cotton
A	fragment	blue		N	N	28.05	35.7			polypropylene
A	fibre	colourless	ribbon	N	N					Cotton
A	fibre	colourless	ribbon	N	N					Cotton
A	fibre	colourless	ribbon	N	N					Cotton
A	fibre	colourless	ribbon	N	N					Cotton
A	fibre	blue	cylindrical	L	N	10.2		P	0.147	polyester
A	fibre	colourless	ribbon	N	N					Cotton

A	fibre	colourless	ribbon	N	N					Cotton
A	fibre	blue	ribbon	N	N					Cotton
A	fibre	colourless	ribbon	N	N					Cotton
A	fibre	colourless	ribbon	N	N					Cotton
A	fibre	colourless	ribbon	N	N					Cotton
A	fibre	colourless	cylindrical	L	N	7.62		P	0.104	polyester
A	fibre	colourless	ribbon	N	N					Cotton
A	fibre	colourless	ribbon	N	N					Cotton
A	fibre	colourless	ribbon	N	N					Cotton
A	fibre	colourless	ribbon	N	N					Cotton
A	fibre	colourless	ribbon	N	N					Cotton
A	fibre	colourless	ribbon	N	N					Cotton
A	fibre	colourless	ribbon	N	N					Cotton
A	fibre	colourless	ribbon	N	N					Cotton
A	fibre	colourless	ribbon	N	N					Cotton
A	fibre	colourless	ribbon	N	N					Cotton
A	fibre	colourless	ribbon	N	N					Cotton
A	fibre	colourless	ribbon	N	N					Cotton
A	fibre	colourless	ribbon	N	N					Cotton
A	fibre	blue	cylindrical	N	N	40.64	246.38			synthetic
A	fibre	colourless	ribbon	N	N					Cotton
A	fibre	colourless	cylindrical	L	N	10.16		P	0.167	polyester
A	fibre	colourless	ribbon	N	N					Cotton
A	fibre	colourless	ribbon	N	N					Cotton
A	fibre	colourless	ribbon	N	N					Cotton
A	fibre	colourless	ribbon	N	N					Cotton
A	fibre	colourless	ribbon	N	N					Cotton
A	fibre	colourless	ribbon	N	N					Cotton
A	fibre	colourless	ribbon	N	N					Cotton
A	fibre	colourless	ribbon	N	N					Cotton
A	fibre	colourless	ribbon	N	N					Cotton
A	fibre	colourless	ribbon	N	N					Cotton
A	fibre	colourless	ribbon	N	N					Cotton
A	fibre	colourless	ribbon	N	N					Cotton
A	fibre	colourless	ribbon	N	N					Cotton
A	fibre	colourless	cylindrical	N	N	7.62		P	0.098	polyester
A	fibre	colourless	ribbon	N	N					Cotton
A	fibre	colourless	ribbon	N	N					Cotton
A	fibre	colourless	ribbon	N	N					Cotton
A	fibre	colourless	ribbon	N	N					Cotton
A	fibre	colourless	ribbon	N	N					Cotton
A	fibre	colourless	ribbon	N	N					Cotton
A	fibre	colourless	ribbon	N	N					Cotton
A	fibre	colourless	ribbon	N	N					Cotton
A	fibre	colourless	ribbon	N	N					Cotton
A	fibre	colourless	ribbon	N	N					Cotton

A	fibre	colourless	ribbon	N	N					Cotton
A	fibre	colourless	ribbon	N	N					Cotton
A	fibre	colourless	ribbon	N	N					Cotton
A	fibre	colourless	ribbon	N	N					Cotton
A	fibre	colourless	ribbon	N	N					Cotton
A	fibre	colourless	ribbon	N	N					Cotton
A	fibre	colourless	ribbon	N	N					Cotton
A	fibre	colourless	ribbon	N	N					Cotton
A	fibre	blue	ribbon	N	N					Cotton
A	fibre	colourless

A	fibre	colourless	ribbon	N	N					Cotton
A	fibre	colourless	ribbon	N	N					Cotton
A	fibre	colourless	ribbon	N	N					Cotton
A	fibre	colourless	ribbon	N	N					Cotton
A	fibre	colourless	ribbon	N	N					Cotton
A	fibre	colourless	bilobal	L	N	25.4		P	0.055	nylon
A	fibre	colourless	ribbon	N	N					Cotton
A	fibre	colourless	ribbon	N	N					Cotton
A	fibre	colourless	ribbon	N	N					Cotton
A	fibre	colourless	ribbon	N	N					Cotton
A	fibre	blue	ribbon	N	N					Cotton
A	fibre	colourless	ribbon	N	N					Cotton
A	fibre	colourless	ribbon	N	N					Cotton
A	fibre	colourless	ribbon	N	N					Cotton
A	fibre	colourless	ribbon	N	N					Cotton
A	fibre	colourless	ribbon	N	N					Cotton
A	fibre	colourless	ribbon	N	N					Cotton
A	fibre	colourless	ribbon	N	N					Cotton
A	fibre	blue	ribbon	N	N					Cotton
A	fibre	blue	ribbon	N	N					Cotton
A	fibre	colourless	ribbon	N	N					Cotton
A	fibre	colourless	ribbon	N	N					Cotton
A	fibre	colourless	ribbon	N	N					Cotton
A	fibre	colourless	ribbon	N	N					Cotton
A	fibre	colourless	ribbon	N	N					Cotton
A	fibre	colourless	cylindrical	M	N	22.86		P	>0.175	polyester
A	fibre	colourless	ribbon	N	N					Cotton
A	fibre	colourless	ribbon	N	N					Cotton
A	fibre	colourless	ribbon	N	N					Cotton
A	fibre	colourless	ribbon	N	N					Cotton
A	fibre	colourless	ribbon	N	N					Cotton
A	fibre	colourless	ribbon	N	N					Cotton
A	fibre	colourless	ribbon	N	N					Cotton
A	fibre	colourless	ribbon	N	N					Cotton
A	fibre	colourless	ribbon	N	N					Cotton
A	fibre	colourless	ribbon	N	N					Cotton
A	fibre	colourless	ribbon	N	N					Cotton
A	fibre	colourless	ribbon	N	N					Cotton
A	fibre	colourless	ribbon	N	N					Cotton
A	fibre	colourless	ribbon	N	N					Cotton
A	fibre	colourless	ribbon	N	N					Cotton
A	fibre	colourless	ribbon	N	N					Cotton
A	fibre	colourless	ribbon	N	N					Cotton
A	fibre	colourless	delta	L	N	10.16		P	0.177	polyester
A	fibre	colourless	ribbon	N	N					Cotton
A	fibre	colourless	ribbon	N	N					Cotton

A	fibre	colourless	ribbon	N	N					Cotton
A	fibre	colourless	ribbon	N	N					Cotton
A	fibre	colourless	ribbon	N	N					Cotton
A	fibre	colourless	ribbon	N	N					Cotton
A	fibre	colourless	ribbon	N	N					Cotton
A	fibre	colourless	irregular	N	crosshatch	17.78		P	0.101	polyester
A	fibre	colourless	ribbon	N	N					Cotton
A	fibre	colourless	ribbon	N	N					Cotton
A	fibre	colourless	ribbon	N	N					Cotton
A	fibre	colourless	ribbon	N	N					Cotton
A	fibre	colourless	ribbon	N	N					Cotton
A	fibre	colourless	ribbon	N	N					Cotton
A	fibre	colourless	ribbon	N	N					Cotton
A	fibre	colourless	irregular	N	N	6.35		P	0.173	polyester
A	fibre	colourless	ribbon	N	N					Cotton
A	fibre	colourless	ribbon	N	N					Cotton
A	fibre	colourless	ribbon	N	N					Cotton
A	fibre	colourless	ribbon	N	N					Cotton
A	fibre	colourless	ribbon	N	N					Cotton
A	fibre	colourless	ribbon	N	N					Cotton
A	fibre	colourless	ribbon	N	N					Cotton
A	fibre	colourless	ribbon	N	N					Cotton
A	fibre	colourless	ribbon	N	N					Cotton
A	fibre	colourless	irregular	M	N	12.7		P	0.094	polyester
A	fibre	colourless	ribbon	N	N					Cotton
A	fibre	colourless	ribbon	N	N					Cotton
A	fibre	colourless	ribbon	N	N					Cotton
A	fibre	colourless	ribbon	N	N					Cotton
A	fibre	colourless	irregular	N	N	12.7	93.98	P	0.098	polyester
A	fibre	colourless	ribbon	N	N					Cotton
A	fibre	colourless	ribbon	N	N					Cotton
A	fibre	colourless	ribbon	N	N					Cotton
A	fibre	colourless	irregular	N	damage	30.48	317.5	P	0.045	nylon
A	fibre	colourless	ribbon	N	N					Cotton
A	fibre	blue	ribbon	N	N					Cotton
A	fibre	colourless	ribbon	N	N					Cotton
A	fibre	colourless	ribbon	N	N					Cotton
A	fibre	colourless	ribbon	N	N					Cotton
A	fibre	colourless	bilobal	N	N	10.12		P	0.046	nylon
A	fibre	colourless	ribbon	N	N					Cotton
A	fibre	colourless	ribbon	N	N					Cotton
A	fibre	colourless	ribbon	N	N					Cotton
A	fibre	colourless	ribbon	N	N					Cotton
A	fibre	colourless	ribbon	N	N					Cotton
A	fibre	colourless	ribbon	N	N					Cotton

A	fibre	colourless	ribbon	N	N					Cotton

A	fibre	colourless	ribbon	N	N					Cotton
A	fibre	colourless	ribbon	N	N					Cotton
A	fibre	colourless	ribbon	N	N					Cotton
A	fibre	colourless	ribbon	N	N					Cotton
A	fibre	colourless	ribbon	N	N					Cotton
A	fibre	colourless	ribbon	N	N					Cotton
A	fragment	blue		N	N	30.48	50.8			synthetic
A	fibre	colourless	ribbon	N	N					Cotton
A	fibre	colourless	ribbon	N	N					Cotton
A	fibre	colourless	ribbon	N	N					Cotton
A	fibre	colourless	ribbon	N	N					Cotton
A	fibre	colourless	ribbon	N	N					Cotton
A	fibre	colourless	ribbon	N	N					Cotton
A	fibre	colourless	ribbon	N	N					Cotton
A	fibre	colourless	ribbon	N	N					Cotton
A	fibre	colourless	ribbon	N	N					Cotton
A	fibre	blue	cylindrical	L	N	7.62		P	0.105	polyester
A	fibre	colourless	ribbon	N	N					Cotton
A	fibre	colourless	ribbon	N	N					Cotton
A	fibre	colourless	ribbon	N	N					Cotton
A	fibre	colourless	ribbon	N	N					Cotton
A	fibre	colourless	ribbon	N	N					Cotton
A	fibre	colourless	ribbon	N	N					Cotton
A	fibre	colourless	ribbon	N	N					Cotton
A	fibre	colourless	ribbon	N	N					Cotton
A	fibre	colourless	ribbon	N	N					Cotton
A	fibre	colourless	ribbon	N	N					Cotton

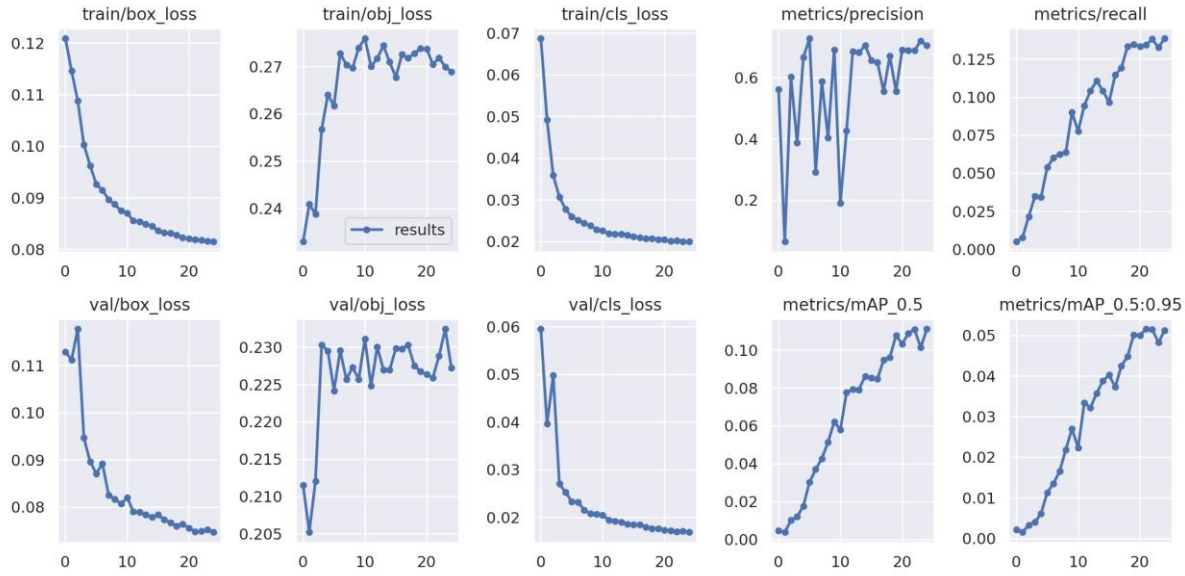

Figure A.8 A series of graphs to evaluate the model's performance when the dataset is trained with YOLOv5 for 25 epochs.

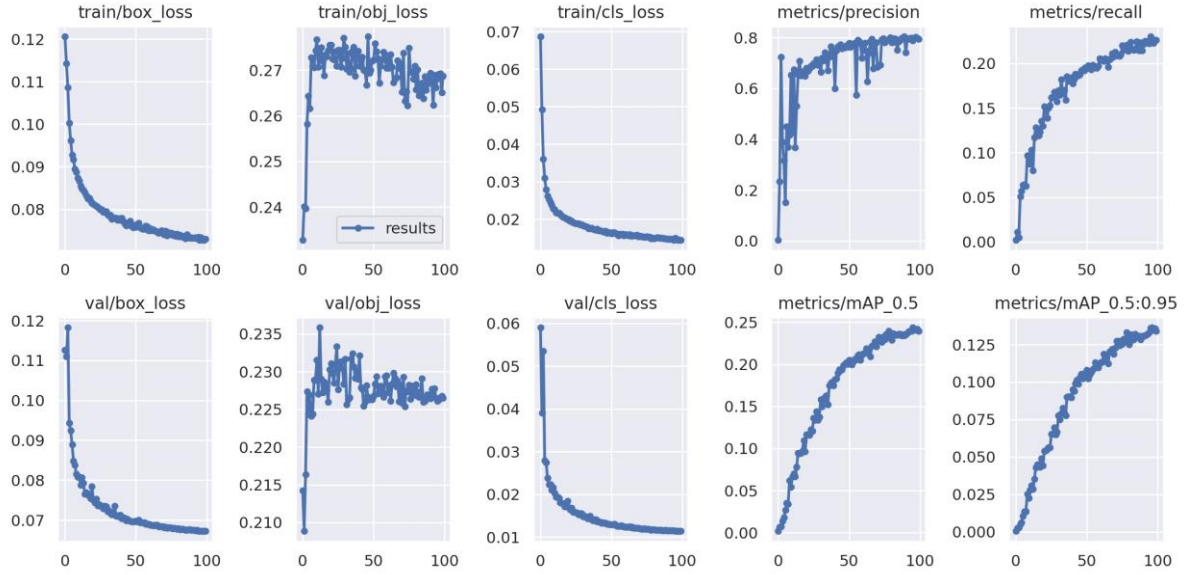

Figure A.9 A series of graphs to evaluate the model's performance when the dataset is trained with YOLOv5 for 100 epochs.

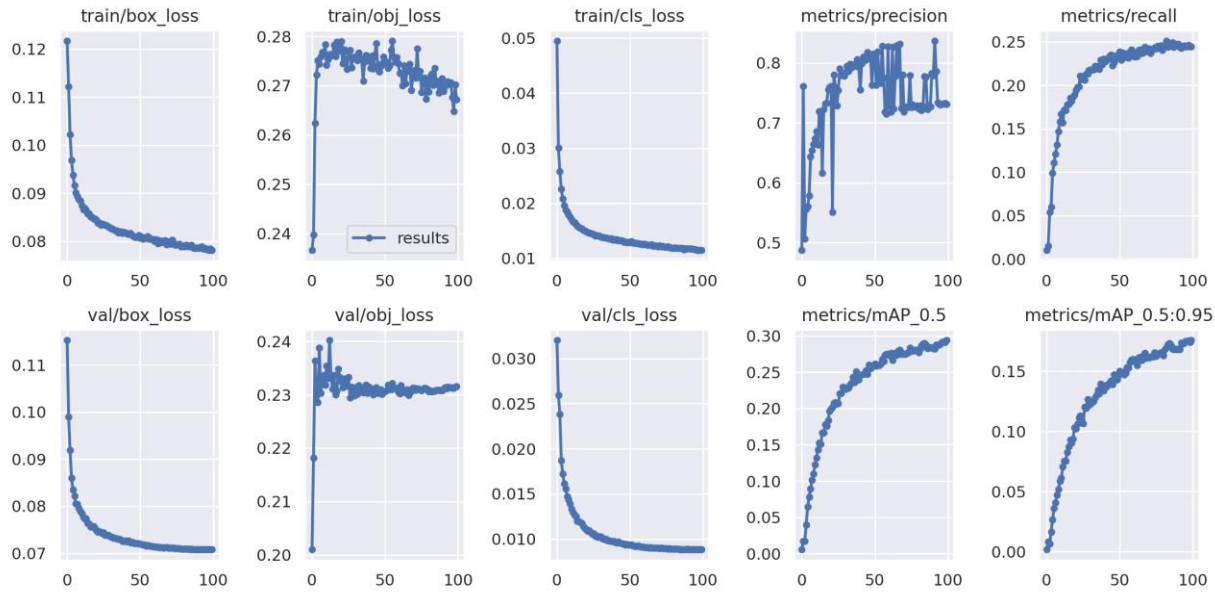

Figure A.10 A series of graphs to evaluate the model's performance when the dataset is trained with augmented images using YOLOv5 for 100 epochs.

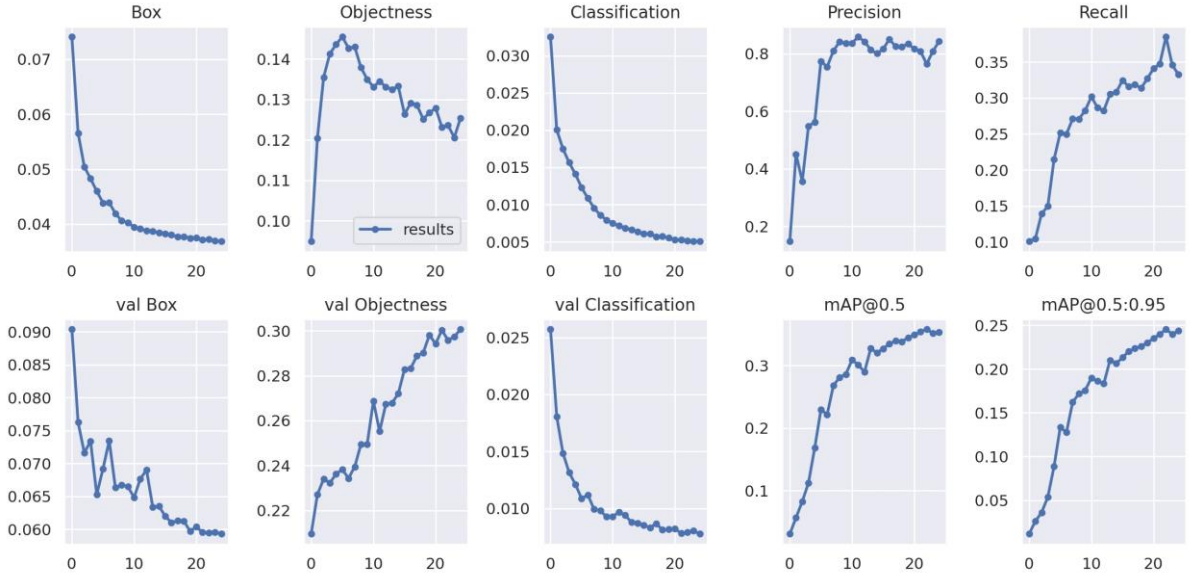

Figure A.11 A series of graphs to evaluate the model's performance when the dataset is trained using YOLOv7 for 25 epochs.

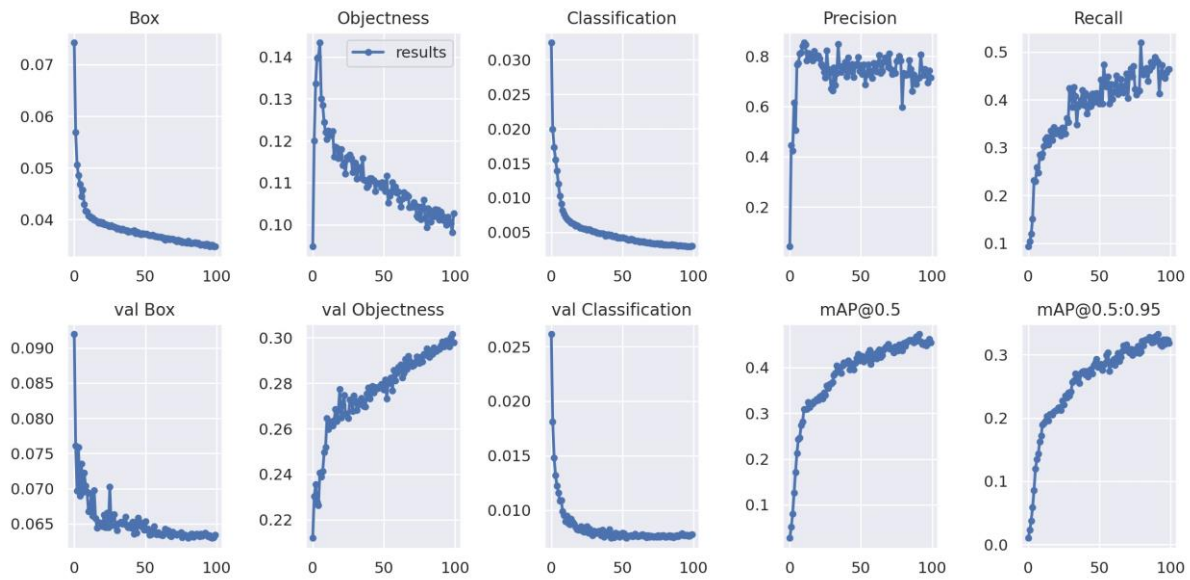

Figure A.12 A series of graphs to evaluate the model's performance when the dataset is trained using YOLOv7 for 100 epochs.

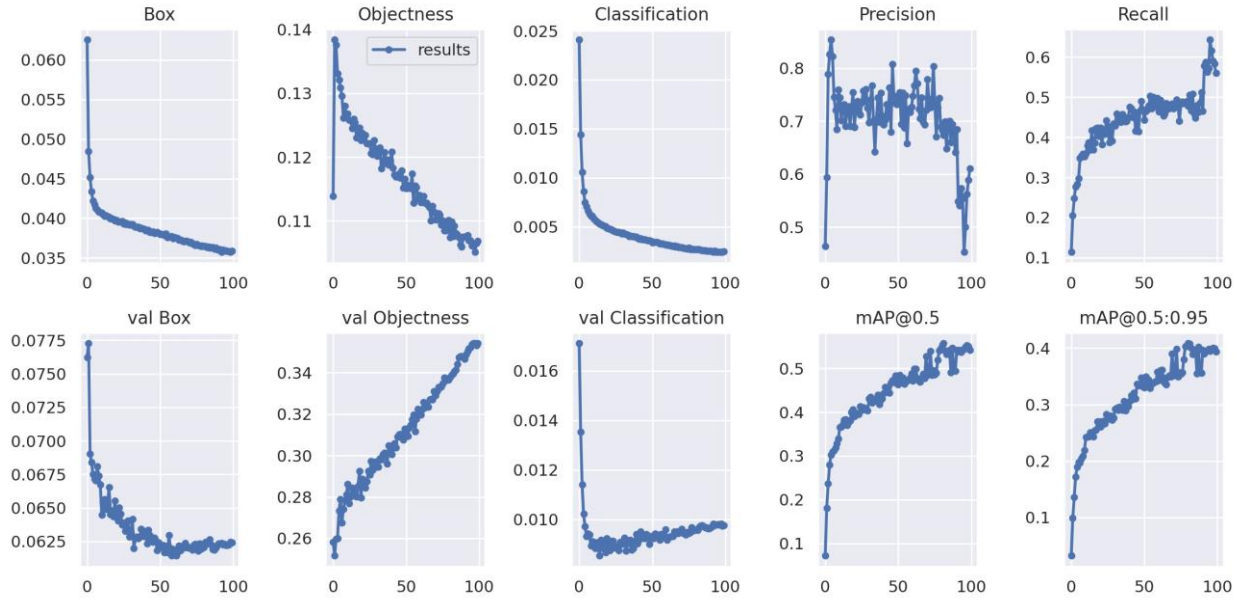

Figure A.13 A series of graphs to evaluate the model's performance when the dataset is trained with augmented images using YOLOv7 for 100 epochs.

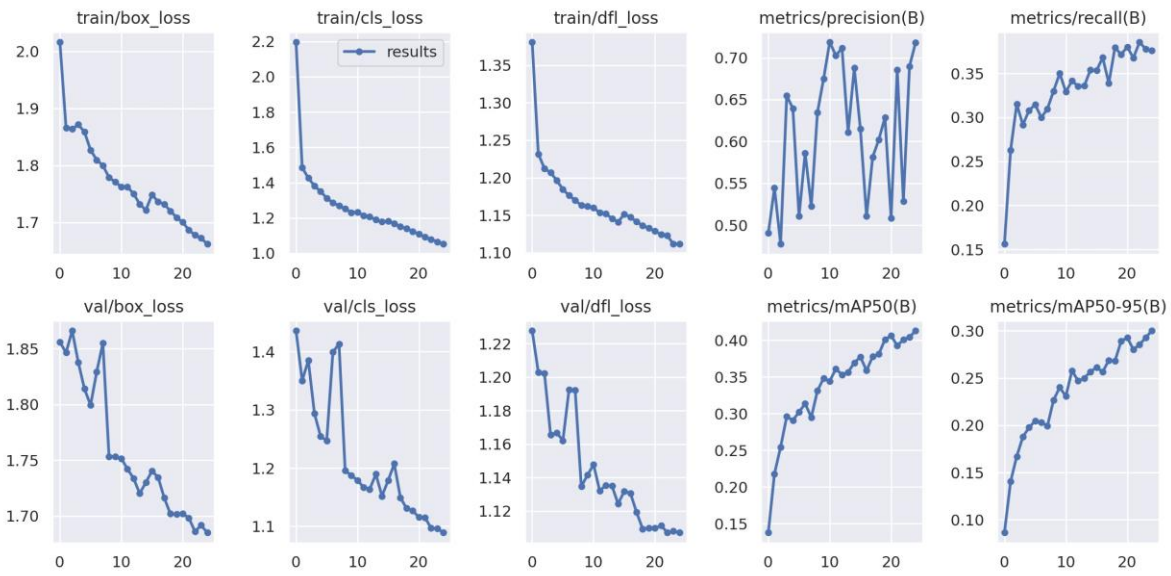

Figure A.14 A series of graphs to evaluate the model's performance when the dataset is trained using YOLOv8 for 25 epochs.

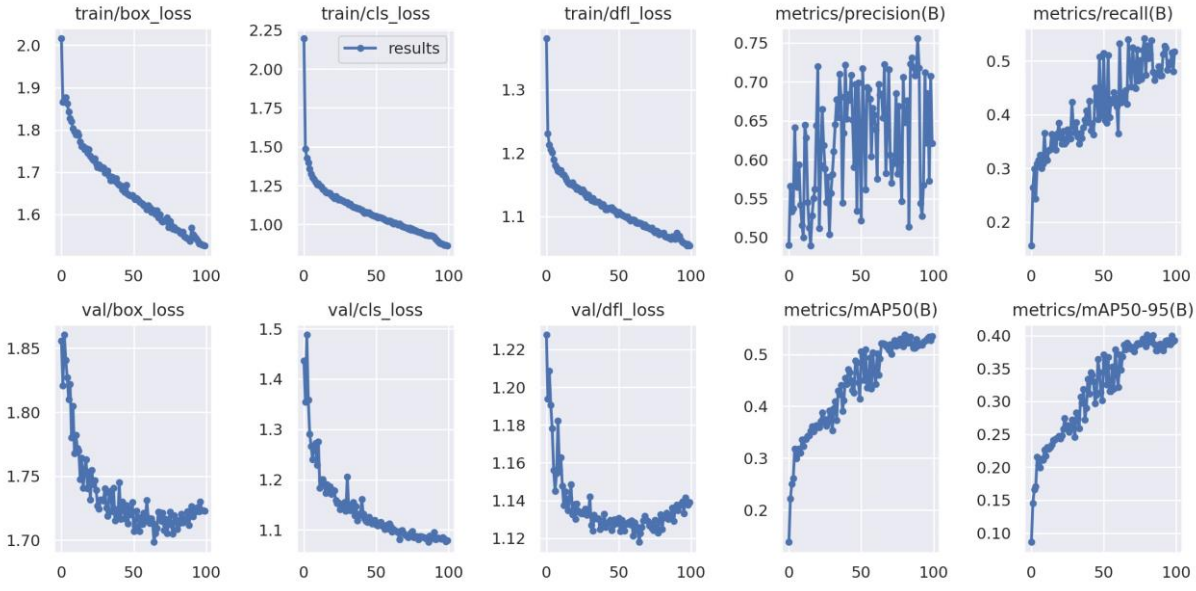

Figure A.14 A series of graphs to evaluate the model's performance when the dataset is trained using YOLOv8 for 100 epochs.

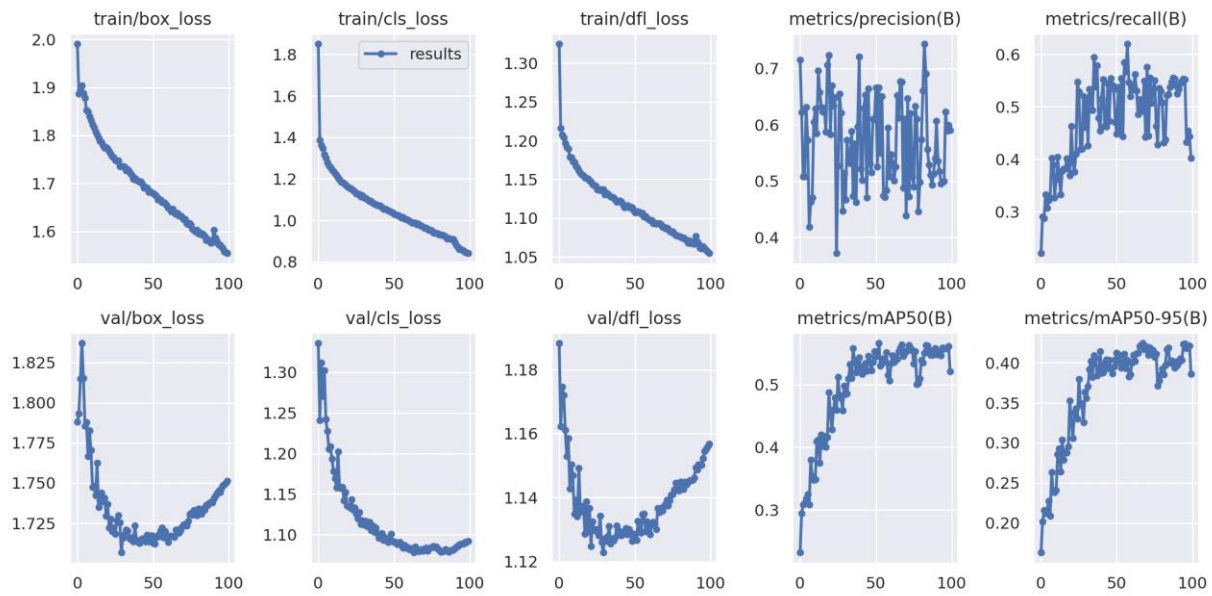

Figure A.15 A series of graphs to evaluate the model's performance when the dataset is trained with augmented images using YOLOv8 for 100 epochs.

Appendix B – Published Papers.

CUNNINGHAM, E. M., SEIJO, N. R., ALTIERI, K. E., AUDH, R. R., BURGER, J. M., BORNMAN, T. G., FAWCETT, S., GWINNETT, C. M. B., OSBORNE, A. O. & WOODALL. L. C. (2022). The transport and fate of microplastic fibres in the Antarctic: The role of multiple global processes. *Frontiers in Marine Science*. 9. pp. 1056081. (Online). Available from: https://doi.org/10.3389/fmars.2022.1056081. [Accessed: 23/11/2022].

GWINNETT, C. HARRISON, E. OSBORNE, A., PIVATO, A. & VARGHESE, G. (2021). Sampling microplastics for environmental forensic applications. *Detritus*. 14. (Online). Available from: https://doi.org/10.31025/2611-4135/2021.14080.

GWINNETT, M. B., OSBORNE, A. O. & JACKSON, A. R. W. (2021). The application of tape lifting for microplastic pollution monitoring. *Environmental Advances*. 5. pp. 100066. (Online). Available from: https://doi.org/10.1016/j.envadv.2021.100066. [Accessed: 26/06/21].

JACKSON, A. R. W., OSBORNE, A. O., GWINNETT, C. M. B. (2021), *Microplastic pollution isolation - a forensic science approach*, Mendeley Data, v1, http://dx.doi.org/10.17632/jzppg7h8j4.1.

MILLER, R. Z., WINSLOW, B., KAPP, K., OSBORNE, A. & GWINNETT, C. (2023). Microplastic and anthropogenic microfiber pollution in the surface waters of the East River and Long Island sound, USA. *Regional studies in marine science*. 70. (Online). https://doi.org/10.1016/j.rsma.2023.103360.

STANTON, T., STANES, E., GWINNETT, C., LEI, X., CAUILAN, M., RAMOS, M., SALLACH, J. B., HARRISON, E., OSBORNE, A., SANDERS, C. H., BAYNES, E., LAW, A., JOHNSON, M., RYVES, D. B., SHERIDAN, K. J., BLACKBURN, R. S. & MCKAY, D. (2023). Shedding off-the-grid: The role of garment manufacturing and textile care in global microfibre pollution. *Journal of Cleaner Production*. 428. (Online). Available from: https://doi.org/10.1016/j.jclepro.2023.139391.

Glossary.

Algorithm – A set of rules that need to be followed for a computer to achieve a certain task or problem-solving processes.

Anthropogenic materials – microplastics and natural materials that have been processed by humans, such as cotton.

Biofilm – A collection of microbial cells including bacteria, fungus, protist and diatoms that form a film on a surface.

Birefringence – an optical property of a material that has two refractive indices, n perpendicular and n parallel. Birefringence is the difference between the two refractive indices. It can give an indication of the polymer type.

Class/classification – The names of the object class e.g. ‘microfibre’ and ‘fragment’.

Convolution – A process where two pieces of information are intertwined.

Crossed polars – The sample is illuminated between two polaroids at 90° to each other to show the specimens interference colours.

Delusterant – An additive for synthetic fibres that removes its lustre (sheen). Most commonly made from titanium dioxide.

Epoch – A complete pass through of the training dataset through an algorithm.

F1 score – The harmonic mean between precision and recall.

False negatives – Where the model incorrectly predicts a classification as being negative.

False positives – Where the model incorrectly predicts a classification is positive.

Kernel – a matrix of weights that performs an element-wise multiplication on the image provided and summarises it in a single pixel.

Interference colours – a colour produced when an object is illuminated under crossed polars it indicated the optical path difference of the material.

Intersection over union (IOU) – An evaluation of an object detection by comparing how close the predicted bounding box is to the ground truth bounding box.

Köhler Illumination – The process of illuminating specimens with the optimum contrast and resolution, with the aim to provide an even illumination across the sample.

mAP50 – A measure of the model's performance with 'easy' identifications where the IOU meets the threshold of 0.50.

mAP50-95 – A more comprehensive view of the model's ability to identify objects at a varying level of detection difficulty calculated from the mean average precision at varying IOU thresholds ranging between 0.50 to 0.95.

Mean average precision (mAP) – a metric to measure a model's performance in object detection tasks.

Microfibre – both natural and synthetic fibres that are anthropogenic in origin. The length is longer than its width.

Microplastic – synthetic polymer materials under 5mm.

Model – The result of training with an algorithm.

Optical path difference – a numerical figure that is the result of the thickness of the specimin being observed and the difference between its two refractive indices.

Plane polarised light – The sample is illuminated with one polaroid in the light path.

Precision – The measure of how many positive identifications were true positives. True positives/ (true positives+ false positives).

Recall – The measure of how many true positives were correctly identified. True positives/ (true positives + false negatives).

Reflective illumination – The sample is illuminated from above; the light will reflect back to the eye pieces allowing the samples surface to become visible.

Sign of elongation – An indication of which of the two refractive indices is bigger than the other, if n perpendicular is bigger than n parallel then there is a positive sign of elongation. Conversely if n parallel is bigger than n perpendicular then there is a negative sign of elongation.

Transmitted illumination – The sample is illuminated from beneath, allowing the light to pass through the sample. This allows the internal structure of thin structures to be observed.

True negatives – Where the model correctly predicts a classification as being negative.

True positives – Where the model correctly predicts a classification as being positive.

You Only Look Once (YOLO) – A single pass object detection algorithm.